Identification of factors affecting the physicochemical behaviour and fate of engineered metallic nanoparticles released into aquatic environments

Frederik Van Koetsem

"You can never cross the ocean
until you have the courage to lose sight of the shore."

~ Christopher Columbus

Promoter:	Prof. dr. ir. Gijs Du Laing Department of Applied Analytical and Physical Chemistry Laboratory of Analytical Chemistry and Applied Ecochemistry
Dean:	Prof. dr. ir. Guido Van Huylenbroeck
Rector:	Prof. dr. Anne De Paepe

Frederik Van Koetsem

IDENTIFICATION OF FACTORS AFFECTING THE PHYSICOCHEMICAL BEHAVIOUR AND FATE OF ENGINEERED METALLIC NANOPARTICLES RELEASED INTO AQUATIC ENVIRONMENTS

Thesis submitted in fulfilment of the requirements for the degree of
Doctor (PhD) in Applied Biological Sciences

Dutch translation of the title:

Identificatie van factoren die het fysicochemisch gedrag en lot van metallische nanopartikels in aquatische milieus beïnvloeden

Cover illustrations:

Front: Picture of the Biobío river (Chile) at base level (Photograph © 2006 Gustavo Burgos, Concepcíon, Chile)

Back: Word cloud created from this thesis with Wordle™

Printed by: University Press, Zelzate, Belgium

Please refer to this thesis as follows:

Van Koetsem, F. (2015). **Identification of factors affecting the physicochemical behaviour and fate of engineered metallic nanoparticles released into aquatic environments.** PhD thesis, Faculty of Bioscience Engineering, Ghent University, Ghent, Belgium, pp. 320.

ISBN: 978-90-5989-798-4

The author and the promoter give the authorisation to consult and to copy parts of this work for personal use only. Every other use is subject to the copyright laws. Permission to reproduce any material contained in this work should be obtained from the author.

Woord vooraf

Every beginning has an end... en hier zijn we dan. Bijna exact 5 jaar na datum is de tijd gekomen om de laatste bladzijde van een boeiend en leerrijk doctoraatsverhaal om te slaan. Een verhaal dat handelde over "de kleine dingen". Maar vooraleer we daaraan toe zijn wil ik graag een kort woordje van dank richten aan iedereen die zowel rechtstreeks als onrechtstreeks heeft bijgedragen tot het finaal tot stand komen van dit werk.

In eerste instantie zou ik heel graag mijn promotor Prof. Gijs Du Laing willen bedanken om me de mogelijkheid aan te reiken mezelf te kunnen verdiepen in de wondere wereld van nanodeeltjes, voor het vertrouwen om me op zelfstandige wijze dit onderzoek te laten uitvoeren en voor het feit dat uw deur ten allen tijde open stond voor de nodige raad en daad. Bovendien koester ik de talloze gezellige momenten, zowel in binnen- als buitenland, maar ben ik er toch ook niet rouwig om dat bepaalde filmpjes m.b.t. mezelf en een glaasje cava van uw gsm verdwenen zijn…

Verder dank ik ook de overige leden van de examencommissie, Prof. Filip Tack, Prof. Jörg Rinklebe, Prof. Stijn Van Hulle, Prof. Diederik Rousseau en Prof. Stefaan de Smet, voor hun grondige evaluatie van dit werk en het formuleren van interessante en constructieve bemerkingen en suggesties.

Gedurende de afgelopen jaren in dienst van het Labo voor Analytische Chemie en Toegepaste Ecochemie ben ik omringd geweest door een zeer fijne groep collega's aan wie ik dan ook van harte wil zeggen: "dikke merci voor alles!" Aan de (ex-)medebezetters van "den bureau op 't 6e" Brecht, Céline, Ellen, Eva, Ivona, Jeroen, Karel, Lies, Natalia, Reinhart, Sofie, Srikanth, Stijn, Pradeep en Yasin, alsook aan Evelien, Evi, Hannele, Maja, Prof. Erik Meers en Prof. Filip Tack, bedankt voor het aangename gezelschap en de leuke tijden! Aan de achterblijvende lichting doctoraatstudenten maar ook aan de nieuwe lichting (Peter en Tsegaye), veel succes met jullie onderzoek! En wat zou een arme doctoraatstudent zijn zonder technische, administratieve en logistieke ondersteuning? Hiervoor wil ik Ann, Joachim, Katty, Martin, Ria en Roseline, dan ook van harte bedanken, evenals voor de vele leuke babbeltjes tussendoor. Ria en Martin, ik hoop dat jullie ondertussen ten volle genieten van jullie welverdiende pensioen! Joachim, jou wil ik toch nog eens extra bedanken voor alle hulp bij de vele labo-analyses en de staalnames "in 't veld". Onze avonturen gedurende het samplen van sediment langsheen de Schelde of het verzamelen van oppervlaktewaterstalen, waarbij bv. menig trechter er op eigen houtje vandoor dreigde te zwemmen, staan voor

eeuwig in mijn geheugen gegrift! Verder kijk ik ook met veel plezier terug op enkele "extra-professionele initiatieven/activiteiten" met jullie allen, zoals o.a. de verjaardagstraktaties, de nieuwjaarsetentjes, de WK-pronostiek, de trappenloop competitie, het bowlen en het zaalvoetballen. Hopelijk kunnen dergelijke tradities in ere blijven…

Ook de collega's vanop "het 3e" wil ik graag bedanken: Prof. Paul Van der Meeren voor de aangename en leerrijke discussies, Quenten voor alle assistentie inzake deeltjesgrootte en deeltjeslading analyses, en ook Saskia, Eric, Katja en Prof. Arne Verliefde voor de aangename babbeltjes en dito samenwerking.

Verder wil ik ook nog Elien en Prof. Kim Verbeken van de vakgroep Toegepaste Materiaalwetenschappen bedanken voor alle ondersteuning m.b.t. TEM analyses en voor de aangename gesprekjes tussendoor.

I would also like to extend my sincerest gratitude to Prof. Jörg Rinklebe and his staff members Björn, Carsten, Claus, Daniel, Felix, Jens, Julia, Kai, Marc, Mareen, Melanie, Moritz, Susanne, and Tina, of the Department of Soil- and Groundwater Management at the University of Wuppertal (Germany), where I spent conducting the final experiments for this research. Not only for their assistance during the experimental work, but also for the very pleasant chats in between. Jörg, many thanks for your supervision and for your kind hospitality, which immediately made me feel like home. I also really enjoyed the BBQ at your place. Björn, the latter could also be said in your case. It appears you Germans like BBQ as much as we Belgians do! *Vielen Dank für alles!*

Samen met mij hebben een aantal thesisstudenten eveneens de wondere wereld van de nanopartikels verkend. Ik bedank Simon, Lynn, Yi, Gebe en Teddy dan ook van harte voor hun inzet en bijdrage aan dit onderzoek.

Vermits het leven natuurlijk veel meer is dan onderzoek alleen wil ik graag mijn familie en vrienden bedanken om op tijd en stond te zorgen voor aangename afleiding en de nodige ontspanning, maar uiteraard ook voor al jullie steun gedurende de drukke tijden en de interesse in mijn werk. Om ontelbare redenen wil ik in de eerste plaats mijn ouders bedanken vanuit de grond van mijn hart! Het warme gezinsnest dat jullie gecreëerd hebben en jullie nimmer aflatende steun door de jaren heen, hebben onomstotelijk bijgedragen tot het succesvol afronden van een lange studieloopbaan. Eeuwige dank voor alles! Hier hebben uiteraard ook mijn broertje en grote zus een groot aandeel in gehad. Dikke merci Mattias en

Katrin, een mens kan zich geen betere “siblings” wensen! Ook bedankt Moeke en Bomma, eindelijk kan ik jullie vertellen dat er een einde gekomen is aan de lange studententijd. Ronny en Carine, jullie eveneens bedankt voor alles gedurende de afgelopen jaren. Verder ook dank aan Peter en Nieke, Pascale en Guy, Celine, Kevin en Lennert, voor jullie interesse en steun en om me op te nemen in de “schoonfamilie” als zijnde één van jullie.
Tenslotte, merci aan de zovele vrienden! Bedankt An, Ben, Bossi, Elie, Gerwin, Ines, Ive, Jeroen, Julie, Micha, Miho, Nicky, Pieter Jan, Rob, Ryan, Saartje, Stephanie, Thierry, Valérie, Valerie, Veronique, Ward, Wim, …, niet enkel voor jullie steun en interesse of de welgekomen ontspanning, maar tevens voor het diepgaande begrip dat ik jullie (zeker gedurende deze laatste maanden) misschien een beetje heb verwaarloosd door het vele werk! Denis, bijna exact 2 jaar geleden plots en veel te vroeg uit onze vriendenkring gerukt, ik weet dat ook jij nog steeds bij me bent. *Miss ya buddy, everyday!*
Hoewel menig onder jullie door uiteenlopende redenen jammer genoeg niet aanwezig kunnen zijn op de publieke doctoraatsverdediging, mogen jullie er gerust in zijn dat ik weet ten allen tijde over jullie onvoorwaardelijke steun te beschikken!

Tot slot, mijn steun en toeverlaat, mijn allerliefste Jessie. Bedankt om er al 10 jaar voor mij te zijn, me te nemen voor wie ik ben, me te steunen door dik en dun en omdat je jouw schema gedurende de afgelopen zeer drukke maanden volledig hebt willen afstemmen op dit doctoraat. Jij zult ongetwijfeld ook tevreden zijn wanneer er een einde komt aan deze hectische doctoraatsperiode vol avond- en weekendwerk, hoewel je van dit laatste zelf ook wel voldoende pap hebt gegeten! Bedankt voor al je steun en onvoorwaardelijke liefde.

Ook bedankt aan alle anderen die ik misschien niet expliciet heb vermeld, maar toch altijd klaarstaan voor mij.

Een einde kan echter ook het begin van iets nieuws inluiden… op nu dus naar een nieuw hoofdstuk in het levensboek.

Frederik, 18 mei 2015

Table of contents

List of abbreviations

A:V	Surface area-to-volume ratio
AFM	Atomic force microscopy
ANOVA	Analysis of variance
APS	Average particle size
AsFl-FFF or AF4	Asymmetrical flow field-flow fractionation
AVS	Acid volatile sulphide
BCC	Body-centred cubic crystal structure
BET	Brunauer-Emmet-Teller
C18	Octadecyl carbon chain
CCC	Critical coagulation concentration
CE	Capillary electrophoresis
CEC	Cation exchange capacity
CFF	Cross flow filtration
CFUF	Cross flow ultrafiltration
Chl	Chlorophyll
Cit	Citrate
CMC	Carboxymethyl cellulose
CNTs	Carbon nanotubes
CT	Computed tomography
DL	Detection limit, determined as: $DL = \frac{3 \times \sigma_B}{m}$, where σ_B is the standard deviation on the response signal obtained from ≥ 10 blank measurements, and m is the slope of the linear calibration curve
DLS	Dynamic light scattering
DLVO	Derjaguin-Landau-Verwey-Overbeek
DM	Dry matter
DOC	Dissolved organic carbon
DR	Dry residue
DW	Dry weight
EC	Electrical conductivity
EC_n	n % effect concentration
EDL	Electrical double layer
EDS or EDX	Energy dispersive X-ray spectroscopy

EELS	Electron energy loss spectrometry
El-FFF	Electrical field-flow fractionation
ELS	Electrophoretic light scattering
EM	Electron microscopy
ENMs	Engineered nanomaterials
ENPs	Engineered nanoparticles
ESEM	Environmental scanning electron microscopy
ETEM	Environmental transmission electron microscopy
FCC	Face-centred cubic crystal structure
FCS	Fluorescence correlation spectroscopy
FFF	Field-flow fractionation
FIB-SEM	Focused ion beam scanning electron microscopy
Fl-FFF	(Hydraulic) Flow field-flow fractionation
FW	Fresh weight
GFC	Gel filtration chromatography
GPC	Gel permeation chromatography
HDC	Hydrodynamic chromatography
HPLC	High performance liquid chromatography
HR-TEM	High resolution transmission electron microscopy
IC	Inorganic carbon
ICP-MS	Inductively coupled plasma mass spectrometry
ICP-OES	Inductively coupled plasma optical emission spectrometry
id	Internal diameter
IEC	Ion exchange chromatography
IEP	Isoelectric point
IS	Ionic strength
l	length
LC_n	*n* % lethal concentration
LEDs	Light emitting diodes
LIBD	Laser induced breakdown detection
LOI	Loss on ignition
m:V	Mass per volume
MA(L)LS	Multi angle (laser) light scattering
MC	Microcosm

MF	Microfiltration
MLSS	Mixed liquor suspended solids
MMF	Multistage membrane filtration
M^{n+}	Metal ions
MRI	Magnetic resonance imaging
MWCO	Molecular weight cut-off
N/A	Not applicable
NF	Nanofiltration
NM	Not measured
NMs	Nanomaterials
NNI	The National Nanotechnology Innitiative
NOM	Natural organic matter
NO_x	Nitrogen oxides
NP-HPLC	Normal phase high performance liquid chromatography
NSOM	Near-field scanning optical microscopy
NTA	Nanoparticle tracking analysis
nZVI	Nanoscale zero valent iron
OD	Optical density
OM	Organic matter
PCS	Photon correlation spectroscopy
PDI	Polydispersity index
PES	Polyethersulfone
PFCAs	Perfluorocarboxylic acids
$PM_{0.1}$	Particulate matter < 0.1 μm or ultrafine particles
PP	Polypropylene
PSD	Particle size distribution
PV	Pore volume
PVDF	Polyvinylidene difluoride
PVP	Polyvinylpyrrolidone
PZC	Point of zero charge
QDs	Quantum dots
QELS	Quasi-elastic light scattering
R&D	Research and development
RC	Regenerated cellulose

ROS	Reactive oxygen species
RP-HPLC	Reverse phase high performance liquid chromatography
SD	Standard deviation
Sd-FFF	Sedimentation field-flow fractionation
SDS	Sodium dodecyl sulphate
SEC	Size exclusion chromatography
SEM	Scanning electron microscopy
SM	Suspended matter
SP-ICP-MS	Single particle inductively coupled plasma mass spectrometry
SPLP	Synthetic precipitation leaching procedure
SPR	Surface plasmon resonance
SRHA	Suwannee River humic acid
SSA	Specific surface area
STM	Scanning tunnelling microscopy
TCLP	Toxicity characteristic leaching procedure
TEM	Transmission electron microscopy
TFF	Tangential flow filtration
Th-FFF	Thermal field-flow fractionation
TN	Total nitrogen
TOC	Total organic carbon
TP	Total phosphorus
TSS	Total suspended solids
UC	Ultracentrifugation
UF	Ultrafiltration
USDA	United States Department of Agriculture
UV	Ultraviolet
UV-Vis	Ultraviolet-visible spectroscopy
WetSEM™	Wet scanning electron microscopy
WetSTEM	Wet scanning transmission electron microscopy
XAS	X-ray absorption spectroscopy
XDLVO	Extended Derjaguin-Landau-Verwey-Overbeek
XRD	X-ray diffraction
ZVI	Zero valent iron
ζ-potential	Zeta potential

Chapter 1

General introduction

1 General Introduction

1.1 Nanoscience and nanotechnology: A preface

To date, a fixed definition of what constitutes nanotechnology still remains undeniably elusive, despite the ever-growing interest in the subject over the last decades (Watlington, 2005). According to the US National Nanotechnology Initiative (NNI), the term "nanotechnology" is generally used as an all-encompassing concept for nanoscale science, engineering, and technology, and nanotechnology can be defined as "*the understanding and control of matter at the nanoscale (1 – 100 nm), which is the size scale between individual atoms and bulk materials, where unique phenomena enable novel applications*" (Sargent, 2013). A report by The Royal Society and The Royal Academy of Engineering (2004) on the other hand, differentiates between nanoscience and nanotechnologies, although recognizing that no sharp distinction between both terms exists, as follows:

- ***Nanoscience*** *is the study of phenomena and manipulation of materials at the atomic, molecular, and macromolecular scales, where properties differ significantly from those at larger scale.*
- ***Nanotechnologies*** *are the design, production, characterization, and application of structures, devices, and systems by controlling shape and size at the nanometre scale.*

The prefix "nano" is derived from the Greek (*νάνος*) or Latin (*nanus*) word for dwarf. One nanometre (nm) is equal to one billionth of a metre (*i.e.*, 10^{-9} m), roughly the width of 3.5 gold or 8 hydrogen atoms arranged side-by-side along a straight line (Sargent, 2013). In comparison, a sheet of paper is nearly 100 000 nm (*i.e.*, 100 μm) thick, while a human hair is on average about 80 000 nm (*i.e.*, 80 μm) wide, and the diameter of an erythrocyte (*i.e.*, a red blood cell) is approximately 2500 nm (*i.e.*, 2.5 μm). Bacteria are typically between 200 nm (*i.e.*, 0.2 μm) and 5 μm in size, whereas the majority of viruses that have been studied over the years measure between 20 and 300 nm. Figure 1.1 depicts the nanoscale (*i.e.*, the size range from 1 to 100 nm) in context to a larger length scale.

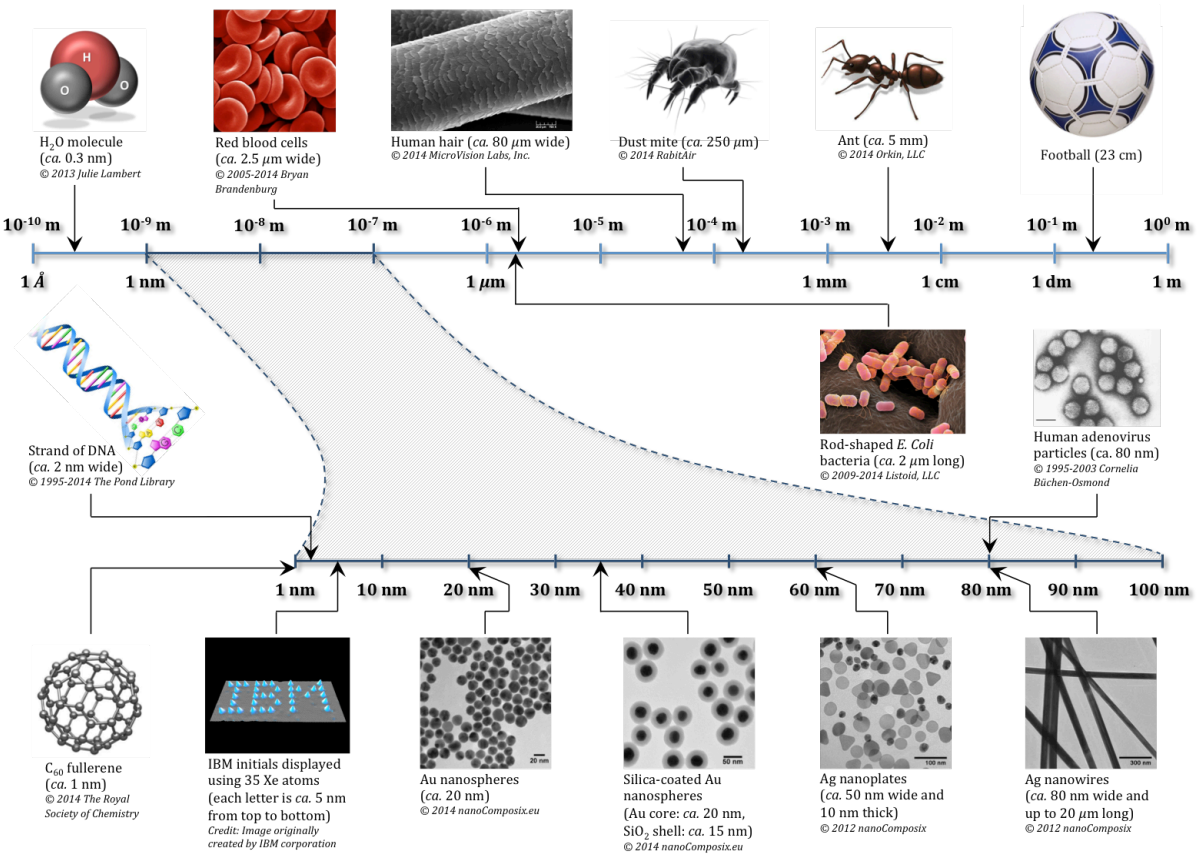

Figure 1.1 – The length scale indicating the size of some materials in the range of 1 to 10^{-10} m (top), and showing the nanoscale (1 – 100 nm) in context (expanded below). Putting nanoscale dimensions into perspective, Earth is about 100 million times larger than a football, which is in turn approximately 100 million times larger than a spherical C_{60} fullerene molecule, also referred to as Buckminsterfullerene or buckyball. [After The Royal Society and The Royal Academy of Engineering (2004)]

The conceptual underpinnings of nanoscience and nanotechnology can be traced back to 1959, when American physicist and Nobel Prize laureate Richard Feynman challenged the scientific community to think small in his brilliant lecture *"There's Plenty of Room at the Bottom"* at the annual meeting of the American Physical Society (Feynman, 1960; Maynard *et al.*, 2006). Feynman envisioned the possibility of manipulating and controlling matter at the scale of individual atoms and molecules, imagining printing all 24 volumes of the *Encyclopaedia Britannica* on the head of a pin, and foreseeing a world where scientists like himself could *"Arrange the atoms the way we want; the very atoms, all the way down!"* (Feynman, 1960; Lane and Kalil, 2005; Klaine *et al.*, 2012). However, he never claimed that "anything goes" at the nanoscale, and warned that the very act of arranging atoms is subject to fundamental principles: *"You cannot put them so that they are chemically unstable, for example."* (Feynman, 1960; Roukes, 2001).

Although Feynman planted the seeds for a new era in science and technology with his talk in 1959, it took until the 1980s and early 1990s for the primary developments in the field of nanoscience and nanotechnology to occur. Moreover, the term "nano-technology" was only mentioned for the first time in 1974 when Japanese scientist Norio Taniguchi used it to refer to his explorations of ultra-precision machining (The Royal Society and The Royal Academy of Engineering, 2004; NNI, n.d.). Additionally, American engineer Eric Drexler is also often credited for coining the term "nanotechnology", as being the first person to describe engineering at the nanoscale in his book on molecular manufacturing *"Engines of Creation: The Coming Era of Nanotechnology"*, which was published in 1986 (Phoenix, 2008; Klaine *et al.*, 2012). It is recognized that two major developments in the 1980s boosted the field of nanotechnology: *(1) the invention of the scanning tunnelling microscope (STM) by Nobel Prize laureates Gerd Binnig and Heinrich Rohrer at IBM in 1981, which allowed scientists to "see" (i.e., create direct spatial images of) individual atoms for the first time; and (2) the invention of the atomic force microscope (AFM) by Gerd Binnig, Calvin Quate, and Christoph Gerber in 1986, which is also capable of viewing, measuring, and manipulating matter down to fractions of a nanometre in size* (NNI, n.d.). In 1989 for instance, IBM researchers Don Eigler and Erhard Schweizer used a custom-build STM to "write" IBM's initials with 35 individual Xe atoms on a chilled crystalline Ni surface (see also Figure 1.1) (The Royal Society and The Royal Academy of Engineering, 2004; NNI, n.d.). Such achievements aided scientists to realize and explore the possibilities of nanoscience and nanotechnology, paving the way for expanding nanotechnology research and development (R&D) (Watlington, 2005).

Nanotechnology is a relatively young field of science, but a dynamic and rapid developing one, and it is considered to be one of the most promising new technologies of the 21st century (Lin *et al.*, 2010; Jośko and Oleszczuk, 2013). By 1998, physicist Neal Lane testified before the US Congress that *"If I were asked for an area of science and engineering that will most likely produce the breakthroughs of tomorrow, I would point to nanoscale science and engineering."* (Lane and Kalil, 2005). Engineered nanoparticles (ENPs) (see also sections below) are some of the most important products of nanotechnology, whose benefits and drawbacks are believed to well exceed those of the industrial revolution (Nel *et al.*, 2006; Hansen *et al.*, 2008; Navarro *et al.*, 2008a). Since the beginning of the 21st century, the annual production of engineered nanomaterials (ENMs) has increased exponentially from about 400 tonnes to an expected 58 000 tonnes in 2011 – 2020 (Maynard, 2006; Navarro *et al.*, 2008a; Sharma, 2009a). Accordingly, the global market for the nanomaterial industry has

grown rapidly from a reported $10 billion in 2005 to a $147 billion value in 2007, and global nanotechnology product revenues are projected to reach a value of $3.1 trillion by 2015 (Sargent, 2013; Subramanian *et al.*, 2014).

1.2 Nanoparticles

1.2.1 Definition

Nanomaterials are generally defined as particulate objects having a size between 1 and 100 nm in at least one dimension. These materials include nanofilms and nanoplates (one dimension on the nanoscale), nanowires and nanotubes (two dimensions on the nanoscale), and nanoparticles (three dimensions on the nanoscale), and may or may not exhibit size-related intensive properties that differ significantly from those observed in larger-sized objects of the same material (*e.g.*, micrometre-sized particulates or bulk materials) (Handy *et al.*, 2008b; Batley *et al.*, 2013). However, this definition of matter smaller than 100 nm is somewhat arbitrary, and has been subject to controversy due to the pragmatic size range and presence of a size-related property it encompasses (Handy *et al.*, 2008b; Auffan *et al.*, 2009; Van Hoecke, 2010). It has for instance been argued that non-bulk properties or so-called "true nano effects" mainly emerge for particles smaller than 20 to 30 nm, whereas particles of several hundred nm (< 300 nm) could already adversely affect the biological activity of biota, and should therefore also be considered when performing nano(eco)toxicological studies for example (Handy *et al.*, 2008b; Auffan *et al.*, 2009). Nevertheless, nanoparticles are currently still defined by consensus as being particulate matter with all three dimensions between 1 and 100 nm.

1.2.2 Types and classification

Nanoparticles occur in aquatic, terrestrial, and atmospheric environments, both from natural sources and as a result of human activities, and can by definition be considered as ultra-fine particles (< 0.1 μm, $PM_{0.1}$) (in the case of air-borne particulates) or as a sub-set of colloidal particles (1 nm – 1 μm) (in aquatic or terrestrial systems) (see also Figure 1.3). They can exist in different forms (*e.g.*, as single, aggregated, or agglomerated particles) and

have various morphologies (*e.g.*, spherical, tubular, or irregular shapes), coatings, and surface functionalities (Nowack and Bucheli, 2007; Klaine *et al.*, 2008).

Nanoparticles can be categorized further depending on their origin, distinguishing between natural (*i.e.*, geogenic, biogenic, pyrogenic or atmospheric), anthropogenic (*i.e.*, unintentionally produced) and engineered nanoparticles (*i.e.*, intentionally manufactured), and be divided according to their chemical composition into organic and inorganic nanoparticles (Figure 1.2).

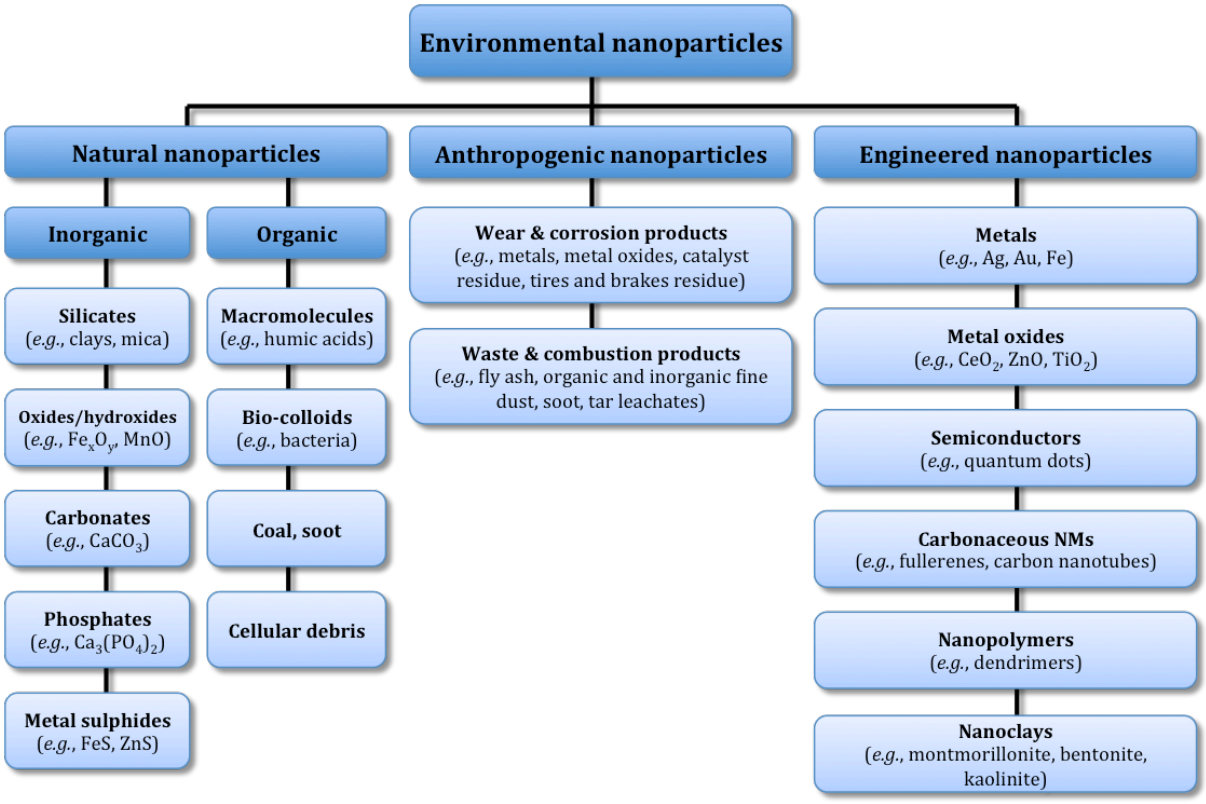

Figure 1.2 – Concise schematic overview of environmental nanoparticles categorized according to origin and composition. [After Christian *et al.* (2008)]

Environmental nanoparticles have existed naturally ever since the beginning of Earth's history. For example, nanoscale particles that are assumed to originate from natural combustion processes have been discovered in 10 000 year-old glacial ice cores (Murr *et al.*, 2004). Moreover, natural iron nanoparticles (16 – 27 nm in size) have been recorded in sediment samples from the Cretaceous-Tertiary boundary layer at Gubbio, Italy (Verma *et al.*, 2002). Many geological or biological processes can create natural nanoparticles in the environment. Geological mechanisms include physicochemical weathering, authigenesis/neoformation, and volcanic activity, and typically produce inorganic

nanoparticles (*e.g.*, clay minerals and iron oxyhydroxides) (Handy *et al.*, 2008a). Numerous biological molecules/entities, such as polysaccharides, proteins, nucleic acids, and viruses, are typically nanometre-sized, while degradation of biological matter can also result in environmental nanoparticles (*e.g.*, humic and fulvic acids) (Handy *et al.*, 2008a; Bhatt and Tripathi, 2011). Figure 1.3 shows the size domains of natural colloids and nanoparticles occurring in the environment.

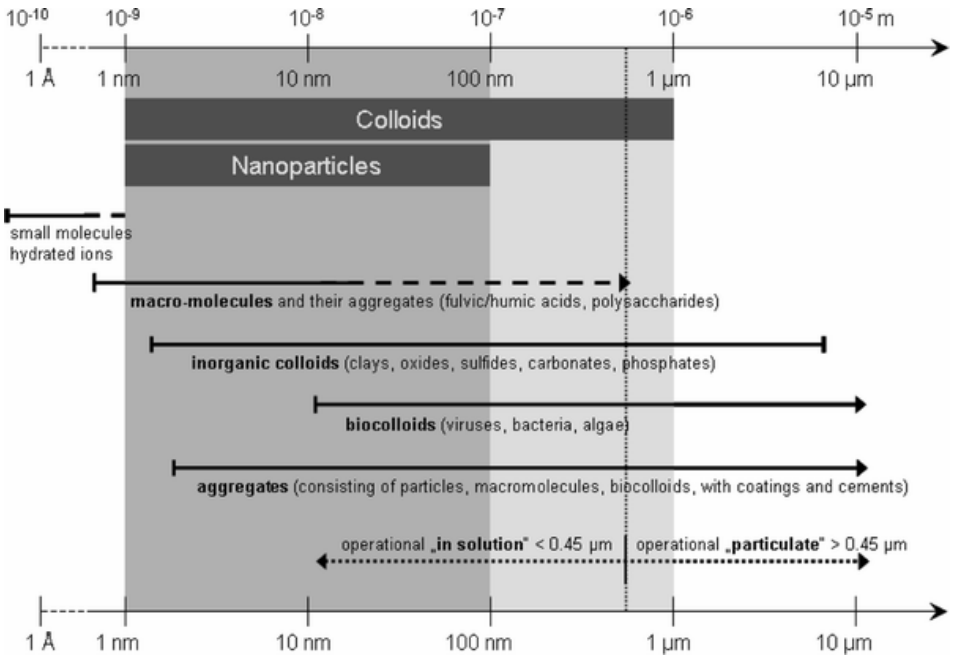

Figure 1.3 – Size domains and typical representatives of naturally occurring colloids and nanoparticles. The operationally defined cut-off between dissolved and particulate matter, which is commonly given for filtration at 0.45 μm, is also shown. [Reprinted from Christian *et al.* (2008), with kind permission from Springer Science and Business Media]

Nanoparticles that are produced as unintended by-products during technological or combustion processes, or other human activities, are referred to as anthropogenic nanoparticles. Such non-natural nanoparticles include both organic and inorganic particulate objects for instance resulting from wear and corrosion products from tires and breaks, catalysts (*e.g.*, Pt, Rh and Pd), and metallic bearings, and from waste and combustion products (*e.g.*, soot, fly ash, and fine dust) (Nowack and Bucheli, 2007; Christian *et al.*, 2008; Klaine *et al.*, 2008).

Engineered nanoparticles (ENPs) on the other hand, are deliberately manufactured to have a specific size, shape, composition, or possess other particular properties. Top-down and bottom-up fabrication are two distinct fundamental approaches for the production of

ENPs. The former involves for instance the application of grinding, milling, etching, or lithographic techniques to reduce the size of a macroscopic piece of material, whereas the latter refers to the concept of synthesizing nanoparticles starting from basic building blocks, such as individual atoms or molecules, and assembling those atomic or molecular precursors until the desired structure is formed (Christian *et al.*, 2008; Klaine *et al.*, 2008; Bhatt and Tripathi, 2011). Bottom-up methods, such as the colloidal synthesis of nanoparticles through chemical reduction of metal ions, are generally better suited to generate uniform particles, and control their size (distribution), shape, and structure (Bhatt and Tripathi, 2011). Engineered nanoparticles can be divided according to their chemical nature into organic and inorganic particles, and can consist of a single element or a mixture of elements. Organic ENPs comprise mainly of carbonaceous materials like carbon black, fullerenes, carbon nanotubes (CNTs), and dendrimers, while inorganic ENPs are primarily represented by metal-containing particulates (*i.e.*, metallic ENPs), including zero valent metals (*e.g.*, Ag, Au, Cu, Fe, and Pt), metal oxides (*e.g.*, CuO, ZnO, CeO_2, SiO_2, TiO_2, and Fe_2O_3), and semiconductor nanocrystals, also known as quantum dots (QDs) (*e.g.*, CdS, CdSe, CdTe, InP, and ZnSe) (Nowack and Bucheli, 2007; Christian *et al.*, 2008; Klaine *et al.*, 2008; Bhatt and Tripathi, 2011; Jośko and Oleszczuk, 2013).

As metallic ENPs are the actual subject of interest of this study, emphasis will be laid primarily on these types of nanoparticles throughout the remainder of this thesis.

1.2.3 Characteristics

Due to their small size, composition, structure, and surface characteristics, (engineered) nanoparticles often exhibit unique physical, chemical, mechanical, and optical properties and reactivities that are not present at a larger scale (Nel *et al.*, 2006; Klaine *et al.*, 2012; NNI, n.d.). The main characteristic responsible for the extraordinary attributes of nanomaterials is their size, which falls in the transitional zone between individual atoms or molecules and the corresponding bulk materials (see also sections above) (Nel *et al.*, 2006; Van Hoecke, 2010). At this scale, material properties become size-dependent (*i.e.*, properties such as melting point, fluorescence, electrical conductivity, and chemical reactivity change as a function of particle size) and so-called quantum effects may dominate the behaviour and characteristics of particles (NNI, n.d.).

Quantum confinement, a term referring to the restricted motion of electrons in space rather than them being able to move randomly in the bulk of a material, for instance enables nanoscale gold to interact differently with light than larger-scale gold, and as a result, Au nanoparticles appear red or purple instead of having the familiar yellowish colour of macroscopic gold (Filipponi and Sutherland, 2013; NNI, n.d.). Such peculiar colour shifts, typically occurring with noble metal nanoparticles (*e.g.*, Au and Ag) and distinguishing them from their bulk counterparts, can actually be attributed to a phenomenon called localized surface plasmon resonance (SPR). This effect is due to the confined collective oscillation of conduction electrons in the metal, driven by specific wavelengths of incident light (Filipponi and Sutherland, 2013). Another example of a size-related optical property is quantum fluorescence, which can be observed in nanoscale semiconductors. Quantum dots of the same material (*e.g.*, CdSe) can absorb/emit various wavelengths of light depending on their size, and thus emit different colours (The Royal Society and The Royal Academy of Engineering, 2004; Filipponi and Sutherland, 2013). Figure 1.4 illustrates some of the remarkable size-dependent optical characteristics of metallic ENPs.

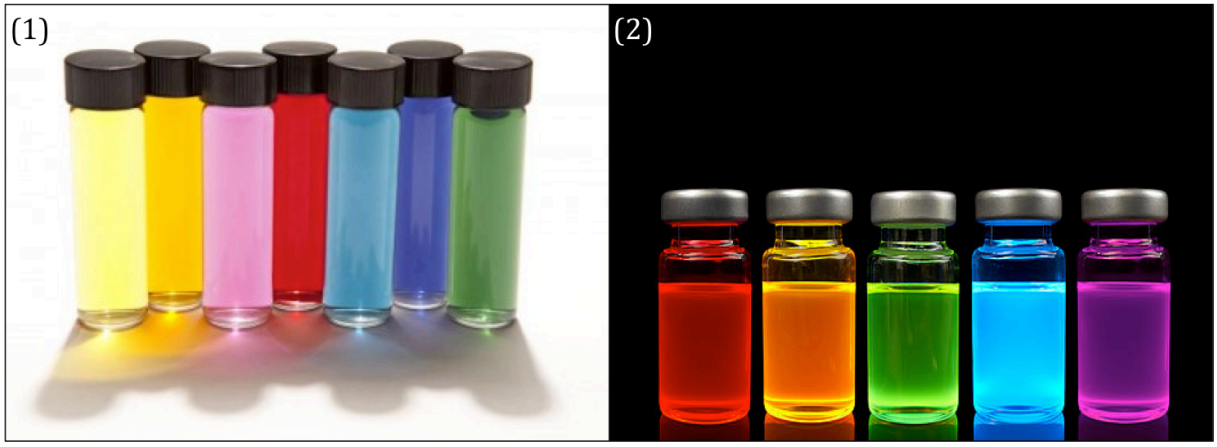

Figure 1.4 – (1) Aqueous suspensions of gold and silver nanoparticles of various sizes and shapes. From left to right: 80 nm Ag nanospheres, 20 nm Ag nanospheres, 40 nm Au nanospeheres, 12 nm Au nanospheres, 200 nm Ag nanoplates, 120 nm Ag nanoplates, and 60 nm Ag nanoplates. (2) Suspensions of cadmium selenide (CdSe) quantum dots (QDs) of different sizes, responding to UV irradiation by emitting visible light. The colours (and specific emission wavelengths) red (610 nm), orange (590 nm), green (560 nm), blue (480 nm), and violet (380 nm) correspond to 5 nm, 4 nm, 3 nm, 2.5 nm, 2 nm, and 1.5 nm CdSe QDs, respectively. [Photograph (1) © 2014 nanoComposix.eu; Photograph (2) © 2012 – 2014 HOLY MOLECULES, BATMAN!]

Aside from impacting optical properties, quantum confinement and the quantization of energy levels (*i.e.*, electrons can only exist in discrete energy states) can also affect the

electrical properties of nanoscale particles. Three categories of materials exist based on their electrical characteristics, which are determined by the energy separation between the valence and conduction band (*i.e.*, the so-called band gap), and the ability to fill their conduction band with electrons: *(1) conductors, (2) semiconductors, and (3) insulators.* At very small dimensions, the band gap energy between the valence and conduction band of a material increases due to quantum confinement, and it is for instance possible that as energy levels are quantified, the band overlap present in metals (*i.e.*, metals are conductors) disappears and an actual band gap forms. This explains why certain metals can become semiconductors as their size is decreased (Filipponi and Sutherland, 2013).

Quantum tunnelling is another potent quantum effect occurring at the nanoscale, which enables the scanning tunnelling microscope and is applied in resonant tunnelling diodes that are used as switching units in fast electronic circuits (*e.g.*, flash memory for computing). The tunnelling phenomenon is attained when a particle of very small mass, such as an electron, violates the principles of classical mechanics by penetrating a potential energy barrier that is higher than the kinetic energy of the particle. This energy barrier may be a form of energy state analogous to a "hill" or "incline" in classical physics, and a fundamental law of classical mechanics suggests that passage over such a barrier would be impossible without sufficient energy (Vasileska and Klimeck, 2008; Filipponi and Sutherland, 2013; NNI, n.d.).

Many of the physical and chemical properties of a material are dependent on its surface characteristics, regardless of whether it concerns bulk or nanoscale matter. However, as the size of a material is decreased, the impact of its surface properties becomes more and more pronounced (Filipponi and Sutherland, 2013). For example, any given nanoparticle, regardless of its chemical constituents, features an exceptionally high surface-area-to-volume ratio (A:V), a parameter that is inversely proportional to the particle radius when considering a sphere for instance. Consequently, the fraction of atoms localized at the surface of a particle also scales inversely with the radius of a spherical particle (Figure 1.5) (Nel *et al.*, 2006; Christian *et al.*, 2008; Van Hoecke, 2010). For example, a solid sphere with a diameter of 1 cm has a total surface area of about 3 cm^2 and a volume of *ca.* 0.5 cm^3, and although a single spherical nanoparticle of 1 nm in diameter only has a tiny surface area of approximately 3 nm^2 (*i.e.*, 3×10^{-14} cm^2), it would take 10^{21} of such 1 nm spheres to occupy the same volume as a 1 cm sphere, which would result in a staggering total surface area of *ca.* 3×10^7 cm^2. Taking for instance spherical Au particles into

consideration and using a face-centred cubic (FCC) unit cell approach with a lattice constant (a) of 0.40782 nm for gold, the fraction of atoms positioned at the surface of a 5 nm Au nanoparticle is calculated to be *ca.* 41 %, whereas a 50 nm Au nanosphere only has about 5 % of its atoms at the surface, and at 1 μm this fraction is decreased further to approximately 0.2 %. Thus, the increase in surface area determines the potential number of reactive sites on the surface of the particle (Nel *et al.*, 2006). Additionally, the chemistry of these sites may also differ from the bulk material or even from the interior of the nanoparticle, for instance depending on variations in the lattice structure at the particle surface (Christian *et al.*, 2008). One result of these features is the enhanced or even unexpected catalytic activity of certain nanoscale objects compared to the bulk material. For example, Au nanoparticles a few nanometres in size have been shown to be extremely effective oxidation catalysts, whereas macroscopic gold is known to be inert (Auffan *et al.*, 2009; NNI, n.d.).

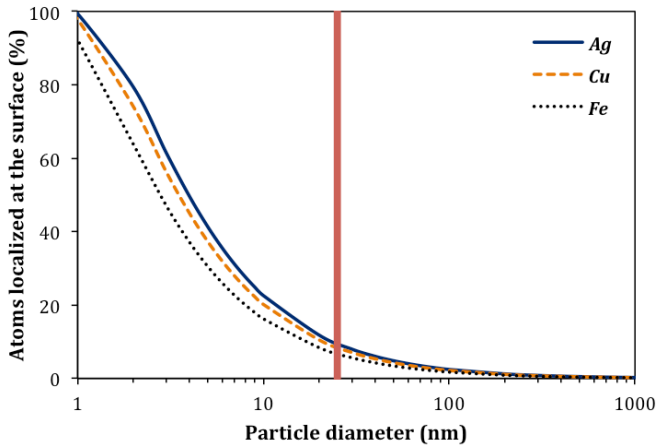

Figure 1.5 – The percentage of atoms localized at the surface of a spherical Ag, Cu, and Fe particle as a function of particle diameter. A face-centred cubic (FCC) or body-centred cubic (BCC) unit cell approach was employed in order to calculate the percentage surface atoms in the case of Ag (a = 0.40853 nm) and Cu (a = 0.36149 nm), or Fe (a = 0.28665 nm) particles, respectively. Non-bulk properties are argued to mainly emerge for particles smaller than 20 to 30 nm in diameter (vertical red line). [After Auffan *et al.* (2009)]

The fact that a significant portion of atoms is retrieved at the surface of a nanoparticle also affects some thermal properties, such as the melting point. As surface atoms are more easily "removed" than bulk atoms, the melting point of the same material will be lower in case it is nano-sized (Auffan *et al.*, 2009; Filipponi and Sutherland, 2013). For example, by decreasing the diameters of In and Sn nanoparticles from 100 to 10 nm,

their melting point has been reported to be reduced by 120 °C and 80 °C, respectively, whereas a decrease in melting point by 850 °C relative to that of the bulk material has been observed in the case of Au nanoparticles smaller than 2 nm (Auffan *et al.*, 2009; Van Hoecke, 2010).

As mentioned before, atoms and molecules at the particle surface exhibit an enhanced reactivity compared to those that exist in the interior of a material. Nanoparticles are therefore also characterized by an excess of energy at the surface and are thermodynamically unstable (Auffan *et al.*, 2009). One way to minimise the inherent high surface energy of nanoparticles, is their strong intrinsic tendency to aggregate or sorb onto available surfaces. To avoid this (generally) unwanted characteristic, engineered nanoparticles are usually coated with surface ligands to stabilize the particles in suspension, or fixed onto a solid substrate prior to being used (Bhatt and Tripathi, 2011; Filipponi and Sutherland, 2013). More detailed information on the aggregation and sorption behaviour of nanoparticles can be found in Chapter 2.

Thus, it is clear that many of the interesting and sometimes unexpected physicochemical properties of nanoparticles like catalytic activity, dispersibility, adhesion, chemical reactivity, gas storage, and electrical resistivity, are also dominated by the nature of the particle surface (Borm *et al.*, 2006; Filipponi and Sutherland, 2013).

1.2.4 Applications: Background and current use

The novel and unparalleled physicochemical properties nanoparticles often possess, have led to a rapid increase in potential applications of ENPs in various areas of the economy, including textiles, electronics, optics, cosmetics, medical devices, food packaging, catalysts, fuel cells, (waste)water treatment, and environmental remediation (Handy *et al.*, 2008b; Navarro *et al.*, 2008a). In September 2014, The Project on Emerging Nanotechnologies (2014) listed 1801 commercially available consumer products incorporating ENMs, produced by 715 different companies in over 30 countries worldwide, in their online inventory. Although not exhaustive, this database has grown by nearly 750 %, as 1589 new nanotechnology-based products have been added since March 2006. Figure 1.6 depicts various ENMs-containing consumer goods that are presently on the market.

Figure 1.6 – A selection of consumer products containing engineered nanomaterials (ENMs), which are available on the market today. [Photograph © 2006 David Hawxhurst, Woodrow Wilson Center]

Even though the rapid development of nanoscience and nanotechnology only took place during the last decades (see also Section 1.1), the use of nanoparticles already dates back for many centuries in human history (Van Hoecke, 2010; NNI, n.d.). For instance, the 4th century Roman Lycurgus cup, which is currently being preserved and displayed at the British Museum in London, contains colloidal gold and silver embedded in the glass matrix, allowing it to appear opaque green when lit from the outside, or translucent red when light is able to pass through from the inside (NNI, n.d.). Ancient ceramic lustreware originating from the 9th – 17th century Islamic world, as well as stained glass windows used in European cathedrals during the 6th – 15th century, have also been found to contain silver, copper, gold chloride, and other metallic nanoparticles (NNI, n.d.). Only by 1857, Michael Faraday discovered colloidal ”ruby” gold and was the first to present scientific reasoning on the properties and synthesis of gold nanoparticles, demonstrating alterations in colour of nanoscale gold solutions under certain lighting conditions (Van Hoecke, 2010; NNI, n.d.).

Since the start of the 21st century, nanotechnology has become big business, and the production and use of ENPs have boomed (see also Section 1.1). Metallic ENPs are amongst the most widely used nanomaterials to date (Mudunkotuwa and Grassian, 2011; Weinberg *et al.*, 2011; The Project on Emerging Nanotechnologies, 2014). Au and Ag ENPs are for instance being used in biomedical applications (*e.g.*, in cancer diagnosis and therapy), as catalysts, as nanoscale optical antennas to improve light harvesting in solar cells and other

devices, or in the pharmaceutical sector (Ju-Nam and Lead, 2008; Sharma *et al.*, 2009b; Fabrega *et al.*, 2011). Au ENPs are also been utilized in electronics in flexible conducting inks and thin films, and have been used to enhance the imaging properties of a variety of MRI and CT-based contrasting agents (Klaine *et al.*, 2008; Jośko and Oleszczuk, 2013; NNI, n.d.). Furthermore, Ag ENPs have been demonstrated to possess antimicrobial properties, which have led to their use in a whole variety of applications, including household appliances, air and water filters, textiles, food packaging, refrigerator coatings, wound dressings, and cosmetics, and are nowadays considered as the largest and fastest growing class of ENPs in product applications (Klaine *et al.*, 2008; Bradford *et al.*, 2009; Fabrega *et al.*, 2011; Ferreira da Silva *et al.*, 2011; Sharma *et al.*, 2014; The Project on Emerging Nanotechnologies, 2014).

At present, Cu ENPs are for example being incorporated in pesticides, fungicides, and coolants, to improve their performance (Jośko and Oleszczuk, 2013).

Owing to its large specific surface area and high reactivity, nanoscale zero valent iron (nZVI or Fe ENPs) has been used for some time for the remediation of groundwater, sediments, and soils that have been polluted with organic or inorganic contaminants, such as halogenated hydrocarbons, organic dyes, pesticides and heavy metals, whereas TiO_2 is considered to be the most commonly used photocatalyst for removal of nitrates or non-biodegradable organic compounds (*e.g.*, nitrobenzene, cyclohexane, and tetrachloroethane) during groundwater and (waste)water treatment (Ju-Nam and Lead, 2008; Klaine *et al.*, 2008; Theron *et al.*, 2008; Sharma *et al.*, 2009a; Grieger *et al.*, 2010; Sánchez *et al.*, 2011; Jośko and Oleszczuk, 2013). Additionally, bi-metallic nanoparticles, such as Fe:Pd, Fe:Ni, and Fe:Ag, have been demonstrated to be even more active and stable than Fe ENPs, thus further improving such environmental remediation applications (Batley and McLaughlin, 2010; Filipponi and Sutherland, 2013).

Nanoscale ZnO has found applications in electronic devices, in photocatalytic remediation, and is used in the production of chemical sensors and solar cells. Moreover, due to their remarkable UV-light absorbing capabilities, ZnO and TiO_2 ENPs are also commonly used in sunscreen lotion and other cosmetics, paints, plastics, and packaging materials (Ju-Nam and Lead, 2008; Batley and McLaughlin, 2010; Filipponi and Sutherland, 2013).

Owing to their increased surface area, CeO_2, Pd, and Pt ENPs have readily been used as fuel-borne catalysts or as catalyst support to improve combustion and thus increase fuel efficiency of diesel fuel driven automobiles, and to reduce and better control vehicle emissions (Batley and McLaughlin, 2010; Van Hoecke, 2010; Nowack *et al.*, 2012).

Due to their interesting size-related and tuneable electronic, magnetic, and optical properties, QDs (*e.g.*, CdSe, CdTe:ZnS, CdS, and PbSe) have for example found applications in light emitting diodes (LEDs), solar cells, transistors, biosensors, medical imaging, and in targeted therapeutics (The Royal Society and The Royal Academy of Engineering, 2004; Ju-Nam and Lead, 2008; Klaine *et al.*, 2008; Batley and McLaughlin, 2010; Filipponi and Sutherland, 2013).

The numerous applications and fields making use of metallic ENPs are off course not solely limited to the selected examples that are highlighted in the paragraphs above, both in regard to the types of nanoparticles and the application categories involved.

1.2.5 (Eco)toxicity

The exceptional properties of nanoparticles (*e.g.*, their small size, large specific surface area, and high reactivity) might not only favour their use in a vast array of applications, but also cause their novel toxicity (Liu *et al.*, 2014). Nanoparticles could potentially infiltrate organisms (*e.g.*, through oral intake, inhalation, or via the skin) and be translocated through tissues, cells, and even into cell organelles in ways that larger particles may not (Lin *et al.*, 2010; Scown *et al.*, 2010). Possible ways of ENPs to penetrate cells may include diffusion through cell membranes and endocytosis (Jośko and Oleszczuk, 2013; Liu *et al.*, 2014). Although the various ways in which ENPs can exert toxic effects (*e.g.*, damage to cell membrane integrity, protein destabilization and oxidation, damage to nucleic acids, and interruption of energy transduction) still need to be fully elucidated, two main toxicity mechanisms have been proposed to explain their toxic activity (Klaine *et al.*, 2008; Bhatt and Tripathi, 2011; Jośko and Oleszczuk, 2013). The first mechanism assumes that nanoparticle toxicity is caused by the release of harmful metal ions, which may for instance act as enzyme inhibitors or interfere with DNA replication (Klaine *et al.*, 2008; Jośko and Oleszczuk, 2013). The second important toxicity mechanism is the generation of reactive oxygen species (ROS), which are known to cause damage to cell membranes, cell organelles, and nucleic acids contained in DNA and RNA (Klaine *et al.*, 2008; Jośko and Oleszczuk, 2013).

(Eco)toxicity measurements are conducted on different trophic levels (*e.g.*, microorganisms, plants, invertebrates, and vertebrates), and test protocols have been standardized (*e.g.*, by the OECD or ISO) for some organisms (*e.g.*, Daphnids, zebrafish, or earthworms) and exposure conditions (*e.g.*, medium composition, exposure time, and endpoint determination) (Joner *et al.*, 2008). Numerous studies have already provided data pointing towards the detrimental impact ENPs might have on living organisms such as bacteria, algae, aquatic invertebrates, fish, benthic organisms, plants, mammals, and humans (Scown *et al.*, 2010; Peralta-Videa *et al.*, 2011; Jośko and Oleszczuk, 2013). The biological response of such organisms to the presence of ENPs may vary *e.g.*, from changes at the DNA level, and individual cells and organs, to disease or death of the entire organism (Jośko and Oleszczuk, 2013).

Bacteria are one of the most commonly studied group of organisms in nanoparticle toxicity tests, and the antimicrobial properties of silver as well as metal oxide nanoparticles (*e.g.*, CeO_2, TiO_2, ZnO, and Al_2O_3 ENPs) have been well established (Scown *et al.*, 2010; Fabrega *et al.*, 2011). For instance, Hwang *et al.* (2008) demonstrated that 24 h exposure of *E. coli* to 0.1 – 1 mg L^{-1} Ag ENPs (10 nm) in culture media resulted in cell membrane/protein damage. Another study reported a 100 % kill rate for bacteria of the *Bacillus* species after 5 d exposure to 0.6 mg L^{-1} or more of 10 nm citrate-stabilized Ag ENPs (El Badawy *et al.*, 2010). Battin *et al.* (2009) explored nanotoxicity of 5 mg L^{-1} TiO_2 ENPs (10 – 20 nm) towards a natural microbial community from surface water and observed cell membrane damage in the microorganisms.

Algae are another group of organisms frequently used in nanotoxicity studies. For example, Van Hoecke *et al.* (2009) observed chronic toxicity of CeO_2 ENPs (14 – 29 nm) to *P. subcapitata*, with 72 h 10 % effect concentrations (72 h-EC_{10}) on algal growth rate between 2.6 and 5.4 mg L^{-1}. Furthermore, no toxic effects were noted for bulk CeO_2. TiO_2 ENPs (25 – 70 nm) have also been shown to be more toxic than bulk TiO_2 with a 48 h-EC_{50} on *P. subcapitata* growth of 5.83 or 35.9 mg L^{-1} for the nano or the bulk form, respectively (Aruoja *et al.*, 2009). Navarro *et al.* (2008b) studied growth inhibition of 25 nm Ag ENPs on *C. reinhardtii* and reported a 1 h-EC_{50} of 3300 nM and a 5 h-EC_{50} of 829 nM, whereby the observed toxicity was mediated by the release of Ag^+ ions from the nanoparticles. A study by Griffitt *et al.* (2008) examined the toxicity of citrate-stabilized Ag ENPs (20 – 30 nm) to *P. subcapitata* and observed a 96 h 50 % lethal concentration (96 h-LC_{50}) of 0.19 mg L^{-1}.

Aquatic invertebrates are considered as one the ultimate recipients of contaminants released into the environment and have thus also been widely used in experiments assessing nanoparticle toxicity (Peralta-Videa *et al.*, 2011). Lee *et al.* (2009) for instance, evaluated the toxic effects of 1 mg L^{-1} CeO_2 (15 – 30 nm) and SiO_2 (7 – 10 nm) ENPs on *D. magna* and the larva of *C. riparius* and observed DNA damage and a 10 to 15 % increase in mortility after exposure during 96 h. Citrate-coated Ag ENPs (20 – 30 nm) were shown to be toxic towards *D. pulex* and *C. dubia* in a study by Griffitt *et al.* (2008), with reported 48 h-LC_{50} values of 0.04 and 0.067 mg L^{-1}, respectively. Lovern and Klaper (2006) observed a 48 h-LC_{50} of 5.5 mg L^{-1} for TiO_2 ENPs (10 – 20 nm) and a 100 % mortality rate at 10 mg L^{-1}. Boron nanoparticles have also been demonstrated to be lethal to *D. magna*, with reported 24 h and 48 h LC_{50} values of 19.5 and 6.7 mg L^{-1}, respectively (Strigul *et al.*, 2009).

Fish are also commonly used as sentinels for chemical exposure and effects in the aquatic environment, and have therefore also been utilized for assessing the toxic effects of ENPs (Scown *et al.*, 2010). Wu *et al.* (2010) for example, evaluated the exposure of Japanese medeka (*O. latipes*) to Ag ENPs (20 – 37 nm) and reported a 48 h-LC_{50} of 1.03 mg L^{-1}. They also observed developmental and morphological changes including abnormalities in the spine, fins, heart, brain, and eyes. Another study examined the effects of citrate-coated Ag ENPs (20 – 30 nm) to zebrafish (*D. rerio*) and reported a 48 h-LC_{50} of 7.07 mg L^{-1} as well as differential toxicity at different developmental stages (Griffitt *et al.*, 2008). The same study also examined Cu ENPs toxicity on *D. rerio* and reported gill injuries and a 48 h-LC_{50} of 0.94 mg L^{-1} (Griffitt *et al.*, 2008).

ENPs have also been shown to induce toxic responses in human and other mammalian cells (Peralta-Videa *et al.*, 2011). For instance, Au ENPs (≤ 1.4 nm) were shown to adversely affect several human cell types (e.g., connective tissue fibroblasts, epithelial cells, and macrophages), with reported 12 h-EC_{50} values for cell death ranging from 30 to 56 μM (Pan *et al.*, 2007). Silver nanoparticles were shown to have cytotoxic effects on mammalian germline stem cells, with cell necrosis occurring at 10 μg L^{-1} or more (Braydich-Stolle *et al.*, 2005). Results from a study on human lung epithelial cells indicated that 18 h exposure to 5 – 50 mg L^{-1} CuO, TiO_2, and ZnO ENPs induced DNA damage and/or oxidative lesions (Karlsson *et al.*, 2008).

1.3 Scope and aim of this research

1.3.1 Scope

Because of the diversity of potential applications, ENPs will inevitably yield considerable benefits to society in terms of general consumer goods and healthcare (Scown *et al.*, 2010). However, *in vitro* studies focusing on the effects of nanoparticles on human health and the environment, so far, have also put a damper on such claims (Navarro *et al.*, 2008a). As the nanotechnology industry grows, and the amount of nanoparticle types and applications increase, so does the likelihood that significant quantities of ENPs will (unintentionally) find their way into the aquatic, terrestrial, and atmospheric environment, where their fate and behaviour are still largely unknown (Navarro *et al.*, 2008a; Scown *et al.*, 2010; Liu *et al.*, 2014). The remarkable properties of ENPs also equip them with the potential to adversely affect humans and the environment, and even though their environmental impact is not sufficiently studied, it is clear that their environmental behaviour, as well as their uptake, distribution, and effects within the bodies of living organisms, are likely to differ in comparison to the bulk material or to other conventional xenobiotics (Scown *et al.*, 2010; Klaine *et al.*, 2012). It is therefore expected that organisms, especially those interacting strongly with their immediate environment (*e.g.*, plants, algae, and fungi), are going to be affected as a result of their exposure to ENPs (Navarro *et al.*, 2008a). Past errors (*e.g.*, the use of asbestos fibres) and the application of a "precautionary principle" in many countries underline the crucial need for intensive research on the potential risks associated with the increasing production and use of ENPs (Thill *et al.*, 2006). Accordingly, there is a consensus amongst both proponents and sceptics that potentially adverse effects ENPs could have on humans as well as whole ecosystems, need to be widely examined in the early phase of nanotechnology (Navarro *et al.*, 2008a). This results in a strong need for a complete life cycle analysis of the behaviour, transport, and fate of ENPs in the environment (Narr *et al.*, 2007).

1.3.2 Objectives

The main objective of this research is to contribute to environmental fate studies of engineered nanoparticles. More specifically, this study aims to further the understanding of

the behaviour, fate, and potential bioavailability of metallic ENPs upon their release into aquatic environments, which is dependent on both the properties of the ENPs and the physicochemical characteristics of the receiving medium, as well as to reveal the kinetics of nanoparticles' transformation processes occurring after such a release. Additionally, environmental factors potentially affecting remobilization of adsorbed or precipitated metallic ENPs in complex aquatic matrices are also studied. Although various studies have already investigated several factors (*e.g.*, pH and ionic strength) impacting the behaviour and fate of ENPs in aqueous systems, the majority of such studies have been performed using simple synthetic media under controlled laboratory conditions. It is however recognized that in more complex natural aquatic systems, the behaviour and fate of ENPs could differ significantly from that in artificial media. The lack of studies on the physicochemical fate of metallic nanoparticles in complex aquatic matrices until now was also driven by a lack of reliable analytical methods to routinely detect, identify, and quantify metallic ENPs in aqueous mixtures containing particles with different sizes and compositions. Therefore, focus is also laid on the application and further development of existing analytical techniques and methodologies (*e.g.*, filtration, centrifugation, and elemental analysis via ICP-OES and ICP-MS) in order to assess the environmental occurrence, behaviour, and fate of metallic ENPs in complex aqueous media. These aims should not hinder the further development of nanotechnology, but rather contribute to its sustainability. The better understanding of for instance the aggregation, deposition, and mobilization behaviour of nanoparticles, should help to better predict their fate in the environment as well as their potential biological effects.

1.4 Outline of this thesis

A review of past and present research regarding the physicochemical behaviour and fate of metallic ENPs in aquatic environments is given in **Chapter 2**. Besides briefly describing potential entry routes of ENPs into the environment, this comprehensive literature review also addresses the main processes and factors expected to affect the behaviour and fate of metallic ENPs in aquatic and terrestrial systems, as well as common analytical methods for physical and chemical characterization of ENPs in environmental fate studies.

Quantification of the (elemental) content of metallic nanoparticles in aqueous matrices by means of ICP-OES or ICP-MS may require a digestion of the sample prior to analysis. Therefore, different digestion methods were compared and optimized for analysis, which is outlined in the brief first part of **Chapter 3**. Moreover, the main focus of this chapter was to investigate the potential interactions of Ag and CeO_2 ENPs with different filter media. Different filtration techniques (*e.g.*, paper filtration, microfiltration, and ultrafiltration), and the impact of initial concentration, matrix composition, and filter type and (pre-)treatment on nanoparticle retation are evaluated.

In **Chapter 4**, the stability and settling of CeO_2 ENPs in ten different natural surface waters during a 7-day time period is reported. A first-order kinetics model was used to describe the observed sedimentation rates, and potential factors (*e.g.*, surface water characteristics) affecting nanoparticle sedimentation behaviour are proposed.

Association of nanoparticles with the submerged aquatic plant *Elodea canadensis* are presented in **Chapter 5**. Batch tests were employed to perform dosing experiments, and to study the effects of solution composition on the uptake of Ag and CeO_2 ENPs, as well as to reveal the kinetics of their removal from the water phase, over a 72-hour time frame.

The partitioning behaviour of ENPs between solid and liquid phases in complex aquatic matrices can provide important information on the mobility and potential bioavailability of ENPs. In **Chapter 6**, the partitioning kinetics and association of Ag and CeO_2 ENPs with sediment constituents in aqueous suspensions, as well as how they are affected by sediment characteristics are evaluated.

A similar experimental set-up was applied to examine the solid-liquid partitioning behaviour and fate of Ag and CeO_2 ENPs in (re)suspended soils in **Chapter 7**. In addition to the identification of soil properties affecting the association of nanoparticles with soil constituents, the impact of dissolved organic matter on the stability of CeO_2 ENPs in suspension in the presence of quartz sand is also discussed.

In **Chapter 8**, the synthesis and characterization of carboxymethyl cellulose (CMC) stabilized FeS ENPs, the impact of the CMC surface coating on the stability of FeS ENPs in aqueous suspension, the transport behaviour of the nanoparticles through soil columns, and the potential of the CMC-stabilized FeS ENPs to mobilize and leach out metals from field-contaminated soils and sediment, are assessed.

Chapter 9 describes the use of automated biogeochemical microcosm set-ups to study the solid-liquid partitioning behaviour and fate of citrate-stabilized and PVP-coated Ag ENPs in aqueous sediment suspensions. The observed consequences of working with either oven-dried sediment or fresh sediment that was (re)incubated in the field at its original sampling location are outlined, and the impact of redox condition as well as the type of surface coating on silver fate are addressed.

Finally, the insights gained from the previous chapters are combined into a brief general discussion in **Chapter 10**. Furthermore, the main conclusions gathered during the course of this PhD research are summarized, and some recommendations for potential future research are presented.

Chapter 2

Assessing the physicochemical behaviour and fate of engineered metallic nanoparticles in aquatic environments: A review

2 Assessing the physicochemical behaviour and fate of engineered metallic nanoparticles in aquatic environments: A review[‡]

2.1 Introduction

The increasing production and widespread use of metallic engineered nanoparticles (ENPs) will inevitably result in their discharge into the environment, where their novel characteristics, such as a high specific surface area and abundant reactive sites on the particle surface, as well as their high mobility and bioavailability due to their small size, could lead to unexpected health and/or environmental hazards (Navarro *et al.*, 2008a; Bhatt and Tripathi, 2011; Liu *et al.*, 2014). It is therefore important to gain extensive knowledge on the physicochemical behaviour and fate of ENPs upon their release into the environment, in order to assess their potential risks (Klaine *et al.*, 2008; Batley *et al.*, 2013).

The sections below provide an overview on the fate and behaviour of metallic ENPs in the aquatic environment, and on the most commonly applied analytical methodologies that can be used to assess their environmental occurrence, behaviour and fate.

2.2 Environmental behaviour and fate of engineered nanoparticles

2.2.1 Potential pathways into the environment

There is a scientific consensus that the manufacturing, transportation, use, and disposal of ENPs will result in their entry into the atmosphere, water bodies, sediment, soil and biota (Lowry *et al.*, 2010; Nowack *et al.*, 2012). Although ENPs are not yet regulated, they are already included in lists of emerging contaminants, and similar to many pollutants, water bodies and soils can receive ENPs from point sources, such as production facilities,

[‡] *Redrafted after: Van Koetsem, F., Rinklebe, J., and Du Laing, G. (in press).* ***Analysis and fate of metal-based engineered nanoparticles in aquatic environments, wetlands and floodplain soils.*** *In: Rinklebe, J. (Ed.), Trace elements in waterlogged soils and sediments. CRC Press, Taylor & Francis Group, Boca Raton, FL, USA.*

landfills, and (waste)water treatment plants, or from non-point sources, including wear from materials containing ENPs. In addition, deliberate introduction of ENPs into the environment also occurs, *e.g.*, upon their application in groundwater or soil remediation or the use of ENPs-containing agrochemicals (Scown *et al.*, 2010; Ferreira da Silva *et al.*, 2011; Gottschalk and Nowack, 2011). Due to the diverse input routes, aquatic systems are highly susceptible to contamination with ENPs. However, very little data on the actual emissions of ENPs from products and their releases into the environment are available (Nowack *et al.*, 2012). Besides quantification of the emissions, it is also important to investigate in which form ENPs are released (*e.g.*, as single nanoparticles, aggregates or agglomerates, or embedded in a matrix) (Gottschalk and Nowack, 2011). For example, Benn and Westerhoff (2008) have demonstrated leaching of both colloidal (100 – 200 nm) and ionic Ag from socks upon repeated washing. Benn *et al.* (2010) reported the emission of Ag ENPs from several consumer products, including a t-shirt, shampoo, and toothpaste. Kaegi *et al.* (2008a) provided evidence for the release of TiO_2 ENPs into the aquatic environment, due to natural weathering of painted house façades. Additionally, Limbach *et al.* (2008) illustrated that a small yet significant fraction (6 wt%) of CeO_2 ENPs fed to a model wastewater treatment plant, could be retrieved in the effluent at concentrations of 2 to 5 mg L^{-1}.

2.2.2 Processes and factors affecting behaviour and fate in aquatic systems

Upon their release into the environment, ENPs can undergo a number of potential physical, chemical, and even biological transformation processes that govern their behaviour and fate, including aggregation, sedimentation, dissolution, interactions with colloidal components, sorption to particulates and other solid surfaces, biological degradation, abiotic degradation (*e.g.*, photolysis), and oxidation and/or reduction. These transformation processes depend on both the characteristics of the nanoparticles (*e.g.*, size, chemical composition, and surface properties), and on the prevailing conditions of the receiving medium (*e.g.*, solution pH, ionic strength, natural organic matter (NOM) content, and clay content). Aggregation and dissolution are considered to be the two most important contributors to environmental impacts of ENPs in aquatic systems (Hotze *et al.*, 2010; Lowry *et al.*, 2010; Scown *et al.*, 2010; Mudunkotuwa and Grassian, 2011; Nowack *et al.*, 2012; Batley *et al.*, 2013). Potential entry routes, as well as occurring transformation processes of ENPs in the environment are depicted in Figure 2.1.

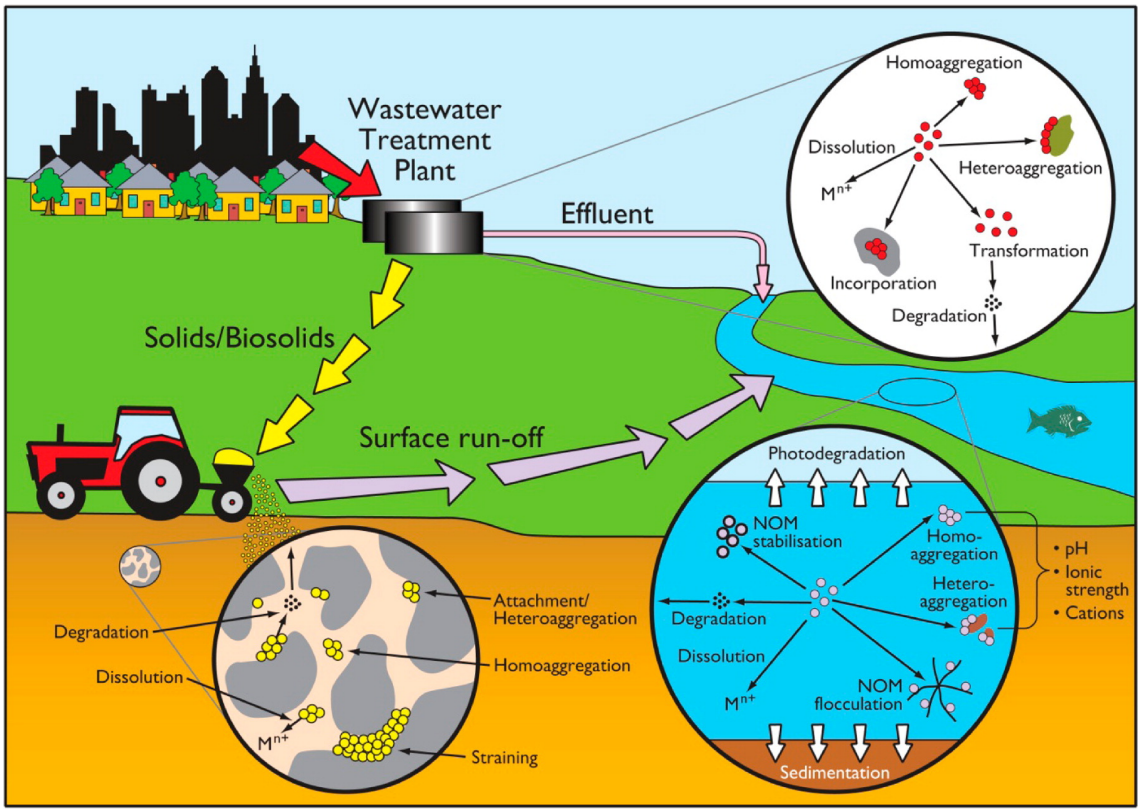

Figure 2.1 – Potential entry routes and transformation processes of ENPs in the environment. [Reprinted from Batley *et al.* (2013), with kind permission from the corresponding author.]

2.2.2.1 Aggregation – sedimentation

Stability in suspension is a key factor controlling the transport and ultimate fate of ENPs in aquatic systems. Aggregation and subsequent sedimentation restricts their mobility and bioavailability, whereas well-dispersed ENPs can be transported widely, thereby increasing the risk for potential harmful interactions with organisms. Aggregation also limits the reactivity of ENPs by reducing the overall specific surface area and interfacial free energy (Boxall *et al.*, 2007; Lin *et al.*, 2010).

Aggregation occurs when particles collide due to physical processes, and thermodynamic interactions allow for particle-particle attachment to take place. These particle-particle collisions originate from three fundamental mechanisms: *(1) Brownian diffusion, leading to perikinetic aggregation; (2) particles moving at different velocities in a shear flow, resulting in orthokinetic aggregation; and (3) particles of different size or density undergoing differential settling.* Considering particles smaller than 100 nm and a fluid at rest, the long-range forces between individual particles, and hence the collisions between particles, are controlled by Brownian motion, and mechanisms (2) and (3) can be neglected.

Contact between particles can result in attachment or repulsion, which is controlled by short-range thermodynamic interactions. Such interactions can be understood in the context of Derjaguin-Landau-Verwey-Overbeek (DLVO) theory (Handy *et al.*, 2008b; Hotze *et al.*, 2010).

According to classical DLVO theory, attachment between spherical particles is determined by the sum of attractive Van der Waals forces (V_{VdW}), and repulsive electrostatic double layer forces (V_{EDL}) (Mudunkotuwa and Grassian, 2011). The total interaction energy (V_T) is therefore:

$$V_T = V_{VdW} + V_{EDL} \quad \textbf{(2.1)}$$

Attractive Van der Waals forces are given by Equation 2.2.

$$V_{VdW} = -\frac{A_H}{6}\left[\frac{2a_1a_2}{R^2-(a_1+a_2)^2} + \frac{2a_1a_2}{R^2-(a_1-a_2)^2} + ln\frac{R^2-(a_1+a_2)^2}{R^2-(a_1-a_2)^2}\right] \quad \textbf{(2.2)}$$

where V_{VdW} [J] is the Van der Waals attraction, A_H [J] is the overall Hamaker constant (taking particle composition into account), a_1 and a_2 [m] are the particle radii, and R [m] is the distance between the centres of adjacent particles.

Repulsive electrostatic forces, which depend on the particle radius (a) and thickness of the electrical double layer ($1/\kappa$), are given by Equation 2.3 and 2.4, in the case of $\kappa a > 5$ or $\kappa a < 5$, respectively.

$$V_{EDL} = 4\pi\varepsilon\psi_0^2\frac{a_1a_2}{a_1+a_2}ln[1+\exp(-\kappa x)] \quad \textbf{(2.3)}$$

$$V_{EDL} = 4\pi\varepsilon Y_1Y_2a_1a_2\left(\frac{k_BT}{e}\right)^2\frac{\exp(-\kappa x)}{a_1+a_2+x} \quad \textbf{(2.4)}$$

with:

$$Y_i = \frac{8\tanh(\frac{e\psi_0}{4k_BT})}{1+\sqrt{\left[1-\frac{2\kappa a_i+1}{(\kappa a_i+1)^2}tanh^2\left(\frac{e\psi_0}{4k_BT}\right)\right]}} \quad \textbf{(2.5)}$$

where V_{EDL} [J] is the electrostatic double layer repulsion, ε [-] is the relative permittivity of the fluid, a_1 and a_2 [m] are the radii of the particles, ψ_0 [V] is the surface potential, k_B [J K^{-1}] is the Boltzmann constant, T [K] is the absolute temperature, e [C] is the elementary charge of an electron, x [m] is the interparticle distance, and κ [m^{-1}] is the inverse Debeye length.

In case the attractive forces are larger than the repulsive forces, aggregation will occur. Summation of these forces also demonstrates that particles can have a net attraction in a primary or secondary minimum. The primary minimum implies irreversible aggregation, whereas reversible aggregation of particles is considered in the secondary minimum (Hotze *et al.*, 2010). The Stern-Gouy-Chapman model of the electrical double layer, as well as particle-particle interaction energy profiles are shown in Figure 2.2.

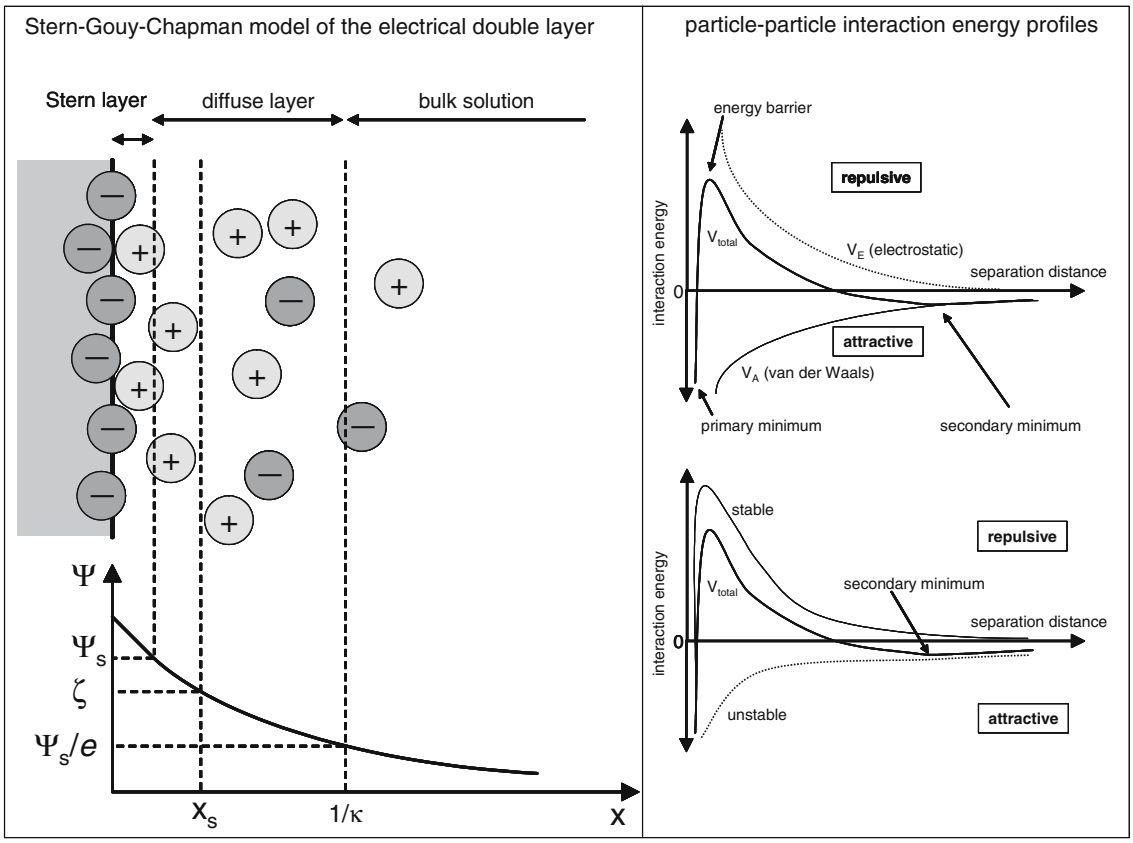

Figure 2.2 – Schematic diagram showing (left panel) the electrical double layer (EDL) on the surface of a particle, with the different potentials to be considered (*i.e.*, the electrostatic potential (ψ), the potential at the Stern layer (ψ_s), the zeta potential (ζ), and the potential at the diffuse layer (ψ_s/e)), the Debeye length ($1/\kappa$) at which the potential has fallen to a value of $1/e$ of the Stern potential, and the shear plane (X_s) where ions and molecules are mobile. An increased ionic strength will effectively compress the EDL, thereby influencing the Debeye length (*e.g.*, from a couple of nm to nearly 1 μm in the case of seawater or ultrapure water, respectively). The right panel shows a simplified graph summarizing the DLVO interaction energies and resulting sum function. The top graph shows a situation where repulsive electrostatic forces are working against attractive Van der Waals forces, and an activation energy is required to achieve particle-particle attachment in either the secondary or primary minimum. The bottom graph shows three possible situations: *a fully stabilized system, a system having a secondary and primary minimum, and a fully destabilized system.* [Reprinted from Handy *et al.* (2008b), with kind permission from Springer Science and Business Media.]

ENPs are most often coated with surface ligands, such as polymers, polyelectrolytes, or NOM, resulting in (electro)steric stabilization of the particles in suspension, arising from elastic and osmotic contributions. Therefore, extended DLVO (XDLVO) theory has been developed to account for these additional repulsion forces. DLVO and XDLVO theories both stem from colloid chemistry, and although these theories have been shown to be able to semi-quantitatively describe aggregation and deposition of ENPs under laboratory conditions, prediction of the aggregation behaviour of ENPs in more complex matrices has proven a lot more challenging. Nevertheless, DLVO and XDLVO theories are important modelling tools in order to gain insight in the processes and influences of diverse parameters affecting aggregation of ENPs (Hotze *et al.*, 2010; Petosa *et al.*, 2010; Mudunkotuwa and Grassian, 2011). For instance, studies by Elzey and Grassian (2010a), Li *et al.* (2010), von der Kammer *et al.* (2010), Bian *et al.* (2011), and Stebounova *et al.* (2011), have successfully applied (X)DLVO theories to investigate the aggregation and sedimentation behaviour of Ag, TiO_2, and ZnO ENPs as a function of aquatic parameters, including pH, ionic strength, and NOM content.

Two types of aggregation of ENPs in the environment can occur, *i.e.*, homo-aggregation and hetero-aggregation. The former refers to the attachment of similar particles, while the latter addresses attachment of dissimilar particles (Hotze *et al.*, 2010). Natural colloids (*e.g.*, clays, iron and manganese hydrous oxides, dissolved organic matter, fibrillar colloids (exopolymers), and microorganisms) are ubiquitous in the aquatic environment, and their concentrations (mg L^{-1}) are typically several orders of magnitude higher than the expected environmental concentrations of ENPs (μg L^{-1} or less). Hence, hetero-aggregation is likely to be the dominant process controlling the fate of most ENPs, and attachment of ENPs to natural colloids followed by sedimentation is considered as the most important removal process of ENPs from natural water bodies. Still, most studies have been focused on examining homo-aggregation, or were performed using artificial suspension media instead of natural aquatic matrices (Lin *et al.*, 2010; Quik *et al.*, 2010; Quik *et al.*, 2012; Batley *et al.*, 2013).

Ionic strength (IS) is a measure for the concentration of dissolved salts in solution, and is an important parameter in regard to colloidal stability. An increase in ionic strength results in compression of the EDL, which leads to a decrease in the repulsion forces and potentially to aggregation of ENPs. The ionic concentration at which the repulsive energy barrier is completely screened and rapid aggregation occurs is called the critical coagulation

concentration (CCC) (Hotze *et al.*, 2010). Additionally, according to the Schulze-Hardy rule, the valence of the counterions also has an important impact on colloidal stability (Lin *et al.*, 2010). ENPs will therefore have a higher tendency to aggregate and settle out of solution in seawater or brackish water, than in freshwater, as was demonstrated in a study by Keller *et al.* (2010). French *et al.* (2009) have also shown that aggregation of TiO_2 ENPs is stimulated by increasing IS and cation valence, whereas Li *et al.* (2010) identified CCC values of 30, 40, and 2 mM for bare 82 ± 1.3 nm Ag ENPs in the case of $NaNO_3$, NaCl, and $CaCl_2$, respectively.

Solution pH also plays a crucial role in the aggregation of ENPs, by affecting the surface charge of particles, or rather their zeta (ζ) potential, which is the potential difference between the dispersion medium and the stationary layer of fluid attached to the particle (see also Figure 2.2), and which actually determines the interparticle forces (Handy *et al.*, 2008b; Lin *et al.*, 2010). Colloids and ENPs having a ζ-potential between -30 mV and +30 mV are generally considered to be unstable in suspension, and tend to aggregate. When the pH of an aquatic system is at the point of zero charge (PZC) or isoelectric point (IEP), the colloidal system exhibits minimum stability (Lin *et al.*, 2010). A pH below the PZC leads to a positively charged particle surface and the ζ-potential will increase further with decreasing pH, whereas a pH above the PZC results in a negatively charged particle surface, and further increasing the pH leads to a decrease in ζ-potential. A high absolute ζ-potential therefore implies stability of ENPs in dispersion. Because the PZC differs between different ENPs, their stability in suspension also varies at a certain solution pH (Lin *et al.*, 2010). Amongst numerous studies, Ghosh *et al.* (2008) for instance examined the colloidal behaviour of Al_2O_3 ENPs as a function of pH, showing that the surface charge of the particles decreased with increasing pH, and reached a PZC at pH 7.9. The effect of pH and NOM on the ζ-potential of CeO_2 ENPs dispersed in deionized water and algae medium is illustrated in Figure 2.3.

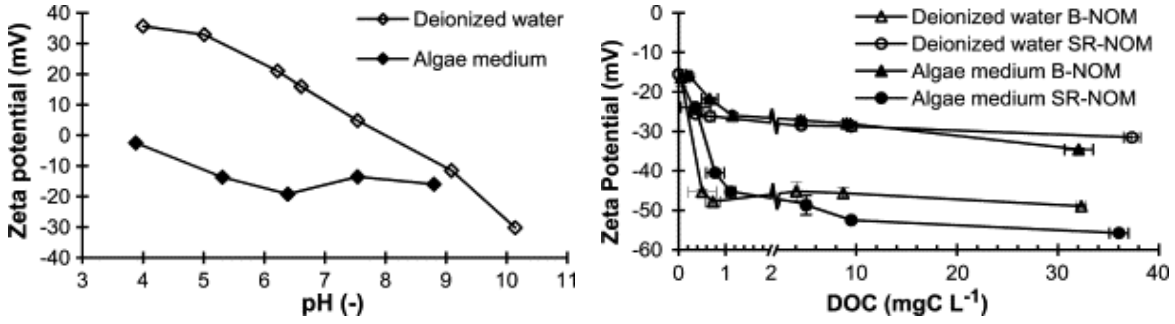

Figure 2.3 – Effect of pH (left graph), and various concentrations Bilhain and Suwannee River NOM (right graph), on the ζ-potential of CeO_2 ENPs dispersed in deionized water and algae medium. [Reprinted from Quik *et al.* (2010), with kind permission from Elsevier.]

As mentioned above, ENPs are often coated with synthetic surface ligands to improve their colloidal stability and overcome rapid aggregation and sedimentation. Limbach *et al.* (2008) have demonstrated that different surface coatings have a major effect on the stability of CeO_2 ENPs in solutions of varying NaCl concentration. Similar results were obtained in a study by Phenrat *et al.* (2007), who compared the sedimentation of coated Fe ENPs with bare Fe ENPs, and in a study by El Badawy *et al.* (2010), who examined the impact of capping agents and environmental conditions (*e.g.*, pH, IS, and background electrolytes) on the surface charge and aggregation potential of Ag ENPs. In addition to stabilization by synthetic ligands, ENPs can also be coated and stabilized by NOM upon their release into the environment. NOM has been shown to sorb onto various metal oxide ENPs (*e.g.*, TiO_2, Al_2O_3, and ZnO), resulting in a decrease in particle ζ-potential and suggesting a higher stability in suspension (Scown *et al.*, 2010). For instance, up to 40 % of CeO_2 ENPs initially spiked to artificial fresh water have been shown to remain stable in suspension in the presence of NOM, over a 12-day period (Quik *et al.*, 2010). Furthermore, von der Kammer *et al.* (2010) found that about 70 to 90 % of initially added TiO_2 ENPs remained in suspension after 15 hours of settling in the presence of NOM. In contrast, ENPs can also be bridged by NOM, resulting in destabilization, aggregation and settling. Whether attachment results in either stabilization or destabilization depends on various factors, such as type and concentration of NOM, as well as solution chemistry (Hotze *et al.*, 2010). Baalousha *et al.* (2008) for example, demonstrated that the start of aggregation of Fe_2O_3 ENPs shifted from a pH of 5 – 6 to a pH of 4 – 5 upon addition of Suwannee River humic acid (SRHA), and that increasingly larger aggregates were formed with increasing SRHA concentration (0 – 25 mg L^{-1}) and pH. In a different study it was also shown that divalent cations (0.04 – 0.06 M Ca^{2+}) could induce aggregation of NOM-coated metal oxide (ZnO, NiO, TiO_2, Fe_2O_3, and SiO_2) ENPs (Zhang *et al.*, 2009).

Contaminants in natural aquatic systems are mostly bound to particle surfaces, or form complexes with for instance NOM. They can be sorbed, co-precipitated, or trapped upon aggregation of ENPs, and thus ENPs could play an important role in the solid-liquid partitioning of pollutants. Interactions between contaminants and ENPs depend on characteristics, such as particle size, structure and composition, and solution chemistry (Christian *et al.*, 2008). Stabilization of ENPs in the environment induces a higher mobility, thereby not only enhancing the risks associated with the ENPs directly, but also increasing the potential exposure to associated contaminants as ENPs could potentially act as co-transporters of other pollutants (Scown *et al.*, 2010).

2.2.2.2 Dissolution

Essentially, dissolution of ENPs can be considered as the transformation of a chemical compound in its nanoparticulate form to individual ions or molecules that are soluble in water (Quik *et al.*, 2011; Nowack *et al.*, 2012). It is a heterogeneous process that takes place on the solid-liquid phase boundaries in two steps: *(1) a reaction at the solid-liquid interface, and (2) a transfer of the dissolved matter away from the reaction site* (Dokoumetzidis *et al.*, 2008). According to Liu *et al.* (2009), a modified Kelvin equation (Equation 2.6) (also known as the Ostwald-Freundlich equation) has commonly been used to describe the thermodynamic size-dependent dissolution of nanoparticles.

$$\frac{S}{S_0} = \exp\left(\frac{2\gamma V}{RTr}\right) \qquad (\mathbf{2.6})$$

where S [mol kg^{-1}] is the solubility of a spherical nanoparticle with radius r [m], S_0 [mol kg^{-1}] is the solubility of the bulk material, γ [J m^{-2}] is the surface free energy, V [m^3 mol^{-1}] is the molecular volume, R [J mol^{-1} K^{-1}] is the gas constant, and T [K] is the absolute temperature.

Following Equation 2.6, the solubility increases exponentially with decreasing particle size, and it is clear that surface energy and particle size strongly influence nanoparticle dissolution. However, due to a lack of detailed knowledge on the surface energy, its size dependency, and its dependency on the details of the surface structure, deviations from predictions rendered by Equation 2.6 can be expected (Mudunkotuwa and Grassian, 2011).

The dissolution behaviour of ENPs is important in terms of understanding their overall stability in the aquatic environment, and especially their potential (eco)toxicity, as the latter has generally been attributed to originate from the release of ionic species rather than being induced by the ENPs themselves (Mudunkotuwa and Grassian, 2011). Most metallic ENPs are hydrophilic and have a finite but often low solubility. Nevertheless, they can still release metal ions in amounts that could be detrimental to the environment, and despite the fact that the soluble ionic metal fraction is considered as the most toxic to aquatic and terrestrial biota, not many studies have been designed to measure this (Lin *et al.*, 2010; Batley *et al.*, 2013). For instance, despite a common believe that ZnO is “insoluble”, ZnO ENPs have been found to dissolve rapidly in a freshwater algal medium buffered at pH 7.5, producing 6 and 16 mg L^{-1} dissolved Zn after 6 and 72 h, respectively. This should not be neglected, considering that 5 mg Zn L^{-1} would already be toxic to most aquatic

organisms (Franklin *et al.*, 2007). In contrast, a similar study by Rogers *et al.* (2010b) found the dissolution of CeO_2 ENPs to be negligible (ng L^{-1}), and demonstrated a greater toxicity to freshwater algae for nanoparticulate CeO_2 compared to bulk CeO_2. Furthermore, the formation of aggregates can hinder dissolution by reducing the active surface area and the average equilibrium solubility, and can lead to kinetic hindrance of the diffusion process (Lin *et al.*, 2010).

In addition to nanoparticle properties, including particle size, morphology, and composition, dissolution of ENPs is also greatly affected by environmental parameters, such as pH, temperature, and NOM content (Lin *et al.*, 2010). The dissolution of Cu ENPs in low pH aqueous suspension was examined by Elzey and Grassian (2010b), and they postulated that copper oxide (CuO:Cu_2O) layers present on the surface of the nanoparticles likely facilitated nanoparticle dissolution. Baalousha *et al.* (2008) have reported that dissolution of Fe_2O_3 ENPs was negligible at pH values above 4, whereas 35 % of total iron from the Fe_2O_3 ENPs was found in the dissolved phase (< 1 kDa) at low pH. Furthermore, Bian *et al.* (2011) found that humic acid can increase the release of Zn^{2+} ions from ZnO ENPs at pH > 9, whereas no effect of the presence of humic acid on dissolution was seen at pH < 6. According to Liu and Hurt (2010), the ionic release from Ag ENPs is a cooperative oxidation process requiring both protons and dissolved oxygen. The ionic release was found to increase with temperature (0 – 37 °C), and decrease with increasing pH, or addition of NOM. Additionally, sea salts appear to have only a minor effect on the release of dissolved silver. Kittler *et al.* (2010) demonstrated that in addition to temperature, surface functionalization of ENPs could also affect nanoparticle dissolution. Considerable differences in the release of Ag^+ ions were observed when examining the rate and degree of dissolution of citrate-stabilized and polyvinylpyrrolidone-stabilized Ag ENPs in ultrapure water over a time scale of several days. In all cases studies, none of the Ag ENPs dissolved completely, however the nanoparticles released up to 90 wt% of silver in some cases. Ag ENPs have been shown to be more toxic than their micrometre-sized counterparts, mainly due to the larger release of dissolved silver (Kittler *et al.*, 2010; Batley *et al.*, 2013).

2.2.2.3 Additional transformation processes

Once released into the environment, ENPs can undergo additional biotic or abiotic alterations, such as biological transformations, disaggregation, photolysis, hydrolysis, and redox transformations, which can alter the size, shape, surface chemistry and surface

coating of nanoparticles, and affect their concentration, persistence, and potential toxicity in the environment (Lowry and Casman, 2009).

Biological uptake and biodegradation are considered as important cleansing routes for environmental contaminants, and can therefore also be of significance for the fate of ENPs. Uptake of ENPs by aquatic organisms generally occurs through normal feeding behaviour and/or through water filtration via gills. Following their uptake, ENPs could pass through the digestive tract, and then be translocated to other body parts, or be excreted (Lin *et al.*, 2010). For instance, it has been reported that exposure to 80 nm Cu ENPs resulted in higher Cu content in the gills of zebrafish, and that this result could not solely be attributed to dissolved Cu, whilst translocation of Ag ENPs to the brain, heart, yolk, and blood of zebrafish embryos has also been observed (Lin *et al.*, 2010). Additionally, microorganisms could be capable of oxidizing or reducing ENPs or their coating, *e.g.*, by electron transport in the *pili* of bacteria, or through direct reduction by membrane bound cytochromes, and could induce localized dissolution. However, detailed information regarding such biological transformation processes is scarce and additional research is required (Lowry and Casman, 2009).

Abiotic redox transformations are also vital processes affecting the environmental fate of ENPs. Redox reactions could result in ionic release in solution, but could also occur at the surface layer of ENPs leading to alterations in their crystalline nature (Auffan *et al.*, 2009). Fe ENPs for instance, have been used for *in situ* remediation and are designed to supply electrons for the reductive dehalogenation of chlorinated solvents or the reductive sequestration of heavy metals (Lowry and Casman, 2009). It has been reported that Fe ENPs could be oxidized over time (*i.e.*, aging) to form iron oxides, such as magnetite, maghemite, hematite, and goethite, and that the surface oxidation affected the redox activity, aggregation, sedimentation, and toxicity of Fe ENPs (Lin *et al.*, 2010). CdSe quantum dots (QDs) have also been shown to release substantial amounts of Cd^{2+} ions, which was attributed to selenide oxidation (Batley *et al.*, 2013). Additionally, redox reactions involving metallic ENPs could also result in the generation of reactive oxygen species (ROS) leading to oxidative stress towards cellular organisms. Strong cytotoxic effects due to oxidative stress have been demonstrated for some bacteria, human, and rodent cells (Auffan *et al.*, 2009).

Metallic nanoparticles and their ionic dissolution products readily react with ionic species (*e.g.*, Cl^-, HS^-, HCO_3^-, $H_2PO_4^-$, S^{2-}, CO_3^{2-}, and HPO_4^{2-}) present in aquatic environments, which could result in the formation of rather insoluble solid compounds that might

precipitate out of solution. The solubility product constants (K_{sp}) of a selection of metal salts are tabulated in Table 2.1. It is for instance recognized that Ag ENPs are not stable in aquatic systems under most prevailing environmental conditions, but will dissolve or transform into other species, of which AgCl and Ag_2S seem to be to most relevant inorganic forms (Levard *et al.*, 2012; Thalmann *et al.*, 2014). E_h-pH conditions as well as solution composition will dictate speciation of metals in natural waters. Low Cl:Ag ratios typically found in freshwater systems are expected to result in $AgCl_{(s)}$ precipitation, whereas high Cl:Ag ratios occurring in seawater, are predicted to lead to the formation of soluble $AgCl_{(aq)}$, $AgCl_2^-$, $AgCl_3^{2-}$, and $AgCl_4^{3-}$ species, under aerobic conditions. However, under anaerobic conditions and in sulphide-rich environments (*e.g.*, anaerobic (waste)water, wetlands, and anoxic sediments), $Ag_2S_{(s)}$ precipitation is expected to predominate, as it is thermodynamically favoured over AgCl formation (Levard *et al.*, 2012; Thalmann *et al.*, 2014). Sequestration of metals through precipitation of metal sulphides in aqueous and subsurface systems, and its environmental implications has been well documented (Kim *et al.*, 2010; Lewis, 2010). Sulphidation is therefore also considered to be an important transformation process affecting the environmental behaviour, fate, transport, and toxicity of metallic ENPs. According to Liu *et al.* (2011), the sulphidation of Ag ENPs can take place via two reaction mechanisms, depending on the amount of sulphides present in solution. At high sulphide concentrations, nanosilver oxysulphidation occurs by a direct particle-fluid heterogeneous reaction at the particle surface, while at low sulphide concentrations, sulphidation proceeds indirectly via oxidative dissolution of Ag to Ag^+ ions followed by precipitation of Ag_2S particles. These two potential nanosilver sulphidation pathways are shown in Figure 2.4. Metal sulphides are generally considered to be very stable compounds (see also Table 2.1) (Lewis, 2010). For instance, the dissolution of Ag_2S upon re-oxidation has been reported to be negligible over a period of months (Thalmann *et al.*, 2014). Moreover, even partial sulphidation of Ag ENPs to Ag:Ag_2S core:shell particles, has been shown to drastically reduce nanosilver toxicity towards aquatic and terrestrial eukaryotic organisms, such as *Danio rerio* (zebrafish), *Fundulus heteroclitus* (killifish), *Caenorhabditis elegans* (nematode worm), and *Lemna minuta* (least duckweed), as a result of a decreased release of Ag^+ ions (Levard *et al.*, 2013). Yet, findings by Ma *et al.* (in press) suggest that sulphidation of CuO ENPs may enhance their apparent solubility, and hence increase their bioavailability and eco-toxicity, which has been attributed to toxic Cu^{2+} ions. The observed increased solubility was caused by the oxidative dissolution of Cu_xS_y clusters. Additionally, Ma *et al.* (2013) have demonstrated that the solubility of partially sulphidized ZnO ENPs is controlled by the ZnO core and is not

quenched by the formation of the ZnS shell, in contrary to what was observed with partially sulphidized Ag ENPs. Sulphidation of ZnO ENPs also led to a decrease in surface charge and to aggregation, suggesting sulphidation alters their behaviour, fate, and toxicity in the environment.

Table 2.1 – Solubility product constants (K_{sp}) at 25 °C of a selection of inorganic compounds.

Compound	Formula	Equilibration reaction	$K_{sp,\ 25\ °C}$
Aluminium hydroxide	$Al(OH)_3$	$AlOH_3 \rightleftharpoons Al^{3+} + 3OH^-$	4.6×10^{-33}
Aluminium phosphate	$AlPO_4$	$AlPO_4 \rightleftharpoons Al^{3+} + PO_4^{3-}$	9.8×10^{-21}
Cadmium hydroxide	$Cd(OH)_2$	$Cd(OH)_2 \rightleftharpoons Cd^{2+} + 2OH^-$	7.2×10^{-15}
Cadmium phosphate	$Cd_3(PO_4)_2$	$Cd_3(PO_4)_2 \rightleftharpoons 3Cd^{2+} + 2PO_4^{3-}$	2.5×10^{-33}
Cadmium sulphide	CdS	$CdS \rightleftharpoons Cd^{2+} + S^{2-}$	1.4×10^{-29}
Copper(I) chloride	$CuCl$	$CuCl \rightleftharpoons Cu^{+} + Cl^-$	1.7×10^{-7}
Copper(I) sulphide	Cu_2S	$Cu_2S \rightleftharpoons 2Cu^{+} + S^{2-}$	2.3×10^{-48}
Copper(II) hydroxide	$CuOH_2$	$CuOH_2 \rightleftharpoons Cu^{2+} + 2OH^-$	1.6×10^{-19}
Copper(II) phosphate	$Cu_3(PO_4)_2$	$Cu_3(PO_4)_2 \rightleftharpoons 3Cu^{2+} + 2PO_4^{3-}$	1.4×10^{-37}
Copper(II) sulphide	CuS	$CuS \rightleftharpoons Cu^{2+} + S^{2-}$	1.3×10^{-36}
Iron(II) carbonate	$FeCO_3$	$FeCO_3 \rightleftharpoons Fe^{2+} + CO_3^{2-}$	3.1×10^{-11}
Iron(II) hydroxide	$Fe(OH)_2$	$Fe(OH)_2 \rightleftharpoons Fe^{2+} + 2OH^-$	4.9×10^{-17}
Iron(II) sulphide	FeS	$FeS \rightleftharpoons Fe^{2+} + S^{2-}$	1.6×10^{-19}
Iron(III) hydroxide	$Fe(OH)_3$	$Fe(OH)_3 \rightleftharpoons Fe^{3+} + 3OH^-$	2.8×10^{-39}
Iron(III) phosphate	$FePO_4$	$FePO_4 \rightleftharpoons Fe^{3+} + PO_4^{3-}$	9.9×10^{-16}
Silver carbonate	Ag_2CO_3	$Ag_2CO_3 \rightleftharpoons 2Ag^{+} + CO_3^{2-}$	8.5×10^{-12}
Silver chloride	$AgCl$	$AgCl \rightleftharpoons Ag^{+} + Cl^-$	1.8×10^{-10}
Silver phosphate	Ag_3PO_4	$Ag_3PO_4 \rightleftharpoons 3Ag^{+} + PO_4^{3-}$	8.9×10^{-17}
Silver sulphide	Ag_2S	$Ag_2S \rightleftharpoons 2Ag^{+} + S^{2-}$	5.9×10^{-51}
Tin(II) hydroxide	$Sn(OH)_2$	$Sn(OH)_2 \rightleftharpoons Sn^{2+} + 2OH^-$	5.5×10^{-27}
Tin(II) sulphide	SnS	$SnS \rightleftharpoons Sn^{2+} + S^{2-}$	3.3×10^{-28}
Zinc carbonate	$ZnCO_3$	$ZnCO_3 \rightleftharpoons Zn^{2+} + CO_3^{2-}$	1.5×10^{-10}
Zinc hydroxide	$Zn(OH)_2$	$Zn(OH)_2 \rightleftharpoons Zn^{2+} + 2OH^-$	3.0×10^{-17}
Zinc sulphide	ZnS	$ZnS \rightleftharpoons Zn^{2+} + S^{2-}$	2.9×10^{-25}

Contents compiled from Reger *et al.* (2010) and Levard *et al.* (2012).

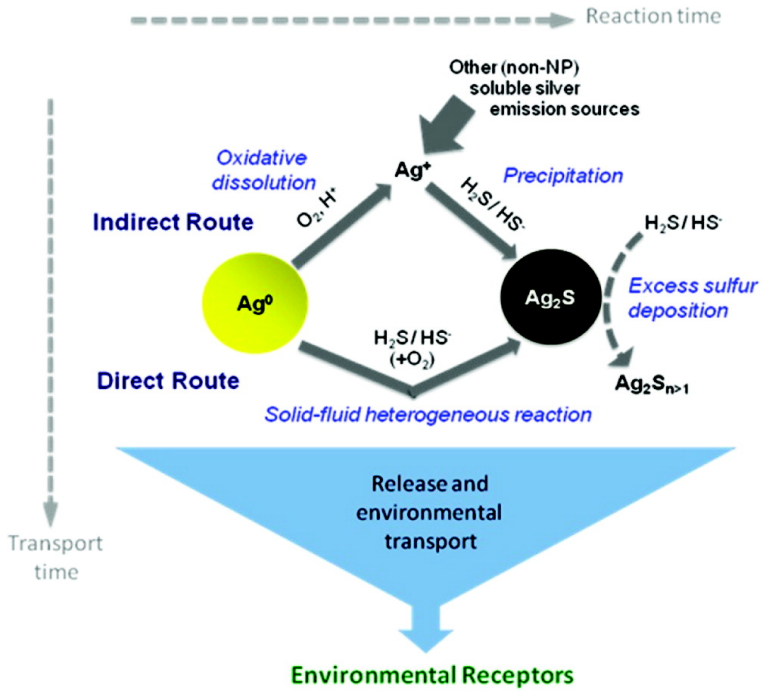

Figure 2.4 – Competing chemical and transport pathways of nanosilver sulphidation. Ag_2S ENPs may be produced by particle-fluid reaction (direct route), or via oxidative dissolution to soluble silver followed by sulphide precipitation (indirect route). The main chemical pathway to Ag_2S will depend on the relative rates of these two reactions as a function of media compositions along the Ag ENPs transport trajectory. Also shown is the possible role of oxygen in direct sulphidation, and the potential formation of super-stoichiometric sulphide phases, as reported by Kim *et al.* (2010). A competition between sulphidation reaction times (horizontal axis) and transport times (vertical axis) determines whether the biologically active ionic Ag^+ and nanoparticulate Ag phases reach sensitive biological receptors before being transformed into the more benign sulphide phases. [Reprinted from Liu *et al.* (2011), with kind permission from The American Chemical Society.]

Disaggregation of ENPs is as substantial as aggregation processes are (Christian *et al.*, 2008). Hetero-aggregation of ENPs with NOM or bio-colloids (*e.g.*, bacteria) could prevent aggregation (see Section 2.2.2.1) but could also promote disaggregation (Hotze *et al.*, 2010). The presence of SRHA has been shown to induce (partial) disaggregation of Ag ENPs aggregates (Fabrega *et al.*, 2011) and Fe_2O_3 ENPs aggregates (Baalousha, 2009). CeO_2 ENPs have been reported to sorb onto the surface of bacteria (15 mg CeO_2 m^{-2}) due to electrostatic attraction, while disaggregation of TiO_2 ENPs in the presence of microorganisms, and enhanced stabilization of Fe ENPs in suspension upon attachment with bacteria has also been mentioned (Hotze *et al.*, 2010).

Certain ENPs are photoreactive (*e.g.*, TiO_2, ZnO, CdS, CdSe, and WO_3), which has also lead to their use in environmental remediation. For instance, TiO_2 ENPs have been

frequently used as a photocatalyst in (waste)water treatment (*e.g.*, for photodegradation of organic pollutants) due to their high catalytic activity resulting from a high surface to volume ratio, low toxicity, chemical stability, low cost, and the large availability of raw materials (Qu *et al.*, 2013). After their release into the environment, photochemical transformations could occur when incident light reaches photoreactive ENPs, thereby for instance inducing excitation and generation of free radicals, or leading to structural degradation at the surface of the particles or disaggregation (Hotze *et al.*, 2010; Nowack *et al.*, 2012). The extent to which such processes could take place depends on for example, the wavelength of the incident light, the capacity of the light to penetrate the outer layers of the particles (*e.g.*, aggregation or particle surface ligands might reduce the light penetration efficiency), and the capacity of the photosensitive portion of the ENPs to be excited or photodegraded (Nowack *et al.*, 2012). Photochemical alterations are fast, with the rate-determining step being the mass transfer from the surface of the particles to the surrounding medium, and could alter interactions of ENPs with environmental components, such as binding to NOM (Nowack *et al.*, 2012). Yin *et al.* (2014) for instance, have studied the effect of natural and synthetic sunlight on the reduction of ionic Au^{3+} complexes by NOM in river water, and reported the photo-induced formation of elemental Au nanoparticles from ionic Au in the presence of SRHA. Furthermore, it was shown that SRHA not only served as a reducing agent, but also as a coating agent, stabilizing the formed Au nanoparticles in dispersion. Li *et al.* (2014) examined photochemical transformations of Ag ENPs in the presence of perfluorocarboxylic acids (PFCAs) under UV irradiation and observed a decrease in dissolution, aggregation, ROS generation, and photo-induced toxicity, suggesting that the lower amounts of Ag^{+} ions and ROS produced from Ag ENPs upon their release into surface waters could be less hazardous to aquatic organisms under natural solar radiation.

2.2.3 Fate in terrestrial systems

Although extensive information on the behaviour and fate of ENPs in terrestrial environments is still lacking, sediments and soils are generally considered to serve as key receptors for ENPs. The physicochemical processes and factors mentioned and described in the sections above are also likely to play a major role in the alterations, transport, and environmental effects of ENPs in soil and sediment environments (Boxall *et al.*, 2007; Lin *et al.*, 2010; Ferreira da Silva *et al.*, 2011; Peralta-Videa *et al.*, 2011; Batley *et al.*, 2013).

2.2.3.1 Dissolution – Aggregation – Deposition – Partitioning

The solid phase present in sediment and soil systems provides a large reactive sink for ENPs. Dissolution of ENPs in sediments and soils could be promoted due to the large available surface area and exchange capacity for cations and anions, by acting as a sink for dissolution products, and providing protons, thereby enhancing dissolution of compounds with a pH-dependent solubility (Batley and McLaughlin, 2010).

Aggregation and deposition are two closely related phenomena that affect the fate and transport of ENPs. Aggregation describes the interaction between two mobile objects, while attachment of a mobile particle onto an immobile phase (*i.e.*, a collector) is referred to as deposition (Navarro *et al.*, 2008a; Hotze *et al.*, 2010). Due to the higher colloidal load and ionic strength of soil pore waters compared to natural water bodies, even greater aggregation of ENPs is expected in soils and sediments (Batley and McLaughlin, 2010).

Studies on partitioning of ENPs between liquid and solid soil phases are scant, however hydrophilic ENPs having a net positive surface charge can be expected to bind strongly to the predominantly negatively charged surfaces of soil minerals and soil organic matter, and thus be retained in soils and sediments. ENPs could however also stay mobile (or be remobilized) depending on particle properties (*e.g.*, surface charge and surface coating), and the (changing) environmental conditions (Batley and McLaughlin, 2010; Peralta-Videa *et al.*, 2011).

Amongst only a handful of studies investigating the fate of ENPs in real soil systems, Cornelis *et al.* (2011 and 2012) examined the retention and dissolution behaviour of citrate-stabilized CeO_2 ENPs, and polyvinylpyrrolidone-stabilized Ag ENPs in different soil solutions, and found homo-aggregation to be unlikely in the studied soil suspensions, and that hetero-aggregation was dominating. Both negatively charged Ag and CeO_2 ENPs were found to primarily bind at positively charged sites on clay particles. Additionally, almost no ionic Ag or Ce was detected, suggesting that either dissolution of the particles was negligible, or the dissolved species partitioned strongly towards the solid phase. In addition, Fang *et al.* (2009) reported that TiO_2 ENPs could remain suspended in real soil solutions even after settling for 10 days, and that the suspended TiO_2 ENPs content after 24 h of settling was positively correlated with NOM and clay content of the soils, whereas negative correlations with ionic strength, pH, and ζ-potential were obtained.

2.2.3.2 Transport – Mobility

The extent of movement of ENPs away from their source, as well as their potential to be removed from (waste)water by filtration, is determined by their transport in environmental matrices (*e.g.*, in porous media) (Lowry *et al.*, 2010). Knowledge on the transport behaviour of ENPs in natural sediment and soil systems is essential for assessing their potential impact on biota (*e.g.*, on plant roots and benthic organisms), but also for the further development of environmental applications, such as groundwater remediation, which requires ENPs to be transported through the soil or sediment (Lin *et al.*, 2010; Peralta-Videa *et al.*, 2011). Generally, columns packed with a porous matrix (*e.g.*, glass beads, quartz sand, or model soils) are used to study the mobility of ENPs, and particle filtration theory can be used to aid in understanding the transport behaviour of ENPs in sediments and soils (Lin *et al.*, 2010).

The transport or filtration of ENPs in porous media like soils, sediments, or aquifers largely depends on the rate of collision and attachment of ENPs to stationary soil or sediment grain surfaces (*i.e.*, the collector). Attachment is mainly a function of electrostatic interactions between the ENPs and the collector, whereas collisions occur as a result of three processes: *Brownian diffusion, interception, and gravitational sedimentation* (Christian *et al.*, 2008). For small particles Brownian diffusion is considered as the dominant transport mechanism, while interception and sedimentation mainly regulate the transport of larger particles and aggregates. Additionally, particles can also be retained by pore size exclusion in case their size is larger than the pore size through which the fluid flows (*i.e.*, straining) (Christian *et al.*, 2008; Hotze *et al.*, 2010; Lin *et al.*, 2010). A schematic diagram of the transport of ENPs in porous media is shown in Figure 2.5.

Transport of ENPs in porous media depends on particle properties (*e.g.*, size, morphology, and surface properties), solution conditions (*e.g.*, pH, ionic strength, NOM content, temperature, and fluid velocity), and collector characteristics (*e.g.*, porosity and grain size) (Christian *et al.*, 2008; Navarro *et al.*, 2008a; Darlington *et al.*, 2009; Lin *et al.*, 2010; Peralta-Videa *et al.*, 2011). Particle transport is theoretically predicted to increase with decreasing particle size, however as ENPs are prone to aggregation, straining of aggregates can greatly inhibit nanoparticle transport (Christian *et al.*, 2008; Lin *et al.*, 2010). A correlation between aggregate size and the transportability of Al ENPs through soils has been demonstrated (Darlington *et al.*, 2009), whereas Cornelis *et al.* (2013) also reported

irreversible attachment of Ag ENPs to mobile soil colloids in natural soil columns, leading to straining and favourable deposition. Surface characteristics (*e.g.*, surface chemistry, charge, and coating) also play a key role. ENPs having a hydrophilic surface will generally be easily dispersed and transported, while hydrophobic ENPs tend to aggregate and settle out of solution, followed by deposition onto a collector surface (Lin *et al.*, 2010). As mentioned earlier, environmental sediment and soil particles are usually negatively charged, ENPs having a negative surface charge will therefore tend to remain more mobile in the terrestrial matrix as a result of the stronger electrostatic repulsion between the ENPs and sediment or soil particles, while positively charged ENPs are readily attracted electrostatically to the collector surfaces (Christian *et al.*, 2008; Darlington *et al.*, 2009; Cornelis *et al.*, 2013). Consequently, several options to modify particle surface properties to enhance or restrict ENPs transport in porous media have been explored (*e.g.*, surface modification with hydrophilic functional groups, surfactants, or polymers) (Christian *et al.*, 2008; Lin *et al.*, 2010; Peralta-Videa *et al.*, 2011). Size and porosity of the terrestrial matrix can also affect ENPs mobility by determining their attachment to the collector surfaces. Generally, nanoparticle transport increases with increasing size of the collectors and porosity of the matrix (Christian *et al.*, 2008; Lin *et al.*, 2010; Cornelis *et al.*, 2013). Solution pH determines the dissolution and surface charge of ENPs, and hence the electrostatic interactions between ENPs and between ENPs and collector surfaces, whereas dissolved counterions will screen the long-range electrostatic interactions of electrostatically stabilized ENPs, thereby reducing their stability and transport through porous matrices (Christian *et al.*, 2008; Darlington *et al.*, 2009; Lin *et al.*, 2010). Fang *et al.* (2009) demonstrated an enhanced retention of TiO_2 ENPs as a function of increasing ionic strength and clay content, when passing through saturated porous columns packed with various soils. They also estimated that the maximum transport distance of TiO_2 ENPs in some soils ranged from 41.3 to 370 cm, indicating a potential risk of transfer of ENPs from soil media to deep soil layers and groundwater. Temperature and flow condition (*e.g.*, flow velocity) are additional solution properties affecting ENPs transport in porous media. Brownian diffusion is temperature dependent, and increases with increasing temperature, leading to an enhanced collision probability of Brownian particles. An increase in temperature can also result in a decrease in solution viscosity, and thus enhance the retention of non-Brownian particles. Moreover, increasing fluid velocity can enhance ENPs collisions and deposition, and hence their transport (Christian *et al.*, 2008; Lin *et al.*, 2010).

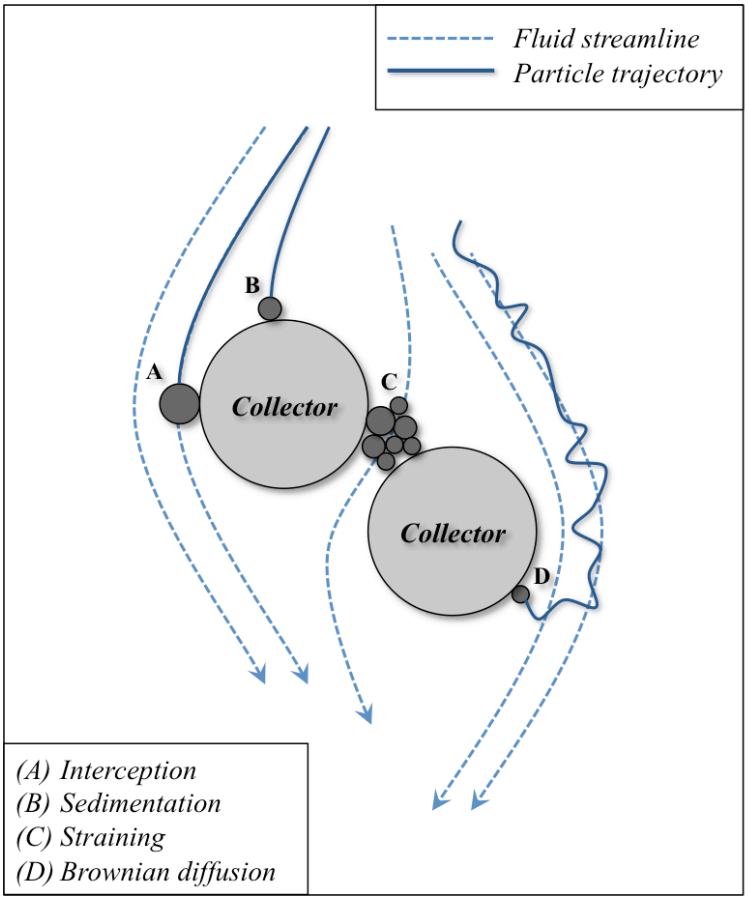

Figure 2.5 – Schematic illustration of basic particle filtration mechanisms affecting the transport of ENPs in porous media. [After Yao *et al.* (1971)]

It has been recognized that sediments can serve as sinks for a variety of organic (*e.g.*, herbicides and pesticides) and inorganic (*e.g.*, heavy metals) contaminants, which have a high tendency to sorb onto colloidal particles (*e.g.*, due to their high specific surface). Understanding the transport behaviour and mobility of ENPs is therefore also important to assess interactions of ENPs with existing contaminants, as association of ENPs with pollutants could potentially lead to particle-facilitated contaminant transport (see also Section 2.2.2.1) (Peralta-Videa *et al.*, 2011). Plathe *et al.* (2010 and 2013) for example, studied the associations between potentially toxic trace metals (*e.g.*, Pb, As, Cu, and Zn) and metal oxide nanoparticles in riverbed sediment, and their transport and distribution in riverine systems. Furthermore, TiO_2 ENPs have been shown to act as Cu carrier, and to potentially facilitate the transport of Cu through soil (Fang *et al.*, 2011).

2.3 Extraction and analysis of nanoparticles

Assessment of the occurrence, fate and behaviour of ENPs in the aquatic environment is a prerequisite to be able to understand and evaluate their potential environmental impact and risks. Therefore, a suitable analytical toolbox that can provide both qualitative and quantitative information is essential. Currently, no single method or protocol to fully characterize nanoparticles in complex environmental media (*e.g.*, natural surface waters, aquatic sediments, and soils) exists, but rather a combination of (complicated) analytical techniques is required (Tiede *et al.*, 2009a; Paterson *et al.*, 2011; Weinberg *et al.*, 2011).

Key parameters that should be considered during characterization analyses of nanoparticles in environmental matrices include: *average particle size and particle size distribution, particle shape and structure, aggregation state, surface charge, surface chemistry and surface area, dissolution potential, particle number, and particle chemical composition and concentration* (Tiede *et al.*, 2009a; Stone *et al.*, 2010; Farré *et al.*, 2011; Paterson *et al.*, 2011).

The sections below provide an overview of a selection of analytical methodologies that are commonly used to physically or chemically characterize nanoparticles when conducting environmental fate studies.

2.3.1 Sample pre-treatment – (pre-)fractionation

Depending on the analytical method(s) that will be used to analyse the sample, sample preparation and/or digestion is often necessary. The main purpose of sample pre-treatment is to extract the nanoparticles from the environmental matrix, or to reduce the complexity or the volume of the original sample prior to analysis. Sample pre-treatment can however impact the dispersion state of nanoparticle, and thus the obtained results could differ when compared to results obtained from direct *in situ* characterization of the nanoparticles. It is therefore recommended to use analytical techniques that do not require (extensive) sample preparation, or to minimize sample perturbation from the point of sampling on to the analysis (Tiede *et al.*, 2008; Simonet and Valcárcel, 2009; Weinberg *et al.*, 2011). The most common traditional techniques for a coarse pre-fractionation of samples are based on settling, centrifugation or filtration methodologies. Advantages of these

analytical tools include simplicity, low cost and short time consumption (Hassellöv *et al.*, 2008; Tiede *et al.*, 2008).

Settling or centrifugation can only remove particles from solution if their settling velocities overcome their Brownian motion. Settling velocities are a function of parameters, such as particle volume and shape, and the density difference between particle and water. As a result, settling or centrifugation is more effective in removing more dense mineral particles than for instance organic particles (Hassellöv *et al.*, 2008; Ferreira da Silva *et al.*, 2011). Centrifugation allows working with a broad range of particle sizes (10 to > 1000 nm), causes only minimum sample perturbation, and requires little sample preparation (*i.e.*, it only requires that particles are in suspension) (Handy *et al.*, 2008b). The technique could however induce aggregation, as settling particles can scavenge other smaller particles as a result of differential settling velocities. Although centrifugation is mainly considered as a pre-fractionation method, it can also be used as a general nanoparticle fractionation technique, especially when applied as ultracentrifugation (UC). For instance, Kaegi *et al.* (2008b) demonstrated a stepwise particle size fractionation approach during drinking water processing, where sedimentation was followed by differential centrifugation, to achieve stepwise size cut-offs stages of 9000 nm, 750 nm, 180 nm, and 12 nm. Whilst Bai *et al.* (2010) applied ultracentrifugation in the separation and concomitant purification of Au, Ag, and CdSe nanoparticles. The authors also successfully separated Au nanowires from their spherical counterparts, hereby showing that nanoparticles cannot only be separated by size but also by morphology.

Traditional membrane filtration (0.2 – 1 μm) and microfiltration (> 0.1 μm) are considered as common pre-fractionation techniques, mainly due to their simplicity of operation, low-cost, field-portability, ability to treat high volumes, and the fact that they only cause low sample perturbation. Conventional, dead-end filtration, is however also prone to artefacts, such as nanoparticle deposition, concentration polarization, surface interactions, and filter-cake formation (Buffle *et al.*, 1992; Morrison and Benoit, 2001). These artefacts become greater with decreasing pore size of the filter membrane (ultra- and nanofiltration).

In order to reduce concentration polarization and pore clogging, cross flow or tangential flow filtration (CFF or TFF), whereby the sample is recirculated on top of the membrane, has been developed (Hassellöv *et al.*, 2008). Liu and Lead (2006) have applied CFF in the separation of colloids and particles, and validated its efficacy against atomic force microscopy (AFM). Cross flow ultrafiltration (CFUF) has been evaluated for the size

fractionation of freshwater colloids and particles (1 nm – 1 μm) against AFM and scanning electron microscopy (SEM), by Doucet *et al.* (2004). They concluded that CFUF is not fully quantitative and that fractionation is not always based solely on size.

Ultrafiltration (UF) (1 nm – 30 nm) is a size fractionation method, applicable to process large sample volumes and capable to produce large quantities of isolated nanomaterials (Hassellöv *et al.*, 2008). When the pore size of the filter membrane is smaller than 1 nm, the filtration method is typically defined as nanofiltration (NF). Although fractionation by filtration is limited to two fractions only (*i.e.*, larger and smaller than the membrane pore size), multistage membrane filtration (MMF) can allow for a crude size fractionation. This method is however extremely labour intensive and time consuming (Hassellöv *et al.*, 2008; Fedotov *et al.*, 2011).

Dialysis is an ultra- or nanofiltration technique, where the driving force of operation relies on the diffusion of solutes across a membrane, arising from concentration gradients and osmotic pressure, rather than driven by a pressure gradient. This mild fractionation technique, can be used to separate "truly dissolved" components (*i.e.*, ions and small molecules) from their (nano)particulate counterparts. Dialysis has been applied to examine nanoparticle dissolution and nanoparticle-solute sorption behaviour (Franklin *et al.*, 2007; Kittler *et al.*, 2010), while Liu and Hurt (2010) investigated the ion release kinetics from Ag ENPs in aqueous solutions by application of centrifugal ultrafiltration.

2.3.2 Fractionation techniques

Analysis of nanoparticles in environmental samples generally requires extraction or separation from the matrix. Therefore, in order to meet detector sensitivity limitations, high pre-concentration factors are required. Chromatographic techniques that have been widely used to separate nanoparticles include: *high performance liquid chromatography (HPLC), size exclusion chromatography (SEC), capillary electrophoresis (CE), hydrodynamic chromatography (HDC), and field-flow fractionation (FFF)*. These techniques are characterized for being sensitive, non-destructive, and for allowing further characterization of the sample by combination with other techniques (Weinberg *et al.*, 2011). In Table 2.2, a summary is presented of these separation techniques, as well as the previously mentioned (pre-)fractionation methods.

Table 2.2 – Summary of a selection of methods applied for (pre-)fractionation of nanoparticles in environmental samples.

Technique		Approximate size range	Fractionation according to	Benefits or advantages	Drawbacks or limitations
Membrane Filtration	Microfiltration	100 nm – 1 μm	Size	Simplicity, low cost, high volume and speed, little sample preparation	Filtration artefacts, clogging, membrane interactions, poor size resolution
	Ultrafiltration	1 – 30 nm	Size		
	Nanofiltration	0.5 – 1 nm	Size		
	Dialysis	0.5 – 100 nm	Size		
Centrifugation	Conventional	10 nm – > 1 μm	Size, density	Low cost, high volume, little sample preparation and perturbation	Low size resolution, can induce aggregation
	UC	100 Da – 10 GDa	Size, density		
Chromatography	HPLC	3 nm – 1 μm	Size, affinity for stationary phase	Allows combination with detection methods, equipment is generally available	Mobile and stationary phase interactions, size range limited by column, poor size resolution
	SEC	0.5 – < 100 nm	Size, shape	Good separation efficiency, simple	Unwanted solvent and column interactions, limited size separation range
	HDC	5 nm – 1.2 μm	Size	Robust, simple, large separation range, independent of particle density	Poor selectivity, poor peak resolution
Field-flow fractionation	Fl-FFF	1 nm – 50 μm	Size, density	High resolution, applicable to a large size range, less interactions compared to SEC or HDC, most selective over 50 nm, analysis of sub-fractions with defined particle size is possible, low sample perturbation	Requires pre-concentration of sample and standards for calibration, prone to errors due to particle shape or density, requires coupling to a detector that can measure nanoparticle number or mass concentration (*e.g.*, ICP-MS, MALLS, UV-Vis)
	Sd-FFF	50 nm – 50 μm	Size, density		
	Th-FFF	30 nm – 10 μm	Size, chemical composition		
	El-FFF	10 nm – 2.5 μm	Size, surface charge		
Capillary electrophoresis	CE	3 nm – > 1μm	Size, shape, surface charge	Sensitivity, direct data on charge, faster than EM, low sample and reagents consumption	Mobile phase interactions, high concentration is necessary, interpretation of migration times can be cumbersome

Contents compiled from Handy *et al.* (2008b), Hassellöv *et al.* (2008), Tiede *et al.* (2008), Simonet and Valcárcel (2009), Ferreira da Silva *et al.* (2011), and Lespes and Gigault (2011).

HPLC is a pressure driven fractionation technique that separates components in a mixture based on the analytes' affinity for a stationary phase. The interactions between analyte, and stationary and mobile phases are based upon dipole-dipole forces, electrostatic interactions, and dispersion forces. As a result, compounds differing in polarity or chemical structure are easier to separate. HPLC can be operated in two modes: *(1) normal phase (NP-HPLC), utilizing a polar stationary phase (e.g., silica) and a non-polar mobile phase (e.g., chloroform); or (2) reversed phase (RP-HPLC), where a non-polar stationary phase (e.g., C18 surface modified silica) and a (moderately) polar mobile phase (aqueous) are used.* Although usually not applied as a particle size fractionation method but in the separation of solutes, Helfrich *et al.* (2006) did achieve size separation of Au nanoparticles by coupling RP-HPLC to inductively coupled plasma mass spectrometry (ICP-MS). It was shown that gold colloids of 5 to 20 nm in diameter could be separated by means of a standard C18 column, owing to size-dependent retention behaviour, comparable to the separation mechanism that occurs during SEC. In a different study, HPLC-ICP-MS has also proven to be a valuable tool in monitoring and characterizing the formation of citrate-stabilized Au nanoparticles (Helfrich and Bettmer, 2011).

SEC is one of the most commonly used and well-known size fractionation techniques for submicron particles, and is frequently combined with detection methods, including voltammetry, multi angle (laser) light scattering (MA(L)LS), dynamic light scattering (DLS), and ICP-MS, to further characterize the particles (Pérez *et al.*, 2009). The sample is brought onto a SEC column, which is packed with porous beads (*i.e.*, the stationary phase), and as the particles pass through the column, they are retained in the pores according to their size and shape, whereby the largest particles are eluted first (Lespes and Gigault, 2011). SEC is often referred to as gel filtration or gel permeation chromatography (GFC or GPC), in case an aqueous or organic solvent is used as the mobile phase, respectively. To ensure an efficient separation, the pore size distribution of the stationary phase has to be in accordance to the size of the particles that are to be separated. As a result, several columns are needed to cover a broad size range. Separation efficiency also depends on column length and mobile phase flow rate (Lespes and Gigault, 2011; Weinberg *et al.*, 2011). Other disadvantages of SEC include possible interactions of the analyte with the stationary phase, leading to irreversible sorption, risk of sample loss, and clogging of the pores when working with complex environmental samples. (Lead and Wilkinson, 2006). Addition of surfactants to the mobile phase has proven to tackle such clogging issues. The anionic surfactant sodium dodecyl sulphate (SDS) has been shown to improve the separation of 5.3 and 38.3 nm

citrate-stabilized Au nanoparticles, by electrostatic repulsion of the negatively charged particles from the stationary phase (Wei and Liu, 1999). SEC has also been used for the characterization of CdSe QDs (Krueger *et al.*, 2005).

Another valuable size-based fractionation tool for nanoparticles is CE, which separates compounds in solution according to their electrophoretic mobility, based on their size-to-charge ratio. The fractionation takes place in the interior of fine capillaries filled with an electrolyte, upon application of a high voltage. Parameters of the electrolyte, such as pH or ionic strength, are important in optimizing nanoparticle fractionation (Fedotov *et al.*, 2011). According to Surugau and Urban (2009), CE represents a major advancement in the size separation of nanoparticles. The technique is less prone to surface effects, in comparison to SEC, is considered faster than electron microscopy (EM), and only requires a low amount of sample and reagents during operation. Additionally, useful information regarding the ζ-potential of the nanoparticles can also be obtained, as the ζ-potential is derived from the electrophoretic mobility (Weinberg *et al.*, 2011). Data interpretation can be quite complex due to the fact that CE does not solely rely on particle size. Additional drawbacks include the need to work with high concentrations, inevitable mobile phase interactions, and the lack of sensitivity of online detectors when working with low sample volumes (Tiede *et al.*, 2008; Fedotov *et al.*, 2011; Weinberg *et al.*, 2011). A variety of examples of successful application of CE in particle separation and characterization are available. Separation of Ag ENPs (17 – 50 nm) (Liu *et al.*, 2005), Au (5 – 60 nm) and Au:Ag core:shell ENPs (24 – 90 nm) (Liu *et al.*, 2007), and CdSe QDs (Oszwałdowski *et al.*, 2011) has been reported in the literature. Surugau and Urban (2009) published an extensive overview on CE techniques used for nanoparticles, and concluded that a consistent correlation exists between electrophoretic mobility and nanoparticle size.

HDC is a chromatographic technique, which separates nanoparticles according to their hydrodynamic radius. Unlike with SEC, a HDC column is packed with non-porous beads creating interstitial voids, which can be considered as capillaries, where particles are separated by flow velocity and velocity gradient across the particle. Within these capillaries, a parabolic flow profile exists, creating regions of slow or fast flow rates (*i.e.*, maximum at the centre of the capillary, minimum near the wall). The migration rate of the particles is influenced by particle size, size of the packing material, and flow rate and composition of the aqueous mobile phase. Since the maximum distance of a particle to the column wall is limited by its radius, smaller particles tend to remain near the capillary walls, while larger

particles are subjected to higher flow velocity regions near the centreline. Consequently, larger particles are eluted faster from the column than smaller particles, similar to SEC (Tiede *et al.*, 2008; Fedotov *et al.*, 2011; Lespes and Gigault, 2011). Depending on column length, HDC allows separation of particles in the range of 5 to 1200 nm, independent of their density, making it a robust method for the analysis of nanoparticles in environmental samples (Tiede *et al.*, 2008; Weinberg *et al.*, 2011). Additional advantages include reduced solid-phase interactions due to the fact that the technique utilizes a non-porous stationary phase, and the potential combination with other detection methods, the most common being a UV-Vis detector (Williams *et al.*, 2002). However, problems of analyte sorption onto packing material, as well as poor selectivity and resolution have been reported (Fedotov *et al.*, 2011). A hyphenated HDC-ICP-MS method to analyse metallic nanoparticles in environmental samples was developed and optimized by Tiede *et al.* (2009b), mentioning rapid analysis time (< 10 min), an extended size range (5 to > 300 nm), and limited sample preparation requirements. In a later study, the method was applied to detect and characterize Ag nanoparticles in activated sewage sludge, showing the technique's potential to study the fate and behaviour of ENPs in complex environmental samples (Tiede *et al.*, 2010). Figure 2.6 shows a typical size calibration curve obtained from the HDC method using Au nanoparticles as sizing standards, as well as the detection and characterization of Ag nanoparticles in sewage sludge supernatant.

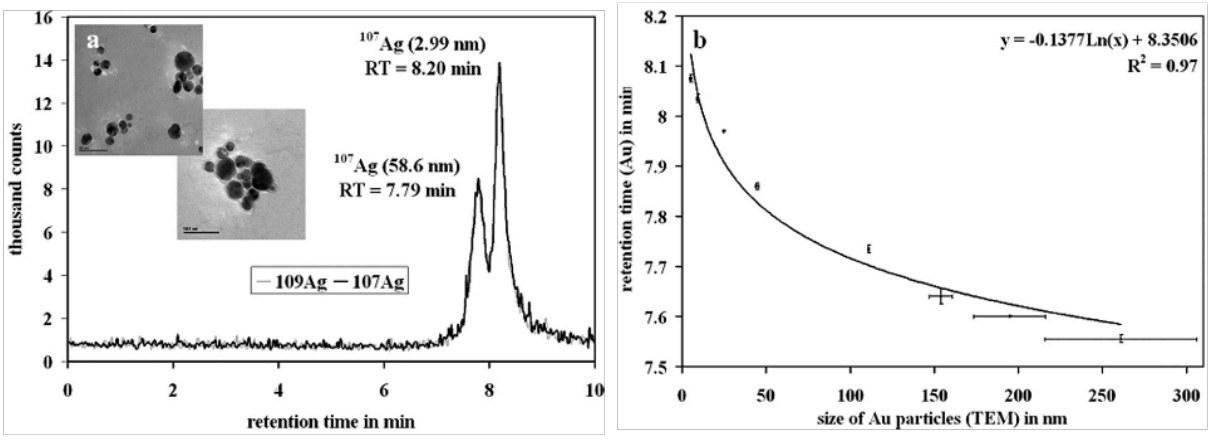

Figure 2.6 – (a) HDC-ICP-MS chromatogram and TEM images obtained from the supernatant of sewage sludge samples spiked with Ag nanoparticles (10 mg Ag L^{-1}, 2 g MLSS L^{-1}), and (b) the corresponding calibration curve using Au nanoparticles as size calibration standards (*y*-axis error bars indicate standard deviation of retention times, while *x*-axis error bars represent standard deviation of Au particle size as determined by TEM). [Reproduced from Tiede *et al.* (2009b), with kind permission from The Royal Society of Chemistry.]

Another chromatography-like fractionation technique that received much attention over the years and showing high promise in the size separation of ENPs in complex matrices is FFF. Unlike other chromatographic methods, FFF does not utilize a stationary phase. Particle fractionation solely relies on physical phenomena occurring in an open channel. Particles are separated by application of an external field (*i.e.*, no solid-phase interactions), which controls the particle transport velocity depending on particle diffusion coefficients, by positioning them in different laminar flow vectors in a very thin channel (Giddings *et al.*, 1976; Giddings, 1993; Handy *et al.*, 2008b; Hassellöv *et al.*, 2008; Tiede *et al.*, 2008; Fedotov *et al.*, 2011). The different FFF sub-techniques are usually categorized according to the nature of the applied external field. The most commonly used FFF sub-techniques are tabulated in Table 2.3. These techniques are also the only ones that are currently commercially available (Lespes and Gigault, 2011). Figure 2.7 shows a schematic overview of the working mechanism of two types of hydraulic flow FFF (Fl-FFF).

Table 2.3 – Overview of the most commonly applied FFF sub-techniques.

FFF sub-technique	Acronym	Applied external field
Hydraulic Flow FFF	Fl-FFF	Two crossed flow streams, superimposed on the same channel; Two types of Fl-FFF: Symmetrical, and Asymmetrical (AsFl-FFF or AF4)
Sedimentation FFF	Sd-FFF	Centrifugation (40 000 *g*) induced force field
Thermal FFF	Th-FFF	Temperature gradient is applied across the channel
Electrical FFF	El-FFF	Electrical potential is applied across the channel

Based on the applied external field and mode of operation, FFF allows the separation and characterization of particles in the range of 1 nm to 200 μm (Lespes and Gigault, 2011; Fedotov *et al.*, 2011). In terms of fractionation range, selectivity, and resolution, FFF is considered as one of the most versatile methods. It provides high-resolution, reduced sample complexity, direct related information between time and size, versatility in mobile phase composition, and the possibility of analysis on obtained sub-fractions with defined particle size (Dubascoux *et al.*, 2008). The most notable drawbacks include that errors may arise due to particle shape and density, the necessity of sizing standards to calibrate the apparatus, and the requirement to be combined with some kind of detector. Most commonly used detectors include UV-Vis, light scattering, and ICP-MS (von der Kammer *et al.*, 2005; Dubascoux *et al.*, 2010; Fedotov *et al.*, 2011). Numerous studies applying FFF in the fractionation and characterization of ENPs have been published in the literature. For instance, Gray *et al.* (2012) have performed a comparison study of AsFl-FFF versus HDC

coupled to ICP-MS, for the analysis of Au nanoparticles in aqueous samples. They concluded that AsFl-FFF is capable of separating mixtures of 5, 20, 50, and 100 nm particles with significantly greater resolution than HDC. However, recoveries tended to be generally lower in the case of AsFl-FFF, and HDC also provided an additional benefit for being able to distinguish dissolved Au from nanoparticulate Au. Ag nanoparticles have also been successfully detected and characterized by AsFl-FFF and Fl-FFF (Bolea *et al.*, 2011; Poda *et al.*, 2011), while Schmidt *et al.* (2011) established an analytical platform consisting of AsFl-FFF – MALLS – DLS – ICP-MS, and used it for separation and quantitative analysis of Au ENPs in aqueous suspensions.

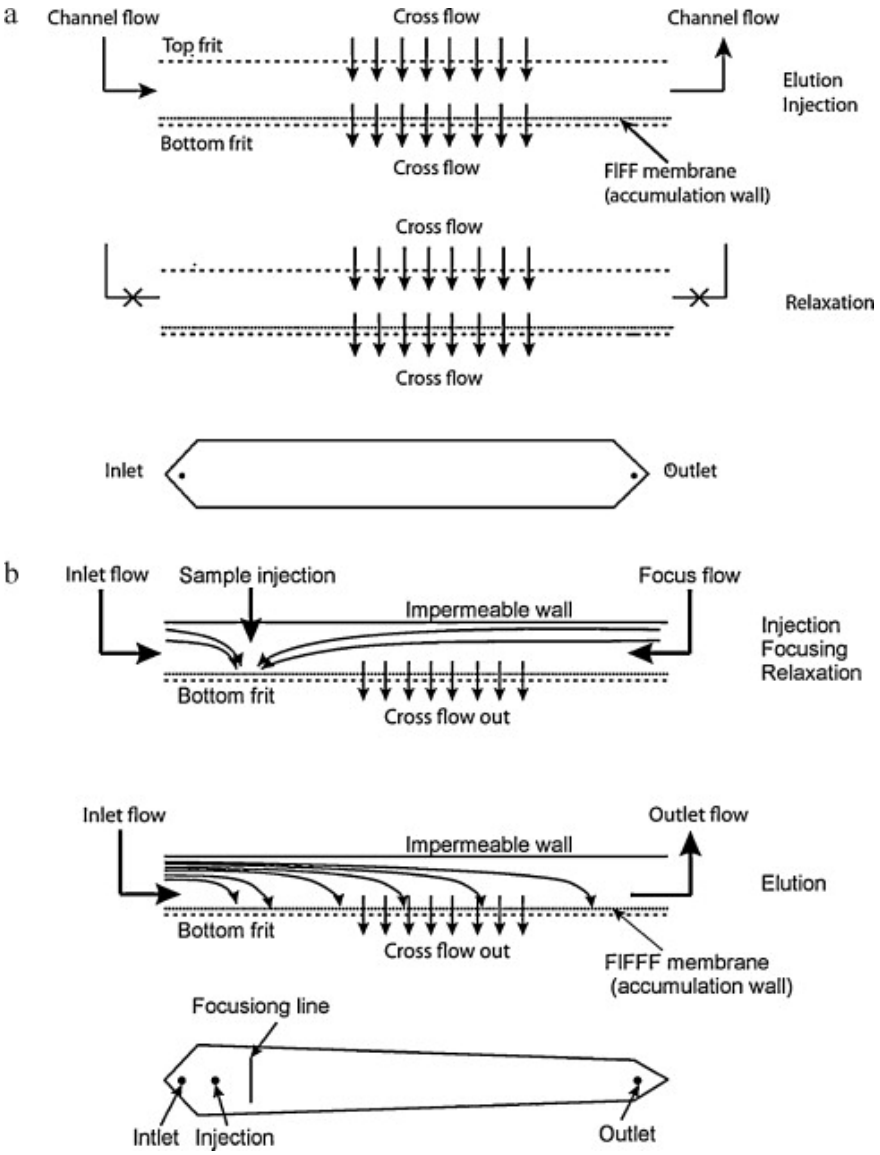

Figure 2.7 – Schematic representation of (a) a symmetrical Fl-FFF flow diagram and channel geometry, and (b) a typical asymmetrical Fl-FFF channel. [Reprinted from Baalousha *et al.* (2011), with kind permission from Elsevier.]

2.3.3 Characterization techniques

2.3.3.1 Particle morphology, size, and size distribution

Particle size distribution and shape are important nanoparticle characteristics. Not only are nanoparticles per definition classified by particle size, size and shape also play fundamental roles in controlling properties of nanoparticles, such as chemical reactivity, transport behaviour, accessibility, diffusivity, and the ability to permeate cell membranes (Brar and Verma, 2011).

An established and traditional technique to determine the size distribution of nanoparticles suspended in a liquid is dynamic light scattering (DLS), also referred to as photon correlation spectroscopy (PCS) or quasi-elastic light scattering (QELS). DLS utilizes a laser beam to probe the random movement (*i.e.*, Brownian motion) of nanoparticles in suspension, causing the laser light to scatter at different intensities. These time-dependent intensity fluctuations are mathematically related to the diffusion coefficient, and consequently to the particle hydrodynamic radius according to the Stokes-Einstein relationship (Equation 2.7) (Filella *et al.*, 1997; Hassellöv *et al.*, 2008; Brar and Verma, 2011).

$$D = \frac{k_B\, T}{6\, \pi\, \eta\, r_h} \qquad (\mathbf{2.7})$$

where D [$m^2\ s^{-1}$] is the diffusion coefficient, k_B [$J\ K^{-1}$] is the Boltzmann's constant, T [K] is the absolute temperature, η [$Pa\ s^{-1}$] is the solution's dynamic viscosity, and r_h [m] is the hydrodynamic radius of a spherical particle.

DLS is a relatively rapid and easy to perform, non-destructive technique that can be combined with other analytical tools, such as SEC, MALLS, and ICP-MS. However, DLS is not suitable to determine very broad size distributions, and due to the fact that it is an intensity-based methodology, the determined particle size results are biased towards large particles (Ledin *et al.*, 1994; Handy *et al.*, 2008b). In addition, DLS is a non-element specific analysis tool and cannot be used to analyse complex environmental samples. However, in combination with a fractionation tool like FFF, it can allow a more thorough characterization of complex matrices (Weinberg *et al.*, 2011; Isaacson and Bouchard, 2010). Römer *et al.*

(2011) applied DLS for studying the aggregation behaviour of Ag nanoparticles in exposure media used for aquatic toxicity tests, and compared it to AsFl-FFF.

Nanoparticle tracking analysis (NTA) is a relatively novel technique that not only allows for size measurements of nanoparticles in suspensions, but can also provide information regarding particle count and concentration (Malloy, 2011). The principle of operation is closely related to DLS, yet where DLS measures the changes in scattering intensities caused by Brownian motion of the particles, NTA measures the observed particle diffusion directly using video microscopy. NTA can thereby overcome the intensity-biased results potentially occurring during DLS (Gallego-Urrea *et al.*, 2011; Malloy, 2011). The method however cannot provide information on elemental composition, and suffers from detection issues for particles smaller than 50 nm (Domingos *et al.*, 2009; Paterson *et al.*, 2011).

Microscopic techniques based on optical (*i.e.*, confocal), and electron or scanning probe approaches, can be applied to visualize and characterize nanoparticles on size, size distribution, aggregation state, shape, structure, and surface topology (Mavrocordatos *et al.*, 2004; Tiede *et al.*, 2008). The typical dimensions of nanoparticles are below the diffraction limit of visible light, and hence below the detection limit of conventional optical microscopy. Near-field scanning optical microscopy (NSOM) can however obtain a spatial resolution of 50 to 100 nm by using a sub-wavelength diameter aperture, and can potentially be used for optical imaging of nanoparticle aggregates (Tiede *et al.*, 2008). Confocal laser scanning microscopy (CLSM) can be used to characterize colloids, as well as thick and fluorescent specimen with resolutions of up to 200 nm, and has been applied in the analysis of more complex systems when combined with fluorescence correlation spectroscopy (FCS) (Lead *et al.*, 2000; Prasad *et al.*, 2007). The most preferred analytical tools for visualization of ENPs are electron and scanning probe microscopy, including scanning and transmission electron microscopy (SEM and TEM), and atomic force microscopy (AFM), due to their high resolving power (*i.e.*, sub-nanometre range) (Tiede *et al.*, 2008). SEM utilizes a low-energy beam of electrons (1 – 30 keV) to scan across the surface of a sample. A microscopic image of the sample interface is then created by detection of the scattered electrons. Focused ion beam SEM (FIB-SEM) makes use of an ion beam to cut into the sample material and allows for 3D imaging of a solid specimen (Dudkiewicz *et al.*, 2011). The principle of TEM is based on interactions of a high-energy electron beam (80 – 300 keV) with a very thin sample (< 200 nm). Electrons that are transmitted through the sample are focused onto a detector,

generating a microscopic image (Dudkiewicz *et al.*, 2011). Both SEM and TEM are quite time consuming and expensive, and often require extensive sample preparation (*e.g.*, dehydration, (cryo)fixation, embedding, and staining), which in turn can lead to unwanted errors when characterizing ENPs in aqueous media (*e.g.*, induced aggregation). Some of these artefacts can however be tackled through the use of relatively new developments in EM, such as environmental SEM and TEM (ESEM and ETEM), and WetSEM™ and WetSTEM, which allow imaging of hydrated or even fully liquid samples (Tiede *et al.*, 2008; Tiede *et al.*, 2009c; Dudkiewicz *et al.*, 2011). AFM is a high resolution type of scanning probe microscopy, utilizing an oscillating cantilever with a silicon or silicon nitride tip to scan the surface of a specimen, producing a topographical image of the surface of the sample with atomic resolution (< 1 nm) (Tiede *et al.*, 2008). The technique is capable of analysing liquid samples, although artefacts might occur due to sample smearing, or attachment of the sample to the probe (Hassellöv *et al.*, 2008; Tiede *et al.*, 2008). Figure 2.8 shows microscopic images of ZnO and TiO_2 ENPs obtained from SEM, AFM, and TEM measurements, while a brief summary of selected techniques applied in nanoparticle size or shape analysis is presented in Table 2.4.

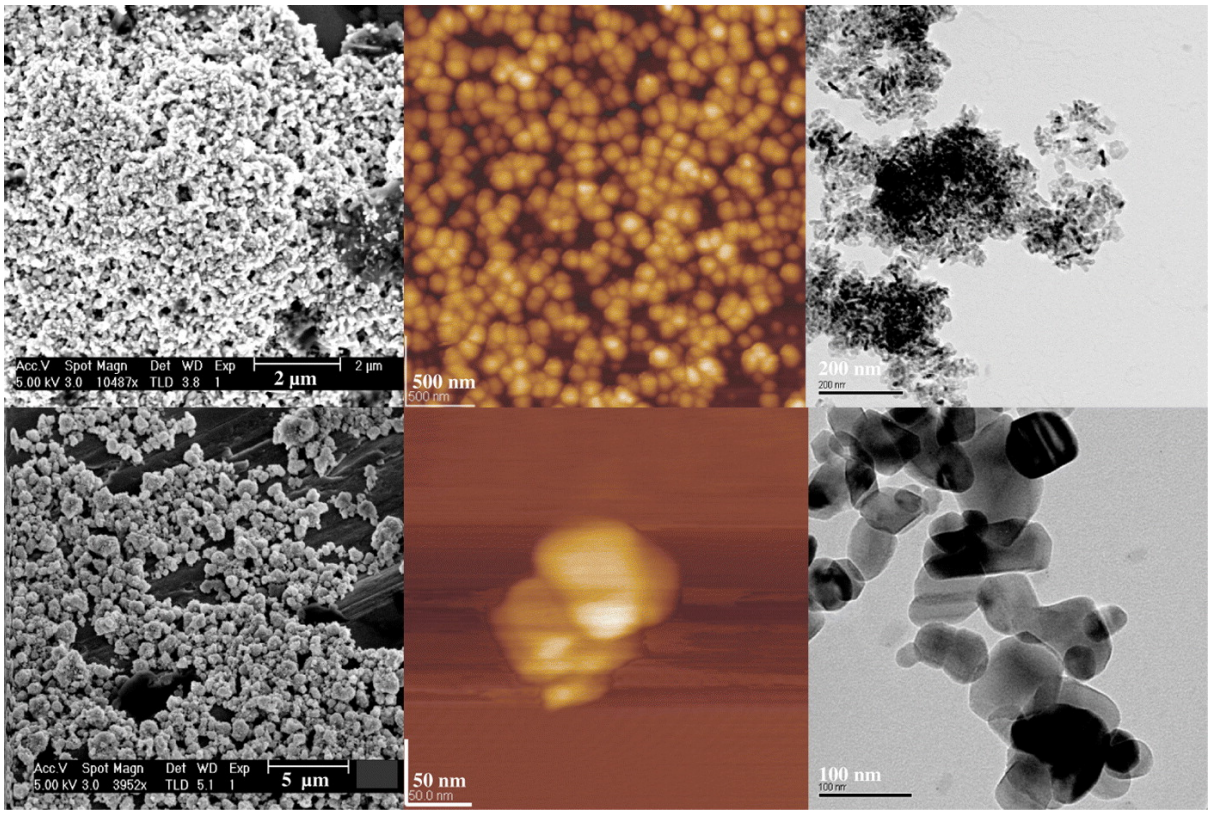

Figure 2.8 – ZnO (1st row) and TiO_2 (2nd row) nanoparticles suspended in distilled water, allowed to dry, imaged in order from left to right by SEM, AFM, and TEM, respectively. [Reprinted from Tiede *et al.* (2008), with kind permission from Taylor & Francis Ltd.]

Table 2.4 – Summary of a selection of characterization techniques applied in determination of the particle size, size distribution, and morphology of nanoparticles in environmental samples.

Technique	Information obtained	Approximate size range	Benefits or advantages	Drawbacks or limitations
DLS (PCS, QELS)	Particle size, size distribution	3 nm – > 1 μm	Rapid, simple, readily available, non-destructive, aggregation process follow-up	Not suitable for complex heterogeneous samples, biased towards large particles
NTA	Particle size, size distribution, particle count	30 nm – > 1 μm	Overcomes intensity-biased results seen in DLS, low sample preparation	Non-element specific, detection issues for particles < 50 nm
NSOM	Particle visualization, size, optical properties	50 nm – > 1 μm	Optical imaging, can provide info on size, topography and optical properties	Spatial resolution, sensitivity, requires thin samples
SEM	Particle visualization, size, shape, structure, aggregation	10 nm – > 1 μm	High resolution, suitable for elemental analysis by complementary techniques (*e.g.*, EDS/EDX)	Requires high vacuum, extensive sample preparation, prone to artefacts, expensive
ESEM	Particle visualization, size, shape	40 nm – > 1 μm	No sample preparation or charging effects, able to handle moist samples	Loss in resolution, contrasting, imaging under atmospheric pressure not possible
WetSEM™	Particle visualization, size, shape	50 nm – > 1 μm	Imaging under fully liquid conditions	Loss in resolution, sensitive membrane
TEM/HR-TEM	Particle visualization, size, shape, structure, aggregation	1 nm – > 1 μm	Very high resolution, suitable for elemental analysis by complementary techniques (*e.g.*, EDS/EDX, EELS)	Requires high vacuum, extensive sample preparation, prone to artefacts, very expensive
AFM	Particle visualization, size, shape, structure, topography, electrical and mechanical properties	40 nm – > 1 μm	Dry, moist samples, or liquid samples under ambient conditions, sub-nm resolution, 3D surface plots	Poor lateral dimension accuracy, artefacts due to particle smearing and attachment to cantilever tip

Contents compiled from Hassellöv *et al.* (2008b), Tiede *et al.* (2008), Tiede *et al.* (2009a), Dudkiewicz *et al.* (2011), Ferreira da Silva *et al.* (2011), Gallego-Urrea *et al.* (2011), Malloy (2011), and Paterson *et al.* (2011).

2.3.3.2 Particle surface and optical properties

Nanoparticles are characterized by a large specific surface area (SSA), hence the particle-liquid interface plays a key-role in the properties and behaviour of nanoparticulate matter. The Brunauer-Emmet-Teller (BET) method is the most commonly applied technique to determine SSA of solids. Under ultra high vacuum conditions, the SSA is determined by measuring the adsorption of N_2-gas on the surface and in the micro-pores of the nanoparticles. The SSA of ENPs can also be calculated from TEM measurements, however this approach is not so straightforward (Handy *et al.*, 2008b; Hassellöv *et al.*, 2008).

One of the most important nanoparticle properties is particle surface charge, since it determines their stability in dispersion and their tendency to aggregate, as well as the possible chemical or biological reactivity at the particle surface. As no easy method to measure the actual net surface charge is available, the surface potential of nanoparticles is assessed by determination of the ζ-potential (see also Section 2.2.2.1) (Tiede *et al.*, 2008; Hassellöv *et al.*, 2008). Electrophoretic light scattering (ELS), also called laser Doppler velocimetry is a well-established technique to determine the electrophoretic mobility by electrophoresis. Using Smoluchowski's theories, the electrophoretic mobility can then be converted to ζ-potential (Hassellöv *et al.*, 2008; Fedotov *et al.*, 2011).

Information on optical properties of nanoparticles, such as reflection, absorption, and transmission characteristics, can be obtained from UV-Vis spectroscopy. The technique can also be applied to confirm the presence of metallic ENPs in suspension, monitor nanoparticles' aggregation processes, and give an indication on particle concentration according to Lambert-Beer's law. UV-Vis is a rapid, simple, and inexpensive technique that does not require extensive sample preparation (Hassellöv *et al.*, 2008; Stebounova *et al.*, 2011). Fluorescence is a property used in many fields, including medical imaging, immunoassays, and photonics. The fluorescent properties of ENPs can be assessed by fluorescence spectroscopy or even via NSOM (Kim and Song, 2007; Hassellöv *et al.*, 2008).

2.3.3.3 Chemical composition and concentration

Laser induced breakdown detection (LIBD) is a quite novel, extremely sensitive technique, suitable for determination of the bulk concentration of nanoparticles in suspension, as well as their number weighted mean diameter. A pulsed laser beam is used to

generate selective dielectric breakdowns on the particles in suspension. The measured breakdown probability depends on total particle count and size. Although considered a highly promising tool, LIBD cannot discriminate between different types of particles, and requires particle-specific calibration (Hassellöv *et al.*, 2008; Tiede *et al.*, 2008). Kaegi *et al.* (2008b) have for instance demonstrated the abilities of LIBD by characterizing colloidal particles in drinking water from a lake source.

X-ray spectroscopic techniques, such as energy dispersive X-ray spectroscopy (EDS or EDX), X-ray absorption spectroscopy (XAS), and X-ray diffraction (XRD), are useful tools in the determination of the chemical composition of single nanoparticles. In EDS, an X-ray spectrum is obtained after exposing a solid sample to a high-energy beam of electrons or X-rays. EDS is generally combined with SEM and TEM for elemental analysis of a sample (Mavrocordatos *et al.*, 2004; Hassellöv *et al.*, 2008). The principle of XAS is based on the fact that each element has unique electron binding energies, resulting in X-ray absorption edges occurring at unique energies. Besides knowledge on elemental composition, XAS also provides information on the oxidation state and structure of nanoparticles (Schulze and Bertsch, 1995; Tiede *et al.*, 2008). XRD makes use of the fact that each crystalline solid generates a unique characteristic X-ray scattering pattern, when irradiated with an X-ray beam. The method is usually applied to determine the crystal structure of mineral particles, but information on elemental composition can also be obtained (Hassellöv *et al.*, 2008). Another technique to determine the chemical and structural composition of single particles is electron energy loss spectrometry (EELS), in which a sample is bombarded with electrons and the resulting loss in energy is determined. The changes in kinetic energy of electrons, caused by inelastic scattering processes when passing through the sample, are element-specific. EELS is often combined with TEM (Hassellöv *et al.*, 2008).

Inductively coupled plasma optical emission spectrometry and mass spectrometry (ICP-OES and ICP-MS) are the most conventional and widely used methods to perform elemental analysis, and determine the elemental concentration of bulk metals or metallic nanoparticles. In ICP-OES, a liquid sample is introduced into a nebulizer, by means of a peristaltic pump, and a fine aerosol is formed using Ar gas. A spray chamber is used to eliminate large aerosol droplets before the fine aerosol is introduced into the plasma torch, where excited atoms and ions that emit electromagnetic radiation specific to a particular element, are generated. The intensity of emission is proportional to the elemental concentration. Sample introduction and ionization in ICP-MS is similar to ICP-OES, but

ICP-MS utilizes a mass spectrometer (*e.g.*, a quadrupole) to detect analytes based on their mass-to-charge ratio. ICP-MS is more sensitive than ICP-OES (*ca.* 3 orders of magnitude), making it the preferred option when maximum detection power is required (Scheffer *et al.*, 2008). Both techniques generally require extensive sample preparation, including acid digestion, making it destructive methods (Ferreira da Silva *et al.*, 2011). However, Allabashi *et al.* (2009) have demonstrated the potential of ICP-MS to analyse Au ENPs directly, without prior dissolving, as illustrated in Figure 2.9. Additionally, recent developments have allowed ICP-MS to gain information on elemental concentration, as well as on nanoparticle size and count when operated in single particle mode (*i.e.*, SP-ICP-MS). In SP-ICP-MS, extremely short measurement times are used in order to ensure detection of the ion pulses resulting from the ionization of individual nanoparticles introduced into the plasma (one ion cloud per particle). The number of observed pulses is related to the particle concentration by the nebulization efficiency and the total number of nanoparticles in the sample, while the pulse intensity is related to the size of the nanoparticles (Degueldre *et al.*, 2006; Mitrano *et al.*, 2012; Tuoriniemi *et al.*, 2012). ICP-MS can also be combined with fractionation techniques (*e.g.*, FFF, HDC, HPLC, and SEC) to create very powerful hyphenated analytical tools that can be applied in nanoparticle environmental fate studies (Stolpe *et al.*, 2005; Tiede *et al.*, 2008; Fedotov *et al.*, 2011; Lespes and Gigault, 2011; Weinberg *et al.*, 2011). Table 2.5 provides a concise summary of techniques used for measuring the surface and optical properties, chemical composition and concentration of nanoparticles.

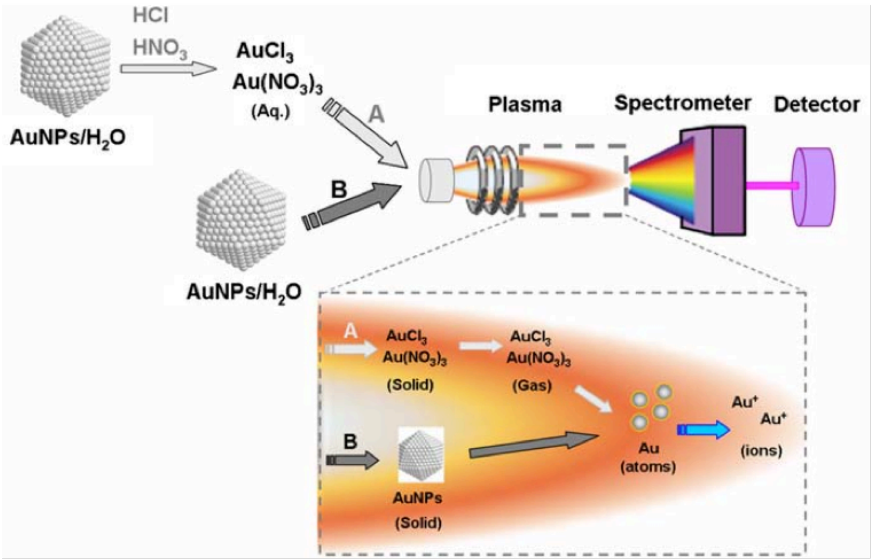

Figure 2.9 – Schematic overview of processes involving ICP-MS analysis of Au nanoparticles with (A), and without (B) previous dissolving. [Reprinted from Allabashi *et al.* (2009), with kind permission from Springer Science and Business Media.]

Table 2.5 – Summary of a selection of characterization techniques applied in determination of the particle surface and optical properties, chemical composition, and concentration of nanoparticles in environmental samples.

Technique	Information obtained	Benefits or advantages	Drawbacks or limitations
BET	Specific surface area, porosity	Well-known technique in material science, high precision, direct measurement of SSA	Artefacts due to sample preparation, requires ultra-high vacuum, solid sample
ELS	ζ-potential	Rapid, simple, minimal sample perturbation	Interferences from complex samples, prone to contamination
UV-Vis	Optical properties, particle concentration, aggregation state	Cheap, rapid, simple, robust, non-destructive, equipment is readily available, little sample preparation	Signal depends on concentration and extinction coefficient, interferences from sample matrix
LIBD	Particle count, size	Sensitivity, accuracy, little sample preparation, non-destructive, info on particle concentration and size	Not element specific, external size calibration required, research-grade instrumentation
EDS (EDX)	Chemical composition	Sensitivity (for heavier elements), rapid, high spatial resolution, combination with EM possible	Biased towards heavier elements, semi-quantitative, measurement uncertainty up to 20 %
XAS	Chemical composition, oxidation state, structure	Non-destructive, solid and liquid samples	Lack of accuracy in identifying scattering from nearest neighbouring atoms
XRD	Chemical composition, crystal structure	Elemental and crystallographic information, well-established method in mineralogy	Low sensitivity and spatial resolution, large sample amount (1 – 3 wt%) required, only solid samples
EELS	Chemical composition, structure	Sensitivity (also for lighter elements), combination with TEM	Complex, expensive, time-consuming, requires thin samples
ICP-OES	Chemical composition, elemental concentration	Sensitivity (mg to μg L^{-1}), specific, multi-element, robust, lower operating cost than ICP-MS	Destructive, possible spectral interferences
ICP-MS	Chemical composition, elemental concentration, particle count, size	Sensitivity (μg to ng L^{-1}), specific, multi-element, isotopic composition, higher selectivity than ICP-OES	Destructive, possible isobaric interferences, expensive equipment,

Contents compiled from Handy *et al.* (2008b), Hassellöv *et al.* (2008), Tiede *et al.* (2008), Tiede *et al.* (2009), Ferreira da Silva *et al.* (2011), and Lespes and Gigault (2011).

2.4 Conspectus

The rapid growth of nanotechnology over the last decade was governed by an increase in a variety of potential applications involving engineered nanomaterials, such as metallic engineered nanoparticles (ENPs). However, the increasing production, distribution, use, and disposal of ENPs will undoubtedly result in enhanced emissions into the environment, raising concerns on their potential impact on human and environmental health. The aquatic environment is considered to be particularly at risk for exposure to ENPs, as it acts as a sink for most environmental contaminants.

Upon their release in the aquatic environment, ENPs can undergo various physical, chemical or biological alterations that depend on the characteristics of both the ENPs and of the receiving environmental matrix. Ultimately, ENPs are expected to accumulate in sediments and soils, due to an increased probability of hetero-aggregation, and subsequent sedimentation and/or deposition in natural aquatic systems.

Existing theories stemming from colloid science have aided in understanding the physicochemical behaviour of ENPs in synthetic media under controlled laboratory conditions, yet predicting their behaviour in more complex matrices has proven to be a lot more challenging. Additionally, it is still not exactly clear how, in what form, and at which concentrations ENPs will be released into the aquatic environment. Therefore, despite recent progress in understanding the transformations, transport, and fate of ENPs in model aquatic systems, there is still a lack of information regarding the physicochemical behaviour and fate of ENPs, especially in real complex environmental media (*e.g.*, surface waters and real sediment and soil solutions).

The lack of studies on the physicochemical fate of ENPs in aquatic systems until now has in part been due to a lack of effective and reliable analytical methods to routinely detect, identify, and quantify ENPs in aqueous mixtures. Characterization of nanoparticles in environmental samples is challenging. For instance, the heterogeneous nature of environmental media, as well as the expected low environmental concentrations of ENPs, might impede the assessment of nano-sized materials in complex environmental matrices. Recently, great progress in the development of analytical tools for analysis of ENPs in environmental samples has been made (*e.g.*, hyphenated techniques). Yet, numerous challenges remain, including how to minimize sampling and handling artefacts, and being

able to distinguish between naturally occurring and anthropogenically generated nanoparticles. Currently, the most reliable way to perform environmental analysis of ENPs involves a combination of analytical methods, including isolation of ENPs by filtration, centrifugation, and size-exclusion techniques, followed by bulk characterization via ICP-OES or ICP-MS, as well as characterization of individual nanoparticulate objects by means of microscopy based techniques (*e.g.*, SEM and TEM), often combined with X-ray spectrometry (*e.g.*, EDS and XRD).

Chapter 3

Use of filtration techniques to study environmental fate of engineered metallic nanoparticles: Factors affecting filter performance

3 Use of filtration techniques to study environmental fate of engineered metallic nanoparticles: Factors affecting filter performance[‡]

3.1 Introduction

The rapid developments in nanoscience and nanotechnology during the last decades have allowed the extraordinary size-related properties of engineered nanoparticles (ENPs) (1 – 100 nm) to be implemented in a variety of commercial and industrial applications including cosmetics, personal care products, textiles, household appliances, food additives, food packaging, paints, coatings, catalysts, fuel additives, fuel cells, electronics, and (waste)water treatment (Wu *et al.*, 2013; Sadik *et al.*, 2014). In October 2013, the Woodrow Wilson database had already listed 1628 nanotechnology-based market available consumer products in their online inventory compared to only 212 in March 2006, representing an increase by approximately 670 % (The Project on Emerging Nanotechnologies, 2014). However, the increasing production and use of ENPs in such applications will also inevitably result in their (unintentional) discharge into aquatic environments (*e.g.*, surface water or groundwater), where they could pose a risk to living organisms and human health (*e.g.*, via drinking water consumption or transfer through the food chain) (Lohwacharin and Takizawa 2009; Wu *et al.*, 2013; Sadik *et al.*, 2014). For instance, ENPs have already been demonstrated to be released from consumer goods (Benn *et al.*, 2010), during washing of textiles (Benn and Westerhoff, 2008; Geranio *et al.*, 2009; Windler *et al.*, 2012), and via surface run-off from coated façades (Kaegi *et al.*, 2008a; Kaegi *et al.*, 2010), and have been detected in effluents from wastewater treatment plants (Kiser *et al.*, 2009; Westerhoff *et al.*, 2011), indicating that conventional (waste)water treatment processes might be insufficient in removing ENPs (Springer *et al.*, 2013; Wu *et al.*, 2013). Therefore, increasing concern has been raised within the scientific community regarding the occurrence, behaviour, and fate of

[‡] *Submitted for publication as: Van Koetsem, F., Verstraete, S., Wallaert, E., Verbeken, K., Van der Meeren, P., and Du Laing, G.* ***Use of filtration techniques to study environmental fate of engineered metallic nanoparticles: Factors affecting filter performance.***

these emerging contaminants in aquatic systems, as well as on their removal and fractionation methodologies (Wu *et al.*, 2014).

Filtration processes are interesting and promising options when studying ENPs, not only for retaining and removing nanoparticles from solution, but also as fractionation techniques during characterization or sample preparation prior to further analysis (Ladner *et al.*, 2012; Wu *et al.*, 2014). Microfiltration (MF) using 0.45 μm cut-off filter membranes is commonly utilized to determine the dissolved metal fraction in *e.g.*, surface waters or soil solutions (Cornelis *et al.*, 2010; Hedberg *et al.*, 2011), while 0.2 μm filtration is routinely used for sterilization of for instance nutrient media (Weltje *et al.*, 2003). However, solely based on size, nanoparticles should be allowed to permeate during MF due to their extremely small dimensions, thereby ending up in the so-called "dissolved" fraction. On the other hand, nanoparticle-membrane interactions (*e.g.*, sorption) or membrane fouling could lead to retention of particulates that are smaller than the filter pore size (Ladner *et al.*, 2012; Wu *et al.*, 2013; Jeong and Kim, 2014). Ultrafiltration (UF) is already being extensively applied during drinking water treatment, and is anticipated to be an effective removal strategy of ENPs from drinking water sources as nanoparticles or their aggregates are often too large to pass through UF filters (Lohwacharin and Takizawa 2009; Wu *et al.*, 2014). In contrast to MF, where the retention capability is basically expressed through size exclusion from a well-defined pore size of the filter membrane (> 0.1 μm), UF membranes are characterized by their molecular weight cut-off (MWCO), which refers to the approximate molecular weight of a compound that is retained for 90 % by the filter membrane (Wu *et al.*, 2013). UF has been regularly utilized in trace metal speciation studies (Singhal *et al.*, 2006; Hedberg *et al.*, 2011), or in studies involving nanoparticles (Dalwadi *et al.*, 2005; Cornelis *et al.*, 2010; Liu *et al.*, 2010; Park *et al.*, 2013; Springer *et al.*, 2013; Dorney *et al.*, 2014; Wu *et al.*, 2014), primarily to investigate removal of (nano)particulate matter from solution, to examine dissolution behaviour by differentiating between (nano)particulate and "truly" dissolved compounds, or to characterize and purify nanoparticle dispersions.

Although numerous studies have investigated membrane-fouling phenomena and other filtration induced artefacts occurring during trace metal analysis (Gardner and Comber 1997; Weltje *et al.*, 2003; Meers *et al.*, 2006; Hedberg *et al.*, 2011), only few studies have thoroughly discussed the removal and retention of metallic ENPs upon filtration of aqueous samples. Especially information regarding nanoparticle-filter interactions and how they are potentially influenced by parameters such as membrane, solution or particle

properties, is scarce (Ladner *et al.*, 2012; Springer *et al.*, 2013; Jeong and Kim, 2014; Wu *et al.*, 2014). Studying factors affecting the separation and removal efficiency, and the underlying mechanisms could promote the potential use of membrane filtration in, for example, the removal of ENPs from water samples (Wu *et al.*, 2013).

Two types of metallic ENPs were chosen for this study based on environmental relevance as well as on particle characteristics, *i.e.*, negatively charged citrate-stabilized Ag ENPs and positively charged CeO_2 ENPs. Currently, Ag ENPs are the most widely used engineered nanomaterials in consumer goods, mainly for their antimicrobial properties (Cornelis *et al.*, 2010; The Project on Emerging Nanotechnologies, 2014), whereas the catalytic and UV-blocking properties of CeO_2 ENPs have lead to their extensive use *e.g.*, as diesel fuel additives or in cosmetics (Cornelis *et al.*, 2010). Both types have already been demonstrated to cause toxic reactions in aquatic organisms (Van Hoecke *et al.*, 2009; Levard *et al.*, 2012).

The main aim of this study was to examine the retention behaviour of aqueous suspensions of Ag and CeO_2 ENPs upon application of several different filtration techniques (*i.e.*, paper filtration, syringe filtration (0.02 and 0.45 μm), and centrifugal micro- and ultrafiltration), in order to aid in providing useful information on for instance, the size fractionation and characterization of nanoparticles in aqueous samples, or on their removal from (waste)water streams, preventing their environmental release, and ultimately, in assessing their behaviour and fate in aquatic environments. In particular, the effects of nanoparticle concentration, matrix composition, and filter type, pore sizes and (pre-)treatments, on the recoveries of silver or cerium in the filtrates were examined, and compared to the recoveries of Ag^+ or Ce^{3+} ions treated in the same way, and potential interaction mechanisms were investigated. Additionally, several nanoparticle digestion methods were assessed for quantification of total silver or cerium content in solution.

3.2 Materials and methods

3.2.1 Nanoparticles and chemical reagents

Citrate-stabilized silver nanoparticles (Ag ENPs, APS: *ca.* 10 nm, 100 mg L^{-1}, ζ-potential: -50 ± 5 mV, pH: 6 – 8) and cerium dioxide nanoparticles (CeO_2 ENPs,

APS: 4 ± 2 nm, 50 000 mg L^{-1}, ζ-potential: +45 ± 5 mV) were obtained from PlasmaChem GmbH (Berlin, Germany) as aqueous dispersions. Ionic silver (as $AgNO_3$) and cerium (as $Ce(NO_3)_3$) reference standard solutions (Plasma HIQU, 1000 ± 2 μg Ag^+ or Ce^{3+} mL^{-1} in 2 – 5 % HNO_3), and analytical grade nitric acid (HNO_3, 65 %, ρ: 1.39 g mL^{-1}, M: 63.01 g mol^{-1}), hydrochloric acid (HCl, 37 %, ρ: 1.19 g mL^{-1}, M: 36.46 g mol^{-1}), hydrogen peroxide (H_2O_2, 30 wt%, ρ: 1.11 g mL^{-1}, M: 34.01 g mol^{-1}), sodium chloride (NaCl, > 99.8 %, ρ: 2.17 g cm^{-3}, M: 58.44 g mol^{-1}), calcium chloride ($CaCl_2.2H_2O$, > 99.5 %, ρ: 1.85 g cm^{-3}, M: 147.02 g mol^{-1}), potassium nitrate (KNO_3, > 99 %, ρ: 2.11 g cm^{-3}, M: 101.10 g mol^{-1}), and copper nitrate ($Cu(NO_3)_2.2½.H_2O$, 99 – 102 %, ρ: 2.05 g cm^{-3}, M: 232.59 g mol^{-1}) were all purchased from ChemLab NV (Zedelgem, Belgium).

3.2.2 Nanoparticle characterization

Photon correlation spectroscopy (PCS) (Malvern PCS-100, Malvern Instruments Ltd., Worcestershire, UK) was applied to determine the particle size distributions (PSDs) of the Ag and CeO_2 ENPs. Sample measurements were performed in quadruplicate, at 25 °C using a 633 nm HeNe laser positioned at a measuring angle of 150 degrees. Cumulant and multi modal analysis were applied to obtain the so-called *Z*-average hydrodynamic particle diameter and PSDs, respectively. The surface charge of the nanoparticles was assessed through zeta (ζ) potential measurements (Zetasizer 3000 HSa, Malvern Instruments Ltd., Worcestershire, UK). Transmission electron microscopy (TEM) equipped with energy dispersive X-ray spectrometry (EDS) (JEM-2200FS, Jeol Ltd., Tokyo, Japan) was used to visualize the ENPs. Absorption spectra were determined via UV-Vis spectroscopy (6400 Spectrophotometer, Jenway, Bibby Scientific Ltd., Staffordshire, UK).

3.2.3 Comparison of nanoparticle digestion methods

Different digestion media were tested for their applicability in the digestion of Ag and CeO_2 ENPs (Table 3.1). The ENPs (10 mL) were digested on a hotplate at 150 °C for 2 h under reflux using a beaker and a watchglass. After cooling down, the samples were transferred quantitatively to 50 mL volumetric flasks (without filtration) and ultrapure water (18.2 MΩ cm^{-1}) (Milli-Q®, EMD Millipore Corp., Billerica, MA, USA) was added to the mark. Prior to determination of the silver and cerium contents by means of inductively coupled plasma optical emission spectrometry (ICP-OES) (Vista-MPX CCD Simultaneous

ICP-OES, Agilent Technologies, Santa Clara, CA, USA), the samples were diluted further with Milli-Q® water to a final concentration of 0.05 or 2 mg L^{-1} in the case of silver or cerium, respectively. In addition to digestion on a hotplate, microwave-assisted digestion using a microwave accelerated reaction system (MARS 5, CEM Corp., Matthews, NC, USA), in both open and closed vessel configuration, was also examined. Table 3.2 shows the applied working conditions in detail. In addition to the ENPs, ionic Ag^{+} and Ce^{3+} samples were treated in the same way. Direct introduction of ENPs or ions into the plasma of the ICP-OES, *i.e.*, without digestion prior to the analysis and using Milli-Q® water as matrix, was also included in the set-up. Prior to being used, all glassware was soaked in diluted nitric acid and thoroughly rinsed with Milli-Q® water. All tests were performed in triplicate.

Table 3.1 – Overview and composition of applied digestion media.

No.	Digestion treatment	Amount and composition of digestion medium
1	HNO_3	4 mL 65 % HNO_3
2	HNO_3 + H_2O_2	4 mL 65 % HNO_3 + 2 mL 30 % H_2O_2
3	HCl	4 mL 37 % HCl
4	*Aqua regia*	1 mL 65 % HNO_3 + 3 mL 37 % HCl
5	Reverse *aqua regia*	3 mL 65 % HNO_3 + 1 mL 37 % HCl

Table 3.2 – Overview of applied conditions during microwave-assisted digestions. The microwave accelerated reaction system operated at 600 W, and for the closed vessel configuration, a pressure limit of 41.4 bar was employed.

	Phase (-)	Temperature (°C)	Ramping time (min)	Holding time (min)
Open vessel	1	55	5	10
	2	75	10	10
	3	100	10	40
Closed vessel	1	120	15	5
	2	195	10	25

3.2.4 Filtration experiments

Ashless filter paper (MN 640 m, average retention capacity: 4 – 12 μm, Macherey-Nagel GmbH & Co. KG, Düren, Germany) was used to filter 15 mL suspensions/solutions of

250 μg L^{-1} Ag ENPs or Ag^+ ions, or 1 mg L^{-1} CeO_2 ENPs or Ce^{3+} ions in Milli-Q® water. The selection of these concentrations was mainly due to practical/analytical limitations. Three different filter (pre-)treatments were compared: filter "wetting" and "rinsing" with Milli-Q® water, filter wetting and rinsing with 1 % HNO_3, and filter wetting with 0.1 M $Cu(NO_3)_2$ followed by rinsing with Milli-Q® water. According to Cornelis *et al.* (2010), preconditioning of filters with 0.1 M $Cu(NO_3)_2$ could reduce adsorption of Ag^+ and Ce^{n+} ions by membrane surfaces. The filtrates were collected in 25 mL volumetric flasks and Milli-Q® water was added to the mark. Afterwards, 10 mL was pipetted from the filtrate (*e*LINE electronic pipette, Sartorius Biohit Liquid Handling Oy, Helsinki, Finland), subjected to open vessel microwave digestion (using 4 mL 65 % HNO_3 or 4 mL *aqua regia* in the case of silver or cerium, respectively), and analysed for total silver or cerium content by means of ICP-OES. All paper filtration tests were performed in triplicate, whereby for each treatment, the three replicate filtrations were performed using the same filter (*i.e.*, to also examine the impact of potential re-use of the filter).

Four different types of disposable syringe filters were used for filtration of Ag and CeO_2 nanoparticle suspensions (15 mL) as well as Ag^+ and Ce^{3+} ionic solutions (15 mL) that were all prepared in Milli-Q® water, and were mutually compared: Chromafil RC-45/25, Chromafil PVDF-45/25, and Chromafil PES-45/25 filters all had a pore size of 0.45 μm and were obtained from Macherey-Nagel GmbH & Co. KG (Düren, Germany), whereas Anatop 25 filters had a pore size of 0.02 μm and were purchased from Whatman International Ltd. (Kent, UK). The filtrates were collected in test tubes, and 10 mL was pipetted and subjected to open vessel microwave digestion using 4 mL 65 % HNO_3 for silver or 4 mL *aqua regia* for cerium, prior to being analysed by means of ICP-OES. Filtration was performed using dry as well as pre-treated (*i.e.*, preconditioned by subsequent filtration of 3 mL 0.1 M $Cu(NO_3)_2$ solution and 3 mL Milli-Q® water as proposed by Cornelis *et al.* (2010)) filters. All syringe filtration experiments were performed in triplicate, whereby for each test, three replicate filtrations were performed over the same filter (*i.e.*, to again also assess the impact of potential re-use of the filter).

Centrifugal micro- and ultrafiltration (MF and UF) was also performed. For this, 4 mL samples of 250 μg L^{-1} Ag ENPs or Ag^+ ions, or 1 mg L^{-1} CeO_2 ENPs or Ce^{3+} ions in Milli-Q® water were pipetted into the centrifugal devices and subjected to centrifugation (Megafuge 1.0, Heraeus, Hanau, Germany) at 4500 rpm (*i.e.*, 3735 *g*) for 15 min (or 60 min in the case of 3 kDa MWCO UF devices). The obtained filtrates were then digested via open

vessel microwave digestion using 4 mL 65 % HNO_3 for silver, or 4 mL *aqua regia* for cerium containing samples, and analysed via ICP-OES. Various types of centrifugal devices were utilized: Amicon Ultra-4 units with a 3, 10, 30, 50, and 100 kDa MWCO that were obtained from EMD Millipore Corp. (Billerica, MA, USA), Vivaspin 6 units having a 100, 300, and 1000 kDa MWCO or a 0.20 μm pore size that were purchased from Sartorius AG (Göttingen, Germany), and Microsep Advance with a 30 and 100 kDa MWCO or a 0.20 and 0.45 μm pore size, which were obtained from Pall Corp. (Port Washington, NY, USA). All centrifugal filtrations were performed in triplicate.

The impact of sample matrix on the retention of the nanoparticles or ions was also examined for 0.02 and 0.45 μm syringe filtration and for 10 kDa centrifugal ultrafiltration. For this, nanoparticle suspensions (250 μg L^{-1} Ag ENPs and 1 mg L^{-1} CeO_2 ENPs) and ionic solutions (250 μg L^{-1} Ag^+ ions and 1 mg L^{-1} Ce^{3+} ions) were prepared in 2 mM $CaCl_2$, 2 mM NaCl, and 2 mM KNO_3 instead of in Milli-Q® water, and were subjected to the same syringe and centrifugal filtration and analysis procedures as described in the paragraphs above. These background electrolytes were chosen based on the expected order of magnitude of their occurrence in *e.g.*, natural surface water or groundwater, and on their potential impact on nanoparticle stability in suspension (*e.g.*, $CaCl_2$ is expected to have a higher negative impact on the stability of Ag ENPs than NaCl and KNO_3). Both $CaCl_2$ and KNO_3 have been mentioned for providing a simplified soil solution matrix (Cornelis *et al.*, 2010; Cornelis *et al.*, 2011).

Finally, stepwise filtration of 0.25 mg L^{-1} Ag ENPs and Ag^+ ions in 2 mM $CaCl_2$, 2 mM NaCl, and 2 mM KNO_3 was performed in order to assess different size fractions of silver present in those aqueous matrices (*i.e.*, the fractions permeating through 0.45 μm, and the portion of these fractions permeating through either 0.02 μm or 10 kDa). For this, the samples were first filtered over a 0.45 μm syringe filter (Chromafil RC, PES, or PVDF), after which the obtained 0.45 μm filtrates were devided up into three parts: (1) 10 mL was pipetted, subjected to open vessel microwave digestion with 4 mL 65 % HNO_3, and analysed for silver via ICP-OES; (2) 4 mL was pipetted into Amicon 10 kDa UF units and subjected to the same centrifugal filtration and analysis procedure as described above; and (3) about 15 mL was filtered over 0.02 μm Anatop syringe filters, after which the obtained 0.02 μm filtrates were subjected to open vessel microwave digestion using 4 mL 65 % HNO_3, and analysed for silver via ICP-OES. All of these filtrations were again performed in triplicate, whereby the three replicate filtrations were performed consecutively using the same filter.

3.2.5 Data processing

Numerical and graphical data processing was performed by means of Excel (Microsoft Corp., Redmond, WA, USA) and SigmaPlot 12.5 (Systat Software, Inc., Chicago, IL, USA) software packages. Statistically significant differences were assessed using SPSS 22 (IBM, Armonk, NY, USA) software. Shapiro-Wilk's test was utilized to check data normality. One-way analysis of variance (ANOVA) or Welch's *t*-test were performed in case Levene's conditions for homogeneity of variances were or were not met, respectively. Statistically significant mean differences observed via ANOVA or Welch's *t*-test were evaluated further via Tukey's HSD or Games-Howell's *post-hoc* tests, respectively.

3.3 Results and discussion

3.3.1 Nanoparticle characterization

TEM imaging revealed an apparent spherical morphology for both Ag and CeO_2 ENPs (Figure 3.1). According to PCS measurements, the *Z*-average size (*i.e.*, the harmonic intensity-averaged hydrodynamic particle diameter (ISO 22412:2008)) of the nanoparticles suspended in Milli-Q® water was 14.5 ± 1.1 nm in the case of Ag ENPs, and 7.3 ± 1.4 nm for CeO_2 ENPs (n = 4). The corresponding particle size distributions (PSDs) are presented in Figure 3.2. For Ag ENPs, the obtained PSDs indicate that although the majority of the nanoparticles were about 10 nm in size, some larger-sized particulates (between 20 and 80 nm) were also present. The relatively higher share in the measured intensity resulting from these few larger particles, as shown by the bimodal distribution, can be explained by light scattering theories. According to the Rayleigh approximation or Mie theory, the scattered light intensity is proportional to the 6^{th} or 4^{th} power of the particle diameter, respectively (Foerter-Barth and Teipel, 2000). Narrow unimodal PSDs were observed for CeO_2 ENPs, indicating a highly monodisperse system. Ag ENPs suspended in Milli-Q® water at pH 5 had a ζ-potential of -46.0 ± 1.8 mV, while this was +52.7 ± 4.2 mV at pH 6.5 in the case of CeO_2 ENPs (n = 4). The UV-Vis absorption spectrum of Ag ENPs shows a peak at 395 nm resulting from surface plasmons, which is characteristic for the presence of silver nanoparticles (Stebounova *et al.*, 2011), whereas no distinguishable absorbance peak but rather a decreasing absorbance gradient in the near-UV region was observed with

CeO_2 ENPs (Figure 3.3). Furthermore, the absorption spectra after storing the nanoparticle suspensions for 12 months at 4 to 6 °C remained virtually unchanged, suggesting nanoparticle size and shape stability over time (Liu and Hurt, 2010).

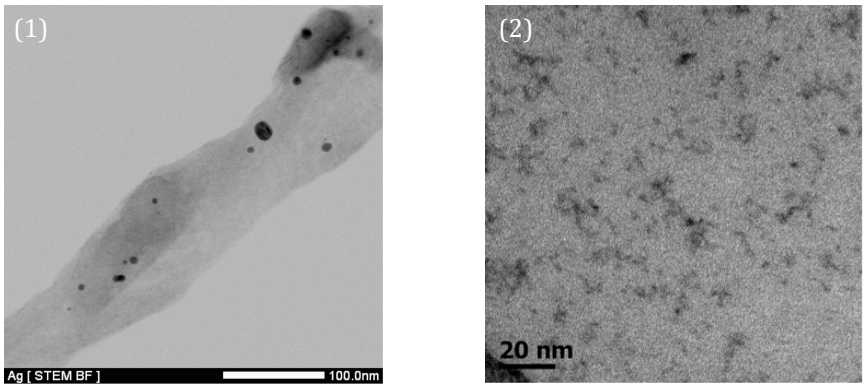

Figure 3.1 – TEM images of Ag ENPs (1) and CeO_2 ENPs (2) suspended in Milli-Q® water.

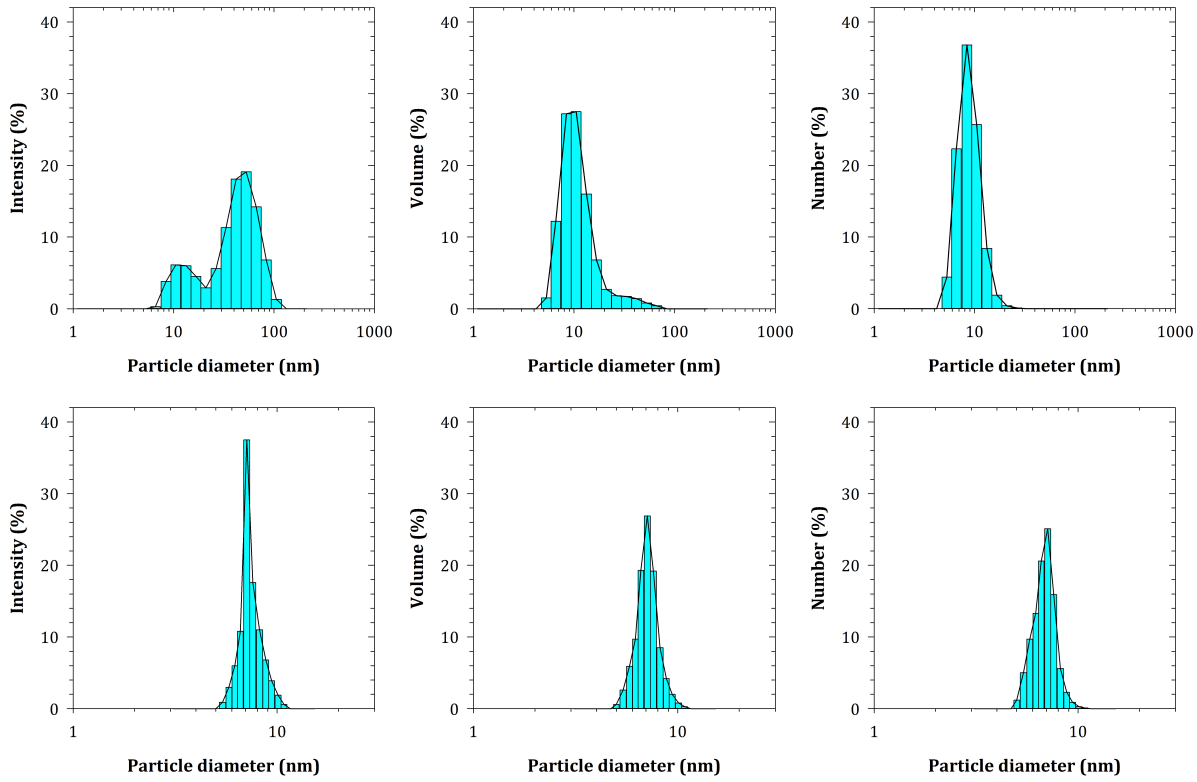

Figure 3.2 – Intensity, volume, and number weighted particle size distributions of Ag ENPs (top three graphs) and CeO_2 ENPs (bottom three graphs) dispersed in Milli-Q® water, obtained from PCS measurements.

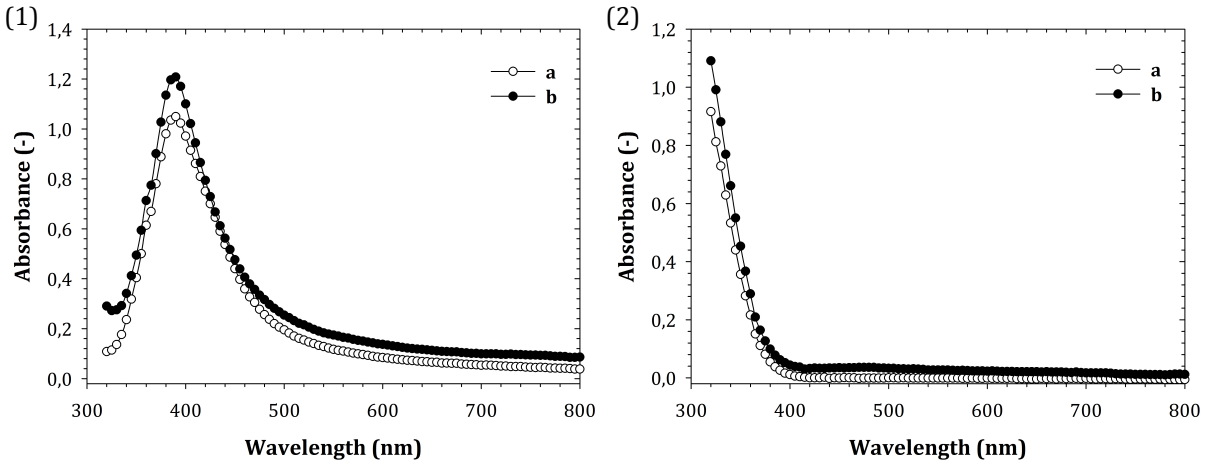

Figure 3.3 – UV-Vis absorption spectra of Ag ENPs (1) and CeO_2 ENPs (2) in Milli-Q® water, measured (a) upon purchase, and (b) after being stored in the fridge at 4 – 6 °C for 12 months.

3.3.2 Nanoparticle digestion

Recoveries (C/C_0) of silver or cerium after subjecting aqueous suspensions/solutions of Ag and CeO_2 ENPs, or Ag^+ and Ce^{3+} ions to various digestion treatments, are shown in Figure 3.4. The results are presented as the ratio between the actual measured concentration (C) and the calculated stock concentration (C_0). Both hotplate and microwave-assisted acid digestions of the nanoparticles resulted in high recoveries, varying between 84 and 94 % for CeO_2 ENPs, and between 99 and 114 % for Ag ENPs. This is in contrast to what has been reported by Cornelis *et al.* (2010), who observed non-quantifiable recoveries of Ag ENPs in digestions involving HCl, presumably due to $AgCl_{(s)}$ precipitation, and reduced recoveries upon digestion of CeO_2 ENPs with HNO_3. Considering our experimental conditions, the formation of soluble AgCl species seems more plausible due to the high chloride concentrations. The reported limited solubility of Ag and CeO_2 ENPs in their study might also have been due to the fact that they digested nanopowders instead of nanodispersions, and the fact that their ENPs were larger than ours.

No statistically significant differences were observed between the applied digestion media during hotplate treatments of the nanoparticles ($p > 0.05$), whereas significant differences were observed between open and closed vessel microwave-assisted digestions ($p < 0.05$). Overall, open vessel digestion resulted in the highest recoveries for both Ag and CeO_2 ENPs. Ionic silver and cerium species were only considered during hotplate acid digestions, and provided recoveries approaching 100 %. Without the addition of an acidic

digestion medium (*i.e.*, just Milli-Q® water), silver or cerium recoveries were *ca.* 10 to 50 % lower compared to the acid-treated samples. Therefore, direct introduction of the Ag or CeO_2 ENPs, or Ag^+ and Ce^{3+} ions used in this study into the plasma of the ICP-OES is not favourable, although Allabashi *et al.* (2009) for example, have demonstrated the successful quantification of the gold content in Au ENPs via ICP-MS without digesting the aqueous suspension prior to the analysis. Consequently, and because of its ease of use, open vessel microwave-assisted digestion using nitric acid or (reverse) *aqua regia* is the preferred method in the case of Ag or CeO_2 ENPs, respectively.

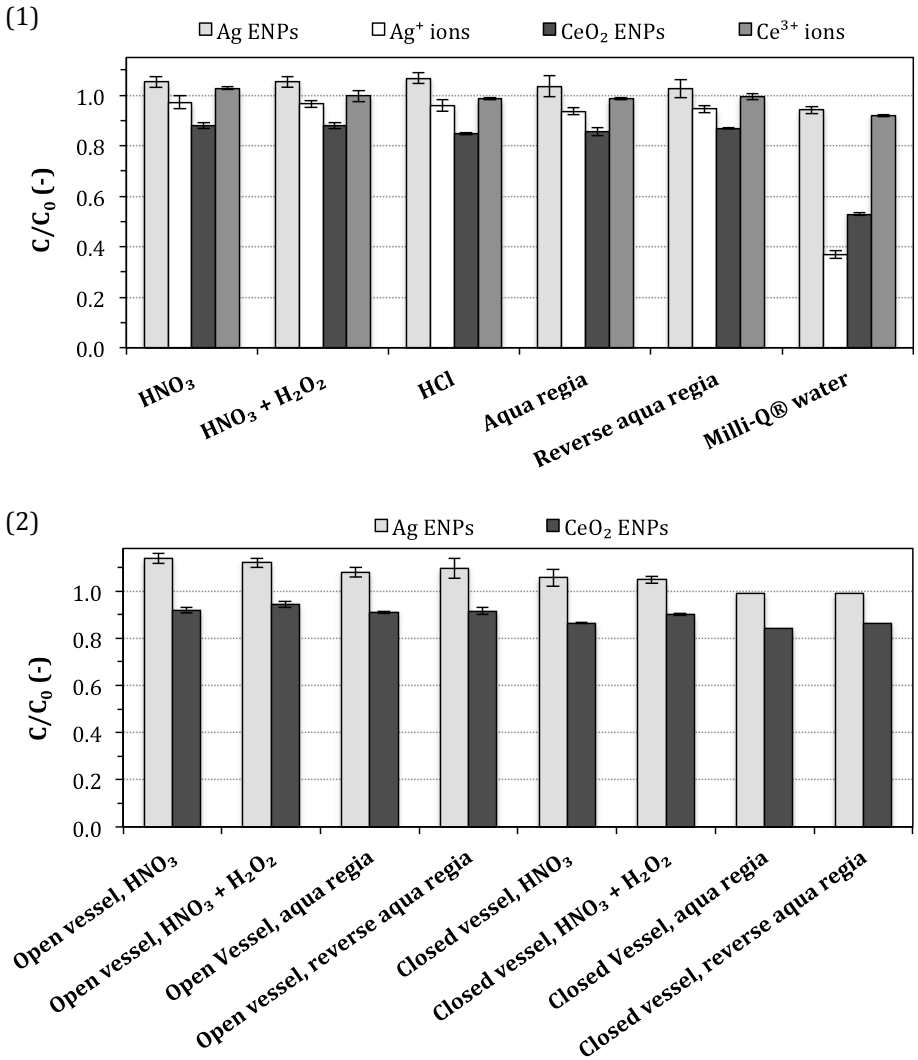

Figure 3.4 – Recoveries of silver or cerium upon digestion of Ag or CeO_2 ENPs, and Ag^+ or Ce^{3+} ions containing suspensions/solutions on a hotplate (1), or via microwave-assisted digestion (2), using various digestion media as outlined in Table 3.1. Results from direct introduction of ENPs or ions into the plasma of the ICP-OES are displayed in the top graph as "Milli-Q® water". Prior to ICP-OES analysis, all of the silver or cerium samples were diluted to a final concentration of 0.05 or 2 mg L^{-1}, respectively. (Bars represent mean values, error bars denote standard deviations, n = 3)

3.3.3 Nanoparticle filtration tests

All filtration recoveries are presented as the ratio between the actual measured silver or cerium concentration in the filtrates (C) and the actual measured silver or cerium content in the samples prior to being subjected to filtration (*i.e.*, controls) (C_0).

3.3.3.1 Paper filtration

The relative amounts (C/C_0) of silver or cerium recovered in the filtrates following paper filtration of Ag or CeO_2 ENPs, and Ag^+ or Ce^{3+} ions in Milli-Q® water are shown in Figure 3.5. Recoveries of Ag ENPs varied between 55 and 67 % depending on the filter (pre-)treatment ($p < 0.05$), whereas for Ag^+ ions, only negligible retention and no significant effect of filter (pre-)treatment was observed ($p = 0.239$). Both CeO_2 ENPs and Ce^{3+} ions were partially retained by the filters, and only (pre-)treatment with 1 % HNO_3 appeared to (positively) affect the recovery ($p < 0.05$). The observed high standard deviation on the recovery of Ce^{3+} ions on the filter paper treated with Milli-Q® water is due to the low recovery of cerium in the filtrate obtained from the first of three consecutive replicate filtrations over the same filter, indicating an initial higher degree of sorption. Meers *et al.* (2006) have also reported retention of metals (*e.g.*, Cd, Cu, Ni, Pb, and Zn) in solution upon paper filtration, whereas loss of metals on micro- and ultrafiltration membranes has been mentioned in the literature as well (Angehrn-bettinazzi, 1990; Weltje *et al.*, 2003; Guo and Santschi, 2007; Hedberg *et al.*, 2011). Filters can possess a certain cation exchange capacity, which enables them to electrostatically bind free metal ions and positively charged complexes (Weltje *et al.*, 2003). In synthetic media, such adsorption phenomena are primarily related to the filter material rather than its pore size (Weltje *et al.*, 2003). However, when considering more complex environmental matrices (*e.g.*, surface water and sediment or soil solutions) containing suspended matter, pore size becomes more important as particulates could clog the filter and thus affect the effective pore size (Weltje *et al.*, 2003; Ferreira da Silva *et al.*, 2011). Additionally, a decrease in solution-pH causes competition between protons and cations to occupy specific binding sites on the filter material, hence reducing metal adsorption (Weltje *et al.*, 2003). Wetting and/or rinsing of the filter with an acidic solution can therefore also result in fewer interactions with metal cations in solution.

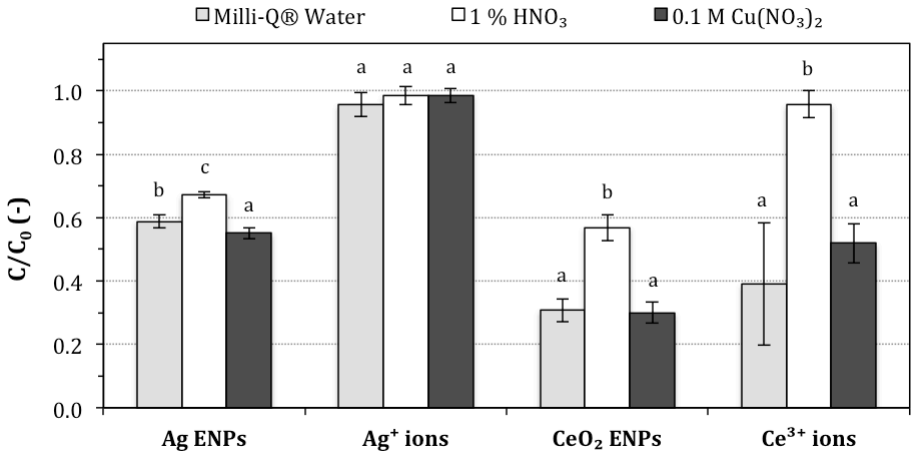

Figure 3.5 – Recoveries of silver or cerium after filtration of 250 μg L^{-1} Ag ENPs and Ag^+ ions, or 1 mg L^{-1} CeO_2 ENPs and Ce^{3+} ions in Milli-Q® water over ashless filter paper, upon application of three different filter (pre-)treatments. (Bars represent mean values, different letters indicate statistically significant differences ($p < 0.05$) between treatments for each species, error bars denote standard deviations, $n = 3$)

3.3.3.2 Syringe filtration

Figure 3.6 depicts the silver or cerium recoveries following microfiltration of 10 mL suspensions/solutions of Ag or CeO_2 ENPs, and Ag^+ or Ce^{3+} ions prepared in Milli-Q® water at various concentrations (*i.e.*, 250, 50, and 25 μg L^{-1} in the case of silver, and 5, 1, and 0.5 mg L^{-1} for cerium). Silver recoveries varied between 49 and 94 % for Ag ENPs, and between 60 and 97 % for Ag^+ ions. For Ce^{3+} ions, recoveries were found to vary between 88 and 100 %, whereas a recovery up to 89 % was observed for 5 mg L^{-1} CeO_2 ENPs. In contrast, filtration of 1 and 0.5 mg L^{-1} CeO_2 ENPs resulted in cerium concentrations in the filtrates below the detection limit (DL_{Ce} = 4.3 μg L^{-1}). Overall, a decrease in initial silver or cerium concentration resulted in notably lower recoveries. These results again suggest potential sorption onto the filter material. Membrane filters have a certain saturation capacity to bind charged species, and thus the amount of metals adsorbed onto a filter is best approached in an absolute manner, as the loss of metals through sorption is more significant at low concentrations in solution. Filtration over dry filters also resulted in high standard deviations on the recoveries, which could again be attributed to a high loss of metals, most likely through adsorption, during the first of three replicate filtrations when reusing the same filter (*i.e.*, up to 50 % lower recoveries compared to the second and third replicates). This effect got more pronounced as the initial concentration decreases. Pre-treatment of the filter with $Cu(NO_3)_2$ generally led to a substantial decrease in the

variations on silver or cerium recoveries, and seemingly also enhanced the recoveries of Ag^+ ions, 25 μg L^{-1} Ag ENPs, and 5 mg L^{-1} CeO_2 ENPs. Cornelis *et al.* (2010) described the recoveries of Ag^+ ions in artificial soil solutions after filtration over 0.45 μm filters, and reported recoveries varying between 10 and 100 %. Preconditioning of the filters with $Cu(NO_3)_2$ was also demonstrated to increase the silver recovery significantly, which was potentially due to the competition of Cu^{2+} and Ag^+ ions to occupy specific binding sites on the membranes, as both ionic species have a high affinity for organic ligands (Cornelis *et al.*, 2010).

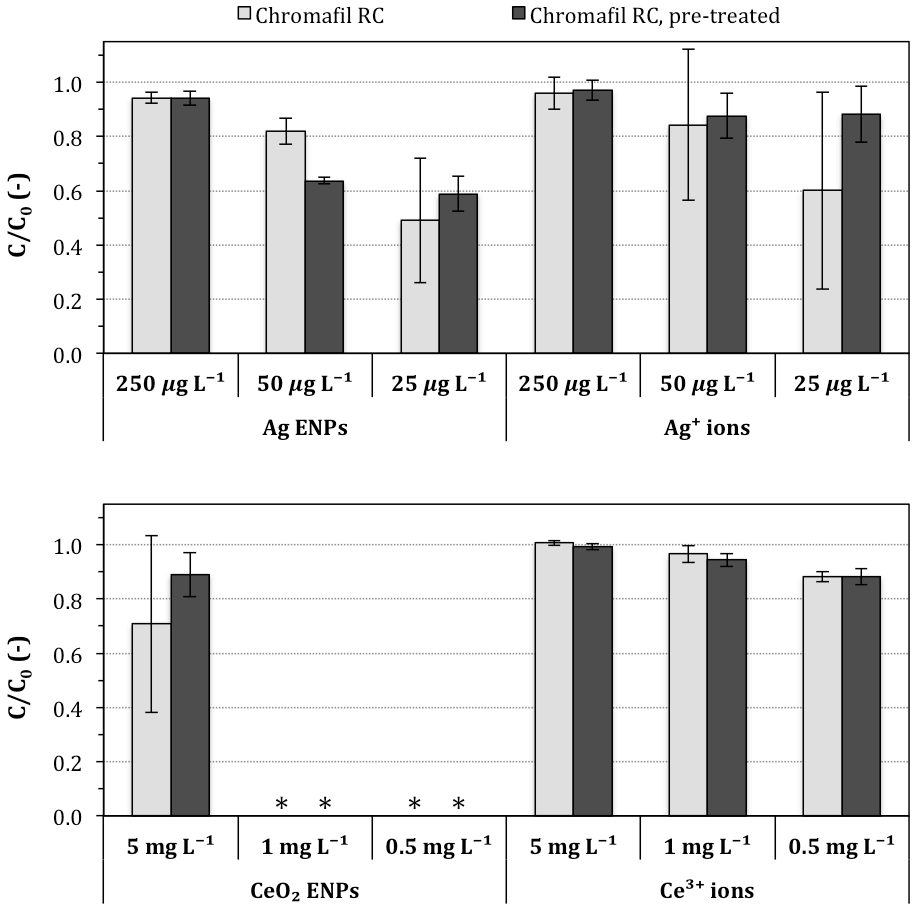

Figure 3.6 – Recoveries of silver or cerium after filtration of 250, 50, and 25 μg L^{-1} Ag ENPs and Ag^+ ions (top graph), or 5, 1, and 0.5 mg L^{-1} CeO_2 ENPs and Ce^{3+} ions (bottom graph) in Milli-Q® water over dry or 0.1 M $Cu(NO_3)_2$ pre-treated 0.45 μm Chromafil RC syringe filters. (Bars represent mean values, values below the detection limit are indicated with an asterisk (DL_{Ce} = 4.3 μg L^{-1}), error bars denote standard deviations, n = 3)

In addition to regenerated cellulose (RC), polyvinylidene difluoride (PVDF) and polyethersulfone (PES) filter membranes (0.45 μm) were also tested for Ag or CeO_2 ENPs, and Ag^+ or Ce^{3+} ions in Milli-Q® water (Figure 3.7). Generally, filtration using a dry filter again resulted in a lower recovery in the first replicate filtrates and hence higher standard deviations compared to filtration using $Cu(NO_3)_2$ pre-treated filters. For both Ag ENPs and Ag^+ ions at 250 $\mu g\ L^{-1}$, comparably high recoveries (91 – 100 %) were observed for all the tested PVDF and PES filters ($p > 0.05$). At lower silver concentrations (50 $\mu g\ L^{-1}$), recoveries ranged between 78 and 89 % or between 72 and 99 % for Ag ENPs or Ag^+ ions, respectively. In contrast to RC filters, PVDF and PES filters did provide quantifiable yet low recoveries (7 – 20 %) for CeO_2 ENPs suspended in Milli-Q® water. Recoveries of Ce^{3+} ions varied between 93 and 101 %, with PES membrane filters providing the highest recoveries at the lowest initial concentration ($p < 0.05$). Polymeric membranes typically possess a negative surface charge upon filtration of aqueous solutions (Ladner *et al.*, 2012; Park *et al.*, 2013). Therefore, with the size of the nanoparticles being a lot smaller than the pore size of the filters, the high retention of CeO_2 ENPs in Milli-Q® water is probably due to electrostatic interactions between the positively charged nanoparticles and negatively charged sites on the surface of the filter membranes, whereas the high recoveries of Ag ENPs in Milli-Q® water could be attributed to both their dimensions and their net negative surface charge, leading to electrostatic repulsion between the nanoparticles and the filter membrane. The high recoveries of Ag^+ or Ce^{3+} ions in Milli-Q® water might have been caused by the presence of residual protons occupying potential adsorption sites, as these solutions were prepared from acidic standard solutions. Higher retention is to be expected at higher, more environmental realistic pH conditions (Meers *et al.*, 2006). Overall, when considering filtration of the nanoparticles or ions in a pure matrix (*i.e.*, Milli-Q® water) over 0.45 μm filters, Chromafil PES filters achieved the highest recoveries.

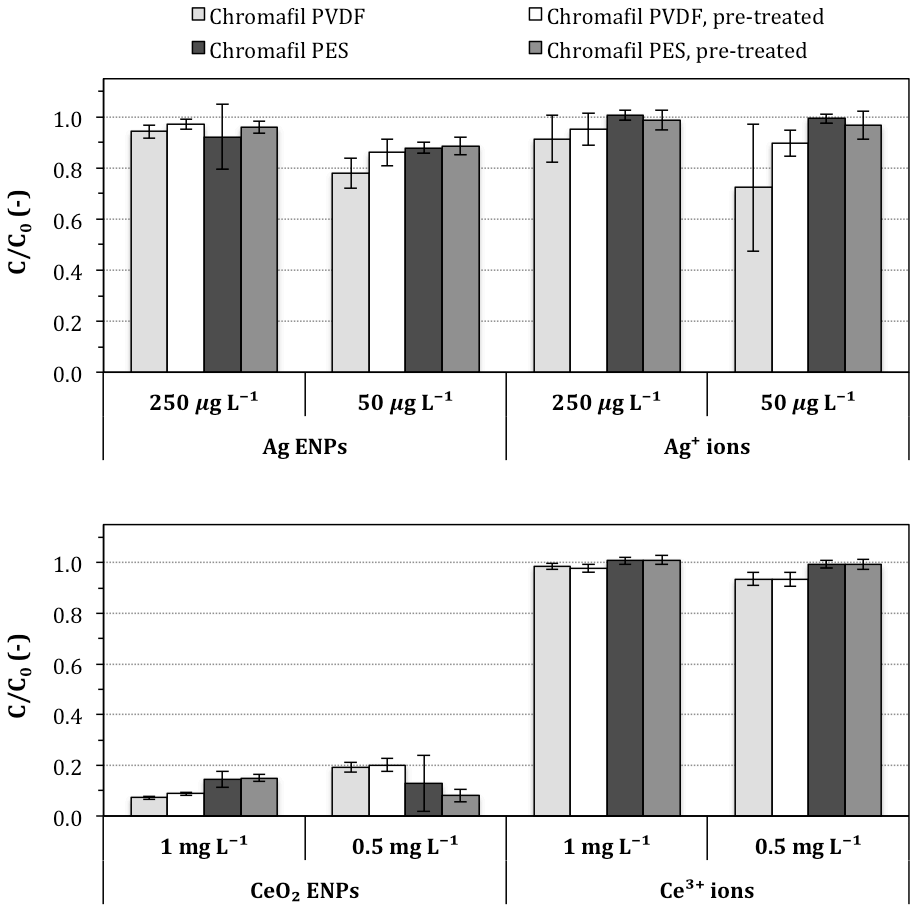

Figure 3.7 – Recoveries of silver or cerium after filtration of 250 and 50 μg L^{-1} Ag ENPs and Ag^+ ions (top graph), or 1 and 0.5 mg L^{-1} CeO_2 ENPs and Ce^{3+} ions (bottom graph) in Milli-Q® water over dry or 0.1 M $Cu(NO_3)_2$ pre-treated 0.45 μm Chromafil PVDF and PES syringe filters. (Bars represent mean values, error bars denote standard deviations, n = 3)

Besides Milli-Q® water, 2 mM KNO_3, NaCl, and $CaCl_2$ solutions were applied to assess the impact of matrix composition on the filtration efficiency and recovery of Ag and CeO_2 ENPs, or Ag^+ and Ce^{3+} ions. The results are presented in Figure 3.8. For both silver species, increasing amounts of silver were retained from the chloride-containing solutions ($p < 0.05$). In the case of Ag ENPs, recoveries varied between 89 and 102 %, between 61 and 78 %, or between 3 and 16 % in the presence of 2 mM KNO_3, NaCl, or $CaCl_2$, respectively, depending on the utilized filter ($p < 0.05$). Recoveries of Ag^+ ions in 2 mM NaCl or $CaCl_2$ were found to vary between 16 and 73 % or between 18 and 61 %, respectively ($p < 0.05$), whereas in 2 mM KNO_3, virtually no Ag^+ ions were retained ($p = 0.849$). Negligible retention of Ce^{3+} ions occurred as recoveries ranged between 97 and 103 %, independent of background electrolyte composition ($p > 0.05$). In contrast, recoveries of CeO_2 ENPs were either low (7 – 29 %) or cerium concentrations in the filtrates were below the detection

limit (DL_{Ce} = 4.3 μg L^{-1}). In chloride-containing matrices the Ag ENPs and Ag^+ ions might have aggregated and/or precipitated as AgCl ($K_{sp,\ 25\ °C}$ = 1.77 × 10^{-10}) (Levard *et al.*, 2012). Furthermore, retention was higher in the presence of divalent cations (Ca^{2+}) compared to monovalent cations (Na^+), which could point towards a higher degree of aggregation in the former case, consistent with the Schulze-Hardy rule on colloidal stability (Lin *et al.*, 2010). El Badawy *et al.* (2010) demonstrated that 10 mM NaCl only had a limited effect on the size and stability of Ag ENPs, whereas 10 mM Ca^{2+} as background electrolyte induced aggregation. Similar observations involving Ag, CeO_2, Fe_2O_3, NiO, TiO_2, and ZnO ENPs have been reported in the literature (Zhang *et al.*, 2009; Buettner *et al.*, 2010; Li *et al.*, 2010).

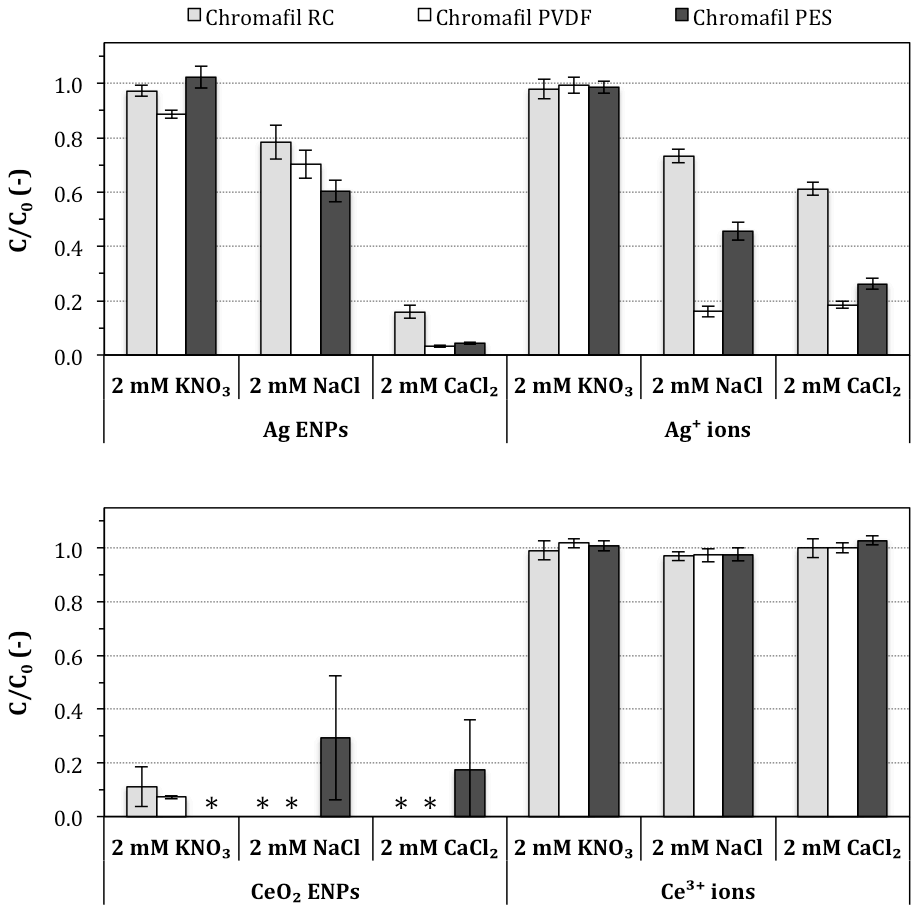

Figure 3.8 – Recoveries of silver or cerium after filtration of 250 μg L^{-1} Ag ENPs and Ag^+ ions (top graph), or 1 mg L^{-1} CeO_2 ENPs and Ce^{3+} ions (bottom graph) in 2 mM KNO_3, NaCl, or $CaCl_2$ over 0.1 M $Cu(NO_3)_2$ pre-treated 0.45 μm Chromafil RC, PVDF and PES syringe filters. (Bars represent mean values, values below the detection limit are indicated with an asterisk (DL_{Ce} = 4.3 μg L^{-1}), error bars denote standard deviations, n = 3)

Figure 3.9 presents the results from filtration of Ag and CeO_2 ENPs, or Ag^+ and Ce^{3+} ions in Milli-Q® water using alumina-based 0.02 μm Anatop syringe filters. Both Ag and CeO_2 ENPs were retained to a large extent, *i.e.*, only up to 7 % of silver or 4 % of cerium was recovered in the filtrates. In the case of Ag^+ and Ce^{3+} ions, recoveries approached 100 %. Preconditioning of the filters with 0.1 M $Cu(NO_3)_2$ did not affect silver or cerium retention ($p > 0.05$). Retention of the nanoparticles is probably due to a combination of size-exclusion and sorption phenomena leading to pore constriction and blockage (Ladner *et al.*, 2012). However, as the Anatop filter material is supposed to be positively charged under the current experimental conditions, adsorption of CeO_2 ENPs is highly unlikely. A possible explanation for the observed high retention of CeO_2 ENPs could be electrostatic exclusion, whereby the small positively charged nanoparticles were electrostatically repelled by the filter membrane, hence impeding their permeation.

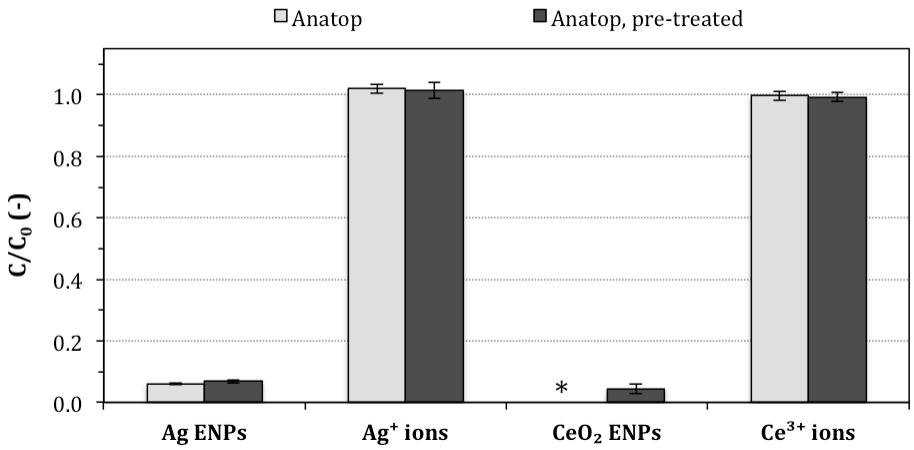

Figure 3.9 – Recoveries of silver or cerium after filtration of 250 μg L^{-1} Ag ENPs and Ag^+ ions, or 1 mg L^{-1} CeO_2 ENPs and Ce^{3+} ions in Milli-Q® water over dry or 0.1 M $Cu(NO_3)_2$ pre-treated 0.02 μm Anatop syringe filters. (Bars represent mean values, values below the detection limit are indicated with an asterisk (DL_{Ce} = 4.3 μg L^{-1}), error bars denote standard deviations, n = 3)

3.3.3.3 Centrifugal filtration

As mentioned in the introduction, UF membranes are operationally defined with a MWCO value by their manufacturers, because their actual pore sizes are difficult to quantify, and in reality there exists a distribution of pore sizes (Ladner *et al.*, 2012). However, according to the work by Ren *et al.* (2006), the geometric mean pore diameter of high quality UF membranes, which are characterized by linear pore size distribution parameters, can be estimated through Equation 3.1. For comparison purposes, calculated average pore

sizes of the tested UF membranes are therefore tabulated in Table 3.3.

$$\sigma = 1.8054 - 0.5608 \frac{D^*}{D_{MWCO}} \qquad \{1.15 \leq \sigma \leq 1.55 \quad (r^2 = 0.999)\} \qquad \textbf{(3.1)}$$

where σ [-] is the geometric standard deviation, D^* [nm] is the geometric mean pore diameter, and D_{MWCO} [nm] is the diameter of a solute molecule that is retained for 90 %, whereby $D_{MWCO} = 0.066 \times (\text{MWCO})^{0.46}$.

Table 3.3 – Estimated pore sizes (D^*) of the utilized UF membranes.

MWCO (kDa)	D_{MWCO} (nm)	D^* ± SD (nm)
3	2.6	2.1 ± 1.3
10	4.6	3.2 ± 2.3
30	7.6	6.2 ± 3.8
50	9.6	7.8 ± 4.8
100	13.2	10.7 ± 6.6
300	21.8	17.7 ± 11.0
1000	38.0	30.8 ± 19.2

SD: standard deviation.

Recoveries from Ag or CeO_2 ENPs, and Ag^+ or Ce^{3+} ions in Milli-Q® water upon application of centrifugal filtration using various MF and UF units are shown in Figure 3.10. Virtually no Ag^+ or Ce^{3+} ions were retained by 3 kDa, 10 kDa, or 0.45 μm centrifugal filters, which were the only three types used to evaluate filtration of the ionic species ($p > 0.05$). However, retention of the ENPs was observed. In the case of Ag ENPs, recoveries were very low (2 – 7 %) when considering all UF units with a MWCO ≤ 300 kDa ($p > 0.05$), whereas centrifugal filtration over 1000 kDa, 0.2 μm, or 0.45 μm resulted in recoveries between 71 and 95 % ($p < 0.05$). Accordingly, the CeO_2 ENPs were also highly retained by the applied centrifugal filters ($p > 0.05$), with the exception of the 0.2 μm Vivaspin filters. These results again suggest a combination of interaction mechanisms between the nanoparticles and filter membranes, as proposed by Ladner *et al.* (2012): *(1) size exclusion of the nanoparticles (or aggregates), leading to accumulation at the membrane interface, (2) strong adsorption and/or particle entrapment, resulting in pore constriction or blockage, or (3) limited or no adsorption affinity, allowing partial or even complete passage of the particles.* Filtration results of the negatively charged Ag ENPs can mostly be related to mechanisms (1) and (3), while in addition to mechanism (1), the high retention of positively charged CeO_2 ENPs is most likely

primarily the result of sorption onto the negatively charged UF and MF membranes, and subsequent constriction and clogging of the filter pores (2). Moreover, the low, yet quantifiable recoveries of silver or cerium after UF of Ag or CeO_2 ENPs suspended in Milli-Q® water, especially at low MWCO such as 3 kDa or 10 kDa, could potentially be the result of minimal fractions occurring as dissolved ionic silver or cerium species in solution, rather than stem from the presence of extremely small particulate matter. However, this conjecture merits further research for eventual confirmation (*e.g.*, via ultracentrifugation). On the other hand, these findings could also be due to the pore size distribution of the filter membranes, as there are always a limited number of "large" pores that are preferentially used.

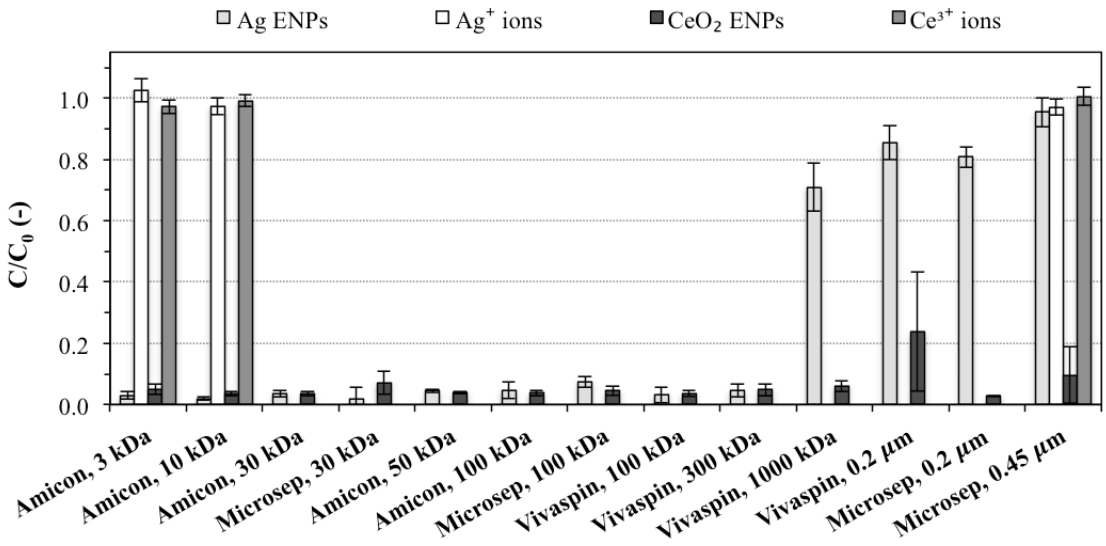

Figure 3.10 – Recoveries of silver or cerium after centrifugal filtration of 250 μg L^{-1} Ag ENPs and Ag^+ ions, or 1 mg L^{-1} CeO_2 ENPs and Ce^{3+} ions in Milli-Q® water at 3735 *g* for 15 min (60 min in the case of 3 kDa UF devices), using various centrifugal filters. Ag^+ and Ce^{3+} ions were only filtered using 3 kDa, 10 kDa, and 0.45 μm filtration units, as indicated by the missing bars for the remaining MF and UF devices. (Bars represent mean values, error bars denote standard deviations, $n = 3$)

It was shown that UF at low MWCO (*e.g.*, 10 kDa) as well as filtration over 0.02 μm might potentially be suitable to separate "(nano)particulate" from "dissolved" compounds, at least considering the tested nanoparticles and ionic species in Milli-Q® water. This was examined further for different matrices (*i.e.*, 2 mM KNO_3, NaCl, and $CaCl_2$) as presented in Figure 3.11. Comparable retention of Ag ENPs, or Ag^+ and Ce^{3+} ions in the different matrices was observed when comparing the results from using Anatop 0.02 μm syringe filters or Amicon 10 kDa UF devices ($p > 0.05$), suggesting that those recoveries might be caused by

ionic silver or cerium species in solution. A high retention of Ag ENPs was observed for all tested matrices, with a slightly higher recovery (up to 10 %) of the nanoparticles in 2 mM KNO_3. In chloride-containing solutions, the recoveries of Ag^+ ions were also low (10 – 12 %), most likely due to the formation of AgCl precipitates, whereas in 2 mM KNO_3, 95 to 100 % of the Ag^+ ions permeated into the filtrates. Recoveries approaching 100 % were also observed for Ce^{3+} ions, independent of the matrix composition. However, in each of the three matrices, significantly higher cerium recoveries from CeO_2 ENPs were found in the 0.02 μm filtrates compared to the 10 kDa filtrates ($p < 0.05$). Just like in a pure Milli-Q® water matrix, CeO_2 ENPs are highly retained by 10 kDa UF and the quantified recoveries (5 – 8 %) can possibly be attributed to ionic cerium in solution, although passage of some extremely small (or other) particulates cannot be ruled out completely. In the 0.02 μm filtrates on the other hand, recoveries of CeO_2 ENPs varied between 59 and 78 %, suggesting that breakthrough of CeO_2 ENPs occurred in the presence of either 2 mM KNO_3, NaCl, or $CaCl_2$, in contrast to what was observed in Milli-Q® water as discussed earlier. Background electrolytes, which are also present in real environmental samples (*e.g.*, in surface or coastal waters), generally reduce interactions between metal cations and filters through competition for specific binding sites (Gardner and Comber, 1997).

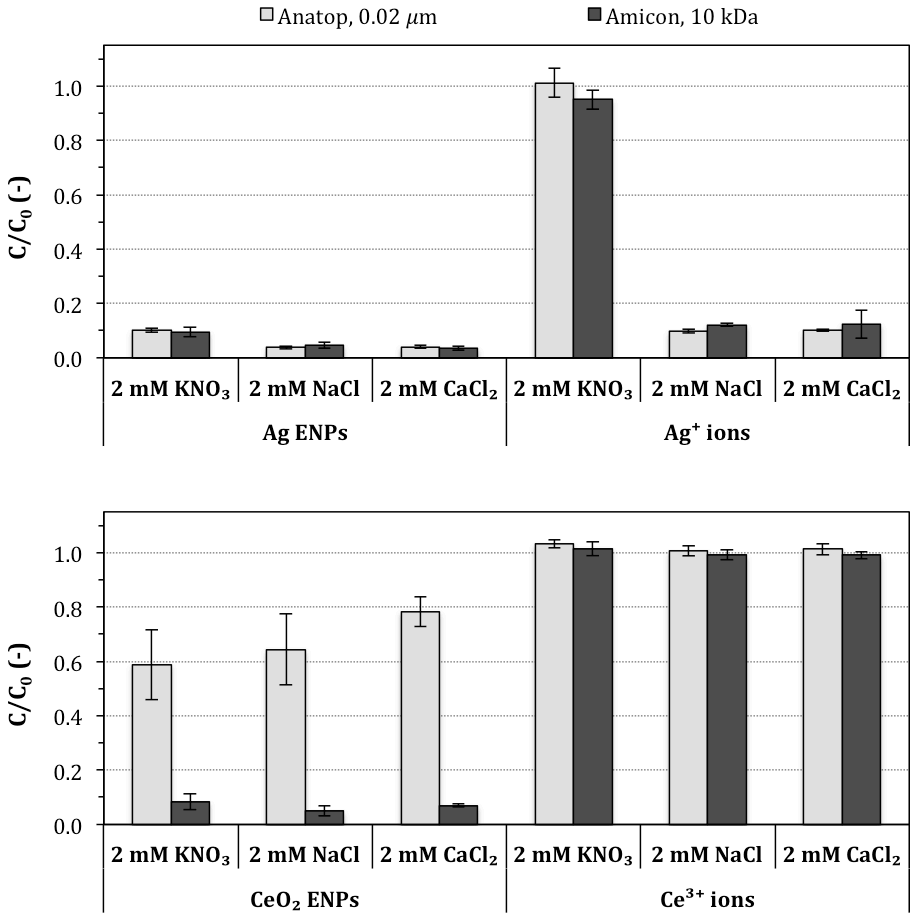

Figure 3.11 – Recoveries of silver or cerium after filtration of 250 μg L^{-1} Ag ENPs and Ag^+ ions (top graph), or 1 mg L^{-1} CeO_2 ENPs and Ce^{3+} ions (bottom graph) in 2 mM KNO_3, NaCl, or $CaCl_2$ over 0.02 μm Anatop syringe filters, or using 10 kDa Amicon UF units. UF was performed at 3735 *g* for 15 min. (Bars represent mean values, error bars denote standard deviations, *n* = 3)

Finally, stepwise filtration was performed by first filtering 250 μg L^{-1} Ag ENPs or Ag^+ ions in 2 mM KNO_3, NaCl, or $CaCl_2$ over 0.45 μm Chromafil RC, PVDF, and PES filters, where after the obtained filtrates were partially filtered again over 0.02 μm Anatop filters and partially via 10 kDa UF units. The results are presented in Figure 3.12. Filtration of Ag ENPs using 0.45 μm filters resulted in similar recoveries as discussed earlier, whereby particle aggregation and possibly AgCl formation most likely caused the increased retention in chloride-containing matrices (*i.e.*, 60 to 90 % recovery in 2 mM NaCl and 5 to 14 % recovery in 2 mM $CaCl_2$). Further filtration of the 0.45 μm filtrates over 0.02 μm or 10 kDa filters led to mutually comparable, low silver recoveries (maximum 17 %, 9 %, or 10 % in 2 mM KNO_3, NaCl, or $CaCl_2$, respectively). For KNO_3 and NaCl, these results indicate permeation of (nano)particulate silver (*e.g.*, Ag or AgCl) and potentially also the presence of ionic silver species (*e.g.*, Ag^+ or $AgCl_2^-$) in solution. In $CaCl_2$, the colloidal stability of Ag ENPs

was decreased to a large extent, inducing the formation of aggregates that are retained by the 0.45 μm filter. Meanwhile, the somewhat comparable silver recoveries in the 0.45 μm, 0.02 μm and 10 kDa filtrates, suggest that the fraction of silver that was allowed to permeate through 0.45 μm was again either present as extremely small (or other) particulate silver or as ionic silver species in solution. This was even more prominent when looking at Ag^+ ions in both chloride-containing matrices, where the silver retention was again most likely caused by the formation of AgCl precipitates. Significant particulate fractions that permeated through 0.45 μm filters could only be distinguished from the "dissolved" fraction (*i.e.*, < 10 kDa or at least < 20 nm) in the case of Ag^+ ions in 2 mM NaCl for Chromafil RC or PES filters, or in 2 mM $CaCl_2$ for Chromafil RC filters ($p < 0.05$). Stepwise filtration of Ag^+ ions in 2 mM KNO_3 over 0.45 μm, and 0.02 μm or 10 kDa resulted in recoveries approaching 100 %.

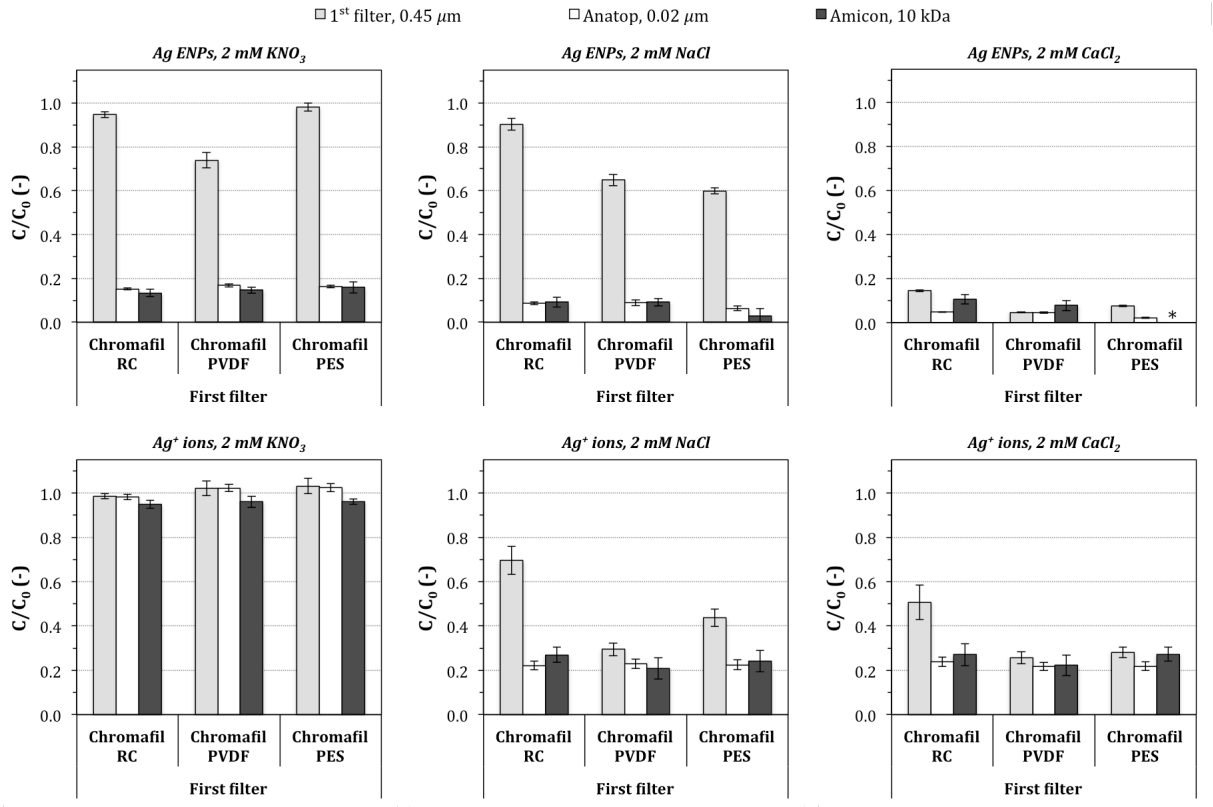

Figure 3.12 – Recoveries of silver after filtration of 250 μg L^{-1} Ag ENPs (top three graphs) and Ag^+ ions (bottom three graphs) in 2 mM KNO_3, NaCl, or $CaCl_2$ over 0.1 M $Cu(NO_3)_2$ pre-treated 0.45 μm Chromafil RC, PVDF and PES syringe filters. The resulting filtrates were then filtered over either 0.02 μm Anatop syringe filters, or were subjected to UF at 3735 *g* for 15 min using 10 kDa Amicon UF devices. (Bars represent mean values, values below the detection limit are indicated with an asterisk (DL_{Ag} = 3.1 μg L^{-1}), error bars denote standard deviations, n = 3)

3.4 Conclusion

This study evaluated the filtration of aqueous (citrate-coated) Ag (14.5 ± 1.1 nm) and CeO_2 (7.3 ± 1.4 nm) ENPs suspensions via several filtration methods (*e.g.*, paper filtration, micro- and ultrafiltration) that are routinely applied during (pre-)treatment of aquatic samples. Nanoparticle retention and potential interaction mechanisms with the filters were discussed comprehensively. As expected, all of the nanoparticles were highly retained by filter membranes having a pore size smaller than the size of the ENPs. Yet, significant retention was also observed with considerably larger filter pore sizes. Adsorptive interactions between negatively charged filters and the positively charged CeO_2 ENPs most likely caused their high retention. The negatively charged Ag ENPs were less prone to adsorption, and were hence less retained, at least in ultrapure water. Such potentially occurring interactions thus need to be taken into account for instance during fractionation for characterization or sample preparation of nanoparticles.

Wetting and rinsing of paper filters with 1 % HNO_3, and preconditioning of filter membranes with 0.1 M $Cu(NO_3)_2$ generally reduced the variations on silver or cerium recoveries, and seemingly also enhanced their recovery. However, considering the filter membranes, the latter might also have been due to a general "wetting" effect instead of an actual blocking of potential sorption sites on the membranes by Cu^{2+} ions, and for instance wetting with just Milli-Q® water could potentially also reduce the variability in recovery. Nevertheless, it was shown that re-use of the filters might potentially be considered for instance to reduce material costs during nanoparticle characterization or sample preparation, in case the filters are pre-treated prior to filtering the samples, at least when working with pure/simple aqueous solutions.

Additionally, the presence of competing electrolytes in solution might reduce (nano)particle-membrane interactions and thus increase their recovery. However, background electrolytes could also affect nanoparticle or ionic (colloidal) stability, for instance as indicated by the enhanced retention of the Ag ENPs and Ag^+ ions in chloride-containing matrices, which was most likely due to particle aggregation and AgCl precipitation. A simple stepwise filtration procedure was performed, allowing for a quick preliminary assessment of the behaviour of Ag ENPs and Ag^+ ions in 2 mM KNO_3, NaCl, or $CaCl_2$, by permitting quantification of the "dissolved" portion (*i.e.*, < 10 kDa or < 20 nm) of the 0.45 μm permeated fractions.

In ultrapure water, permeation appears to be determined more by particle properties than by membrane characteristics, at least for the filters under consideration in this study, as indicated by retention similarities between the different membrane types. Yet in general, PES did achieve slightly higher recoveries. In the presence of 2 mM KNO_3, NaCl, or $CaCl_2$ however, more significant differences in recoveries were observed between the different membrane materials, and the use of RC membranes generally provided the highest recoveries in these matrices. This suggests these membrane types might be best suited during for example nanoparticle fractionation in (simple) aqueous matrices.

Ultrafiltration using 10 kDa centrifugal filters is proposed for the removal of the ENPs from aqueous solution, due to the ease of use and the fact that centrifugation only took 15 min to complete the filtration in comparison to 60 min for 3 kDa filters, and might potentially also be suitable to fractionate (nano)particulate from dissolved matter. However, definitive confirmation of the latter requires additional research (*e.g.*, by subjecting the 10 kDa filtrates to ultracentrifugation).

It should further be noted that in real, more complex environmental samples, the filtration efficiency and retention of nanoparticles is most likely to be influenced by additional parameters, *e.g.*, by the presence of colloidal matter, as well as by the method of operation, *e.g.*, dead-end versus tangential flow filtration. Furthermore, the results discussed in this work could benefit from the application of more advanced analytical tools, such as transmission electron or a combination of electrophoresis, streaming potential, and particle size analysis, in order to elucidate the actual underlying nanoparticle-membrane interactions to a further extent. For instance, to clarify if the nanoparticles *e.g.*, remain attached on the surface of the filter membrane or become entrapped within the membrane pores, or to determine the charge of the particles and membranes and demonstrate particle aggregation for example.

Chapter 4

Stability of engineered nanomaterials in complex aqueous matrices: Settling of CeO_2 nanoparticles in natural surface waters

4 Stability of engineered nanomaterials in complex aqueous matrices: Settling of CeO_2 nanoparticles in natural surface waters[‡]

4.1 Introduction

Over the past decade, the production and use of engineered nanoparticles (ENPs) have increased exponentially. This will inherently lead to their emission into the environment (*e.g.*, surface water or groundwater), where their often unique and size-related properties could pose a threat to the ecosystem and public health (Klaine *et al.*, 2012; Liu *et al.*, 2013; The Project on Emerging Nanotechnologies, 2014). Particularly metal oxide nanoparticles, including CeO_2 ENPs, are increasingly being incorporated into a wide range of industrial and commercial products (Keller *et al.*, 2010). CeO_2 ENPs have for instance been used as polishing agents, as fuel additives, as automotive exhaust catalysts, and as electrolytes in solid oxide fuel cells, and have recently also gained interest for biomedical applications (*e.g.*, in radio therapy and cancer treatment) due to their antioxidant properties (Karakoti *et al.*, 2012; Shah *et al.*, 2012). However, evidence of their toxicity to (aquatic) organisms and even human cells is also emerging, making a thorough understanding of their environmental behaviour and fate imperative in order to examine potential exposure routes and further improve risk assessment (Fang *et al.*, 2009; Keller *et al.*, 2010; Tso *et al.*, 2010; Karakoti *et al.*, 2012; Shah *et al.*, 2012).

The stability of ENPs in complex aquatic media such as natural surface waters is a key parameter governing their fate and potential toxicological risks. Well-dispersed nanoparticles could persist longer in the environment, be transported over larger distances, or could also potentially be involved in particle-facilitated contaminant transport, hence increasing their possible bioavailability or influencing the bio-accessibility of other toxic pollutants (Gimbert *et al.*, 2007; Fang *et al.*, 2009; Quik *et al.*, 2010; Liu *et al.*, 2013). Aggregation, sedimentation, and dissolution are some of the main physicochemical

[‡] *Submitted for publication as: Van Koetsem, F., Verstraete, S., Van der Meeren, P., and Du Laing, G.* ***Stability of engineered nanomaterials in complex aqueous matrices: Settling behaviour of CeO_2 nanoparticles in natural surface waters.***

processes affecting the stability and ultimate fate of ENPs in natural waters, and are highly influenced by both nanoparticle properties as well as the characteristics of the receiving medium (Boxall *et al.*, 2007; Batley and McLaughlin, 2010; Velzeboer *et al.*, 2014). Numerous studies have already addressed the effects of individual aqueous parameters such as pH, ionic strength (IS), cation valence, or the type and amount of natural organic matter (NOM) on these processes (Domingos *et al.*, 2009; French *et al.*, 2009; El Badawy *et al.*, 2010; Quik *et al.*, 2010; Liu *et al.*, 2013). However, the vast majority of these studies have done so using simplified artificial solutions, where the full complexity and heterogeneity of real environmental systems is lacking (*i.e.*, the combined effect of pH, IS, NOM, suspended solids, and other properties of the aqueous media) (Keller *et al.*, 2010; Tso *et al.*, 2010; Quik *et al.*, 2012; Velzeboer *et al.*, 2014). Therefore, there is still a need to study and elucidate the physicochemical behaviour and fate of ENPs in complex natural aquatic samples.

This study aimed to contribute to the general knowledge on the fate of nanoparticles in aquatic environments, by assessing the stability and sedimentation kinetics of CeO_2 ENPs in natural aqueous media, and identifying potential physicochemical factors affecting their behaviour in such complex environmental matrices. Therefore, CeO_2 ENPs were dispersed in 10 distinct natural surface waters (5 mg L^{-1}), and the evolution of their mass concentration over time (7 d), under stagnant and isothermal conditions (4 – 6 °C), was measured and evaluated by means of a first-order settling rate model proposed by Quik *et al.* (2012). Additionally, Ce^{3+} ions were treated in the same way for comparison purposes.

4.2 Materials and methods

4.2.1 Surface water sampling and characterization

Surface water samples (± 20 L) were collected from 10 different locations in the Flanders region (Belgium) (Table 4.1), and were characterized thoroughly within 48 h upon arrival at the lab. All samples were stored at 4 – 6 °C under dark conditions and settling experiments were initiated 48 h after sample collection. Electrical conductivity (EC) was measured using a type LF537 conductivity probe (WTW, Weilheim, Germany). A model 520A pH electrode (Orion Research Inc., Boston, MA, USA) was used to acquire the solution-pH. Total organic carbon (TOC) and inorganic carbon (IC) content were determined by means of a TOC analyser (TOC-V_{CPN}, Shimadzu, Kyoto, Japan). Dry residue (DR) was

obtained by evaporating 100 mL of surface water sample in a pre-weighed beaker at 105 °C, and recording the mass difference. The total suspended solids (TSS) content was obtained after (vacuum) filtration of 100 mL of water sample over pre-dried and pre-weighed 0.45 μm filters (Porafil RC, Macherey-Nagel GmbH & Co. KG, Düren, Germany), and determining the mass difference. Ion exchange chromatography (IEC) (761 Compact IC, Metrohm AG, Herisau, Switzerland) was applied to quantify anionic species (F^-, Cl^-, NO_3^-, SO_4^{2-}, and PO_4^{3-}) present in the water samples. Colorimetric determination of nitrite (NO_2^-) was carried out by first adding 1 mL sulfanilic acid solution (*i.e.*, 1.5 g sulfanilic acid and 50 mL 37 % HCl in 200 mL H_2O), 1 mL α-naphthylamine hydrochloride solution (*i.e.*, a filtered solution of 1.2 g α-naphthylamine in 2 mL 37 % HCl added to 200 mL H_2O), and 1 mL sodium acetate solution (*i.e.*, 135 mg sodium acetate trihydrate in 500 mL H_2O) to 20 mL of surface water sample. Then, this solution was shaken and allowed to fully react for 15 min prior to analysis using a Jenway 6400 Spectrophotometer (Bibby Scientific Ltd., Staffordshire, UK) at 520 nm. Concentrations of main elements (Na, K, Ca, and Mg), trace elements (Al, Cd, Co, Cr, Cu, Fe, Mn, Ni, Pb, and Zn), and cerium in the surface waters were determined by inductively coupled plasma optical emission spectrometry (ICP-OES) (Vista-MPX CCD Simultaneous ICP-OES, Agilent Technologies, Santa Clara, CA, USA) after being digested (*i.e.*, 50 mL of surface water sample was boiled for 2 h on a hotplate at 150 °C under reflux using a beaker and a watch glass, after 5 mL 65 % HNO_3 and 2 mL 30 % H_2O_2 had been added, and was quantitatively transferred to 100 mL volumetric flasks).

Table 4.1 – Detailed overview of the different sampled surface waters.

Sample ID	Surface water	Type	Location	Coordinates	
				Latitude	Longitude
PUM	Putse Moer	Fen	Kalmthout	51° 22’ 49” N	04° 26’ 09” E
SC1	Scheldt	River	Doel	51° 17’ 47” N	04° 16’ 56” E
SC2	Scheldt	River	Linkeroever (Antwerp)	51° 12’ 21” N	04° 22’ 02” E
GAL	Galgenweel	Lake	Linkeroever (Antwerp)	51° 12’ 47” N	04° 22’ 43” E
RUP	Rupel	River	Niel	51° 05’ 53” N	04° 20’ 09” E
NIK	Nielse Kleiputten	Lake	Niel	51° 06’ 28” N	04° 20’ 25” E
OLS	Old Scheldt	Stream	Weert	51° 06’ 20” N	04° 12’ 06” E
DEN	Dender	River	Oudegem	51° 00’ 41” N	04° 04’ 16” E
GTC	Ghent-Terneuzen Canal	Canal	Zelzate	51° 11’ 50” N	03° 48’ 03” E
COC	Coupure Canal	Canal	Ekkergem (Ghent)	51° 03’ 11” N	03° 42’ 35” E

4.2.2 Nanoparticles

The CeO_2 ENPs (APS: 4 ± 2 nm, ζ-potential: +40 ± 5 mV concentration: 50 000 mg L^{-1}) were obtained from PlasmaChem GmbH (Berlin, Germany) in the form of an aqueous dispersion. Additional particle size analysis was performed by means of photon correlation spectroscopy (PCS) (Malvern PCS-100, Malvern Instruments Ltd., Worcestershire, UK). PCS measurements were performed in quadruplicate, at 25 °C using a HeNe laser (633 nm) positioned at a scattering angle of 150 degrees. The so-called *Z*-average hydrodynamic particle size was obtained through cumulant analysis, while particle size distributions (PSDs) were obtained via multi modal analysis. Furthermore, the nanoparticles were visualized via transmission electron microscopy (TEM) (JEM-2200FS, Jeol Ltd., Tokyo, Japan) equipped with energy dispersive X-ray spectrometry (EDS), subjected to UV-Vis spectroscopy (6400 Spectrophotometer, Jenway, Bibby Scientific Ltd., Staffordshire, UK), and to zeta (ζ) potential measurements (Zetasizer 3000 HSa, Malvern Instruments Ltd., Worcestershire, UK) to assess the nanoparticles surface charge. Ionic cerium (as $Ce(NO_3)_3$) (Plasma HIQU, 10 000 ± 20 μg Ce^{3+} mL^{-1} in 2 – 5 % HNO_3) reference standard solution was purchased from ChemLab NV (Zedelgem, Belgium). All chemicals used were of analytical grade.

4.2.3 Settling experiments

Firstly, a screening experiment was conducted to examine the suitability of two potential settling recipients (*i.e.*, conical-bottomed polypropylene or borosilicate glass tubes). After soaking the recipients in diluted nitric acid followed by a thorough rinsing with ultrapure water (Milli-Q®, 18.2 MΩ cm^{-1}, EMD Millipore Corp., Billerica, MA, USA), 40 mL solutions of 5 and 0.5 mg L^{-1} CeO_2 ENPs or Ce^{3+} ions were transferred into the tubes and stored at 4 to 6 °C in a fridge for 7 d. At the start (t_0) and after 7 d, 10 mL aliquots were pipetted at about the middle of the liquid height (after first gently mixing the samples manually), subjected to open vessel microwave digestion (for 1.5 h after addition of 4 mL *aqua regia*) using a microwave accelerated reaction system (MARS 5, CEM Corp., Matthews, NC, USA), and analysed for total cerium content by means of ICP-OES.

The different surface waters (200 mL) were transferred to 250 mL Erlenmeyer flasks, spiked with CeO_2 ENPs or Ce^{3+} ions to a final concentration of 5 mg L^{-1}, and allowed to

equilibrate for 5 min by shaking on an orbital shaker. Afterwards, 40 mL aliquots were transferred into polypropylene settling tubes (separate tubes for each of the intended sampling times), which were then capped and briefly shaken vigorously by hand, before finally being placed on a steady surface in a fridge at 4 to 6 °C, allowing the settling to occur under isothermal conditions at a low temperature to minimize eventual biofilm growth in the sample vials. Moreover, by shielding the samples from light, potential photolytic degradation of the ENPs was also minimized. At designated times (*i.e.*, at t_0 and after 1, 3, and 7 d), 10 mL aliquots were sampled from the specified vials close to the liquid surface, to minimize turbulence. Additional polypropylene tubes containing 40 mL of 5 mg L^{-1} CeO_2 ENPs or Ce^{3+} ions in all the different surface waters were also included to examine possible losses of cerium due to sorption of ENPs or ions onto the inner walls of the settling recipients. These solutions were sampled (10 mL) after 7 d, after first being shaken vigorously by hand. Controls (*i.e.*, spiked Milli-Q® water) were also included in the experimental set-up, and sampled in a similar manner. All of the sampled aliquots were then digested and analysed for cerium content in the same way as described in the paragraph above.

Finally, ionic release from CeO_2 ENPs in the different surface water samples was examined by means of centrifugal ultrafiltration (UF). For this, 4 mL aliquots were sampled at t_0 and after 7 d residing in the fridge (after first shaking the sample vials manually), transferred to UF devices (Amicon Ultra-4, EMD Millipore Corp., Billerica, MA, USA) having a 10 kDa molecular weight cut-off (MWCO), and subjected to centrifugation (Megafuge 1.0, Heraeus, Hanau, Germany) at 4500 rpm (*i.e.*, 3735 *g*) for 15 min. Afterwards, the resulting filtrates were diluted with 2 % *aqua regia*, and were analysed directly for cerium content by means of ICP-OES (*cf.* Chapter 3).

4.2.4 Data processing

SPSS Statistics 22 (IBM, Armonk, NY, USA) was used to perform analysis of variance (ANOVA), Pearson's product-moment correlation analysis and non-linear least squares regression. Normality of data was checked via Shapiro-Wilk's test. Excel (Microsoft Corp., Redmond, WA, USA) and SigmaPlot 12.5 (Systat Software, Inc., Chicago, IL, USA) software packages were used for numerical and graphical data processing.

4.3 Results

4.3.1 Nanoparticle characterization

PCS measurements of the CeO_2 ENPs suspended in Milli-Q® water revealed a *Z*-average hydrodynamic particle diameter of 7.3 ± 1.4 nm, and a narrow unimodal particle size distribution (see also Figure 3.2 in Chapter 3), indicating a highly monodisperse system. The nanoparticles had a ζ-potential of +52.7 ± 4.2 mV when dispersed in Milli-Q® water at pH 6.5. Overall, both the determined average particle size and surface charge are in line with what was claimed by the manufacturer. According to TEM analysis the nanoparticles appeared to possess a spherical morphology (see also Figure 3.1 in Chapter 3). The UV-Vis absorption spectrum of CeO_2 ENPs showed a decreasing absorbance gradient in the near-UV region, which also remained virtually unchanged after storing the nanoparticle suspensions for 12 months at 4 to 6 °C (see also Figure 3.3 in Chapter 3), suggesting nanoparticle size and shape stability over time (Liu and Hurt, 2010).

4.3.2 Surface water properties

The natural surface waters were characterized for various physicochemical properties in order to examine the potential impact of water properties on the stability and settling of the CeO_2 ENPs (Tables 4.2 and 4.3). Solution-pH was generally slightly alkaline (7.28 – 8.08), except for PUM, which had pH of 4.95. Between the different samples, variations up to three orders of magnitude were observed for EC (39 – 4863 μS cm^{-1}), TSS (6.5 – 213 mg L^{-1}), and DR (35 – 3123 mg L^{-1}). The TOC content ranged from 7.0 to 13.6 mg L^{-1}. PUM and GAL had the lowest IC content (0.3 and 8.6 mg L^{-1}, respectively), whereas values between 30.1 and 49.6 mg L^{-1} were obtained for the other water samples. The amounts of anions, as well as major and trace elements present in solution were noticeably lower for PUM, in comparison to the other surface waters.

Table 4.2 – Physicochemical properties of the different surface water samples. Data is presented as mean ± standard deviation (n = 3).

Parameter		PUM	SC1	SC2	GAL	RUP	NIK	OLS	DEN	GTC	COC
pH	**(-)**	4.95 ± 0.09	7.46 ± 0.13	7.57 ± 0.38	7.40 ± 0.17	7.28 ± 0.18	8.08 ± 0.06	7.80 ± 0.26	7.75 ± 0.18	7.61 ± 0.35	7.65 ± 0.30
EC	**(μS cm^{-1})**	39 ± 1	2257 ± 15	725 ± 2	4863 ± 12	720 ± 4	892 ± 4	723 ± 2	680 ± 1	1323 ± 7	776 ± 5
TSS	**(mg L^{-1})**	6.5 ± 0.7	89 ± 6	144 ± 8	7.2 ± 2.6	213 ± 13	13 ± 3	8.0 ± 2.8	62 ± 5	16 ± 6	12 ± 1
DR	**(mg L^{-1})**	53 ± 6	1497 ± 64	626 ± 45	3123 ± 115	727 ± 33	624 ± 44	464 ± 30	501 ± 27	822 ± 52	497 ± 39
TOC	**(mg L^{-1})**	13.6 ± 0.9	8.5 ± 0.6	10.0 ± 3.2	7.0 ± 0.4	8.7 ± 0.6	9.5 ± 0.5	12.9 ± 0.8	8.1 ± 0.7	7.9 ± 1.3	7.7 ± 1.2
IC	**(mg L^{-1})**	0.3 ± 0.1	40.0 ± 2.5	35.0 ± 2.8	8.6 ± 0.6	30.1 ± 3.0	45.2 ± 2.6	49.3 ± 2.9	47.3 ± 2.6	48.7 ± 2.3	49.6 ± 2.7
Cl^-	**(mg L^{-1})**	6.4 ± 2.2	486 ± 71	128 ± 30	408 ± 12	147 ± 1	90 ± 3	110 ± 1	89 ± 1	268 ± 17	101 ± 1
F^-	**(mg L^{-1})**	< 0.25	0.51 ± 0.11	0.31 ± 0.03	NM	0.26 ± 0.01	0.76 ± 0.01	0.34 ± 0.04	0.34 ± 0.02	0.40 ± 0.08	0.33 ± 0.03
NO_2^-	**(μg L^{-1})**	14 ± 2	107 ± 19	94 ± 4	40 ± 16	134 ± 56	34 ± 9	52 ± 13	106 ± 27	221 ± 138	173 ± 52
NO_3^-	**(mg L^{-1})**	0.96 ± 0.41	24.6 ± 2.9	20.6 ± 0.1	43.8 ± 3.6	18.4 ± 0.1	1.37 ± 0.12	3.33 ± 0.13	19.7 ± 0.3	22.6 ± 0.2	26.9 ± 2.5
SO_4^{2-}	**(mg L^{-1})**	4.3 ± 0.3	136 ± 7	64 ± 4	268 ± 20	61 ± 1	195 ± 13	45 ± 3	55 ± 1	99 ± 5	78 ± 11
PO_4^{3-}	**(mg L^{-1})**	< 0.25	0.49 ± 0.07	0.38 ± 0.25	NM	< 0.25	0.43 ± 0.04	0.30 ± 0.10	0.61 ± 0.10	0.79 ± 0.26	1.10 ± 0.48

Data presented as "<" indicate values below the detection limit (DL). NM: Not measured.

Table 4.3 – Main and trace elements content of the various surface water samples. Data is presented as mean values ± standard deviations (n = 3).

Element		PUM	SC1	SC2	GAL	RUP	NIK	OLS	DEN	GTC	COC
K	**(mg L^{-1})**	0.75 ± 0.01	16.4 ± 2.5	9.12 ± 0.24	33.9 ± 1.8	8.72 ± 0.34	18.3 ± 2.2	6.78 ± 0.38	7.79 ± 0.05	12.3 ± 1.4	8.75 ± 0.14
Na	**(mg L^{-1})**	3.13 ± 0.08	138 ± 21	44.4 ± 1.5	482 ± 26	30.9 ± 8.5	38.7 ± 1.6	38.8 ± 0.6	21.8 ± 5.8	88.7 ± 0.8	37.7 ± 0.2
Ca	**(mg L^{-1})**	1.22 ± 0.32	111 ± 1	89.9 ± 1.1	60.1 ± 1.6	102 ± 4	121 ± 14	98.3 ± 4.4	110 ± 17	109 ± 1	113 ± 8
Mg	**(mg L^{-1})**	0.27 ± 0.15	39.0 ± 1.9	10.0 ± 0.4	104 ± 3	9.38 ± 1.03	24.0 ± 2.2	9.48 ± 0.82	13.5 ± 1.7	19.2 ± 1.0	10.0 ± 0.9
Al	**(mg L^{-1})**	0.29 ± 0.03	1.48 ± 0.17	3.39 ± 0.44	0.10 ± 0.01	4.00 ± 0.39	0.24 ± 0.02	0.15 ± 0.01	1.82 ± 0.31	0.38 ± 0.04	0.38 ± 0.05
Fe	**(mg L^{-1})**	0.75 ± 0.03	3.57 ± 0.16	7.42 ± 0.51	0.08 ± 0.01	17.7 ± 3.2	0.27 ± 0.01	0.59 ± 0.02	2.79 ± 0.42	0.60 ± 0.03	0.55 ± 0.07
Cr	**(μg L^{-1})**	< 4.0	8.36 ± 1.50	16.9 ± 0.6	< 4.0	19.9 ± 2.1	< 4.0	< 4.0	5.10 ± 1.19	< 4.0	< 4.0
Cu	**(μg L^{-1})**	< 10	< 10	15.4 ± 2.3	< 10	20.1 ± 1.9	< 10	< 10	< 10	< 10	< 10
Mn	**(μg L^{-1})**	< 5.0	138 ± 14	225 ± 23	< 5.0	335 ± 53	13.0 ± 1.0	530 ± 39	99.0 ± 30.0	86.9 ± 14.5	65.1 ± 21.6
Ni	**(μg L^{-1})**	< 12	< 12	16.5 ± 6.1	< 12	17.4 ± 6.4	< 12	< 12	< 12	< 12	< 12
Zn	**(μg L^{-1})**	31.1 ± 0.7	50.2 ± 4.0	101 ± 6	< 20	199 ± 21	59.1 ± 6.3	< 20	39.3 ± 8.2	< 20	22.3 ± 3.1

Data presented as "<" indicate values below the detection limit (DL). In all of the water samples, Ce, Cd, Co, and Pb concentrations were below the detection limit (DL_{Ce} = 6.3 μg L^{-1}; DL_{Cd} = 4.0 μg L^{-1}; DL_{Co} = 40 μg L^{-1}; DL_{Pb} = 40 μg L^{-1}).

4.3.3 Screening of settling recipients

Figure 4.1 shows the cerium recoveries (*i.e.*, the ratio between the final (C) and the actual measured initial (C_0) cerium concentration) after incubating CeO_2 ENPs or Ce^{3+} ions in Milli-Q® water at 4 to 6 °C during 7 d in borosilicate glass or polypropylene (PP) settling vessels. Recoveries approaching 100 % were observed for 5 mg L^{-1} CeO_2 ENPs, and in the case of 5 and 0.5 mg L^{-1} Ce^{3+} ions, for both glass and PP tubes (p > 0.05). However, for 0.5 mg L^{-1} CeO_2 ENPs, recoveries substantially decreased and varied between 10 and 58 % (p = 0.005), indicating potential adsorptive interactions of CeO_2 ENPs with the inner walls of the settling recipients. Therefore, PP tubes were chosen to serve as settling recipients during further experiments, and a sufficiently high initial test concentration (*i.e.*, 5 mg L^{-1}) was utilized, in order to minimize potential losses due to sorption, and to still be able to accurately quantify potentially low cerium contents remaining in solution after settling by means of ICP-OES.

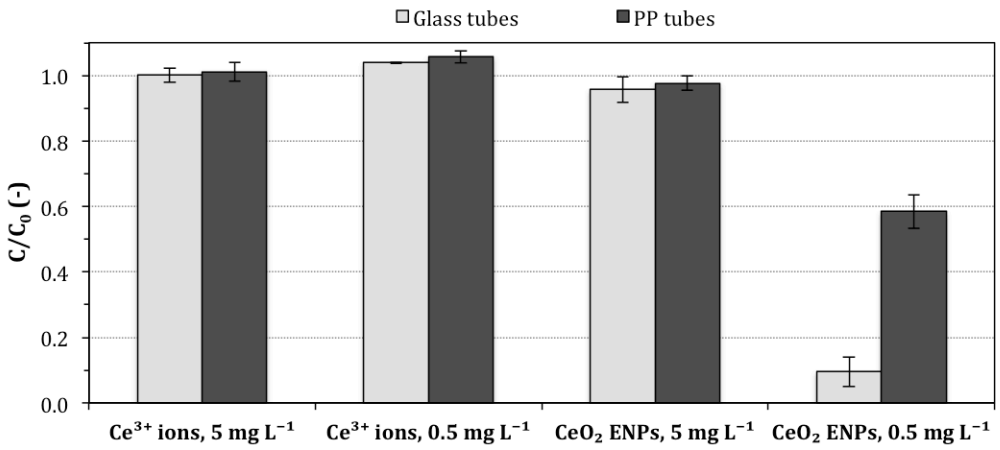

Figure 4.1 – Relative cerium content remaining in solution after 7 d incubation of CeO_2 ENPs or Ce^{3+} ions in Milli-Q® water at 4 – 6 °C, in either borosilicate glass or polypropylene (PP) settling recipients. Samples were shaken vigorously prior to determining the initial cerium concentration (C_0) and the cerium concentration after 7 d (C). (Bars represent mean values, error bars denote standard deviations, n = 3)

4.3.4 Settling of CeO_2 ENPs in natural surface waters

The depletion of 5 mg L^{-1} CeO_2 ENPs or Ce^{3+} ions in various (natural) aqueous matrices during 7 d is presented in Figure 4.2. For clarity purposes, error bars indicating standard deviations of the mean values were omitted from this figure, but have been included in Figure B.2 in Appendix B. Both the nanoparticles and ions remained stable in Milli-Q® water (Control) over the entire experimental time frame. Similarly, virtually no sedimentation was observed in the case of CeO_2 ENPs in PUM, and for Ce^{3+} ions in PUM and GAL. However, for all the other natural surface waters, between 85 and 96 % of the CeO_2 ENPs were already removed from the water phase after just 1 d of settling, and cerium recoveries near the liquid surface were reduced further in function of time (*i.e.*, more than 92 or 95 % removal after 3 or 7 d of settling, respectively). In the case of Ce^{3+} ions, between 16 and 50 % removal near the liquid surface was observed after 1 d, whereas after 3 or 7 d, a reduction of up to 53 or 68 % of the initial cerium concentration was noted, respectively.

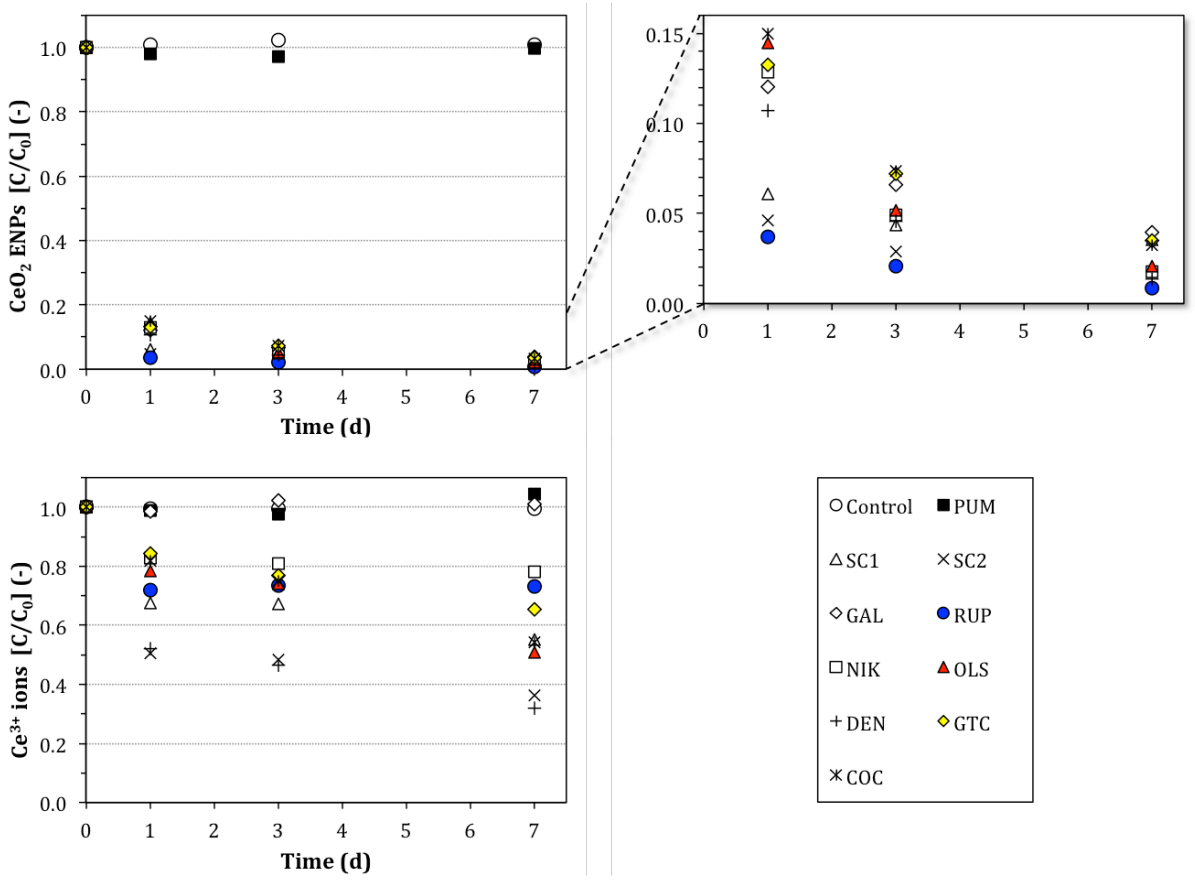

Figure 4.2 – Relative cerium content remaining in solution near the liquid surface after spiking 10 distinct natural surface waters as well as Milli-Q® water (Control) with 5 mg L^{-1} CeO_2 ENPs (top graph) or Ce^{3+} ions (bottom graph), and allowing the samples to settle for 1, 3, or 7 d under isothermal conditions (4 – 6 °C). (Data points represent mean values, n = 3)

It was also shown that losses due to potential sorption of ENPs or ions onto the inner walls of the settling recipients were minimal (*i.e.*, maximum 6 %) (Figure B.1 in Appendix B). Furthermore, no increase in "truly" dissolved cerium species (defined here as the fraction < 10 kDa) was observed after 7 d incubation of CeO_2 ENPs in natural surface waters. Actually, cerium contents in all of the 10 kDa UF filtrates were below the detection limit (DL_{Ce} = 4.0 μg L^{-1}), both at t_0 and after 7 d. These results, in combination with the observed low residual cerium contents, suggest that CeO_2 ENPs removal from the water column can be explained as sedimentation. The observed data were therefore interpreted by means of a semi-empirical first-order settling rate model (Equation 4.1), which was adapted from Quick *et al.* (2012) and can be used to describe the time-dependent removal of nanoparticles from the water phase.

$$\frac{C_t}{C_0} = \left(1 - \frac{C_{res}}{C_0}\right) e^{-k_{sed}t} + \frac{C_{res}}{C_0} \tag{4.1}$$

where C_t [mg L^{-1}] is the concentration at time t, C_0 [mg L^{-1}] is the initial concentration, C_{res} [mg L^{-1}] is the residual concentration, k_{sed} [d^{-1}] is the sedimentation or settling rate constant, and t [d] is the settling time.

Non-linear least squares regression analysis was employed to estimate the model parameters (Table 4.4), in order to test how this first-order sedimentation kinetics model is able to quantitatively describe the observed experimental data. Very good model fits were obtained ($R^2 \geq 0.998$) for CeO_2 ENPs settling in natural surface waters, except in the case of PUM (R^2 = 0.182). Moreover, the extent to which Equation 4.1 is able to describe the removal of Ce^{3+} ions from the water phase was also examined. Although the estimated model parameters indicate that the applied first-order model can describe the removal of CeO_2 ENPs from the water phase more accurately, good model fits were still also obtained in the case of Ce^{3+} ions for the majority of the surface water samples ($R^2 \geq 0.812$), with the exception of PUM (R^2 = 0.280) and GAL (R^2 = 0.166).

Graphs displaying the experimental data as well as the fitted regression curves describing the time-dependent settling of CeO_2 ENPs and depletion of Ce^{3+} ions in the different natural surface waters can be retrieved in Appendix B (Figure B.2).

Table 4.4 – Non-linear least squares regression estimated model parameters for Equation 4.1, describing the depletion of 5 mg L^{-1} CeO_2 ENPs or Ce^{3+} ions in 10 natural surface waters.

Sample ID	CeO_2 ENPs			Ce^{3+} ions		
	k_{sed} (d^{-1})	C_{res}/C_0 (-)	R^2 (-)	k_{sed} (d^{-1})	C_{res}/C_0 (-)	R^2 (-)
PUM	-	-	-	-	-	-
SC1	3.817	0.040	1.000	1.665	0.608	0.906
SC2	3.753	0.023	1.000	1.875	0.419	0.958
GAL	2.634	0.052	0.999	-	-	-
RUP	3.795	0.015	1.000	22.664	0.728	0.981
NIK	2.279	0.030	0.999	1.927	0.800	0.964
OLS	2.174	0.035	0.999	0.276	0.440	0.812
DEN	2.519	0.029	0.999	1.406	0.383	0.938
GTC	2.473	0.053	0.999	0.453	0.649	0.951
COC	2.266	0.052	0.998	0.275	0.479	0.893

C_{res}/C_0 is the relative residual concentration after infinite time, based on the data obtained after 7 d of settling.

R^2 is the determination coefficient.

The aggregation and sedimentation behaviour of nanoparticles in complex aqueous matrices depends on various solution characteristics, such as pH, ionic strength, and the presence of natural colloidal matter (Lin *et al.*, 2010; Tso *et al.*, 2010; Quik *et al.*, 2012). Pearson correlation analysis was performed to examine potential relationships between the physicochemical properties of the natural surface waters and the estimated model parameters k_{sed} and C_{res}/C_0 describing the settling of CeO_2 ENPs (Table 4.5). The data of PUM was omitted from the correlation analysis due to the low determination coefficient of the model fit. Statistically significant relationships were observed between k_{sed} and pH, TSS, Al, and Fe content, and between C_{res}/C_0 and TSS, PO_4^{3-}, Al, Fe, and Zn content.

Table 4.5 – Pearson correlation coefficients (r) and statistical significances (p) between surface water properties and the estimated model parameters describing the settling of 5 mg L^{-1} CeO_2 ENPs.

		pH	TSS	PO_4^{3-}	Al	Fe	Zn
k_{sed}	r	-0.673 *	0.873 **	-0.300	0.824 **	0.750 *	0.641
	p	0.047	0.002	0.484	0.006	0.020	0.171
C_{res}/C_0	r	-0.001	-0.774 *	0.780 *	-0.791 *	-0.753 *	-0.827 *
	p	0.997	0.014	0.038	0.018	0.019	0.043

** Correlation is significant at the 0.01 level (2-tailed).

* Correlation is significant at the 0.05 level (2-tailed).

Relationships between the estimated model parameters describing the removal of Ce^{3+} ions from the water phase and water properties were also studied (Table 4.6). As a result of the low determination coefficients of the model fits for PUM and GAL, these samples were excluded from the calculations. Statistically significant correlations were observed between k_{sed} and TSS, IC, Al, Fe, and Zn content, whereas C_{res}/C_0 correlated significantly with the amount of SO_4^{2-} and K in solution.

Table 4.6 – Pearson correlation coefficients (r) and statistical significances (p) between surface water properties and the estimated model parameters describing the depletion of 5 mg L^{-1} Ce^{3+} ions.

		TSS	IC	SO_4^{2-}	K	Al	Fe	Zn
k_{sed}	r	0.804 *	-0.765 *	-0.200	-0.169	0.715 *	0.932 **	0.931 **
	p	0.016	0.027	0.635	0.689	0.046	0.001	0.007
C_{res}/C_0	r	0.117	-0.277	0.716 *	0.708 *	-0.033	0.231	0.410
	p	0.782	0.506	0.046	0.049	0.939	0.582	0.007

** Correlation is significant at the 0.01 level (2-tailed).

* Correlation is significant at the 0.05 level (2-tailed).

4.4 Discussion

4.4.1 Settling of CeO_2 ENPs in natural surface waters

The sedimentation of CeO_2 ENPs and depletion of Ce^{3+} ions in 10 distinct natural surface waters was examined during 7 d, under isothermal conditions (4 – 6 C°). A first-order kinetics model proposed by Quick *et al.* (2012) was then applied to the experimental data in an attempt to quantitatively describe the time-dependent removal of nanoparticles and ions from the water column. The model parameters (k_{sed} and C_{res}/C_0) were estimated for each surface water sample by means of non-linear least squares regression. Finally, potential physicochemical factors affecting the sedimentation behaviour were investigated.

A significant reduction of CeO_2 ENPs near the liquid surface was observed for all but one of the tested surface waters, and the first-order model was able to describe the evolution of cerium concentration over time in those samples very well ($R^2 \geq 0.998$). However, similar to the controls (*i.e.*, Milli-Q® water), no considerable removal of CeO_2 ENPs was observed in PUM, and the model was therefore not appropriate to describe the

experimentally observed data in this case. Additionally, the proposed model was also capable of describing the time-dependent removal of Ce^{3+} ions from the water phase reasonably well ($R^2 \geq 0.812$) for 8 out of 10 water samples. In all cases, CeO_2 ENPs appeared to be less stable in suspension compared to Ce^{3+} ions, as indicated by the higher settling rate constants and the lower residual fractions.

The fate and transport of natural colloids is controlled by aggregation and sedimentation processes. Removal of particulates from suspension is determined by their settling velocity, which in turn depends on particle size, density, and friction factor (Quick *et al.*, 2010). Particle aggregation results in larger particulates that generally settle much more rapidly and to a greater extent. Aggregation occurs as a consequence of collision and attachment of two particulates, and is affected by both particle properties as well as the physicochemical characteristics of the receiving medium (Hotze *et al.*, 2010).

Solution-pH plays a crucial role in the colloidal stability of nanoparticles by affecting their surface charge and hence their potential propensity to aggregate. When the pH of an aquatic system is at the isoelectric point (IEP) the colloidal system exhibits minimal stability and the particles tend to aggregate and settle from the water column (Lin *et al.*, 2010; Hotze *et al.*, 2010). Although not experimentally determined in this study, the IEP of CeO_2 ENPs in water has been reported to be situated around pH 8 (Van Hoecke *et al.*, 2009; Quik *et al.*, 2010). Therefore, the low pH of PUM (4.95) is most likely the dominant factor governing the high stability of the CeO_2 ENPs in this water sample by providing an enhanced electrostatic repulsion between the particles, whereas the pH of all the other surface waters was more closely situated near the expected IEP, leading to particle aggregation and subsequent sedimentation.

The ionic strength (IS) of a solution, which is a function of the concentration of all dissolved ionic species, can also influence the fate and behaviour of nanoparticles. An increase in IS (at fixed pH) induces a compression of the electrical double layer of dispersed nanoparticles, thereby reducing the repulsive forces and promoting potential particle aggregation and subsequent sedimentation (Hotze *et al.*, 2010). However, no significant relationship between the EC (which is a measure for the IS) and the settling rate or the residual content was observed in this study. This could be due to the fact that no linear relationship exists between IS and the attachment efficiency. Furthermore, pH as well as the type and valence of background electrolytes also affect the attachment efficiency (*e.g.*, a higher IS with NaCl will be less detrimental than a lower IS with $CaCl_2$) (Lin *et al.*, 2010;

Hotze *et al.*, 2010). Within a certain range, a reaction-controlled regime may dominate and an increase in IS results in a higher attachment efficiency. Yet, above a certain threshold (*i.e.*, the critical coagulation concentration), a diffusion-controlled regime exists, where the attachment efficiency is barely affected by the IS (Liu *et al.*, 2011). The EC data (*i.e.*, very low EC for PUM compared to high EC values for all the other water samples) suggest that the latter regime might be dominant in the tested surface waters (except for PUM), which would also be a further consequence from the fact that the pH of all waters (except for PUM) approaches the IEP of the CeO_2 ENPs.

The concentration of total suspended solids (TSS) in the surface waters was determined as the fraction of compounds retained on a 0.45 μm filter. Quik *et al.* (2012) already reported that hetero-aggregation with or deposition onto natural colloidal matter might be the dominant mechanism for nanoparticle removal from the water column. In this study, significant correlations between TSS and the estimated model parameters were also obtained, indicating that a higher amount of TSS leads to a higher settling rate and a lower residual fraction of the nanoparticles and ions. Additionally, similar significant relationships were observed for Al and Fe content, potentially suggesting association and co-precipitation of CeO_2 ENPs and Ce^{3+} ions with aluminium- and iron-containing compounds. The predicted very high k_{sed} value (22.664 d^{-1}) for Ce^{3+} ions in RUP is a consequence of the fact that the residual cerium content was already attained at the first sampling time point (1 d), which is potentially the result of association of the Ce^{3+} ions with natural suspended matter as this water sample was characterized by the highest TSS content. As the amount of suspended solids was shown to be an important factor in describing the removal of CeO_2 ENPs from the water phase, the observed high stability of CeO_2 ENPs in PUM might possibly in part also be explained by the low amount of TSS in this sample. Similarly, the high residual cerium fractions of Ce^{3+} ions in PUM and GAL might also be due to their low TSS contents. Furthermore, a higher PO_4^{3-} or lower Zn content appeared to increase the residual cerium fraction of CeO_2 ENPs remaining in suspension. Surface adsorption of phosphate, resulting in a net negative charge, has already been demonstrated to increase the stability and transport of CeO_2 and Al_2O_3 ENPs (Darlington *et al.*, 2009; Cornelis *et al.*, 2011).

The impact of initial concentration (C_0) on the sedimentation of CeO_2 ENPs was not studied in this work. According to previous reports, a higher C_0 results in a higher settling rate and a lower residual concentration (Keller *et al.*, 2010; Quik *et al.*, 2012). Therefore it should be mentioned that because the concentrations of CeO_2 ENPs in natural surface

waters are expected to be less than the C_0 used in this study (*i.e.*, 5 mg L^{-1}), settling rates might potentially be lower under more realistic environmental conditions. Moreover, for extrapolation of the observed results towards for instance other systems or nanoparticulate species, one should bear in mind the increasing complexity of the natural environment (*e.g.*, an increased shear stress due to turbulent flow conditions or potential interactions with (micro)organisms), as stated by Quik *et al.* (2012). Furthermore, it should be noted that the time-dependent settling of CeO_2 ENPs was described on a mass concentration basis, and it is plausible that the physicochemical properties of the particles remaining suspended might have altered over time and thus differ from the characteristics of the initially added nanoparticles, this however merits further investigation.

4.4.2 Ionic release from CeO_2 ENPs in natural surface waters

From an (eco)toxicological point of view it is interesting to study the dissolution behaviour of nanoparticles, as differences often exist in bioavailability and toxicity towards organisms between nanoparticles and dissolved ions. Actually, the majority of induced toxic effects are generally attributed to the ionic species released from the particles rather than to stem from the nanoparticles themselves (Mudunkotuwa and Grassian, 2011). Dissolution is a surface-controlled process and smaller particulates will dissolve more easily due to their larger specific surface area. For instance, Elzey and Grassian (2010a) have demonstrated that Ag ENPs (10 nm) dissolved more easily than bulk Ag particles (10 μm) under the same controlled conditions. In this study, dissolution was assessed by means of 10 kDa UF, and although no dissolved cerium was detected after 7 d, this does not necessarily mean that entirely no ionic release from the particle surface has occurred. For instance, dissolved ions could have associated with NOM or suspended solids, inhibiting them to permeate into the UF filtrates. However, CeO_2 ENPs have been found to be relatively insoluble under various experimental conditions (Van Hoecke *et al.*, 2009; Rogers *et al.*, 2010a; Cornelis *et al.*, 2011). These observations together with the obtained low residual cerium fractions do suggest that dissolution of the CeO_2 ENPs was most likely negligible. Nevertheless, real environmental risks may still exist, as this study has shown that CeO_2 ENPs could remain stable in suspension under certain conditions, potentially leading to a high mobility and bioavailability, and because previous studies have already demonstrated CeO_2 ENPs to induce toxic effects in for example bacteria, freshwater algae, and human lung cells (Thill *et al.*, 2006; Van Hoecke *et al.*, 2009; Rogers *et al.*, 2010a; Zhang *et al.*, 2011a).

4.5 Conclusion

For the majority of the tested natural surface waters, substantial removal of CeO_2 ENPs from near the liquid surface was observed. In all cases, reduction of CeO_2 ENPs from the water column was considerably higher compared to Ce^{3+} ions. The observed time-dependent removal could be described well by means of a first-order kinetics model, in case significant sedimentation occurred over time. Solution-pH appeared to be a prime determinant governing nanoparticle colloidal stability, as virtually no sedimentation occurred in case the pH differed considerably from the isoelectric point. Furthermore, the amount of suspended matter also appeared to be an important factor affecting the settling rate and residual fraction of cerium remaining in solution, and results indicated potential association of CeO_2 ENPs as well as Ce^{3+} ions with aluminium- and iron-containing natural compounds. This in combination with additional physicochemical water properties (*e.g.*, ionic strength) eventually determined nanoparticle stability and subsequent sedimentation kinetics. The CeO_2 ENPs seemingly remained stable in suspension in surface water characterized by a low pH, ionic strength, and suspended solids content. Furthermore, dissolution of the nanoparticles in all natural surface water samples appeared to be negligible during the 7 d experimental time frame.

Further research is needed in order to extrapolate the observed results towards natural systems. For instance, the expected nanoparticle concentrations in natural waters will be a lot lower compared to the initial concentrations tested in this work. Furthermore, increased shear stress due to turbulent flow conditions, or possible interactions with organisms, are also factors to be reckoned with. Therefore, additional experimental studies are required in order to describe and identify factors affecting the settling and dissolution behaviour of distinct engineered nanoparticles, and elucidate their physicochemical behaviour and ultimate fate in aquatic environments.

Chapter 5

Impact of water composition on association of Ag and CeO_2 nanoparticles with aquatic macrophyte *Elodea canadensis*

5 Impact of water composition on association of Ag and CeO_2 nanoparticles with aquatic macrophyte *Elodea canadensis*[‡]

5.1 Introduction

Engineered nanoparticles (ENPs) can be defined as particles having all three dimensions at the nanoscale (1 – 100 nm), which have been deliberately manufactured to have a particular size, composition, or possess other specific properties (Handy *et al.*, 2008b; Gubbins *et al.*, 2011). In recent years, these particles have increasingly been implemented in a wide spectrum of products and applications, including cosmetics, pharmaceuticals, electronics, textiles, catalysts, and environmental remediation, due to their often unique and size-related properties (Handy *et al.*, 2008b; Klaine *et al.*, 2008). However, the increased production and use of ENPs in combination with their extraordinary characteristics have also raised concern within the scientific community in regard to the potential adverse impact these materials may have on terrestrial and aquatic ecosystems, upon their expected inevitable release into the environment (Nowack and Bucheli, 2007; Handy *et al.*, 2008b; Klaine *et al.*, 2012). Engineered nanomaterials may enter the aquatic environment via various pathways, including spills, product use and disposal, storm events, erosion, leaching, surface run-off, and effluent discharges. (Glenn *et al.*, 2012; Glenn and Klaine, 2013). Extensive knowledge on their environmental behaviour and fate is thus essential and can aid in improving risk assessment (Keller *et al.*, 2010; Juhel *et al.*, 2011; Glenn *et al.*, 2012).

To date, metallic nanoparticles such as Ag and CeO_2 ENPs are amongst the most widely used engineered nanomaterials (Keller *et al.*, 2010; Fabrega *et al.*, 2011). The antimicrobial properties of Ag ENPs have led to their widespread use in many consumer products (*e.g.*, textiles, cosmetics, detergents, and food packaging) (Wijnhoven *et al.*, 2009; Fabrega *et al.*, 2011), while CeO_2 ENPs have for instance been used as diesel fuel additives, polishing agents, electrolytes in fuel cells, and in cosmetics (Keller *et al.*, 2010; Karakoti *et al.*, 2012;

[‡] *Submitted for publication as: Van Koetsem, F., Xiao, Y., Luo, Z., and Du Laing, G.* ***Impact of water composition on association of Ag and CeO_2 nanoparticles with aquatic macrophyte Elodea canadensis.***

Shah *et al.*, 2012). Yet, evidence of their potential toxicity towards (aquatic) organisms and even human cells is also emerging, especially in the case of Ag ENPs (Thill *et al.*, 2006; Blaser *et al.*, 2008; Navarro *et al.*, 2008a; Van Hoecke *et al.*, 2009; Rogers *et al.*, 2010a; Ma *et al.*, 2011; Zhang *et al.*, 2011a; Levard *et al.*, 2012; Karakoti *et al.*, 2012; Shah *et al.*, 2012; Jiang *et al.*, 2014).

Aquatic plants constitute a key community within aquatic ecosystems, as they can be primary producers, provide surface area for bacteria, serve as a food source for various organisms, provide oxygen and a habitat for invertebrates, fish, and amphibians, and play a role in the biogeochemical cycling of nutrients and pollutants (Gubbins *et al.*, 2011; Jiang *et al.*, 2011; Larras *et al.*, 2013). Thus, aquatic plants represent a large interface for potential interactions with nanoparticles, and could play a crucial part in the fate and transport of ENPs through plant uptake and bioaccumulation from the water column and/or from the sediment bed, potentially facilitating trophic transfer (Monica and Cremonini, 2009; Glenn *et al.*, 2012; Glenn and Klaine, 2013). However, detailed studies on the interactions between metallic ENPs and aquatic plants are still very scarce, especially in regard to submerged plant species such as *Elodea canadensis* (Navarro *et al.*, 2008a; Ma *et al.*, 2010; Glenn *et al.*, 2012; Glenn and Klaine, 2013).

Moreover, besides the existing uncertainties concerning the probable nanoparticle-plant uptake, translocation and toxicity mechanisms, there is also a paucity of information regarding the factors affecting their bioavailability and association with aquatic plants (Rico *et al.*, 2011; Miralles *et al.*, 2012; Glenn and Klaine, 2013). These factors may include nanoparticle characteristics such as size, morphology, composition, and surface chemistry, as well as water quality parameters including pH, ionic strength, electrolyte composition, and natural organic matter content, which can influence nanoparticle aggregation and stability in suspension (Keller *et al.*, 2010; Rico *et al.*, 2011; Miralles *et al.*, 2012; Glenn and Klaine, 2013). For instance, Glenn *et al.* (2012) reported that root uptake of Au ENPs by submerged aquatic plants was dependent on particle size and on plant species, while a later study also demonstrated that absorption of Au ENPs by the aquatic plants decreased in the presence of dissolved organic carbon (Glenn and Klaine, 2013).

E. canadensis is considered as a good model candidate for metal accumulation and phytotoxicity tests because it is a widespread, well-studied species that has been shown to accumulate metal pollutants (*e.g.*, Cd, Cr, Cu, Pb, and Zn) from both water and sediments (Kähkönen *et al.*, 1997; Fritioff and Greger, 2007; Nyquist and Greger 2007; Thiébaut *et al.*,

2010; Chu *et al.*, 2014). However, studies investigating potential interactions between metallic ENPs and *E. canadensis* are very scant (Johnson *et al.*, 2011; Jacob *et al.*, 2013), and to the best of our knowledge, no research reports concerning the potential uptake of Ag or CeO_2 ENPs by *E. canadensis* nor their possible phytotoxic effects on this submerged aquatic macrophyte have been published at present.

The main objective of this study was to examine the potential association of Ag and CeO_2 ENPs with *E. canadensis* and determine factors which may affect the partitioning of the nanoparticles between plant biomass and the water phase in complex (natural) aqueous matrices, in order to contribute to the existing knowledge on the fate and behaviour of metallic nanoparticles in aquatic environments. Therefore, 72-hour lasting batch experiments were set up whereby *E. canadensis* plants were incubated in five distinct (natural) water samples and exposed to varying concentrations of Ag or CeO_2 ENPs. For comparison purposes, experiments with Ag^+ and Ce^{3+} ions were performed in the same way.

5.2 Materials and methods

5.2.1 Nanoparticles and chemical reagents

Aqueous dispersions of citrate-coated Ag ENPs (100 mg L^{-1}, APS: *ca.* 10 nm, ζ-potential: -50 ± 5 mV, pH: 6 – 8) and CeO_2 ENPs (50 000 mg L^{-1}, APS: 4 ± 2 nm, ζ-potential: +40 ± 5 mV) were acquired from PlasmaChem GmbH (Berlin, Germany). Additional information on particle size, morphology, and apparent surface charge of these ENPs was obtained by means of photon correlation spectroscopy (PCS) (Malvern PCS-100SM, Malvern Instruments Ltd., Worcestershire, UK), transmission electron microscopy (TEM) (JEM-2200FS, Jeol Ltd., Tokyo, Japan), and zeta (ζ) potential measurements (Zetasizer 3000 HSa, Malvern Instruments Ltd., Worcestershire, UK), respectively. PCS measurements were performed in triplicate, at 25 °C, using a laser (HeNe, 633 nm) scattering angle of 150 degrees. Cumulant analysis provided the so-called *Z*-average hydrodynamic particle size, whereas particle size distributions (PSDs) were obtained through multi modal analysis. Silver (as $AgNO_3$) (Plasma HIQU, 1000 ± 2 μg Ag^+ mL^{-1} in 2 – 5 % HNO_3) and cerium (as $Ce(NO_3)_3$) (Plasma HIQU, 10 000 ± 20 μg Ce^{3+} mL^{-1} in 2 – 5 % HNO_3) reference standard solutions were purchased from ChemLab NV (Zedelgem, Belgium), and were utilized as the ionic counterparts (*i.e.*,

Ag^+ ions and Ce^{3+} ions) of Ag and CeO_2 ENPs in the batch experiments (see Section 5.2.4). All chemicals used in this study were of analytical grade, and were either obtained from ChemLab NV or from Merck KGaA (Darmstadt, Germany). Prior to being used, all recipients were acid-washed with 10 % HNO_3, disinfected with a 5 % ethanol solution, and thoroughly rinsed with ultrapure water (18.2 MΩ cm^{-1}) (Milli-Q®, EMD Millipore Corp., Billerica, MA, USA).

5.2.2 Test plant species

Elodea canadensis plants, which were purchased from a reputed nursery and distributor of aquatic plants (Van der Velde Waterplanten BV, Bleiswijk, The Netherlands), were cultivated in glass aquarium tanks containing a modified 10 % Hoagland's solution (Table 5.1), at room temperature, and under a 14 h:10 h light:dark illumination cycle. The growth medium in the water tanks was renewed every 7 d. All plants that were selected for this study appeared healthy and had no visible periphyton growth. Prior to experimental use, all selected plants were rinsed with Milli-Q® water, gently patted dry with disposable tissue wipes, and weighed.

Table 5.1 – Composition of the modified 10 % Hoagland's E-medium.

	Compound	**Molar mass (g mol^{-1})**	**Concentration (μM)**
Macronutrients	$MgSO_4.7H_2O$	246.48	99.8
	$Ca(NO_3)_2.4H_2O$	236.15	230
	KH_2PO_4	136.09	50
	KNO_3	101.11	250
Micronutrients	H_3BO_3	61.83	2.31
	$MnCl_2.4H_2O$	197.84	0.460
	$ZnSO_4.7H_2O$	287.54	0.038
	$Na_2MoO_4.2H_2O$	241.95	0.019
	$CuSO_4.5H_2O$	249.68	0.018
Fe-chelate	$FeCl_3.6H_2O$	270.33	3.58
	EDTA	292.24	10.3

After the UTCC formulation of Hoagland's E-medium by Acreman (2013).

5.2.3 Surface water sampling and characterization

Three different surface water sources were sampled (± 20 L) in Flanders, Belgium (Table 5.2). The collected surface water samples, together with tap water, as well as the modified 10 % Hoagland's solution, were thoroughly characterized before being put to experimental use. A pH electrode (Model 520A, Orion Research Inc., Boston, MA, USA) was used to directly measure the pH values of the water samples. The Electrical conductivity (EC) was measured by means of a conductivity probe (LF537, WTW, Weilheim, Germany). A TOC analyser (TOC-V_{CPN}, Shimadzu, Kyoto, Japan) was used to determine the total organic carbon (TOC) and inorganic carbon (IC) content of the different samples directly. The amount of total suspended solids (TSS) was acquired via (vacuum) filtration of 250 mL of water sample over pre-dried (at 105 °C) and pre-weighed 0.45 μm membrane filters (Porafil RC, Macherey-Nagel GmbH & Co. KG, Düren, Germany), and recording the mass difference after drying the used filters again in an oven at 105 °C for at least 1 h. In a comparable manner, the dry residue (DR) was determined by evaporating 100 mL of water sample in pre-weighed glass beakers in an oven at 105 °C until a constant mass, and recording the final mass difference. Anions (*i.e.*, F^-, Cl^-, NO_3^-, PO_4^{3-}, and SO_4^{2-}) present in the water samples were measured via ion exchange chromatography (IEC) (761 Compact IC, Metrohm AG, Herisau, Switzerland). Finally, the main elements content (*i.e.*, K, Na, Ca, and Mg) as well as the Ag and Ce concentration in the different water samples was quantified by means of inductively coupled plasma optical emission spectrometry (ICP-OES) (Vista-MPX CCD Simultaneous ICP-OES, Agilent Technologies, Santa Clara, CA, USA), after being subjected to liquid digestion (*i.e.*, 5 mL 65 % HNO_3 and 2 mL 30 % H_2O_2 was added to 50 mL of water sample, and the mixture was boiled on a hotplate for 2 h under reflux using a beaker and a watch glass) and filtration over acid-resistant filter paper (MN 640 m, Macherey-Nagel GmbH & Co. KG, Düren, Germany).

Table 5.2 – Detailed overview of the different surface waters that were sampled.

Sample ID	Surface water	Type	Location	Coordinates	
				Latitude	Longitude
MB	Mostbeek	Stream	Lochristi	51° 03' 36" N	03° 51' 03" E
GG	Grote Geule	Creek	Assenede	51° 14' 45" N	03° 44' 42" E
CC	Coupure Canal	Canal	Ekkergem (Ghent)	51° 03' 11" N	03° 42' 35" E

5.2.4 Nanoparticle exposure experiments

A first set of batch experiments was performed to examine the dose-dependent removal of Ag and CeO_2 ENPs, as well as Ag^+ and Ce^{3+} ions by *E. canadensis*. Individual plants with approximately the same fresh weight (FW) (1 ± 0.5 g) and size (*ca.* 16 cm) were selected, transferred into 100 mL polypropylene cylindrical recipients (250 × 33 mm), and exposed to varying concentrations of nanoparticles or ions (*i.e.*, 0, 0.05, 0.1, 0.25, 0.5, and 1 mg L^{-1} of Ag ENPs or Ag^+ ions, and 0, 0.5, 1, 5, 10, and 50 mg L^{-1} in the case of CeO_2 ENPs or Ce^{3+} ions). Tap water, which was chosen to limit nutrients and restrict potential periphyton growth, was used to prepare the various incubation solutions (100 mL). The aquatic macrophytes were all entirely immersed in solution, and were incubated at room temperature for 72 h under a fixed 14 h:10 h light:dark photoperiod. Five replicates were included in the set-up for each treatment, three of which for silver, cerium, and total phosphorous (TP) determination, and two for total nitrogen (TN) and chlorophyll (Chl) analysis (see Section 5.2.6). All treatment solutions were sampled before immersing the plants (t_0) as well as after 72 h of incubation, and the remaining silver and cerium concentrations were determined (see Section 5.2.5).

A second and final series of batch tests were carried out to evaluate the effect of water composition on the removal of Ag and CeO_2 ENPs, or Ag^+ and Ce^{3+} ions from the water phase by *E. canadensis*. The experimental outline was similar as described above, with the exception that *E. canadensis* plants were only exposed to one fixed concentration of nanoparticles or ions (*i.e.*, 0.1 mg L^{-1} of Ag ENPs or Ag^+ ions, or 1 mg L^{-1} in the case of CeO_2 ENPs or Ce^{3+} ions), and that five water types differing in physicochemical properties (*i.e.*, tap water, 10 % Hoagland's solution, and three natural surface waters: *MB, GG, and CC*) were used to prepare the incubation solutions. Each treatment consisted of three replicate plants, which were harvested after 72 h of incubation at room temperature under a 14 h:10 h light:dark photoperiod, and were analysed for silver and cerium content. Control samples (*i.e.*, without exposure to ENPs or ions) were again also included in the set-up. Additionally, in order to assess the removal kinetics of ENPs or ions from the water phase in the presence of *E. canadensis*, aliquots were sampled at t_0, and after 2, 6, 10, 24, 48, and 72 h, and the silver and cerium concentrations were determined (see Section 5.2.5).

5.2.5 Water aliquots analysis

Prior to sampling 2 mL aliquots from the water phase at the designated time points, each incubation recipient was gently inversed manually to (re)homogenize the treatment solution. The sampled aliquots were then acidified with 4 mL 65 % HNO_3 and left to stand under a fume hood overnight. Subsequently, the aliquots were subjected to open vessel microwave digestion at 100 °C for 1.5 h using a microwave accelerated reaction system (MARS 5, CEM Corp., Matthews, NC, USA) operating at 600 W, and were analysed for silver or cerium content via ICP-OES or inductively coupled plasma mass spectrometry (ICP-MS) (Elan DRC-e, PerkinElmer Inc., Waltham, MA, USA).

5.2.6 Plant sampling and analysis

E canadensis plants were harvested after 72 h of exposure, allowed to drip dry, and carefully patted with disposable tissue wipes, and weighed. The plants were not rinsed after being harvested to retain any ENPs or ions that might be sorbed onto the surface of the aquatic macrophytes. Three plant replicates (out of five) were then dried in an oven at 55 °C for 24 h and weighed again. Afterwards, the dried plants were pre-digested with 5 mL 65 % HNO_3 overnight under a fume hood, before being subjected to open-vessel microwave digestion (under the same operating conditions as mentioned in Section 5.2.5). Finally, the amount of silver and cerium in the digested plant samples was measured by means of ICP-OES or ICP-MS, whereas the amount of TP was obtained via the colorimetric method of Scheel (Van Ranst *et al.*, 1999). The two remaining plant replicates (only for the "dose experiments") were combined and divided up for TN and Chl analysis. The TN content was determined according to the modified Kjeldahl method by digesting 0.1 g dried plant material with 7 mL sulphuric/salicylic acid reagent, followed by alkalization with NaOH and steam distillation using a Vapodest Kjeldahl distillation system (Gerhardt GmbH & Co. KG, Königswinter, Germany) (Van Ranst *et al.*, 1999). The Chl *a*, *b*, and *c* was established according to a standard spectrophotometric procedure (*i.e.*, the trichromatic method) after addition of 15 mL aqueous acetone to 0.5 g fresh plant material and macerating the sample (Clasceri *et al.*, 1999). Additional details on TP, TN, and Chl determination are outlined in Appendix C.

5.2.7 Data processing

Analysis of variance (ANOVA), Pearson's product-moment correlation analysis, and linear and non-linear least squares regression analysis were performed using SPSS Statistics 22 (IBM, Armonk, NY, USA). Shapiro-Wilk's test was utilized to check for normality of data. Levene's test was employed to test for homogeneity of variances, and Welch's *t*-test was used instead of ANOVA in case the conditions from Levene's test were violated. Significant mean differences were further examined via Tukey's HSD or Games-Howell's *post-hoc* tests in the case of ANOVA or Welch's *t*-test, respectively. Excel (Microsoft Corp., Redmond, WA, USA) and SigmaPlot 12 (Systat Software Inc., Chicago, IL, USA) were utilized for numerical and graphical data processing.

5.3 Results and discussion

5.3.1 Nanoparticle characterization

According to PCS measurements, the *Z*-average particle size of the Ag and CeO_2 ENPs dispersed in Milli-Q® water was 14.1 ± 1.0 nm and 6.7 ± 1.2 nm, respectively. The Ag ENPs had a ζ-potential of -43.4 ± 5.0 mV (at pH 5), whereas this was +51.1 ± 5.6 mV (at pH 6.5) for the CeO_2 ENPs (n = 3). On overall, both the measured particle size and apparent surface charge are thus in agreement with what was stated by the manufacturer. TEM analyses indicated that all nanoparticles seemingly possess a spherical morphology (Figure C.1 in Appendix C). Furthermore, although the majority of the Ag ENPs were indeed confirmed to be approximately 10 nm in size, both visualisation via TEM and the particle size distributions obtained via PCS also suggested the presence of larger-sized particles (between 10 and 80 nm) in suspension (Figure C.1 in Appendix C). In contrast, the CeO_2 ENPs showed a narrow unimodal particle size distribution (Figure C.1 in Appendix C), which indicates a highly monodisperse system.

5.3.2 Water characterization

Table 5.3 presents various physicochemical characteristics of the (surface) water samples, which were shown to differ significantly amongst each other. The pH of the water

samples was slightly alkaline (7.6 – 8.0), except for the 10 % Hoagland's medium which had a pH of 5.8. On overall, GG contained the largest amount of anionic species and major elements, and had the highest EC (2240 μS cm^{-1}), DR (1274 mg L^{-1}), and IC content (67 mg L^{-1}). In contrast, the 10 % Hoagland's solution was characterized by the lowest EC (108 μS cm^{-1}), and DR (64 mg L^{-1}) content, and generally also contained the least amount of anions and main elements. Furthermore, the highest TOC (10.7 mg L^{-1}), SO_4^{2-} (192 mg L^{-1}), and Ca (114 mg L^{-1}) content, as well as the lowest NO_3^- (13.6 mg L^{-1}) and K (2.73 mg L^{-1}) concentrations were noted for MB. Finally, the highest amount of TSS (16 mg L^{-1}) and the lowest TOC content were observed for CC and tap water, respectively.

Table 5.3 – Physicochemical properties of the different (surface) water samples. Data is presented as mean ± standard deviation (n = 3). Different letters indicate statistically significant differences (p < 0.05) between samples for each parameter.

Parameter		Tap water	10 % Hoagland's	MB	GG	CC
pH	**(-)**	7.7 ± 0.1 ^{bc}	5.8 ± 0.2 ^{a}	7.9 ± 0.1 ^{bc}	8.0 ± 0.2 ^{c}	7.6 ± 0.1 ^{b}
EC	**(μS cm^{-1})**	614 ± 3 ^{b}	108 ± 1 ^{a}	711 ± 3 ^{c}	2240 ± 6 ^{e}	871 ± 2 ^{d}
TSS	**(mg L^{-1})**	< 0.3	< 0.3	14 ± 1 ^{b}	6.0 ± 1.9 ^{a}	16 ± 1 ^{b}
DR	**(mg L^{-1})**	298 ± 10 ^{b}	64 ± 10 ^{a}	497 ± 8 ^{c}	1274 ± 17 ^{e}	548 ± 26 ^{d}
TOC	**(mg L^{-1})**	< 0.25	0.54 ± 0.09 ^{a}	10.7 ± 0.2 ^{d}	5.7 ± 0.9 ^{c}	2.6 ± 0.3 ^{b}
IC	**(mg L^{-1})**	35 ± 1 ^{b}	< 0.25	19 ± 1 ^{a}	67 ± 1 ^{d}	54 ± 1 ^{c}
Cl^-	**(mg L^{-1})**	34 ± 3 ^{b}	2.3 ± 1 ^{a}	46 ± 1 ^{c}	490 ± 3 ^{e}	79 ± 1 ^{d}
F^-	**(mg L^{-1})**	< 0.25	< 0.25	< 0.25	0.40 ± 0.01	< 0.25
NO_3^-	**(mg L^{-1})**	21.9 ± 1.1 ^{b}	36.4 ± 0.2 ^{d}	13.6 ± 0.9 ^{a}	36.4 ± 0.8 ^{d}	26.7 ± 0.6 ^{c}
SO_4^{2-}	**(mg L^{-1})**	68.1 ± 0.6 ^{b}	9.8 ± 0.1 ^{a}	192 ± 1 ^{e}	97.9 ± 0.6 ^{d}	76.6 ± 0.3 ^{c}
PO_4^{3-}	**(mg L^{-1})**	< 1.0	2.26 ± 0.06	< 1.0	< 1.0	< 1.0
K	**(mg L^{-1})**	2.73 ± 0.01 ^{a}	5.90 ± 0.13 ^{b}	8.90 ± 0.24 ^{c}	16.2 ± 0.2 ^{e}	9.55 ± 0.03 ^{d}
Na	**(mg L^{-1})**	22.8 ± 0.6 ^{a}	< 6.3	22.5 ± 0.4 ^{a}	205 ± 4 ^{c}	43.8 ± 0.7 ^{b}
Ca	**(mg L^{-1})**	81.3 ± 0.4 ^{b}	11.1 ± 0.1 ^{a}	114 ± 1 ^{e}	103 ± 1 ^{c}	106 ± 1 ^{d}
Mg	**(mg L^{-1})**	7.97 ± 0.03 ^{b}	2.78 ± 0.02 ^{a}	9.32 ± 0.10 ^{c}	45.1 ± 0.4 ^{e}	10.7 ± 0.1 ^{d}

Data presented as "<" indicate values below the detection limit (DL). In all of the water samples, Ag and Ce concentrations were below the detection limit (DL_{Ag} = 5.3 μg L^{-1}; DL_{Ce} = 6.7 μg L^{-1}).

5.3.3 Dose-dependent removal of Ag and CeO_2 ENPs by *E. canadensis*

Figure 5.1 depicts the dose-dependent depletion of silver or cerium in solution upon incubation of *E. canadensis* for 72 h in tap water spiked with Ag or CeO_2 ENPs, and Ag^+ or Ce^{3+} ions. For all treatments, the silver and cerium concentrations remaining in solution were significantly reduced after 72 h in the presence of the plants ($p < 0.05$). The remaining silver contents varied between 20 and 57 %, or between 26 and 54 % of the initially added amounts of Ag ENPs or Ag^+ ions, respectively. In the case of CeO_2 ENPs or Ce^{3+} ions, the remaining cerium concentrations ranged between 22 and 66 %, or between 19 and 63 % of the initial concentrations, respectively.

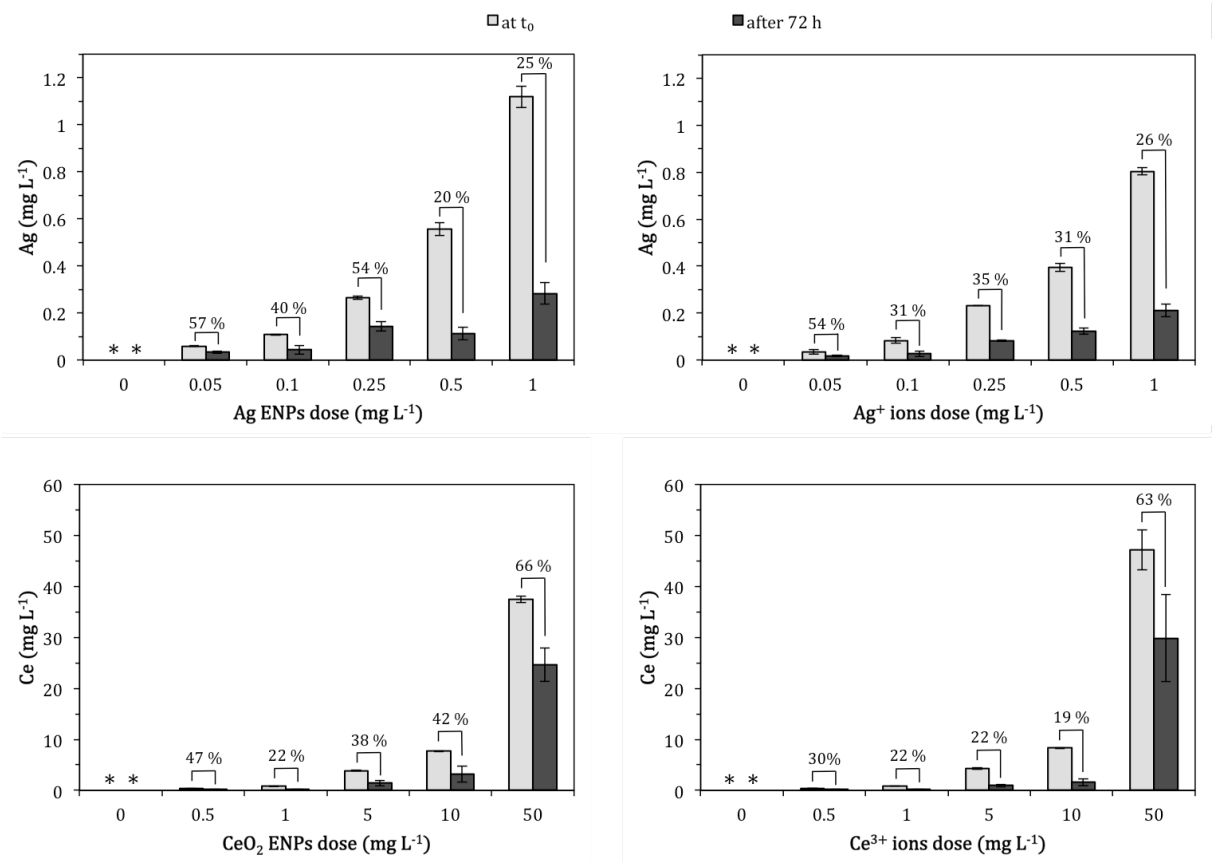

Figure 5.1 – Silver or cerium contents remaining in solution (tap water) after exposure of *E. canadensis* to varying concentrations of Ag ENPs and Ag^+ ions (top two graphs), or CeO_2 ENPs and Ce^{3+} ions (bottom two graphs) for 72 h. The percentages remaining for each dose are also displayed. (Bars represent mean values, values below the detection limit are indicated with an asterisk (DL_{Ag} = 5.3 μg L^{-1}; DL_{Ce} = 6.7 μg L^{-1}), error bars denote standard deviations, n = 3)

Part of the nanoparticles or ions were removed from solution by the plants, and as shown in Figure 5.2, both the silver and the cerium content in the biomass of *E. canadensis* significantly increased with increasing exposure concentration ($p < 0.05$). Furthermore, exposure to ions always resulted in higher concentrations in plant biomass compared to the nanoparticle treatments ($p < 0.05$), except for 0.05 mg L^{-1} Ag ENPs and Ag^+ ions ($p = 0.141$) and for 0.25 mg L^{-1} Ag ENPs and Ag^+ ions ($p = 0.331$). The dose-dependent silver content increased from 23 to 111 mg kg^{-1} DW for Ag ENPs and from 27 to 812 mg kg^{-1} DW in the case of Ag^+ ions, whereas the cerium content increased from 0.08 to 1.9 g kg^{-1} DW, or from 0.13 to 19 g kg^{-1} DW after treatment with CeO_2 ENPs or Ce^{3+} ions, respectively. Comparable results were reported by Jiang *et al.* (2012), who also observed a dose-dependent silver accumulation from Ag ENPs and $AgNO_3$ in *S. polyrhiza* (*i.e.,* greater duckweed), with a significantly higher uptake of the ionic silver species.

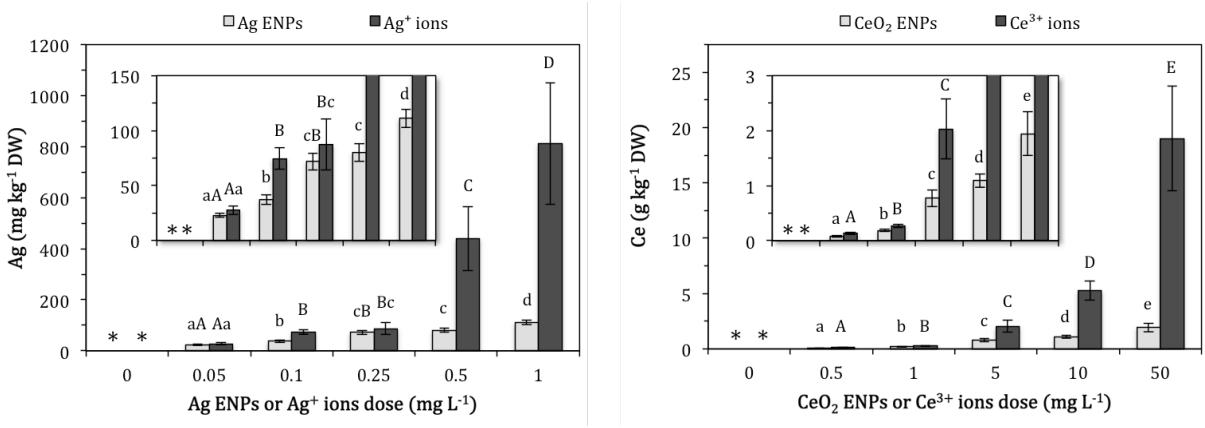

Figure 5.2 – Impact of the amount of Ag ENPs or Ag^+ ions (left graph), and CeO_2 ENPs or Ce^{3+} ions (right graph) on the silver or cerium content in the biomass of *E. canadensis* after 72 h of exposure. The insets show close-ups of the lower range Ag and Ce biomass concentrations. (Bars represent mean values, values below the detection limit are displayed with an asterisk (DL_{Ag} = 1.1 mg kg^{-1} DW; DL_{Ce} = 1.3 mg kg^{-1} DW), different letters indicate statistically significant differences ($p < 0.05$), error bars denote standard deviations, $n = 3$)

It should be noted that according to mass balance calculations, the amount of silver or cerium retrieved in the plant biomass was always lower than the total amount that was removed from the water after 72 h (Table 5.4). These discrepancies were most likely caused by aggregation, sedimentation, and precipitation of the nanoparticles or ions, in combination with potential losses that might have occurred *e.g.*, during dry dripping and patting of the plants after incubation.

Table 5.4 – Fractions of silver or cerium that were removed from solution and could be retrieved in plant biomass after 72 h of exposure.

	Exposure dose (mg L^{-1})							
	0.05	**0.1**	**0.25**	**0.5**	**1**	**5**	**10**	**50**
Ag ENPs	89 %	78 %	79 %	70 %	69 %	N/A	N/A	N/A
Ag^+ ions	97 %	96 %	86 %	97 %	97 %	N/A	N/A	N/A
CeO_2 ENPs	N/A	N/A	N/A	77 %	69 %	79 %	68 %	78 %
Ce^{3+} ions	N/A	N/A	N/A	76 %	71 %	99 %	96 %	97 %

N/A: Not applicable

Uptake of metals by *E. canadensis* predominantly occurs at the leaf surface (Nyquist and Greger, 2007; Jacob *et al.*, 2013), and metal accumulation in the plant biomass could be due to absorption and internalization by the plants via cell wall pores, or to adsorption onto plant surfaces (Glenn *et al.*, 2012; Jiang *et al.*, 2012). Although, the exact mechanisms of nanoparticle uptake by (aquatic) plants are still largely unknown (Lin and Xing, 2008; Navarro *et al.*, 2008a; Rico *et al.*, 2011; Sabo-Attwood *et al.*, 2011; Miralles *et al.*, 2012; Jiang *et al.*, 2012), it has been reported that any particle larger than 5 nm would encounter difficulties passing through the cell wall pores (Dietz and Herth, 2011). This might help explain the higher biomass concentrations resulting from exposure to the Ag^+ and Ce^{3+} ions compared to the Ag and CeO_2 ENPs used in this study. Furthermore, the (negatively charged) citrate coating of the Ag ENPs might also hinder their uptake, as plants normally exude organic compounds (*e.g.*, malate or citrate) (Glenn *et al.*, 2012). The smaller size, positive surface charge, and absence of an organic surface coating of the CeO_2 ENPs could thus potentially explain their apparent higher uptake, as higher biomass contents of cerium were observed compared to the silver contents when considering a similar dose of Ag and CeO_2 ENPs (*e.g.*, 111 versus 186 mg kg^{-1} DW at 1 mg L^{-1}). Another possible uptake route might be dissolution of the nanoparticles at the plant surface and subsequent absorption of the dissolved species (Jiang *et al.*, 2012), which is however less likely for CeO_2 ENPs due to their expected very low solubility (Van Hoecke *et al.*, 2009; Rogers *et al.*, 2010a; Cornelis *et al.*, 2011). A study by Glenn *et al.* (2012) already reported that interactions of Au ENPs with freshwater aquatic plants are particle size and plant species dependent, and demonstrated that both 4 and 18 nm Au ENPs adsorbed onto *A. caroliniana*, *M. simulans*, and *E. densa*, whereas absorption was only noted for 4 and 18 nm Au ENPs by *A. caroliniana*, and for 4 nm Au ENPs by *M. simulans*. However, additional research is required in order to elucidate the specifically occurring adsorptive and/or absorptive nanoparticle-plant interactions for *E. canadensis*. Furthermore, the colloidal stability of nanoparticles may also be an important

aspect, as for instance particle aggregation and sedimentation could affect plant exposure and thus plant uptake (see also Section 5.3.4).

None of the treatments had a significant impact on plant biomass after 72 h of exposure ($p > 0.05$) (Tables C.1 and C.2 in Appendix C). However, given the short experimental time frame and hence low percentage growth of the control plants, additional longer-term experiments focused on the impact of ENPs on *E. canadensis* growth need to be undertaken. Several other studies have reported a dose-dependent growth inhibition of aquatic plants by Ag ENPs and/or ionic silver *e.g.*, for duckweeds such as *L. minor* at exposure concentrations as low as 5 μg L^{-1} for 14 d (Gubbins *et al.*, 2011), *L. paucicostata* at doses equal to or above 1 mg L^{-1} during 7 d (Kim *et al.*, 2011), *S. polyrhiza* at exposure to 0.5 mg L^{-1} or more during 72 h (Jiang *et al.*, 2012), and *L. gibba* after 7 d exposure to 10 μg L^{-1} or more (Oukarroum *et al.*, 2013), whereas CeO_2 ENPs (at 5.6 mg L^{-1} or more during 72 h) have also been reported to inhibit the growth of the green alga *P. subcapitata* (Van Hoecke *et al.*, 2009; Van Hoecke *et al.*, 2011). On the other hand, nanoparticles could potentially also enhance growth, as was demonstrated for Al_2O_3 ENPs on *L. minor* plants (Juhel *et al.*, 2011).

Both nitrogen and phosphorous are essential plant elements that are related to cell division and growth, and which could influence the synthesis of photosynthetic pigments (Jiang *et al.*, 2012). In the case of CeO_2 ENPs or Ce^{3+} ions, generally no impact on total nitrogen (TN), total phosphorous (TP), or chlorophyll (Chl) content was observed ($p > 0.05$) (Table C.2 in Appendix C). These results indicate that neither CeO_2 ENPs nor Ce^{3+} ions showed an apparent toxicity towards *E. canadensis*, at least not for the considered exposure concentrations and experimental time frame. In contrast, Chu *et al.* (2014) demonstrated that Ce^{3+} ions did induce dose-dependent toxic effects on *E. canadensis* after exposure to 5 mg L^{-1} or more during 7 d, which included a reduction in photosynthetic pigments, disruption of nutrient elements, and signs of oxidative stress. Additionally, CeO_2 ENPs have also been shown to induce toxic responses in for example bacteria, algae, and even human cells (Thill *et al.*, 2006; Van Hoecke *et al.*, 2009; Rogers *et al.*, 2010a; Zhang *et al.*, 2011a). For Ag ENPs or Ag^+ ions also no effect on the plants TN content was observed ($p > 0.05$) (Table C.1 in Appendix C). However, the TP content did increase slightly upon exposure to Ag ENPs or Ag^+ ions ($p < 0.05$), whereas a significant decrease in Chl *a*, *b*, and *c* content was also noted ($p < 0.05$). Furthermore, a colour change of the plants from green to yellow was visually noticeable after 72 h of exposure to 0.25 mg L^{-1} Ag ENPs or Ag^+ ions or more. These

results suggest that both Ag ENPs and Ag^+ ions might potentially be toxic towards *E. canadensis*. A dose-dependent decrease in the Chl content upon exposure to Ag ENPs has for instance also been reported for *S. polyrhiza* (Jiang *et al.*, 2012), and for the microalgae *C. vulgaris* and *D. tertiolecta* (Oukarroum *et al.*, 2012). Numerous studies have already demonstrated Ag ENPs to be toxic towards various aquatic organisms, whereby the induced toxicity is often but not exclusively attributed to the release of ionic silver from the particles (Navarro *et al.*, 2008a; Gaiser *et al.*, 2009; Gubbins *et al.*, 2011; Zhao and Wang, 2011; Levard *et al.*, 2012; Jiang *et al.*, 2012; Oukarroum *et al.*, 2013; Thwala *et al.*, 2013; Jiang *et al.*, 2014). Yet, no specific ecotoxicity studies of Ag (or CeO_2) ENPs on *E. canadensis* have currently been published, and any research reports regarding nanoparticles and *E. canadensis* are very scarce in general for that matter (Johnson *et al.*, 2011; Jacob *et al.*, 2013). And although *E. canadensis* is considered to be a metal tolerant plant species (Nyquist and Greger, 2007), various dissolved metals have already been shown to be potentially phytotoxic to this plant (Brown and Rattigan, 1979; Thiébaut *et al.*, 2010; Chu *et al.*, 2014). Thus, more studies investigating the potential toxic effects of metallic nanoparticles on *E. canadensis* are needed.

5.3.4 Ag and CeO_2 ENPs depletion in complex aqueous media in the presence of *E. canadensis*

Figure 5.3 shows the time-dependent removal of Ag or CeO_2 ENPs, and Ag^+ or Ce^{3+} ions from solution upon incubation of *E. canadensis* in various (natural) aquatic matrices during 72 h. Error bars indicating relative standard deviations of the mean values were omitted from the figure for clarity purposes yet were on average 4, 3, 6, and 4 % for the Ag ENPs, Ag^+ ions, CeO_2 ENPs, and Ce^{3+} ions, respectively, and did not exceed 12 % in any case. In all five water samples, the relative amounts of Ag and CeO_2 ENPs remaining in suspension gradually decreased over the course of 72 h to reach a final 19 to 35 % or 4 to 10 % of the initial silver or cerium content, respectively. In the case of Ag^+ ions, a rapid decrease could be observed during the first 6 h where between 47 to 81 % of the initially added silver was removed. Afterwards, a more gradual decrease was noted and after 72 h between 10 and 22 % still remained in solution. A similar trend was observed for the Ce^{3+} ions in 10 % Hoagland's medium, where about 17 and 4 % of the added cerium remained in solution after 6 and 72 h, respectively. In the natural surface waters (*i.e.*, MB, GG, and CC) on the other hand, the relative amounts of Ce^{3+} ions showed a gradual decrease

during the 72 h incubation period, until finally between 14 and 21 % of the initially added cerium content remained in solution. In tap water, the removal behaviour of Ce^{3+} ions in the presence of *E. canadensis* seemingly laid in between that of the natural water samples and the 10 % Hoagland's medium, whereby approximately 52 and 80 % removal was observed during the first 24 and 48 h, respectively, and finally about 18 % of the initial cerium content remained in the water phase after 72 h of incubation. Thus, the nanoparticles and ions appeared to behave differently, and their depletion in the presence of *E. canadensis* also seems to be affected by the properties of the aquatic medium.

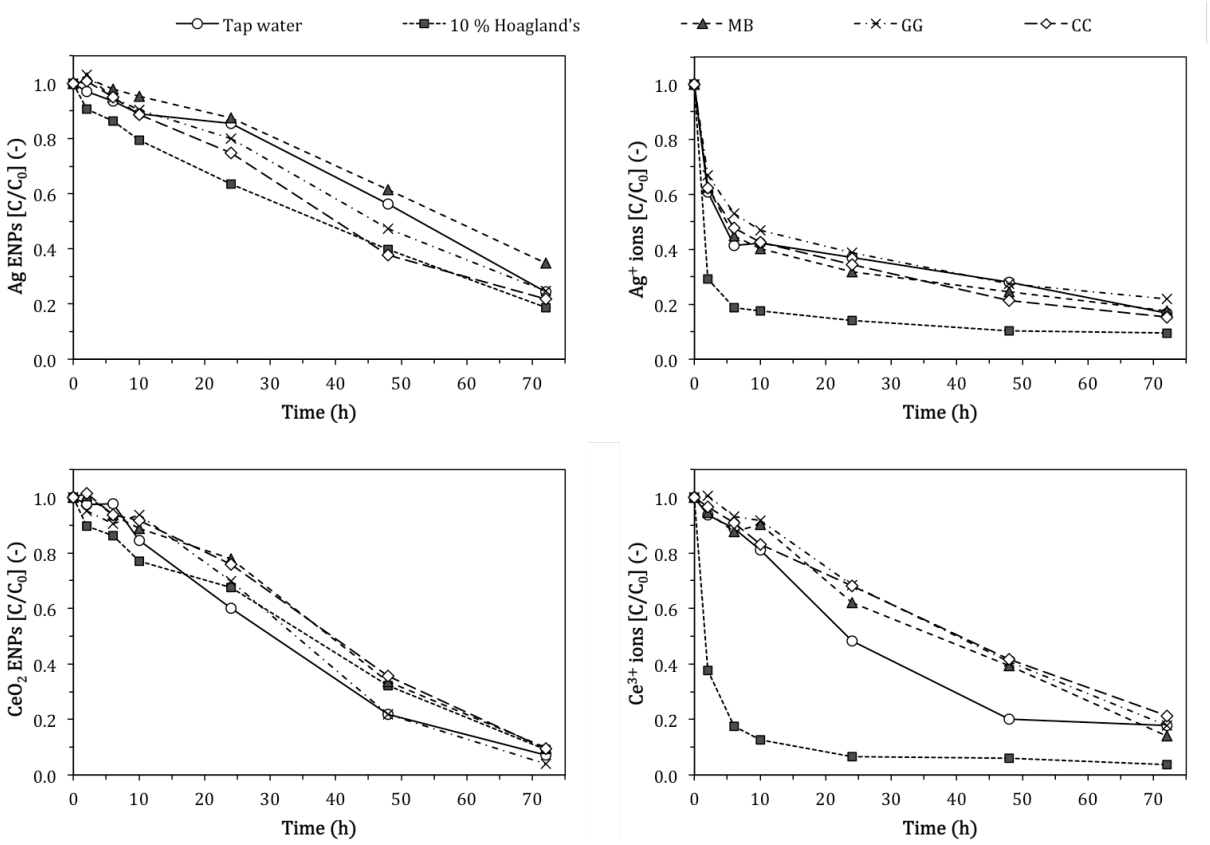

Figure 5.3 – Relative amounts of silver or cerium remaining in solution during 72 h, upon exposure of *E. canadensis* to 0.1 mg L^{-1} Ag ENPs or Ag^{+} ions (top two graphs), and 1 mg L^{-1} CeO_2 ENPs or Ce^{3+} ions (bottom two graphs), in five distinct aqueous matrices (*i.e.*, tap water, 10 % Hoagland's solution, and three natural surface waters: MB, GG, and CC). (Data points indicate mean values, n = 3)

The method of integrated rate law was used to assess the removal rate of the nanoparticles and ions in the presence of *E. Canadensis*, and thus models describing zero-order (Equation 5.1), first-order (Equation 5.2), and second-order (Equation 5.3) reaction kinetics were applied to the experimental data.

$$C_t = -kt + C_0 \quad \textbf{(5.1)}$$

$$C_t = C_0\, e^{-k_1 t} \quad \textbf{(5.2)}$$

$$C_t = \frac{C_0}{1 + k_2 t C_0} \quad \textbf{(5.3)}$$

where C_t [mg L^{-1}] is the concentration at time t, C_0 [mg L^{-1}] is the initial concentration, t [h] is the exposure time, and k [mg L^{-1} h^{-1}], k_1 [h^{-1}], and k_2 [L mg^{-1} h^{-1}] are the zero-, first-, and second-order reaction rate constants, respectively.

Linear and non-linear least squares regression analysis was performed in order to estimate the reaction rate constants and test to what extent the different kinetic models are able to describe the observed data (Table 5.5). Under the considered experimental conditions, the removal of both Ag and CeO_2 ENPs could be characterized best by a zero-order rate law ($R^2 \geq 0.929$), although good model fits were also obtained via first-order reaction kinetics ($R^2 \geq 0.897$). On the other hand, second-order kinetics appear to best be able to describe the depletion of Ag^+ ions in the presence of *E. canadensis* ($R^2 \geq 0.774$). For Ce^{3+} ions, application of the zero- or first-order kinetic model provided the best model fits (*i.e.*, $R^2 \geq 0.962$ or $R^2 \geq 0.955$, respectively) in the case of the natural water samples (*i.e.*, MB, GG, and CC), while their depletion in tap water or in 10 % Hoagland's solution could be best described via a first-order ($R^2 = 0.972$) or second-order ($R^2 = 0.991$) rate law, respectively. Although mainly serving a descriptive purpose, these results indicate that the observed time-dependent removal of the Ag and CeO_2 ENPs or the Ag^+ and Ce^{3+} ions from the waters in the presence of *E. canadensis* differed amongst the nanoparticulate and ionic species as well as amongst the different water samples.

Table 5.5 – Estimated model parameters for Equations 5.1 to 5.3, describing the depletion of 0.1 mg L^{-1} Ag ENPs or Ag^{+} ions, and 1 mg L^{-1} CeO_2 ENPs or Ce^{3+} ions from solution during 72 h in the presence of *E. canadensis*.

	Water sample	k (mg L^{-1} h^{-1})	R^2 (-)	k_1 (h^{-1})	R^2 (-)	k_2 (L mg^{-1} h^{-1})	R^2 (-)
Ag ENPs	**Tap water**	1.04×10^{-2}	0.963	1.36×10^{-2}	0.909	1.68×10^{-2}	0.850
	10 % Hoagland's	1.22×10^{-2}	0.929	2.08×10^{-2}	0.968	3.16×10^{-2}	0.942
	MB	8.44×10^{-3}	0.957	1.09×10^{-2}	0.911	1.36×10^{-2}	0.859
	GG	1.11×10^{-2}	0.947	1.51×10^{-2}	0.914	1.91×10^{-2}	0.861
	CC	1.14×10^{-2}	0.976	1.77×10^{-2}	0.955	2.45×10^{-2}	0.897
Ag^{+} ions	**Tap water**	-	-	9.06×10^{-2}	0.442	1.45×10^{-1}	0.774
	10 % Hoagland's	-	-	5.08×10^{-1}	0.843	8.19×10^{-1}	0.938
	MB	-	-	9.53×10^{-2}	0.597	1.50×10^{-1}	0.866
	GG	-	-	5.73×10^{-2}	0.533	1.03×10^{-1}	0.839
	CC	-	-	8.40×10^{-2}	0.649	1.43×10^{-1}	0.888
CeO_2 ENPs	**Tap water**	8.22×10^{-4}	0.958	2.57×10^{-2}	0.948	6.50×10^{-1}	0.872
	10 % Hoagland's	8.88×10^{-4}	0.929	2.38×10^{-2}	0.945	5.50×10^{-1}	0.896
	MB	7.70×10^{-4}	0.968	1.99×10^{-2}	0.913	4.58×10^{-1}	0.836
	GG	7.85×10^{-4}	0.948	2.40×10^{-2}	0.897	6.20×10^{-1}	0.812
	CC	7.24×10^{-4}	0.973	1.97×10^{-2}	0.913	4.77×10^{-1}	0.836
Ce^{3+} ions	**Tap water**	1.11×10^{-3}	0.873	2.80×10^{-2}	0.972	5.36×10^{-1}	0.932
	10 % Hoagland's	-	-	4.03×10^{-1}	0.946	$9{,}06 \times 10^{0}$	0.991
	MB	1.05×10^{-3}	0.971	2.08×10^{-2}	0.966	3.63×10^{-1}	0.912
	GG	8.70×10^{-4}	0.976	1.85×10^{-2}	0.955	3.52×10^{-1}	0.896
	CC	9.63×10^{-4}	0.962	1.87×10^{-2}	0.972	3.26×10^{-1}	0.935

R^2 is the determination coefficient.

Table 5.6 presents the amounts of silver or cerium in plant biomass after 72 h incubation of *E. canadensis* in the different aqueous matrices. Exposure to ions always resulted in higher biomass concentrations compared to exposure to nanoparticles ($p < 0.05$). Potential explanations for this observation have already been discussed in Section 5.3.3. The silver content varied between 27.7 and 57.7 mg kg^{-1} DW for 0.1 mg L^{-1} Ag ENPs and between 67.7 and 124 mg kg^{-1} DW in the case of 0.1 mg L^{-1} Ag^{+} ions, whereby the lowest biomass contents were observed for GG, and the highest for tap water or MB in the case of Ag ENPs or Ag^{+} ions, respectively. Exposure to 1 mg L^{-1} CeO_2 ENPs resulted in cerium concentrations between 110 and 240 mg kg^{-1} DW, whereas this was between 195 and 404 mg kg^{-1} DW upon treatment with 1 mg L^{-1} Ce^{3+} ions. The highest amounts of cerium in plant biomass were observed for the 10 % Hoagland's medium, while the lowest cerium

uptake was noted for CC or GG in the case of CeO_2 ENPs or Ce^{3+} ions, respectively. These results clearly indicate that association of the nanoparticles or ions with *E. canadensis* is affected by the characteristics of the water sample.

Table 5.6 – Silver or cerium concentrations in the biomass of *E. canadensis,* after 72 h of exposure to 0.1 mg L^{-1} Ag ENPs or Ag^+ ions, and 1 mg L^{-1} CeO_2 ENPs or Ce^{3+} ions in five different aquatic media (mean ± standard deviation, n = 3). Different letters indicate statistically significant differences ($p < 0.05$) between samples for each nanoparticulate or ionic species.

Water sample	**Ag (mg kg^{-1} DW)**		**Ce (mg kg^{-1} DW)**	
	Ag ENPs	**Ag^+ ions**	**CeO_2 ENPs**	**Ce^{3+} ions**
Tap water	57.7 ± 5.4 ^{c}	102 ± 18 ^{bc}	191 ± 41 ^{bc}	241 ± 36 ^{ab}
10 % Hoagland's	40.6 ± 4.5 ^{b}	95.2 ± 6.5 ^{bc}	240 ± 25 ^{c}	404 ± 25 ^{c}
MB	40.5 ± 3.6 ^{b}	124 ± 22 ^{c}	215 ± 37 ^{bc}	277 ± 42 ^{b}
GG	27.7 ± 5.4 ^{a}	67.7 ± 5.8 ^{a}	145 ± 1 ^{b}	195 ± 27 ^{a}
CC	41.5 ± 4.8 ^{b}	71.7 ± 5.3 ^{a}	110 ± 12 ^{a}	203 ± 11 ^{ab}

In all of the controls, Ag and Ce concentrations were below the detection limit (DL_{Ag} = 1.1 mg kg^{-1} DW; DL_{Ce} = 1.3 mg kg^{-1} DW).

As presentend in Table 5.7, it should again be noted that the mass balance calculations revealed that the amount of silver or cerium retrieved in the plant biomass was always lower than the total amount that was removed from the different waters after 72 h. This was again most likely due to aggregation, sedimentation, and precipitation of the nanoparticles or ions, together with potential losses that might have occurred during or following the harvesting of the plants (*e.g.*, during dry dripping and patting of the plants after incubation).

Table 5.7 – Fractions of silver or cerium that were removed from solution and could be retrieved in plant biomass after 72 h of exposure.

	Tap water	**10 % Hoagland's**	**MB**	**GG**	**CC**
Ag ENPs	67 %	61 %	69 %	66 %	60 %
Ag^+ ions	81 %	73 %	74 %	68 %	76 %
CeO_2 ENPs	67 %	69 %	69 %	63 %	63 %
Ce^{3+} ions	76 %	85 %	75 %	73 %	68 %

N/A: Not applicable

Significant relationships were obtained between the silver concentration in the plant biomass and the EC, DR, Cl^-, K, Na, and Mg content for Ag ENPs, while the EC, IC, Cl^-, NO_3^-, Na, and Mg content significantly correlated with the silver uptake in the case of Ag^+ ions (Table 5.8). For CeO_2 ENPs, the cerium content in the plants significantly correlated with EC, DR, IC, and Ca content, while significant relationships between cerium uptake and pH, EC, DR, IC, Cl^-, Ca, and Mg content were observed in the case of Ce^{3+} ions (Table 5.9).

Table 5.8 – Pearson correlation coefficients (*r*) and statistical significances (*p*) between water characteristics and the silver content in the biomass of *E. canadensis* after 72 h of exposure to 0.1 mg L^{-1} Ag ENPs and Ag^+ ions.

		EC	DR	IC	Cl^-	NO_3^-	K	Na	Mg
Ag ENPs	***r***	-0.606*	-0.643**	-0.323	-0.676**	-0.448	-0.852**	-0.669**	-0.655**
	p	0.017	0.010	0.240	0.006	0.094	< 0.0005	0.006	0.008
Ag^+ ions	***r***	-0.521*	-0.491	-0.872**	-0.553*	-0.661**	-0.496	-0.598*	-0.526*
	p	0.046	0.063	< 0.0005	0.032	0.007	0.060	0.040	0.044

** Correlation is significant at the 0.01 level (2-tailed).

* Correlation is significant at the 0.05 level (2-tailed).

Table 5.9 – Pearson correlation coefficients (*r*) and statistical significances (*p*) between water properties and the cerium content in the biomass of *E. canadensis* after 72 h of exposure to 1 mg L^{-1} CeO_2 ENPs and Ce^{3+} ions.

		pH	EC	DR	IC	Cl^-	Ca	Mg
CeO_2 ENPs	***r***	-0.500	-0.549*	-0.553*	-0.731**	-0.436	-0.566*	-0.445
	p	0.058	0.034	0.033	0.007	0.105	0.028	0.097
Ce^{3+} ions	***r***	-0.837**	-0.688**	-0.691**	-0.739**	-0.527*	-0.821**	-0.562*
	p	< 0.0005	0.005	0.004	0.006	0.044	< 0.0005	0.029

** Correlation is significant at the 0.01 level (2-tailed).

* Correlation is significant at the 0.05 level (2-tailed).

A higher EC, which is a measure for the ionic strength (IS) of a solution, could promote particle aggregation and thus potentially reduce association of the nanoparticles with the plant, as their reactivity and bioavailability is decreased by the formation of larger particle aggregates (Hotze *et al.*, 2010). El Badawy *et al.* (2010) for instance demonstrated that aggregation of Ag ENPs was stimulated by increasing IS and cation valence, while similar observations have also been reported for CeO_2 ENPs (Buettner *et al.*, 2010). On the other hand, the observed reduced interactions between the nanoparticles or ions and *E. canadensis* in waters characterized by a high EC might possibly also be the result of potential adaptation mechanisms certain (aquatic) plants utilize in order to survive in more

saline environments, which may include biochemical pathways that exclude ions or physical alterations such as modifications of cell walls or the membrane structure (Perida and Das, 2004; Glenn *et al.*, 2012). Glenn *et al.* (2012) hypothesized that enhanced exclusion mechanism resulting from salinity tolerance could impact the uptake and partitioning of Au ENPs in aquatic plants. Furthermore, the formation of virtually insoluble precipitates such as AgCl, Ag_2CO_3, or $Ce_2(CO_3)_3$ could potentially also impede the uptake of Ag^+ or Ce^{3+} ions by *E. canadensis*, as was noted for the waters having a higher Cl^- or IC content.

In addition, despite the fact that no significant correlations were obtained between the silver or cerium content in the plant biomass and for instance the amount of TSS or TOC in this study, these factors could definitely also play an important role in the bioavailability of the nanoparticles or their ionic counterparts. Association of the nanoparticles or ions with suspended solids would reduce their bio-accessibility. For instance, Quik *et al.* (2012) argued that hetero-aggregation of nanoparticles with natural colloidal material and subsequent sedimentation might be the dominant mechanism for their depletion in natural waters. The presence of natural organic matter (NOM) on the other hand, has been observed to reduce nanoparticle aggregation by (electro)sterically hindering particle-particle or particle-collector interactions, and thus increasing their stability and potential bioavailability (Johnson *et al.*, 2009; Hotze *et al.*, 2010; Keller *et al.*, 2010; Quik *et al.*, 2010; Scown *et al.*, 2010; Thio *et al.*, 2011). However, a recent study by Glenn and Klaine (2013) demonstrated that the presence of dissolved organic carbon besides minimizing nanoparticle aggregation, also reduced the interactions of 4 and 18 nm Au ENPs with the aquatic plants *A. caroliniana*, *M. simulans*, and *E. densa*. Nevertheless, for all water samples significant silver or cerium biomass concentrations were observed, indicating interactions between the Ag and CeO_2 ENPs and *E. canadensis* have occurred in complex (natural) aquatic matrices, which could in time prove to be detrimental to either the plant itself or to the surrounding aquatic environment (*e.g.*, through trophic transfer).

5.4 Conclusion

This study examined the potential association of citrate-stabilized Ag ENPs (14.1 ± 1.0 nm) and CeO_2 ENPs (6.7 ± 1.2 nm), as well as their ionic counterparts, with *E. canadensis* in complex (natural) aquatic media. The results indicate that Ag and CeO_2 ENPs as well as Ag^+ and Ce^{3+} ions interacted with the aquatic plant under

consideration. A dose-dependent increase of silver or cerium in the plant biomass was observed for both the nanoparticles and the ions, whereby 72 h exposure to the latter systematically resulted in significantly higher biomass concentrations. Moreover, when comparing similar exposure concentrations, the partitioning of CeO_2 ENPs towards plant biomass was higher than was the case for Ag ENPs. These findings suggest that association with *E. canadensis* might be affected by particle properties such as size, composition, solubility, surface charge, and surface coating. Furthermore, the stability of the nanoparticles or ions in suspension/solution may be another important aspect affecting plant exposure and uptake. It was shown that association of Ag or CeO_2 ENPs, as well as Ag^+ or Ce^{3+} ions with *E. canadensis* is influenced by the physicochemical properties of the aquatic medium. In the case of Ag ENPs, significant relationships were obtained between the silver biomass concentration and the EC, DR, Cl^-, K, Na, and Mg content, whereas the silver uptake from Ag^+ ions significantly correlated with the EC, IC, Cl^-, NO_3^-, Na, and Mg content. The cerium biomass concentration was found to correlate with the EC, DR, IC, and Ca content in the case of CeO_2 ENPs, or with the pH, EC, DR, IC, Cl^-, Ca, and Mg content in the case of Ce^{3+} ions.

However, as the current study does not allow identifying the specifically occurring uptake mechanisms of the Ag or CeO_2 ENPs by *E. canadensis*, additional research is required in order to clarify as well as to differentiate between the potential absorptive and/or adsorptive nanoparticle-plant interactions. Nevertheless, significant silver or cerium biomass contents were obtained after 72 h of exposure for all treatments and so, regardless of the nanoparticles being adsorbed onto the surface or absorbed within the biomass, plant uptake could be an important determinant in the fate of ENPs in aquatic environments and could potentially facilitate trophic transfer, thereby posing a risk to other aquatic biota.

Treatment with the ENPs or ions seemingly did not affect the biomass of the plants, and no clear indications of phytotoxicity were observed in the case of CeO_2 ENPs or Ce^{3+} ions. A dose-dependent decrease in the chlorophyll content was however established for the Ag ENPs and Ag^+ ions, as well as a colour change of the plants from green to yellow after exposure to a dose of 0.25 mg L^{-1} or more during 72 h. Although these findings suggest that Ag ENPs and Ag^+ ions might potentially be toxic towards *E. canadensis*, they are mainly indicative as detailed nanoparticle or ionic induced phytotoxicity fell outside the scope of this study. Additional studies focused on the possible toxic effects of metallic nanoparticles such as Ag ENPs on *E. canadensis* are thus also needed.

Chapter 6

Factors affecting interactions of Ag and CeO_2 nanoparticles with (re)suspended sediments

6 Factors affecting interactions of Ag and CeO_2 nanoparticles with (re)suspended sediments[‡]

6.1 Introduction

The increasing production and commercial use of engineered nanoparticles (ENPs) will inevitably lead to their (unintentional) release into aquatic or terrestrial environments (Darlington *et al.*, 2009). Due to their small size, nanoparticles can exhibit a variety of unique properties that differ significantly from their bulk counterparts, and can hence pose a threat to human health and ecosystems (Handy *et al.*, 2008b; Klaine *et al.*, 2008). On the other hand, these unique properties also form the foundation of their utilization in commercial, industrial, agricultural, and environmental technology applications (Handy *et al.*, 2008a). Therefore, extended knowledge of their environmental behaviour and fate is essential in order to evaluate possible exposure routes, and improve risk assessment (Fang *et al.*, 2009).

Partitioning of ENPs between the solid and liquid phase in complex environmental media can provide important information on their mobility, bioavailability and toxicity. Association of ENPs with solid phase constituents will result in limited mobility, and will therefore render them less bio-accessible (Gimbert *et al.*, 2007). The major physicochemical processes that control the fate of ENPs in natural waters include: *dissolution, sorption, aggregation and sedimentation* (Batley and McLaughlin, 2010). In turn, the environmental behaviour and fate of ENPs highly depends on particle characteristics (*e.g.*, type, size and surface properties), as well as on the conditions of the environmental medium (*e.g.*, pH, ionic strength, and dissolved organic matter content) (Boxall *et al.*, 2007). Natural organic matter for instance, has been demonstrated to decrease aggregation (Quik *et al.*, 2010), while high concentrations of Ca^{2+} or Mg^{2+} could promote aggregation and deposition of nanoparticles (Fang *et al.*, 2009).

[‡] *Redrafted after: Van Koetsem, F., Geremew, T.T., Wallaert, E., Verbeken, K., Van der Meeren, P., and Du Laing, G. (in press).* ***Fate of engineered nanomaterials in surface water: Factors affecting interactions of Ag and CeO_2 nanoparticles with (re)suspended sediments.*** *Ecol. Eng., DOI: 10.1016/j.ecoleng.2014.07.024.*

Sediments can serve as a sink for a variety of contaminants like heavy metals or organic pollutants, whose emissions into the environment are the result of increasing industrial, agricultural, and household activities (Rakowska *et al.*, 2012). The high tendency of metals in general to sorb onto colloids, which in turn aggregate and settle out of solution, leads to accumulation in the sediments, but also results in the depletion of pollutants from the water phase. This important process, referred to as self-purification, is also likely to occur in the case of ENPs (Klaine *et al.*, 2008). Therefore, although extensive information on the interactions of ENPs with suspended sediments is lacking, some studies suggest that upon aggregation and subsequent sedimentation, the sediment bed and benthic organisms could be considered as key receptors for ENPs upon their release in *e.g.*, surface waters (Batley and McLaughlin, 2010; Boxall *et al.*, 2007; Christian *et al.*, 2008; Klaine *et al.*, 2008). Stabilization or (re)mobilization of ENPs in the aquatic environment on the other hand, can not only enhance the risks directly associated with the nanoparticulate materials in question, but can also lead to particle-facilitated contaminant transport. Contaminants can be associated with ENPs or their resulting aggregates, and can be carried-forward over large distances under conditions favouring colloidal transport. Sorption or incorporation of contaminants is again influenced by particle properties (*e.g.*, composition, morphology, and surface charge), as well as solution characteristics (Zhang *et al.*, 2003; Christian *et al.*, 2008; Klaine *et al.*, 2008).

Ag and CeO_2 ENPs are amongst the most widely used nanoparticles to date (Maynard and Michelson, 2007). The antimicrobial nature of Ag ENPs has lead to their application in consumer goods, including cosmetics, textiles, medical and other household products (Wijnhoven *et al.*, 2009). CeO_2 ENPs, on the other hand, are for instance used in the automotive or cosmetic sector, as fuel additives or UV-blocking agents, respectively (Masui *et al.*, 2000; Fall *et al.*, 2007). Both Ag and CeO_2 ENPs have been shown to potentially induce toxic effects in aquatic and terrestrial organisms (Navarro *et al.*, 2008b; Roh *et al.*, 2009; Van Hoecke *et al.*, 2009). Still, insufficient knowledge exists on their transport, stability, mobility, and deposition behaviour, when in contact with sediments.

The aim of this study was to examine the solid-liquid partitioning behaviour of Ag and CeO_2 ENPs in different sediment suspensions, in order to assess their potential mobility upon release in the environment. Partitioning kinetics and interactions with sediment constituents were investigated, as well as how they are affected by sediment properties. Therefore, batch experiments were set up under oxic conditions, aimed at contributing to

the identification of factors affecting the physicochemical fate of these nanoparticulate materials in aquatic environments.

6.2 Materials and methods

6.2.1 Sediment sampling and characterization

Intertidal sediment samples (top 0 – 30 cm) were collected from four different locations (*i.e.*, Doel, Linkeroever, Bornem, and Mariekerke) along the river Scheldt (Belgium) (Figure 6.1). All collected sediment samples were first air-dried at 25 °C, followed by a final drying step in an oven at 65 °C. Afterwards, the different sediment samples were crushed manually and/or ground in a cross beater mill if necessary, and passed through a 1 mm mesh sieve. Organic matter content (OM) was determined as loss on ignition (LOI) after incineration of 3 g oven-dried sediment in a muffle furnace at 550 °C for 2 h (Salehi *et al.*, 2011). Deionized water (1:10 (m:V)) was used as extraction reagents in the determination of soluble organic constituents in the sediments (Jones and Willet, 2006). After mixing for 24 h on an orbital shaker and following paper filtration (MN 640 m, Macherey-Nagel GmbH & Co. KG, Düren, Germany), the dissolved organic carbon (DOC) content was measured in the filtrates using a TOC analyser (TOC-V_{CPN}, Shimadzu, Kyoto, Japan). Particle size analysis was performed according to the Bouyoucos hydrometer method after removing organic matter by adding H_2O_2 (Gee *et al.*, 1986; van Reeuwijk, 2002; Sartori *et al.*, 2013). Sediment-pH (pH-H_2O) was measured in 1:5 (m:V) sediment:deionized water suspensions after equilibration during 16 h (Van Ranst *et al.*, 1999). The dry matter (DM) content was determined by recording the mass difference after drying 100 g dried sediment in an oven at 105 °C for 24 h. The electrical conductivity (EC) was measured in the filtrates (MN 640 m, Macherey-Nagel GmbH & Co. KG, Düren, Germany) of 1:5 (m:V) sediment:deionized water suspensions after shaking for 1 h (Van Ranst *et al.*, 1999). The cation exchange capacity was determined by percolation of 150 ml 1 M NH_4OAc through a percolation tube filled with a mixture of 5 g sediment and 12.5 g quartz sand, followed by washing through the excess with 150 mL denatured ethanol. The exchangeable ammonium ions were then eluted with 250 mL 1 M KCl and analysed in the percolate by means of a steam distillation (Vapodest Kjeldahl distillation system, Gerhardt GmbH & Co. KG, Königswinter, Germany). To determine the chloride (Cl^-) content, 10 g sediment was suspended in 50 mL 0.15 M HNO_3,

shaken for 30 min. The filtrate was titrated with 0.05 M $AgNO_3$ using potentiometric end-point detection (Van Ranst *et al.*, 1999). The total carbonate ($CaCO_3$) content was determined by back-titration (with 0.5 M NaOH) of an excess 0.25 M H_2SO_4 added to 1 g sediment (Van Ranst *et al.*, 1999). The total nitrogen (TN) content was determined according to the modified Kjeldahl method by digestion of 1 g sediment with 7 mL sulphuric/salicylic acid reagent, followed by alkalization with NaOH and steam distillation using a Vapodest Kjeldahl distillation system (Gerhardt GmbH & Co. KG, Königswinter, Germany) (Van Ranst *et al.*, 1999). The total phosphorous (TP) content was determined according to the colorimetric method of Scheel after *aqua regia* destruction of 1 g sediment (Van Ranst *et al.*, 1999). Pseudo-total main (Na, K, Ca, Mg) and trace elements contents (including Ag and Ce) were determined by an *aqua regia* destruction of 1 g sediment (Van Ranst *et al.*, 1999), followed by analysis via inductively coupled plasma optical emission spectrometry (ICP-OES) (Vista-MPX CCD Simultaneous ICP-OES, Varian, Agilent Technologies, Santa Clara, CA, USA) (Van Ranst *et al.*, 1999). Additional details on the employed sediment characterization procedures can be retrieved in Appendix A.

6.2.2 Nanoparticle dispersions and ionic standard solutions

Ag ENPs (Citrate-stabilized, APS: *ca.* 10 nm, ζ-potential: -50 ± 5 mV, pH: 6 – 8, concentration: 100 mg L^{-1}) and CeO_2 ENPs (APS: 4 ± 2 nm, ζ-potential: +40 ± 5 mV, concentration: 50 000 mg L^{-1}) were purchased from PlasmaChem GmbH (Berlin, Germany) as aqueous dispersions. These nanoparticle stock dispersions were further characterized for particle size distribution (PSD) via photon correlation spectroscopy (PCS) (Malvern PCS-100SM, Malvern Instruments Ltd., Worcestershire, UK), visualized and detected using transmission electron microscopy (TEM) (JEM-2200FS, Jeol Ltd., Tokyo, Japan) equipped with energy dispersive X-ray spectrometry (EDS), and subjected to zeta (ζ) potential measurements (Zetasizer 3000 HSa, Malvern Instruments Ltd., Worcestershire, UK) to assess their surface charge. PCS measurements were performed in quadruplicate, at 25 °C, and using a 633 nm HeNe laser positioned at a scattering angle of 150 degrees. The so-called *Z*-average hydrodynamic diameter obtained by cumulant analysis was considered, whereas particle size distributions were obtained by multi modal analysis. Cerium (as $Ce(NO_3)_3$) (Plasma HIQU, 10 000 ± 20 μg Ce^{3+} mL^{-1} in 2 – 5 % HNO_3) and silver (as $AgNO_3$) (Plasma HIQU, 10 000 ± 20 μg Ag^+ mL^{-1} in 2 – 5 % HNO_3) reference standard solutions were obtained from ChemLab NV (Zedelgem, Belgium), and applied as ionic spikes (*i.e.*, Ag^+ ions and

Ce^{3+} ions) in the batch experiments. All chemicals used were of analytical grade.

6.2.3 Batch experiments

Sediment suspensions were prepared with Milli-Q® water (18.2 MΩ cm^{-1}) (EMD Millipore Corp., Billerica, MA, USA) in a 1:10 ratio (m:V) in 50 mL centrifuge tubes, and spiked with a known amount of metallic nanoparticles or ions (either 10 mg L^{-1} in the case of CeO_2 ENPs or Ce^{3+} ions, or 2 mg L^{-1} in the case of Ag ENPs or Ag^+ ions). The suspensions were continuously shaken for 10 min (t0), 2 h (t2), or 24 h (t24) on an orbital shaker. At these time intervals, the suspensions were removed from the shaker and subjected to 10 min of centrifugation (Megafuge 1.0, Heraeus, Hanau, Germany) at 500 or 2000 rpm (*i.e.*, 46 or 738 *g*, respectively), or left for gravitational settling (0 rpm) for 10 min. The supernatants were analysed for total metal content via ICP-OES (Vista-MPX CCD Simultaneous ICP-OES, Varian, Agilent Technologies, Santa Clara, CA, USA) after being digested (*i.e.*, digestion on a hotplate at 150 °C for 2 h with *aqua regia* for cerium, or with 65 % HNO_3 and 30 % H_2O_2 in the case of silver spiked sediment suspensions). Blanks (*i.e.*, un-spiked sediment suspensions) and controls (*i.e.*, spiked Milli-Q® water) were also included in the set-up.

The impact of centrifugation speed on the amount of suspended matter (SM) and total organic carbon (TOC) in the supernatant was also studied. In this experiment, sediment suspensions were prepared by adding 30 mL of Milli-Q® water to 3 g of sediment in 50 mL centrifuge tubes. These suspensions were shaken thoroughly for 24 h before being subjected to centrifugation for 10 min at different chosen speeds (*i.e.*, at 500, 1000, 1500, 2000 or 2500 rpm, which corresponds to 46, 184, 415, 738, or 1153 *g*, respectively), or left for 10 min of gravitational settling (0 rpm). Afterwards, the centrifuged samples were gently placed onto a steady horizontal surface to not disturb the sample, and 20 mL of the supernatant was pipetted with an electronic pipette into proper pre-dried and pre-weighed disposable aluminium evaporation dishes. Finally, the concentration of sediment still present in solution (*i.e.*, in the supernatant) was determined in function of centrifugation speed, by determining the mass remaining inside the evaporation recipients after drying in an oven at 105 °C for at least 6 h. TOC content in function of centrifugation speed (*i.e.*, 0, 500, and 2000 rpm) was determined by sampling 10 mL from the supernatants and analysing these samples directly using a TOC analyser (TOC-V_{CPN}, Shimadzu, Kyoto, Japan).

A final set of batch experiments was designed to mimic the behaviour of Ag and CeO_2 ENPs in the water column in contact with sediments. For this, two of the sampled sediments were selected (*i.e.*, Doel and Bornem), 1:10 (m:V) suspensions were prepared with Milli-Q® water in conical flasks, covered with Parafilm, and put on an orbital shaker for 24 h. Afterwards, the suspensions were subjected to different treatments (*i.e.*, 10 min gravitational settling (0 rpm) or 10 min centrifugation at 500 or 2000 rpm) and the resulting supernatant from each treatment was collected. These different supernatants (*i.e.*, sediment extracts) were transferred into 50 mL centrifuge tubes, and were spiked (with CeO_2 ENPs, Ce^{3+} ions, Ag ENPs, or Ag^{+} ions), further treated, and analysed, in a comparable manner as described in the first text paragraph above, with the sole exception that only one sampling time point (t2) was selected.

6.2.4 Data processing

Analysis of variance (ANOVA) and Pearson's product-moment correlation analysis were performed using SPSS Statistics 21 (IBM, Armonk, NY, USA). Normality of data was checked via Shapiro-Wilk's test. Welch's *t*-test was used to examine equality of means in case the conditions for homogeneity of variances resulting from Levene's test were not met. Tukey's HSD or Games-Howell's *post-hoc* tests were used if significant mean differences were observed after running ANOVA or Welch's *t*-test, respectively. Not normally distributed data was also assessed via Kruskal-Wallis' *H*-test, and if necessary, pairwise comparisons were performed as *post-hoc* analysis using Dunn's procedure with a Bonferroni correction for multiple comparisons. Excel (Microsoft Corp., Redmond, WA, USA) and SigmaPlot 12 (Systat Software Inc., Chicago, IL, USA) software packages were used for numerical and graphical data processing.

6.3 Results

6.3.1 Sediment properties

The physicochemical properties of the sampled sediments are presented in Table 6.1. The pH of the sediments sampled along the Scheldt River was slightly alkaline (7.55 – 7.89), and the total amount of carbonates present ranged from 10.1 to 15.2 %. A higher EC was

observed for Doel (1929 μS cm^{-1}) compared to the three other sampling sites. The organic matter content varied between 3.47 and 9.35 %, at Bornem and Mariekerke, respectively. Additionally, the highest CEC (24.3 cmol$_c$ kg^{-1}), and DOC (879 mg kg^{-1}), TN (3.41 g kg^{-1}), TP (2.89 g kg^{-1}), and clay (26.7 %) content were also observed in the latter sediment sample. Chloride content was highest for Doel (1632 mg kg^{-1}) and decreased to 138 mg kg^{-1} at Mariekerke, as the sampling distance to the river mouth increased. According to the USDA's soil texture classification system, Doel and Linkeroever samples can be classified as loamy sediments, whereas Bornem and Mariekerke samples are classified as sandy loam and clayey loam sediments, respectively.

Table 6.1 – Physicochemical properties of the sampled sediments. Data is presented as mean ± standard deviation (n = 3). Different letters denote statistically significant differences (p < 0.05) between samples for each parameter.

Parameter		Doel	Linkeroever	Bornem	Mariekerke
pH-H_2O	**(-)**	7.89 ± 0.06 ^{b}	7.88 ± 0.02 ^{b}	7.56 ± 0.02 ^{a}	7.55 ± 0.03 ^{a}
EC	**(μS cm^{-1})**	1929 ± 26 ^{c}	864 ± 8 ^{a}	861 ± 14 ^{a}	930 ± 11 ^{b}
CEC	**(cmol$_c$ kg^{-1})**	10.7 ± 0.1 ^{b}	12.6 ± 0.2 ^{c}	9.44 ± 0.10 ^{a}	24.3 ± 0.2 ^{d}
OM	**(%)**	4.75 ± 0.10 ^{b}	5.08 ± 0.05 ^{c}	3.47 ± 0.04 ^{a}	9.35 ± 0.13 ^{d}
DOC	**(mg kg^{-1})**	386 ± 15 ^{b}	381 ± 14 ^{b}	320 ± 31 ^{a}	879 ± 3 ^{c}
$CaCO_3$	**(%)**	14.3 ± 0.9 ^{b}	15.2 ± 0.5 ^{b}	10.1 ± 0.8 ^{a}	10.2 ± 0.5 ^{a}
TN	**(g kg^{-1})**	1.20 ± 0.01 ^{a}	1.46 ± 0.09 ^{b}	1.21 ± 0.08 ^{a}	3.41 ± 0.02 ^{c}
TP	**(g kg^{-1})**	1.51 ± 0.01 ^{a}	1.54 ± 0.01 ^{a}	1.88 ± 0.05 ^{b}	2.89 ± 0.03 ^{c}
Cl^-	**(mg kg^{-1})**	1632 ± 13 ^{d}	649 ± 1 ^{c}	234 ± 1 ^{b}	138 ± 2 ^{a}
Sand	**(%)**	41.8 ± 0.4 ^{b}	45.0 ± 0.4 ^{c}	61.0 ± 0.1 ^{d}	26.0 ± 0.1 ^{a}
Silt	**(%)**	46.0 ± 0.2 ^{c}	40.0 ± 1.1 ^{b}	28.3 ± 0.9 ^{a}	47.3 ± 0.5 ^{c}
Clay	**(%)**	12.1 ± 0.2 ^{a}	14.2 ± 0.5 ^{b}	10.7 ± 0.9 ^{a}	26.7 ± 0.7 ^{c}

The total amount of main and trace elements in the sediments is tabulated in Table 6.2. In general, Mariekerke contained the highest amounts of main and trace elements, with the exception of the total Na, Ca, and Ce content. All sampled sediments can be considered being contaminated with heavy metals, as the measured concentrations of As, Cd, Cr, Cu, Pb, Ni, and Zn surpass the reference values imposed by the Flemish government (De Saedeleer *et al.*, 2010).

Table 6.2 – Major and trace elements content in the sampled sediments (mean ± standard deviation, n = 3). Different letters denote statistically significant differences (p < 0.05) between samples for each element.

Element		Doel	Linkeroever	Bornem	Mariekerke
Na	**(g kg^{-1})**	2.26 ± 0.05 ^{c}	1.17 ± 0.05 ^{b}	0.55 ± 0.04 ^{a}	0.64 ± 0.04 ^{a}
K	**(g kg^{-1})**	3.45 ± 0.33 ^{a}	4.17 ± 0.33 ^{a}	3.18 ± 0.10 ^{a}	5.81 ± 0.02 ^{b}
Ca	**(g kg^{-1})**	66.7 ± 2.5 ^{b}	67.4 ± 1.1 ^{b}	51.7 ± 2.0 ^{a}	54.5 ± 0.9 ^{a}
Mg	**(g kg^{-1})**	5.95 ± 0.26 ^{b}	5.58 ± 0.13 ^{b}	3.94 ± 0.17 ^{a}	6.47 ± 0.13 ^{c}
Al	**(g kg^{-1})**	10.8 ± 0.3 ^{b}	12.1 ± 1.0 ^{b}	8.43 ± 0.59 ^{a}	22.3 ± 0.7 ^{c}
Fe	**(g kg^{-1})**	25.0 ± 0.1 ^{b}	27.3 ± 1.6 ^{b}	19.6 ± 1.1 ^{a}	41.9 ± 1.6 ^{c}
Co	**(mg kg^{-1})**	< 3.9	< 3.9	< 3.9	5.33 ± 0.73
Pb	**(mg kg^{-1})**	41.1 ± 0.6 ^{a}	44.5 ± 0.7 ^{a}	43.6 ± 2.5 ^{a}	90.9 ± 2.6 ^{b}
Cr	**(mg kg^{-1})**	20.8 ± 0.3 ^{a}	24.1 ± 0.6 ^{b}	19.2 ± 1.2 ^{a}	41.7 ± 1.1 ^{c}
As	**(mg kg^{-1})**	17.1 ± 1.6 ^{ab}	18.2 ± 3.3 ^{b}	10.8 ± 1.9 ^{a}	20.7 ± 2.5 ^{b}
Cd	**(mg kg^{-1})**	1.79 ± 0.07 ^{a}	2.14 ± 0.14 ^{b}	2.38 ± 0.17 ^{b}	3.70 ± 0.05 ^{c}
Mn	**(mg kg^{-1})**	446 ± 2 ^{a}	588 ± 40 ^{b}	449 ± 29 ^{a}	1234 ± 29 ^{c}
Ni	**(mg kg^{-1})**	15.5 ± 0.1 ^{a}	17.4 ± 0.1 ^{b}	15.1 ± 1.2 ^{a}	31.7 ± 0.5 ^{c}
Cu	**(mg kg^{-1})**	24.6 ± 0.7 ^{a}	28.1 ± 0.3 ^{b}	26.2 ± 1.4 ^{ab}	61.0 ± 2.2 ^{c}
Zn	**(mg kg^{-1})**	195 ± 1 ^{a}	229 ± 4 ^{b}	233 ± 11 ^{ab}	471 ± 12 ^{c}
Ce	**(mg kg^{-1})**	27.3 ± 0.8 ^{b}	28.4 ± 0.5 ^{b}	37.9 ± 0.8 ^{c}	25.2 ± 0.1 ^{a}
Ag	**(mg kg^{-1})**	0.53 ± 0.06 ^{a}	0.61 ± 0.10 ^{a}	0.54 ± 0.05 ^{a}	1.10 ± 0.06 ^{b}

Data presented as "< " indicate values below the detection limit (DL).

6.3.2 Nanoparticle characterization

PCS analyses revealed a Z-average hydrodynamic diameter of 14.8 ± 1.3 nm for Ag ENPs, and of 6.2 ± 0.5 nm in the case of CeO_2 ENPs, when dispersed in Milli-Q® water, which is in agreement with what was claimed by the manufacturer. The obtained particle size distributions shown in Figure 6.1, together with visualisation of the ENPs via TEM (Figure 6.2), suggest that the majority of the Ag ENPs were indeed approximately 10 nm in size, but a few larger particles in the range of 20 – 70 nm were also present in suspension. All nanoparticles appeared to be spherical in morphology. The obtained ζ-potentials were -40.7 ± 6.2 mV and +52.3 ± 1.9 mV, for Ag and CeO_2 ENPs, respectively, when dispersed in Milli-Q® water, at a pH of 5 for Ag ENPs or 6.5 in the case of CeO_2 ENPs (n = 4).

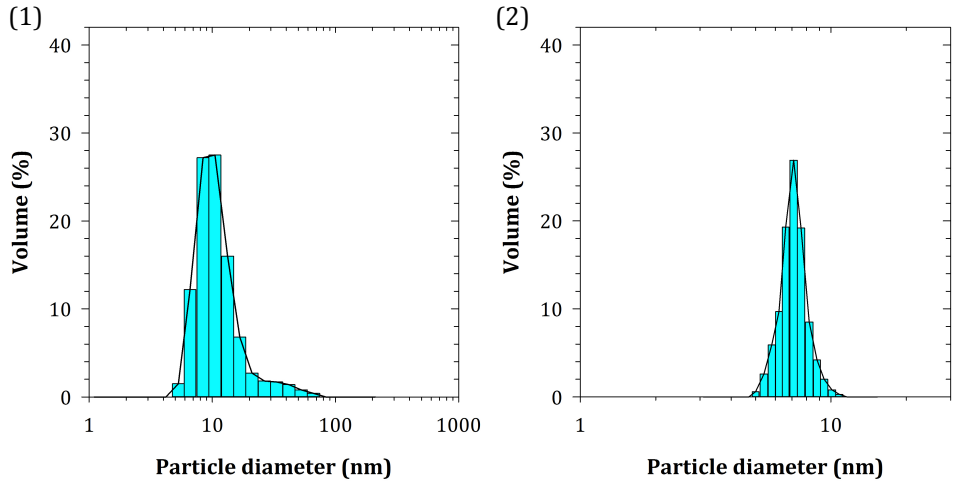

Figure 6.1 – Volume weighted particle size distribution of Ag ENPs (1) and CeO_2 ENPs (2) dispersed in Milli-Q® water, obtained from PCS measurements.

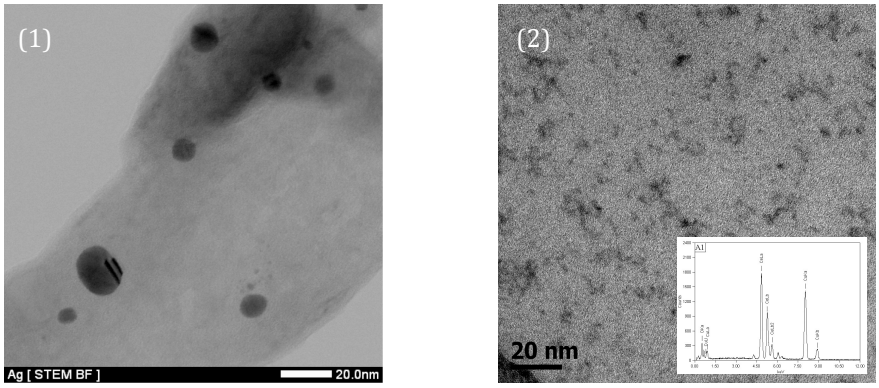

Figure 6.2 – TEM images of Ag ENPs (1) and CeO_2 ENPs (2) dispersed in Milli-Q® water. The inset shows the EDS spectrum of CeO_2 ENPs taken during TEM analysis.

6.3.3 Ag and CeO_2 ENPs stability in ultrapure water

Figure 6.3 shows that the concentration of Ag ENPs (p = 0.158), Ag^+ ions (p = 0.703), CeO_2 ENPs (p = 0.061), and Ce^{3+} ions (p = 0.144), measured as total silver or cerium in solution (C_0), remained unchanged over a 24-hour time period, suggesting that no sorption on recipients' inner walls occurred. Additionally, no significant effect of centrifugation speed on the amount of Ag ENPs (p = 0.349), Ag^+ ions (p = 0.317), CeO_2 ENPs (p = 0.501), and Ce^{3+} ions (p = 0.864) sampled close to the liquid surface was observed, indicating that the respective ENPs and ions remained stable in suspension/solution (*i.e.*, did not aggregate nor precipitate) during the 24-hour time frame. The pH of the nanoparticles dispersed in Milli-Q® water was approximately 5 or 6, in the case of Ag or CeO_2 ENPs, respectively.

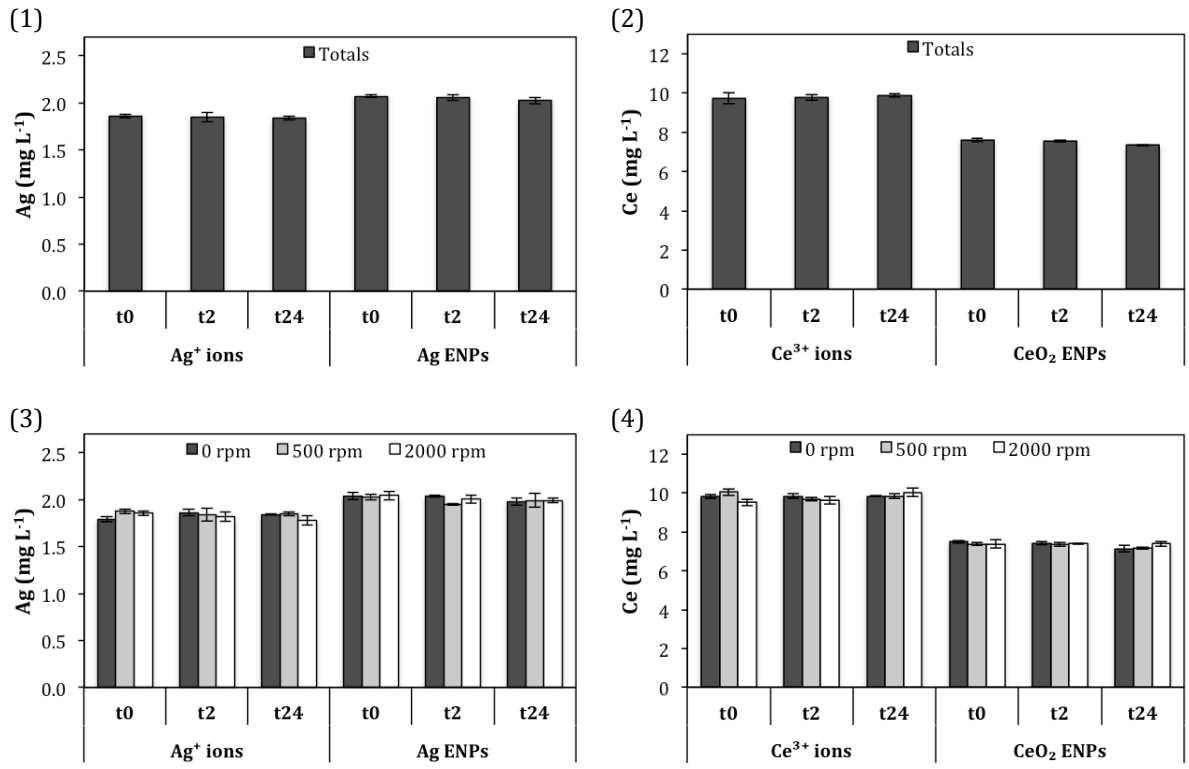

Figure 6.3 – Stability of *ca.* 2 mg L^{-1} Ag ENPs and Ag^+ ions, and *ca.* 10 mg L^{-1} CeO_2 ENPs and Ce^{3+} ions in Milli-Q® water (*i.e.*, controls), by determination of the silver or cerium concentration (C_0) in solution: (1) and (2) after shaking for 10 min (t0), 2 h (t2), or 24 h (t24), without being subjected to settling or centrifugation; (3) and (4) after being subjected to 10 min of gravitational settling (0 rpm) or 10 min of centrifugation (at 500 or 2000 rpm) at different time intervals. (Bars represent mean values, error bars indicate standard deviations, $n = 3$)

6.3.4 Ag and CeO_2 ENPs partitioning in sediment suspensions

The relative amounts (C/C_0) of Ag or CeO_2 ENPs, and Ag^+ or Ce^{3+} ions remaining in the liquid phase after spiking of the sediment suspensions and subjecting them to different centrifugation treatments are presented in Figure 6.4. The addition of nanoparticles to the sediment suspensions always resulted in higher silver or cerium content remaining in the supernatant, when compared to spiking with ions ($p < 0.05$). In the case of Ag^+ ions, maximum 32 % of silver remained in the supernatant after spiking of the sediment suspensions, whereas up to 59 % of added silver could be retrieved after spiking with Ag ENPs. The maximum amount of cerium detected in the liquid phase of the different sediment suspensions varied between 6 and 51 % or 22 and 91 % of the original spike concentration in the case of Ce^{3+} ions or CeO_2 ENPs, respectively. Generally, centrifugation

speed significantly affected the silver or cerium content remaining in the liquid phase in an inversely proportional manner ($p < 0.05$), with the exception of Doel and Linkeroever (t0, t2) spiked with Ag ENPs, Doel (t0, t24) spiked with Ag^+ ions, Doel (t2) and Linkeroever (t24) spiked with Ce^{3+} ions, and Linkeroever (t0, t24) spiked with CeO_2 ENPs ($p > 0.05$). The effect of centrifugation speed also appears to be greater in the case of CeO_2 ENPs and Ce^{3+} ions compared to Ag ENPs and Ag^+ ions, definitely looking at Doel and Linkeroever sediments. Moreover, the results obtained from adding nanoparticles or ions to Doel and Linkeroever sediment suspensions seem comparable to some extent, while the results from spiking Bornem and Mariekerke also show similarities. In the case of Bornem and Mariekerke sediments, the silver or cerium content in solution decreased with increasing equilibration time ($p < 0.05$). However, no clearly definable trend in the effect of equilibration time could be obtained when considering Doel and Linkeroever sediments, although statistically significant differences were also observed ($p < 0.05$). The pH of the sediment suspensions spiked with Ag or CeO_2 ENPs varied from 7.7 to 8.2, and no effect on pH was observed over time, nor when compared to blank sediment suspensions.

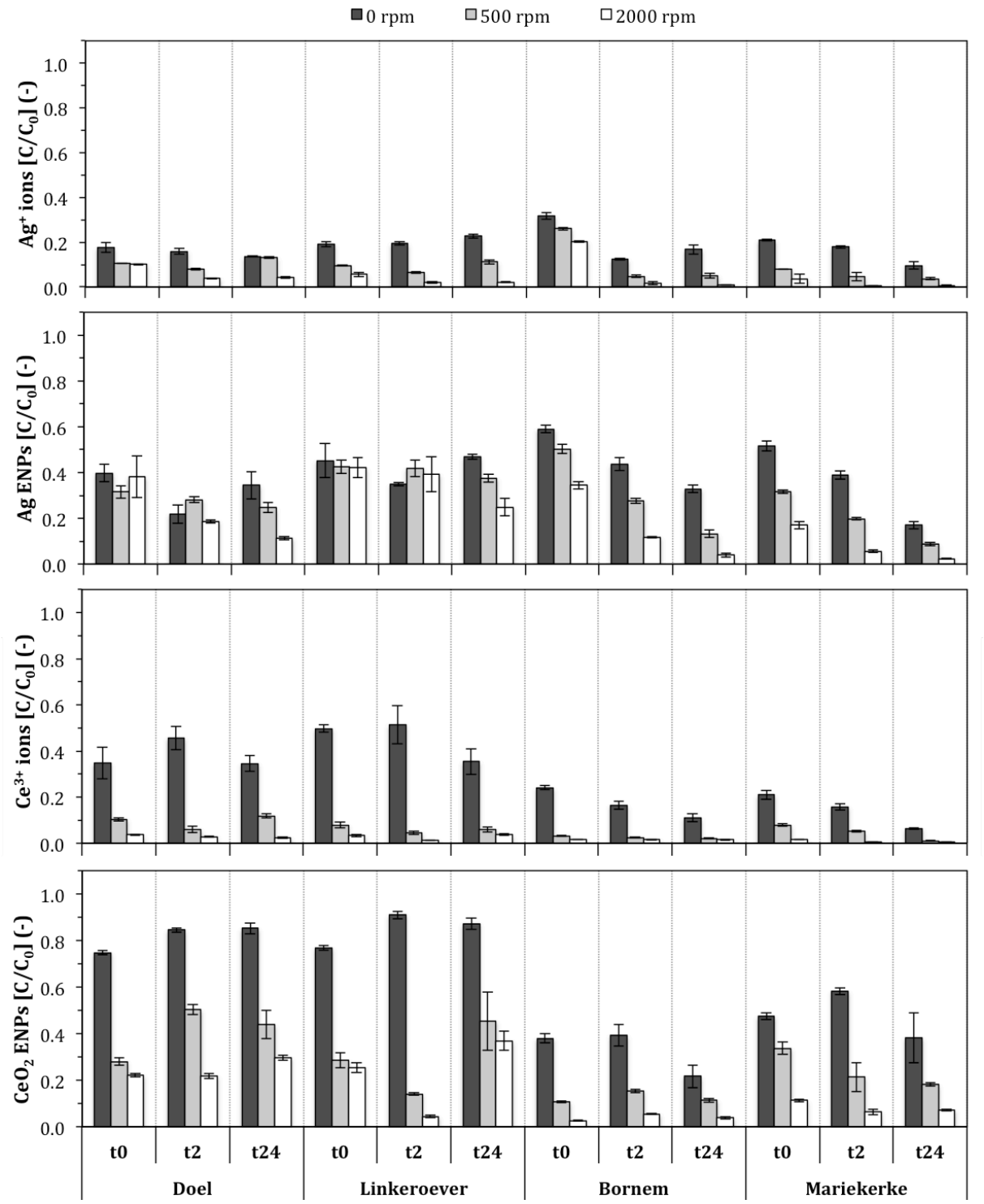

Figure 6.4 – Relative amounts of silver or cerium in the supernatant, 10 min (t0), 2 h (t2), or 24 h (t24) after spiking the different sediment suspensions with 2 mg L^{-1} Ag^{+} ions or Ag ENPs (top two graphs), or 10 mg L^{-1} Ce^{3+} ions or CeO_2 ENPs (bottom two graphs). Supernatants were obtained by subjecting the samples to 10 min of gravitational settling (0 rpm), or 10 min of centrifugation (at 500 or 2000 rpm). (Bars represent mean values, missing bars indicate values below the detection limit (DL_{Ag} = 12 μg L^{-1}; DL_{Ce} = 25 μg L^{-1}), error bars denote standard deviations, n = 3)

6.3.5 Impact of centrifugation speed on amount of suspended matter and TOC

The impact of centrifugation speed on the amount of suspended material and of TOC remaining in suspension is presented in Figure 6.5. After 10 min of gravitational settling, the percentage of suspended matter varied between 1.5 and 3.6 %. At a centrifugation speed of 500 rpm these amounts have already decreased to 0.8 – 1.5 %, whereas the suspended matter content dropped below 1 % and became independent of centrifugation speed above 1000 rpm ($p > 0.05$).

The TOC content remaining in suspension also decreased with increasing centrifugation speed ($p < 0.05$), as shown in Figure 6.5. The highest decrease was observed for Doel sediment, where the TOC concentration in the supernatant dropped from 246 to 100 and finally 43 mg L^{-1}.

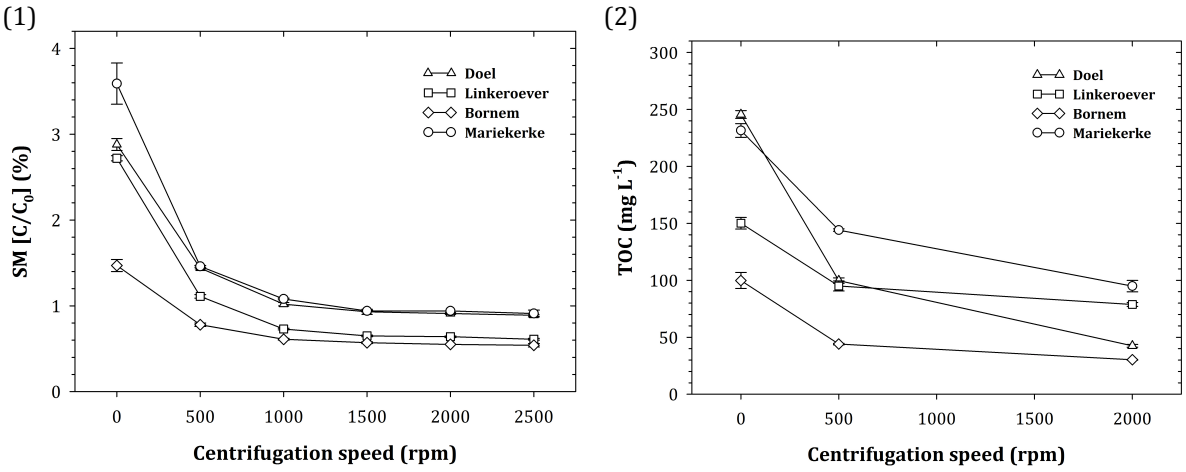

Figure 6.5 – Amount of suspended matter (1) and TOC content (2) remaining in suspension as affected by centrifugation speed, after centrifugation for 10 min. The speed of 0 rpm represents 10 min of gravitational settling. (Data shown are mean values, error bars indicate standard deviations, $n = 4$)

6.3.6 Fate of Ag and CeO_2 ENPs in sediment extracts

Figure 6.6 shows the relative amounts of Ag or CeO_2 ENPs, and Ag^+ or Ce^{3+} ions remaining in the supernatant after spiking different Doel and Bornem sediment extracts, and subjecting them to centrifugation. For Doel extracts, 6 to 21 % of the added silver remained in the liquid phase after spiking with either Ag ENPs or Ag^+ ions, and these amounts seem fairly independent of type of sediment extract (*i.e.*, Doel 0, 500, and 2000).

Significant differences were only observed for Doel (0, 0 rpm), Doel (0, 500 rpm), and Doel (500, 0 rpm) extracts ($p < 0.05$). The amounts of remaining silver in Bornem extracts were generally higher compared to Doel extracts, up to 61 % of the original spike of Ag ENPs or Ag^+ ions. Results show that up to 93 % of the added CeO_2 ENPs was found in the liquid phase, and even up to 100 % could be retrieved in the case of Ce^{3+} ions. Overall, the remaining amounts of silver or cerium decreased with increasing centrifugation speed. However, this effect seems to diminish when comparing the 0, 500, and 2000 extracts. For instance, no significant effect of centrifugation speed was observed when Ce^{3+} ions had been spiked to Doel 2000 ($p = 0.077$) and Bornem 2000 ($p = 0.761$) extracts.

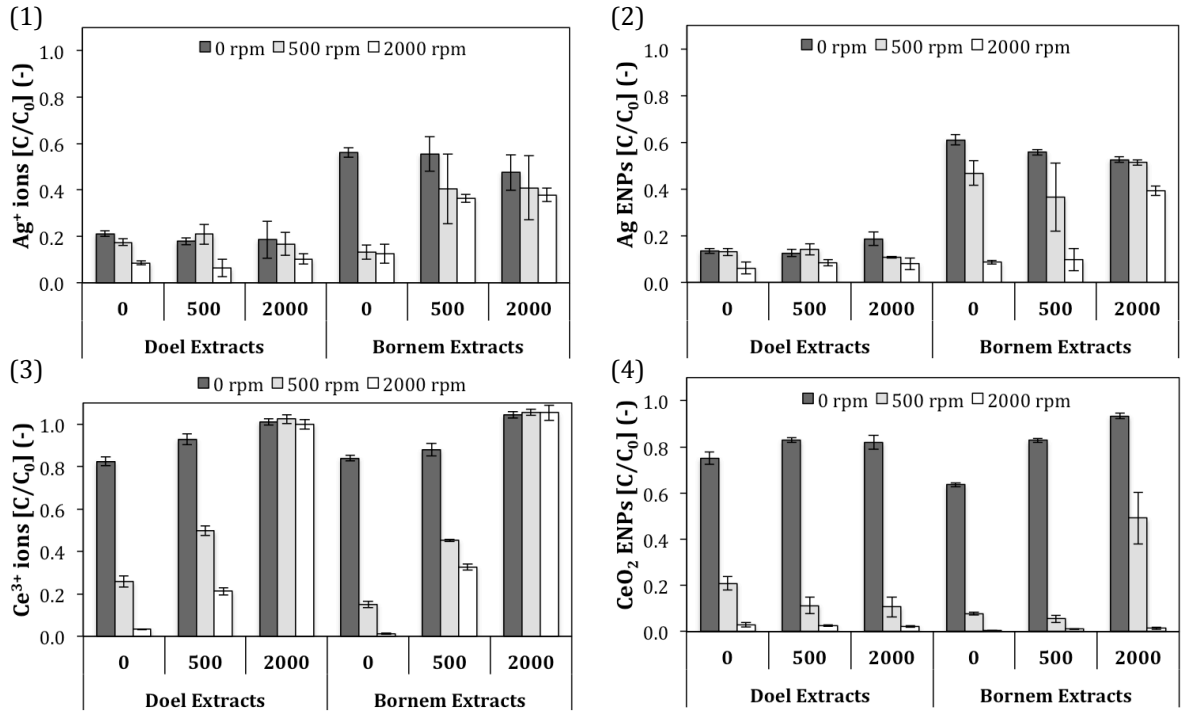

Figure 6.6 – Relative amounts of silver or cerium in the supernatant, 2 h after spiking the different Doel and Bornem sediment extracts (0, 500, and 2000) with 2 mg L^{-1} Ag^+ ions (1) or Ag ENPs (2), or 10 mg L^{-1} Ce^{3+} ions (3) or CeO_2 ENPs (4). Supernatants were obtained by subjecting the spiked Doel or Bornem sediment extracts to 10 min of gravitational settling (0 rpm), or 10 min of centrifugation (at 500 or 2000 rpm). (Bars represent mean values, missing bars indicate values below the detection limit (DL_{Ag} = 12 μg L^{-1}; DL_{Ce} = 25 μg L^{-1}), error bars denote standard deviations, $n = 3$)

6.4 Discussion

6.4.1 Sediment characteristics

In this work, the partitioning of Ag and CeO_2 ENPs in the presence of (re)suspended sediments was studied, and compared to the distribution of Ag^+ and Ce^{3+} ions between the liquid and solid phase. Sediments can indeed serve as a sink for trace metal contamination, as observed from the elevated background levels of *e.g.,* As, Cd, Cr, Cu, Pb, and Zn, obtained during characterization analyses. Additionally, it was shown that the sediment containing the highest amount of trace metals (Mariekerke) was also characterized by the highest OM, CEC, and clay content. Highly significant correlations between these parameters and metal content in floodplain soils have already been reported in the literature (Du Laing *et al.*, 2009). Overall, the physicochemical properties of the sampled intertidal sediments were in accordance with previous work conducted by Du Laing *et al.* (2007) on Scheldt river sediments.

6.4.2 Behaviour in ultrapure water

Prior to spiking the sediment suspensions with either Ag or CeO_2 ENPs, or Ag^+ or Ce^{3+} ions, their behaviour in Milli-Q® water was examined. All respective nanoparticles and ions remained unaffected by centrifugation speed in this pure matrix over the 24-hour time period, implying no significant alterations of their properties or appearance occurred, and thereby justifying these samples to serve as controls. These controls were used to normalise all partitioning results, allowing for a more straightforward comparison of the obtained results between sediments, spikes, and the applied treatments. All partitioning results were blank corrected prior to normalisation, although blank sediment suspensions yielded very low amounts of silver or cerium remaining in the liquid phase (*i.e.*, maximum 0.03 mg Ag L^{-1} or 0.35 mg Ce L^{-1}) (Figure D.1 in Appendix D).

6.4.3 Solid-liquid partitioning behaviour and fate in (re)suspended sediments

Partitioning of Ag and CeO_2 ENPs was examined over a course of batch experiments, during which the effect of centrifugation speed and equilibration time on the distribution between liquid and solid phase was also studied. Higher concentrations of silver and cerium were detected in the liquid phase when the sediments were spiked with nanoparticles compared to ions, suggesting that Ag and CeO_2 ENPs are more mobile despite having a high surface reactivity. A possible explanation for the enhanced mobility could be stabilization of the ENPs by natural organic matter (NOM) in solution. An additional set of experiments has indeed demonstrated that the stabilization of CeO_2 ENPs in the presence of quartz sand could be attributed to NOM in solution (see Chapter 7). Capping of Ag ENPs with organic molecules like citrate or polyvinylpyrrolidone (PVP) as surface ligands increases the stabilization in suspension, and could hence promote a higher mobility (El Badawy *et al.*, 2010). In contrast, the findings of a study by Lowry *et al.* (2012) showed that 70 % of initially spiked PVP-coated Ag ENPs ended up in wetland sediment. A higher mobility of citrate-stabilized CeO_2 ENPs compared to Ce^{3+} and Ce^{4+} ions in soils has also been reported in the literature by Cornelis *et al.* (2011).

The distribution of silver and cerium was significantly affected upon application of increasing settling forces, indicating alterations in the physicochemical properties of the nanoparticles have taken place. The nanoparticles may have aggregated to larger particles (homo-aggregation) or have associated with solid sediment particles (hetero-aggregation), becoming more susceptible to settling out of solution. Additionally, ionic release from the particle surface and subsequent complexation by dissolved organic matter and/or sorption onto sediment particles could have occurred. However, the results obtained when comparing the addition of nanoparticles versus ions, in addition to results from centrifugal ultrafiltration (UF, 10 kDa) of the liquid phase after 24 h (results not shown), indicate that dissolution from the particle surface was probably negligible during the experimental time frame, or that at least no free Ag or Ce ions (*i.e.*, measured in the 10 kDa UF filtrates) were detected. Upon application of Stokes' law, the settling velocity of a spherical particle dispersed in a fluid can be calculated (Equation 6.1). Subsequently, an approximate size range of particles (or particle aggregates) affected by centrifugation can be obtained. When considering a settling distance of 8 cm, more than 99 % of Ag particles smaller than 236 nm (< 295 nm for CeO_2) remain virtually unaffected (*i.e.*, remain in suspension) by centrifugation at 500 rpm for 10 min (at 20 °C), while Ag particles between 236 and

2365 nm (295 – 2944 nm for CeO_2) partially, and Ag and CeO_2 particles larger than 2365 nm or 2944 nm, respectively, completely settle out of solution. In the case of centrifugation at 2000 rpm for 10 min, Ag particles smaller than 60 nm (< 74 nm for CeO_2) remain fully suspended, whereas Ag particles between 60 and 591 nm (74 – 736 nm for CeO_2) partially, and Ag particles larger than 591 nm (> 736 nm for CeO_2) fully settle out of solution.

$$v_s = \frac{1}{18}\, g\, \frac{(\rho_s - \rho_l)}{\mu_l}\, d_s^2 \qquad \textbf{(6.1)}$$

where v_s [m s^{-1}] is the particle's settling velocity, g [m s^{-2}] is the gravitational (or centrifugal) acceleration, ρ_s and ρ_l [kg m^{-3}] are the mass densities of the solid particle (10 501 kg m^{-3} for Ag and 7132 kg m^{-3} for CeO_2) and the fluid medium (998.2 kg m^{-3} for water at 20 °C), respectively, μ_l [Pa s] is the dynamic viscosity of the liquid medium, and d_s [m] is the particle diameter.

The solid-liquid partitioning of nanoparticles is governed by their sorption, aggregation, precipitation, and dissolution behaviour, which in turn are linked to the characteristics of the environmental matrix (Boxall *et al.*, 2007). For instance, El Badawy *et al.* (2010) suggested that aggregation of Ag ENPs is favoured in conditions of high ionic strength and in the presence of Ca^{2+}, while Liu and Hurt (2010) concluded that pH and dissolved oxygen content greatly impact Ag ENPs dissolution rate. Sediment characteristics directly influence the solution chemistry (Baalousha, 2009; Keller *et al.*, 2010). Association of nanoparticles and ions therefore depends on sediment properties. The observed significant differences in silver or cerium content remaining in the supernatant when comparing different sediment samples, supports this suggestion. Moreover, the similarities in results observed after spiking Doel and Linkeroever sediments, and Bornem and Mariekerke sediments, could be caused by their, to some extent, pairwise comparable physicochemical characteristics (*e.g.*, pH, $CaCO_3$ content, and texture).

In the case of blank sediment suspensions, a strong positive correlation was found between the TOC content and the amount of suspended matter remaining in the liquid phase ($r = 0.919$, $p < 0.0005$), taking all four sediment samples into account (Figure 6.7).

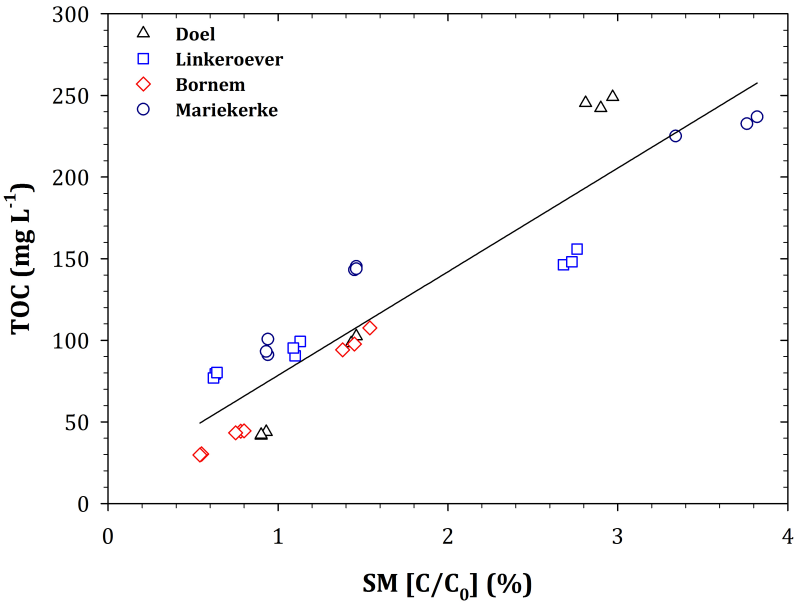

Figure 6.7 – Relationship between the amount of suspended matter and the TOC content, in the supernatant of blank sediment suspensions (r = 0.919, p < 0.0005).

In turn, when looking at relationships between suspended matter or TOC content and the amount of silver or cerium remaining in the supernatant after addition of Ag or CeO_2 ENPs, or Ag^+ or Ce^{3+} ions, moderate to strong positive correlations could be obtained when considering all sediment samples together (Table 6.3).

Table 6.3 – Pearson correlation coefficients (r) and statistical significances (p) between the relative amounts of silver and cerium and the suspended matter or TOC content, remaining in the liquid phase of sediment suspensions spiked with Ag or CeO_2 ENPs, or Ag^+ or Ce^{3+} ions.

		Ag^+ ions	**Ag ENPs**	**Ce^{3+} ions**	**CeO_2 ENPs**
SM	***r***	0.612 **	0.434 **	0.644 **	0.651 **
	p	< 0.0005	0.008	< 0.0005	< 0.0005
TOC	***r***	0.467 **	0.382 *	0.595 **	0.629 **
	p	0.004	0.021	< 0.0005	< 0.0005

** Correlation is significant at the 0.01 level (2-tailed).

* Correlation is significant at the 0.05 level (2-tailed).

However, differences in the slopes of best linear fits were demonstrated, resulting in even stronger positive correlations when considering the relationships between individual sediment samples, as presented in Figures 6.8 and 6.9, and in Tables D.2 to D.9 in Appendix D. All of this suggests that the partitioning behaviour of Ag and CeO_2 ENPs,

although strongly related to the amount of organic matter and suspended solids in solution, also depends on additional sediment characteristics. Cornelis *et al.* (2011) demonstrated that the amount of clay, phosphate, and pH could play a key role in the solid-liquid distribution of citrate-capped CeO_2 ENPs, whereas also CEC is mentioned as a factor determining the partitioning of Ce^{3+} in soils. Additionally, other reports have also suggested organic carbon content and the presence of natural occurring colloids to be important parameters (Fang *et al.*, 2009; Benoit *et al.*, 2013), hereby supporting the findings from this study.

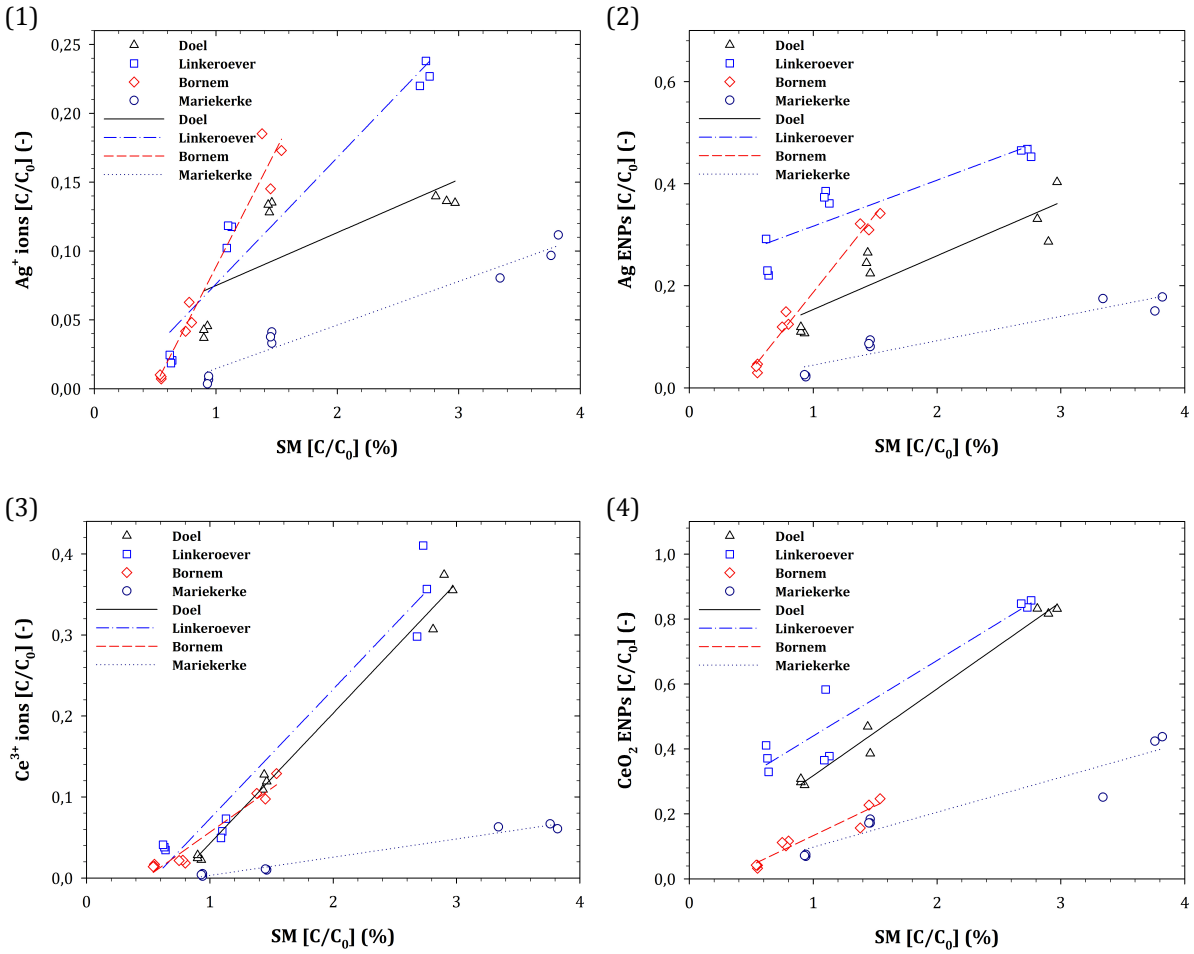

Figure 6.8 – Relationship between the relative amounts of Ag^+ ions (1), Ag ENPs (2), Ce^{3+} ions (3), and CeO_2 ENPs (4) and the amount of suspended matter, in the supernatant of spiked sediment suspensions.

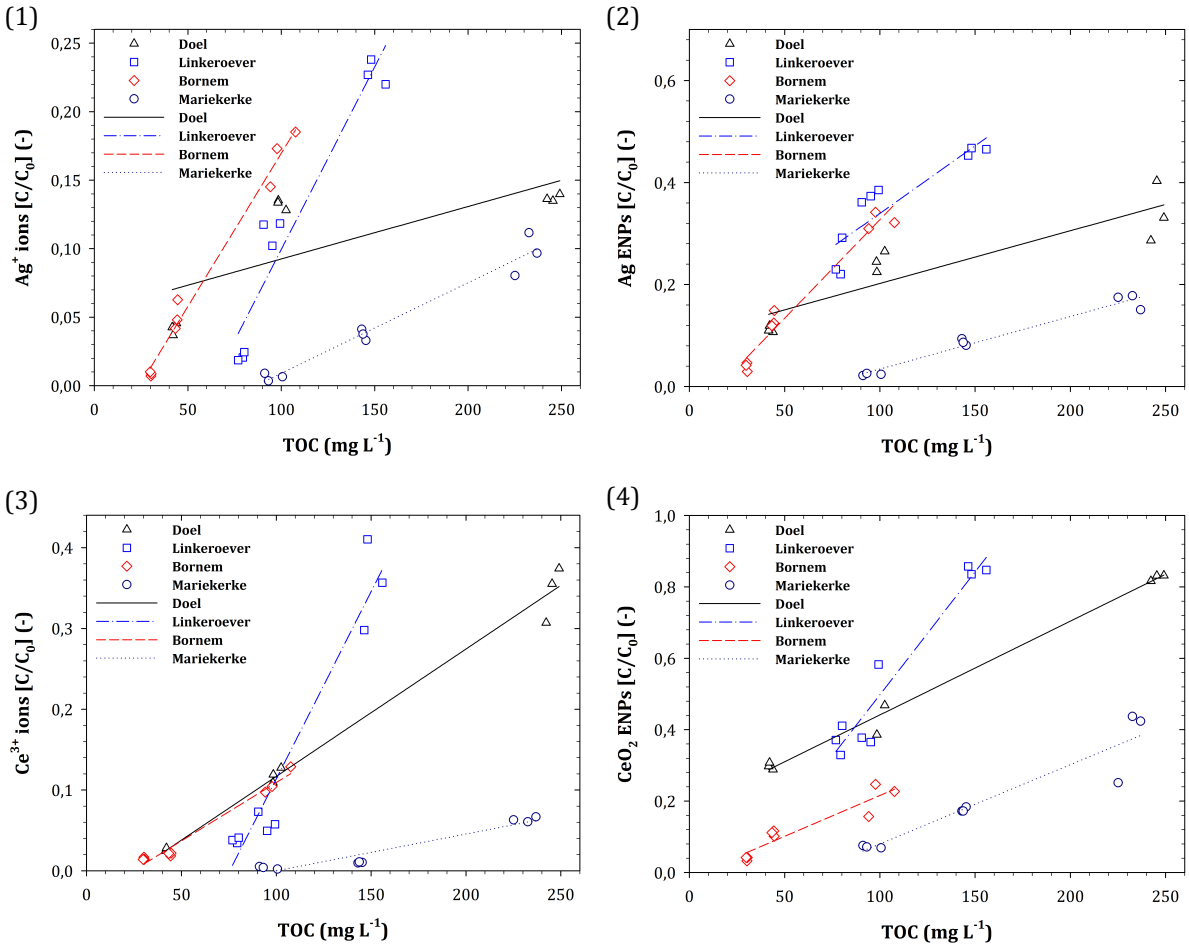

Figure 6.9 – Relationship between the TOC content and the relative amounts of Ag^+ ions (1), Ag ENPs (2), Ce^{3+} ions (3), and CeO_2 ENPs (4), in the supernatant of spiked sediment suspensions.

Indeed, when looking at other sediment characteristics, the remaining amount of silver in solution resulting from Ag ENPs could also be correlated to the pH, OM, $CaCO_3$, TN, CEC, TP, and clay content, as well as to the Ca, Cd, Cr, Ni, Fe, Mn, Pb, Cu, Zn and Al content. In addition to the pH, $CaCO_3$, and TP content, also the amounts of Cl^-, Ca, Na, and Cd were significantly correlated in the case of CeO_2 ENPs. An extensive overview of these Pearson correlation analysis results can be retrieved in Tables D.10 and D.11 in Appendix D. Although, caution should be employed when drawing definitive conclusions from these results, as the sediment dataset used for these correlation analyses was only comprised of four different sediments, still they can provide a good indication of factors affecting the solid-liquid partitioning of Ag and CeO_2 ENPs, given the fact that the results are in agreement with what is reported in the literature.

6.4.4 Behaviour and fate in sediment extracts

The behaviour of Ag and CeO_2 ENPs in different sediment extracts was examined and compared to the fate of Ag^+ and Ce^{3+} ions. Generally, an increase in silver or cerium content remaining in solution was observed when comparing sediment extracts "0" to "500" to "2000". At the same time, a decline in the effect of centrifugation speed was also demonstrated. These results again suggest that when less colloidal material is present in solution, the probability for hetero-aggregation and possible co-precipitation decreases, and nanoparticle bioavailability is potentially enhanced. Additionally, for Bornem extracts it was shown that up to 60 % of the initially spiked Ag ENPs could be retrieved in solution, compared to only 20 % in the case of Doel extracts. A possible explanation for these findings could be the higher chloride content in the original Doel sediment compared to Bornem sediment. The same trend was observed in the case of Ag^+ ions. Silver chloride (AgCl) is quite insoluble ($K_{sp,\ 25\ °C}$ = 1.77 × 10^{-10}) and Ag ENPs could form precipitates with Cl^- even without complete dissolution of the entire nanoparticle first (Choi *et al.*, 2009). For CeO_2 ENPs even up to 90 % of the initial spike could be retrieved in solution. However, upon application of centrifugation these amounts are drastically reduced, indicating that transformations of the nanoparticles, *e.g.*, the formation of aggregates, have occurred. Nevertheless, it seems that even in complex environmental aquatic matrices, Ag and CeO_2 ENPs still appear to remain quite mobile, at least over a 2-hour period and be it no longer in their pristine form.

6.5 Conclusion

This study aimed to contribute to the knowledge on the potential fate of engineered nanoparticles in aquatic environments, by examining the solid-liquid partitioning behaviour of Ag and CeO_2 ENPs in sediment suspensions. In the absence of sediment, Ag and CeO_2 ENPs as well as Ag^+ and Ce^{3+} ions remained stable in suspension/solution during 24 h, whereas a significant decrease of silver or cerium content remaining in suspension was observed in the presence of natural sediments. Nevertheless, substantial fractions of silver or cerium could still be retrieved in the aqueous phase of the different sediment suspensions after 24 h, indicating a relatively high potential mobility and bioavailability of the nanoparticles. Furthermore, it was demonstrated that Ag^+ and Ce^{3+} ions are seemingly retained more

strongly by the sediment solid phase compared to their nanoparticulate counterparts, rendering the Ag and CeO_2 ENPs more mobile. It was shown that aggregation, or association of Ag and CeO_2 ENPs with sediment constituents, is influenced by sediment properties and that the solid-liquid partitioning of the nanoparticles as well as their ionic counterparts was strongly related to the amount of dissolved organic carbon and the suspended solids content. When less colloidal material is present, the probability for hetero-aggregation and possible co-precipitation is reduced, and the migration potential of the nanoparticles might be enhanced.

As this study was performed under fully oxic conditions, using prepared sediment samples and upon application of quite high spike concentrations, the main focus was merely pointed towards physicochemical interactions. However, further research is needed to elucidate the fate and behaviour of nanoparticles in more realistic environmental conditions. For instance, the presence of a biofilm of (micro)organisms might have an influence on the solid-liquid partitioning or dissolution behaviour of nanoparticles. Additionally, longer-term experiments should be performed and a larger set of sediments and soils should be studied, in order to receive better insight in the environmental fate of engineered nanoparticles. Finally, more specialized and technologically advanced analytical techniques (*e.g.*, field-flow fractionation and electron microscopy) could provide important additional information in the appearance, behaviour, and fate of ENPs in aquatic media.

Chapter 7

Fate of Ag and CeO_2 nanoparticles and effect of natural organic matter on CeO_2 nanoparticles stability in soil suspensions

7 Fate of Ag and CeO_2 nanoparticles and effect of natural organic matter on CeO_2 nanoparticles stability in soil suspensions[‡]

7.1 Introduction

Due to their exceptionally small size (< 100 nm), engineered nanoparticles (ENPs) often possess unique size-related properties (*e.g.*, a high surface-to-volume ratio and surface reactivity) that are not observed in bulk materials (Akaighe *et al.*, 2013). These particles have received a lot of attention and concern recently due to their rapidly increasing applications in various areas of the economy, such as textiles, electronics, optics, pharmaceutics, medical devices, cosmetics, food packaging, biosensors, catalysts, fuel cells, (waste)water treatment and environmental remediation (Handy *et al.*, 2008b; Klaine *et al.*, 2008). The growing manufacturing and use of ENPs increases the likelihood that they will find their way into aquatic or terrestrial environments such as soils, where they might be transported via pore water and potentially end up in groundwater (Tian *et al.*, 2010; Liang *et al.*, 2013b). Hence, there exists a public concern about the potential harmful interactions with the natural environment and adverse effects ENPs might have on organisms and human health (Klaine *et al.*, 2008; Gottschalk *et al.*, 2013). The extent of such detrimental effects is dependent on *e.g.*, the concentration, bioavailability, and possible transformations of ENPs in the environment (Cornelis *et al.*, 2013; Cornelis *et al.*, 2014). Therefore, it is of considerable importance to gain extensive knowledge on the environmental behaviour and fate of ENPs (Fang *et al.*, 2009; Sagee *et al.*, 2012).

Metallic nanoparticles, including Ag, Au, Fe, CeO_2, TiO_2, and ZnO ENPs, are currently the most widely utilized engineered nanomaterials (Liu *et al.*, 2012; Tourinho *et al.*, 2012; Benoit *et al.*, 2013). Ag ENPs have been used in numerous commercial products, such as cosmetics, textiles, and medical products, mostly because of their antimicrobial properties (Benoit *et al.*, 2013; Liang *et al.*, 2013a), and have already been shown to be toxic to a wide range of aquatic and terrestrial organisms (Levard *et al.*, 2012; Tourinho *et al.*, 2012). The

[‡] *Submitted for publication as: Van Koetsem, F., Woldetsadik, G.S., and Du Laing, G.* ***Fate of Ag and CeO_2 nanoparticles and effect of natural organic matter on CeO_2 nanoparticles stability in soil suspensions.***

high oxygen storage and UV absorbing capacity of CeO_2 ENPs have for instance led to their use as catalysts in the automotive industry for reducing NO_x and particulate emissions of diesel engines, and in fuel cells, polishing materials, and a variety of pharmaceutical and agricultural products (Cornelis *et al.*, 2011; Li *et al.*, 2011). CeO_2 ENPs have also been demonstrated to induce toxic effects in bacteria, algae, and even in human cells (Thill *et al.*, 2006; Van Hoecke *et al.*, 2009; Rogers *et al.*, 2010a; Zhang *et al.*, 2011a).

As a major environmental compartment, soils are considered to be a potential sink for engineered nanomaterials (Cornelis *et al.*, 2014). Main exposure pathways of terrestrial environments to metallic nanomaterials, such as Ag and CeO_2 ENPs, include the application of wastewater biosolids to agricultural land as soil amendments, leakage from landfills, deposition of airborne particulates, accidental spills, and deliberate use in for instance soil remediation or agrochemicals (Zhang and Elliot, 2006; Klaine *et al.*, 2008; Limbach *et al.*, 2008; Gottschalk *et al.*, 2009; Kiser *et al.*, 2009). Consecutively, soils are expected to be a source of ENPs to aquatic environments *e.g.*, through erosion and surface runoff (Whitley *et al.*, 2013). Still, relatively little information on the behaviour and fate of metallic ENPs in the soil compartment has been generated (Tourinho *et al.*, 2012).

The stability of nanoparticles in complex aquatic matrices such as soil solutions, is a prime determinant of their fate, and possibly their bioavailability and toxicity (Gimbert *et al.*, 2007; Liu *et al.*, 2012). Preferential partitioning of ENPs towards the solid phase reduces their mobility and hence bio-accessibility, whereas well-dispersed nanoparticles could persist longer in the environment, be transported more easily over longer distances, and potentially be involved in particle-facilitated contaminant transport (Gimbert *et al.*, 2007; Fang *et al.*, 2009). The nature and extend of their partitioning between solid and liquid soil compartments, which is suggested to be highly affected by solution chemistry and hence soil properties, are therefore essential aspects to consider in order to assess the potential environmental risks engineered nanomaterials may pose (Cornelis *et al.*, 2012; Sagee *et al.*, 2012). Soils are comprised of a large collection of reactive surfaces, which could impact the bioavailability and mobility of nanoparticles *e.g.*, through deposition (Batley *et al.*, 2013). Additionally, environmental conditions such as pH, ionic strength, and dissolved organic matter, have already been demonstrated to affect the behaviour of ENPs (Ben-Moshe *et al.*, 2013). For instance, at ionic strengths higher than the critical coagulation concentration, ENPs will quickly aggregate and settle out of solution, whereas natural organic matter on the other hand could sorb onto nanoparticles and stabilize them in suspension, thereby

increasing their mobility potential (Johnson *et al.*, 2009; Liu *et al.*, 2012; Liang *et al.*, 2013a; Whitley *et al.*, 2013). However, the majority of studies examining for instance the retention and transport behaviour of ENPs, have done so utilizing highly idealized systems using model porous media such as well-defined glass beads or homogeneous quartz sand (Petosa *et al.*, 2010; Tian *et al.*, 2010; Kanel and Al-Abed, 2011; Li *et al.*, 2011; Liang *et al.*, 2013a). Although studies employing such simplified systems have provided fundamental mechanistic insights and valuable knowledge on physicochemical parameters affecting nanoparticle transport and deposition, they are not able to account for the full complexity and heterogeneity of natural soil systems (Cornelis *et al.*, 2013; Liang *et al.*, 2013b). Only few studies have investigated the solid-liquid distribution of ENPs using natural soils or sediments (Fang *et al.*, 2009; Cornelis *et al.*, 2010; Cornelis *et al.*, 2011, Cornelis *et al.*, 2012; Van Koetsem *et al.*, in press), and how their retention behaviour and mobility is affected by physicochemical soil properties has not been examined systematically (Cornelis *et al.*, 2012). Therefore, to date there is still a paucity of information regarding the factors affecting the partitioning behaviour of ENPs, and to a further extent, their transport behaviour and general environmental fate, especially in natural soil systems (Akaighe *et al.*, 2013; Benoit *et al.*, 2013; Whitley *et al.*, 2013).

The current study aimed to contribute to the general understanding of the environmental behaviour and fate of engineered nanomaterials in aqueous systems, by examining the solid-liquid partitioning of Ag and CeO_2 ENPs as well as their ionic counterparts in soil suspensions. In particular, the partitioning kinetics and association of these nanoparticles and corresponding ions with soil constituents, such as colloidal matter and dissolved organic carbon, were investigated, as well as how they are influenced by soil properties, in order to assess their stability and potential mobility in complex aqueous media, and aid in the identification of factors affecting the physicochemical behaviour and fate of nanoparticles in aquatic and terrestrial environments. Therefore, 24-hour lasting batch experiments were performed under oxic conditions, using three distinct natural soils and one model soil (*i.e.*, quartz sand) that were thoroughly characterized prior to being (re)suspended with ultrapure water and spiked with nanoparticles or ions, and finally being subjected to gravitational settling or centrifugation.

7.2 Materials and methods

7.2.1 Soil sampling and characterization

Samples (top 0-25 cm) of three soils in the region of Ghent (Belgium) (*i.e.*, in Lembeke, Wannegem-Lede, and Zwijnaarde) were collected. The collected soils were air-dried in a greenhouse at 25 °C, before being crushed manually if necessary, and passed through a 2 mm mesh sieve. In addition to the sampled soils, quartz sand and peat were purchased at local stores. Prior to characterization, the quartz sand was rinsed with diluted nitric acid and deionized water, dried in an oven at 65 °C, and sieved over a 1 mm mesh. Loss on ignition (LOI) after incineration of 3 g oven-dried soil in a muffle furnace at 550 °C for 2 h, was employed to determine the organic matter content (OM) (Salehi *et al.*, 2001). After extraction with deionized water (1:10 (m:V)) on an orbital shaker for 24 h, the dissolved organic carbon (DOC) content was measured in the extracts after filtration over ashless filter paper (MN 640 m, Macherey-Nagel GmbH & Co. KG, Düren, Germany) using a TOC analyser (TOC-V_{CPN}, Shimadzu, Kyoto, Japan) (Jones and Willet, 2006). Soil texture was determined according to the Bouyoucos hydrometer method after removing organic matter by addition of H_2O_2 (Gee *et al.*, 1986; van Reeuwijk, 2002; Sartori *et al.*, 2013). The pH (pH-H_2O) was measured in 1:5 (m:V) soil:deionized water suspensions after equilibration during 16 h (Van Ranst *et al.*, 1999). The dry matter (DM) content was determined by drying 100 g dried soil in an oven at 105 °C for 24 h and recording the mass difference. The electrical conductivity (EC) was measured in the filtrates (MN 640 m, Macherey-Nagel GmbH & Co. KG, Düren, Germany) of 1:5 (m:V) soil:deionized water suspensions after shaking for 1 h (Van Ranst *et al.*, 1999). The cation exchange capacity was determined by percolating 150 ml 1 M NH_4OAc through a percolation column filled with a mixture of 5 g soil and 12.5 g quartz sand, followed by washing through the excess with 150 mL denatured ethanol. The exchangeable ammonium ions were then eluted with 250 mL 1 M KCl and analysed in the percolate by means of a steam distillation (Vapodest Kjeldahl distillation system, Gerhardt GmbH & Co. KG, Königswinter, Germany). The total carbonate ($CaCO_3$) content was determined by back-titration (with 0.5 M NaOH) of an excess 0.25 M H_2SO_4 added to 1 g soil (Van Ranst *et al.*, 1999). The total nitrogen (TN) content was determined according to the modified Kjeldahl method by digestion of 1 g soil with 7 mL sulphuric/salicylic acid reagent, followed by alkalization with NaOH and steam distillation using a Vapodest Kjeldahl distillation system (Gerhardt GmbH & Co. KG, Königswinter,

Germany) (Van Ranst *et al.*, 1999). The total phosphorous (TP) content was determined according to the colorimetric method of Scheel after *aqua regia* destruction of 1 g soil (Van Ranst *et al.*, 1999). Pseudo-total main (Na, K, Ca, Mg) and trace elements contents (including Ag and Ce) were determined by an *aqua regia* destruction of 1 g soil (Van Ranst *et al.*, 1999), followed by analysis via inductively coupled plasma optical emission spectrometry (ICP-OES) (Vista-MPX CCD Simultaneous ICP-OES, Varian, Agilent Technologies, Santa Clara, CA, USA) (Van Ranst *et al.*, 1999). More details regarding the employed soil characterization procedures are outlined in Appendix A.

7.2.2 Nanoparticles and ionic solutions

Citrate-stabilized Ag ENPs (100 mg L^{-1}, APS: *ca.* 10 nm, ζ-potential: -50 ± 5 mV, pH: 6 – 8) and CeO_2 ENPs (50 000 mg L^{-1}, APS: 4 ± 2 nm, ζ-potential: +40 ± 5 mV), obtained as aqueous stock dispersions from PlasmaChem GmbH (Berlin, Germany), were analysed further via photon correlation spectroscopy (PCS) (Malvern PCS-100SM, Malvern Instruments Ltd., Worcestershire, UK) to determine the particle size distributions (PSDs), subjected to zeta (ζ) potential measurements to assess their surface charge (Zetasizer 3000 HSa, Malvern Instruments Ltd., Worcestershire, UK), and visualized via transmission electron microscopy (TEM) (JEM-2200FS, Jeol Ltd., Tokyo, Japan) equipped with energy dispersive X-ray spectrometry (EDS). PCS analyses were performed in quadruplicate, at 25 °C, using a measuring angle of 150 degrees. PSDs were obtained via multi modal analysis, whereas the *Z*-average hydrodynamic diameter was obtained by cumulant analysis. Ionic silver (as $AgNO_3$) (Plasma HIQU, 10 000 ± 20 μg Ag^+ mL^{-1} in 2 – 5 % HNO_3) and cerium (as $Ce(NO_3)_3$) (Plasma HIQU, 10 000 ± 20 μg Ce^{3+} mL^{-1} in 2 – 5 % HNO_3) reference standard solutions were acquired from ChemLab NV (Zedelgem, Belgium), and used as the ionic spikes (*i.e.*, Ag^+ ions and Ce^{3+} ions) in the batch experiments. All chemical reagents used in this study were of analytical grade.

7.2.3 Batch experiments

Ultrapure water (18.2 MΩ cm^{-1}) (Milli-Q®, EMD Millipore Corp., Billerica, MA, USA) was used to prepare 1:10 (m:V) soil suspensions in 50 mL centrifuge tubes. These suspensions were spiked with either Ag ENPs (2 mg L^{-1}), CeO_2 ENPs (10 mg L^{-1}), Ag^+ ions (2 mg L^{-1}) or Ce^{3+} ions (10 mg L^{-1}), prior to being placed on an orbital shaker for 10 min (t0),

2 h (t2), or 24 h (t24). At these time intervals, the suspensions were either subjected to centrifugation (Megafuge 1.0, Heraeus, Hanau, Germany) at 500 or 2000 rpm (*i.e.*, 46 or 738 *g*, respectively) for 10 min, or left for 10 min of gravitational settling (0 rpm). Finally, after proper digestion (*i.e.*, on a hotplate at 150 °C for 2 h with *aqua regia* for cerium, or with 65 % HNO_3 and 30 % H_2O_2 in the case of silver), the supernatants were analysed for total silver or cerium content by means of ICP-OES (Vista-MPX CCD Simultaneous ICP-OES, Varian, Agilent Technologies, Santa Clara, CA, USA). The set-up also included blank (*i.e.*, un-spiked soil suspensions) and control (*i.e.*, spiked Milli-Q® water) samples.

Comparable experimental procedures were employed to examine the impact of centrifugation speed on the amount of suspended matter (SM) and the total organic carbon content (TOC) remaining in the supernatant of soil suspensions. The 1:10 (m:V) soil suspensions were prepared with Milli-Q® water in 50 mL centrifuge tubes, and shaken for 24 h on an orbital shaker. Afterwards, the suspensions were subjected to centrifugation for 10 min at selected gyration velocities (*i.e.*, at 500, 1000, 1500, 2000 or 2500 rpm, which corresponds to 46, 184, 415, 738, or 1153 *g*, respectively) (merely at 500 or 2000 rpm in the case of TOC determinations), or left for 10 min of gravitational settling (0 rpm). The centrifuged samples were then gently placed onto a steady horizontal surface to not disturb the sample, and a 20 mL aliquot of the supernatants was pipetted into pre-dried and pre-weighed disposable aluminium evaporation dishes. Finally, the amount of soil still present in solution (*i.e.*, in the supernatant) was determined in function of centrifugation speed, by determining the mass difference after drying in an oven at 105 °C for a minimum of 6 h. The TOC content was measured directly using a TOC analyser (TOC-V_{CPN}, Shimadzu, Kyoto, Japan), after sampling 10 mL from the different supernatants.

A final set of batch experiments was performed to explore the impact of natural organic matter (NOM) on the stability of CeO_2 ENPs in the aqueous phase of quartz sand mixtures. Peat extracts containing various concentrations of NOM (*i.e.*, 0, 0.5, 1, 5, 10, and 50 mg TOC L^{-1}) were prepared with Milli-Q® water, and 40 mL aliquots were transferred to 50 mL centrifuge tubes already containing 4 g of quartz sand. The NOM and quartz sand containing suspensions were then spiked with CeO_2 ENPs (10 mg L^{-1}), put on an orbital shaker for 10 min (t0), 2 h (t2), or 24 h (t24), and subjected to centrifugation at 2000 rpm or left to settle (0 rpm) for 10 min. Finally, the supernatant was sampled, digested, and analysed for total cerium content via ICP-OES in a similar manner as described above.

7.2.4 Data processing

SPSS Statistics 22 (IBM, Armonk, NY, USA) was used to perform analysis of variance (ANOVA) and Pearson's product-moment correlation analysis. Shapiro-Wilk's test was used to check for normality of data. In case the conditions for homogeneity of variances resulting from Levene's test were violated, Welch's *t*-test was employed to examine equality of means instead of ANOVA. Significant mean differences were further examined via Tukey's HSD or Games-Howell's *post-hoc* tests. Violations of data normality were also assessed by employing Kruskal-Walli's *H*-test, followed by pairwise comparisons as *post-hoc* analysis using Dunn's procedure with a Bonferroni correction for multiple comparisons. Numerical and graphical data processing was performed via Excel (Microsoft Corp., Redmond, WA, USA) and SigmaPlot 12.5 (Systat Software Inc., Chicago, IL, USA) software packages.

7.3 Results and discussion

7.3.1 Nanoparticle characterization

The measured *Z*-average size of the Ag and CeO_2 ENPs dispersed in Milli-Q® water was 14.8 ± 1.3 nm and 6.2 ± 0.5 nm, respectively. The ζ-potential of the Ag ENPs was determined to be -40.7 ± 6.2 mV, whereas the CeO_2 ENPs had a ζ-potential of +52.3 ± 1.9 mV, when dispersed in Milli-Q® water at a pH of 5 or 6.5, respectively. On overall, both the obtained average particle size and surface charge of the Ag and CeO_2 ENPs are therefore in accordance to what was claimed by the manufacturer. However, although visualisation via TEM together with the obtained particle size distributions from PCS measurements indeed confirmed that the majority of the Ag ENPs were *ca.* 10 nm in size, they also indicated the presence of some larger-sized particles between 10 and 70 nm (see also Figures 6.2 and 6.3 in Chapter 6). All nanoparticles observed via TEM seemed to have a spherical morphology.

7.3.2 Soil characterization

The physicochemical properties of the soils are tabulated in Table 7.1, the main and trace elements content in Table 7.2. According to the USDA's soil texture classification system, Lembeke, Wannegem-Lede, and Zwijnaarde can be classified as sandy, loamy sand,

and silt loamy soils, respectively. Soil-pH varied from moderately acidic at Lembeke (5.41) to slightly alkaline at Wannegem-Lede (7.53). The highest EC (229 μS cm^{-1}), and silt (50.9 %) and clay (11.3 %) content were also observed in the latter soil sample. In general, Wannegem-Lede contained the highest amounts of main and trace elements, Lembeke the lowest (not taking quartz sand into account). The higher geogenic cerium content in Wannegem-Lede (35.5 mg kg^{-1}) may be explained by the soil texture, as concentrations of rare earth elements such as Ce, have been observed to increase with increasing clay or silt content (Mihajlovic *et al.*, 2014). Zwijnaarde had the highest OM (4.61 %), DOC (688 mg kg^{-1}), TN (1.8 g kg^{-1}), and TP (715 mg kg^{-1}) content. The CEC of the three soils was comparable and ranged between 8.49 and 9.27 $cmol_c$ kg^{-1}. On overall, Lembeke and Zwijnaarde soils showed quite some similarities. However, the amount of exchangeable cations varied significantly between these two soils, probably due to the difference in pH and the fact that the CEC was determined after buffering at neutral pH.

Table 7.1 – Physicochemical characteristics of the sampled soils and purchased quartz sand (mean value ± standard deviation, n = 3). Different letters indicate statistically significant differences ($p < 0.05$) between samples for each parameter.

Parameter		Lembeke	Wannegem-Lede	Zwijnaarde	Quartz sand
pH-H_2O	**(-)**	5.41 ± 0.04 ^{a}	7.53 ± 0.07 ^{d}	7.06 ± 0.01 ^{c}	6.76 ± 0.06 ^{b}
EC	**(μS cm^{-1})**	113 ± 1 ^{b}	229 ± 2 ^{d}	170 ± 3 ^{c}	12 ± 1 ^{a}
CEC	**($cmol_c$ kg^{-1})**	8.67 ± 0.71 ^{b}	9.27 ± 0.25 ^{b}	8.49 ± 0.26 ^{b}	0.29 ± 0.06 ^{a}
OM	**(%)**	3.68 ± 0.07 ^{c}	3.11 ± 0.01 ^{b}	4.61 ± 0.19 ^{d}	0.07 ± 0.01 ^{a}
DOC	**(mg kg^{-1})**	589 ± 51 ^{a}	545 ± 52 ^{a}	688 ± 25 ^{b}	NM
$CaCO_3$	**(%)**	< 0.75	< 0.75	< 0.75	< 0.75
TN	**(g kg^{-1})**	1.3 ± 0.1 ^{c}	1.2 ± 0.1 ^{b}	1.8 ± 0.1 ^{d}	0.2 ± 0.1 ^{a}
TP	**(mg kg^{-1})**	564 ± 12 ^{b}	692 ± 6 ^{c}	715 ± 16 ^{c}	39 ± 2 ^{a}
Sand	**(%)**	90.8 ± 2.0 ^{c}	37.8 ± 0.1 ^{a}	84.7 ± 0.8 ^{b}	100 $^{\#}$
Silt	**(%)**	8.0 ± 1.1 ^{a}	50.9 ± 1.6 ^{b}	11.0 ± 0.1 ^{a}	0 $^{\#}$
Clay	**(%)**	1.2 ± 0.9 ^{a}	11.3 ± 1.1 ^{b}	4.3 ± 0.7 ^{a}	0 $^{\#}$

Data presented as "< " indicate values below the detection limit (DL). NM: not measured. $^{\#}$ Assumed values as no texture analysis was performed on the quartz sand.

Table 7.2 – Major and trace elements content in the sampled soils and purchased quartz sand (mean value ± standard deviation, n = 3). Different letters indicate statistically significant differences ($p < 0.05$) between samples for each element.

Element		Lembeke	Wannegem-Lede	Zwijnaarde	Quartz sand
Ca	**(mg kg^{-1})**	500 ± 16 ^{a}	3863 ± 96 ^{c}	1950 ± 23 ^{b}	< 4.0
K	**(mg kg^{-1})**	405 ± 21 ^{b}	2169 ± 56 ^{d}	771 ± 36 ^{c}	56.1 ± 3.4 ^{a}
Mg	**(mg kg^{-1})**	204 ± 9 ^{b}	2030 ± 83 ^{d}	657 ± 24 ^{c}	14.7 ± 0.6 ^{a}
Na	**(mg kg^{-1})**	85.7 ± 12.2 ^{b}	125 ± 20 ^{c}	48.8 ± 5.0 ^{a}	36.5 ± 3.5 ^{a}
Al	**(mg kg^{-1})**	2819 ± 76 ^{b}	10 538 ± 329 ^{d}	5534 ± 167 ^{c}	343 ± 35 ^{a}
Fe	**(mg kg^{-1})**	1381 ± 40 ^{b}	14 461 ± 1336 ^{d}	5048 ± 271 ^{c}	83.0 ± 10.4 ^{a}
Cr	**(mg kg^{-1})**	7.94 ± 0.39 ^{a}	32.6 ± 1.4 ^{c}	10.7 ± 0.7 ^{b}	< 0.4
Cu	**(mg kg^{-1})**	7.85 ± 0.30 ^{a}	15.3 ± 0.5 ^{c}	12.9 ± 0.2 ^{b}	< 1.0
Mn	**(mg kg^{-1})**	16.9 ± 0.5 ^{a}	411 ± 18 ^{c}	93.9 ± 1.1 ^{b}	< 0.5
Ni	**(mg kg^{-1})**	1.99 ± 0.19 ^{a}	16.1 ± 0.1 ^{c}	4.91 ± 0.13 ^{b}	< 1.2
Pb	**(mg kg^{-1})**	14.6 ± 0.8 ^{a}	19.4 ± 1.8 ^{b}	26.1 ± 1.4 ^{c}	< 4.0
Zn	**(mg kg^{-1})**	5.11 ± 0.68 ^{a}	43.0 ± 0.6 ^{c}	34.4 ± 0.6 ^{b}	< 2.0
Ce	**(mg kg^{-1})**	5.60 ± 0.19 ^{b}	35.5 ± 0.9 ^{d}	9.10 ± 0.15 ^{c}	< 1.3

Data presented as "< " indicate values below the detection limit (DL). In all of the soil samples, Ag, As, and Cd concentrations were below the detection limit (DL_{Ag} = 0.1 mg kg^{-1}; DL_{As} = 10 mg kg^{-1}; DL_{Cd} = 0.4 mg kg^{-1}).

7.3.3 Suspended matter and TOC content in soil suspensions as affected by centrifugation

Figure 7.1 depicts the impact of centrifugation on the suspended matter (SM) and TOC content remaining in the liquid phase of soil suspensions. The amount of SM in the supernatant after 10 min of gravitational settling (0 rpm) was *ca.* 3.8 % in the case of Wannegem-Lede, and around 1 % for Lembeke and Zwijnaarde (p = 0.180). Due to their sandy texture, Lembeke and Zwijnaarde contain more coarse soil particulates, which settle out of suspension more easily. After 10 min of centrifugation at 500 rpm, the percentage SM dropped to about 1.1 % or 0.4 % in the case of Wannegem-Lede or Lembeke and Zwijnaarde, respectively. Taking the latter two soils into account, no significant impact of centrifugation speed on SM content remaining in suspension was observed when considering centrifugation velocities higher than 500 rpm ($p > 0.05$). For Wannegem-Lede, the amount of SM decreased further to *ca.* 0.5 % at 1500 rpm and became independent of centrifugation speed from that point on ($p > 0.05$).

As presented in Figure 7.1, the amount of TOC remaining in suspension also decreased with increasing centrifugation velocity ($p < 0.05$). After 10 min of gravitational settling (0 rpm), the highest TOC content was observed for Lembeke (345 mg L^{-1}), while *ca.* 250 mg TOC L^{-1} remained in solution for Wannegem-Lede and Zwijnaarde ($p = 609$). Centrifugation for 10 min at 500 rpm resulted in comparable TOC values for all soils ($p = 0.309$), whereas at 2000 rpm around 30 mg TOC L^{-1} remained in solution in the case of Lembeke and Wannegem-Lede ($p = 0.213$), and about 85 mg TOC L^{-1} for Zwijnaarde. The TOC content remaining in the liquid phase of quartz sand mixtures was very low (8.7 – 1.3 mg L^{-1}). These results indicate that the type of dissolved organic matter differed between the tested soils, with Lembeke and Zwijnaarde containing the densest and lightest kind of NOM, respectively.

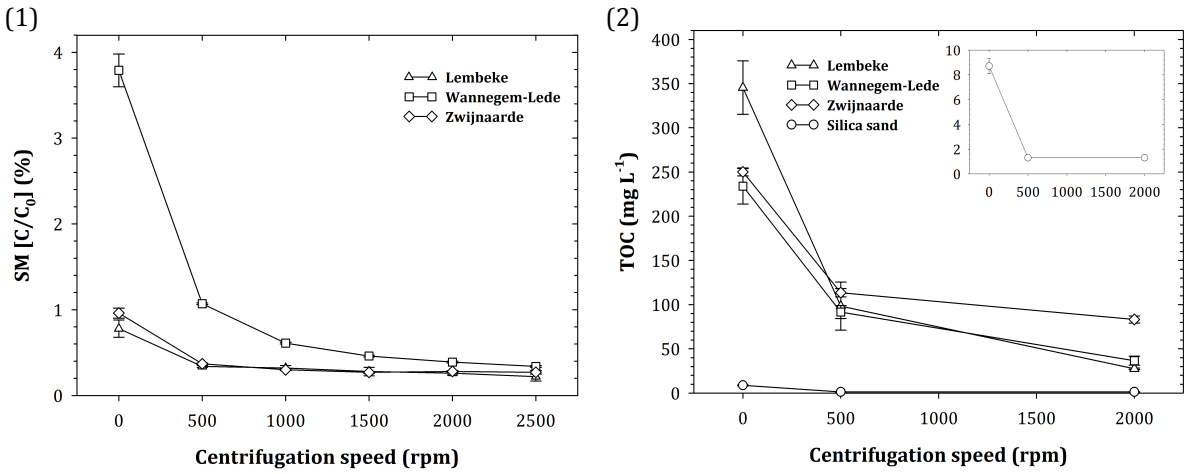

Figure 7.1 – Effect of centrifugation speed on (1) the amount of suspended matter and (2) the TOC content remaining in suspension, after centrifugation for 10 min, or after 10 min of gravitational settling (0 rpm). Data points for quartz sand have been omitted in graph (1), as already less than 0.02 % remained in suspension after just 10 min of gravitational settling. The inset in graph (2) zooms in on the evolution of TOC as affected by centrifugation speed in the case of quartz sand. (Data shown are mean values, error bars indicate standard deviations, $n = 4$)

A moderate positive correlation was found between the amount of SM and the TOC content remaining in the aqueous phase of the blank soil suspensions ($r = 0.460$, $p = 0.016$). However, when considering each soil individually, very strong positive correlations between the TOC and SM content were obtained, as presented in Figure 7.2 and in Table E.1 in Appendix E.

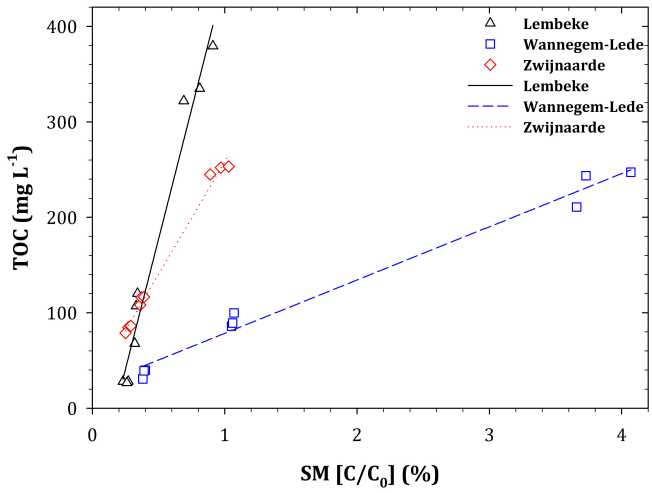

Figure 7.2 – Linear regression analysis between the amount of suspended matter and the TOC content in the supernatant of the different soil suspensions. [Lembeke (r = 0.986, p < 0.0005), Wannegem-Lede (r = 0.992, p < 0.0005), Zwijnaarde (r = 0.996, p < 0.0005)]

7.3.4 Partitioning behaviour and fate of Ag and CeO_2 ENPs in soil suspensions

Prior to spiking the different soils with nanoparticles or ions, a reference experiment was performed whereby the stability of Ag and CeO_2 ENPs, and Ag^+ and Ce^{3+} ions in Milli-Q® water was examined. In the absence of soil, the concentrations of Ag^+ ions (p = 0.317), Ag ENPs (p = 0.349), Ce^{3+} ions (p = 0.864), and CeO_2 ENPs (p = 0.501), determined as total Ag or Ce content in solution (C_0), remained unaffected during a period of 24 h, regardless of the applied centrifugation speed (see also Figure 6.3 in Chapter 6). These results indicate that neither sorption on the recipients' inner walls, nor aggregation and/or precipitation of nanoparticles or ions in solution occurred during the experimental time frame, and suggest that no significant alterations in their appearance or characteristics have taken place. Consequently, these control samples were applied to normalise all partitioning results and calculate relative silver or cerium contents remaining in solution (C/C_0), allowing for a more straightforward comparison of the different soils and treatments. Furthermore, although blank soil suspensions yielded very low background concentrations of Ag or Ce in solution (*i.e.*, maximum 0.02 mg Ag L^{-1} or 0.19 mg Ce L^{-1}) (Figure E.1 in Appendix E), partitioning results were blank corrected prior to normalisation.

Figure 7.3 presents the relative amounts of Ag or CeO_2 ENPs, and Ag^+ or Ce^{3+} ions remaining in the supernatant of soil suspensions after being spiked and subjected to centrifugation. The pH of the soil suspensions remained unaffected by spiking with nanoparticles or ions. The silver or cerium content in the aqueous phase of "real" soil suspensions was always significantly higher after exposure to Ag or CeO_2 ENPs in comparison to the addition of Ag^+ or Ce^{3+} ions ($p < 0.05$). Between 51 and 95 % of the initially spiked Ag ENPs could be retrieved in the supernatants, while 29 to 97 % of the added CeO_2 ENPs cerium remained suspended. The silver or cerium recovery in solution resulting from exposure to Ag^+ or Ce^{3+} ions varied between 2 and 35 % or between 0.3 and 54 %, respectively. Thus, ions seemingly interact more strongly with soil constituents, suggesting a higher mobility and potential bioavailability of nanoparticles compared to their ionic counterparts in natural soils, which is in agreement with results from previous studies investigating the fate of Ag and CeO_2 ENPs in (re)suspended soils and sediments (Cornelis *et al.*, 2010; Cornelis *et al.*, 2011; Cornelis *et al.*, 2012; Van Koetsem *et al.*, in press). Under environmentally relevant conditions, mineral soil particulates and organic substances predominantly exhibit a net negative surface charge (Batley and McLaughlin, 2010; Petosa *et al.*, 2010). Electrostatic interactions between Ag^+ and Ce^{3+} ions and oppositely charged soil constituents could therefore explain the observed strong retention of these ionic species by the solid phase in natural soil suspensions, whereas electrostatic repulsion due the negative surface charge of the citrate-stabilized Ag ENPs probably resulted in their overall enhanced stability in suspension (Fabrega *et al.*, 2009; El Badawy *et al.*, 2010; Bae *et al.*, 2013; Whitley *et al.*, 2013). As the CeO_2 ENPs have a positive surface charge, their high stability in the aqueous phase of real soil suspensions can most likely be attributed to stabilization by natural organic matter. Stabilization of nanoparticles by natural organic compounds such as humic and fulvic acids, is a phenomenon widely recognized to affect the behaviour and fate of nanoparticles in aqueous soil systems (Johnson *et al.*, 2009; Peralta-Videa *et al.*, 2011; Coutris *et al.*, 2012; Tourinho *et al.*, 2012; Batley *et al.*, 2013; Cornelis *et al.*, 2014). Additionally, surface adsorption of phosphate, resulting in a net negative charge, has also been reported to reduce association of CeO_2 and Al_2O_3 ENPs with soils and hence increase their mobility (Darlington *et al.*, 2009; Cornelis *et al.*, 2011).

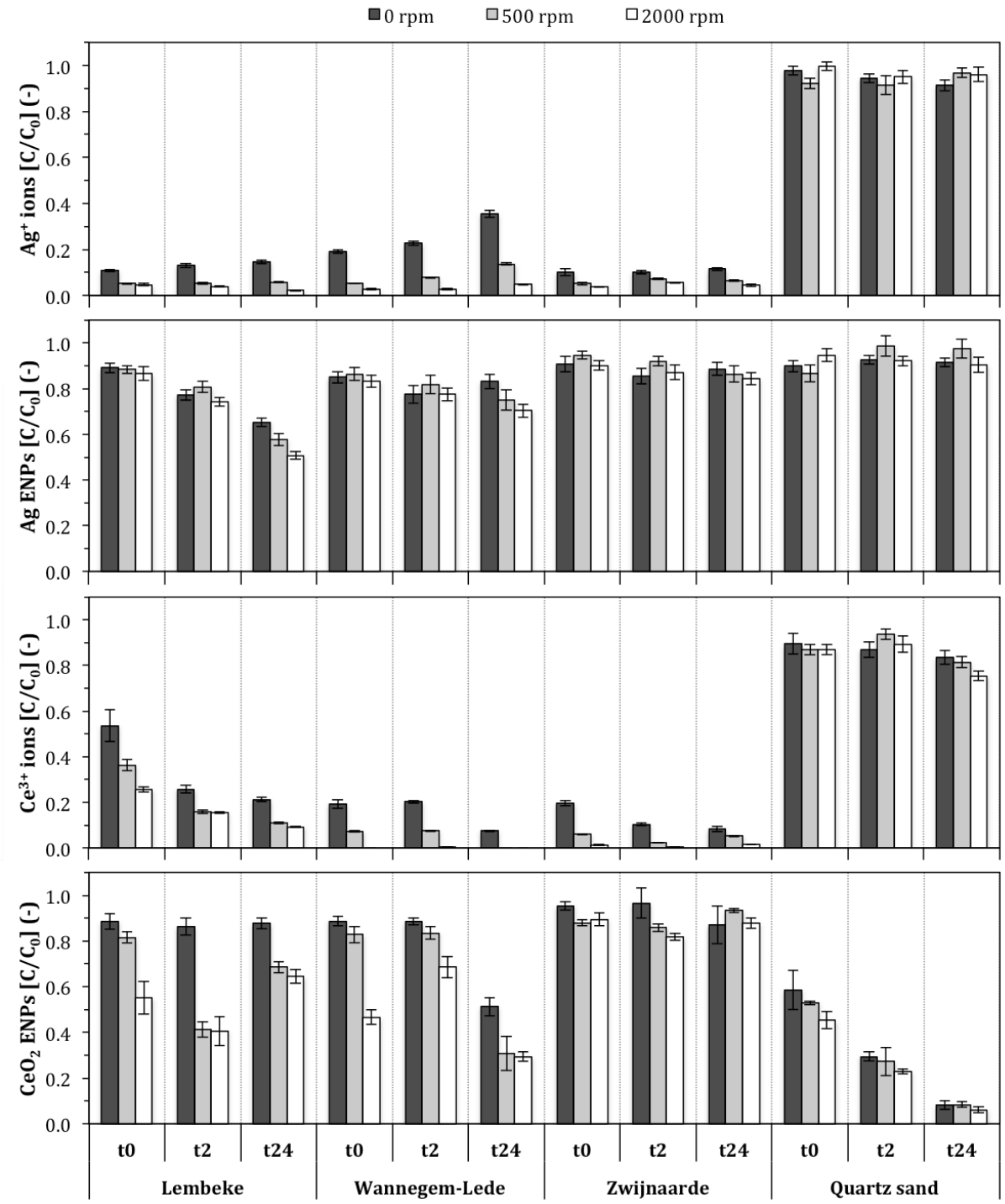

Figure 7.3 – Relative amounts of silver or cerium in the supernatant, 10 min (t0), 2 h (t2), or 24 h (t24) after spiking the different soil suspensions with 2 mg L^{-1} Ag^{+} ions or Ag ENPs (top two graphs), or 10 mg L^{-1} Ce^{3+} ions or CeO_2 ENPs (bottom two graphs). Supernatants were obtained by subjecting the samples to 10 min of gravitational settling (0 rpm), or 10 min of centrifugation (at 500 or 2000 rpm). (Bars represent mean values, missing bars indicate values below the detection limit (DL_{Ag} = 12 μg L^{-1}; DL_{Ce} = 25 μg L^{-1}), error bars denote standard deviations, n = 3)

In the presence of pure quartz sand, both Ag ENPs as well as Ag^+ ions showed a very high potential mobility (*i.e.*, between 87 and 100 % remained stable in the aqueous phase), and no statistically significant differences in the behaviour between these two species were observed ($p > 0.05$). The addition of Ce^{3+} ions also resulted in limited sorption onto the quartz sand solid phase as between 75 and 94 % remained in solution. In contrast, the fraction of CeO_2 ENPs remaining stable in suspension in the presence of quartz sand was maximum 59 % and displayed a dynamic (*i.e.*, time-dependent) decrease to 29 % (after 2 h), and finally 8 % (after 24 h) ($p < 0.05$). Although not determined experimentally, quartz sand has a net negative surface charge under the given experimental conditions (reported ζ-potential values at pH 6 – 7 vary between -70 and -30 mV, and the isoelectric point (IEP) is mentioned to lie around pH 2) (Cerda, 1988; Kim and Lawler, 2005; Darlington *et al.*, 2009; Jiang *et al.*, 2010; Kanel and Al-Abed, 2011; Vitorge *et al.*, 2013). Accordingly, the retention of the CeO_2 ENPs in quartz sand suspensions could be explained by electrostatic attraction, whereas electrostatic repulsion probably lead to the high stability of the Ag ENPs. Previous studies examining the transport behaviour of nanoparticles through porous media have also reported limited retention of negatively charged Ag and Au ENPs by quartz sand matrices (Darlington *et al.*, 2009; Sagee *et al.*, 2012; Liang *et al.*, 2013a).

The fate and behaviour of Ag and CeO_2 ENPs and Ag^+ and Ce^{3+} ions in (re)suspended soils is affected by equilibration time as indicated by statistically significant differences obtained from statistical analyses. However in general, no clearly definable trend was observed. A dynamic decrease of cerium remaining in the liquid phase was observed for all natural soils exposed to Ce^{3+} ions ($p < 0.05$), whereas for Ag^+ ions even a time-dependent increase of silver in solution was seen for Lembeke and Wannegem-Lede ($p < 0.05$), the latter suggesting potential remobilization of previously retained silver over the experimental 24-hour time frame. The relative amounts of Ag and CeO_2 ENPs remaining suspended decreased continuously over time only in the case of Lembeke and quartz sand, respectively, but additional statistically significant differences were also observed for the other soils ($p < 0.05$).

Overall, application of centrifugation significantly affected the solid-liquid distribution of Ag and CeO_2 ENPs, and Ag^+ and Ce^{3+} ions, indicating transformations in the physicochemical appearance of the nanoparticles or ions have occurred. In general, increasing centrifugation velocities resulted in a decreased silver or cerium content remaining in the aqueous phase of soil suspensions ($p < 0.05$), suggesting potential

nanoparticle aggregation or association with colloidal matter, leading to the formation of larger clusters that settle out of solution more easily upon increasing settling forces (Van Koetsem *et al.*, in press). However, no impact of centrifugation was observed in the case of Lembeke (t0, t2), Wannegem-Lede (t0, t2), and Zwijnaarde exposed to Ag ENPs, for Zwijnaarde (t2, t24) spiked with CeO_2 ENPs ($p > 0.05$). Moreover, the observed time-dependent decrease of CeO_2 ENPs in quartz sand mixtures was also not affected by increasing settling forces upon application of centrifugation ($p > 0.05$), suggesting adsorption of the nanoparticles onto quartz sand particulates and subsequent sedimentation as the sole removal mechanism of the nanoparticles from solution in this pure matrix.

As indicated by the observed differences in the solid-liquid distribution of nanoparticles or ions in distinct soil suspensions and the impact of different centrifugation treatments, their behaviour and fate in soils is influenced by solution characteristics, which in turn depend on soil properties (Boxall *et al.*, 2007; Saleh *et al.*, 2008; Baalousha, 2009; Keller *et al.*, 2010; Peralta-Videa *et al.*, 2011; Tourinho *et al.*, 2012; Batley *et al.*, 2013; Cornelis *et al.*, 2014). For instance, the difference in partitioning behaviour of Ag ENPs when comparing Lembeke and Zwijnaarde could be caused by the relatively acidic prevailing conditions of the former, which for instance might have resulted in surface charge titration, leading to aggregation and consecutive sedimentation, or in ionic release from the surface of the nanoparticles, and subsequent association with soil constituents and concurrent removal from the liquid phase. A strong positive correlation between the relative amount of Ag ENPs remaining in suspension and soil-pH was indeed observed ($r = 0.787$, $p = 0.002$), thereby supporting this suggestion. Environmental parameters such as pH, dissolved oxygen, and the presence of NOM, surface coatings and sulphides have been reported to affect the dissolution kinetics and thermodynamics of Ag ENPs considerably (Liu and Hurt, 2010; Liu *et al.*, 2011; Zhang *et al.*, 2011b; Benoit *et al.*, 2013). In addition, the relative amount of Ag ENPs remaining in the aqueous phase was also found to correlate significantly with the Pb, Cu, and Zn content, whereas in the case of CeO_2 ENPs significant correlations were obtained for CEC, OM, DOC, TN, TP, silt, and clay content, as well as for the amounts of Ca, Cr, Ni, Mn, Cu, and Zn (see also Tables E.10 and E.11 in Appendix E for an extensive overview of these Pearson correlation analysis results). It should be mentioned however that these results were obtained from a limited collection of different soils, thus caution should be employed when drawing definitive conclusions. Nevertheless, as these results are also in agreement with what is mentioned in the literature, they can still provide a good

indication of factors affecting the solid-liquid partitioning behaviour of Ag and CeO_2 ENPs in aqueous matrices under environmentally relevant conditions. For instance, pH, ionic strength, OM content, and colloidal and granulometric clay particles have been demonstrated to affect retention of Ag, Au, Fe, Al_2O_3, CeO_2, TiO_2, and ZnO ENPs in soils (Saleh *et al.*, 2008; Darlington *et al.*, 2009; Fang *et al.*, 2009; Johnson *et al.*, 2009; Solovitch *et al.*, 2010; Cornelis *et al.*, 2011; Coutris *et al.*, 2012; Zhou *et al.*, 2012; Cornelis *et al.*, 2013; Benoit *et al.*, 2013; Liang *et al.*, 2013b).

Furthermore, when looking at the relationships between the suspended matter or TOC content and the relative amount of Ag or CeO_2 ENPs, or Ag^+ or Ce^{3+} ions remaining in the aqueous phase of (re)suspended natural soils as depicted in Figures 7.4 and 7.5, very strong correlations could be obtained when considering each soil sample individually, with the exception of Zwijnaarde, where the correlations were statistically significant only in the case of Ag^+ and Ce^{3+} ions (see also Tables E.2 to E.9 in Appendix E). These results again indicate that besides association of nanoparticles or ions with suspended solids and organic compounds, their partitioning behaviour and ultimate fate in soils also strongly depends on additional physicochemical properties of the environmental matrix.

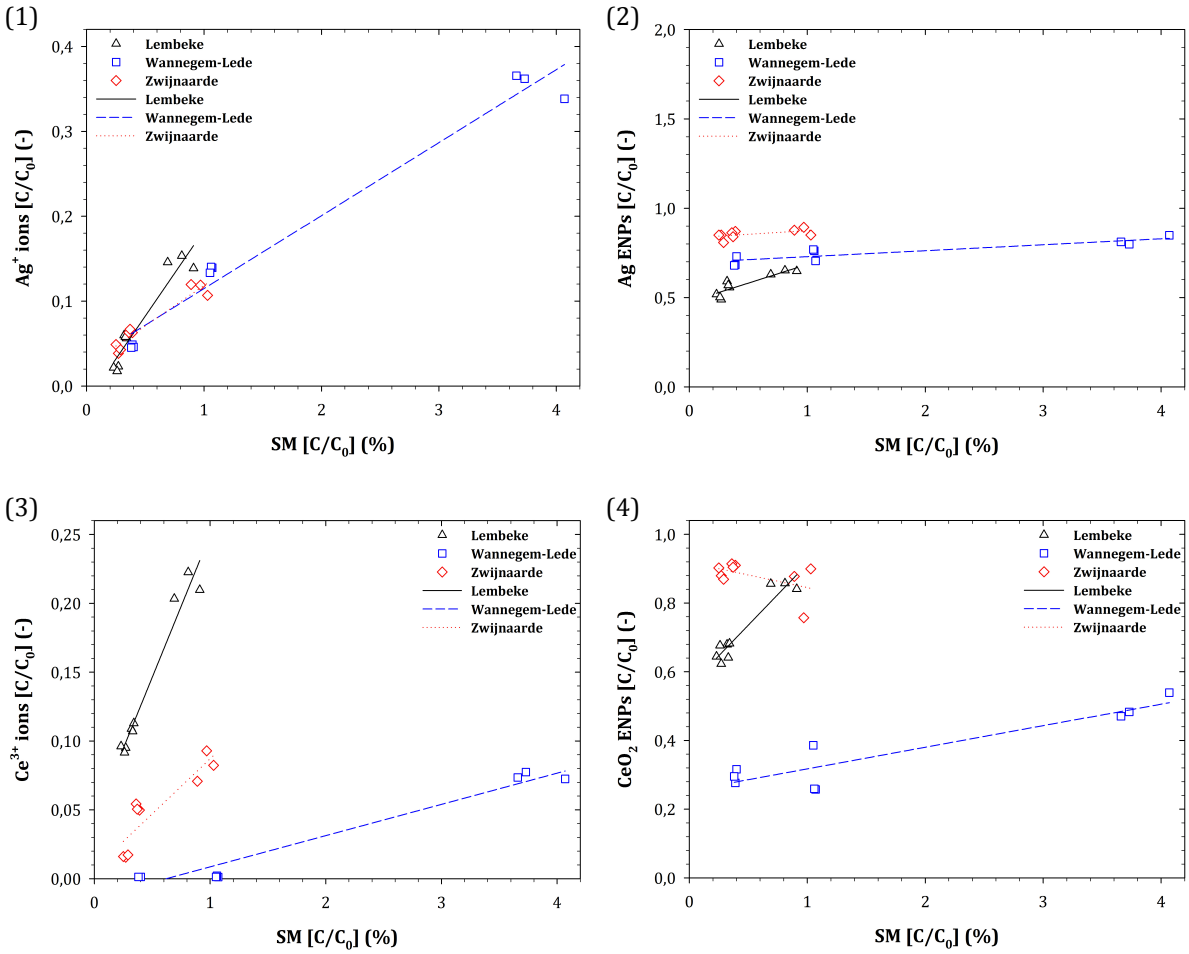

Figure 7.4 – Linear regression analysis between the relative amounts of Ag^{+} ions (1), Ag ENPs (2), Ce^{3+} ions (3), and CeO_2 ENPs (4) and the amount of suspended matter, in the supernatant of the different soil suspensions.

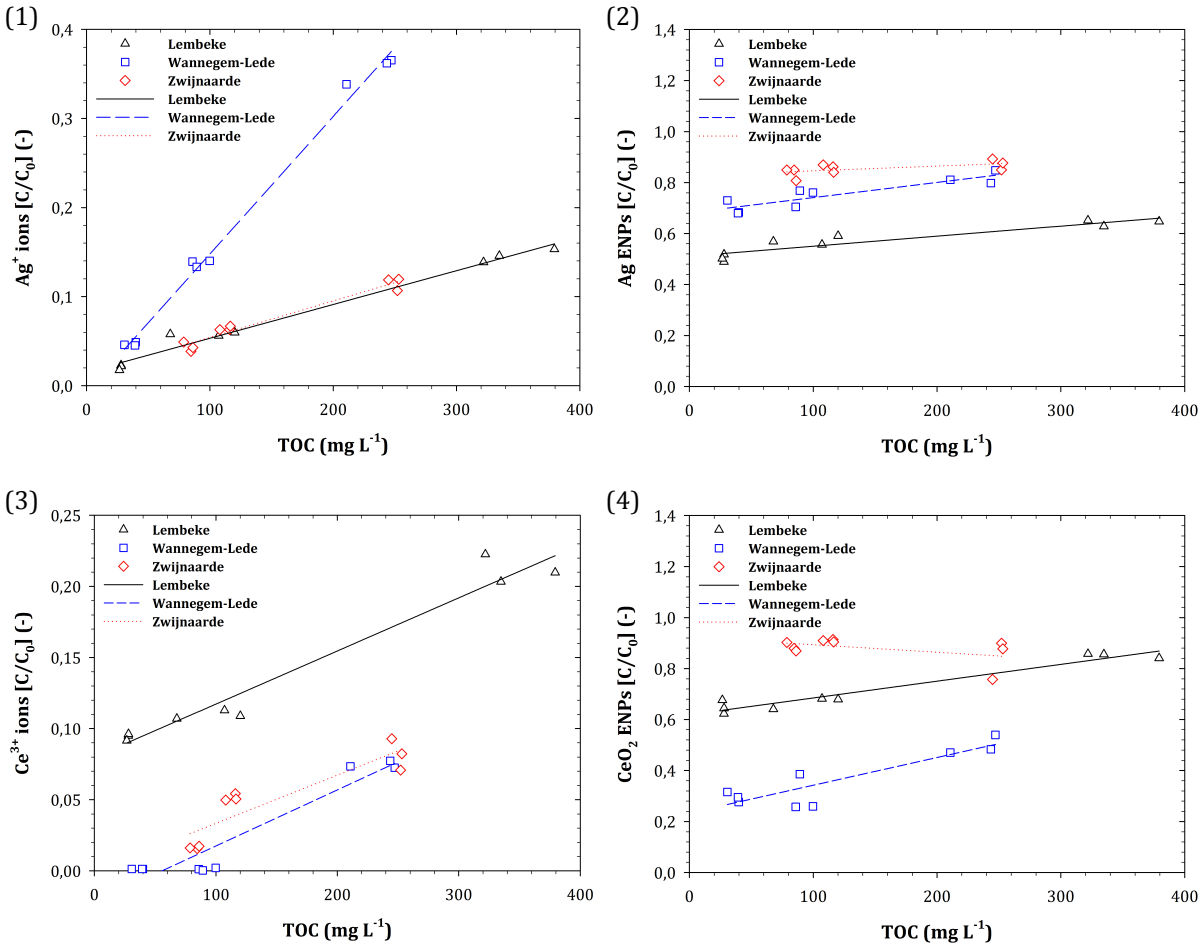

Figure 7.5 – Linear regression analysis between the TOC content and the relative amounts of Ag^+ ions (1), Ag ENPs (2), Ce^{3+} ions (3), and CeO_2 ENPs (4), in the supernatant of the soil suspensions.

7.3.5 Impact of NOM on CeO_2 ENPs stability in suspension

The effect of dissolved natural organic matter on the relative amount of CeO_2 ENPs remaining in the aqueous phase of quartz sand suspensions is shown in Figure 7.6. A concentration of 1 mg L^{-1} NOM had no significant impact on the stability of CeO_2 ENPs in suspension (p > 0.05). At 5 mg L^{-1} NOM, the initial amount of CeO_2 ENPs remaining suspended (t0) after 10 min gravitational settling (0 rpm) was not affected (p > 0.05). However, a time-dependent decrease of the relative CeO_2 ENPs content was no longer observed (p = 0.188), already indicating stabilization of the nanoparticles in suspension. In contrast, 10 min centrifugation at 2000 rpm did impact the amount of CeO_2 ENPs remaining in the aqueous phase during the 24-hour time frame (p < 0.05). These results suggest that at 5 mg L^{-1} NOM association of CeO_2 ENPs with natural organic compounds has occurred, either in clusters large enough to be affected by the increased settling forces, or that

potential (electro)steric repulsion between distinct clusters was overcome at 2000 rpm, resulting in their settling out of solution. Furthermore, in the presence of 10 mg L^{-1} NOM or more, little or no effect of centrifugation was observed and between 90 and 98 % of the initially spiked amount of CeO_2 ENPs remained stable in suspension during the 24-hour experimental time period. Quik *et al.* (2010) also demonstrated the stabilizing effect of NOM on CeO_2 ENPs in aqueous matrices and reported that after 12 days of settling up to 88 % or 41 % of the initially added nanoparticles remained suspended in deionized water or model fresh water (*i.e.*, algae growth medium), respectively. Adsorption of organic matter resulted in a decrease in ζ-potential from -15 to -55 mV, thereby increasing electrostatic repulsion. Additionally, NOM has also been shown to negatively affect the deposition and retention of Ag, Fe, TiO_2, and ZnO ENPs by quartz sand (Johnson *et al.*, 2009; Jiang *et al.*, 2010; Thio *et al.*, 2011; Sagee *et al.*, 2012).

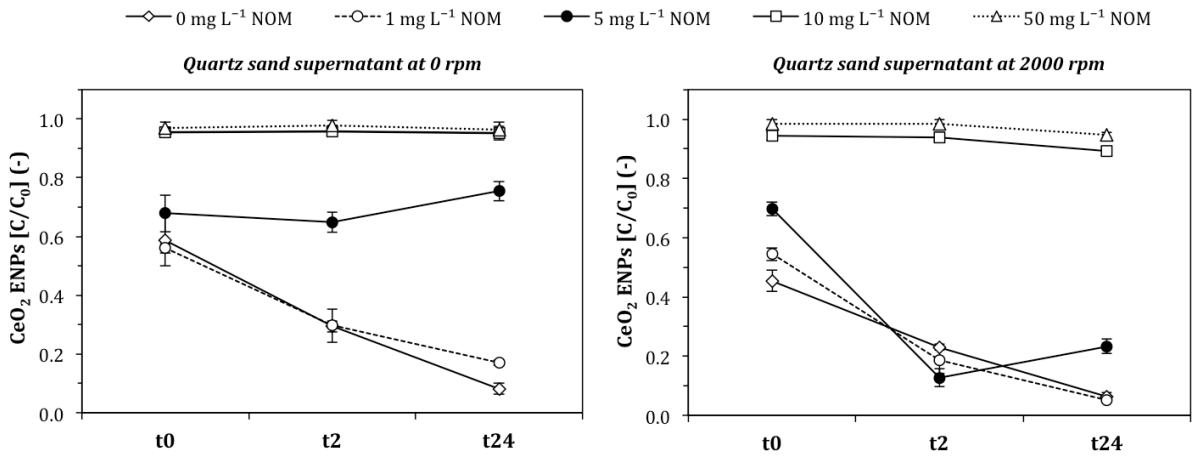

Figure 7.6 – Effect of NOM on CeO_2 ENPs (10 mg L^{-1}) stability in suspension in the presence of quartz sand (1:10 (m:V)): after 10 min of gravitational settling (left graph), and after 10 min of centrifugation at 2000 rpm (right graph). NOM (determined as mg TOC L^{-1}) was obtained by extracting pure peat with Milli-Q® water. (Data plotted are mean values, error bars represent standard deviations, n = 3)

7.4 Conclusion

The stability of nanoparticles in complex aquatic matrices such as soil solutions is an important aspect to consider when assessing the potential risks nanomaterials may pose to the environment. In the present study, the solid-liquid distribution of Ag and CeO_2 ENPs as well as their ionic counterparts in soil suspensions was examined, in order to contribute to

the existing knowledge on the behaviour and fate of engineered nanomaterials in aquatic systems. A substantial fraction of silver or cerium resulting from the addition of Ag or CeO_2 ENPs could be retrieved in the aqueous phase of (re)suspended soils after 24 h of equilibration. Thus, the migration potential for Ag and CeO_2 ENPs appears to be high, despite their high surface reactivity. Moreover, in natural soils, the partitioning of Ag^+ and Ce^{3+} ions to the solid phase was more pronounced in comparison to their nanoparticulate counterparts, rendering the nanoparticles more mobile and potentially bioavailable. However, in the presence of quartz sand, the mobility of CeO_2 ENPs appears to be lower than for Ce^{3+} ions, whereas no difference between Ag ENPs and Ag^+ ions was observed. This distinct behaviour again underlines the importance of differentiating between "real" and "model" soils when studying the environmental fate of nanoparticles. In the absence of soil, Ag and CeO_2 ENPs as well as their ionic counterparts remained stable in suspension/solution during 24 h, whereas significant differences were observed in the presence of natural soils or quartz sand, indicating that their partitioning behaviour is influenced by soil properties. It was demonstrated that the physicochemical appearance and the solid-liquid partitioning of Ag and CeO_2 ENPs is influenced by soil properties such as pH, CEC, texture, TN, TP, SM, TOC, and main and trace elements content. Furthermore, the potential of natural organic matter to stabilize CeO_2 ENPs in suspension was also clearly demonstrated.

It should however be noted that as the current study was performed under fully oxic conditions, using environmentally unrealistic spike concentrations due to instrumental and experimental limitations, the main focus was to gain insight in the physicochemical interactions between ENPs and natural soil constituents. Furthermore, it is also unlikely that real aquatic or terrestrial environments are exposed to unmodified nanoparticles (Cornelis *et al.*, 2012). Therefore, the present study should be extended towards a larger selection of soils, nanoparticle species and concentrations, and longer-term experiments should be performed, in order to elucidate the behaviour and ultimate fate of nanoparticles in aquatic and terrestrial systems under more realistic environmental conditions.

Chapter 8

Impact of carboxymethyl cellulose coating on FeS nanoparticles stability, transport, and mobilization potential of trace metals present in soils and sediment

8 Impact of carboxymethyl cellulose coating on FeS nanoparticles stability, transport, and mobilization potential of trace metals present in soils and sediment[‡]

8.1 Introduction

Contamination of water bodies, sediments, and soils with heavy metals (or metalloids) such as As, Cd, Co, Cr, Cu, Hg, Ni, Pb, and Zn is considered to be a worldwide problem, primarily originating from anthropogenic activities (*e.g.*, ore mining and processing, fossil fuel combustion, industrial waste disposal, or usage of pesticides, paints, fertilizer, and sewage sludge), although geogenic processes (*e.g.*, natural geological weathering) could also lead to elevated trace metal concentrations (Du Laing *et al.*, 2009; Plathe *et al.*, 2010; Hou *et al.*, 2013; Plathe *et al.*, 2013; Frohne *et al.*, 2014). Whatever the source, heavy metals are known to induce toxicological responses in humans and organisms and are believed to be hazardous to public health and ecosystems, even at trace levels (Hua *et al.*, 2012; Plathe *et al.*, 2013). For instance, As, Pb, Hg, and Cd were ranked 1st, 2nd, 3rd, and 7th, respectively, in the 2013 Priority List of Hazardous Substances reported by the Agency for Toxic Substances and Disease Registry (ATSDR, 2013).

As major environmental compartments, sediments and soils are considered to be a large sink for metal contaminants, and opposed to organic pollutants, most metals are not readily susceptible to microbial or chemical degradation to non-toxic end products *in situ* and will therefore persist in the environment (Kostal *et al.*, 2005; Wuana and Okieimen, 2011; Hou *et al.*, 2013). Alterations in their physicochemical appearance potentially affecting metal mobility, bioavailability, and toxicity are however possible, and depending on the environmental conditions, the metals could for instance be re-suspended and transported via pore water and end up in ground- or surface water causing a secondary contamination zone, and thus soils and sediments can act both as a sink and a source of

[‡] *Submitted for publication as: Van Koetsem, F., Van Havere, L., and Du Laing, G.* ***Impact of carboxymethyl cellulose coating on iron sulphide nanoparticles stability, transport, and mobilization of trace metals present in soils and sediment.***

prolonged metal contamination in the aquatic environment (Wuana and Okieimen, 2011; Hou *et al.*, 2013). Effective and sustainable remediation options are therefore required in order to adequately restore and protect contaminated aquatic and terrestrial ecosystems (Wuana and Okieimen, 2011).

Numerous techniques have been developed and employed in order to remediate water or soil systems contaminated with heavy metals both *in* and *ex situ*, including but not limited to immobilization, soil washing, chemical extraction, membrane filtration, and phytoremediation technologies (Huang *et al.*, 2011; Wuana and Okieimen, 2011; Hua *et al.*, 2012; Mallampati *et al.*, 2013). Moreover, with the advances in nanotechnology over the recent years, nanomaterial-based techniques have also been proposed as promising and even more efficient, durable, and cost-effective remediation options compared to traditional technologies (Cundy *et al.*, 2008; Karn *et al.*, 2009; Sánchez *et al.*, 2011; Hua *et al.*, 2012; Liu and Lal, 2012). The two main advantages nanomaterials possess over traditional remediation options, which stem from their exceptionally small dimensions (typically < 100 nm), are a higher specific surface area and reactivity, and an enhanced deliverability of the small-sized particles in the subsurface of porous media such as soils or sediments (Hua *et al.*, 2012; Liu and Lal, 2012). Examples of nanomaterials showing great potential for treatment of heavy metal-contaminated aqueous or terrestrial systems include nanosized zeolites, zerovalent iron (ZVI), iron oxides, aluminium oxides, manganese oxides, titanium oxides, cerium oxides, phosphates, iron sulphides, and carbon nanotubes. Remediation using these materials is generally based on immobilization and/or reduction of the metal contaminants (Hua *et al.*, 2012; Liu and Lal, 2012). For instance, ZVI engineered nanoparticles (ENPs) have been used to reduce aqueous Cr(VI) and Pb^{2+} to Cr^{3+} and Pb, respectively, thereby decreasing the solubility/mobility and toxicity of those metals (Ponder *et al.*, 2000; Cao and Zhang, 2006). ZVI ENPs have also been shown to be able to treat other potentially toxic elements such as Ag, As, Cd, Hg, and Ni in aqueous and soil media, whereby the decontamination mechanisms again included reduction of the metal ions on the ZVI surface and/or adsorption of the metals on the ZVI shell, consisting of a layer of iron oxides (Kanel *et al.*, 2005; Kanel *et al.*, 2006; Li and Zhang, 2006; Li and Zhang, 2007; Alidokht *et al.*, 2011; Liu and Lal, 2012).

According to previous reports, injection of iron sulphide (FeS) nanoparticles into soils and sediments can be applied to immobilize heavy metal contaminants (*e.g.*, As and Hg) and hence render them unavailable to organisms and plants (Xiong *et al.*, 2009; Zhang *et al.*,

2010; Gong *et al.*, 2012). However, as the particle size is reduced from the microscale to the nanoscale, the particle surface energy increases, and thus nanoparticles are inherently less stable and more prone to aggregation due to inter-particle interactions (*e.g.*, Van der Waals forces). Consequently, the high chemical reactivity, sorption capacity, and mobility of the particles rapidly diminishes or even vanishes due to the formation of larger clusters, and hence the particles are not particularly suitable for *in situ* delivery in the subsurface (He *et al.*, 2007; Hua *et al.*, 2012). Therefore, stabilizing surface coatings (*e.g.*, thiols, carboxylic acids, surfactants, or polymers) are often used in order to enhance nanoparticle dispersibility and reduce aggregation, either through electrostatic repulsion, by providing steric hindrance, or via a combination of both (He *et al.*, 2007). As a low-cost and environmentally friendly "green" product, carboxymethyl cellulose (CMC) has been proposed as a potential suitable stabilizing agent (He and Zhao, 2007; He *et al.*, 2007; Xu and Zhao, 2007). CMC-stabilized FeS ENPs have already been demonstrated to display a much greater physical stability, soil deliverability, and reactivity compared to non-stabilized particles (Xiong *et al.*, 2009; Gong *et al.*, 2012).

However, the greatly amplified stability and mobility of such CMC-coated particles together with their high sorption capacity of metal contaminants could potentially also lead to enhanced contaminant extraction and/or particle-facilitated contaminant transport in the environment instead of immobilization of the pollutants. Such well-dispersed nanoparticles could thus impart an elevated environmental risk as they may persist longer in the environment and be transported more easily over longer distances, which might result in an expansion of the contaminated area (Fang *et al.*, 2009; Plathe *et al.*, 2010; Plathe *et al.*, 2013). For example, As, Cr, Cu, Pb, and Zn have already been demonstrated to bind with natural Fe- and Ti-containing nanoparticles or small aggregates of them, which could remain suspended and highly mobile in surface water (*e.g.*, through (electro)steric stabilization by natural organic matter) (Plathe *et al.*, 2010; Plathe *et al.*, 2013). Thus, the stability and transport behaviour of nanoparticles in complex environmental matrices are key factors not only governing their own ultimate fate, but also the fate, mobility, and potential bioavailability and toxicity of trace metal contaminants (Gimbert *et al.*, 2007; Liu *et al.*, 2012; Plathe *et al.*, 2013).

This study primarily aimed at investigating the stability and transport of CMC-coated FeS ENPs as well as their concurrent impact on trace metal scavenging and mobility in field-contaminated soils and sediment, in order to contribute to the knowledge on their

behaviour and fate in aqueous and terrestrial environments and invoke awareness on potential environmental risks associated with the use of such nanoparticles, *e.g.*, as an *in situ* environmental remediation option. Therefore, bare and CMC-stabilized FeS particles were synthesized and thoroughly characterized to examine the effect of CMC. Batch and column experiments were set up to study CMC-FeS ENPs affinity for trace metal contaminants present in soils and sediment, and to investigate their transport behaviour. Finally, the effect of the nanoparticles on the batch-leachability of trace metals was also explored.

8.2 Materials and methods

8.2.1 Synthesis of CMC-stabilized FeS ENPs

CMC-stabilized FeS ENPs were synthesized based on a method developed by Xiong *et al.* (2009). Firstly, a 1 wt% CMC solution was prepared by dissolving carboxymethyl cellulose sodium salt (VWR International, LLC, Radnor, PA, USA) in ultrapure water (18.2 MΩ cm^{-1}) (Milli-Q®, EMD Millipore Corp., Billerica, MA, USA) using an ultrasonic bath (Sonorex Super RK103H, Bandelin electronic GmbH, Berlin, Germany). A 7.5 mL aliquot from this CMC solution was added to 112.5 mL N_2-purged Milli-Q® water, and the solution was further purged with N_2 for 20 min to eliminate dissolved oxygen. Under continuous purging with N_2, 20 mL of a freshly prepared 0.043 M $FeSO_4$ solution ($FeSO_4.7H_2O$, Merck KGaA, Darmstadt, Germany) was added, resulting in the formation of CMC-Fe^{2+} complexes. Finally, 10 mL of freshly prepared 0.085 M Na_2S solution (*i.e.*, a Fe:S molar ratio of 1:1) ($Na_2S.3H_2O$, VWR International LLC, Radnor, PA, USA) was added drop-wise using a 718 STAT Titrino (Metrohm AG, Herisau, Switzerland) under vacuum and continuous stirring on an orbital shaker, to yield the CMC-FeS ENPs. The resulting black nanoparticle suspension (0.05 % CMC, 500 mg L^{-1} FeS) was shaken for an additional 5 min under vacuum to ensure complete reaction, and was transferred to airtight recipients to prevent oxidation of the ENPs prior to being characterized or utilized in the experiments. Non-stabilized FeS particles were also synthesized in a similar manner but in the absence of CMC. All Milli-Q® water was purged with N_2 prior to being used. All reagents used in this study were of analytical grade.

8.2.2 Characterization of FeS ENPs

Particle size distributions (PSDs) and *Z*-average particle sizes were determined by means of photon correlation spectroscopy (PCS) (Malvern PCS-100, Malvern Instruments Ltd., Worcestershire, UK), via multi modal and cumulant analysis, respectively. All sample measurements were performed in triplicate at 25 °C, using a 633 nm HeNe laser positioned at a 150 ° measuring angle. UV-Vis absorption spectra of synthesized CMC-FeS ENPs and bare FeS particulates, as well as of the individual components (*i.e.*, CMC, Fe^{2+}, S^{2-}, and CMC-Fe^{2+} solutions), were obtained using a 6400 Spectrophotometer (Jenway, Bibby Scientific Ltd., Staffordshire, UK) over a 320 – 1000 nm measuring range.

The stability of CMC-coated and bare FeS particles in suspension was examined, (1) through visual inspection of the time-dependent sedimentation behaviour of the prepared ENPs, and (2) by concurrently following up on the evolution of the iron concentration near the liquid surface. For the latter, 2 mL aliquots were sampled at designated times (*i.e.*, after 0, 0.5, 2, 5, 15, 30, 60, 240, and 1200 min), digested (*i.e.*, via open vessel microwave-assisted digestion (MARS 5, CEM Corp., Matthews, NC, USA) with 4 mL *aqua regia*), and analysed for total iron content by means of inductively coupled plasma optical emission spectrometry (ICP-OES) (Vista-MPX CCD Simultaneous ICP-OES, Varian, Agilent Technologies, Santa Clara, CA, USA). All sedimentation tests were performed on a steady surface at room temperature, using airtight recipients to avoid potential oxidation of the FeS particles through contact with air. In addition to gravitational settling, the synthesized CMC-FeS ENPs were also subjected to centrifugation (Megafuge 1.0, Heraeus, Hanau, Germany) for 10 min at 2000, 3000, and 4500 rpm (*i.e.*, 738, 1660, and 3735 *g*, respectively). Afterwards, the "supernatant" was gently sampled (2 mL) close to the liquid surface to avoid sample disturbance, digested, and analysed using ICP-OES to determine the total iron concentration.

The impact of filtration was studied using four different types of syringe filters: 0.02 μm Anatop 25 filters (Whatman International Ltd., Kent, UK); 0.10 μm Minisart High-Flow filters (Sartorius Stedim Biotech GmbH, Goettingen, Germany); and 0.20 and 0.45 μm Chromafil RC filters (Macherey-Nagel GmbH & Co. KG, Düren, Germany). The obtained filtrates were again analysed for total iron content via ICP-OES, after being subjected to open vessel microwave digestion with *aqua regia*.

8.2.3 Soil and sediment characterization

Three different soil/sediment samples (pre-dried, pre-sieved, and homogenized) were used during batch and/or column experiments: a mercury polluted soil (S1), a historically polluted soil originating from Lommel (Campine region, Flanders, Belgium) containing Cd, Pb, and Zn as most important contaminants (S2), and an intertidal sediment from the Scheldt river (Belgium) (S3). All samples were thoroughly characterized according to standard methods. After digestion of 1 g of soil/sediment sample with *aqua regia* on a hotplate at 150 °C for 2 h, major and trace elements concentations were determined via ICP-OES (Vista-MPX CCD Simultaneous ICP-OES, Varian, Agilent Technologies, Santa Clara, CA, USA), while the Hg content was determined with a QuickTrace M-7500 Mercury analyser (Cetac Technologies, Omaha, NE, USA) (Van Ranst *et al.*, 1999). Soil/sediment texture was obtained via the Bouyoucos hydrometer method after removing organic matter by addition of H_2O_2 (Gee *et al.*, 1986; van Reeuwijk, 2002; Sartori *et al.*, 2013). The pH (pH-H_2O) was measured in 1:5 (m:V) soil/sediment suspensions prepared with Milli-Q® water after equilibration for 16 h (Van Ranst *et al.*, 1999). The electrical conductivity (EC) was measured in the filtrates (MN 640 m, Macherey-Nagel GmbH & Co. KG, Düren, Germany) of 1:5 (m:V) soil/sediment suspensions after shaking for 1 h (Van Ranst *et al.*, 1999). The cation exchange capacity was determined by percolation of 150 ml 1 M NH_4OAc through a percolation column filled with a mixture of 5 g soil/sediment and 12.5 g quartz sand, followed by washing through the excess with 150 mL denatured ethanol. Then, the exchangeable ammonium ions were eluted with 250 mL 1 M KCl and analysed in the percolate by means of a steam distillation (Vapodest Kjeldahl distillation system, Gerhardt GmbH & Co. KG, Königswinter, Germany). The organic matter content (OM) was calculated through loss on ignition (LOI) after incineration of 3 g oven-dried soil/sediment sample in a muffle furnace at 550 °C for 2 h (Salehi *et al.*, 2011). The total carbonate ($CaCO_3$) content was determined by back-titration (with 0.5 M NaOH) of an excess 0.25 M H_2SO_4 added to 1 g soil/sediment (Van Ranst *et al.*, 1999). The total nitrogen (TN) content was determined according to the modified Kjeldahl method by digestion of 1 g soil/sediment with 7 mL sulphuric/salicylic acid reagent, followed by alkalization with NaOH and steam distillation using a Vapodest Kjeldahl distillation system (Gerhardt GmbH & Co. KG, Königswinter, Germany) (Van Ranst *et al.*, 1999). The total phosphorous (TP) content was determined according to the colorimetric method of Scheel after *aqua regia* destruction of 1 g soil/sediment (Van Ranst *et al.*, 1999). More details on the employed soil and sediment characterization procedures can be retrieved in Appendix A.

8.2.4 Batch leaching experiments

In addition to Milli-Q® water, three different standard leaching procedures that are commonly used to assess the mobility of inorganic contaminants were applied to investigate the leachability of trace metals from the three soil/sediment samples: (1) extraction with 0.01 M $CaCl_2$, a procedure commonly used to determine the bio-available fraction of elements in soils (Houba *et al.*, 2000); (2) extraction with extraction liquid #1 (*i.e.*, 5.7 mL 99 – 100 % acetic acid, and 64.3 mL 1 M NaOH in 1 L Milli-Q® water, pH 4.93 ± 0.05) according to TCLP (US EPA, 1992), a method designed to simulate material sitting inside a landfill for years, and then determine the mobility of organic and inorganic contaminants present in a sample and whether the generated leachates would classify the material as hazardous; and (3) extraction with extraction liquid #2 (*i.e.*, a 3:2 (m:m) H_2SO_4:HNO_3 mixture in Milli-Q® water, pH 5.00 ± 0.05) according to SPLP (US EPA, 1994), a procedure designed to evaluate the impact of contaminated soils on groundwater, by simulating material sitting *in-situ* and assessing its leaching potential (*i.e.*, the mobility of organic and inorganic analytes) under acidic rain conditions. For this, 2 g of soil/sediment was transferred into 50 mL centrifuge tubes, and 40 mL extraction liquid was added to obtain a 1:20 (m:V) ratio. The samples were then shaken on an end-over-end shaker for 18 h, before being subjected to centrifugation at 3000 rpm for 10 min. Afterwards, the supernatant was removed, acidified with 2 drops 65 % HNO_3, and analysed for trace elements content by means of ICP-OES or a Hg analyser.

Leaching of trace metals from the three soil/sediment samples, after first being treated with CMC-FeS ENPs, was examined through sequential extraction tests by application of the three leaching procedures (*i.e.*, $CaCl_2$, TCLP, and SPLP) explained in the paragraph above. In the treatment step, centrifuge tubes were filled with 1.5 g soil/sediment and 15 mL 500 mg L^{-1} CMC-FeS ENPs suspension (*i.e.*, a ratio of 1:10 (m:V)), sealed from the air, and shaken for 24 h on an end-over-end shaker. The samples were then subjected to centrifugation at 3000 rpm for 10 min, where after the supernatant was removed, digested, and analysed for trace metals content. After removal of the supernatant, 15 mL of extraction liquid was added to the remaining soil/sediment residue, and the samples were again shaken for 24 h, before being subjected to centrifugation. The supernatant was again removed, digested, and analysed for the presence of trace elements. These extraction steps were repeated three times. Control samples (*i.e.*, untreated soil/sediment samples) where 15 mL Milli-Q® water was used during the "treatment step", were also included in the set-up.

Trace elements analysis occurred via ICP-OES, inductively coupled plasma mass spectrometry (ICP-MS) (Elan DRC-e, PerkinElmer Inc., Waltham, MA, USA), or a Hg analyser. All batch tests were performed in triplicate.

8.2.5 Column tests

Glass columns (*id*: 2 cm, *l*: 40 cm) were filled with 12 g of soil sample S2, packed in between two layers of 7 g quartz sand (pre-sieved, pre-rinsed, and pre-dried), on top of a sintered glass disc of 0.3 cm in height at the bottom of the column. The purpose of the quartz sand is to act as a buffer layer to physically protect the top layer of the soil sample, and to prevent the surface of the soil to run dry. Next, 170 mL (*i.e.*, 22.7 pore volumes (PVs)) of a 500 or 83.3 mg L^{-1} CMC-FeS ENPs suspension was passed through the soil column gravitationally at a steady flow rate, and effluent samples were collected, digested, and analysed via ICP-OES or ICP-MS. The samples were analysed for total iron as well as for trace metals content, to examine transport of the ENPs through the soil column, and the impact of the ENPs on the leachability of trace elements, respectively. Filtration using 0.10 μm syringe filters was applied on selected samples in order to quantify leached trace metals associated with CMC-FeS ENPs. These filtrates were analysed directly via ICP-MS after being diluted ten times with internal standard solution (*i.e.*, 10 μg L^{-1} Rh in 2 % HNO_3). A tracer test using a 50 mg L^{-1} KBr solution was also performed in a similar manner. The collected samples were analysed for Br^- by means of ion exchange chromatography (IEC) (761 Compact IC, Metrohm AG, Herisau, Switzerland). All column tests were performed in triplicate.

8.3 Results and discussion

8.3.1 Nanoparticle characterization

PCS analyses revealed a *Z*-average hydrodynamic particle diameter of 154.5 ± 5.8 nm for the synthesized CMC-FeS ENPs, whereas no valid PCS measurements could be performed in the case of bare FeS particles due to their larger size and hence rapid settling out of solution. The CMC-FeS ENPs had a polydispersity index (PDI) of 0.167 ± 0.027, suggesting a quite monodisperse system. Yet, the obtained particle size distributions also indicate the

presence of particles with sizes spanning from 90 to 350 nm, as shown in Figure 8.1.

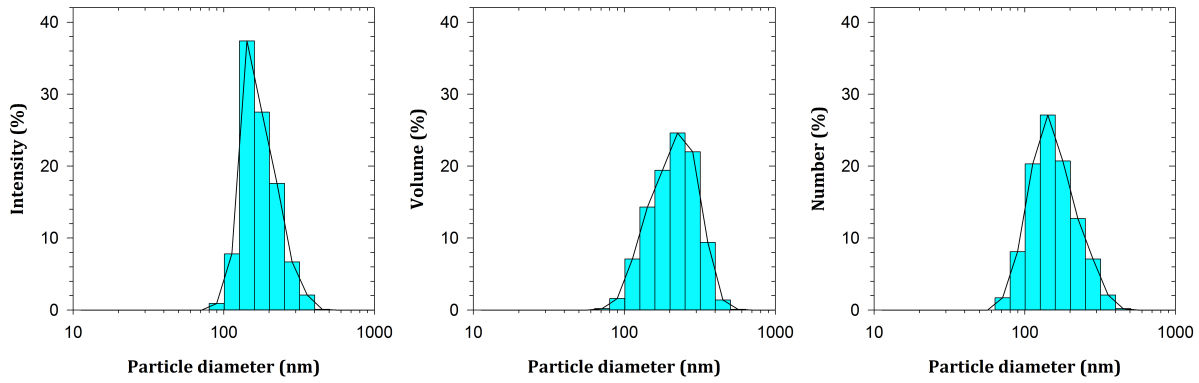

Figure 8.1 – Intensity, volume, and number weighted particle size distribution of the synthesized CMC-FeS ENPs, obtained from PCS measurements.

UV-Vis spectroscopy can provide a convenient indication of the formation of nanoparticles, as indicated by the differences in absorption spectra for CMC-FeS ENPs, FeS particulates, and the individual homogeneous solutions of CMC, Fe^{2+}, CMC-Fe^{2+} complexes, or S^{2-} (Figure 8.2). Virtually no absorption was observed for the latter solutions over the considered wavelength range (320 – 1000 nm), and all of these solutions appeared transparent. However, addition of S^{2-} into the CMC-Fe^{2+} solution immediately turned its colour black, and a dark homogeneous suspension was formed, which absorbed strongly between 320 and 1000 nm. Furthermore, the UV-Vis absorption of CMC-FeS ENPs was considerably higher than that of bare FeS particles, especially between 320 and 900 nm.

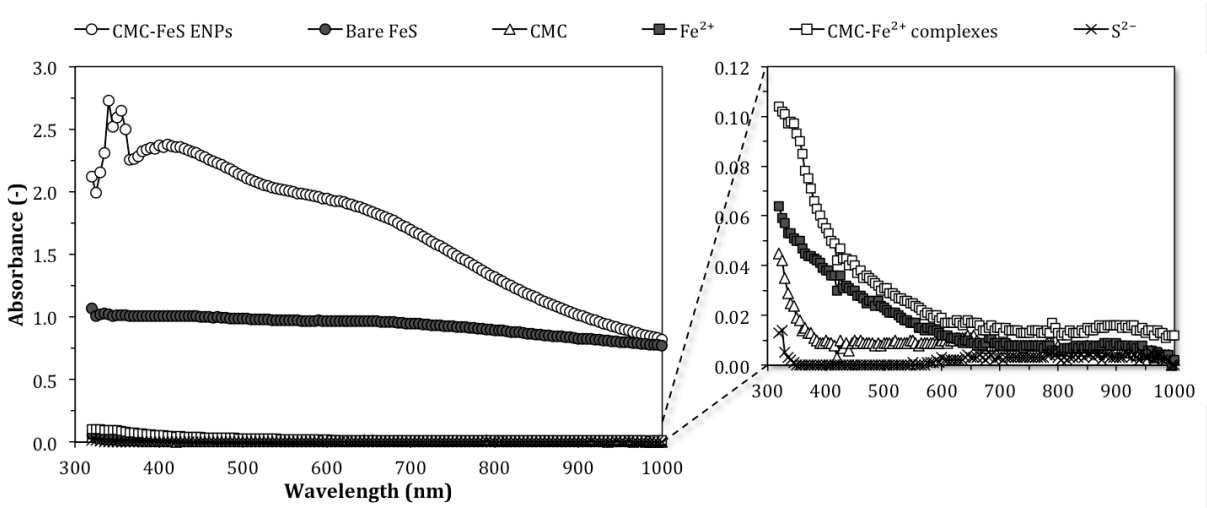

Figure 8.2 – UV-Vis absorption spectra of 50 mg L^{-1} CMC-FeS ENPs and bare FeS particles, and of the individual components used or generated during synthesis *(i.e.*, 0.05 % CMC, 318 mg L^{-1} Fe^{2+}, CMC-Fe^{2+} complexes (0.05 % CMC, 318 mg L^{-1} Fe^{2+}), and 182 mg L^{-1} S^{2-}).

Figure 8.3 depicts the impact of 0.05 % CMC on the stability of 500 mg L^{-1} FeS particles in suspension. CMC-FeS ENPs were shown to remain stable in suspension for at least 24 h after allowing the samples to stand on a steady surface and settle gravitationally at room temperature, as visually no sedimentation was noticeable. Additionally, the relative iron content near the liquid surface also remained virtually constant (98 – 102 %) during the first 20 h. In contrast, bare FeS particles quickly aggregated and precipitated already after only a couple of minutes. Accordingly, the relative iron content near the liquid surface rapidly decreased to 9 % after just 15 min of settling and reached a steady state of approximately 5 % after 4 h. The CMC molecules most likely encapsulated the FeS ENPs, thereby providing the nanoparticles with both electrostatic and steric stabilization, and hence preventing particle aggregation and subsequent sedimentation (He and Zhao, 2007; He *et al.*, 2007). Evidence that attachment of CMC onto the surface of FeS particles induced strong electrostatic repulsion between the negatively charged particles was also provided by Gong *et al.* (2012), who reported zeta potential values between -43 and -68 mV over a pH-range of 5 to 11 and a point of zero charge (PZC) below pH 2.5, which is much lower than the PZC of bare FeS which is reported to lie around pH 7.5 (Wolthers *et al.*, 2005). Furthermore, when stored in sealed vials under anaerobic conditions at room temperature, the CMC-FeS ENPs did not display any visual sedimentation over a period of several weeks. However, the nanoparticles were quickly oxidized when coming in contact with air, turning the black suspension into a yellowish-orange coloured solution.

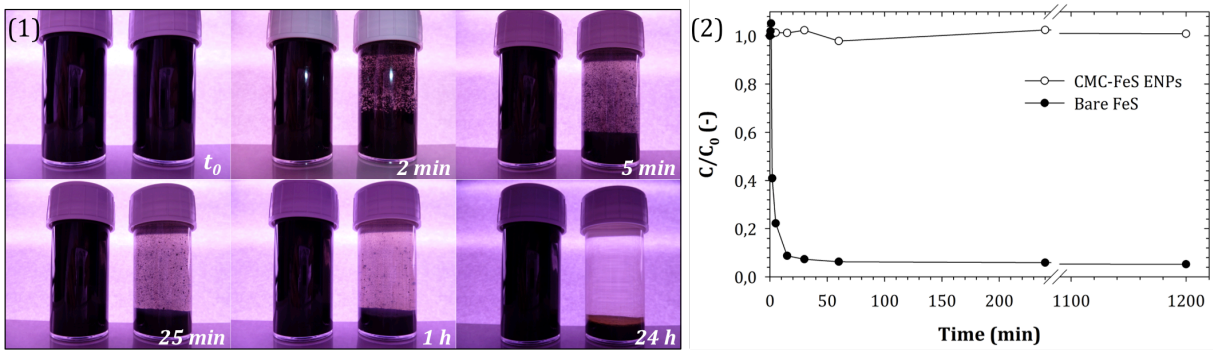

Figure 8.3 – Stability of 500 mg L^{-1} CMC-FeS ENPs and bare FeS particulates in suspension: (1) photographs displaying the time-dependent sedimentation behaviour of CMC-stabilized (left vials) and bare (right vials) FeS particles, and (2) evolution of the relative iron content (C/C_0) remaining in solution near the liquid surface in function of settling time.

The impact of centrifugation and filtration of CMC-FeS ENPs are presented in Figure 8.4. In addition to gravitational settling, the stability of CMC-FeS ENPs in suspension

also appeared to be unaffected upon application of centrifugation at 2000, 3000, and 4000 rpm for 10 min, as between 97 and 100 % of the initial iron content near the liquid surface was recovered. Approximately 98 % of the CMC-FeS ENPs were retained upon filtration over 0.10 μm, while filtration over 0.20 or 0.45 μm only retained about 72 or 8 %, respectively. Furthermore, filtration over 0.02 μm was found to be impossible and thus no quantitative data could be obtained for this type of filter. These results suggest that filtration over 0.10 μm might be best suited to distinguish the (nano)particulate from the dissolved fraction.

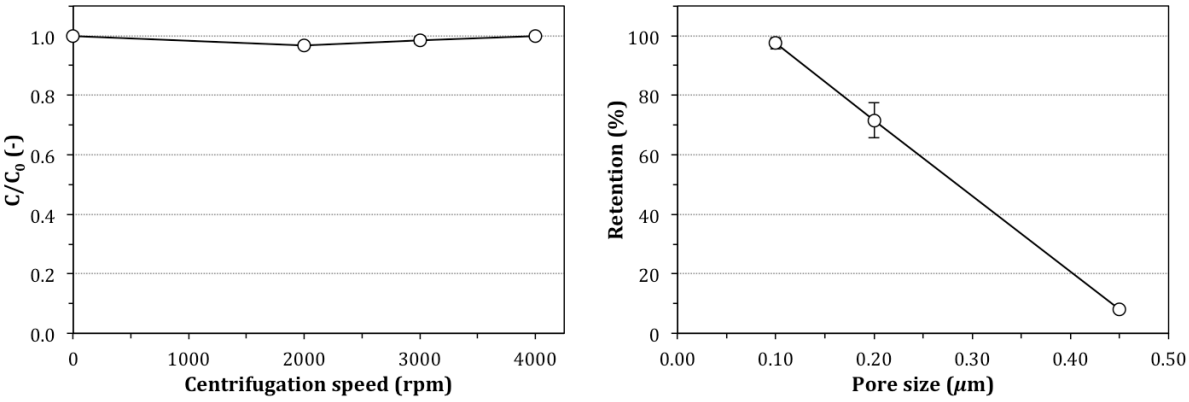

Figure 8.4 – The relative iron content (C/C_0) remaining near the liquid surface after subjecting 500 mg L^{-1} CMC-FeS ENPs suspensions to centrifugation at 2000, 3000, or 4000 rpm for 10 min (left graph), and the fraction of CMC-FeS ENPs retained by filtration over 0.45, 0.20, or 0.10 μm, as determined from the total iron content in the resulting filtrates (right graph). (Data points represent mean values, error bars indicate standard deviations, n = 3)

8.3.2 Leaching of trace metals: Batch experiments

Three distinct soil/sediment samples were utilized during the batch leaching experiments: S1, a Hg contaminated (20.8 mg kg^{-1}) sandy soil; S2, a sandy soil mainly contaminated with Cd (11.3 mg kg^{-1}), Pb (273 mg kg^{-1}), and Zn (651 mg kg^{-1}); and S3, a clayey loam sediment containing Cd (3.84 mg kg^{-1}), Cr (41.7 mg kg^{-1}), Cu (61.0 mg kg^{-1}), Ni (33.3 mg kg^{-1}), Pb (87.7 mg kg^{-1}), and Zn (455 mg kg^{-1}) as main contaminants (Vlarebo, 2008). Additional major and trace elements content and physicochemical characteristics can be retrieved in Tables F.2 and F.3 in Appendix F, respectively. Batch leaching of trace elements from S1, S2, and S3 was examined using four standard extraction procedures (*i.e.*, TCLP, SPLP, 0.1 M $CaCl_2$, and Milli-Q® water) (Figures F.1 to F.3 in Appendix F). The leaching of trace metals appeared to depend strongly on the specific metal under consideration. For

instance, between 2 and 7 μg Hg L^{-1} leached from S1, between 6 and 108 μg Cd L^{-1}, < 40 and 75 μg Pb L^{-1}, and 0.5 and 7 mg Zn L^{-1} from S2, and between 6 and 11 μg Cr L^{-1}, 27 and 64 μg Cu L^{-1}, 23 and 43 μg Ni L^{-1}, and 53 and 960 μg Zn L^{-1} in the case of S3. Furthermore, no general trend was observed when comparing the different extraction procedures between elements.

The impact of CMC-FeS ENPs on the leaching of trace metals from S1, S2, and S3 was examined in batch mode, and the results hereon are presented in Figures 8.5, 8.6, and 8.7 (for the primary contaminants of each sample) and in Figures F.4 and F.5 in Appendix F. Treatment of the samples with 500 mg L^{-1} CMC-FeS ENPs always resulted in higher amounts of metals released into the aqueous phase when compared to the control treatments with Milli-Q® water, already indicating the strong ability of the nanoparticles for scavenging metals from the solid soil/sediment phase. In case of Hg for S1 this was 104 versus 27 μg L^{-1}, accounting for 5 or 1.3 % of the total Hg initially present in the soil, respectively. For S2 these values were 354 versus 15 μg L^{-1} of Cd (*i.e.*, 31 or 1.3 %, respectively), 4.1 mg L^{-1} versus 170 μg L^{-1} of Pb (*i.e.*, 15 or 0.6 %, respectively), and 34 compared to 1.1 mg L^{-1} of Zn (*i.e.*, 52 or 1.8 %, respectively). Finally, for S3 this was 187 compared to 8.3 μg L^{-1} of Cr (*i.e.*, 4.5 or 0.2 %, respectively), 676 versus 100 μg L^{-1} of Cu (*i.e.*, 11 or 1.6 %, respectively), 122 versus 29 μg L^{-1} of Ni (*i.e.*, 3.7 or 0.9 %, respectively), and 2.6 mg L^{-1} versus 168 μg L^{-1} of Zn (*i.e.*, 5.7 or 0.4 %, respectively). Additionally, the iron content in the supernatants was also determined (data not shown), and indicated that only limited retention of the nanoparticles by the soil/sediment solid phase occurred (*i.e.*, 5, 21, or 37 % for S1, S2, or S3, respectively). The higher retention in S3 might be attributed to the sediment's finer texture compared to soils S1 or S2. Previous studies also demonstrated the high affinity of FeS (nano)particles for trace elements like Hg (Xiong *et al.*, 2009; Gong *et al.*, 2012) or As in soils (Zhang *et al.*, 2010), and Xiong *et al.* (2009) mentioned adsorption (surface complexation), inclusion, precipitation/co-precipitation, and solid solution formation as potential processes involved in the immobilization of Hg by stabilized FeS (nano)particles in soil or groundwater. However, the high affinity of CMC-FeS ENPs for metals together with their high stability in suspension (see Section 8.3.1) and low retention by the solid phase, as observed in this work, already suggests that association of trace metals with the nanoparticles could potentially lead to particle-facilitated contaminant transport in case conditions favouring colloidal transport are prevailing.

After the nanoparticle or control treatment step, the remaining solid soil/sediment residues were subjected to three-way sequential extractions according to TCLP or SPLP or using 0.1 M $CaCl_2$ (see also Figures 8.5 to 8.7 and Figures F.4 and F.5 in Appendix F). Although differences in extractable trace metal contents were observed when comparing the soils/sediment treated with CMC-FeS ENPs to the controls, no clear distinctive trend could be observed and metal leaching appeared to be dependent on the element in question as well as on the type of extraction liquid and on soil/sediment properties. In general, the $CaCl_2$- and TCLP-extractable Cd, Cu and Zn concentrations from S2 and S3 were lower for soil/sediment treated with nanoparticles. Yet, it cannot just be assumed that treatment with CMC-FeS ENPs reduced the metal leachability in these cases, as high amounts of metals were already scavenged from the soil/sediment during the nanoparticle treatment step, thereby increasing the likelihood that fewer quantities are removed during consecutive extractions. Furthermore, treatment with CMC-FeS ENPs appeared to have even enhanced the overall SPLP-extractability of trace metals from S1, S2, and S3, as well as the TCLP-leachable amount of Hg from S1, whereas seemingly no differences between nanoparticle and control treatments were observed in all remaining cases. In contrast, Xiong *et al.* (2009) and Gong *et al.* (2012) both reported a substantial reduction (between 26 and 99 %) of TCLP-leachable Hg content upon treatment of soil with stabilized FeS (nano)particles. However, in both studies these TCLP-leachable Hg concentrations were determined in either 0.05 or 0.22 μm filtrates of the supernatants, thus potentially neglecting any Hg associated with larger-sized (FeS) particulates that could remain well-dispersed in the aquatic environment for a certain amount of time, and be eventually mobile and bio-accessible (Fang *et al.*, 2009).

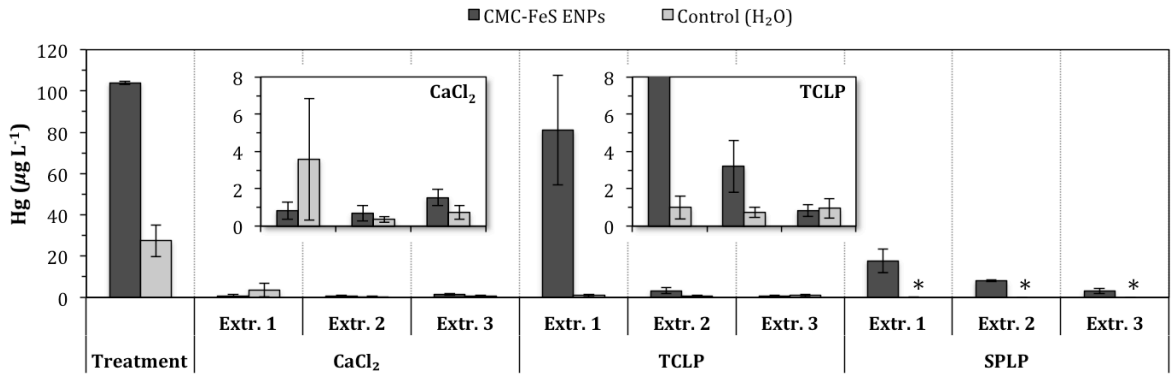

Figure 8.5 – Leaching of Hg upon treatment of S1 with 500 mg L^{-1} CMC-FeS ENPs, and following a threefold sequential extraction of the treated soil residue with $CaCl_2$, TCLP, or SPLP solution. Milli-Q® water was used for the control treatment. The insets show close-ups of the sequential extraction of Hg using $CaCl_2$ or TCLP solution. (Bars represent mean values, values below the detection limit are indicated with an asterisk (DL_{Hg} = 0.02 μg L^{-1}), error bars denote standard deviations, n = 3)

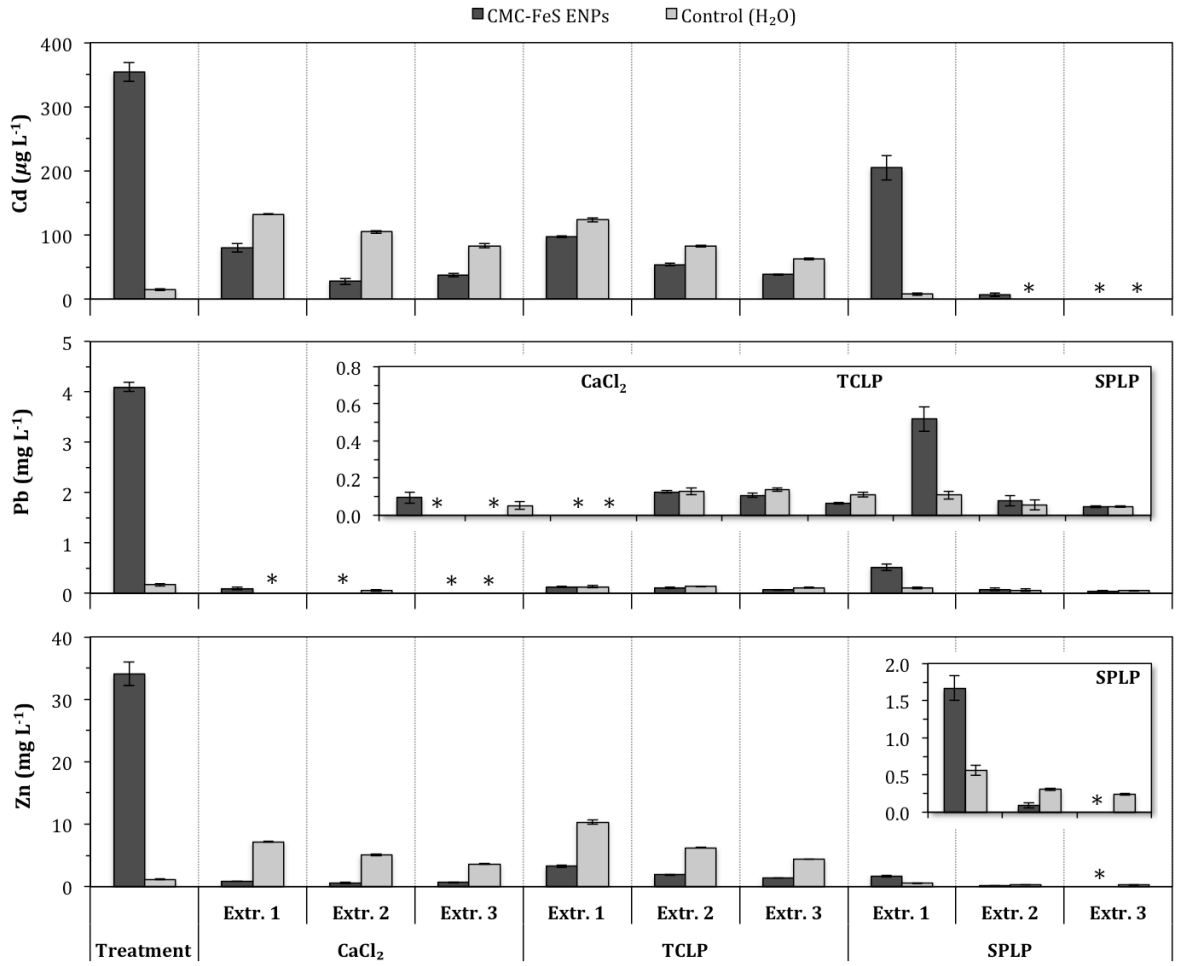

Figure 8.6 – Leaching of Cd, Pb, and Zn upon treatment of S2 with 500 mg L^{-1} CMC-FeS ENPs, and following a threefold sequential extraction of the treated soil residue with $CaCl_2$, TCLP, or SPLP solution. Milli-Q® water was used for the control treatment. The insets show close-ups of the sequential extraction of Pb using $CaCl_2$, TCLP, or SPLP solution (middle graph), and of Zn using SPLP solution (bottom graph). (Bars represent mean values, values below the detection limit are indicated with an asterisk (DL_{Cd} = 4.0 μg L^{-1}; DL_{Pb} = 40 μg L^{-1}; DL_{Zn} = 20 μg L^{-1}), error bars denote standard deviations, n = 3)

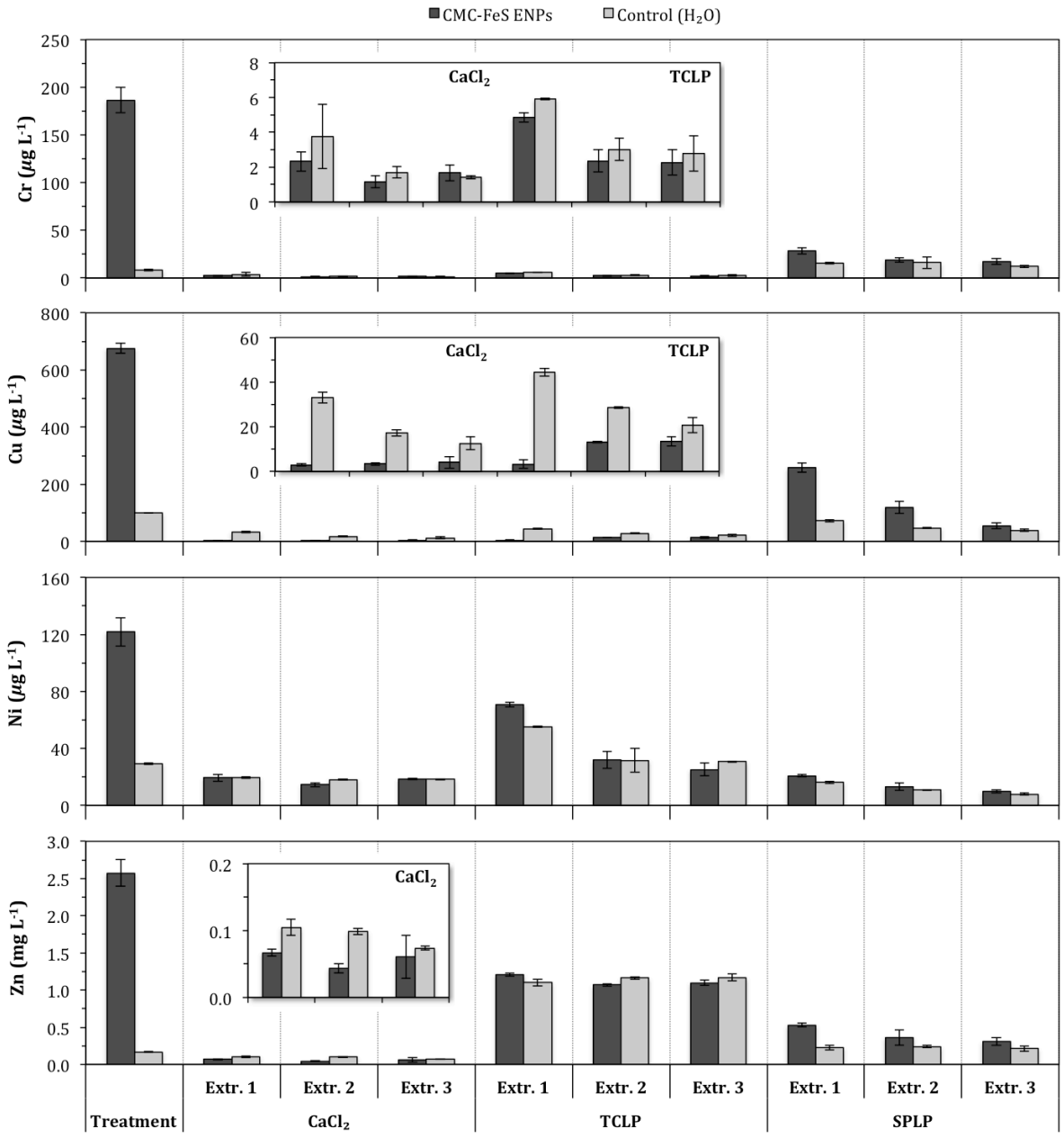

Figure 8.7 – Leaching of Cr, Cu, Ni, and Zn upon treatment of S3 with 500 mg L^{-1} CMC-FeS ENPs, and following a threefold sequential extraction of the treated sediment residue with $CaCl_2$, TCLP, or SPLP solution. Milli-Q® water was used for the control treatment. The insets show close-ups of the sequential extractions of Cr and Cu using $CaCl_2$ or TCLP solution (top two graphs), and of Zn using $CaCl_2$ solution (bottom graph). (Bars represent mean values, error bars denote standard deviations, n = 3)

8.3.3 Transport of FeS ENPs and mobilization of trace metals: Column tests

During the batch experiments discussed in Section 8.3.2, it was shown that only limited retention of 500 mg L^{-1} CMC-FeS ENPs by the solid phase occurred (*i.e.*, 21 % in the

case of S2). Therefore, prior to performing the column experiments with S2, a final set of batch tests was carried out to examine the effect of the initial CMC-FeS ENPs concentration on nanoparticle retention by the solid soil phase (Figure 8.8). The different nanoparticle concentrations were obtained by dilution of the 500 mg L^{-1} stock suspension with N_2-purged Milli-Q® water. A concentration of 83.3 mg L^{-1} resulted in the lowest relative iron content remaining in solution and hence the highest uptake of iron from the nanoparticles by the soil, suggesting 75 % of the ENPs were retained. This concentration was therefore also included during the column experiments.

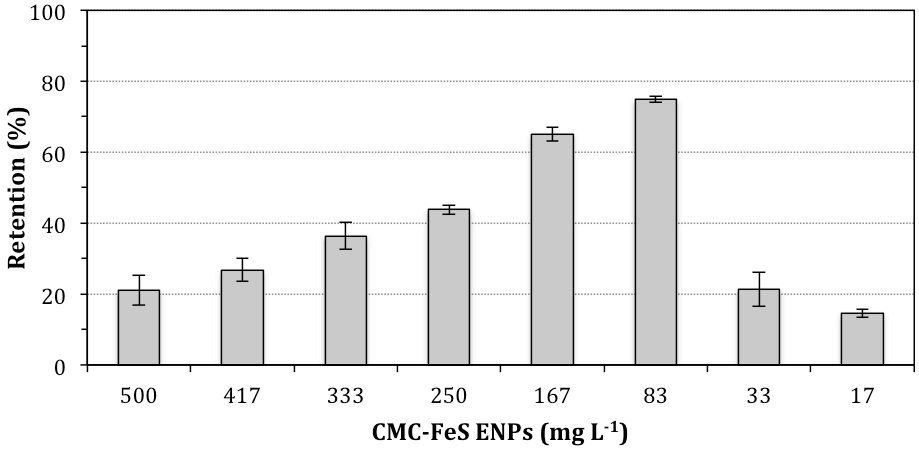

Figure 8.8 – Fraction of CMC-FeS ENPs retained by the S2 solid phase upon batch treatment of the soil with different nanoparticle concentrations, as determined from the total iron content remaining in the aqueous phase after 24 h of shaking and following centrifugation at 3000 rpm for 10 min. (Bars represent mean values, error bars indicate standard deviations, n = 3)

Column breakthrough tests were performed to examine the transport behaviour of the nanoparticles through S2. Breakthrough curves of CMC-FeS ENPs as well as of a KBr tracer through a column packed with S2 are presented in Figure 8.9. Maximal breakthrough of the nanoparticles occurred after about 10 or 16 pore volumes (PVs) for 83.3 or 500 mg L^{-1} CMC-FeS ENPs, respectively, whereas complete breakthrough ($C/C_0 \approx 1$) of the tracer was observed after approximately 1 PV (*i.e.*, 7.5 mL). Both nanoparticle suspensions showed comparable breakthrough profiles, although a higher degree of variation was noted for 500 mg L^{-1}, and reached a steady state at about 93 %, indicating that *ca.* 7 % of the nanoparticles were retained by the soil after 22.7 PVs. These results indicate that the CMC-FeS ENPs are highly mobile in the tested sandy soil, which is most likely due to a combination of the small particle size, the negative surface charge resulting from the CMC stabilizer attached to the particles, and soil properties (*e.g.*, pore size and structure,

accessible surface area, and surface chemistry) (He *et al.*, 2009; Lin *et al.*, 2010; Peralta-Videa *et al.*, 2011). In contrast, both Xiong *et al.* (2009) and Gong *et al.* (2012) have also demonstrated that bare FeS particles were nearly completely retained (> 99.7 %) on top of a sediment column, suggesting that CMC is essential for enhanced particle transport. From an *in situ* remediation point of view, a high mobility is off course required in order for the nanoparticles to reach the targeted contamination zone (Gong *et al.*, 2012). An enhanced stability and mobility could however also expand the contaminated area by carrying-forward contaminants associated with the nanoparticles. According to He *et al.* (2009), who studied the transport behaviour of CMC-Fe ENPs in porous media, the nanoparticles could be transported from as little as a few centimetres to over a 146 m from the point of injection, depending on the prevailing groundwater flow conditions. Based in that study, Xiong *et al.* (2009) and Gong *et al.* (2012) also concluded that upon release of the external pressure that was used to inject CMC-FeS ENPs into the soil, the nanoparticles would remain virtually immobile under typical groundwater flow conditions. The preliminary findings from the current study however indicate that the transport of CMC-FeS ENPs and the potential spread of contaminants associated herewith do merit sufficient attention, as these nanoparticles were shown to percolate easily through soil even without the use of an external injection pressure.

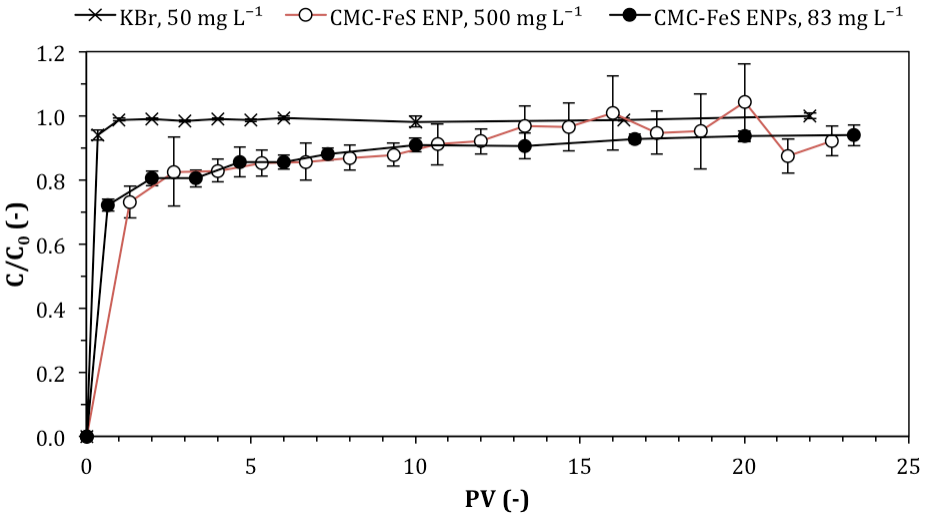

Figure 8.9 – Breakthrough curves of a 50 mg L^{-1} KBr tracer solution, and of 500 and 83.3 mg L^{-1} CMC-FeS ENPs suspensions after percolating gravitationally through S2. (Data points represent mean values, error bars denote standard deviations, n = 3)

The elution profiles of Cd, Pb, and Zn from S2 upon gravitationally percolating 500 or 83.3 mg L^{-1} CMC-FeS ENPs through the soil column are shown in Figure 8.10. Initial peaking

of total Cd (up to 717 μg L^{-1}), Pb (up to 3.9 mg L^{-1}), and Zn (up to 14 mg L^{-1}) was observed during the first 5 to 10 PVs, followed by a long tailing situated around 60 μg L^{-1} for Cd, around 0.5 to 1.1 mg L^{-1} for Pb, and around 0.7 to 2 mg L^{-1} for Zn after 22.7 PVs, indicating that the most efficient metal mass transfer occurred within these first PVs. During percolation with 500 mg L^{-1} nanoparticles, a total of 19, 8.7, or 11 % of the respective Cd, Pb, or Zn originally present in the soil was eluted after 22.7 PVs, whereas this was 13, 4.2, or 2.2 % in the case of the 83.3 mg L^{-1} treatment. Furthermore, filtration of selected samples over 0.10 μm revealed that the vast majority of the eluted metals were associated with the nanoparticles (*i.e.*, only a small fraction occurred as "dissolved" Cd, Pb, or Zn), again confirming the strong affinity of CMC-FeS ENPs towards metals. Gong *et al.* (2012) reported similar observations for Hg, stating that the nanoparticle treatment is primarily a process where water-extractable Hg is transferred from the solid sediment matrix to the more thermodynamically stable CMC-FeS ENPs. Although Xiong *et al.* (2009) and Gong *et al.* (2012) both claimed that the delivered nanoparticles would remain virtually immobile upon removal of the exerted hydraulic head, the findings in this study suggest this might not always be the case and awareness should be raised regarding potential particle-facilitated contaminant transport.

On the other hand, as CMC is biodegradable, the stabilizing coating is believed to diminish and eventually vanish over time (in days, weeks, or even months), leading to nanoparticle aggregation and precipitation, or sorption onto solid soil/sediment surfaces, and hence immobilization of the associated contaminants (Gong *et al.*, 2012). However, additional research regarding elucidating such processes is required. Furthermore, it should also be noted that as FeS particulates are typically unstable under aerobic conditions and are easily oxidized to soluble sulphate species by air, their sorption capacity is also lost and any associated contaminants are released and potentially remobilized (Liu and Lal, 2012). According to Liu and Lal (2012), it is in practice difficult to maintain anaerobic conditions in soil/sediment environments for an extended amount of time, and thus changes in redox potential could potentially lead to a secondary contamination problem affiliated with FeS immobilization treatments. On the other hand, the high metal scavenging ability of the CMC-FeS ENPs in combination with their enhanced stability and mobility might allow the particles to possibly be considered as a feasible extraction agent for removal of metal contaminants from soils and sediments rather than an immobilization tool, in case they were shown to be competitive with other (organic) extraction agents that are currently being employed in soil remediation. This suggestion however merits further research.

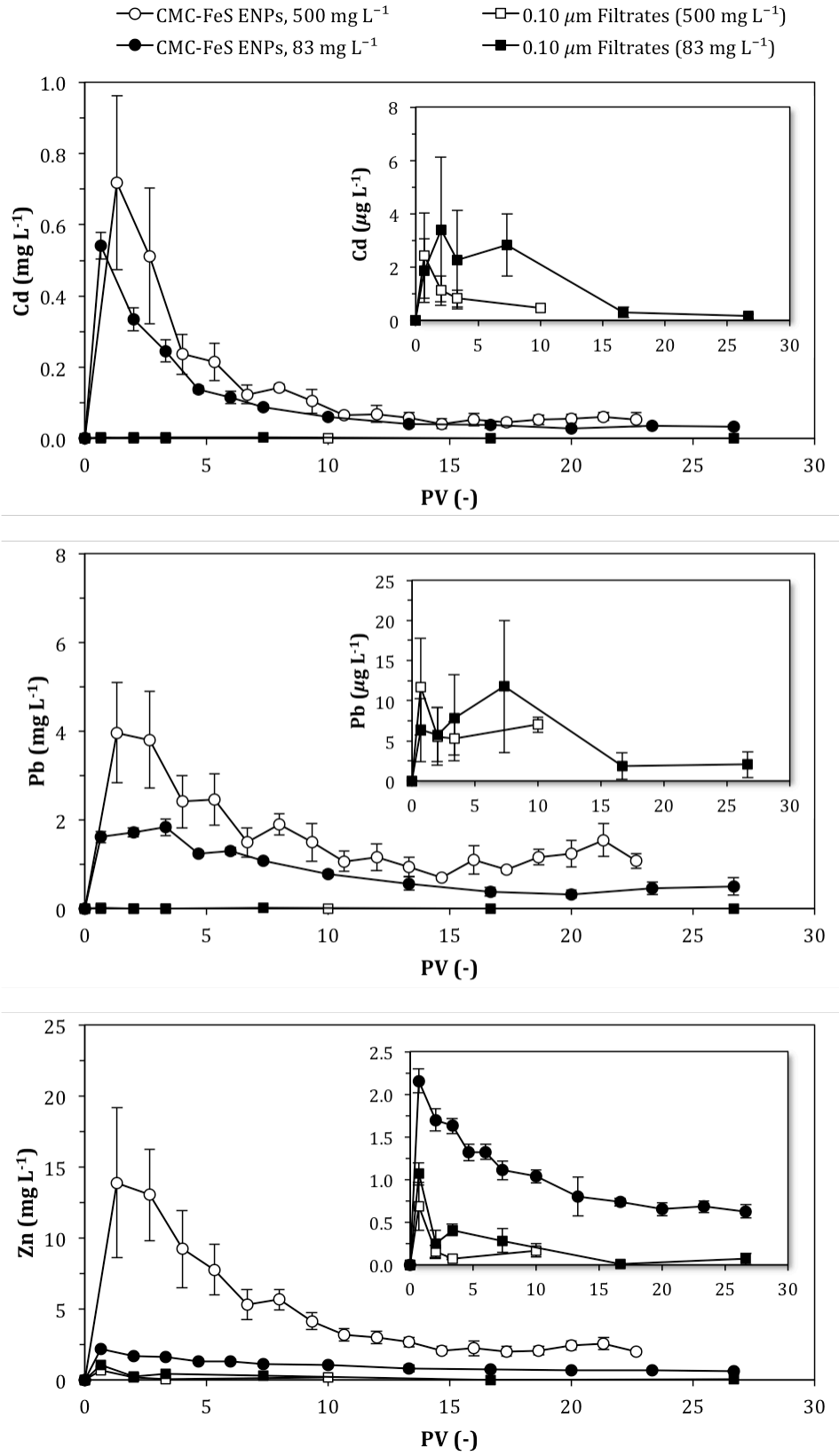

Figure 8.10 – Elution of total and dissolved (*i.e.*, the fraction < 0.10 μm) Cd, Zn, and Pb upon gravitational percolation of 500 and 83.3 mg L^{-1} CMC-FeS ENPs suspensions through S2. (Data points represent mean values, error bars denote standard deviations, n = 3)

8.4 Conclusion

From the preliminary findings of this study it may be concluded that the carboxymethyl cellulose (CMC) stabilizer is a prime determinant of FeS ENPs size, stability, and transport. In the presence of CMC, smaller FeS particles (154.5 ± 5.8 nm) were formed, which remained stable in suspension for a prolonged period of time (several weeks) when kept under anaerobic conditions, whereas bare FeS particles quickly aggregated and precipitated within minutes.

Additionally, batch and column tests have shown that the synthesized CMC-FeS ENPs possess a high affinity for metals, as high amounts of metal contaminants (*e.g.*, Cd, Cr, Cu, Hg, Ni, Pb, and Zn) could be extracted from field-contaminated soil/sediment samples, while filtration of the aqueous phase over 0.10 μm indicated that the vast majority of the extracted metals were associated with the nanoparticles. Furthermore, the CMC-FeS ENPs were demonstrated to remain quite stable in suspension even in the presence of soil/sediment, as only limited fractions (< 37 %) were retained by the solid phase, at least at an initial concentration of 500 mg L^{-1}. At a concentration of 83.3 mg L^{-1} CMC-FeS ENPs, batch retention in soil S2 apparently increased to around 75 %. Yet, no significant differences in the transport behaviour were observed between both concentrations when percolating CMC-FeS ENPs gravitationally through S2, and the nanoparticles showed a very high mobility through the soil column even without exerting an external pressure.

From an *in situ* environmental remediation perspective, a high affinity for the metal contaminants as well as a high particle mobility in order to be effectively deliverable to the targeted contamination zone, are important criteria that need to be satisfied. However, from an environmental behaviour and fate point of view, a high stability and mobility could allow the nanoparticles to persist longer in the environment and be transported more easily over longer distances, thereby augmenting potential environmental risks by expanding the contamination area through particle-facilitated contaminant transport (unless the particles can for instance be pumped up again following injection). On the other hand, CMC is believed to (bio)degrade over time, thereby stripping the FeS ENPs of their stabilizing coating and inducing immobilization of the particles and their associated contaminants through aggregation and precipitation, or sorption onto solid surfaces. Yet, as for instance the time span of CMC degradation has been mentioned to vary from days to even months, more research regarding such processes is required. Moreover, the CMC-FeS ENPs are also

highly susceptible to oxidation by air, thereby transforming them into soluble species that are deprived of their contaminant-sorption capacity, resulting in release and potential remobilization of formerly associated contaminants. Therefore, caution should be employed when considering such type of nanoparticles for *in situ* environmental remediation purposes. However, the feasibility of the CMC-FeS ENPs to serve as an extraction agent for heavy metal removal from contaminated soils and sediments as opposed to an immobilization option might potentially be taken under consideration, yet, requires additional research (*e.g.*, a comparison of their extraction performance to that of other commonly used extractants such as organic chelating agents).

Chapter 9

Partitioning behaviour of Ag nanoparticles in suspensions of field-incubated sediment under controlled redox conditions

9 Partitioning behaviour of Ag nanoparticles in suspensions of field-incubated sediment under controlled redox conditions[‡]

9.1 Introduction

Previous chapters have already stressed the relevance of studying the environmental behaviour and fate of Ag ENPs, as well as the significance of thoroughly understanding their partitioning between solid and liquid phases in complex (natural) aquatic systems. However, the experiments focused on the solid-liquid distribution behaviour of ENPs in sediment or soil suspensions that were performed in previous chapters, and even the majority of comparable studies currently available in the literature for that matter, have employed prepared (*i.e.*, dried, ground, and sieved) sediment or soil, have been performed over a relatively short experimental time frame, or have utilized relatively high nanoparticle exposure concentrations. Although such studies have already generated, and still can provide important and valuable information, there is also a strong necessity to elucidate the behaviour and fate of ENPs under more realistic environmental conditions. Therefore, the main objective of the present study was to examine the potential impact of field-incubated sediment on the solid-liquid partitioning behaviour and fate of Ag ENPs, as compared to oven-dried sediment.

Upon their release into the aquatic environment, Ag ENPs could undergo various transformation processes, including aggregation, flocculation, oxidation, dissolution, or sulphidation, which will impact their ultimate form and may affect their mobility, bioavailability and potential toxicity (Lowry *et al.*, 2012; Sharma *et al.*, 2014). These transformations are highly dependent on the prevailing environmental conditions, such as pH, redox potential (E_h), natural organic matter (NOM) content, ionic strength, or electrolyte composition, as well as on particle properties (*e.g.*, particle size or surface coating) (Lowry *et al.*, 2012; Kaegi *et al.*, 2013). The E_h is generally considered to be an important parameter dictating the stability and mobility of trace metals in soils and sediments, either directly or indirectly through related alterations in *e.g.*, pH, dissolved organic carbon, or Fe, Mn, and S

[‡] *In preparation for publication*

chemistry (Du Laing *et al.*, 2009; Frohne *et al.*, 2011; Frohne *et al.*, 2014). For example, metal immobilization can occur due to formation of largely insoluble metal sulphides under anaerobic conditions (Du Laing *et al.*, 2008). It is therefore not illogical to assume that the E_h could also significantly affect the ultimate fate of metallic ENPs. Under aerobic conditions, Ag ENPs can for instance be oxidized to Ag_2O that may dissolve to form Ag^+ ions or complexed Ag species, whereas in the presence of inorganic or biogenic sulphide (usually under anaerobic conditions), Ag ENPs may become partially or fully sulphidized and potentially immobilized as Ag_2S (Liu *et al.*, 2011; Levard *et al.*, 2012; Lowry *et al.*, 2012). Thus, the secondary aims of this work were to investigate the possible impact E_h might have on the solid-liquid distribution of Ag ENPs in (re)suspended sediment, as well as to examine the effects of particle properties by comparing the behaviour and fate of three different silver species (*i.e.*, Ag^+ ions, citrate-coated Ag ENPs, and polyvinylpyrrolidone-coated Ag ENPs).

9.2 Materials and methods

9.2.1 Sediment

Sediment from a depth of about 80 cm below the surface was excavated at Kijkverdriet (Steendorp, Belgium), an intertidal marsh situated approximately 95 km from the mouth of the river Scheldt (Belgium), which is vegetated by reed plants and is regularly flooded by the river. The collected sediment was transported back to the lab in plastic containers, where leaf litter, plant roots, and rhizomes were removed by hand. The sediment was then air-dried at room temperature, before being dried in an oven at 105°C for 48 h. Afterwards, the sediment was crushed, ground in a cross beater mill, passed through a 1 mm mesh sieve, and homogenized.

The homogenized sediment was characterized according to standard procedures. The pH-H_2O was measured in 1:5 (m:V) sediment:deionized water suspensions after equilibration during 16 h, whereas the pH-$CaCl_2$ was determined after adding 25 mL 0.01 M $CaCl_2$ to 10 g sediment and allowing to equilibrate for 30 min (Van Ranst *et al.*, 1999). The electrical conductivity (EC) was measured in the filtrates (MN 640 m, Macherey-Nagel GmbH & Co. KG, Düren, Germany) of 1:5 (m:V) sediment:deionized water suspensions after shaking for 1 h (Van Ranst *et al.*, 1999). The cation exchange capacity was determined by

percolation of 150 ml 1 M NH_4OAc through a percolation tube filled with a mixture of 5 g sediment and 12.5 g quartz sand, followed by washing through the excess with 150 mL denatured ethanol. The exchangeable ammonium ions were then eluted with 250 mL 1 M KCl and analysed in the percolate by means of a steam distillation (Vapodest Kjeldahl distillation system, Gerhardt GmbH & Co. KG, Königswinter, Germany). The organic matter (OM) content was determined by measuring the weight loss after incineration of 3 g oven-dried sample in a muffle furnace at 550 °C for 2 h (Salehi *et al.*, 2011). A TOC analyser (TOC-V_{CPN}, Shimadzu, Kyoto, Japan) was used to determine the dissolved organic carbon (DOC) content in sediment extracts, which were prepared with ultrapure water (18.2 MΩ cm^{-1}) (Milli-Q®, EMD Millipore Corp., Billerica, MA, USA) in a 1:10 (m:V) ratio, mixed for 24 h using an orbital shaker, and filtered over ashless filter paper (MN 640 m, Macherey-Nagel GmbH & Co. KG, Düren, Germany) (Jones and Willet, 2006). The total carbonate ($CaCO_3$) content was determined by back-titration (with 0.5 M NaOH) of an excess 0.25 M H_2SO_4 added to 1 g sediment (Van Ranst *et al.*, 1999). The total nitrogen (TN) content was determined according to the modified Kjeldahl method by digestion of 1 g sediment with 7 mL sulphuric/salicylic acid reagent, followed by alkalization with NaOH and steam distillation using a Vapodest Kjeldahl distillation system (Gerhardt GmbH & Co. KG, Königswinter, Germany) (Van Ranst *et al.*, 1999). The total phosphorous (TP) content was determined according to the colorimetric method of Scheel after *aqua regia* destruction of 1 g sediment (Van Ranst *et al.*, 1999). Particle size analysis was performed via the Bouyoucos hydrometer method after removing organic matter by adding H_2O_2 (Gee *et al.*, 1986; van Reeuwijk, 2002; Sartori *et al.*, 2013). Pseudo-total main and trace elements (*i.e.*, Ag, Al, As, Ca, Cd, Co, Cr, Cu, Fe, K, Mg, Mn, Na, Ni, Pb, S, and Zn) concentrations were determined via inductively coupled plasma optical emission spectrometry (ICP-OES) (Vista-MPX CCD Simultaneous ICP-OES, Varian, Agilent Technologies, Santa Clara, CA, USA) following an *aqua regia* destruction of 1 g sediment (Van Ranst *et al.*, 1999). More details regarding the employed characterization procedures can be found in Appendix A.

Following characterization, a fraction of the homogenized oven-dried sediment was (re)incubated in the field at the original sampling location, either under "oxic" or under "anoxic" conditions. For this, individual litterbags were custom-made using nylon filter cloth (41 μm mesh, Prosep BVBA, Zaventem, Belgium), filled with 205 g of dry sediment, and were either incubated at about 5 cm beneath the surface or buried at 80 to 100 cm depth for a period of 3 months (January – March 2014). The litterbag material should allow water and microorganisms to pass through, while retaining the sediment itself inside the bags. After

field incubation, the litterbags were dug up, transported back to the lab in sealed plastic containers, and stored in a refrigerator at 4 °C, before being utilized in the microcosm batch experiments (see Section 9.2.3) within 24 h after collection. In the case of the anoxically (re)incubated samples, the retrieved litterbags were immediately covered up completely under a thick layer of mud from the site to minimize exposure to the air, and were kept anoxic prior to being used in the batch tests.

Throughout the remainder of this chapter, the homogenized oven-dried sediment is referred to as "dry sediment", whereas the terms "oxic fresh sediment" or "anoxic fresh sediment" are used to refer to the oxically or anoxically (re)incubated sediment, respectively.

9.2.2 Nanoparticle dispersions and chemical reagents

Aqueous dispersions of spherical 40 nm NanoXact™ citrate- and polyvinylpyrrolidone-coated silver nanoparticles (Cit-Ag and PVP-Ag ENPs) were purchased from nanoComposix Europe (nanoComposix Inc., San Diego, CA, USA). The obtained Cit-Ag ENPs were 40.6 ± 4.1 nm in size, had a zeta (ζ) potential of -39.4 mV, and a surface area of 13.8 m^2 g^{-1}, and were provided as 22 mg Ag L^{-1} in aqueous 2mM citrate. The PVP-Ag ENPs had a particle diameter of 39.0 ± 5.2 nm, a surface area of 14.2 m^2 g^{-1}, and a ζ-potential of -44.3 mV, and were provided as 23 mg Ag L^{-1} in Milli-Q® water. Additional characterization info can be retrieved in Appendix G. Silver (as $AgNO_3$) reference standard solution (Plasma HIQU, 1000 ± 2 μg Ag^+ mL^{-1} in 2 – 5 % HNO_3) was purchased from ChemLab NV (Zedelgem, Belgium), and was applied to serve as the ionic counterpart (*i.e.*, Ag^+ ions) of the Ag ENPs in the batch experiments. All chemical reagents used in this study were of analytical grade.

9.2.3 Biogeochemical microcosm set-up

An automated biogeochemical microcosm system was used to examine the behaviour and fate of Ag ENPs in (re)suspended sediment under controlled redox conditions (Figure 9.1). This configuration allows for a continuous monitoring and control of redox potential (E_h), pH, and temperature in sediment or soil suspensions. For instance, predefined redox conditions can be established by (automatically) flushing the suspensions

with oxygen (O_2) (to increase E_h) or nitrogen (N_2) (to decrease E_h) via an automated-valve gas regulation system. This set-up was already successfully employed in several previous studies, *e.g.*, for quantification of trace gas emissions from flooded soils (Yu *et al.*, 2007; Rinklebe *et al.*, 2010), for examining mercury methylation in wetland soils (Frohne *et al.*, 2012), and for determination of the dynamics of trace metals in floodplain soils (Rupp *et al.*, 2010; Frohne *et al.*, 2011; Frohne *et al.*, 2014; Shaheen *et al.*, 2014), and has been described in detail by Frohne *et al.* (2011), and Yu and Rinklebe (2011).

The current study was performed using 40 independently operated microcosms (MCs) in total, allowing for three replicates of both the dry and the fresh sediments exposed to three different silver treatments (*i.e.*, Ag^+ ions, Cit-Ag ENPs, and PVP-Ag ENPs) under two predefined redox conditions (see below), as well as four (unreplicated) control treatments (*i.e.*, dry and fresh sediment without exposure to silver nanoparticles or ions). Each 2.88 L MC vessel was filled with 200 g dry or fresh sediment and 1.6 L Milli-Q® water (which was purged with either O_2 or N_2) to obtain a 1:8 (m:V) ratio, and was hermetically sealed with an airtight lid. All MC vessels were wrapped in aluminium foil to avoid exposure to (day)light, preventing eventual algae growth and photolysis of the ENPs. Homogeneous conditions were achieved by continuously stirring the slurries. The sediment suspensions were spiked with either Ag^+ ions, Cit-Ag ENPs or PVP-Ag ENPs to a final concentration of 200 μg Ag L^{-1}, and were incubated at room temperature for 192 h under controlled redox conditions. Incubation of the oxic fresh sediment occurred under constant aerobic conditions (O_2) (*i.e.*, by continuously flushing the MCs with O_2 for the first 24 h, followed by periodical flushing with O_2 during the remainder of the experiment). The anoxic fresh sediment on the other hand, was subjected to a variable (two-phasic) anaerobic-aerobic treatment (N_2/O_2) whereby phase I of the incubation occurred under reducing conditions for a duration of 144 h (*i.e.*, the MCs were continuously flushed with N_2 for the first 24 h, followed by periodical flushing with N_2 during the remaining 120 h of phase I), whereas the remainder of the incubation (*i.e.*, phase II) was performed under oxidizing conditions (*i.e.*, immediately following Phase I, the MCs were flushed with O_2 for the final 48 h). The dry sediment underwent both the O_2 and the N_2/O_2 incubation treatments. Redox potential, pH, and temperature in each MC were automatically monitored online via a E_h electrode (EMC 33), a pH electrode (EGA 153), and a temperature probe (Pt 100), which were all obtained from Sensortechnik Meinsberg GmbH (Waldheim, Germany), and data values were recorded every 10 min by a data logger (LogTrans 16-GPRS, UIT, Dresden, Germany).

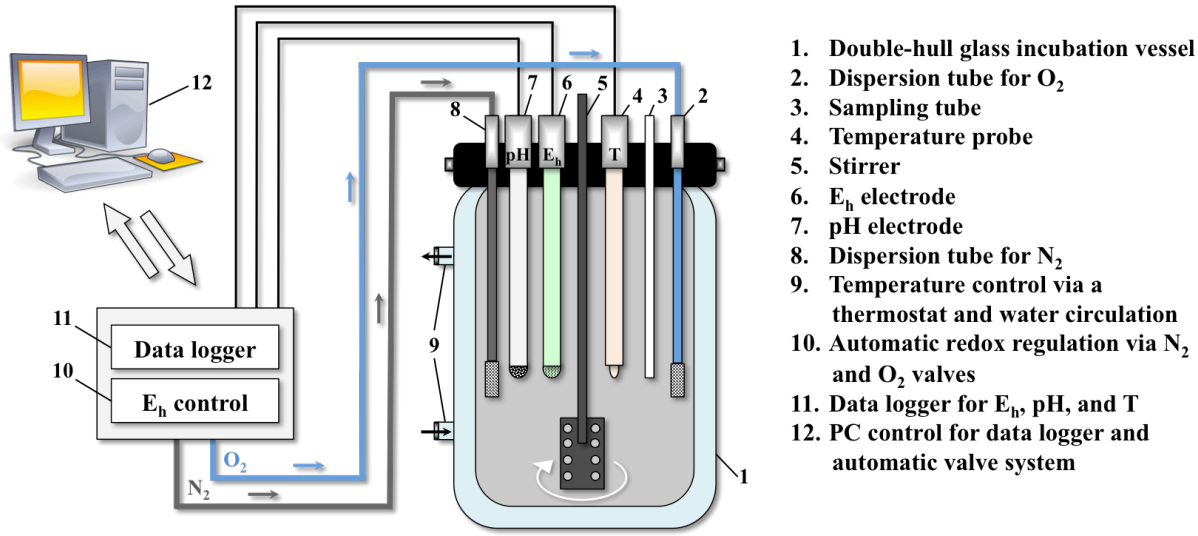

Figure 9.1 – Schematic representation of the components of one biogeochemical microcosm set-up. [After Yu and Rinklebe (2011)]

9.2.4 Slurry sampling and analysis

At designated time points (*i.e.*, after 24, 72, 144, and 192 h of incubation), 50 mL aliquots were sampled from the sediment suspensions using a 100 mL syringe connected to PTFE tubing, under continuous stirring of the slurries. Through this procedure, the 1:8 solid:liquid ratio was maintained throughout the entire experiment. In the case of N_2/O_2 treatments, an additional sampling point was included after 168 h of incubation, due to the switch of reducing (phase I) to oxidizing (phase II) redox conditions occurring after 144 h of MC incubation. The sampled slurry from each MC was then immediately centrifuged at 1000 rpm (*i.e.*, 184 *g*) for 10 min (Heraeus Megafuge 16, Thermo Fisher Scientific Inc., Waltham, MA, USA). Afterwards, 20 mL subsamples were collected from the resulting supernatants, acidified by adding 2 mL 65 % HNO_3, and stored at 4 °C in a refrigerator for a maximum of 2 weeks, prior to being analysed for Ag content via inductively coupled plasma mass spectrometry (ICP-MS) (Elan DRC-e, PerkinElmer Inc., Waltham, MA, USA). Additionally, 20 mL subsamples from the supernatants were filtered over 0.45 μm disposable syringe filters (Spartan 30 RC, Whatman, GE Healthcare Life Sciences, Buckinghamshire, UK) and the filtrates were stored in a freezer at -20 °C, before being analysed for TOC, and IC content using a TOC analyser (TOC-V_E, Shimadzu, Kyoto, Japan), and for Cl^-, NO_3^-, PO_4^{3-}, and SO_4^{2-} content by ion exchange chromatography (IEC) (761 Compact IC, Metrohm AG, Herisau, Switzerland).

Additionally, the potential ionic release of silver from the Cit-Ag and PVP-Ag ENPs in (re)suspended sediment, as affected by the prevailing redox conditions, was examined via centrifugal ultrafiltration (UF). Therefore, UF devices (Amicon Ultra-4, EMD Millipore Corp., Billerica, MA, USA) having a molecular weight cut-off (MWCO) of 10 kDa were used to differentiate between (nano)particulate and "dissolved" silver (*i.e.*, here defined as the fraction < 10 kDa). A third set of subsamples (4 mL) was pipetted from the supernatants obtained from centrifuging slurry that was sampled from the MCs after 144 h and 192 h incubation (see paragraph above), transferred into UF devices, and subjected to centrifugation at 4500 rpm (*i.e.*, 3735 *g*) for 30 min. The resulting filtrates were acidified with 100 μL 65 % HNO_3, and stored at 4 °C in a fridge for a maximum of 48 h, before being analysed for Ag content via ICP-MS.

9.2.5 Sulphide determination

The amount of acid volatile sulphide (AVS) was determined on selected samples (*i.e.*, on the original dry and anoxic fresh sediment, on the dry and anoxic fresh sediment controls after 144 h and 192 h of N_2/O_2 MC incubation, and on the dry and anoxic fresh sediment exposed to silver nanoparticles or ions after 144 h and 192 h of N_2/O_2 MC incubation), according to US EPA method 821-R-91-100 (Allen *et al.*, 1991). Briefly, the sulphides (S^{2-}) present in the sediment samples are first converted to H_2S by acidification with HCl. The formed H_2S is then purged from the samples with N_2 and trapped in a zinc acetate solution as ZnS. An equivalent amount of I_2, which is formed from a KIO_3 and KI mixture, reacts with the sulphides in an acidic environment to form elemental sulphur and I^-, where after the excess I_2 is back-titrated with $Na_2S_2O_3$.

9.2.6 Data processing

SPSS Statistics 22 (IBM, Armonk, NY, USA) was utilized to perform analysis of variance (ANOVA) and Pearson's product-moment correlation analysis. Shapiro-Wilk's test was used to check for normality of data. Welch's *t*-test was applied instead of ANOVA in case Levene's conditions for homogeneity of variances were not met. Tukey's HSD or Games-Howell's *post-hoc* tests ware used in case significant mean differences were observed after performing ANOVA's or Welch's *t*-tests, respectively. Graphical and numerical data processing occurred by means of Excel (Microsoft Corp., Redmond, WA, USA).

9.3 Results

9.3.1 Sediment characterization

The physicochemical properties of the dry sediment are tabulated in Table 9.1. The sediment had a neutral pH (6.96) and a relatively high CEC (39.2 $cmol_c\ kg^{-1}$), which could be attributed to the very high organic matter (20.6 %) and substantial clay content (46.7 %). According to the USDA's soil texture classification system the sediment can be classified as "silty clay". Furthermore, the sediment contained considerable amounts of trace metal contaminants, and was also characterized by a high S (5.78 g kg^{-1}), Al (31.7 g kg^{-1}), Fe (55.3 g kg^{-1}), and Mn (2.92 g kg^{-1}) content. The K (8.26 g kg^{-1}), Ca (31.0 g kg^{-1}), and Mg (6.94 g kg^{-1}) content were also significantly higher than the Na content (673 mg kg^{-1}).

Table 9.1 – Physicochemical properties of the dry sediment. Data is presented as mean ± standard deviation (n = 3).

Parameter		Dry sediment	Parameter		Dry sediment
pH-H_2O	**(-)**	6.96 ± 0.09	**Mg**	**(g kg^{-1})**	6.94 ± 0.02
pH-$CaCl_2$	**(-)**	6.80 ± 0.04	**Al**	**(g kg^{-1})**	31.7 ± 0.3
EC	**($\mu S\ cm^{-1}$)**	995 ± 25	**Fe**	**(g kg^{-1})**	55.3 ± 0.7
CEC	**($cmol_c\ kg^{-1}$)**	39.2 ± 1.0	**Mn**	**(g kg^{-1})**	2.92 ± 0.07
OM	**(%)**	20.6 ± 0.1	**S**	**(g kg^{-1})**	5.78 ± 0.21
DOC	**(mg kg^{-1})**	1137 ± 36	**Ag**	**(mg kg^{-1})**	2.89 ± 0.07
$CaCO_3$	**(%)**	9.42 ± 1.38	**As**	**(mg kg^{-1})**	76.2 ± 0.5
TN	**(g kg^{-1})**	6.78 ± 0.29	**Cd**	**(mg kg^{-1})**	22.1 ± 0.3
TP	**(g kg^{-1})**	7.94 ± 0.68	**Co**	**(mg kg^{-1})**	23.8 ± 0.3
Sand	**(%)**	4.7 ± 0.6	**Cr**	**(mg kg^{-1})**	296 ± 3
Silt	**(%)**	48.7 ± 0.6	**Cu**	**(mg kg^{-1})**	151 ± 1
Clay	**(%)**	46.7 ± 0.8	**Ni**	**(mg kg^{-1})**	74.0 ± 0.5
Na	**(mg kg^{-1})**	673 ± 23	**Pb**	**(mg kg^{-1})**	222 ± 2
K	**(g kg^{-1})**	8.26 ± 0.17	**Zn**	**(mg kg^{-1})**	820 ± 5
Ca	**(g kg^{-1})**	31.0 ± 0.2			

9.3.2 Solid-liquid distribution of Ag ENPs in (re)suspended sediment under controlled redox conditions

The evolution of E_h and pH of the sediment suspensions during the different MC incubations are depicted in Figures 9.2 to 9.5. During the 192 h-lasting experiments, the pH typically ranged between 6.3 and 7.3 or between 6.8 and 7.8 in the case of the O_2 or N_2/O_2 treatments, respectively. The apparent decrease in pH during O_2 incubation is likely caused by dissolution of CO_2, whereas the periodical small peaks coincided with the periodical flushing of the MCs and thus the evacuation of CO_2 from solution resulting in small pH increases. Furthermore, during O_2 incubations the E_h either remained constant around 375 mV (for the dry sediment), or sharply increased from somewhere in between 0 and 50 mV to about 300 mV during the first 2 h of incubation followed by a slow increase to around 375 mV over the remainder of the experimental time frame (for the oxic fresh sediment). In the case of dry sediment incubated under N_2/O_2 conditions on the other hand, the E_h typically decreased from about 350 mV to around 50 mV during the first 24 h followed by a more gradual decrease to about -75 mV after a final 144 h of incubation under N_2 conditions. At that point, switching to O_2 conditions immediately increased the E_h to around 250 mV, where after a more gradual increase to about 350 mV was observed until 192 h of incubation. Similar trends were noted for the anoxic fresh sediment, with the exception that the sediment suspensions were already in reduced condition (between *ca.* -50 and -150 mV) at the start of the MC incubations and remained fairly constant at that E_h until the switch to O_2 conditions after 144 h.

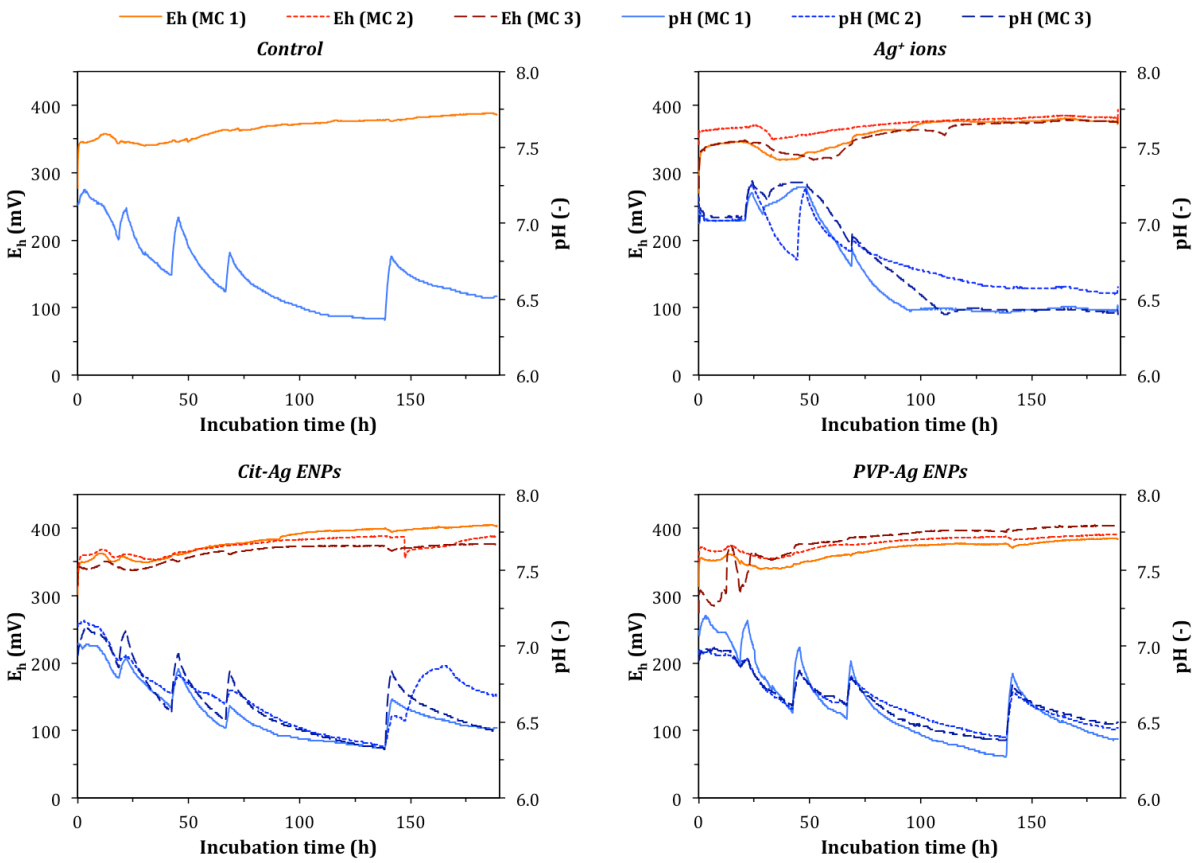

Figure 9.2 – E_h-pH relations during 192 h MC incubation of (re)suspended dry sediment under O_2 redox conditions during for the control treatment (top left graph), and the treatments with 200 μg L^{-1} Ag^+ ions (top right graph), Cit-Ag ENPs (bottom left graph), and PVP-Ag ENPs (bottom right graph). The control treatment consisted of 1 MC, whereas all silver treatments were performed in triplicate.

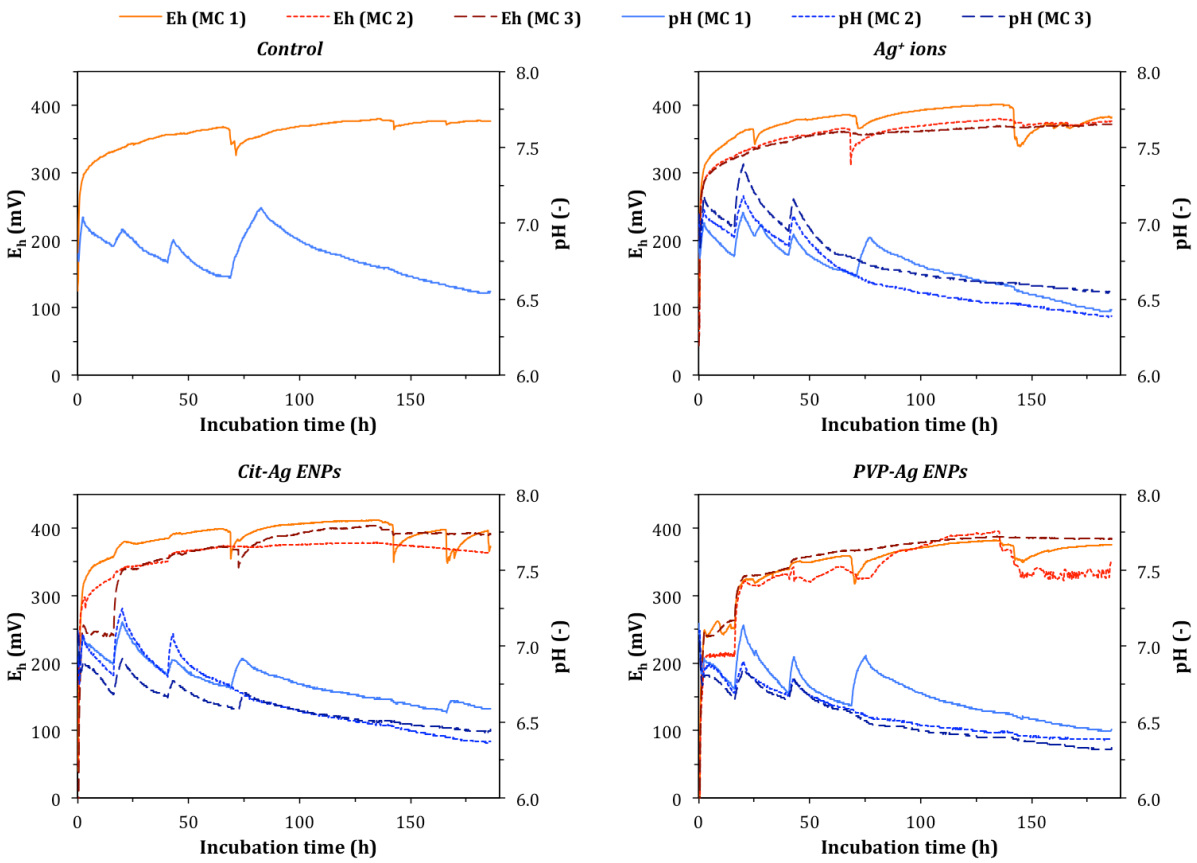

Figure 9.3 – E_h-pH relations during 192 h MC incubation of (re)suspended oxic fresh sediment under O_2 redox conditions for the control treatment (top left graph), and the treatments with 200 μg L^{-1} Ag^+ ions (top right graph), Cit-Ag ENPs (bottom left graph), and PVP-Ag ENPs (bottom right graph). The control treatment consisted of 1 MC, whereas all silver treatments were performed in triplicate.

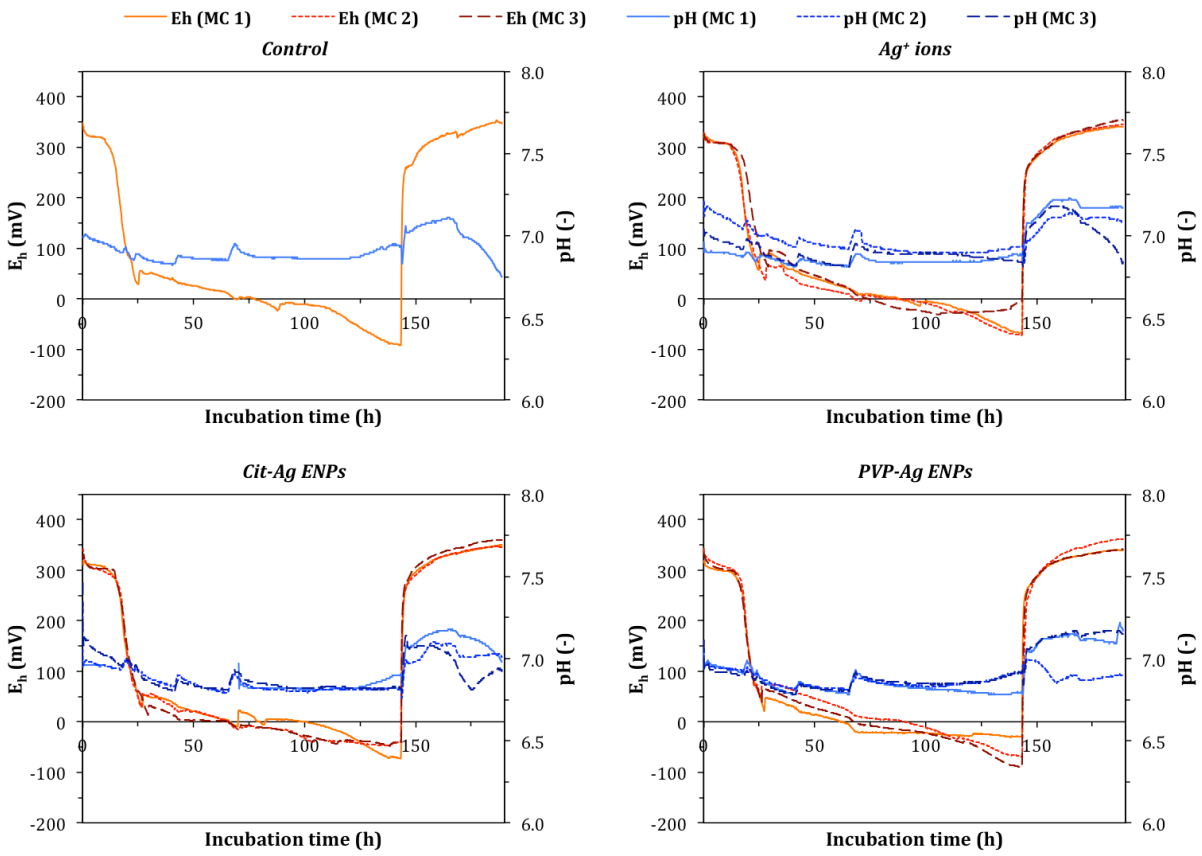

Figure 9.4 – E_h-pH relations during 192 h MC incubation of (re)suspended dry sediment under N_2/O_2 redox conditions (*i.e.*, under reducing conditions during the first 144 h and under oxidizing conditions during the final 48 h) for the control treatment (top left graph), and the treatments with 200 μg L^{-1} Ag^+ ions (top right graph), Cit-Ag ENPs (bottom left graph), and PVP-Ag ENPs (bottom right graph). The control treatment consisted of 1 MC, whereas all silver treatments were performed in triplicate.

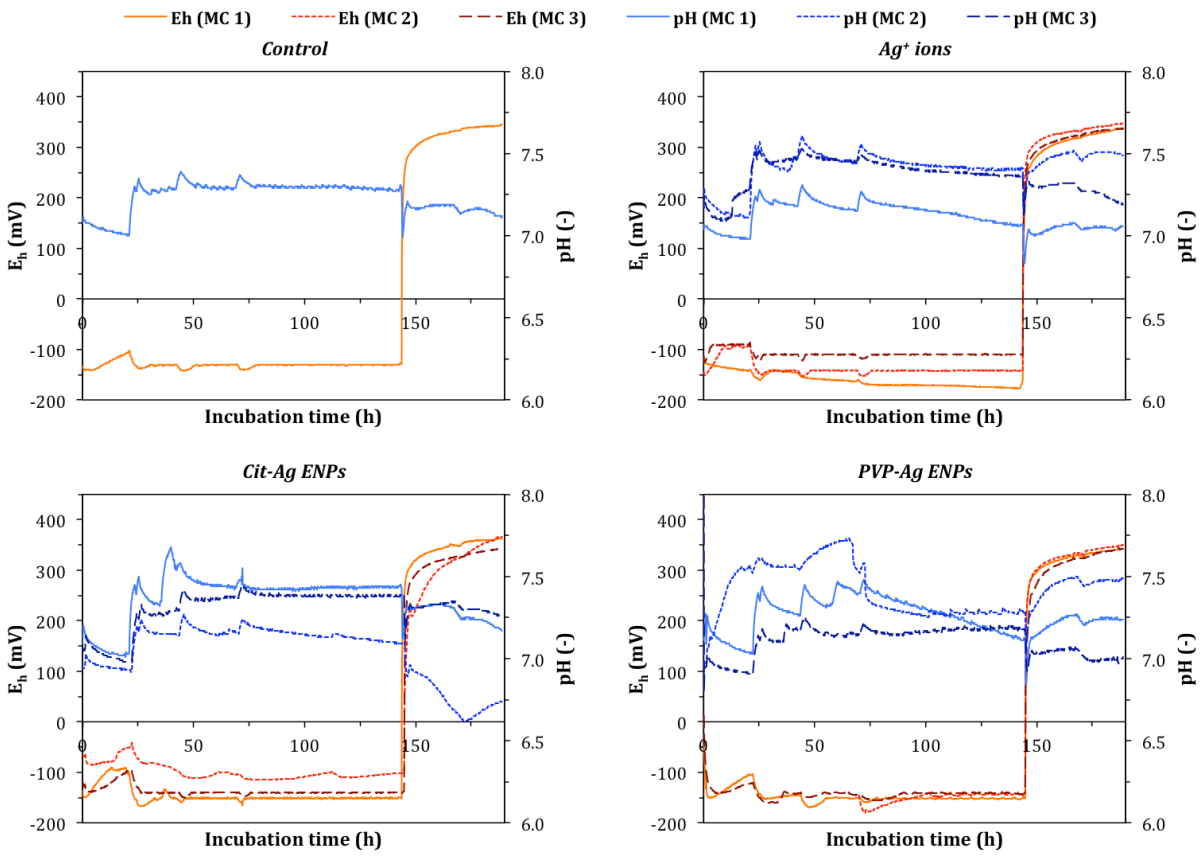

Figure 9.5 – E_h-pH relations during 192 h MC incubation of (re)suspended anoxic fresh sediment under N_2/O_2 redox conditions (*i.e.*, under reducing conditions during the first 144 h and under oxidizing conditions during the final 48 h) for the control treatment (top left graph), and the treatments with 200 μg L^{-1} Ag^+ ions (top right graph), Cit-Ag ENPs (bottom left graph), and PVP-Ag ENPs (bottom right graph). The control treatment consisted of 1 MC, whereas all silver treatments were performed in triplicate.

The silver concentrations in solution of the controls were low and ranged between 1.5 and 3.9 μg L^{-1} during the O_2 incubations, and between 2.3 and 3.6 μg L^{-1} for the N_2/O_2 treatments (Table G.2 in Appendix G). Table 9.2 presents the relative silver content remaining in solution of sediment suspensions spiked with 200 μg L^{-1} Ag^+ ions during 192 h of MC incubation. For the dry sediment, only between 1.1 and 2.3 % of the added silver remained in solution during the entire course of the experiments. On the other hand, in the case of the oxic fresh sediment approximately 16 % remained after 24 h and this amount decreased to about 4.4 % after 192 h. In contrast, an increase from 6.6 to 25 % was observed in the case of the anoxic fresh sediment.

Table 9.2 – Relative amounts of silver remaining in the supernatant of sediment suspensions treated with 200 μg L^{-1} Ag^{+} ions, after 24, 72, 144, 168, and 192 h of MC incubation under O_2 or N_2/O_2 redox conditions. The supernatants were obtained from centrifuging 50 mL slurry samples at 1000 rpm for 10 min. Data is presented as mean ± standard deviation (n = 3). Different small or capital letters denote statistically significant differences (p < 0.05) between treatments for each sampling time or between sampling times for each treatment, respectively.

Sediment type	Redox condition	Ag content in solution (%)				
		24 h	**72 h**	**144 h**	**168 h**	**192 h**
Dry	**O_2**	2.3 ± 0.9 ^{aA}	2.3 ± 0.5 ^{aA}	2.2 ± 0.5 ^{aA}	-	1.7 ± 0.4 ^{aA}
Oxic fresh	**O_2**	16 ± 5 ^{bB}	12 ± 5 ^{bAB}	5.8 ± 2.5 ^{aAB}	-	4.4 ± 3.3 ^{aA}
Dry	**N_2/O_2**	1.6 ± 0.3 ^{aAB}	1.7 ± 0.1 ^{aAB}	1.1 ± 0.2 ^{aA}	2.1 ± 0.6 ^{aB}	1.8 ± 0.3 ^{aAB}
Anoxic fresh	**N_2/O_2**	6.6 ± 3.9 ^{aA}	15 ± 3 ^{bAB}	19 ± 5 ^{bABC}	18 ± 3 ^{bABC}	25 ± 3 ^{bBC}

The relative silver contents remaining in solution of the sediment suspensions spiked with 200 μg L^{-1} Cit-Ag ENPs during 192 h of MC incubation are presented in Table 9.3. Considering the dry sediment, between about 1.1 and 4.4 % of the added silver could be retrieved over the whole experimental time frame. However, around 34 % remained in the case of the oxic fresh sediment after 24 h of incubation, which decreased to about 4.0 % after 192 h. For the anoxic fresh sediment, an increase from *ca.* 2.5 to up to 19 % was observed.

Table 9.3 – Relative amounts of silver remaining in the supernatant of sediment suspensions treated with 200 μg L^{-1} Cit-Ag ENPs, after 24, 72, 144, 168, and 192 h of MC incubation under O_2 or N_2/O_2 redox conditions. The supernatants were obtained from centrifuging 50 mL slurry samples at 1000 rpm for 10 min. Data is presented as mean ± standard deviation (n = 3). Different small or capital letters denote statistically significant differences (p < 0.05) between treatments for each sampling time or between sampling times for each treatment, respectively.

Sediment type	Redox condition	Ag content in solution (%)				
		24 h	**72 h**	**144 h**	**168 h**	**192 h**
Dry	**O_2**	2.4 ± 0.6 ^{aA}	2.5 ± 0.7 ^{aA}	2.0 ± 0.1 ^{aA}	-	1.3 ± 0.2 ^{aA}
Oxic fresh	**O_2**	34 ± 8 ^{bB}	22 ± 7 ^{bB}	7.0 ± 2.1 ^{bA}	-	4.0 ± 1.1 ^{aA}
Dry	**N_2/O_2**	4.4 ± 2.2 ^{aA}	2.5 ± 0.4 ^{aA}	1.4 ± 0.2 ^{aA}	2.3 ± 0.1 ^{aA}	2.3 ± 0.7 ^{aA}
Anoxic fresh	**N_2/O_2**	2.5 ± 0.3 ^{aA}	15 ± 4 ^{bB}	16 ± 1 ^{cB}	15 ± 1 ^{bB}	19 ± 5 ^{bB}

Table 9.4 presents the relative amounts of silver remaining in solution of the sediment suspensions spiked with 200 μg L^{-1} PVP-Ag ENPs during 192 h of MC incubation. Over the course of 192 h, between 1.3 and 3.5 % of the initially added amount of silver could be retrieved in the case of the dry sediment. For the oxic fresh sediment, the remaining silver content decreased from 23 to 3.0 % over 192 h, whereas a relatively constant amount of silver (7.4 – 15 %) remained in solution in the case of the anoxic fresh sediment.

Table 9.4 – Relative amounts of silver remaining in the supernatant of sediment suspensions treated with 200 μg L^{-1} PVP-Ag ENPs, after 24, 72, 144, 168, and 192 h of MC incubation under O_2 or N_2/O_2 redox conditions. The supernatants were obtained from centrifuging 50 mL slurry samples at 1000 rpm for 10 min. Data is presented as mean ± standard deviation (n = 3). Different small or capital letters denote statistically significant differences (p < 0.05) between treatments for each sampling time or between sampling times for each treatment, respectively.

Sediment type	Redox condition	Ag content in solution (%)				
		24 h	72 h	144 h	168 h	192 h
Dry	**O_2**	3.2 ± 0.4 ^{aA}	2.8 ± 0.4 ^{aA}	2.3 ± 0.2 ^{aA}	-	2.6 ± 1.3 ^{aA}
Oxic fresh	**O_2**	23 ± 7 ^{bC}	10 ± 3 ^{bB}	4.5 ± 1.1 ^{aA}	-	3.0 ± 0.4 ^{aA}
Dry	**N_2/O_2**	3.5 ± 0.3 ^{aC}	2.7 ± 0.4 ^{aBC}	1.4 ± 0.4 ^{aA}	2.5 ± 0.4 ^{aB}	2.3 ± 0.4 ^{aAB}
Anoxic fresh	**N_2/O_2**	7.4 ± 5.3 ^{aA}	12 ± 5 ^{bA}	13 ± 3 ^{bA}	15 ± 1 ^{bA}	14 ± 5 ^{bA}

Furthermore, very low silver concentrations (< 0.14 μg L^{-1}) were detected in all of the 10 kDa filtrates obtained through centrifugal ultrafiltration, indicating that the silver remaining in the supernatant of the sediment suspensions spiked with silver nanoparticles occurred in (nano)particulate form, or that at least virtually no "truly" dissolved silver species were present.

In addition to the amounts of silver remaining in the supernatant of the sediment suspensions, the TOC, IC, NO_3^-, Cl^-, SO_4^{2-}, and PO_4^{3-} concentrations were concurrently determined (Tables G.3 to G.6 in Appendix G). In all cases, NO_3^- and PO_4^{3-} contents were generally below 1.8 and 1.6 mg L^{-1}, respectively. For the dry sediment, the TOC content ranged between 95 and 242 mg L^{-1} and generally decreased over time, while values between 41 and 72 mg L^{-1} or between 97 and 136 mg L^{-1} were obtained in the case of the oxic or anoxic fresh sediment, respectively. The IC content varied between 9 and 53 mg L^{-1}, whereby a general increasing trend over time was only seen for the oxic fresh sediment. The Cl^- content generally increased during all MC incubations, and varied between 34 and

79 mg L^{-1} for the dry and anoxic fresh sediment, or between 11 and 37 mg L^{-1} for the oxic fresh sediment. An overall increasing trend was also observed for the SO_4^{2-} content during dry and oxic fresh sediment O_2 incubations, with values ranging from 192 to 632 mg L^{-1} and from 75 to 400 mg L^{-1}, respectively. During N_2/O_2 treatments, the SO_4^{2-} content varied between 147 and 303 or between 5 and 180 mg L^{-1} in the case of the dry or anoxic fresh sediment, respectively, whereby a considerable increase was generally observed upon switching from reducing to oxidizing conditions after 144 h of incubation. The latter could already indicate the potential presence of sulphides and their subsequent conversion to sulphates upon changing redox conditions. Screening of AVS indeed confirmed the presence of sulphides in the anoxic fresh sediment (Table G.7 in Appendix G), where about 3.1 mg S^{2-} g^{-1} DM was observed prior to MC incubation, and between 2.7 and 3.1 mg S^{2-} g^{-1} DM during incubation under N_2 conditions. In contrast, negligible AVS contents (< 0.17 mg S^{2-} g^{-1} DM) were obtained upon switching to O_2 conditions in the case of the anoxic fresh sediment, as well as for the dry sediment prior to or during O_2 and N_2/O_2 incubations.

9.4 Discussion

9.4.1 Sediment properties

Characterization analyses revealed that the sediment was considerably polluted with metal(loid) contaminants, as the determined concentrations of As, Cd, Cr, Cu, Pb, Ni, and Zn surpass the reference and target values for soil quality imposed by the Flemish government (Vlarebo, 2008). Sediments can thus indeed serve as a sink for heavy metal pollution. The very high amounts of trace metals are most likely due to the highly reduced, sulphidic nature of the original sediment, which was already indicated by the characteristic and pungent odour that was noticed upon excavation, as well as from some physicochemical characteristics (*e.g.*, the high organic matter and total sulphur content), and was eventually confirmed via AVS determination. Moreover, these results as well as the other sediment properties were in good agreement with previously reported observations by Du Laing *et al.* (2008), who studied heavy metal availability and mobility in intertidal sediment that was sampled at approximately the same location.

9.4.2 Partitioning behaviour and fate of Ag ENPs in (re)suspended sediment under controlled redox conditions

Addition of silver nanoparticles or ions to the (re)suspended dry sediment always resulted in comparably low silver concentrations remaining in solution ($p > 0.05$), indicating a strong and relatively fast partitioning of the Ag^+ ions and the Cit- and PVP-Ag ENPs towards the sediment solid phase, and a similar behaviour of the silver species under consideration. Furthermore, the prevailing redox conditions did not appear to significantly affect the partitioning behaviour of the silver nanoparticles or ions during the dry sediment incubations ($p > 0.05$). Studies by for instance Kaegi *et al.* (2013) and Whitley *et al.* (2013) have also demonstrated a high removal of Cit- and PVP-Ag or Au ENPs in sludge batch experiments, irrespective of particle size or coating, stating that particle type was of minor importance compared to the degree of ENP removal. The observed high removal of silver from the liquid phase could for instance be due to hetero-aggregation with sediment solid constituents, to homo-aggregation and subsequent sedimentation, or to the formation and precipitation of rather insoluble solid compounds, such as AgCl ($K_{sp,\ 25\ °C} = 1.8 \times 10^{-10}$) or Ag_2CO_3 ($K_{sp,\ 25\ °C} = 8.5 \times 10^{-12}$) (Hotze *et al.*, 2010; Levard *et al.*, 2012; Lowry *et al.*, 2012; Van Koetsem *et al.*, in press). Significant correlations between the IC ($r = -0.426$, $p < 0.0005$), as well as the Cl^- ($r = -0.398$, $p < 0.0005$) content and the amount of silver remaining in solution during the dry sediment incubations could be noticed. Association with natural colloids has been suggested to be a dominant factor controlling the removal of ENPs from natural water bodies and affecting their ultimate fate in soils or sediments (Quik *et al.*, 2012; Batley *et al.*, 2013; Van Koetsem *et al.*, in press). Several studies have reported a higher retention of Ag ENPs in soils or sediments having a higher clay content, suggesting interactions between the nanoparticles and solid phases such as clay minerals, may be important in determining the mobility of ENPs (Cornelis *et al.*, 2010; Cornelis *et al.*, 2012; Cornelis *et al.*, 2013; Navarro *et al.*, 2014; Van Koetsem *et al.*, in press).

When considering the oxic fresh sediment suspensions on the other hand, a substantial fraction of the initially added amount of silver still remained in the liquid phase after 72 h of incubation for all three tested silver species or even after 144 h in the case of Cit-Ag ENPs ($p < 0.05$), suggesting the latter might be the most mobile, persistent, and potentially bioavailable species under the prevailing conditions. In general, significant differences in the silver content remaining in solution were no longer observed upon incubation of the silver nanoparticles or ions for more than 72 h using the oxic fresh

sediment, nor when compared to the dry sediment treatments ($p > 0.05$). The use of oxically (re)incubated sediment thus clearly affected the partitioning behaviour of both the silver ions and silver nanoparticles. The apparent higher mobility of the silver species could potentially be caused by the presence of a biofilm. Disaggregation of TiO_2 ENPs in the presence of microorganisms, and even enhanced stabilization of CeO_2 and Fe ENPs in suspension upon attachment onto the surface of bacteria have been mentioned in the literature (Hotze *et al.*, 2010). Furthermore, it was noticed that after 24 h of MC incubation for instance the TOC and Cl^- content had significantly decreased in comparison to the dry sediment treatments, suggesting potential leaching of salts and dissolved organic carbon, or enhanced biodegradation of organic matter might have occurred during (re)incubation of the sediment in the field under oxic conditions. In turn, the decreased amounts of Cl^- (and possibly other electrolytes) and TOC might thus also have affected silver partitioning. An increase in the ionic strength of a solution is known to potentially promote nanoparticle aggregation, whereas dissolved organic matter could improve resistance to aggregation by stabilizing the nanoparticles in suspension (Hotze *et al.*, 2010; Lin *et al.*, 2010; Quik *et al.*, 2010; Scown *et al.*, 2010; von der Kammer *et al.*, 2010; Sharma *et al.*, 2014). On the other hand, natural organic matter (NOM) could also promote aggregation via bridging mechanisms, and whether association with NOM results in stabilization or destabilization is dependent on the type and concentration of the NOM as well as on solution chemistry (Hotze *et al.*, 2010; Keller *et al.*, 2010). Additionally, the amount of silver remaining in solution during the oxic fresh sediment incubations significantly correlated with the IC ($r = -0.689$, $p < 0.0005$), Cl^- ($r = -0.716$, $p < 0.0005$), and SO_4^{2-} ($r = -0.790$, $p < 0.0005$) content. Further research is however required in order to elucidate the potential occurrence and impact of a biofilm on the behaviour and fate of the nanoparticles (and vice versa), as well as to reveal the exact appearance of the silver species remaining in the liquid phase.

Considerable amounts of silver remaining in solution could also be noticed in the case of anoxic fresh sediment incubations, indicating that (re)incubation of the sediment in the field under anoxic conditions also affected the solid-liquid distribution of the silver ions and nanoparticles. However, in contrast to the oxic fresh sediment treatments, the silver recoveries generally increased over time ($p < 0.05$). After 24 h of incubation under N_2 conditions, the remaining amount of silver was still similarly low compared to the dry sediment treatments ($p > 0.05$) but significantly increased after 72 h of incubation, after which no further increase was noticed until the end of the experiment. Switching between N_2 and O_2 conditions after 144 h of incubation had therefore no apparent impact on the

silver species remaining in the liquid phase. Furthermore, the silver ions and nanoparticles appeared to behave similarly, as no significant differences were observed when comparing the different silver species ($p > 0.05$). Due to the relatively high AVS content of the anoxic fresh sediment prior to as well as during the anoxic phase of the MC incubations, low silver concentrations remaining in the liquid phase were expected as a result of sulphidation. Silver is known to have a high affinity for sulphur containing compounds, and both Ag^+ ions and Ag ENPs readily react with inorganic and organic sulphur species, *e.g.*, to form virtually insoluble Ag_2S precipitates ($K_{sp,\ 25\ °C} = 5.9 \times 10^{-51}$) or Ag-organosulphur (thiols) complexes, especially under anaerobic conditions (Liu *et al.*, 2011; Levard *et al.*, 2012; Thalmann *et al.*, 2014). Furthermore, Lombi *et al.* (2013) reported the transformation of Ag ENPs to Ag_2S particles of a similar size as the original nanoparticles during a wastewater treatment process, and that this process occurred independently of the original nanoparticle surface coating. However, there is still a great paucity of information regarding the surface properties of nano-sized Ag_2S, as well as on the potential impact environmental parameters such as NOM might have on their formation and environmental stability and bioavailability (Levard *et al.*, 2012; Lowry *et al.*, 2012). For example, NOM could potentially act as a competing ligand, which might prevent or retard the sulphidation process, as a passivating layer that could inhibit or limit interactions between the particle surface and other ligands, or as a stabilizing ligand rendering the particles more mobile (Levard *et al.*, 2012). The amount of silver remaining in the liquid phase could be correlated with the TOC content ($r = 0.374$, $p = 0.016$), while significant relationships were also obtained for the IC ($r = -0.798$, $p < 0.0005$), Cl^- ($r = 0.776$, $p < 0.0005$), and SO_4^{2-} ($r = 0.378$, $p = 0.015$) content. Moreover, the presence of a biofilm that might also affect particle stability and mobility, as well as the mechanisms and kinetics of nano-sized Ag_2S oxidation in contact with air or resulting from microbial conversion to the considerably more soluble Ag_2SO_4 ($K_{sp,\ 25\ °C} = 1.2 \times 10^{-5}$), require to be further addressed (Levard *et al.*, 2012). Additional work is thus needed to determine the occurring bioavailable form(s) of silver during the MC incubations, as well as the time-span over which the silver might remain bioavailable under the prevailing conditions.

9.5 Conclusion

The solid-liquid distribution of *ca.* 40 nm citrate- and PVP-coated silver nanoparticles as well as silver ions in (re)suspended sediment was examined by means of microcosm (MC) batch experiments operating under controlled redox conditions. The partitioning behaviour of the silver ions and nanoparticles was shown to be significantly affected by application of sediment that was (re)incubated in the field under oxic or anoxic conditions as opposed to utilizing oven-dried sediment. Considerable amounts of silver remained in the liquid phase up to 72 h of MC incubation using the oxic fresh sediment, or even after 192 h in the case of the anoxic fresh sediment incubations. In contrast, addition of silver ions or nanoparticles to the dry sediment resulted in low silver recoveries during the entire 192 h of incubation. Furthermore, predefined redox settings did not appear to significantly impact silver partitioning in the case of the dry sediment incubations, whereas the redox condition of the field-incubated sediment on the other hand did have a profound effect on silver dynamics, as a time-dependent decrease or even an increase of the silver content remaining in solution was observed when considering the oxic or anoxic fresh sediment incubations, respectively. Generally, no substantial differences in the behaviour of the different silver species were observed (except in the case of Cit-Ag ENPs during the oxic fresh sediment incubation), suggesting that particle properties (*e.g.*, the type of surface coating) were of minor importance in regard to the degree of silver removal from the liquid phase, at least under the prevailing experimental conditions.

The observations from the current study thus indicate that (re)incubation of sediments or soils in the field prior to putting them to experimental use might impart considerable alterations in their properties, which in turn could significantly affect nanoparticle behaviour and should therefore be taken into account when investigating the ultimate environmental behaviour and fate of ENPs in for instance aqueous sediment or soil matrices. Additional research is however needed in order to reveal the exact appearance of the silver species remaining in the aqueous phase during the different MC incubations, to elucidate the potential presence and impact of a biofilm on nanoparticle behaviour and fate and vice versa, and to further examine the time-span over which the silver might remain bioavailable under similar and other prevailing conditions.

Chapter 10

Synthesis

10 Synthesis

10.1 General discussion

The worldwide manufacturing and use of metallic ENPs, which has increased exponentially over recent years, will inevitably result in their emission into the aquatic environment (Gottschalk *et al.*, 2013; Liu *et al.*, 2014). It has also been recognized that their often extraordinary and size-related characteristics could possibly lead to unexpected health and environmental hazards, as for instance evidence of their potential toxicity (or that of their transformation products) towards various (aquatic) organisms and even human cells is systematically emerging (Scown *et al.*, 2010; Klaine *et al.*, 2012). In order to fully understand the environmental implications of ENPs and address the possible risks involved with the advancements in nanotechnology *e.g.*, by adapting or developing exposure assessment methodologies, detailed knowledge of their behaviour and fate in the environment is required (Klaine *et al.*, 2012; Batley *et al.*, 2013). The potentially occurring physical, chemical, or biological transformation processes (*e.g.*, aggregation, sedimentation, and dissolution) that govern the eventual environmental behaviour and fate of metallic ENPs in aquatic systems are highly dependent on nanoparticle properties as well as on the physicochemical characteristics of the receiving medium (Boxall *et al.*, 2007; Keller *et al.*, 2010; Velzeboer *et al.*, 2014).

This work aimed to aid in the identification of parameters affecting the fate of metallic ENPs in the aquatic environment. Therefore, in this section, selected factors potentially affecting their behaviour and fate in complex (natural) aqueous matrices are briefly discussed in view of the experimental data obtained during the course of this PhD research.

10.1.1 Particle properties affecting the environmental behaviour and fate of metallic ENPs in the aquatic environment

Nanoparticles are characterized by several key parameters such as size, surface properties, chemical composition, and morphology (Batley and McLaughlin, 2010). Besides providing nanoparticles with often unique properties and reactivities (**Chapter 1**), the physicochemical characteristics of ENPs are also key elements in determining their

behaviour, fate, and potential bioavailability and toxicity when released in the aquatic environment (Scown *et al.*, 2010; Bhatt and Tripathi, 2011). These nanoparticle properties, which are interrelated, and hence their impact on the ultimate behaviour and fate of ENPs, are in turn also strongly affected by the prevailing environmental conditions (*e.g.*, pH, ionic strength, and natural organic matter content) of the receiving medium (**Chapter 2**).

10.1.1.1 Particle size

Besides being a key defining criteria for a nanomaterial (**Chapter 1**), size is one of the main characteristics responsible for the often extraordinary attributes of nanoparticles and is an important parameter in determining *e.g.*, their stability, mobility, and potential bio-accessibility and toxicity in the aquatic environment (**Chapters 1 and 2**). From simplistic calculations, the small size of nanoparticles (< 100 nm) would imply the formation of stable dispersions as they are subject to Brownian motion to a significant degree, which controls the long-range forces between individual nanoparticles (Christian *et al.*, 2008; Hotze *et al.*, 2010). However, this would be neglecting the high surface energy of nanoparticles, as a decrease in particle size results in a greater percentage of atoms existing at the particle surface and hence, the electronic structure, surface charge behaviour, and reactivity can be altered (Hotze *et al.*, 2010; Liu *et al.*, 2014). Nanoparticles are therefore inherently prone to aggregation and subsequent sedimentation (Christian *et al.*, 2008). Such a phenomenon could for instance be observed during the synthesis of bare FeS particles, which quickly aggregated and precipitated out of solution in a matter of minutes (**Chapter 8**). To overcome this (generally) unwanted behaviour, ENPs are usually coated with surface ligands to enhance their stability in suspension (see Section 10.1.1.2).

The dissolution of metallic ENPs in the aquatic environment is important in terms of their overall stability, persistence, and potential toxicity, as dissolution generates metal ions that could be detrimental to (aquatic) organisms (**Chapter 2**). In theory, equilibrium solubility increases with decreasing particle size. However, aggregation could impede dissolution by reducing the average equilibrium solubility of the nanoparticulate system, and by introducing kinetic hindrance to the diffusion process (Lin *et al.*, 2010). On the other hand, dissolution could also cause disaggregation as the particles within aggregates dissolve over time (Mudunkotuwa and Grassian, 2011). Although most metallic ENPs are hydrophilic and possess a finite yet often low solubility, substantial ionic release from the surface of *e.g.*, Ag and ZnO ENPs, which has been demonstrated to increase with decreasing particle size,

has been reported in numerous publications (Franklin *et al.*, 2007; Elzey and Grassian, 2010; Quik *et al.*, 2011; Angel *et al.*, 2013). In contrast, no substantial ionic release (determined as the total silver or cerium content in 10 kDa filtrates following centrifugal ultrafiltration) from Ag or CeO_2 ENPs was observed during the experiments performed in this work, which could suggest that under the considered experimental conditions dissolution of the nanoparticles was negligible or that at least no free silver or cerium ions were present (**Chapters 3, 4, 6, and 9**).

The transport of nanoparticles is theoretically predicted to increase with decreasing particle size, however, the tendency of nanoparticles to aggregate can also greatly inhibit their transport. Aggregate straining (*e.g.*, in porous media such as sediments and soils) is for instance an important component of nanoparticle capture (**Chapter 2**). Nevertheless, smaller sized particles are considered to be more mobile and hence potentially bioavailable for interactions with living systems. Uptake of Au ENPs by aquatic plants has for instance been reported to depend on nanoparticle size (Glenn *et al.*, 2012; Glenn and Klaine, 2013). A possible explanation for the observed higher apparent uptake of 6.7 nm CeO_2 ENPs compared to 14.1 nm Ag ENPs (*e.g.*, 111 vs. 186 mg kg^{-1} DW at an exposure concentration of 1 mg L^{-1}) by the aquatic plant *E. canadensis* could therefore be the smaller size of the former (**Chapter 5**).

10.1.1.2 Surface characteristics

Many of the interesting and sometimes unexpected characteristics of ENPs are dominated by the nature of the particle surface (**Chapter 1**). Furthermore, the surface properties of nanoparticles such as their surface charge or coating also play a crucial role in their stability and mobility as colloidal suspensions, or their aggregation into larger particulates and deposition in the aquatic environment (**Chapter 2**). Nanoparticles having a near neutral surface charge will rapidly aggregate and precipitate out of solution, which will usually result in the loss of their unique properties. Therefore, ENPs are generally functionalized with specific surface coatings (*e.g.*, carboxylic acids, surfactants, polymers, and polyelectrolytes) that provide electrostatic and/or steric stabilization of the particles in dispersion (He *et al.*, 2007; Christian *et al.*, 2008; Hotze *et al.*, 2010; Sharma *et al.*, 2014). This was for instance shown for FeS ENPs, where the presence of a carboxymethyl cellulose (CMC) surface coating caused the nanoparticles to remain stable in suspension for a prolonged period of time, most likely by providing the particles with electrosteric repulsion

and thus preventing aggregation and subsequent sedimentation (**Chapter 8**). Moreover, CeO_2 ENPs having a net positive surface charge were also shown to remain in stable dispersion in ultrapure water during 7 d sedimentation experiments, which can be attributed to electrostatic stabilization (**Chapter 4**). In contrast, the amount of CeO_2 ENPs remaining suspended in the presence of pure quartz sand were shown to decrease over time, whereas no significant decrease was observed in the case of negatively charged citrate-stabilized Ag ENPs, suggesting that the enhanced retention of the CeO_2 ENPs in quartz sand suspensions was caused by electrostatic attraction between the positively charged nanoparticles and the negatively charged quartz sand (**Chapter 7**). Similarly, the retention of Ag and CeO_2 ENPs upon filtration over filters having considerably larger pore sizes than the size of the ENPs, could in part also be attributed to electrostatic interactions between the nanoparticles and the filter material (**Chapter 3**). In addition to their larger size, the negative surface charge and/or the presence of the organic citrate coating on the surface of Ag ENPs might also have contributed to the apparent higher uptake of CeO_2 ENPs by *E. canadensis* (**Chapter 5**).

Any nanoparticle is characterized by an exceptionally high surface-area-to-volume ratio resulting in an enhanced reactivity compared to larger sized particles composed of the same material (**Chapter 1**). Upon their release in the aquatic environment, the surface of nanoparticles will thus be the first aspect experienced by environmental constituents and could directly interact with biota in a potential adverse manner (Christian *et al.*, 2008; Scown *et al.*, 2010; Van Hoecke, 2010). Potential interactions between ENPs and environmental constituents such as natural colloids, dissolved ionic species, sediment and soil particles, and dissolved organic matter, which are ubiquitous in aqueous systems, and their impact on the behaviour and fate of ENPs are further discussed in Section 10.1.2. The high specific surface area of nanoparticles also provides an enhanced ability to bind environmental contaminants, and as stabilization of ENPs in the environment induces a higher mobility by inhibiting attachment between the nanoparticles and media surfaces, ENPs have the potential to act as vectors for the delivery of attached pollutants (Batley and McLaughlin, 2010; Lin *et al.*, 2010; Scown *et al.*, 2010; Liu *et al.*, 2014). The presence of CMC as a stabilizing agent was not only shown to enhance the stability and mobility of FeS ENPs in aqueous soil and sediment matrices, but to potentially also lead to particle-facilitated contaminant transport in case conditions favouring colloidal transport are prevailing, as the CMC-stabilized FeS ENPs were also demonstrated to possess a very high affinity to associate with heavy metal contaminants (**Chapter 8**).

10.1.1.3 Chemical composition

Aside from equipping ENPs with specific intrinsic properties (**Chapter 1**), the chemical composition of nanoparticles also affects their behaviour (*e.g.*, aggregation and dissolution) and fate in aqueous matrices, as well as their potential (eco)toxicity (Hotze *et al.*, 2010; Scown *et al.*, 2010; Quik *et al.*, 2011). According to classical colloid science, the impact of chemical composition on particle aggregation is captured through the Hamaker constant (A_H), which governs Van der Waals attraction (**Chapter 2**). When considering the same surface and solution chemistry, particles possessing a high A_H have a higher tendency to aggregate in comparison to particles with a low A_H. For instance, the A_H values for gold, silver, and polystyrene are 45.3, 39.8, and 9.8 × 10^{-20} J, respectively, and the Van der Waals forces are hence approximately five times stronger for gold than for polystyrene particles (Hotze *et al.*, 2010). As the chemical composition of nanoparticles alters the surface potential by dissociation or ion adsorption by surface atoms, the surface charge of (uncoated) nanoparticles is in part governed by the type of atoms at the particle surface, although the core of (common) core:shell particles can also influence the charge of surface atoms (Hotze *et al.*, 2010). Furthermore, the chemical composition of nanoparticles, specifically at solid-liquid interface, is also the basis for their dissolution behaviour (Quik *et al.*, 2011). Various metallic ENPs have been demonstrated to have a great range in degree of solubility. For example, CeO_2 and TiO_2 ENPs have been reported to be virtually insoluble, whereas Ag, Al_2O_3, CuO, and ZnO ENPs have been demonstrated to be able to (easily) dissolve under natural conditions (Quik *et al.*, 2011). As mentioned earlier, no significant dissolution of Ag or CeO_2 ENPs was observed during any of the experiments performed in this work (**Chapters 3, 4, 6, and 9**). However, as particle dissolution was determined by means of centrifugal ultrafiltration (UF), it cannot entirely be excluded that ionic release from the particle surface, followed by interactions with natural constituents present in solution (*e.g.*, organic matter, suspended solids, or dissolved ionic species) and hence retention upon performing UF, did occur, especially in the case of Ag ENPs.

10.1.2 Impact of abiotic environmental parameters on the behaviour and fate of metallic ENPs in aquatic systems

Upon their emission into the aquatic environment, ENPs are subjected to various transformation and transport processes, the nature and degree of which can be perceived in

physicochemical, macromolecular, or even biologically mediated interactions (**Chapter 2**). Consequently, *e.g.*, the aggregation, deposition, sedimentation, and dissolution of ENPs, which are some of the main (interrelated) transformation processes governing their stability, mobility, and hence their potential bioavailability and (eco)toxicity, are considered to be highly dependent on the characteristics of the receiving natural aquatic system (*e.g.*, pH, ionic strength and composition, natural organic matter content and type, amount and type of suspended solids, and redox condition) (**Chapter 2**). The stability of ENPs in complex aqueous matrices (*e.g.*, natural surface waters or sediment and soil solutions) is a prime determinant controlling their ultimate environmental fate, as well-dispersed nanoparticles could persist longer in the environment, be transported over larger distances, and could potentially be involved in particle-facilitated contaminant transport, whereas nanoparticle aggregation and subsequent sedimentation greatly restricts their transport and bio-accessability and thus reduces the change for potentially harmful interactions with (aquatic) organisms (Fang *et al.*, 2009; Lin *et al.*, 2010; Liu *et al.*, 2013).

10.1.2.1 pH

The pH plays a crucial role in the stability of metallic ENPs in natural aquatic environments by controlling their aggregation as well as impacting their dissolution (**Chapter 2**). Surface charge titration by H^+ or OH^- is the primary way of pH to promote nanoparticle aggregation. At a low pH (excess of H^+), particle surfaces are normally positively charged, while a high pH (excess OH^-) normally yields a negative surface charge (Hotze *et al.*, 2010). For any given aqueous system, the pH at which the concentration of H^+ or OH^- causes the suspended ENPs to have a neutral surface charge is called the point of zero charge (PZC) or isoelectric point (IEP) (**Chapter 2**). As the pH moves towards this point, the electrostatic repulsion between particles decreases and aggregation is promoted by Van der Waals attraction (Hotze *et al.*, 2010; Lin *et al.*, 2010). Charge reversal could dramatically affect the behaviour of ENPs, as the majority of the surfaces present in environmental media (*e.g.*, natural colloids or sediment and soil particles) possess a negative surface charge at near neutral pH (Hotze *et al.*, 2010). The potential effect of solution-pH on the stability of positively charged CeO_2 ENPs released in natural surface waters was for instance shown in **Chapter 4**, as the nanoparticles remained in stable dispersion during 7 d in surface water characterized by a low pH (4.95) under stagnant and isothermal conditions. In surface waters having a higher pH (7.28 – 8.08) on the other hand, considerable sedimentation of

the CeO_2 ENPs was observed over time (**Chapter 4**). Furthermore, pH was also shown to impact the solid-liquid partitioning behaviour of Ag and CeO_2 ENPs in (re)suspended sediments and soils, and hence their potential mobility and bioavailability in environmental matrices (**Chapters 6 and 7**).

10.1.2.2 Ionic strength and composition

The ionic strength (IS), which is a measure for the concentration of all dissolved ionic species in solution, is an important parameter in regard to colloidal stability, and can therefore greatly influence the behaviour and fate of ENPs in aquatic systems (**Chapter 2**). A higher IS leads to compression of the electrical double layer (EDL) (*i.e.*, by reducing the thickness of the diffuse layer) surrounding dispersed nanoparticles, which in turn results in a decrease in electrostatic repulsion forces between particles and thus potentially to aggregation, deposition, and sedimentation of the ENPs (**Chapter 2**). Association of Ag and CeO_2 ENPs with the submerged aquatic plant *E. canadensis*, was demonstrated to be affected by the electrical conductivity (EC) of the aqueous matrix, which is a measure for the IS, suggesting that a higher EC could reduce nanoparticle-plant interactions and thus their bio-accessibility, potentially as a result of nanoparticle aggregation (**Chapter 5**). Furthermore, in addition to the low pH, the low IS of the natural surface water PUM might have also contributed to the observed colloidal stability of CeO_2 ENPs during the experimental 7 d time frame (**Chapter 4**).

Additionally, the type and valence of the counterions also has a profound impact on nanoparticle stability (**Chapter 2**). Divalent cations have for instance been demonstrated to have a stronger influence (*ca.* 50 – 60 fold) on the aggregation of negatively charged citrate-stabilized Ag ENPs compared to monovalent cations (Baalousha *et al.*, 2013). Similarly, a higher degree of aggregation of citrate-stabilized Ag ENPs in the presence of Ca^{2+} ions was suggested in **Chapter 3**, as retention of the Ag ENPs upon 0.45 μm filtration was considerably higher in a 2 mM $CaCl_2$ matrix compared to 2 mM NaCl or KNO_3 solutions. Metallic ENPs and their ionic dissolution products can also react with certain types of dissolved ionic species (*e.g.*, Cl^-, HS^-, HCO_3^-, $H_2PO_4^-$, S^{2-}, CO_3^{2-}, and HPO_4^{2-}) to form rather insoluble solid compounds that could for instance precipitate from solution, or form a passivating surface layer that could inhibit or limit interactions between the particle surface and other environmental constituents (**Chapter 2**). The formation of AgCl precipitates in chloride-containing matrices (*i.e.*, 2 mM NaCl and $CaCl_2$) was for example indicated in

Chapter 3. Association of Ag ENPs with *E. canadensis* was also shown to significantly decrease with increasing Cl^- content (**Chapter 5**). Moreover, although no substantial correlation was obtained between the settling rate of CeO_2 ENPs in natural surface waters and the PO_4^{3-} content, the residual fraction of CeO_2 ENPs remaining in suspension was demonstrated to be significantly higher at higher PO_4^{3-} concentrations (**Chapter 4**). Adsorption of phosphate on the surface of CeO_2 and Al_2O_3 ENPs has already been reported to enhance their stability and mobility (Darlington *et al.*, 2009; Cornelis *et al.*, 2011). Moreover, the amount of CO_3^{2-} in solution was also shown to impart a negative impact on the association of CeO_2 ENPs with *E. canadensis* (**Chapter 5**), and on the stability of Ag and CeO_2 ENPs in (re)suspended sediments (**Chapter 6**), presumably either by contributing to the overall impact of IS on particle aggregation, by the formation of sparingly soluble precipitates such as Ag_2CO_3 or $Ce_2(CO_3)_3$, or by a combination of both. The solid-liquid distribution behaviour of Ag ENPs during 10 days in sediment suspensions under controlled redox conditions was also found to correlate significantly to the Cl^- and CO_3^{2-} content (**Chapter 9**).

10.1.2.3 Natural organic matter

As mentioned earlier (see Section 10.1.1.2), synthetic surface coatings are often used to improve the colloidal stability of ENPs and overcome their rapid aggregation and sedimentation. In addition, ENPs can also be coated and stabilized in suspension by natural organic matter (NOM), which is omnipresent in the aquatic environment (**Chapter 2**). Stabilization of ENPs by association with NOM can either be caused by electrostatic repulsion, steric hindrance, or a combination of both (Hotze *et al.*, 2010; Lin *et al.*, 2010; Quik *et al.*, 2010; Sharma *et al.*, 2014). In contrast, NOM could also promote aggregation and sedimentation through charge neutralization or bridging mechanisms, and whether interactions between ENPs and NOM result in stabilization or destabilization depends on NOM type and concentration, as well as on solution chemistry (Christian *et al.*, 2008; Hotze *et al.*, 2010; Keller *et al.*, 2010; Batley *et al.*, 2013). Furthermore, NOM has also been mentioned to potentially be involved in the disaggregation of nanoparticle aggregates (Chritstian *et al.*, 2008; Hotze *et al.*, 2010). It was shown that the solid-liquid partitioning behaviour of Ag and CeO_2 ENPs in sediment and soil suspensions was strongly related to the total organic carbon (TOC) concentration in solution, which can be used as an estimate for the NOM content, suggesting an enhanced stability and potential mobility of the ENPs at

higher TOC concentrations (**Chapters 6 and 7**). Comparably, NOM was also found to impact the solid-liquid distribution dynamics of Ag ENPs in anoxic (re)suspended sediment, as a higher TOC content resulted in a higher amount of silver remaining in the liquid phase (**Chapter 9**). Furthermore, the propensity of NOM to stabilize ENPs was clearly demonstrated in **Chapter 7**, as NOM extracted from pure peat was shown to considerably enhance the amount of CeO_2 ENPs remaining in suspension in the presence of quartz sand.

10.1.2.4 Suspended matter

Due to their high specific surface area and reactivity, nanoparticles have a large potential to interact with aquatic colloids (*e.g.*, clays, aluminosilicates, iron oxyhydroxides, dissolved organic matter, and bacteria) and solid sediment and soil particles, which are ubiquitous in natural aquatic systems (**Chapter 2**). As such environmental constituents are often subject to sedimentation, preferential partitioning of ENPs towards solid phases and probable co-precipitation with suspended matter will substantially restrict their mobility and hence bioavailability (**Chapter 2**). Quik *et al.* (2012) already argued that hetero-aggregation of ENPs with natural colloidal material and subsequent sedimentation might be the dominant mechanism for their removal from the water column. In this work, significant correlations were obtained between the amount of total suspended solids (TSS) and the dynamics of CeO_2 ENPs in natural surface waters during 7 d, indicating that a higher TSS content leads to a higher sedimentation rate and generates a lower residual fraction of nanoparticles remaining suspended (**Chapter 4**). It was also suggested that the CeO_2 ENPs might have sorbed and co-precipitated with aluminium- and iron-containing natural compounds, as similar significant relationships were noticed in regard to the Al and Fe content of the different water bodies, and that the observed high stability of CeO_2 ENPs in PUM might also be related to the low amount of TSS in this surface water (**Chapter 4**). Furthermore, the amount of suspended matter was also shown to significantly affect the fraction of Ag and CeO_2 ENPs remaining in the liquid phase of sediment and soil suspensions, suggesting that when less colloidal material is present in solution, the probability for hetero-aggregation and potential co-precipitation decreases, and their mobility and potential bioavailability is enhanced (**Chapters 6 and 7**). In addition, the amount of clay also appeared to play an important role in the behaviour and fate of Ag and CeO_2 ENPs in (re)suspended sediments and soils (**Chapters 6 and 7**), which confirmed

earlier reports suggesting the scavenging of ENPs by clay particulates (Cornelis *et al.*, 2011; Cornelis *et al.*, 2012).

10.1.2.5 Redox condition

In combination with *e.g.*, pH and solution composition, occurring redox conditions can also have a significant impact on the behaviour and fate of ENPs, for instance by affecting the transformation and/or remobilization of the nanoparticles following their release in aquatic environments (**Chapter 2**). Redox reactions could for example contribute to nanoparticle dissolution or lead to alterations in their crystalline nature and composition (Auffan *et al.*, 2009; Lombi *et al.*, 2013). For instance, AgCl or Ag_2S are expected to be the two most relevant inorganic silver species into which Ag ENPs will transform under aerobic or anaerobic environmental conditions, respectively, and such transformations might have a considerable influence on nanoparticle stability, mobility, and potential bio-accessibility and (eco)toxicity (Levard *et al.*, 2012; Thalmann *et al.*, 2014). The solid-liquid partitioning of Ag ENPs in (re)suspended sediment during 8 d under controlled redox conditions was shown to differ significantly when comparing the use of aerobically to anaerobically incubated sediment, whereby a time-dependent decrease in the fraction of Ag ENPs remaining in liquid phase was observed during treatments under oxidizing conditions as opposed to a seemingly (and unexpected) time-dependent increase in the case of treatments under reducing conditions, the latter indicating potential remobilization of silver over time (**Chapter 9**).

10.2 General conclusion

The main objective of this research was to contribute to the general knowledge on the environmental fate of metallic ENPs and further the understanding of their behaviour and fate in the aquatic environment, by aiding in the identification of potential factors affecting for instance nanoparticle stability, mobility, and possible bioavailability upon their release in complex (natural) aqueous systems, as well as to reveal the kinetics of transformation processes occurring after such a release. Furthermore, assessment of the occurrence, behaviour, and fate of metallic ENPs in the aquatic environment requires a suitable analytical toolbox comprised of a combination of reliable analytical techniques that are able

to provide both qualitative and quantitative information. Therefore, attention was also given to the analytical aspect and the potential implications the use of certain existing (traditional) analytical techniques (*e.g.*, filtration, centrifugation, and elemental analysis via ICP-OES and ICP-MS) might have when studying the environmental fate of metallic ENPs.

The use of basic filtration methods (*e.g.*, paper filtration, micro- and ultrafiltration), which are routinely utilized during (pre-)treatment of aquatic samples or as particle size fractionation tools, was evaluated for aqueous dispersions of Ag and CeO_2 ENPs, and as expected, filtration was well suited for retaining nanoparticles that were larger than the pore size of the filter membrane. However, significant retention was also observed for considerably larger filter pore sizes, and thus filtration artefacts for instance resulting from nanoparticle-membrane interactions need to be taken into consideration.

The stability and mobility of metallic ENPs in complex aquatic media (*e.g.*, natural surface waters or sediment and soil solutions) are prime determinants governing their ultimate environmental fate and potential (eco)toxicological risks, and are highly influenced by the characteristics of the ENPs as well as the properties of the receiving medium. Upon their release in natural surface waters, a substantial depletion of CeO_2 ENPs from the water column was observed for 9 out of 10 tested water samples, and the observed time-dependent sedimentation in those 9 samples could be well described by a first-order kinetics settling model. The pH appeared to be a prime determinant governing nanoparticle colloidal stability. Furthermore, the amount of suspended matter was also shown to be an important factor affecting nanoparticle sedimentation rate as well as the residual fraction of CeO_2 ENPs remaining in suspension. In contrast, no sedimentation of the CeO_2 ENPs during 7 d was observed in surface water characterized by a low pH, ionic strength, and suspended matter content, indicating these parameters had a significant impact on nanoparticle stability. Additionally, the physicochemical properties of natural surface water as well as particle properties (*e.g.*, size, surface charge, coating, and composition) were also shown to affect the association of Ag and CeO_2 ENPs with the submerged aquatic plant *Elodea canadensis* significantly, suggesting these parameters should be taken into account for instance when performing environmental risk assessment or (eco)toxicity studies. Furthermore, although the solid-liquid partitioning behaviour of Ag and CeO_2 ENPs in (re)suspended sediments and soils was demonstrated to be highly related to the amount of suspended material and the natural organic matter (NOM) content, considerable fractions of the nanoparticles remained stable in suspension even after 24 h, despite their high surface

reactivity and the large abundance of solid sediment or soil constituents. This might indicate a high mobility and potential bioavailability of the ENPs and thus an enhanced environmental risk. In the case of the positively charged CeO_2 ENPs, the high nanoparticle stability in suspensions could possibly be attributed to electrosteric stabilization by NOM adsorption on the surface of the nanoparticles, while the negatively charged citrate coating of the Ag ENPs potentially provided electrostatic stabilization. Applying a carboxymethyl cellulose (CMC) surface coating on FeS ENPs was also found to greatly enhance their stability and mobility, even in the presence of soil or sediment. These observations in combination with the very high affinity of the CMC-FeS ENPs towards metal contaminants (*e.g.*, Cd, Cr, Cu, Hg, Ni, Pb, and Zn) and the observed ability of CMC-FeS ENPs to extract those pollutants from field-contaminated soils and sediment, suggest such nanoparticles might persist longer in the environment and be transported more easily over greater distances, and could thus pose an environmental threat by potentially expanding a contamination zone through particle-facilitated contaminant transport. Finally, the use of field-incubated sediment compared to homogenized dry sediment was also demonstrated to have a significant impact on the solid-liquid distribution behaviour of Ag ENPs under controlled redox conditions, whereby considerably larger fractions of the Ag ENPs remained in the aqueous phase in the case of field-incubated sediments. Moreover, the redox condition of the field-incubated sediment was also shown to have a profound impact on silver dynamics. These findings suggest that (re)incubation of sediments or soils in the field prior to putting them to experimental use might impart substantial alterations in their characteristics, which in turn could significantly affect nanoparticle behaviour and should therefore be taken into account when studying the environmental behaviour, and fate of ENPs in for example aqueous sediment or soil matrices.

10.3 Future research perspectives

In this section, some recommendations for potential future research are presented based on the current knowledge and on the experiences and insights gained during this research.

- It is generally acknowledged that the analysis of ENPs in environmental matrices is challenging and the assessment of their behaviour in aquatic environments requires a combination of (complicated) analytical techniques. And although already a considerable collection of analytical tools was utilized during the experiments performed in this study, in recent years, great progress has been made in the analytical aspect for providing added fundamental qualitative and quantitative information of ENPs in complex environmental samples. Therefore, it is recognized that additional studies focused on the occurrence, behaviour and fate of metallic ENPs in natural aquatic media should greatly benefit from the application and further development of more novel and technologically advanced analytical tools (*e.g.*, field-flow fractionation hyphenated set-ups and specialized electron microscopy-based techniques).

- From an environmental risk assessment point of view, a future challenge should be to undertake behaviour and fate studies of metallic ENPs in natural water, sediment, and soil systems at even lower, more environmentally realistic nanoparticle concentrations in order to avoid potential artefacts associated with the use of relatively high exposure concentrations.

- In order to extrapolate the observed results towards natural aquatic systems and further the understanding of the stability, mobility, and ultimate environmental fate of metallic ENPs, longer-term experiments are required that are performed under even more complex and realistic environmental conditions (*e.g.*, accounting for potential effects stemming from temporal changes in flow rate, temperature, pH, and redox conditions), and that utilize a broader collection of nanoparticulate species having distinct particle properties (*e.g.*, for assessing the eventual impact of chemical composition, particle size, morphology, and type of surface coating).

- To date, there is still a great paucity of information regarding the exact underlying interaction mechanisms between metallic nanoparticles and aquatic plants.

Additional research is thus necessary in order to clarify as well as differentiate between the potentially occurring absorptive and/or adsorptive nanoparticle-plant interactions, and elucidate the parameters responsible for these different plant uptake mechanisms. Additionally, potential translocation and trophic transfer processes also merit further investigation.

- As certain metallic ENPs were shown to possess a relatively high stability and probable mobility even in complex aqueous matrices, the possible environmental risks stemming from the nanoparticles themselves or affiliated to potential particle-facilitated contaminant transport require additional attention. Therefore, from the point of nanoparticle emission, their exact appearance and how this evolves over time as a consequence of specifically occurring nanoparticle transformation processes, which are mediated by prevailing abiotic and biotic environmental conditions, needs to be further addressed. For example, many uncertainties still exist regarding the mechanisms and time-span for (bio)degradation or alterations of nanoparticle surface coatings and the subsequent environmental implications, as well as the potential impact the presence of (micro)organisms might have on the behaviour and fate of metallic ENPs in the aquatic environment.

- This study contributed considerably to the understanding of the environmental behaviour and fate of pristine metallic ENPs released into complex aquatic systems. However, there currently still is insufficient knowledge on for instance, the amount and the exact nature of nanoparticles that are actually released, the behaviour, impact, and fate of altered and aged ENPs in natural systems and how this is affected by varying environmental conditions, the influence of particle properties on nanoparticle transformation processes and vice versa, the long-term effects of nanoparticle transformation on their (eco)toxicity, product-specific nanoparticle fate processes, and product-specific time scales for nanoparticle alteration and transport processes in the environment. These issues, amongst others, thus require to be further addressed in order to be able to perform adequate risk assessment and in turn establish correct regulatory directions, as it is most likely that not pristine, but altered and product-specific nanoparticles are actually (going to be) present in the environment.

References

Acreman, J. (2013). **Synthetic media for growing duckweeds.** University of Toronto Culture Collection of Algea and Cyanobacteria (UTCC), Toronto, Ontario, Canada. *Available from http://www.mobot.org/jwcross/duckweed/media.htm (Accessed on February 25, 2014)*

Akaighe, N., Depner, S.W., Banerjee, S., and Sohn, M. (2013). **Transport and deposition of Suwannee river humic acid/natural organic matter formed silver nanoparticles on silica matrices: The influence of solution pH and ionic strength.** Chemosphere 92, 406-412.

Alidokht, L., Khataee, A.R., Reyhanitabar, A., and Oustan, S. (2011). **Cr(VI) immobilization process in a Cr-spiked soil by zerovalent iron nanoparticles: Optimization using response surface methodology.** Clean-Soil Air Water 39, 633-640.

Allabashi, R., Stach, W., de la Escosura-Muñiz, A., Liste-Calleja, L., and Merkoçi, A. (2009). **ICP-MS: A powerful technique for quantitative determination of gold nanoparticles without previous dissolving.** J. Nanopart. Res. 11, 2003-2011.

Allen, H.E., Fu, G., Boothman, W., DiToro, M., and Mahony, J.D. (1991). **Determination of acid volatile sulfide and selected simultaneously extractable metals in sediment.** EPA-821-R-91-100 Analytical method, Office of Water, United States Environmental Protection Agency (US EPA), Washington, DC, USA, 1-18.

Angehrn-bettinazzi, C. (1990). **Factors affecting the investigation of heavy metal speciation in forest soils using thin-channel ultrafiltration.** Int. J. Environ. Analyt. Chem. 39, 81-89.

Angel, B.M., Batley, G.E., Jarolimek, C.V., and Rogers, N.J. (2013). **The impact of size on the fate and toxicity of nanoparticulate silver in aquatic systems.** Chemosphere 93, 359-365.

Aruoja, V., Dubourguier, H.-C., Kasemets, K., and Kahru, A. (2009). **Toxicity of CuO, ZnO, and TiO2 to microalgae *Pseudokirchneriella subcapitata*.** Sci. Total Environ. 407, 1461-1468.

ATSDR (2013). **Priority list of hazardous substances**. Agency for Toxic Substances and Disease Registry (ATSDR), Atlanta, GA, USA. *Available from http://www.atsdr.cdc.gov/spl/ (Accessed on January 16, 2015)*

Auffan, M., Rose, J., Bottero, J.-Y., Lowry, G.V., Jolivet, J.-P., and Wiesner, M.R. (2009). **Towards a definition of inorganic nanoparticles from an environmental, health and safety perspective.** Nat. Nanotechnol. 4, 634-641.

Baalousha, M. (2009). **Aggregation and disaggregation of iron oxide nanoparticles: Influence of particle concentration, pH and natural organic matter.** Sci. Total Environ. 407, 2093-2101.

Baalousha, M., Nur, Y., Römer, I., Tejamaya, M., and Lead, J.R. (2013). **Effect of monovalent and divalent cations, anions and fulvic acid on aggregation of citrate-coated silver nanoparticles.** Sci. Total Environ. 454-455, 119-131.

Baalousha, M.A., Manciulea, A., Cumberland, S., Kendall, K., and Lead, J.R. (2008). **Aggregation and surface properties of iron oxide nanoparticles: Influence of pH and natural organic matter.** Environ. Toxicol. Chem. 27, 1875-1882.

Baalousha, M.A., Stolpe, B., and Lead, J.R. (2011). **Flow field-flow fractionation for the analysis and characterization of natural colloids and manufactured nanoparticles in environmental systems: A critical review.** J. Chromatogr. A 1218, 4078-4103.

Bae, S., Hwang, Y.S., Lee, Y.-J., and Lee, S.-K. (2013). **Effects of water chemistry on aggregation and soil adsorption of silver nanoparticles.** Environ. Health Toxicol. 28, 1-7.

Bai, L., Ma, X., Junfeng, L., Sun, X., Zhao, D., and Evans, D.G. (2010). **Rapid separation and purification of nanoparticles in organic density gradients.** J. Am. Chem. Soc. 132, 2333-2337.

Batley, G. E., and McLaughlin, M. J. (2010). **Fate of Manufactured Nanomaterials in the Australian Environment.** CSIRO Niche Manufacturing Flagship report, Lucas Heights, NSW, Australia, pp. 85. *Available from http://www.environment.gov.au/node/21212. (Accessed on December 18, 2014)*

Batley, G.E., Kirby, J.K., and McLaughlin, M.J. (2013). **Fate and risks of nanomaterials in aquatic and terrestrial environments.** Acc. Chem. Res. 46, 854-862.

Battin, T.J., Von der Kammer, F., Weilhartner, A., Ottofuelling, S., and Hofmann, T. (2009). **Nanostructured TiO_2: transport, behaviour and effects on aquatic microbial communities under environmental conditions.** Environ. Sci. Technol. 43, 8098-8104.

Ben-Moshe, T., Frenk, S., Dror, I., Minz, D., and Berkowitz, B. (2013). **Effects of metal oxide nanoparticles on soil properties.** Chemosphere 90, 640-646.

Benn, T., and Westerhoff, P. (2008). **Nanoparticle silver released into water from commercially available sock fabrics.** Environ. Sci. Technol. 42, 4133-4139.

Benn, T., Cavanagh, B., Hristovski, K., Posner, J.D., and Westerhoff, P. (2010). **The release of nanosilver form consumer products used in the home.** J. Environ. Qual. 39, 1875-1882.

Benoit, R., Wilkinson, K.J., and Sauvé, S. (2013). **Partitioning of silver and chemical speciation of free Ag in soils amended with nanoparticles.** Chem. Cent. J. 7, 1-7.

Bhatt, I., and Tripathi, B.N. (2011). **Interaction of engineered nanoparticles with various components of the environment and possible strategies for their risk assessment.** Chemosphere 82, 308-317.

Bian, S.-W., Mudunkotuwa, I.A., Rupasinghe, T., and Grassian, V.H. (2011). **Aggregation and dissolution of 4 nm ZnO nanoparticles in aqueous environments: Influence of pH, ionic strength, size, and adsorption of humic acid.** Langmuir 27, 6059-6068.

Blaser, S.A., Scheringer, M., MacLeod, M., and Hungerbuhler, K. (2008). **Estimation of cumulative aquatic exposure and risk due to silver: Contribution of nano-functionalized plastics and textiles.** Sci. Total Environ. 390, 396-409.

Bolea, E., Jiménez-Lamana, J., Laborda, F., and Castillo, J.R. (2011). **Size characterization and quantification of silver nanoparticles by asymmetric flow field-flow fractionation coupled with inductively coupled plasma mass spectrometry.** Anal. Bioanal. Chem. 401, 2723-2732.

Borm, P.J.A., Robbins, D., Haubold, S., Kuhlbusch, T., Fissan, H., Donaldson, K., Schins, R., Stone, V., Kreyling, W., Lademann, J., Krutmann, J., warheit, D., and Oberdorster, E. (2006). **The potential risks of nanomaterials: A review carried out for ECETOC.** Part. Fibre Toxicol. 3, pp. 35.

Boxall, A.B.A., Tiede, K., and Chaudry, Q. (2007). **Engineered nanoparticles in soils and water: how do they behave and could they pose a risk to human health?** Nanomedicine 2, 919-927.

Bradford, A., Handy, R.H., Readman, J.W., Atfield, A., and Mühling, M. (2009). **Impact of silver nanoparticle contamination on genetic diversity of natural bacterial assemblages in estuarine sediments.** Environ. Sci. technol. 43, 4530-4536.

Brar, S.K., and Verma, M. (2011). **Measurement of nanoparticles by light-scattering techniques.** Trends Anal. Chem. 30, 4-17.

Braydich-Stolle, L., Hussain, S., Schlager, J.J., and Hofmann, M.C. (2005). **In vitro cytotoxicity of nanoparticles in mammalian germline stem cells.** Toxicol. Sci. 88, 412-419.

Brown, B.T., and Rattigan, B.M. (1979). **Toxicity of soluble copper and other metal ions to *Elodea canadensis*.** Environ. Pollut. 20, 303-314.

Buettner, K.M., Rinciog, C.I., and Mylon, S.E. (2010). **Aggregation kinetics of cerium oxide nanoparticles in monovalent and divalent electrolytes.** Colloids Surfaces A: Physicochem. Eng. Aspects 366, 74-79.

Buffle, J., Perret, J., and Newman, J. (1992). **The use of filtration and ultrafiltration for size fractionation of aquatic particles, colloids and macromolecules.** In: Buffle, J., and van Leeuwen, H.P. (Eds.), Environmental particles I. Lewis Publishers, Chelsea, MI, USA, pp. 171-230.

Cao, J.S., and Zhang, W.X. (2006). **Stabilization of chromium ore processing residue (COPR) with nanoscale iron particles.** J. Hazard. Mater. B 132, 213–219.

Cerda, C.M. (1988). **Mobilization of quartz fines in porous media.** Clays Clay Miner. 36, 491-497.

Choi, O., Clevenger, T.E., Deng, B., Surampalli, R.Y., Ross Jr., L., and Hu, Z. (2009). **Role of sulfide and ligand strength in controlling nanosilver toxicity.** Water Res. 43, 1879-1886.

Christian, P., von der Kammer, F., Baalousha, M., and Hofmann, T. (2008). **Nanoparticles: Structure, properties, preparation and behaviour in environmental media.** Ecotoxicology 17, 326 – 343.

Chu, W.Y., Cai, S.J., Fu, Y.Y., Li, F.F., Xu, T., Qiu, H., and Xu, Q.S. (2014). **The toxicity of cerium nitrate to *Elodea canadensis*: Subcellular distribution, chemical forms and physiological effects.** Acta Physiol. Plant. 36, 2491-2499.

Clasceri, L.S., Greenberg, A.E., and Eaton, A.D. (Eds.) (1999). **SM 10200 H. Chlorophyll.** In: Standard methods for the examination of water and wastewater, 20th edition. 10200 Plankton. American Public Health Association, Washington, DC, USA, pp. 1325.

Cornelis, G., Brooke, R., McLaughlin, M.J., Kirby, J.K., Beak, D., and Chittleborough, D. (2011). **Solubility and batch retention of CeO_2 nanoparticles in soils.** Environ. Sci. Technol. 45, 2777-2782.

Cornelis, G., Doolette, C., Thomas, M., McLaughlin, M.J., Kirby, J.K., Beak, D.G., and Chittleborough, D. (2012). **Retention and dissolution of engineered silver nanoparticles in natural soils.** Soil Sci. Soc. Am. J. 76, 891-902.

Cornelis, G., Hund-Rinke, K., Kuhlbusch, T., van den Brink, N., and Nickel, C. (2014). **Fate and bioavailability of engineered nanoparticles in soils: A review.** Crit. Rev. Env. Sci. Tech. 44, 2720-2764.

Cornelis, G., Kirby, J.K., Beak, D., Chittleborough, D., and McLaughlin, M.J. (2010). **A method for determination of retention of silver and cerium oxide manufactured nanoparticles in soils.** Environ. Chem. 7, 298-308.

Cornelis, G., Pang, L., Doolette, C., Kirby, J.K., and McLaughlin, M.J. (2013). **Transport of silver nanoparticles in saturated columns of natural soils.** Sci. Total Environ. 463-464, 120-130.

Cundy, A.B., Hopkinson, L., and Whitby, R.L.D. (2008). **Use of iron-based technologies in contaminated land and groundwater remediation: A review.** Sci. Total Environ. 400, 42-51.

Dalwadi, G., Benson, H.A.E., and Chen, Y. (2005). **Comparison of diafiltration and tangential flow filtration for purification of nanoparticle suspensions.** Pharmaceut. Res. 22, 2152-2162.

Darlington, T.K., Neigh, A.M., Spencer, M.T., Nguyen, O.T., and Oldenburg, S.J. (2009). **Nanoparticle characteristics affecting environmental fate and transport through soil.** Environ. Toxicol. Chem. 28, 1191-1199.

De Saedeleer, V., Cappuyns, V., De Cooman, W., and Swennen, R. (2010). **Influence of major elements on heavy metal composition of river sediments.** Geol. Belg. 13, 257-268.

Degueldre, C., Favarger, P.-Y., and Wold, S., 2006. **Gold colloid analysis by inductively coupled plasma-mass spectrometry in a single particle mode.** Anal. Chim. Acta 555, 263-268.

Dietz, K.J., and Herth, S. (2011). **Plant nanotoxicology.** Trends. Plant. Sci. 16, 582-589.

Dokoumetzidis, A., Papadopoulou, V., Valsami, G., and Macheras, P. (2008). **Development of a reaction-limited model of dissolution: Application to official dissolution test experiments.** Int. J. Pharm. 355, 114-125.

Domingos, R.F., Baalousha, M.A., Ju-Nam, Y., Reid, M.M., Tufenkji, N., Lead, J.R., Leppard, G.G., and Wilkinson, K.J. (2009). **Characterizing manufactured nanoparticles in the environment: Multimethod determination of particle sizes.** Environ. Sci. Technol. 43, 7277-7284.

Dorney, K.M., Baker, J.D., Edwards, M.L., Kanel, S.R., O'Malley, M., and Sizemore, I.E.P. (2014). **Tangential flow filtration of colloidal silver nanoparticles: A "green" laboratory experiment for chemistry and engineering students.** J. Chem. Educ. 91, 1044-1049.

Doucet, F.J., Maguire, L., and Lead, J.R. (2004). **Size fractionation of aquatic colloids and particles by cross-flow filtration: Analysis by scanning electron and atomic force microscopy.** Anal. Chim. Acta 522, 59-71.

Du Laing, G., De Meyer, B., Meers, E., Lesage, E., Van de Moortel, A., Tack, F.M.G., and Verloo, M.G. (2008). **Metal accumulation in intertidal marshes: Role of sulphide precipitation.** Wetlands 28, 735-746.

Du Laing, G., Rinklebe, J., Vandecasteele, B., Meers, E., and Tack, F.M.G. (2009). **Trace metal behaviour in estuarine and riverine floodplain soils and sediments: A review.** Sci. Total Environ. 407, 3972-3985.

Du Laing, G., Vandecasteele, B., De Grauwe, P., Moors, W., Lesage, E., Meers, E., Tack, F.M.G., and Verloo, M.G. (2007). **Factors affecting metal concentrations in the upper sediment layer of intertidal reedbeds along the river Scheldt.** J. Environ. Monit. 9, 449-455.

Dubascoux, S., Le Hécho, I., Hassellöv, M., von der Kammer, F., Potin Gautier, M., and Lespes, G. (2010). **Field-flow fractionation and inductively coupled plasma mass spectrometry coupling: History, development and applications.** J. Anal. At. Spectrom. 25, 613-623.

Dubascoux, S., von der Kammer, F., Le Hécho, I., Potin Gautier, M., and Lespes, G. (2008). **Optimisation of asymmetrical flow field flow fractionation for environmental nanoparticles separation.** J. Chrom. A 1206, 160-165.

Dudkiewicz, A., Tiede, K., Loeschner, K., Helene, L., Jensen, S., Jensen, E., Wierzbicki, R., Boxall, A.B.A., and Molhave, K. (2011). **Characterization of nanomaterials in food by electron microscopy.** Trends Anal. Chem. 30, 28-43.

El Badawy, A.M., Luxton, T.P., Silva, R.G., Scheckel, K.G., Suidan, M.T., and Tolaymat, T.M. (2010). **Impact of environmental conditions (pH, ionic strength, and electrolyte type) on the surface charge and aggregation of silver nanoparticles suspensions.** Environ. Sci. Technol. 44, 1260-1266.

Elzey, S., and Grassian, V.H. (2010a). **Agglomeration, isolation and dissolution of commercially manufactured silver nanoparticles in aqueous environments.** J. Nanopart. Res. 12, 1945-1958.

Elzey, S., and Grassian, V.H. (2010b). **Nanoparticle dissolution from particle perspective: Insights from particle sizing measurements.** Langmuir 26, 12505-12508.

Fabrega, J., Fawcett, S.R., Renshaw, J.C., and Lead, J.R. (2009). **Silver nanoparticle impact on bacterial growth: Effect of pH, concentration, and organic matter.** Environ. Sci. Technol. 43, 7285-7290.

Fabrega, J., Luoma, S.N., Tyler, C.R., Galloway, T.S., and Lead, J.R. (2011). **Silver nanoparticles: Behaviour and effects in the aquatic environment.** Environ. Int. 37, 517-531.

Fall, M., Guerbet, M., Park, B., Gouriou, F., Dionnet, F., and Morin, J.P. (2007). **Evaluation of cerium oxide and cerium oxide based fuel additive safety on organotypic cultures of lung slices.** Nanotoxicology 1, 227-234.

Fang, J., Shan, X.-q., Wen, B., Lin, J.-m., and Owens, G. (2009). **Stability of Titania nanoparticles in soil suspensions and transport in saturated homogeneous soil columns.** Environ. Pollut. 157, 1101-1109.

Fang, J., Shan, X.-q., Wen, B., Lin, J.-m., Owens, G., and Zhou, S.-r. (2011). **Transport of copper as affected by Titania nanoparticles in soil columns.** Environ. Pollut. 159, 1248-1256.

Farré, M., Sanchís, J., and Barceló, D. (2011). **Analysis and assessment of the occurrence, the fate and the behavior of nanomaterials in the environment.** Trends Anal. Chem. 30, 517-527.

Fedotov, P.S., Vanifatova, N.G., Shkinev, V.M., and Spivakov, B.Y. (2011). **Fractionation and characterization of nano- and microparticles in liquid media.** Anal. Bioanl. Chem. 400, 1787-1804.

Ferreira da Silva, B., Pérez, S., Gardinalli, P., Singhal, R.K., Mozeto, A.A., and Barceló, D. (2011). **Analytical chemistry of metallic nanoparticles in natural environments.** Trends Anal. Chem. 30, 528-540.

Feynman, R.P. (1960). **There's plenty of room at the bottom.** Caltech Engineering and Science 23, 22-36.

Filella, M., Zhang, J., Newman, M.E., and Buffle, J. (1997). **Analytical applications of photon correlation spectroscopy for size distribution measurements of natural colloidal suspensions: Capabilities and limitations.** Colloids Surf. A 120, 27-46.

Filipponi, L., and Sutherland, D. (2013). **Nanotechnologies: Principles, applications, implications, and hands-on activities.** A compendium for educators, EUR 24957, Directorate-General for Research and Innovation Industrial Technologies (NMP) programme, European Commission, Brussels, Belgium, pp. 416. *Available from http://ec.europa.eu/research/industrial_technologies/pdf/nano-hands-on-activities_en.pdf (Accessed on September 5, 2014)*

Foerter-Barth, U., and Teipel, U. (2000). **Characterization of particles by means of laser light diffraction and dynamic light scattering.** In: Massacci, P. (Ed.), Proceedings of the XXI International Mineral Processing Congress. Developments in Mineral Processing 13, C1:1-C1:8.

Franklin, N.M., Rogers, N.J., Apte, S.C., Batley, G.E., Gadd. G.E., and Casey, P.S. (2007). **Comparative toxicity of nanoparticulate ZnO, bulk ZnO, and ZnCl2 to a freshwater microalga (*Pseudokirchneriella subcapitata*): The importance of particle solubility.** Environ. Sci. Technol. 41, 8484-8490.

French, R.A., Jacobsen, A.R., Kim, B., Isley, S.L., Penn, R.L., and Baveye, P.C. (2009). **Influence of ionic strength, pH, and cation valence on aggregation kinetics of titanium dioxide nanoparticles.** Environ. Sci. Technol. 43, 1354-1359.

Fritioff, Å., and Greger, M. (2007). **Fate of cadmium in *Elodea canadensis*.** Chemosphere 67, 265-375.

Frohne, T., Rinklebe, J., and Diaz-Bone, R.A. (2014). **Contamination of floodplain soils along the Wupper river, Germany, with As, Co, Cu, Ni, Sb, and Zn and the impact of pre-definite redox variations on the mobility of these elements.** Soil Sediment Contam. 23, 779-799.

Frohne, T., Rinklebe, J., Diaz-Bone, R. A., and Du Laing, G. (2011). **Controlled variation of redox conditions in a floodplain soil: Impact on metal mobilization and biomethylation of arsenic and antimony.** Geoderma, 160, 414-424.

Frohne, T., Rinklebe, J., Langer, U., Du Laing, G., Mothes, S., and Wennrich, R. (2012). **Biogeochemical factors affecting mercury methylation rate in two contaminated floodplain soils.** Biogeosciences 9, 493-507.

Gaiser, B., Fernandes, T., Jepson, M., Lead, J.R., Tyler, C.R., and Stone, V. (2009). **Assessing exposure, uptake and toxicity of silver and cerium dioxide nanoparticles from contaminated environments.** Environ. Health 8(Suppl 1):S2, pp. 4.

Gallego-Urrea, J.A., Tuoriniemi, J., and Hassellöv, M. (2011). **Applications of particle-tracking analysis to the determination of size distributions and concentrations of nanoparticles in environmental, biological and food samples.** Trends Anal. Chem. 30, 473-483.

Gardner, M., and Comber, S. (1997). **Sample filtration as a source of error in the determination of trace metals in marine waters.** Analyst 122, 1029-1032.

Gee, G.W., and Bauder, J.W. (1986). **Particle size analysis.** In: Klute, A.L. (Ed.), Methods of soil analysis, Part 1, Physical and mineral methods. Second edition. Agronomy Monograph 9, American Society of Agronomy, Madison, WI, USA, pp. 383-411.

Geranio, L., Heuberger, M., and Nowack, B. (2009). **The behavior of silver nanotextiles during washing.** Environ. Sci. Technol. 43, 8113-8118.

Ghosh, S., Mashayekhi, H., Pan, B., Bhowmik, P., and Xing, B. (2008). **Colloidal behavior of aluminum oxide nanoparticles as affected by pH and natural organic matter.** Langmuir 24, 12385-12391.

Giddings, J.C. (1993). **Field-flow fractionation: Analysis of macromolecular, colloidal, and particulate materials.** Science 260, 1456-1465.

Giddings, J.C., Yang, F.J., and Myers, M.N. (1976). **Flow field-flow fractionation – Versatile new separation method.** Science 193, 1244-1245.

Gimbert, L.J., Hamon, R.E., Casey, P.S., and Worsfold, P.J. (2007). **Partitioning and stability of engineered ZnO nanoparticles in soil suspensions using field-flow fractionation.** Environ. Chem. 4, 8-10.

Glenn, J.B., and Klaine, S.J. (2013). **Abiotic and biotic factors that influence the bioavailability of gold nanoparticles to aquatic macrophytes.** Environ. Sci. Technol. 47, 10223-10230.

Glenn, J.B., White, S.A., and Klaine, S.J. (2012). **Interactions of gold nanoparticles with freshwater aquatic macrophytes are size and species dependent.** Environ. Toxicol. Chem. 31, 194-201.

Gong, Y., Liu, Y., Xiong, Z., Kaback, D., and Zhao, D. (2012). **Immobilization of mercury in field soil and sediment using carboxymethyl cellulose stabilized iron sulfide nanoparticles.** Nanotechnology 23, 294007, pp. 13.

Gottschalk, F., and Nowack, B. (2011). **The release of engineered nanomaterials to the environment.** J. Environ. Monit. 13, 1145-1155.

Gottschalk, F., Kost, E., and Nowack, B. (2013). **Engineered nanomaterials in water and soils: A risk quantification based on probabilistic exposure and effect modeling.** Environ. Toxicol. Chem. 32, 1278-1287.

Gottschalk, F., Sonderer, T., Scholz, R.W., and Nowack, B. (2009). **Modeled environmental concentrations of engineered nanomaterials (TiO_2, ZnO, Ag, CNT, Fullerenes) for different regions.** Environ. Sci. Technol. 43, 9216-9222.

Gray, E.P., Bruton, T.A., Higgins, C.P., Halden, R.U., Westerhoff, P., and Ranville, J.F. (2012). **Analysis of gold nanoparticle mixtures: A comparison of hydrodynamic chromatography (HDC) and asymmetrical flow field-flow fractionation (AF4) coupled to ICP-MS.** J. Anal. At. Spectrom. 27, 1532-1539.

Grieger, K.D., Fjordbøge, A., Hartmann, N.B., Eriksson, E., Bjerg, P.L., and Baun, A. (2010). **Environmental benefits and risks of zero-valent iron nanoparticles (nZVI) for *in situ* remediation: Risk mitigation or trade-off?** J. Contam. Hydrol. 118, 165-183.

Griffitt, R.J., Luo, J., Gao, J., Bonzongo, J.C., Barber, D.S. (2008). **Effects of particle composition and species on toxicity of metallic nanomaterials in aquatic organisms.** Environ. Toxicol. chem. 27, 1972-1978.

Gubbins, E.J., Batty, L.C., and Lead, J.R. (2011). **Phytotoxicity of silver nanoparticles to *Lemna minor* L.** Environ. Pollut. 159, 1551-1559.

Guo, L.D., and Santschi, P.H. (2007). **Ultrafiltration and its applications to sampling and characterisation of aquatic colloids.** In: Wilkinson, K.J., and Lead, J.R. (Eds.), Environmental Colloids and Particles, Behaviour, Separation and Characterisation. John Wiley & Sons, Ltd., Chichester, UK, pp. 159-222.

Hammes, J., Gallego-Urrea, J.A., and Hassellöv, M. (2013). **Geographically distributed classification of surface water chemical parameters influencing fate and behavior of nanoparticles and colloid facilitated contaminant transport.** Water Res. 47, 5350-5361.

Handy, R.D., Owen, R., and Valsami-Jones, E. (2008a). **The ecotoxicology of nanoparticles and nanomaterials: Current status, knowledge gaps, challenges, and future needs.** Ecotoxicology 17, 315-325.

Handy, R.D., von der Kammer, F., Lead, J.R., Hassellöv, M., Owen, R., and Crane, M. (2008b). **The ecotoxicology and chemistry of manufactured nanoparticles.** Ecotoxicology 17, 287-314.

Hansen, S.F., Maynard, A., Baun, A., and Tickner, J.A. (2008). **Late lessons from early warnings for nanotechnology.** Nat. Nanotechnol. 3, 444-447.

Hassellöv, M., Readman, J.W., Ranville, J.F., and Tiede, K. (2008). **Nanoparticle analysis and characterization methodologies in environmental risk assessment of engineered nanoparticles.** Ecotoxicology 17, 344-361.

He, F., and Zhao, D. (2007). **Manipulating the size and dispersibility of zerovalent iron nanoparticles by use of carboxymethyl cellulose stabilizers.** Environ. Sci. Technol. 41, 6216-6221.

He, F., Zhang, M., Qian, T., and Zhao, D. (2009). **Transport of carboxymethyl cellulose stabilized iron nanoparticles in porous media: Column experiments and modeling.** J. Colloid Interf. Sci. 334, 96-102.

He, F., Zhao, D., Liu, J.C., and Roberts, C.B. (2007). **Stabilization of Fe-Pd nanoparticles with sodium carboxymethyl cellulose for enhanced transport and dechlorination of trichloroethylene in soil and groundwater.** Ind. Eng. Chem. Res. 46, 29-34.

Hedberg, Y., Herting, G., and Wallinder, I.O. (2011). **Risks of using membrane filtration for trace metal analysis and assessing the dissolved metal fraction of aqueous media – A study on zinc, copper and nickel.** Environ. Pollut. 159, 1144-1150.

Helfrich, A., and Bettmer, J. (2011). **Analysis of gold nanoparticles using ICP-MS-based hyphenated and complementary ESI-MS techniques.** Int. J. Mass Spectrom. 307, 92-98.

Helfrich, A., Brüchert, W., and Bettmer, J. (2006). **Size characterisation of Au nanoparticles by ICP-MS coupling techniques.** J. Anal. At. Spectrom. 21, 431-434.

Hotze, E.M., Phenrat, T., and Lowry, G.V. (2010). **Nanoparticle aggregation: Challenges to understanding transport and reactivity in the environment.** J. Environ. Qual. 39, 1909-1924.

Hou, D., He, J., Lü, C., Ren, L., Fan, Q., Wang, J., and Xie, Z. (2013). **Distribution characteristics and potential ecological risk assessment of heavy metals (Cu, Pb, Zn, Cd) in water and sediments from lake Dalinouer, China.** Ecotox. Environ. Safe. 93, 135-144.

Houba, V.J.G., Temminghoff, E.J.M., Gaikhorst, G.A., and Vark, W. (2000). **Soil analysis procedures using 0.01 M calcium chloride as extraction reagent.** Commun. Soil Sci. Plant Anal. 31, 1299-1396.

Hua, M., Zhang, S., Pan, B., Zhang, W., Lu, L., and Zhang, Q. (2012). **Heavy metal removal from water/wastewater by nanosized metal oxides: A review.** J, Hazard. Mater. 211-212, 317-331.

Huang, Y.-T., Hseu, Z.-Y., and His, H.-C. (2011). **Influences of thermal decontamination on mercury removal, soil properties, and repartitioning of coexisting heavy metals.** Chemosphere 84, 1244-1249.

Hwang, E.T., Lee, J.H., Chae, Y.J., Kim, Y.S., Kim, B.C., Sang, B.I., and Gu, M.B. (2008). **Analysis of the toxic mode of action of silver nanoparticles using stress-specific bioluminescent bacteria.** Small 4, 746-750.

Isaacson, C.W., and Bouchard, D. (2010). **Asymmetric flow field flow fractionation of aqueous C60 nanoparticles with size determination by dynamic light scattering and quantification by liquid chromatography atmospheric pressure photo-ionization mass spectrometry.** J. Chrom. A 1217, 1506-1512.

ISO 22412:2008. **Particle size analysis -- Dynamic light scattering (DLS).** International Organisation for Standardization (ISO), Geneva, Switzerland, pp. 17.

Jacob, D.L., Borchardt, J.D., Navaratnam, L., Otte, M.L., and Bezbaruah, A.N. (2013). **Uptake and translocation of Ti from nanoparticles in crops and wetland plants.** Int. J. Phytoremediat. 15, 142-153.

Jeong, S.-W., and Kim, H. (2014). **Filtration of fullerene and copper oxide nanoparticles using surface-modified microfilters.** Environ. Monit. Assess. 186, 5855-5864.

Jiang, H.-S., Li, M., Chang, F.-Y., Li, W., and Yin, L.-Y. (2012). **Physiological analysis of silver nanoparticles and $AgNO_3$ toxicity to *Spirodela polyrhiza*.** Environ. Toxicol. Chem. 31, 1880-1886.

Jiang, H.-S., Qiu, X.-N., Li, G.B., Li, W., and Yin, L.-Y. (2014). **Silver nanoparticles induced accumulation of reactive oxygen species and alteration of antioxidant systems in the aquatic plant *Spirodela polyrhiza*.** Environ. Toxicol. Chem. 33, 1398-1405.

Jiang, X., Tong, M., Li., H., and Yang, K. (2010). **Deposition kinetics of zinc oxide nanoparticles on natural organic matter coated surfaces.** J. Colloid Interf. Sci. 350, 427-434.

Johnson, M.E., Ostroumov, S.A., Tyson, J.F., and Xing, B. (2011). **Study of the interactions between *Elodea canadensis* and CuO nanoparticles.** Russ. J. Gen. Chem. 81, 2688-2693.

Johnson, R.L., Johnson, G.O'B., Nurmi, J.T., and Tratnyek, P.G. (2009). **Natural organic matter enhanced mobility of nano zerovalent iron.** Environ. Sci. Technol. 43, 5455-5460.

Joner, E.J., Hartnik, T., and Amundsen, C.E. (2008). **Environmental fate and ecotoxicity of engineerend nanoparticles.** Norwegian Pollution Control Authority, Report no. TA 2304/2007, Bioforsk, Ås, pp. 64.

Jones, D.L., and Willet, V.B. (2006). **Experimental evaluation of methods to quantify dissolved organic nitrogen (DON) and dissolved organic carbon (DOC) in soil.** Soil Biol. Biochem. 38, 991-999.

Jośko, I., and Oleszczuk, P. (2013). **Manufactured nanomaterials: The connection between environmental fate and toxicity.** Crit. Rev. Environ. Sci. Technol. 43, 2581-2616.

Ju-Nam, Y., and Lead, J.R. (2008). **Manufactured nanoparticles: An overview of their chemistry, interactions and potential environmental implications.** Sci. Total Environ. 400, 396-414.

Juhel, G., Batisse, E., Hugues, Q., Daly, D., van Pelt, F.N.A.M., O'Halloran, J., and Jansen, M.A.K. (2011). **Alumina nanoparticles enhance growth of *Lemna minor*.** Aquat. Toxicol. 105, 328-336.

Kaegi, R., Sinnet, B., Zuleeg, S., Hagendorfer, H., Mueller, E., Vonbank, R., Boller, M., and Burkhardt, M. (2010). **Release of silver nanoparticles from outdoor facades.** Environ. Pollut. 158, 2900-2905.

Kaegi, R., Ulrich, A., Sinnet, B., Vonbank, R., Wichser, A., Zuleeg, S., Simmler, H., Brunner, S., Vonmont, H., Burkhardt, M., and Boller, M. (2008a). **Synthetic TiO_2 nanoparticle emission from exterior facades into the aquatic environment.** Environ. Pollut. 156, 233-239.

Kaegi, R., Voegelin, A., Ort, C., Sinnet, B., Thalmann, B., Krismer, J., Hagendorfer, H., Elumelu, M., and Mueller, E. (2013). **Fate and transformation of silver nanoparticles in urban wastewater systems.** Water Res. 47, 3866-3877.

Kaegi, R., Wagner, T., Hetzer, B., Sinnet, B., Tzvetkov, G., and Boller, M. (2008b). **Size, number and chemical composition of nanosized particles in drinking water determined by analytical microscopy and LIBD.** Water Res. 42, 2778-2786.

Kähkönen, M.A., Pantsar-Kallio, M., and Manninen, P.K.G. (1997). **Analysing heavy metal concentrations in the different parts of *Elodea canadensis* and surface sediment with PCA in two boreal lakes in southern Finland.** Chemosphere 35, 2645-2656.

Kanel, S.R., and Al-Abed, S.R. (2011). **Influence of pH on transport of nanoscale zinc oxide in saturated porous media.** J. Nanopart. Res. 13, 4035-4047.

Kanel, S.R., Greneche, J.M., and Choi, H. (2006). **Arsenic(V) removal from groundwater using nano scale zero-valent iron as a colloidal reactive barrier material.** Environ. Sci. Technol. 40, 2045-2050.

Kanel, S.R., Manning, B., Charlet, L., and Choi, H. (2005). **Removal of arsenic(III) from groundwater by nanoscale zero-valent iron.** Environ. Sci. Technol. 39, 1291-1298.

Karakoti, A.S., Munusamy, P., Hostetler, K., Kodali, V., Kuchibhatla, S., Orr, G., Pounds, J.G., Teeguarden, J.G., Thrall, B.D., and Baer, D.R. (2012). **Preparation and characterization challenges to understanding environmental and biological impacts of ceria nanoparticles.** Surf. Interface Anal. 44, 882-889.

Karlsson, H.L., Cronholm, P., Gustafsson, J., and Möller, L. (2008). **Copper oxide nanoparticles are highly toxic: A comparison between metal oxide nanoparticles and carbon nanotubes.** Chem. Res. Toxicol. 21, 1726-1732.

Karn, B., Kuiken, T., and Otto, M. (2009). **Nanotehcnology and *in situ* remediation: A review of the benefits and potential risks.** Environ. Health Perspect. 117, 1823-1831.

Keller, A.A., Wang, G., Zhou, D., Lenihan, H.S., Cherr, G., Cardinale, B.J., Miller, R., and Ji, Z. (2010). **Stability and aggregation of metal oxide nanoparticles in natural aqueous matrices.** Environ. Sci. Technol. 44, 1962-1967.

Kim, B., Park, C.-S., Murayama, M., and Hochella Jr., M.F. (2010). **Discovery and characterization of silver sulfide nanoparticles in final sewage sludge products.** Environ. Sci. Technol. 44, 7509-7514.

Kim, E., Kim, S.H., Kim, H.C., Lee, S.G., Lee, S.J., and Jeong, S.W. (2011). **Growth inhibition of aquatic plant caused by silver and titanium oxide nanoparticles.** J. Toxicol. Environ. Health Sci. 3, 1-6.

Kim, J., and Lawler, D.F. (2005). **Characteristics of zeta potential distribution in silica particles.** Bull. Korean Chem. Soc. 26, 1083-1089.

Kim, J., and Song, K.-B. (2007). **Recent progress of nano-technology with NSOM**. Micron 38, 409-426.

Kiser, M.A., Westerhoff, P., Benn, T., Wang, Y., Pérez-Rivera, J., and Hristovski, K. (2009). **Titanium nanomaterial removal and release from wastewater treatment plants.** Environ. Sci. Technol. 43, 6757-6763.

Kittler, S., Greulich, C., Diendorf, J., Köller, M., and Epple, M. (2010). **Toxicity of silver nanoparticles increases during storage because of slow dissolution under release of silver ions.** Chem. Mater. 22, 4548-4554.

Klaine, S.J., Alvarez, P.J.J., Batley, G.E., Fernandes, T.F., Handy, R.D., Lyon, D.Y., Mahendra, S., McLaughlin, M.J., and Lead, J.R. (2008). **Nanomaterials in the environment: Behavior, fate, bioavailability, and effects.** Environ. Toxicol. Chem. 27, 1825-1851.

Klaine, S.J., Koelmans, A.A., Horne, N., Carley, S., Handy, R.D., Kaputska, L., Nowack, B., and von der Kammer, F. (2012). **Paradigms to assess the environmental impact of manufactured nanomaterials.** Environ. Toxicol. Chem. 31, 3-14.

Kostal, J., Prabhukumar, G., Lao, U.L., Chen, A., Matsumoto, M., Mulchandani, A., and Chen, W. (2005). **Customizable biopolymers for heavy metal remediation.** J. Nanopart. Res. 7, 517-523.

Krueger, K.M., Al-Somali, A.M., Falkner, J.C., and Colvin, V.L. (2005). **Characterization of nanocrystalline CdSe by size exclusion chromatography.** Anal. Chem. 77, 3511-3515.

Ladner, D.A., Steele, M., Weir, A., Hristovski, K., and Westerhoff, P. (2012). **Functionalized nanoparticle interactions with polymeric membranes.** J. Hazard. Mater. 211-212, 288-295.

Lane, N., and Kalil, T. (2005). **The National Nanotechnology Initiative: Present at the creation.** Issues Sci. Technol. 21, 49-54.

Larras, F., Regier, N., Planchon, S., Poté, J., Renaut, J., and Cosio, C. (2013). **Physiological and proteomic changes suggest an important role of cell walls in the high tolerance to metals of *Elodea nuttallii*.** J. Hazard. Mater. 263, 575-583.

Lead, J.R., and Wilkinson, K.J. (2006). **Aquatic colloids and nanoparticles: Current knowledge and future trends.** Environ. Chem. 3, 159-171.

Lead, J.R., Wilkinson, K.J., Starchev, K., Canonica, S., and Buffle, J. (2000). **Determination of diffusion coefficients of humic substances by fluorescence correlation spectroscopy: Role of solution conditions.** Environ. Sci. Technol. 34, 1365-1369.

Ledin, A., Karlsson, S., Düker, A., and Allard, B. (1994). **Measurements *in situ* of concentration and size distribution of colloidal matter in deep groundwaters by photon correlation spectroscopy.** Water Res. 28, 1539-1545.

Lee, S.W., Kim, S.M., and Choi, J. (2009). **Genotoxicity and ecotoxicity assays using the freshwater crustacean Daphnia magna and the larva of the aquatic midge *Chironomus riparius* to screen the ecological risks of nanoparticle exposure.** Environ. Toxicol. Pharmacol. 28, 86-91.

Lespes, G., and Gigault, J. (2011). **Hyphenated analytical techniques for multidimensional characterisation of submicron particles: A review.** Analyt. Chim. Acta 692, 26-41.

Levard, C., Hotze, E.M., Colman, B.P., Dale, A.L., Truong, L., Yang, X.Y., Bone, A.J., Brown Jr., G.E., Tanguay, R.L., Di Giulio, R.T., Bernhardt, E.S., Meyer, J.N., Wiesner, M.R., and Lowry, G.V. (2013). **Sulfidation of silver nanoparticles: Natural antidote to their toxicity.** Environ. Sci. Technol. 47, 13440-13448.

Levard, C., Hotze, E.M., Lowry, G.V., and Brown Jr., G.E. (2012). **Environmental transformations of silver nanoparticles: Impact on stability and toxicity.** Environ. Sci. Technol. 46, 6900-6914.

Lewis, A.E. (2010). **Review of metal sulphide precipitation.** Hydrometallurgy 104, 222-234.

Li, X., Lenhart, J.J., and Walker, H.W. (2010). **Dissolution-accompanied aggregation kinetics of silver nanoparticles.** Langmuir 26, 16690-16698.

Li, X.Q., and Zhang, W.X. (2006). **Iron nanoparticles: The core-shell structure and unique properties for Ni(II) sequestration.** Langmuir 22, 4638-4642.

Li, X.Q., and Zhang, W.X. (2007). **Sequestration of metal cations with zerovalent iron nanoparticles – A study with high resolution x-ray photoelectron spectroscopy (HR-XPS).** J. Phys. Chem. C 111, 6939-6946.

Li, Y., Niu, J., Shang, E., and Crittenden, J. (2014). **Physicochemical transformations and photoinduced toxicity reduction of silver nanoparticles in the presence of perfluorocarboxylic acids under UV irradiation.** Environ. Sci. Technol. 48, 4946-4953.

Li, Z., Sahle-Demessie, E., Hassan, A.A., and Sorial, G.A. (2011). **Transport and deposition of CeO_2 nanoparticles in water-saturated porous media.** Water Res. 45, 4409-4418.

Liang, Y., Bradford, S.A., Simunek, J., Heggen, M., Vereecken, H., and Klumpp, E. (2013b). **Retention and remobilization of stabilized silver nanoparticles in an undisturbed loamy sand soil.** Environ. Sci. Technol. 47, 12229-12237.

Liang, Y., Bradford, S.A., Simunek, J., Vereecken, H., and Klumpp, E. (2013a). **Sensitivity of the transport and retention of stabilized silver nanoparticles to physicochemical factors.** Water Res. 47, 2572-2582.

Limbach, L.K., Bereiter, R., Müller, E., Krebs, R., Gälli, R., and Stark, W.J. (2008). **Removal of oxide nanoparticles in a model wastewater treatment plant: Influence of agglomeration and surfactants on clearing efficiency.** Environ. Sci. Technol. 42, 5828-5833.

Lin, D., and Xing, B. (2008). **Root uptake and toxicity of ZnO nanoparticles.** Environ. Sci. Technol. 42, 5580-5585.

Lin, D., Tian, X., Wu, F., and Xing, B., 2010. **Fate and transport of engineered nanomaterials in the environment.** J. Environ. Qual. 39, 1896-1908.

Liu, F.-K., Ko, F.-H., Huang, P.-W., Wu, C.-H., and Chu, T.-C. (2005). **Studying the size/shape separation and optical properties of silver nanoparticles by capillary electrophoresis.** J. Chrom. A 1062, 139-145.

Liu, J., and Hurt, R.H. (2010). **Ion release kinetics and particle persistence in aqueous nano-silver colloids.** Environ. Sci. Technol. 44, 2169-2175.

Liu, J., Aruguete, D.M., Murayama, M., and Hochella Jr., M.F. (2009). **Influence of size and aggregation on the reactivity of an environmentally and industrially relevant nanomaterial (PbS).** Environ. Sci. Technol. 43, 8178-8183.

Liu, J., Pennell, K.G., and Hurt, R.H. (2011). **Kinetics and mechanisms of nanosilver oxysulfidation.** Environ. Sci. Technol. 45, 7345-7353.

Liu, R., and Lal, R. (2012). **Nanoenhanced materials for reclamation of mine lands and other degraded soils: A review.** J. Nanotechnol. 2012, 461468, pp. 18.

Liu, R., and Lead, J.R. (2006). **Partial validation of cross flow ultrafiltration by atomic force microscopy.** Anal. Chem. 78, 8105-8112.

Liu, R., Lead, J.R., and Baker, A. (2007). **Fluorescence characterization of cross flow ultrafiltration derived freshwater colloidal and dissolved organic matter.** Chemosphere 68, 1304-1311.

Liu, W., Sun, W., Borthwick, A.G.L., and Ni, J. (2013). **Comparison on aggregation and sedimentation of titanium dioxide, titanate nanotubes and titanate nanotubes-TiO_2: Influence of pH, ionic strength and natural organic matter.** Colloids Surfaces A: Physicochem. Eng. Aspects 434, 319-328.

Liu, X., Chen, G., and Su, C. (2012). **Influence of collector surface composition and water chemistry on the deposition of cerium dioxide nanoparticles: QCM-D and column experiment approaches.** Environ. Sci. Technol. 46, 6681-6688.

Liu, X., Wazne, M., Chou, T., Xiao, R., and Xu, S. (2011). **Influence of Ca^{2+} and Suwannee River Humic Acid on aggregation of silicon nanoparticles in aqueous media.** Water Res. 45, 105-112.

Liu, Y., Tourbin, M., Lachaize, S., and Guiraud, P. (2014). **Nanoparticles in wastewaters: Hazards, fate and remediation.** Powder Technol. 255, 149-156.

Lohwacharin, J., and Takizawa, S. (2009). **Effects of nanoparticles on the ultrafiltration of surface water.** J. Membrane Sci. 326, 354-362.

Lombi, E., Donner, E., Taheri, S., Tavakkoli, E., Jaemting, A.K., McClure, S., Naidu, R., Miller, B.W., Scheckel, K.G., and Vasilev, K. (2013). **Transformation of four silver/silver chloride nanoparticles during anaerobic treatment of wastewater and post-processing of sewage sludge.** Environ. Pollut. 176, 193-197.

Lovern, S.B., and Klaper, R. (2006). ***Daphnia magna* mortality when exposed to titanium dioxide and fullerene (C_{60}) nanoparticles.** Environ. Toxicol. Chem. 25, 1132-1137.

Lowry, G.V., and Casman, E.A. (2009). **Nanomaterial transport, transformation, and fate in the environment. A risk based perspective on research needs.** In: Linkov, I., and Steevens, J. (Eds.), Nanomaterials: Risks and Benefits. Springer Science + Business media B.V., GX Dordrecht, The Netherlands, pp. 125-137.

Lowry, G.V., Espinasse, B.P., Badireddy, A.R., Richardson, C.J., Reinsch, B.C., Bryant, L.D., Bone, A.J., Deonarine, A., Chae, S., Therezien, M., Colman, B.P., Hsu-Kim, H., Bernhardt, E.S., Matson, C.W., and

Wiesner, M.R. (2012). **Long-term transformation and fate of manufactured Ag nanoparticles in a simulated large scale freshwater emergent wetland.** Environ. Sci. Technol. 46, 7027-7036.

Lowry, G.V., Hotze, E.M., Bernhardt, E.S., Dionysiou, D.D., Pedersen, J.A., Wiesner, M.R., and Xing, B. (2010). **Environmental occurrences, behavior, fate, and ecological effects of nanomaterials: An introduction to the special series.** J. Environ. Qual. 39, 1867-1874.

Ma, J.W., Lu, X.Y., and Huang, Y. (2011). **Genomic analysis of cytotoxicity response to nanosilver in human dermal fibroblasts.** J. Biomed. Nanotechnol. 7, 263-275.

Ma, R., Levard, C., Michel, F.M., Brown Jr., G.E., and Lowry, G.V. (2013). **Sulfidation mechanisms for zinc oxide nanoparticles and the effect of sulfidation on their solubility.** Environ. Sci. Technol. 47, 2527-2534.

Ma, R., Stegemeier, J., Levard, C., Dale, J.G., Noack, C.W., Yang, T., Brown Jr., G.E., and Lowry, G.V. (in press). **Sulfidation of copper oxide nanoparticles and properties of resulting copper sulfide.** Environ. Sci.: Nano, *DOI: 10.1039/c4en00018h*

Ma, X., Geiser-Lee, J., Deng, Y., and Kolmakov, A. (2010). **Interactions between engineered nanoparticles (ENPs) and plants: Phytotoxicity, uptake and accumulation.** Sci. Total Environ. 408, 3053-3061.

Mallampati, S.R., Mitoma, Y., Okuda, T., Sakita, S., and Kakeda, M. (2013). **Total immobilization of soil heavy metals with nano-Fe/Ca/CaO dispersion mixtures.** Environ. Chem. Lett. 11, 119-125.

Malloy, A. (2011). **Count, size and visualize nanoparticles.** Mater. Today 14, 170-173.

Masui, T., Yamamoto, M., Sakata, T., Mori, H., and Adachi, G.Y. (2000). **Synthesis of BN-coated CeO_2 fine powder as new UV blocking material.** J. Mater. Chem. 10, 353-357.

Mavrocordatos, D., Pronk, W., and Boller, M. (2004). **Analysis of environmental particles by atomic force microscopy, scanning and transmission electron microscopy.** Water Sci. Technol., 50, 9-18.

Maynard, A.D. (2006). **Nanotechnology: A research strategy for addressing risk.** Report for The Project on Emerging Nanotechnologies, Woodrow Wilson International Center for Scholars, Washington DC, USA, pp. 45. *Available from http://www.nanotechproject.org/publications/page5 (Accessed on August 22, 2014)*

Maynard, A.D., and Michelson, E. (2007). **The nanotechnology consumer products inventory.** Project on Emerging Nanotechnologies, Woodrow Wilson International Center for Scholars, Washington, DC, USA. *Available from http://www.nanotechproject.org (Accessed on January 15, 2014)*

Maynard, D., Aitken, R.J., Butz, T., Colvin, V., Donaldson, K., Oberdörster, G., Philbert, M.A., Ryan, J., Seaton, A., Stone, V., Tinkle, S.S., Tran, L., Walker, N.J., and Warheit, D.B. (2006). **Safe handling of nanotechnology.** Nature 444, 267-269.

Meers, E., Du Laing, G., Unamuno, V.G., Lesage, E., Tack, F.M.G., and Verloo, M.G. (2006). **Water extractability of trace metals from soils: some pitfalls.** Water Air Soil Pollut. 176, 21-35.

Mihajlovic, J., Giani, L., Stärk, H.-J., and Rinklebe, J. (2014). **Concentrations and geochemical fractions of rare earth elements in two different marsh soil profiles at the North Sea, Germany.** J. Soils Sediments 14, 1417-1433.

Miralles, P., Church, T.L., and Harris, A.T. (2012). **Toxicity, uptake, and translocation of engineered nanomaterials in vascular plants.** Environ. Sci. Technol. 46, 9224-9239.

Mitrano, D.M., Barber, A., Bednar, A., Westerhoff, P., Higgins, C.P., and Ranville, J.F. (2012). **Silver nanoparticle characterization using single particle ICP-MS (SP-ICP-MS) and asymmetrical flow field flow fractionation ICP-MS (AF4-ICP-MS).** J. Anal. At. Spectrom. 27, 1131-1142.

Monica, R.C., and Cremonini, R. (2009). **Nanoparticles and higher plants.** Caryologia 62, 161-165.

Morrison, M.A., and Benoit, G. (2001). **Filtration artifacts caused by overloading membrane filters.** Environ. Sci. Technol. 35, 3774-3779.

Morrisson, A.R., Park, J.S., and Sharp, B.L. (1990). **Application of high-performance size-exclusion liquid chromatography to the study of copper speciation in waters extracted from sewage sludge treated soils.** Analyst 115, 1429-1433.

Mudunkotuwa, I.A., and Grassian, V.H. (2011). **The devil is in the details (or the surface): Impact of surface structure and surface energetics on understanding the behavior of nanomaterials in the environment.** J. Environ. Monit. 13, 1135-1144.

Murr, L.E., Esquivel, E.V., Bang, J.J., de la Rosa, G., and Gardea-Torresdey, J.L. (2004). **Chemistry and nanoparticulate compositions of a 10,000 year-old ice core melt water.** Water Res. 38, 4282-4296.

Narr, J., Viraraghavan, T., and Jin, Y.-C. (2007). **Applications of nanotechnology in water/wastewater treatment: A review.** Fresen. Environ. Bull. 16, 320-329.

Navarro, D.A., Kirby, J.K., McLaughlin, M.J., Waddington, L., and Kookana, R.S. (2014). **Remobilisation of silver and silver sulphide nanoparticles in soils.** Environ. Pollut. 193, 102-110.

Navarro, E., Baun, A., Behra, R., Hartmann, N.B., Filser, J., Miao, A.J., Quigg, A., Santschi, P.H., and Sigg, L. (2008a). **Environmental behavior and ecotoxicity of engineered nanoparticles to algae, plants, and fungi.** Ecotoxicology 17, 372-386.

Navarro, E., Piccapietra, F., Wagner, B., Marconi, F., Kaegi, R., Odzak, N., Sigg, L., and Behra, R. (2008b). **Toxicity of silver nanoparticles to *Chlamydomonas reinhardtii*.** Environ. Sci. Technol. 42, 8959-8964.

Nel, A., Xia, T., Mädler, L., and Li, N. (2006). **Toxic potential of materials at the nanolevel.** Science 311, 622-627.

NNI (n.d.). **Nanotechnology 101**. The US National Nanotechnology Initiative, Arlington, VA, USA. *Available from http://www.nano.gov/nanotech-101 (Accessed on August 8, 2014)*

Nowack, B., and Bucheli, T.D. (2007). **Occurrence, behavior and effects of nanoparticles in the environment.** Environ. Pollut. 150, 5-22.

Nowack, B., Ranville, J.F., Diamond, S., Gallego-Urrea, J.A., Metcalfe, C., Rose, J., Horne, N., Koelmans, A.A., and Klaine, S.J. (2012). **Potential scenarios for nanomaterial release and subsequent alteration in the environment.** Environ. Toxicol. Chem. 31, 50-59.

Nyquist, J., and Greger, M. (2007). **Uptake of Zn, Cu, and Cd in metal loaded *Elodea canadensis*.** Environ. Exper. Bot. 60, 219-226.

Oszwałdowski, S., Zawistowska-Gibuła, K., and Roberts, K.P. (2011). **Capillary electrophoretic separation of nanoparticles.** Anal. Bioanal. Chem. 399, 2831-2842.

Oukarroum, A., Barhoumi, L., Pirastru, L., and Dewez, D. (2013). **Silver nanoparticle toxicity effect on growth and cellular viability of the aquatic plant *Lemna gibba*.** Environ. Toxicol. Chem. 32, 902-907.

Oukarroum, A., Bras, S., Perreault, F., and Popovic, R. (2012). **Inhibitory effects of silver nanoparticles in two green algae, *Chlorella vulgaris* and *Dunaliella tertiolecta*.** Ecotoxicol. Environ. Safe. 78, 80-85.

Pan, Y., Neuss, S., Leifert, A., Fischler, M., Wen, F., Simon, U., Schmid, G., Brandau, W., and Jahnen-Dechent, W. (2007). **Size-dependent cytotoxicity of gold nanoparticles.** Small 3, 1941-1949.

Park, J.Y., Lim, S., and Park, K. (2013). **A new approach for determination of fouling potential by colloidal nanoparticles during reverse osmosis (RO) membrane filtration of seawater.** J. Nanopart. Res. 15:1548, pp. 1-9.

Paterson, G., Macken, A., and Thomas, K.V. (2011). **The need for standardized methods and environmental monitoring programs for anthropogenic nanoparticles.** Anal. Methods 3, 1461-1467.

Peralta-Videa, J.R., Zhao, L., Lopez-Moreno, M.L., de la Rosa, G., Hong, J., and Gardea-Torresdey, J.L. (2011). **Nanomaterials and the environment: A review for the biennium 2008-2010.** J. Hazard. Mater. 186, 1-15.

Pérez, S., Farré, M., and Barceló, D. (2011). **Analysis, behavior and ecotoxicity of carbon-based nanomaterials in the aquatic environment.** Trends Anal. Chem. 28, 820-832.

Perida, A.K., and Das, A.B. (2004). **Salt tolerance and salinity effects on plants: A review.** Ecotoxicol. Environ. Safe. 60, 324-349.

Petosa, A.R., Jaisi, D.P., Quevedo, I.R., Elimelech, M., and Tufenkji, N. (2010). **Aggregation and deposition of engineered nanomaterials in aquatic environments: Role of physicochemical interactions.** Environ. Sci. Technol. 44, 6532-6549.

Phenrat, T., Saleh, N., Sirk, K., Tilton, R.D., and Lowry, G.V. (2007). **Aggregation and sedimentation of aqueous nanoscale zero valent iron dispersions.** Environ. Sci. Technol. 41, 284-290.

Phoenix, C. (2008). **History of nanotechnology.** Nanotechnology Press Kit, Nanotechnology Now. *Available from http://www.nanotech-now.com/Press_Kit/nanotechnology-history.htm (Accessed on August 8, 2014)*

Plathe, K.L., von der Kammer, F., Hassellöv, M., Moore, J.N., Murayama, M., Hofmann, T., and Hochella Jr., M.F. (2010). **Using FlFFF and aTEM to determine trace metal-nanoparticle associations in riverbed sediment.** Environ. Chem. 7, 82-93.

Plathe, K.L.,von der Kammer, F., Hassellöv, M., Moore, J.N., Murayama, M., Hofmann, T., and Hochella Jr., M.F. (2013). **The role of nanominerals and mineral nanoparticles in the transport of toxic trace metals: Field-flow fractionation and analytical TEM analyses after nanoparticle isolation and density separation.** Geochim. Cosmochim. Acta 102, 213-225.

Poda, A.R., Bednar, A.J., Kennedy, A.J., Harmon, A., Hull, M., Mitrano, D.M., Ranville, J.F., and Steevens, J. (2011). **Characterization of silver nanoparticles using flow-field flow fractionation interfaced to inductively coupled plasma mass spectrometry.** J. Chrom. A 1218, 4219-4225.

Ponder, S.M., Darab, J.G., and Mallouk, T.E. (2000). **Remediation of Cr(VI) and Pb(II) aqueous solutions using supported, nanoscale zero-valent iron.** Environ. Sci. Technol. 34, 2564-2569.

Prasad, V., Semwogerere, D., and Weeks, E.R. (2007). **Confocal microscopy of colloids.** J. Phys.: Condens. Matter 19, 1-25.

Qu, X., Alvarez, P.J.J., Li, Q. (2013). **Applications of nanotechnology in water and wastewater treatment.** Water Res. 47, 3931-3946.

Quik, J.T.K., Lynch, I., Van Hoecke, K., Miermans, C.J.H., De Schamphelaere, K.A.C., Janssen, C.R., Dawson, K.A., Cohen Stuart, M.A., and Van De Meent, D. (2010). **Effect of natural organic matter on cerium dioxide nanoparticles settling in model fresh water.** Chemosphere 81, 711-715.

Quik, J.T.K., Stuart, M.C., Wouterse, M., Peijnenburg, W., Hendriks, A.J., and Van De Meent, D. (2012). **Natural colloids are the dominant factor in the sedimentation of nanoparticles.** Environ. Toxicol. Chem. 31, 1019-1022.

Quik, J.T.K., Vonk, J.A., Hansen, S.F., Baun, A., and Van De Meent, D. (2011). **How to assess exposure of aquatic organisms to manufactured nanoparticles?** Environ. Int. 37, 1068-1077.

Rakowska, M.I., Kupryianchyk, D., Harmsen, J., Grotenhuis, T., and Koelmans, A.A. (2012). **In situ remediation of contaminated sediments using carbonaceous materials.** Environ. Toxicol. Chem. 31, 693-704.

Reger, D.L., Goode, S.R., and Ball, D.W. (2010). **Appendix F: Solubility product, acid, and base constants.** In: Chemistry: Principles and practice, 3rd edition. Brooks/Cole, Cengage Learning Inc., Belmont, CA, USA, pp. A.17-A.18.

Ren, J., Li, Z., and Wong, F.-S. (2006). **A new method for the prediction of pore size distribution and MWCO of ultrafiltration membranes.** J. Membrane Sci. 279, 558-569.

Rico, C.M., Majumdar, S., Duarte-Gardea, M., Peralta-Videa, J.R., and Gardea-Torresdey, J.L. (2011). **Interaction of nanoparticles with edible plants and their possible implications in the food chain.** J. Agric. Food Chem. 59, 3485-3498.

Rinklebe, J., During, A., Overesch, M., Du Laing, G., Wennrich, R., Stärk, H.-J., and Mothes, S. (2010). **Dynamics of mercury fluxes and their controlling factors in large Hg-polluted floodplain areas.** Environ. Pollut. 158, 308-318.

Rogers, N.J., Franklin, N.M., Apte, S.C., Batley, G.E., Angel, B.M., Lead, J.R., and Baalousha, M. (2010a). **Physico-chemical behaviour and algal toxicity of nanoparticulate CeO_2 in freshwater.** Environ. Chem. 7, 50-60.

Rogers, N.J., Franklin, N.M., Apte, S.C., Spadaro, D., Angel, B., Batley, G.E., Lead, J.R., and Baalousha, M.A. (2010b). **Behaviour and toxicity to algae of nanoparticulate CeO_2 in freshwater.** Environ. Chem. 7, 50-60.

Roh, J.-Y., Sim, S.J., Yi, J., Park., K., Chung, K.H., Ryu, D.-Y., and Choi, J. (2009). **Ecotoxicity of silver nanoparticles on the soil nematode *Caenorhabditis elegans* using functional ecotoxicogenomics.** Environ. Sci. Technol. 43, 3933-3940.

Römer, I., White, T.A., Baalousha, M.A., Chipman, K., Viant, M.R., and Lead, J.R. (2011). **Aggregation and dispersion of silver nanoparticles in exposure media for aquatic toxicity tests.** J. Chrom. A 1218, 4226-4233.

Roukes, M. (2001). **Plenty of room, indeed.** Sci. Am. 285, 48-57.

Rupp, H., Rinklebe, J., Bolze, S., and Meissner, R. (2010). **A scale depended approach to study pollution control processes in wetland soils using three different techniques.** Ecol. Eng. 36, 1439-1447.

Sabo-Attwood, T., Unrine, J.M., Stone, J.W., Murphy, C.J., Ghoshroy, S., Blom, D., Bertsch, P.M., and Newman, L.A. (2011). **Uptake, distribution and toxicity of gold nanoparticles in tobacco (*Nicotiana xanthi*) seedlings.** Nanotoxicology 6, 353-360.

Sadik, O.A., Du, N., Kariuki, V., Okello, V., and Bushlyar, V. (2014). **Current and emerging technologies for the characterization of nanomaterials.** ACS Sustainable Chem. Eng. 2, 1707-1716.

Sagee, O., Dror, I., and Berkowitz, B. (2012). **Transport of silver nanoparticles (AgNPs) in soil.** Chemosphere 88, 670-675.

Saleh, N., Kim, H.-J., Phenrat, T., Matyjaszewski, K., Tilton, R.D., and Lowry, G.V. (2008). **Ionic strength and composition affect the mobility of surface-modified Fe^0 nanoparticles in water-saturated sand columns.** Environ. Sci. Technol. 42, 3349-3355.

Salehi, M.H., Hashemi Beni, O., Beigi Harchegani, H., Esfandiarpour Borujeni, I., and Motaghian, H.R. (2011). **Refining soil organic matter determination by loss-on-ignition.** Pedosphere 21, 473-482.

Sánchez, A., Recillas, S., Font, X., Casals, E., González, E., and Puntes, V. (2011). **Ecotoxicity of, and remediation with, engineered inorganic nanoparticles in the environment.** Trends Anal. Chem. 30, 507-516.

Sánchez, A., Recillas, S., Font, X., Casals, E., González, E., Puntes, V. (2011). **Ecotoxicity of, and remediation with, engineered inorganic nanoparticles in the environment.** Trends Anal. Chem. 30, 507-516.

Sargent Jr., J.F. (2013). **The National Nanotechnology Initiative: Overview, reauthorization, and appropriations issues.** RL34401, CRS report for US Congress, Congressional Research Service, Washington, DC, USA, pp. 69. *Available from https://opencrs.com/document/RL34401 (Accessed on August 22, 2014)*

Sartori, F, Clayton, M., and Stills, D. (2013). **Procedure for determining soil particle size using the hydrometer method.** Standard Operating Procedure, METH004.01, California Department of Pesticide Regulation, Environmental Monitoring Branch, Sacramento, CA, USA, pp. 10. *Available from http://www.cdpr.ca.gov/docs/emon/pubs/ sopmethdta.htm (Accessed on September 19, 2014)*

Scheffer, A., Engelhard, C., Sperling, M., and Buscher, W. (2008). **ICP-MS as a new tool for determination of gold nanoparticles in bioanalytical applications.** Anal. Bioanal. Chem. 390, 249-252.

Schmidt, B., Loeschner, K., Hadrup, N., Mortensen, A., Sloth, J.J., Koch, C.B., and Larsen, E.H. (2011). **Quantitative characterization of gold nanoparticles by field-flow fractionation coupled online with light scattering detection and inductively coupled plasma mass spectrometry.** Anal. Chem. 83, 2461-2468.

Schulze, D.G., and Bertsch, P.M. (1995). **Synchrotron X-ray techniques in soil, plant, and environmental research.** Adv. Argon. 55, 1-66.

Scown, T.M., van Aerle, R., and Tyler, C.R. (2010). **Review: Do engineered nanoparticles pose a significant threat to the aquatic environment?** Crit. Rev. Toxicol. 40, 653-670.

Shah, V., Shah, S., Shah, H., Rispoli, F.J., McDonnell, K.T., Workeneh, S., Karakoti, A., Kumar, A., and Seal, S. (2012). **Antibacterial activity of polymer coated cerium oxide nanoparticles.** PLoS ONE 7, e47827, pp. 12.

Shaheen, S.M., Rinklebe, J., Frohne, T., White, J.R., and DeLaune, R.D. (2014). **Biogeochemical factors governing cobalt, nickel, selenium, and vanadium dynamics in periodically flooded Egyptian North Nile Delta rice soils.** Soil Sci. Soc. Am. J. 78, 1065-1078.

Sharma, V.K. (2009a). **Aggregation and toxicity of titanium dioxide nanoparticles in aquatic environment – A review.** J. Environ. Sci. Health A 44, 1485-1495.

Sharma, V.K., Siskova, K.M., Zboril, R., and Gardea-Torresdey, J.L. (2014). **Organic-coated silver nanoparticles in biological and environmental conditions: Fate, stability and toxicity.** Adv. Colloid Interface Sci. 204, 15-34.

Sharma, V.K., Yngard, R.A., and Lin, Y. (2009b). **Silver nanoparticles: Green synthesis and their antimicrobial activities.** Adv. Colloid Interface Sci. 145, 83-96.

Simonet, B.M., and Valcárcel, M. (2009). **Monitoring nanoparticles in the environment.** Anal. Bioanal. Chem. 393, 17-21.

Singhal, R.K., Preetha, J., Karpe, R., Tirumalesh, K., Kumar, S.C., and Hegde, A.G. (2006). **The use of ultra filtration in trace metal speciation studies in sea water.** Environ. Int. 32, 224-228.

Solovitch, N., Labille, J., Rose, J., Chaurand, P., Borschneck, D., Wiesner, M.R., and Bottero, J.-Y. (2010). **Concurrent aggregation and deposition of TiO_2 nanoparticles in a sandy porous media.** Environ. Sci. Technol. 44, 4897-4902.

Springer, F., Laborie, S., and Guigui, C. (2013). **Removal of SiO_2 nanoparticles from industry wastewaters and subsurface waters by ultrafiltration: Investigation of process efficiency, deposit properties and fouling mechanism.** Sep. Purif. Technol. 108, 6-14.

Stebounova, L.V., Guio, E., and Grassian, V.H. (2011). **Silver nanoparticles in simulated biological media: a study of aggregation, sedimentation, and dissolution.** J. Nanopart. Res. 13, 233-244.

Stolpe, B., Hassellöv, M., Andersson, K., and Turner, D.R. (2005). **High resolution ICPMS as an on-line detector for flow field-flow fractionation; multi-element determination of colloidal size distributions in a natural water sample.** Analyt. Chim. Acta 535, 109-121.

Stone, V., Nowack, B., Baun, A., van den Brink, N., von der Kammer, F., Dusinska, M., Handy, R., Hankin, S., Hassellöv, M., Joner, E., and Fernandes, T.F. (2010). **Nanomaterials for environmental studies: Classification, reference material issues, and strategies for physic-chemical characterisation.** Sci. Total Environ. 408, 1745-1754.

Strigul, N., Vaccari, L., Galdun, C., Wazne, M., Liu, X., Christodoulatos, C., and Jasinkiewicz, K. (2009). **Acute toxicity of boron, titanium dioxide, and aluminum nanoparticles to *Daphnia magna* and *Vibrio fischeri*.** Desalination 248, 771-782.

Subramanian, V., Semenzin, E., Hristozov, D., Marcomini, A., and Linkov, I. (2014). **Sustainable nanotechnology: Defining, measuring and teaching.** Nano Today 9, 6-9.

Surugau, N., and Urban, P.L. (2009). **Electrophoretic methods for separation of nanoparticles.** J. Sep. Sci. 32, 1889-1906.

Thalmann, B., Voegelin, A., Sinnet, B., Morgenroth, E., and Kaegi, R. (2014). **Sulfidation kinetics of silver nanoparticles reacted with metal sulfides.** Environ. Sci. Technol. 48, 4885-4892.

The Project of Emerging Nanotechnologies (2014). **Consumer products inventory.** *Available from http://www.nanotechproject.org/cpi (Accessed on December 18, 2014)*

The Royal Society and The Royal Academy of Engineering (2004). **Nanoscience and nanotechnologies: Opportunities and uncertainties.** RS Policy document 19/04, The Royal Society, London, UK, pp. 113. *Available from http://royalsociety.org/policy/publications/2004/nanoscience-nanotechnologies (Accessed on August 8, 2014)*

Theron, J., Walker, J.A., and Cloete, T.E. (2008). **Nanotechnology and water treatment: Applications and emerging opportunities.** Crit. Rev. Microbiol. 34, 43-69.

Thiébaut, G., Gross, Y., Gierlinski, P., and Boiché, A. (2010). **Accumulation of metals in Elodea Canadensis and Elodea nuttallii: Implications for plant-macroinvertebrate interactions.** Sci. Total Environ. 408, 5499-5505.

Thill, A., Zeyons, O., Spalla, O., Chauvat, F., Rose, J., Auffan, M., and Flank, A.M. (2006). **Cytotoxicity of CeO_2 nanoparticles for *Escherichia coli.* Physico-chemical insight of the cytotoxicity mechanism.** Environ. Sci. Technol. 40, 6151-6156.

Thio, B.J.R., Zhou, D., and Keller, A.A. (2011). **Influence of natural organic matter on the aggregation and deposition of titanium dioxide nanoparticles.** J. Hazard. Mater. 189, 556-563.

Thwala, M., Musee, N., Sikhwivhilu, L., and Wepener, V. (2013). **The oxidative toxicity of Ag and ZnO nanoparticles towards the aquatic plant *Spirodela punctuta* and the role of testing media parameters.** Environ. Sci.: Processes Impacts 15, 1830-1843.

Tian, Y., Gao, B., Silvera-Batista, C., and Ziegler, K. (2010). **Transport of engineered nanoparticles in saturated porous media.** J. Nanopart. Res. 12, 2371-2380.

Tiede, K., Boxall, A.B.A., Tear, S.P., Lewis, J., David, H., and Hassellöv, M. (2008). **Detection and characterization of engineered nanoparticles in food and the environment.** Food Addit. Contam. 25, 795-821.

Tiede, K., Boxall, A.B.A., Tiede, D., Tear, S.P., David, H., and Lewis, J. (2009b). **A robust size-characterisation methodology for studying nanoparticle behaviour in 'real' environmental samples, using hydrodynamic chromatography coupled to ICP-MS.** J. Anal. At. Spectrom. 24, 964-972.

Tiede, K., Boxall, A.B.A., Wang, X., Gore, D., Tiede, D., Baxter, M., David, H., Tear, S.P., and Lewis, J. (2010). **Application of hydrodynamic chromatography-ICP-MS to investigate the fate of silver nanoparticles in activated sludge.** J. Anal. At. Spectrom. 25, 1149-1154.

Tiede, K., Hassellöv, M., Breitbarth, E., Chaudhry, Q., and Boxall, A.B.A. (2009a). **Considerations for environmental fate and ecotoxicity testing to support environmental risk assessments for engineered nanoparticles.** J. Chrom. A 1216, 503-509.

Tiede, K., Tear, S.P., David, H., and Boxall, A.B.A. (2009c). **Imaging of engineered nanoparticles and their aggregates under fully liquid conditions in environmental matrices.** Water Res. 43, 3335-3343.

Tourinho, P.S., van Gestel, C.A.M., Lofts, S., Svendsen, C., Soares, A.M.V.M., and Loureiro, S. (2012). **Metal-based nanoparticles in soil: Fate, behavior, and effects on soil invertebrates.** Environ. Toxicol. Chem. 31, 1679-1692.

Tso, C-p., Zhung, C.-m., Shih, Y.-h., Tseng, Y.-M., Wu, S.-c., and Doong, R.-a. (2010). **Stability of metal oxide nanoparticles in aqueous solutions.** Water Sci. Technol. 61, 127-133.

Tuoriniemi, J., Cornelis, G., and Hassellöv, M. (2012). **Size determination and detection capabilities of single-particle ICPMS for environmental analysis of silver nanoparticles.** Anal. Chem. 84, 3965-3972.

US EPA (1992). **Toxicity characteristic leaching procedure.** Method 1311, United States Environmental Protection Agency, Washington, DC, USA, pp. 31. *Available from http://www.epa.gov/wastes/hazard/testmethods/sw846/pdfs/1311.pdf (Accessed on July 30, 2014)*

US EPA (1994). **Synthetic precipitation leaching procedure.** Method 1312, United States Environmental Protection Agency, Washington, DC, USA, pp. 30. *Available from http://www.epa.gov/wastes/hazard/testmethods/sw846/pdfs/1312.pdf (Accessed on July 30, 2014)*

Van Hoecke, K. (2010). ***In vitro* and *in vivo* evaluation of the ecotoxicity of nanoparticles.** PhD thesis, Faculty of Bioscience Engineering, Ghent University, Ghent, Belgium, pp. 293.

Van Hoecke, K., De Schamphelaere, K.A.C., Van der Meeren, P., Smagghe, G., and Janssen, C.R. (2011). **Aggregation and ecotoxicity of CeO_2 nanoparticles in synthetic and natural waters with variable pH, organic matter concentration and ionic strength.** Environ. Pollut. 159, 970-976.

Van Hoecke, K., Quik, J.T.K., Mankiewicz-Boczek, J., De Schamphelaere, K.A.C., Elsaesser, A., Van der Meeren, P., Barnes, C., McKerr, G., Howard, C.V., Van De Meent, D., Rydzyński, K., Dawson, K.A., Salvati, A., Lesniak, A., Lynch, I., Silversmit, G., De Samber, B., Vincze, L., and Janssen, C.R. (2009). **Fate and effects of CeO_2 nanoparticles in aquatic ecotoxicity tests.** Environ. Sci. Technol. 43, 4537-4546.

Van Koetsem, F., Geremew, T.T., Wallaert, E., Verbeken, K., Van der Meeren, P., and Du Laing, G. (in press). **Fate of engineered nanomaterials in surface water: Factors affecting interactions of Ag and CeO_2 nanoparticles with (re)suspended sediments.** Ecol. Eng., *DOI: 10.1016/j.ecoleng.2014.07.024.*

Van Ranst, E., Verloo, M., Demeye, A., and Pouwels, J.M. (1999). **Manual for the soil chemistry and fertility laboratory: Analytical methods for soils and plants, equipment, and management of consumables.** Ghent University, Ghent, Belgium, pp. 243.

van Reeuwijk, L.P. (Ed.) (2002). **Procedures for soil analysis, sixth edition.** Technical Paper 9, International Soil Reference and Information Center, Food and Agriculture Organization of the United Nations, AJ Wageningen, The Netherlands, pp. 120. *Available from http://www.isric.org/content/technical-papers16-1 (Accessed on September 19, 2014)*

Vasileska, D., and Klimeck, G. (2008). Quantum mechanics: Tunneling. *Available from http://nanohub.org/resources/4945 (Accessed on September 5, 2014)*

Velzeboer, I., Quik, J.T.K., van de Meent, D., and Koelmans, A.A. (2014). **Rapid settling of nanoparticles due to heteroaggregation with suspended sediment.** Environ. Toxicol. Chem. 33, 1766-1773.

Verma, H.C., Upadhyay, C., Tripathi, A., Tripathi, R.P., and Bhandari, N. (2002). **Thermal decomposition pattern and paricle size estimation of iron minerals associated with the Cretaceous-Tertiary boundary at Gubbio.** Meteorit. Planet. Sci. 37, 901-909.

Vitorge, E., Szenknect, S., Martins, J.M.F., and Gaudet, J.-P. (2013). **Size- and concentration-dependent deposition of fluorescent silica colloids in saturated sand columns: Transport experiments and modeling.** Environ. Sci. Process. Impacts 15, 1590-1600.

Vlarebo (2008). **Besluit van de Vlaamse regering houdende de vaststelling van het Vlaams reglement betreffende de bodemsanering en de bodembescherming. Order of the Flemish government of 14 December 2007 establishing the Flemish soil remediation and protection regulations.** The Environment, Nature, and Energy Department, Flemish Government, Brussels, Belgium, pp. 114. *Available from https://navigator.emis.vito.be/milnav-consult/ (Accessed on January 6, 2015)*

von der Kammer, F., Baborowski, M., and Friese, K. (2005). **Field-flow fractionation coupled to multi-angle laser light scattering detectors: Applicability and analytical benefits for the analysis of environmental colloids.** Analyt. Chim. Acta 552, 166-174.

von der Kammer, F., Ottofuelling, S., and Hofmann, T. (2010). **Assessment of the physico-chemical behavior of titanium dioxide nanoparticles in aquatic environments using multi-dimensional parameter testing.** Environ. Pollut. 158, 3472-3481.

Watlington, K. (2005). **Emerging nanotechnologies for site remediation and wastewater treatment.** National Network for Environmental Management Studies fellowship report prepared for the US Environmental Protection Agency, North Carolina State University, Raleigh, NC, USA pp. 55. *Available from http://nepis.epa.gov/Adobe/PDF/P1003FG4.PDF (Accessed on August 22, 2014)*

Wei, G.-T., and Liu, F.-K. (1999). **Separation of nanometer gold particles by size exclusion chromatography.** J. Chrom. A 836, 253-260.

Weinberg, H., Galyean, A., and Leopold, M. (2011). **Evaluating engineered nanoparticles in natural waters.** Trends Anal. Chem. 30, 72-83.

Weltje, L., den Hollander, W., and Wolterbeek, H.T. (2003). **Adsorption of metals to membrane filters in view of their speciation in nutrient solution.** Environ. Toxicol. Chem. 22, 265-271.

Westerhoff, P., Song, G.X., Hristovski, K., and Kiser, M.A. (2011). **Occurrence and removal of titanium at full scale wastewater treatment plants: Implications for TiO_2 nanomaterials.** J. Environ. Monit. 13, 1195-1203.

Whitley, A.R., Levard, C., Oostveen, E., Bertsch, P.M., Matocha, C.J., von der Kammer, F., and Unrine, J.M. (2013). **Behavior of Ag nanoparticles in soil: Effects of particle surface coating, aging and sewage sludge amendment.** Environ. Pollut. 182, 141-149.

Wijnhoven, S.W.P., Peijnenburg, W., Herberts, C.A., Hagens, W.I., Oomen, A.G., Heugens, E.H.W., Roszek, B., Bisschops, J., Gosens, I., Van De Meent, D, Dekkers, S., De Jong, W.H., van Zijverden, M., Sips, A.J.A.M., and Geertsma, R.E. (2009). **Nano-silver – a review of available data and knowledge gaps in human and environmental risk assessment.** Nanotoxicology 3, 109-138.

Williams, A., Varela, E., Meehan, E., and Tribe, K. (2002). **Characterisation of nanoparticulate systems by hydrodynamic chromatography.** Int. J. Pharm. 242, 295-299.

Windler, L., Lorenz, C., von Goetz, N., Hungerbühler, K., Amberg, M., Heuberger, M., and Nowack, B. (2012). **Release of titanium dioxide from textiles during washing.** Environ. Sci. Technol. 46, 8181-8188.

Wolthers, M., Charlet, L., van Der Linde, P.R., Rickard, D., and van Der Weijden, C.H. (2005). **Surface chemistry of disordered mackinawite (FeS).** Geochim. Cosmochim. Acta 69, 3469-3481.

Wu, N., Wyart, Y., Liu, Y., Rose, J., and Moulin, P. (2013). **An overview of solid/liquid separation methods and size fractionation techniques for engineered nanomaterials in aquatic environment.** Environ. Technol. Rev.2, 55-75.

Wu, N., Wyart, Y., Siozade, L., Georges, G., and Moulin, P. (2014). **Characterization of ultrafiltration membranes fouled by quantum dots by confocal laser scanning microscopy.** J. Membrane Sci. 470, 40-51.

Wu, Y., Zhoua, Q., Li, H., Liua, W., Wanga, T., and Jianga, G. (2010). **Effects of silver nanoparticles on the development and histopathology biomarkers of Japanese medeka (*Oryzias latipes*) using the partial-life test.** Aquat. Toxicol. 100-2, 160-167.

Wuana, R.A., and Okieimen, F.E. (2011). **Heavy metals in contaminated soils: A review of sources, chemistry, risks and best available strategies for remediation.** ISRN Ecology 2011, 402647, pp. 20.

Xiong, Z., He, F., Zhao, D., and Barnett, M.O. (2009). **Immobilization of mercury in sediment using stabilized iron sulphide nanoparticles.** Water Research, 43, 5171-5179.

Xu, Y., and Zhao, D. (2007). **Reductive immobilization of chromate in water and soil using stabilized iron nanoparticles.** Water Res. 41, 2101-2108.

Yao, K.-M., Habibian, M.T., and O'Melia, C.R. (1971). **Water and waste water filtration: Concepts and applications.** Environ. Sci. Technol. 5, 1105-1112.

Yin, Y., Yu, S., Liu, J., and Jiang, G. (2014). **Thermal and photoinduced reduction of ionic Au(III) to elemental Au nanoparticles by dissolved organic matter in water: Possible source of naturally occurring Au nanoparticles.** Environ. Sci. Technol. 48, 2671-2679.

Yu, K., and Rinklebe, J. (2011). **Advancement in soil microcosm apparatus for biogeochemical research.** Ecol. Eng. 37, 2071-2075.

Yu, K., Böhme, F., Rinklebe, J., Neue, H.-U., and DeLaune, R.D. (2007). **Major biogeochemical processes in soils – A microcosm incubation from reducing to oxidizing conditions.** Soil Sci. Soc. Am. J. 71, 1406-1417.

Zhang, H., He, X., Zhang, Z., Zhang, P., Li, Y., Ma, Y., Kuang, Y., Zhao, Y., and Chai, Z. (2011a). **Nano-CeO_2 exhibits adverse effects at environmental relevant concentrations.** Environ. Sci. Technol. 45, 3725-3730.

Zhang, M.Y., Wang, Y., Zhao, D.Y., and Pan, G. (2010). **Immobilization of arsenic in soils by stabilized nanoscale zero-valent iron, iron sulfide (FeS), and magnetite (Fe_3O_4) particles.** Chinese Sci. Bull. 55, 365-372.

Zhang, W.-X. (2003). **Nanoscale iron particles for environmental remediation: An overview.** J. Nanopart. Res. 5, 323-332.

Zhang, W.-X., and Elliot, D. (2006). **Applications of iron nanoparticles for groundwater remediation.** Remediation 16, 7-21.

Zhang, W., Yao, Y., Sullivan, N., and Chen, Y. (2011b). **Modeling the primary size effects of citrate-coated silver nanoparticles on their ion release kinetics.** Environ. Sci. Technol. 45, 4422-4428.

Zhang, Y., Chen, Y., Westerhoff, P., and Crittenden, J. (2009). **Impact of natural organic matter and divalent cations on the stability of aqueous nanoparticles.** Water Res. 43, 4249-4257.

Zhao, C.M., and Wang, W.X. (2011). **Comparison of Acute and Chronic Toxicity of Silver Nanoparticles and Silver Nitrate to *Daphnia magna*. Environ.** Toxicol. Chem. 30, 885-892.

Zhou, D., Abdel-Fattah, A., and Keller, A.A. (2012). **Clay particles destabilize engineered nanoparticles in aqueous environments.** Environ. Sci. Technol. 46, 7520-7526.

Summary

Metallic engineered nanoparticles (ENPs) are generally defined as metal-containing particulate objects having a size between 1 and 100 nm in all three dimensions that have been manufactured intentionally to possess specific characteristics (*e.g.*, size, composition, morphology, or surface chemistry). Due to their exceptionally small size, ENPs often display extraordinary size-related properties and reactivities that differ significantly from their larger-sized bulk counterparts, which has led to a rapid increase in their potential applications in various areas of the economy, including textiles, electronics, optics, cosmetics, medical devices, food packaging, catalysts, fuel cells, (waste)water treatment, and environmental remediation. However, the increasing production and widespread use of ENPs will inevitably also result in their discharge into the (aquatic) environment, where their novel characteristics, such as a high specific surface area and abundant reactive sites on the particle surface, as well as their high potential mobility and bioavailability due to their small size, could lead to unexpected health and/or environmental hazards. Therefore, a consensus exists within the scientific and public community underlining the importance to gain extensive knowledge on the behaviour, transport and fate of ENPs upon their release into the (aquatic) environment, in order to evaluate probable exposure routes and improve risk assessment.

This PhD research aimed to contribute to the general knowledge on the environmental fate of metallic ENPs and improve the understanding of their behaviour and fate in the aquatic environment, by aiding in the identification of potential factors affecting for instance nanoparticle stability, mobility, and possible bioavailability upon their release in complex (natural) aqueous systems (*e.g.*, surface water or sediment and soil solutions) (**Chapter 1**).

An overview on past and present research regarding the physicochemical behaviour and fate of metallic ENPs in aquatic environments is given in **Chapter 2**. Aside from briefly describing potential entry routes of ENPs into the environment, this comprehensive literature review also addresses the main processes and factors expected to affect the ultimate behaviour and fate of metallic ENPs in aquatic and terrestrial systems, and provides an extensive survey on the most commonly used analytical methodologies that can be applied to physically and chemically characterize ENPs while performing environmental fate studies.

Filtration processes are interesting and promising options not only for retaining and removing nanoparticles from solution, but also as fractionation techniques during characterization or sample preparation prior to further analysis when studying the

environmental fate of ENPs. In **Chapter 3**, aqueous suspensions of negatively charged (citrate-stabilized) Ag (14.5 ± 1.1 nm) and positively charged CeO_2 (7.3 ± 1.4 nm) ENPs were subjected to different filtration methods (*e.g.*, paper filtration, micro- and ultrafiltration), and the impact of initial concentration, matrix composition, and filter type and filter (pre-)treatment on nanoparticle retention was evaluated. For comparison purposes, solutions of Ag^+ and Ce^{3+} ions were tested in the same way. Significant retention of nanoparticles was observed even for filters having considerably larger pore sizes than the size of the ENPs, indicating sorption. Retention also seemingly increased with decreasing initial concentration, but generally decreased upon treatment of the paper filters with diluted nitric acid or by preconditioning of the filter membranes with 0.1 M $Cu(NO_3)_2$. Additionally, the presence of background electrolytes (*i.e.*, 2 mM KNO_3, NaCl, or $CaCl_2$) affected nanoparticle stability in suspension, *e.g.*, resulting in enhanced retention of Ag ENPs. Results from centrifugal ultrafiltration (UF) recommend the use of 10 kDa filters for removal of the ENPs from solution, and suggest these filters might potentially be suitable to differentiate between (nano)particulate and dissolved species. Furthermore, several digestion methods were assessed for quantification of total silver or cerium in the ENPs via ICP-OES or ICP-MS. For the purpose of this study, open vessel microwave-assisted digestions using concentrated nitric acid and *aqua regia* were preferred in the case of Ag and CeO_2 ENPs, respectively, due the provided high recoveries and their ease of use.

The stability and mobility of ENPs in complex aquatic matrices are prime determinants governing their environmental fate and potential (eco)toxicological hazards towards the aquatic environment and human health. The stability and settling of CeO_2 ENPs (7.3 ± 1.4 nm) as well as the depletion of Ce^{3+} ions in 10 distinct natural surface waters during 7 d was examined in **Chapter 4**, under stagnant and isothermal experimental conditions. For the majority of the surface waters, a substantial depletion (> 95 %) of the initially added CeO_2 ENPs was observed near the liquid surface after 7 d of storage. In all cases, the reduction was considerably higher for CeO_2 ENPs than for Ce^{3+} ions (≤ 68 %). A first-order kinetics model was able to describe the observed time-dependent removal of CeO_2 ENPs (R^2 ≥ 0.998) as well as Ce^{3+} ions (R^2 ≥ 0.812) from the water column, at least in case notable sedimentation occurred over time. Solution-pH appeared to be a prime factor governing nanoparticle colloidal stability. Moreover, the suspended solids (TSS) content also seemed to be an important factor affecting the settling rate and residual fraction of CeO_2 ENPs as well as Ce^{3+} ions in natural surface waters. Correlation results also suggest potential association and co-precipitation of CeO_2 ENPs with aluminium- and

iron-containing natural compounds. The CeO_2 ENPs remained stable in dispersion in surface water characterized by a low pH, ionic strength (IS), and TSS content, indicating the eventual stability and settling of the nanoparticles was likely determined by a combination of physicochemical parameters. Finally, ionic release from the nanoparticle surface was also examined and appeared to be negligible in all of the tested natural waters.

A key community of aquatic systems comprises of aquatic plants, which mainly acquire their nutrients from the water column. Thus, it is not illogical to presume that aquatic plants might also take up nanoparticles from a water body. In **Chapter 5**, the potential association of (citrate-stabilized) Ag (14.1 ± 1.0 nm) and CeO_2 (6.7 ± 1.2 nm) ENPs, or their ionic counterparts, with the submerged aquatic plant *Elodea canadensis* was studied and in particular, parameters affecting the partitioning of the nanoparticles (or metal ions) between plant biomass and the water phase were assessed using five distinct aqueous matrices (*i.e.*, tap water, 10 % Hoagland's solution, and three natural surface waters). Individual plants were exposed to varying concentrations of Ag and CeO_2 ENPs or Ag^+ and Ce^{3+} ions during 72 hour-lasting batch experiments. The results showed a dose-dependent increase of silver or cerium in the plant biomass for both the nanoparticles and the ions, whereby exposure to the latter systematically resulted in significantly higher biomass concentrations. Furthermore, the apparent plant uptake of CeO_2 ENPs appeared to be higher than for Ag ENPs, as higher cerium biomass contents were observed compared to the silver biomass contents when considering comparable nanoparticle exposure concentrations (*e.g.*, 111 versus 186 mg kg^{-1} DW at 1 mg L^{-1}). These findings suggested that association with *E. canadensis* might be affected by particle characteristics such as size, composition, surface charge, or surface coating. Moreover, the stability of the nanoparticles or ions in suspension/solution may be another important aspect affecting plant exposure and uptake. Association of the nanoparticles or ions with *E. canadensis* was also clearly influenced by the properties of the water sample. The silver biomass concentration was found to correlate significantly with the electrical conductivity (EC), dry residue (DR), Cl^-, K, Na, and Mg content in the case of Ag ENPs, or with the EC, inorganic carbon (IC), Cl^-, NO_3^-, Na, and Mg content in the case of Ag^+ ions, whereas significant relationships between the cerium biomass concentration and the EC, DR, IC, and Ca content, or the pH, EC, DR, IC, Cl^-, Ca, and Mg content were obtained for CeO_2 ENPs or Ce^{3+} ions, respectively.

The distribution of ENPs between solid and liquid phases in complex aquatic media can provide important information on their mobility and potential bioavailability. Therefore, the

solid-liquid partitioning behaviour of (citrate-stabilized) Ag (14.8 ± 1.3 nm) and CeO_2 (6.2 ± 0.5 nm) ENPs in (re)suspended sediments (**Chapter 6**) and soils (**Chapter 7**) was examined during a 24 h time frame, and compared to that of Ag^+ and Ce^{3+} ions. Particularly, the association of these nanoparticles and their corresponding ions with sediment and soil constituents was studied. It was shown that after 24 h of equilibration, substantial fractions of Ag or CeO_2 ENPs could be retrieved in the liquid phase of (re)suspended sediments and soils, and that the silver or cerium content remaining in solution was dependent on equilibration time and was affected by the applied centrifugation treatment. Centrifugation also had a significant impact on the amount of suspended matter as well as the total organic carbon (TOC) content present in the supernatant of the different sediment and soil suspensions. In the absence of sediment or soil on the other hand, the Ag and CeO_2 ENPs as well as their ionic counterparts were unaffected by centrifugation over a 24 h time period, indicating that sediment and soil properties had a significance influence on their colloidal stability and mobility. Statistically significant correlations were observed between the amount of silver or cerium remaining in suspension and the TOC and suspended matter content, suggesting interactions of the nanoparticles with sediment and soil colloidal matter. It was also clearly shown that dissolved organic matter might stabilize CeO_2 ENPs in the aqueous phase (**Chapter 7**). Furthermore, in "real" sediment and soil suspensions, Ag^+ and Ce^{3+} ions seemingly interacted more strongly with sediment or soil constituents compared to their nanoparticulate counterparts, rendering the Ag and CeO_2 ENPs more mobile and potentially bio-accessible. However, the nanoparticles and ions behaved differently in a "model" system (*i.e.*, pure quartz sand suspensions). In the presence of quartz sand, CeO_2 ENPs appear to be less mobile than Ce^{3+} ions, whereas no difference in the solid-liquid distribution was observed between Ag ENPs or Ag^+ ions. Therefore, the migration potential of CeO_2 ENPs in real sediments or soils seems to be higher.

Injection of FeS ENPs into soils and sediments can be used to immobilize heavy metal contaminants and make them unavailable to organisms and plants. Coating these particles with carboxymethyl cellulose (CMC) was previously reported to be an interesting option to provide them with a much greater physical stability, soil deliverability, and reactivity. However, the increased mobility of such particles could potentially lead to enhanced contaminant extraction and particle-facilitated contaminant transport in the environment instead of immobilization of the contaminants. Therefore, the stability and transport behaviour of CMC-FeS ENPs and resulting mobility of trace metal contaminants in field-contaminated soils and sediments was studied in **Chapter 8**, through a series of batch

and column experiments. The synthesized CMC-FeS ENPs had a hydrodynamic diameter of 154.5 ± 5.8 nm and remained stable in suspension for a prolonged period of time (several weeks) when kept under anaerobic conditions. In the absence of CMC, much larger (microscale) FeS particles were formed, which quickly aggregated and precipitated within a matter of minutes. Batch experiments indicated that the CMC-FeS ENPs possess a high affinity for metal contaminants (*e.g.*, Cd, Cr, Cu, Hg, Ni, Pb, and Zn), as high amounts of these trace metals could be retrieved in the aqueous phase after treatment of the soils and sediment with the nanoparticles (*i.e.*, up to 29 times more compared to the water-leachable metal contents). Furthermore, batch retention of the nanoparticles by the solid phase was low (< 37 %), suggesting a high particle stability and potential mobility. Column breakthrough tests demonstrated that the CMC-FeS ENPs were highly mobile in a sandy soil, even without the use of an external pressure (*i.e.*, just via gravitational percolation). Maximal breakthrough of the nanoparticles was observed after approximately 10 or 16 pore volumes (PVs) for 83.3 or 500 mg L^{-1} CMC-FeS ENPs, respectively, and only about 7 % of the nanoparticles were retained after 22.7 PVs. Simultaneous elution of trace elements showed that up to 19, 8.7, or 11 % of the respective Cd, Pb, or Zn content originally present in the soil was extracted after 22.7 PVs, with initial peaking occurring during the first 5 to 10 PVs. Moreover, filtration of the percolates over 0.10 μm (which was shown to be able to retain *ca.* 98 % of the CMC-FeS ENPs) indicated that the vast majority of these extracted metals were associated with the nanoparticles and thus did not occur as "dissolved" species. The high affinity of CMC-FeS ENPs for metals in combination with their high stability and mobility indicated that association of trace metals with the nanoparticles could potentially lead to particle-facilitated contaminant transport in the environment, in case conditions favouring colloidal transport are prevailing.

In **Chapter 9**, automated biogeochemical microcosms were employed to study the solid-liquid partitioning behaviour of Ag ENPs (*ca.* 40 nm) and Ag^{+} ions in (re)suspended field-incubated sediment under controlled redox conditions during 8 d. Particularly, the potential implications of utilizing fresh field-incubated sediment compared to oven-dried sediment on nanoparticle behaviour and fate were assessed. Additionally, the impact of redox condition as well as particle properties (*i.e.*, citrate (Cit) or polyvinylpyrrolidone (PVP) surface coating) on the solid-liquid distribution of silver were also examined. Application of fresh sediment that was (re)incubated in the field under oxic or anoxic conditions was demonstrated to have a significant impact on the eventual silver behaviour and fate, as compared to the use of oven-dried sediment. Considerable fractions of silver

remained in the aqueous phase of oxic fresh sediment suspensions up until 72 h after exposure (up to 22 %), or even after 192 h in the case of the anoxic fresh sediment treatments (up to 25 %), whereas addition of silver ions or nanoparticles to the dry sediment resulted in much lower silver recoveries (< 4.4 %) during the entire 192 h experimental time frame, indicating a higher stability and potential bioavailability in the presence of fresh sediment. Furthermore, predefined redox conditions did not appear to significantly impact silver partitioning in the case of the dry sediment treatments, while a time-dependent decrease in silver content remaining in solution was observed for the tests utilizing oxic fresh sediment and even a time-dependent increase in the case of anoxic fresh sediment treatments. Generally, no substantial differences in the behaviour of the different silver species were observed (except in the case of Cit-Ag ENPs during the oxic fresh sediment treatments), suggesting that particle properties (*e.g.*, the type of surface coating) were of minor importance in regard to the degree of silver removal from the liquid phase under the prevailing experimental conditions.

Finally, selected factors (*i.e.*, particle properties and environmental parameters) that were identified during this PhD research to potentially affect the behaviour and fate of metallic ENPs upon their emission into complex (natural) aquatic matrices were discussed in **Chapter 10**. Moreover, this chapter also provides a summarized overview of the main conclusions as well as some possible future research perspectives based on the experiences and insights gained during the course of this research.

Samenvatting

Metallisch nanopartikels (ENPs) worden courant gedefinieerd als zijnde metaal bevattende deeltjes met een grootte tussen 1 en 100 nm in alle drie dimensies. Door hun exceptioneel kleine afmetingen vertonen ENPs vaak unieke eigenschappen (bv. een grote specifieke oppervlakte en reactiviteit, en kwantum effecten) die niet aanwezig zijn bij het corresponderende bulkmateriaal. Zulke eigenschappen kunnen van nut zijn voor verscheidene toepassingen in een brede waaier van economische sectoren (bv. de transportsector, farmaceutische sector, cosmeticasector, consumptiegoederensector, en de milieu-technologische sector). Echter, de stijgende productie en het veelvuldige gebruik van deze ENPs zal ontegensprekelijk ook resulteren in emissies in het (aquatische) milieu, waar de buitengewone eigenschappen van deze partikels mogelijk tot onverwachte milieu- en gezondheidsrisico's kunnen leiden. Er bestaat dan ook een consensus binnen de wetenschappelijke en publieke gemeenschap dat het van vitaal belang is om uitgebreide kennis te verwerven inzake het gedrag van ENPs volgend op hun emissie in het (aquatische) milieu, en zodoende mogelijke blootstellingsroutes te evalueren en risicoanalyses te verbeteren.

Het doel van dit doctoraatsonderzoek was om bij te dragen tot de algemene expertise omtrent het fysicochemisch gedrag van metallische ENPs in aquatische milieus door factoren te identificeren die mogelijk een impact hebben op bijvoorbeeld hun colloïdale stabiliteit, mobiliteit, en potentiële bio-beschikbaarheid in complexe (natuurlijke) aquatische systemen (bv. oppervlakte water of sediment- en bodemoplossingen) (**Hoofdstuk 1**).

In **Hoofdstuk 2** wordt een overzicht gegeven inzake de huidige kennis met betrekking tot het fysicochemisch gedrag van metallische ENPs in aquatische milieus. Deze uitgebreide literatuurstudie beschrijft kort de mogelijke emissieroutes van ENPs in het milieu en gaat dieper in op enkele kernprocessen en parameters die verwacht worden hun uiteindelijke gedrag in het milieu te beïnvloeden. Verder worden ook de meest algemeen toegepaste analytische technieken besproken die aangewend kunnen worden om nanopartikels fysisch en chemisch te karakteriseren.

Filtratietechnieken bieden interessante mogelijkheden om nanopartikels te verwijderen vanuit een oplossing alsook om te dienen als fractioneringstechniek gedurende deeltjeskarakterisering of staalvoorbereiding voorafgaand aan verdere analyse. In **Hoofdstuk 3** werden waterige dispersies van negatief geladen Ag (14.5 ± 1.1 nm) en positief geladen CeO_2 (7.3 ± 1.4 nm) ENPs onderworpen aan verscheidene filtratiemethoden

(bv. papierfiltratie, micro- en ultrafiltratie) en het effect van initiële NP concentratie, matrix samenstelling, en filtertype en -voorbehandeling op het retentiegedrag van de deeltjes werd geëvalueerd. Oplossing van Ag^{+} en Ce^{3+} ionen werden op eenzelfde wijze getest. Een significante fractie van de nanodeeltjes werd weerhouden zelfs bij het gebruik van filters met een poriegrootte die ettelijke malen groter was dan de afmetingen van de ENPs, duidend op sorptie. De retentie nam ook toe bij dalende initiële concentratie, maar nam af bij voorbehandeling van de papieren plooifilters met verdund salpeterzuur of bij pre-conditionering van de synthetische membraanfilters met 0.1 M $Cu(NO_3)_2$. De aanwezigheid van achtergrondelektrolyten (2 mM KNO_3, NaCl, of $CaCl_2$) had een invloed op de colloïdale stabiliteit van de ENPs wat bijvoorbeeld resulteerde in een verhoogde retentie van Ag ENPs. Centrifugale ultrafiltratie gebruik makend van 10 kDa cutoff filters werd aanbevolen om ENPs vanuit een oplossing te verwijderen en werd gesuggereerd als mogelijke optie om gesuspendeerd (nano)particulair van opgelost materiaal te onderscheiden. Verder werd ook het gebruik van microgolf-geassisteerde digestie met geconcentreerd salpeterzuur of met koningswater naar voren geschoven voor het oplossen van respectievelijk Ag en CeO_2 ENPs ten gevolgen van de resulterende hoge recovery's en het gebruiksgemak.

De colloïdale stabiliteit en mobiliteit van ENPs in complexe aquatische matrices spelen een belangrijke rol in hun uiteindelijke gedrag en mogelijke (eco)toxicologische risico's voor het aquatisch milieu en de mensheid. In **Hoofdstuk 4** werd de colloïdale stabiliteit en het sedimentatiegedrag van CeO_2 ENPs (7.3 ± 1.4 nm) alsook van Ce^{3+} ionen in tien verschillende natuurlijke oppervlakte waters bestudeerd gedurende 7 d onder stagnerende en isotherme experimentele condities. In de meerderheid van de water stalen werd na 7 d een aanzienlijke verwijdering (> 95 %) van de initieel toegevoegde CeO_2 ENPs waargenomen net onder het vloeistofoppervlak. Deze verwijdering was in alle gevallen groter voor de nanodeeltjes in vergelijking met de ionen (≤ 68 %). Het sedimentatiegedrag van zowel de CeO_2 ENPs (R^2 ≥ 0.998) als de Ce^{3+} ionen (R^2 ≥ 0.812) kon goed beschreven worden met behulp van een semi-empirisch eerste-orde kinetiek model, ten minste in de gevallen dat er een merkbare vermindering was van het ceriumgehalte aan het vloeistofoppervlak in functie van de tijd. De pH bleek een prominente invloed te hebben op de colloidale stabiliteit van de nanopartikels. Bovendien werd ook aangetoond dat het gehalte aan gesuspendeerd materiaal (TSS) een belangrijke factor was die de sedimentatiesnelheid alsook de residuele fractie aan CeO_2 ENPs en Ce^{3+} ionen in de oppervlakte waters beïnvloedde. Aan de hand van correlatieanalyse werd ook de

mogelijkheid van associatie en co-precipitatie van CeO_2 ENPs met ijzer- en aluminium-houdende natuurlijke colloïden gesuggereerd. Daarentegen bleken de CeO_2 ENPs stabiel in dispersie te blijven in oppervlakte water gekenmerkt door een lage pH, ionensterkte (IS) en TSS gehalte. De colloïdale stabiliteit en het uiteindelijke sedimentatiegedrag van de nanodeeltjes werd daardoor hoogstwaarschijnlijk bepaald door een combinatie van fysicochemische factoren. Finaal bleek ook dat de vrijstelling van ionen uit de nanopartikels in alle oppervlaktewaters verwaarloosbaar was.

Waterplanten maken een belangrijk deel uit van natuurlijk aquatische systemen. Vermits de meerderheid van deze planten hun nutriënten opnemen vanuit de waterkolom is het niet onlogisch te veronderstellen dat ze eveneens nanodeeltjes zouden kunnen opnemen. In **Hoofdstuk 5** werd de mogelijke associatie van citraat-gestabiliseerde Ag (14.1 ± 1.0 nm) en CeO_2 (6.7 ± 1.2 nm) ENPs alsook van Ag^+ en Ce^{3+} ionen met de ondergedompelde waterplant *Elodea canadensis* (brede waterpest) onderzocht. Meer bepaald, mogelijke factoren die een invloed hebben op het verdelingsgedrag van de ENPs (of ionen) tussen de waterfase en de plant werden bestudeerd in vijf verschillende aquatische matrices (kraantjeswater, 10 % Hoagland's oplossing, en drie natuurlijke oppervlakte waters). Tijdens 72 uur durende batchtesten werden individuele plantjes blootgesteld aan variërende dosissen nanodeeltjes of ionen, wat resulteerde in een dosis-afhankelijke stijging van het zilver of ceriumgehalte in de plantjes waarbij de opname van ionen systematisch hoger lag dan de opname van de ENPs. Verder bleek ook dat bij een gelijke blootstellingsdosis de opname van CeO_2 ENPs hoger lag dan van Ag ENPs (bv. 111 t.o.v. 186 mg kg^{-1} DW bij een dosis van 1 mg L^{-1}), wat suggereert dat opname van ENPs door *E. canadensis* mogelijk afhankelijk is van deeltjeseigenschappen (bv. de grootte, samenstelling, oppervlaktelading en oppervlaktecoating). Verder kan ook de stabiliteit van de nanopartikels of ionen in suspensie/oplossing een belangrijke invloed uitoefenen op blootstelling aan en interactie met de plant. Associatie van de nanodeeltjes of ionen met *E. canadensis* werd ook duidelijk beïnvloed door de eigenschappen van de waterstalen. Zodoende werden statistisch significante correlaties verkregen tussen het zilvergehalte in de plant en de geleidbaarheid (EC), droogrest (DR), Cl^-, K, Na en Mg concentraties in het geval van Ag ENPs, of met de EC, anorganische koolstof (IC), Cl^-, NO_3^-, Na en Mg concentraties in het geval van Ag^+ ionen. Er werden ook significant verbanden aangetoond tussen het ceriumgehalte in de plant en de EC, DR, IC en Ca concentraties of met de pH, EC, DR, IC, Cl-, Ca en Mg concentraties in het respectievelijke geval van CeO_2 ENPs of Ce^{3+} ionen.

Vermits de distributie van nanodeeltjes tussen vaste en vloeibare fases in complexe aquatische systemen belangrijke informatie kan verschaffen met betrekking tot hun mobiliteit en mogelijke bio-beschikbaarheid, werd het verdelingsgedrag nagegaan van Ag (14.8 ± 1.3 nm) en CeO_2 (6.2 ± 0.5 nm) ENPs in sedimentsuspensies (**Hoofdstuk 6**) en in bodemsuspensies (**Hoofdstuk 7**) gedurende 24 uur en vergeleken met dat van Ag^+ en Ce^{3+} ionen. Vooral de associatie van deze nanodeeltjes en ionen met sediment- en bodembestanddelen werd bestudeerd. Het werd aangetoond dat na 24 uur nog steeds substantiële fracties van Ag of CeO_2 ENPs konden teruggevonden worden in het supernatans van sediment- en bodemsuspensies en dat deze zilver- of ceriumgehaltes afhankelijk waren van equilibreertijd alsook van de toegepaste centrifugebehandeling. De verschillende centrifugebehandelingen hadden ook een significante impact op gehalte aan gesuspendeerd materiaal (SM) evenals de concentratie aan totaal organische koolstof (TOC) in het supernatans van de verscheidene sediment- en bodemsuspensies. Echter, de verschillende centrifugebehandelingen hadden geen significante invloed op de nanodeeltjes (of ionen) wanneer er geen sediment of bodem aanwezig was (dus in zuiver water), waardoor sediment- en bodemeigenschappen een belangrijke invloed lijken te hebben op hun colloïdale stabiliteit en mobiliteit gedurende 24 uur. Statistisch significante correlaties werden verkregen tussen het zilver- of ceriumgehalte in de vloeistoffase en de concentratie aan SM en TOC, wijzend op sterke interacties tussen de ENPs en natuurlijk colloïdaal sediment- en bodemmateriaal. Verder werd ook duidelijk aangetoond dat NOM CeO_2 ENPs zou kunnen stabilizeren in de waterige fase (**Hoofdstuk 7**). In "natuurlijke" sediment- en bodemsuspensies bleken de Ag^+ en Ce^{3+} ionen sterker te associëren met sediment- of bodembestanddelen in vergelijking met de Ag of CeO_2 ENPs waardoor de nanodeeltjes dus een grotere mobiliteit en mogelijke bio-beschikbaarheid zouden kunnen bezitten. In een "model" systeem (gebruik makend van zuiver kwartszand) daarentegen gedroegen de nanodeeltjes en ionen zich anders. In de aanwezigheid van kwartszand bleken de CeO_2 ENPs namelijk minder mobiel dan Ce^{3+} ionen terwijl er voor Ag ENPs en Ag^+ ionen geen significante verschillen in het verdelingsgedrag waargenomen werden. Het migratiepotentieel van de CeO_2 ENPs lijkt dus hoger te zijn in natuurlijke sedimenten of bodems.

Het injecteren van FeS ENPs in bodems en sedimenten kan gebruikt worden om zware metalen te immobiliseren en deze zodoende onbeschikbaar te stellen voor organismen en planten. Volgens eerdere studies kunnen zulke partikels gecoat worden met carboxymethylcellulose (CMC) om hun fysische stabiliteit, injecteerbaarheid en reactiviteit

te verhogen. De verhoogde mobiliteit van dergelijk deeltjes kan echter ook potentieel resulteren in een verhoogde uitloogbaarheid en co-transport van contaminanten in het milieu in plaats van immobilisatie. In **Hoofdstuk 8** werd daarom via batch en kolomtesten de stabiliteit en het transportgedrag van CMC-FeS ENPs in gecontamineerde bodems en sediment onderzocht, alsook de resulterende mobiliteit van zware metalen. De gesynthetiseerde CMC-FeS ENPs hadden een hydrodynamische diameter van 154.5 ± 5.8 nm en vertoonden een langdurige colloïdale stabiliteit (gedurende meerder weken) indien bewaard onder anaerobe omstandigheden. Zonder CMC werden daarentegen veel grotere (microschaal) FeS deeltjes geproduceerd die binnen luttele minuten aggregeerden en precipiteerden. Batchtesten toonden aan dat de CMC-FeS ENPs een hoge affiniteit bezitten voor metallische contaminanten (bv. Cd, Cr, Cu, Hg, Ni, Pb en Zn) aanwezig in bodems en sediment, alsook een hoge stabiliteit en mogelijke mobiliteit daar batchretentie door de vaste fase laag was (< 37 %). Ook kolomtesten toonden aan dat de CMC-FeS ENPs een hoge mobiliteit bezitten doorheen een zanderige bodem, zelfs zonder gebruik te maken van een externe druk (dus gewoon via gravitationeel percoleren). Er werd een maximale doorbraak van de nanodeeltjes waargenomen na respectievelijk *ca.* 10 of 16 porievolumes (PVs) in het geval van 83.3 of 500 mg L^{-1} CMC-FeS ENPs. Bovendien bleek slechts 7 % van de ENPs weerhouden te zijn geworden na het percoleren van in totaal 22.7 PVs. Gelijktijdige elutie van sporenelementen wees uit dat respectievelijk tot 19, 8.7, of 11 % van het oorspronkelijk aanwezige gehalte aan Cd, Pb, of Zn uitgeloogd was uit de bodem na 22.7 PVs, waarbij initiële piekconcentraties voorkwamen gedurende de eerste 5 tot 10 PVs. Via filtratie van de percolaten over 0.10 μm filters (die ongeveer 98 % van de CMC-FeS ENPs weerhielden) werd verder ook aangetoond dat de overgrote meerderheid van de geëxtraheerde metalen geassocieerd was met de nanopartikels en dus niet voorkwam in opgeloste vorm. De hoge affiniteit van CMC-FeS ENPs voor metalen combinatie met de waargenomen hoge stabiliteit en mobiliteit suggereren dat associatie van sporenmetalen met de nanodeeltjes mogelijk tot contaminant co-transport kan leiden in het milieu in het geval dat er milieucondities heersen die colloïdaal transport mogelijk maken.

In **Hoofdstuk 9** werden geautomatiseerde biogeochemische microkosmos opstellingen aangewend om het verdelingsgedrag van Ag ENPs (*ca.* 40 nm) en Ag^{+} ionen te onderzoeken in suspensies van veld-geïncubeerd sediment onder gecontroleerde redoxomstandigheden gedurende 8 d. Vooral de mogelijke implicaties die het gebruik van vers veld-geïncubeerd sediment in vergelijking met voorbereid gedroogd sediment met zich meebrengt op het gedrag van de nanodeeltjes werden bestudeerd. Verder werden ook de impact van

redoxconditie en het effect van deeltjeseigenschappen (zijnde een citraat (Cit) of polyvinylpyrrolidon (PVP) oppervlaktecoating) op het verdelingsgedrag van zilver onderzocht. Het aanwenden van vers sediment dat geïncubeerd werd in het veld onder aerobe of anaerobe omstandigheden bleek een significante impact te hebben op het resulterende verdelingsgedrag van zilver in sedimentsuspensies. Het gebruik maken van gedroogd sediment resulteerde namelijk in lage relatieve zilvergehaltes (< 4.4 %) die achterbleven in de vloeistoffase van sedimentsuspensies gedurende het volledige 24 uur durende experimentele tijdsverloop. Daarentegen werden tot 72 uur na aanvang van de experimenten met vers aeroob sediment nog aanzienlijk grotere zilverfracties teruggevonden in de vloeistoffase (tot 22 %), of in het geval van vers anaeroob sediment zelfs tot aan het einde van de testen (tot 25 % na 192 uur). Dit suggereert een hogere colloïdale stabiliteit en potentiële bio-beschikbaarheid in de aanwezigheid van vers sediment. Verder bleken voorgedefinieerde redoxcondities geen significante impact te hebben op het verdelingsgedrag van zilver in het geval van de behandelingen met gedroogd sediment, in tegenstelling tot het aanwenden van vers aeroob en anaeroob sediment waar respectievelijk een afname en toename van het zilvergehalte in de vloeistoffase werd waargenomen in functie van de tijd. Over het algemeen werden geen substantiële in het gedrag van de verschillende zilverspecies waargenomen (behalve voor Cit-Ag ENPs tijdens de behandelingen met vers aeroob sediment), waardoor de impact van deeltjeseigenschappen (bv. het type van oppervlaktecoating) van ondergeschikt belang was op de mate van zilververwijdering vanuit de waterige fase, ten minste voor de geteste experimentele omstandigheden.

Een selectie van factoren (deeltjeseigenschappen en milieuparameters) die gedurende dit doctoraatsonderzoek geïdentificeerd werden als parameters die mogelijk het gedrag van metallische ENPs in complexe (natuurlijke) aquatische matrices kunnen beïnvloeden, werd bondig besproken in **Hoofdstuk 10**. Verder werden ook de belangrijkste conclusies evenals enkele potentiële onderzoeksperspectieven voor de toekomst opgesomd, gebaseerd op de ervaringen en inzichten vergaard gedurende het verloop van deze studie.

Curriculum vitae

Personal information

Full name	Van Koetsem, Frederik
Address	Schriek 350
	2180 Ekeren, Antwerpen (Belgium)
Telephone	+32 (0) 486 77 47 70
E-mail	Frederik.VanKoetsem@UGent.be
	frederik.vankoetsem@gmail.com
Date of birth	2 September 1983
Place of birth	Brasschaat (Belgium)
Nationality	Belgian

Education

2004 – 2007	Bachelor in Chemistry: Process Technology
	Karel de Grote University College, Hoboken, Antwerp (Belgium)
2006 – 2007	Internship at BASF Antwerp in completion of Bachelor's thesis
Topic:	*"Optimization of the distillative separation of benzene, toluene, and ethyl benzene"*
2007 – 2008	Bachelor of Science (**BSc**) in Applied Chemical Engineering
	Karel de Grote University College, Hoboken, Antwerp (Belgium)
2008 – 2009	Master of Science (**MSc**) in Applied Chemical Engineering
	Karel de Grote University College, Hoboken, Antwerp (Belgium)
2008 – 2009	Internship at Bayer Antwerp NV in completion of Master's thesis
Topic:	*"Simulation of the debottlenecking of the adiabatic aniline production process"*
2010 – Present	Doctor (**PhD**) in Applied Biological Sciences
	Ghent University, Faculty of Bioscience Engineering, Department of Applied Analytical and Physical Chemistry, Laboratory of Analytical Chemistry and Ecochemistry, Ghent (Belgium)
Topic:	*"Identification of factors affecting the physicochemical behaviour and fate of engineered metallic nanoparticles released into aquatic environments"*

Professional activities during PhD research

Tutor of 11 thesis students

Langebein, M., Van Geert, Y., Van Hauwermeiren, D., and Vos, P. (2012). **Vergelijking van saneringsopties voor kwikvervuilde bodems.** Project report submitted in partial fulfilment of the requirements for the degree of Bachelor of Science in Bioscience Engineering, Ghent University, Ghent, Belgium, pp. 48.

Geremew, T.T. (2012). **Physicochemical fate of engineered metallic nanoparticles in aquatic environments.** Thesis submitted in partial fulfilment of the requirements for the degree of Master of Science in Environmental Sanitation, Ghent University, Ghent, Belgium, pp. 70.

Woldetsadik, G.S. (2012). **Fate of metallic nanoparticles in soils and their applicability as nanocatalyst in environmental remediation.** Thesis submitted in partial fulfilment of the requirements for the degree of Master of Science in Environmental Sanitation, Ghent University, Ghent, Belgium, pp. 62.

Verstraete, S. (2013). **Fysicochemisch gedrag van metallische nanopartikels in oppervlaktewater.** Thesis submitted in partial fulfilment of the requirements for the degree of Master of Science in Bioscience Engineering: Environmental Technology, Ghent University, Ghent, Belgium. pp. 83.

Van Havere, L. (2013). **Synthese en gedrag van carboxymethylcellulose FeS nanopartikels en hun toepasbaarheid in bodemsanering.** Thesis submitted in partial fulfilment of the requirements for the degree of Master of Science in Bioscience Engineering: Environmental Technology, Ghent University, Ghent, Belgium, pp. 83.

Xiao, Y. (2013). **Metal-based engineered nanoparticles in treatment wetlands: interactions with aquatic macrophytes and impact on the performance of microbial communities.** Thesis submitted in partial fulfilment of the requirements for the joint academic degree of International Master of Science in Environmental Technology and Engineering, Ghent University, Ghent, Belgium, pp. 76.

Sultana, U.T. (2013). **Removal of arsenic from water by application of cerium oxide (CeO_2) engineered nanoparticles.** Thesis submitted in partial fulfilment of the requirements for the joint academic degree of International Master of Science in Environmental Technology and Engineering, Ghent University, Ghent, Belgium, pp. 57.

Bai, Y. (2014). **Potential of conventional treatment processes for removal of metallic nanoparticles in drinking water production.** Thesis submitted in partial fulfilment of the requirements for the joint academic degree of International Master of Science in Environmental Technology and Engineering, Ghent University, Ghent, Belgium, pp. 83.

External jury member of the evaluation committee of 2 thesis defences

Asere, T.G. (2013). **Exploring potential environmental applications of selenium nanoparticles.** Thesis submitted in partial fulfilment of the requirements for the joint academic degree of International Master of Science in Environmental Technology and Engineering, Ghent University, Ghent, Belgium, pp. 61.

Jingyue, T. (2013). **Use of biomaterials for removal of platinum compounds from aqueous systems.** Thesis submitted in partial fulfilment of the requirements for the joint academic degree of International Master of Science in Environmental Technology and Engineering, Ghent University, Ghent, Belgium, pp. 45.

Institutional contributions

Gave a presentation entitled "**Identification of factors affecting physicochemical fate of metallic nanoparticles in aquatic environments**" at a PhD research seminar for visiting Russian Professors, Faculty of Bioscience Engineering, Ghent University, Ghent, Belgium, 24 February 2011.

Gave a lecture entitled "**An introductory view on the physical and chemical analysis of Nanomaterials**" at IMETE Summer School 2013, Advanced course on nanotechnology for water treatment, Faculty of Bioscience Engineering, Ghent University, Ghent, Belgium, 9 – 13 September 2013.

Presented a poster entitled "**Nanotechnology and its potential impact on the environment**" at FBE Open House 2013, Faculty of Bioscience Engineering, Ghent University, Ghent, Belgium, 2 March 2013.

Assisted in the organization and supervision of several practical courses such as **Inorganic Chemistry: Instrumental Analysis, Analysis of Trace Elements and Isotopes, Soil Chemistry,** and during **IMETE Summer School 2013,** Faculty of Bioscience Engineering, Ghent University, Ghent, Belgium.

Other

Acted as a Belgian delegate (substituting Prof. G. Du Laing) at the **1st Meeting of the Management Committee of COST Action ES 1205: The transfer of engineered nanomaterials from wastewater treatment and storm water to rivers,** COST Office, Brussels, Belgium, 5 April 2013.

Publications

Van Koetsem, F., and Du Laing, G. (2013). **Partitioning and dissolution behavior of metal-based engineered nanoparticles in sediment and soil suspensions.** E3S Web of Conferences 1, 16003, pp. 1-3, *DOI: 10.1051/e3sconf/20130116003.*

Van Koetsem, F., and Du Laing, G. (2013). **Partitioning behavior of Ag and CeO_2 engineered nanoparticles in soil suspensions.** In: Selim, M., and Seaman, J. (Eds.), ICOBTE 2013 Proceedings of the International Conference on the Biogeochemistry of Trace Elements, 20-00247, pp. 307-308.

Van Koetsem, F., Geremew, T.T., Wallaert, E., Verbeken, K., Van der Meeren, P., and Du Laing, G. (in press). **Fate of engineered nanomaterials in surface water: Factors affecting interactions of Ag and CeO_2 nanoparticles with (re)suspended sediments.** Ecol. Eng., *DOI: 10.1016/j.ecoleng.2014.07.024.*

Van Koetsem, F., Rinklebe, J., and Du Laing, G. (in press). **Analysis and fate of metal-based engineered nanoparticles in aquatic environments, wetlands and floodplain soils.** In: Rinklebe, J. (Ed.), Trace elements in waterlogged soils and sediments. CRC Press, Taylor & Francis Group, Boca Raton, FL, USA.

Van Koetsem, F., Woldetsadik, G.S., and Du Laing, G. **Fate of Ag and CeO_2 engineered nanoparticles and effect of NOM on CeO_2 nanoparticles stability in soil suspensions.** Submitted for publication in *Environ. Technol. Innov.*

Van Koetsem, F., Verstraete, S., Wallaert, E., Verbeken, K., Van der Meeren, P., and Du Laing, G. **Use of filtration techniques to study environmental fate of engineered metallic nanoparticles: Factors affecting filter performance.** Submitted for publication in *J. Nanopart. Res.*

Van Koetsem, F., Verstraete, S., Van der Meeren, P., and Du Laing, G. **Stability of engineered nanomaterials in aqueous matrices: Settling behaviour of CeO_2 engineered nanoparticles in natural surface waters.** Submitted for publication in *Environ. Res.*

Van Koetsem, F., Van Havere, L., and Du Laing, G. **Impact of carboxymethyl cellulose coating on iron sulphide nanoparticles stability, transport, and mobilization potential of trace metals present in soils and sediment.** Submitted for publication in *J. Environ. Manage.*

Van Koetsem, F., Xiao, Y., Luo, Z., and Du Laing, G. **Impact of water composition on association of Ag and CeO_2 nanoparticles with aquatic macrophyte *Elodea canadensis*.** Submitted for publication in *Environ. Sci. Pollut. Res.*

Van Koetsem, F., Frohne, T., Rinklebe, J., and Du Laing, G. (in prep.). **Partitioning behaviour and fate of Ag nanoparticles in (re)suspended field-incubated sediment under controlled aerobic conditions.**

Van Koetsem, F., Frohne, T., Rinklebe, J., and Du Laing, G. (in prep.). **Partitioning behaviour and fate of Ag nanoparticles in suspensions of field-incubated sediment under controlled anaerobic and aerobic conditions.**

Conference, workshop, and seminar contributions

Oral or poster presentations

ICEENN 2012, 7th International Conference on the Environmental Effects of Nanoparticles and Nanomaterials, The Banff Centre, Banff, Alberta, Canada, 10 – 12 September 2012.

ICHMET 2012, 16th International Conference on Heavy Metals in the Environment, Angelicum Congres Centre, Rome, Italy, 22 – 27 September 2012.

ICOBTE 2013, 12th International Conference on the Biogeochemistry of Trace Elements, UGA Conference Centre, Athens, Georgia, USA, 16 – 20 June 2013.

WETPOL 2013, 5th International Symposium on Wetland Pollutant Dynamics and Control, la Cité Nantes Events Center, Nantes, France, 13 – 17 October 2013.

Other

Laborama 2011, Trade Show for Laboratory Professionals, Brussels Kart Expo, Groot-Bijgaarden, Belgium, 25 March 2011.

ICEENN 2011, 6th International Conference on the Environmental Effects of Nanoparticles and Nanomaterials, The Royal Society, London, UK, 19 – 21 September 2011.

Waters Consumables - de nieuwste ontwikkelingen, Seminar, Holiday Inn Gent Expo, Ghent, Belgium, 5 October 2011.

Thermo Scientific User Meetings, ICP-MS Seminar, Business Faculty, Neder-over-Heembeek, Brussels, Belgium, 25 November 2011.

BMG Theme Night, Membrane filtration and Particles Separation Seminar, Faculty of Bioscience Engineering, Ghent University, Ghent, Belgium, 28 March 2012.

Awards

Student Travel Award, 7th International Conference on the Environmental Effects of Nanoparticles and Nanomaterials, The Banff Centre, Banff, Alberta, Canada, 10 – 12 September 2012.

Stays abroad

University of Aveiro, NANOTOX 2012, SETAC Summer School Course, Advanced Workshop Studies in Biology and Applied Biosciences, Implications of Nanomaterials: A hands on course on synthesis, characterization, and ecotoxicology, 4th edition, Department of Biology and CESAM, Aveiro, Portugal, 28 May – 1 June 2012.

University of Wuppertal, Collaborative scientific research project to study the fate and behaviour of silver nanoparticles in (re)suspended sediments under selected physicochemical conditions utilizing custom-built automated biogeochemical microcosm set-ups, Department D, Soil- and Groundwater-management, Wuppertal, Germany, March – June 2014.

Appendices

Appendix A

Standard procedures for the physicochemical characterization analysis of sediments and soils

Unless stated otherwise, the Manual for the Soil Chemistry and Fertility Laboratory (Van Ranst *et al.*, 1999) was employed as a reference guide for the determination of the physicochemical characteristics of sediments or soils, as described in the following sections. All glassware and recipients were subsequently washed in a laboratory dishwasher, soaked in diluted nitric acid (10 %), and thoroughly rinsed with deionized water, prior to being utilized. All chemical reagents used were of analytical grade.

pH

pH-H_2O

About 50 mL of Milli-Q® water (18.2 MΩ cm^{-1}) (EMD Millipore Corp., Billerica, MA, USA) was added to a 50 mL glass beaker containing 10 g of sediment or soil, and after stirring with a glass rod, the resulting suspensions were allowed to equilibrate for 16 h. Afterwards, the pH was measured using a model 520A pH meter (Orion Research Inc., Boston, MA, USA).

pH-KCl

The pH-KCl of sediments and soils was determined in a comparable manner as the pH-H_2O value, with the exception that 25 mL 1 M KCl was used instead of 50 mL Milli-Q® water, and that the equilibration time was only 10 min.

pH-$CaCl_2$

The determination of the pH-$CaCl_2$ value of sediments and soils was again similar to the previously described pH values, except that 25 mL 0.01 M $CaCl_2$ was utilized and that the suspensions were allowed to equilibrate for 30 min.

Dry matter (DM)

The DM content was determined by drying 100 g (air-)dried soil or sediment in an oven at 105 °C for 24 h, and recording the mass difference before and after drying.

Electrical conductivity (EC)

Suspensions were prepared in a 1:5 (m:V) ratio by adding 50 mL Milli-Q® water into 250 mL Erlenmeyer flasks containing 10 g soil or sediment, and shaken for 60 min on an orbital shaker, before being filtered using ashless filter paper (MN 640 m, Macherey-Nagel GmbH & Co. KG, Düren, Germany). The EC was measured in the resulting filtrates immediately using a type LF537 conductivity meter (WTW, Weilheim, Germany).

Chlorides (Cl^-)

To determine the chloride content, 1:5 (m:V) suspensions were prepared by adding 50 mL 0.15 M HNO_3 to 10 g sediment or soil in an Erlenmeyer flask, and shaking the mixtures for 30 min on an orbital shaker. The suspensions were then filtered over ashless MN 640 m filter paper, and the resulting filtrates were titrated with 0.05 M $AgNO_3$ potentiometric end-point detection using a titration instrument (718 STAT Titrino, Metrohm AG, Herisau, Switzerland).

Total nitrogen (TN)

A modified Kjeldahl method was employed in the determination of the TN content in sediment or soil samples. For this, 1 g sediment or soil and 7 mL of a combined reagent of sulphuric and salicylic acid (*i.e.*, 50 g salicylic acid in 1 L 95 – 97 % H_2SO_4) were transferred into glass Kjeldahl digestion flasks, and the mixtures were allowed to react for 30 min. Afterwards, 0.5 g $Na_2S_2O_3.5H_2O$ was added, and the samples were allowed to react for an additional 15 min before consecutively adding 5 mL 95 – 97 % H_2SO_4, 0.2 g of digestion catalyst (*i.e.*, 100 g K_2SO_4, 20 g $CuSO_4$, and 2 g Se), and 4 mL 30 % H_2O_2. The samples were then digested at 380 °C for at least 1 h until a clear solution was obtained. After allowing the samples to cool down to room temperature, 30 mL Milli-Q® water was added and the

solutions were stirred. Subsequently, *ca.* 50 mL 30 % (m:V) NaOH was added to convert the ammonium (NH_4^+) originating from N-containing compounds in the sediment or soil to volatile ammonia (NH_3), and each sample was distilled via a Vapodest Kjeldahl distillation system (Gerhardt GmbH & Co. KG, Königswinter, Germany). The distilled ammonia was recovered in boric acid, which was then titrated with 0.01 M HCl using a titration apparatus (718 STAT Titrino).

Total phosphorous (TP)

To determine the TP content in sediments and soils, the colorimetric method of Scheel was applied. Firstly, 2.5 mL Milli-Q® water and 10 mL *aqua regia* (*i.e.*, 7.5 mL 37 % HCl and 2.5 mL 65 % HNO_3) were added to 1 g sediment or soil, and the samples were allowed to react at room temperature under a fume hood overnight. Afterwards, each sample was digested for 2 h on a hot plate at 150 °C under reflux by using a beaker and a watch glass. After cooling down sufficiently, the samples were filtered using acid-resistant MN 640 m filter paper into 50 mL volumetric flasks. After dilution with Milli-Q® water, 1 mL from the filtrates was transferred into test tubes and 5 mL Milli-Q® water, 1 mL Scheel solution I (*i.e.*, 1 g 4-(methylamino)phenol sulphate, 5 g $Na_2SO_3.7H_2O$, and 150 g $NaHSO_3$ in 1 L Milli-Q® water), and 1 mL Scheel solution II (*i.e.*, 50 g $(NH_4)_6Mo_7O_{24}.4H_2O$ and 140 mL 95 – 97 %. H_2SO_4 in 1 L Milli-Q® water) was added, successively. Each mixture was then homogenized by shaking manually and was allowed to react for 15 min, before 2 mL Scheel solution III (*i.e.*, 205 g sodium acetate in 1 L Milli-Q® water) was added. Afterwards, each mixture was shaken again and allowed to react for an additional 15 min, before the absorbance at 700 nm was measured using a Jenway 6400 spectrophotometer (Bibby Scientific Ltd., Staffordshire, UK).

Total carbonate ($CaCO_3$)

The determination of the amount of $CaCO_3$ present in sediments and soils is based on the acid-base reaction A.1. First, 25 mL 0.25 M H_2SO_4 (excess) and 125 mL Milli-Q® water was added to 1 g sediment or soil in a 250 mL Erlenmeyer flask. Each sample was allowed to react for 1 h in a water bath at 90 °C. After allowing the samples to cool down to room temperature, about 0.5 mL of mixed indicator solution (*i.e.*, 100 mL phenolphthalein solution (1 g in 100 mL 96 % ethanol), 60 mL methyl red solution (0.1 g in 100 mL 96 %

ethanol), and 40 mL bromocresol green solution (0.04 g in 80 mL Milli-Q® water + 5.7 mL 0.01 M NaOH)) was added, and the excess acid was back-titrated with 0.5 M NaOH using a 718 STAT Titrino titration system.

$$CaCO_3 + H_2SO_4 \rightleftharpoons CaSO_4 + CO_2 + H_2O \qquad \textbf{(A.1)}$$

Cation exchange capacity (CEC) at pH 7

A three-step procedure was utilized to determine the CEC of sediment and soil samples was with ammonium acetate at pH 7: *(1) extraction of exchangeable bases by saturation of the adsorption complex with NH_4^+ ions, (2) eliminating the excess ammonium solution by washing with ethanol, and (3) quantitative analysis of sorbed NH_4^+ ions after desorption by K^+ ions.* Therefore, 150 mL 1 M ammonium acetate was percolated through a glass percolation column containing a mixture of 5 g sediment or soil and 12.5 g quartz sand in between 2 layers of 5 g quartz sand. Then, 150 mL denatured ethanol was passed through the column, washing away the excess ammonium filling up the pore voids. The sorbed exchangeable NH_4^+ ions were then eluted with 250 mL 1 M KCl solution, and these final percolates were collected in 250 mL volumetric flasks. Afterwards, 50 mL of the KCl extracts were transferred into Kjeldahl distillation receptacles, and after addition of a spoonful of MgO, the extracts were distilled immediately by means of a Vapodest Kjeldahl distillation system and the obtained distillates were titrated with 0.01 M HCl using a 718 STAT Titrino titrating instrument (*cf.* Section Total Nitrogen).

Main and trace elements

For the pseudo-total analysis of main and trace elements (*e.g.*, Ag, Al, As, Ca, Cd, Ce, Co, Cr, Cu, Fe, K, Mg, Mn, Na, Ni, Pb, S, Se, and Zn), 1 g sediment or soil was first digested by wetting the samples with 2.5 mL Milli-Q® water, adding 10 mL *aqua regia* (*i.e.*, 7.5 mL 37 % HCl and 2.5 mL 65 % HNO_3), allowing the samples to react for 12 h under a fume hood, and boiling them during 2 h at 150 °C on a hotplate under reflux using beakers covered with watch glasses. Afterwards, each sample was allowed to cool down to room temperature before being filtered over acid-resistant MN 640 m ashless filter paper into 50 mL volumetric flasks. Finally, the resulting filtrates were diluted with Milli-Q® water and were analysed by

means of inductively coupled plasma optical emission spectrometry (ICP-OES) (Vista-MPX CCD Simultaneous ICP-OES, Agilent Technologies, Santa Clara, CA, USA).

Particle size analysis

The texture of sediments and soils was determined according to the Bouyoucos hydrometer method (Gee *et al.*, 1986; van Reeuwijk, 2002; Sartori *et al.*, 2013). Briefly, 40 g of sediment or soil was pre-treated with H_2O_2 to oxidize and remove organic matter. The samples were then dispersed by quantitatively transferring the pre-treated sediments or soils into 1 L sealable plastic recipients, adding 100 mL dispersing agent (*i.e.*, 40 g $(NaPO_3)_6$ and 10 g Na_2CO_3 in 1 L Milli-Q® water) and 250 mL Milli-Q® water, and shaking the samples thoroughly overnight using an orbital shaker. The dispersed samples were then transferred into 1 L glass sedimentation cylinders, and Milli-Q® water was added to the 1 L mark, where after the samples were allowed to equilibrate thermally in a water bath at 20 °C. Afterwards, the sedimentation cylinders were capped with rubber stoppers, shaken thoroughly by hand, and placed back in the water bath, before a number of density readings were performed at 20 °C over a 24 h period using standard ASTM 152H hydrometers. The resulting readings were used to determine the sand (*i.e.*, between 2 mm and 50 μm), silt (*i.e.*, between 50 μm and 2 μm) and clay (*i.e.*, < 2 μm) fractions of the different sediment and soil samples.

Appendix B

Supplementary information to Chapter 4

"Stability of engineered nanomaterials in complex aqueous matrices: Settling of CeO_2 nanoparticles in natural surface waters"

Sorption onto the inner walls of settling recipients

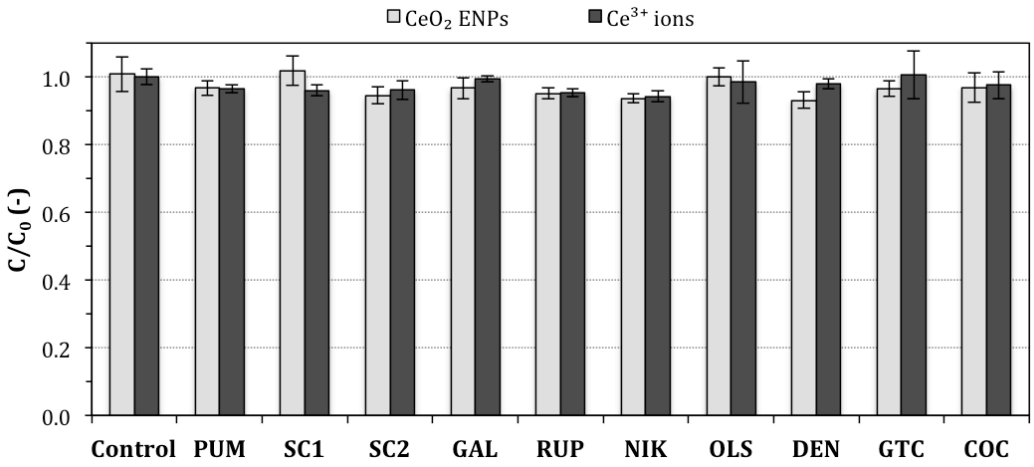

Figure B.1 – Relative cerium content remaining in solution after spiking 10 different natural surface waters as well as Milli-Q® water (Control) with 5 mg L^{-1} CeO_2 ENPs or Ce^{3+} ions, and incubating the samples for 7 d under isothermal conditions (4 – 6 °C). Samples were shaken vigorously prior to determining the initial cerium concentration (C_0) and the cerium concentration after 7 d (C). (Bars represent mean values, error bars denote standard deviations, n = 3)

Settling of CeO_2 ENPs in natural surface waters

Figure B.2 depicts the experimental data as well as the modelled regression curves describing the time-dependent depletion of 5 mg L^{-1} CeO_2 ENPs or Ce^{3+} ions in 10 different natural surface waters during 7 d. The model $\frac{C_t}{C_0} = \left(1 - \frac{C_{res}}{C_0}\right) e^{-k_{sed}t} + \frac{C_{res}}{C_0}$ was fitted to the observed settling data by means of non-linear least squares regression.

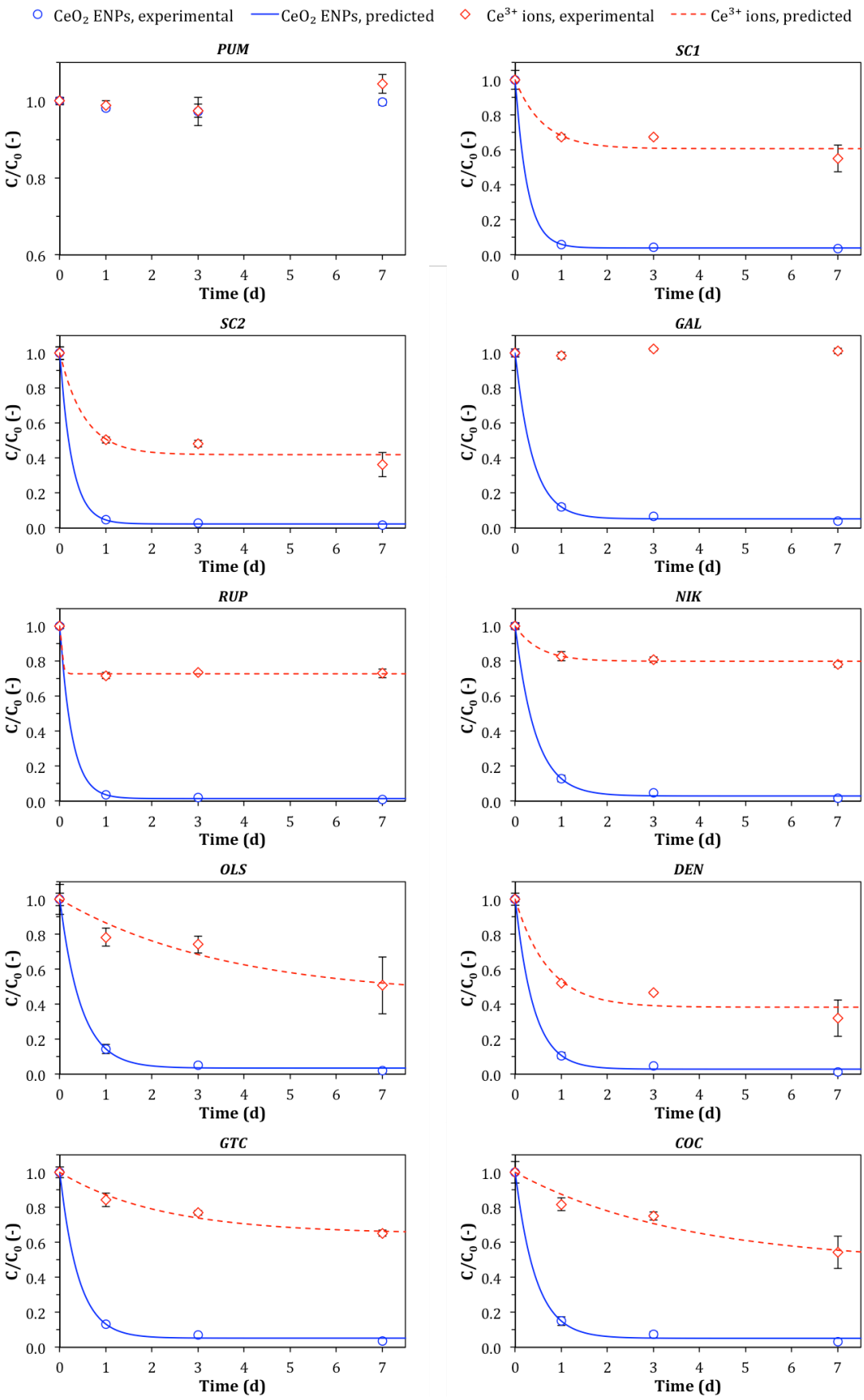

Figure B.2 – Time-dependent depletion of 5 mg L^{-1} CeO_2 ENPs or Ce^{3+} ions in 10 distinct surface waters. (Data points represent mean values, error bars indicate standard deviations, n = 3)

Appendix C

Supplementary information to Chapter 5

"Impact of water composition on association of Ag and CeO_2 nanoparticles with aquatic macrophyte *Elodea canadensis*"

Nanoparticle characterization

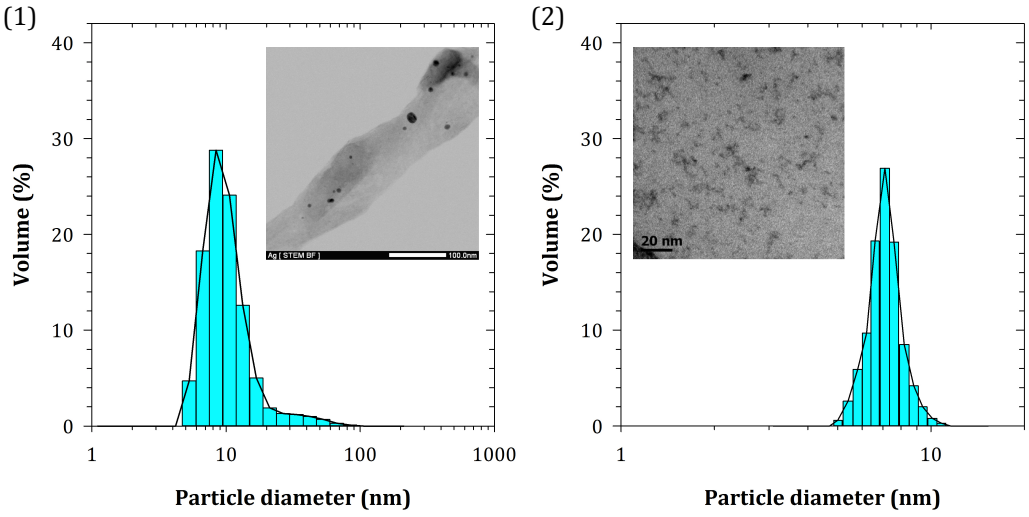

Figure C.1 – Volume weighted particle size distribution of Ag ENPs (1) and CeO_2 ENPs (2) dispersed in Milli-Q® water, obtained through PCS measurements. The insets in (1) and (2) display the corresponding TEM images.

Plant analysis

Total phosphorus (TP) determination

After acid digestion of the harvested *E. canadensis* plants, the samples were diluted with Milli-Q® water and 1 mL was transferred into test tubes. Successively, 5 mL Milli-Q® water, 1 mL Scheel solution I (*i.e.*, 1 g 4-(methylamino)phenol sulphate, 5 g $Na_2SO_3.7H_2O$, and 150 g $NaHSO_3$ in 1 L Milli-Q® water), and 1 mL Scheel solution II (*i.e.*, 50 g $(NH_4)_6Mo_7O_{24}.4H_2O$ and 140 mL 95 – 97 %. H_2SO_4 in 1 L Milli-Q® water) was added. Each mixture was homogenized by shaking manually and was allowed to react for 15 min, before 2 mL Scheel solution III (*i.e.*, 205 g sodium acetate in 1 L Milli-Q® water) was added. Afterwards, each mixture was

shaken again and allowed to react for an additional 15 min. Finally, the absorbance at 700 nm was measured using a Jenway 6400 spectrophotometer (Bibby Scientific Ltd., Staffordshire, UK).

Total nitrogen (TN) determination

Approximately 0.1 g dried plant material was transferred into glass digestion flasks, 7 mL of a combined reagent of sulphuric and salicylic acid (*i.e.*, 50 g salicylic acid in 1 L 95 – 97 % H_2SO_4) was added, and the mixtures were allowed to react for 30 min. Then, 0.5 g $Na_2S_2O_3.5H_2O$ was added, and after allowing the samples to react for an additional 15 min, 5 mL 95 – 97 % H_2SO_4 together with 0.2 g digestion catalyst (*i.e.*, 100 g K_2SO_4, 20 g $CuSO_4$, and 2 g Se) and 4 mL 30 % H_2O_2 was added. Each mixture was then digested at 380 °C for at least 1 h until a clear solution was obtained. After allowing the samples to cool down to room temperature, 30 mL Milli-Q® water was added and the solutions were stirred. Subsequently, 50 mL 30 % (m:V) NaOH was added to convert ammonium (NH_4^+) to volatile ammonia (NH_3), and each mixture was distilled using a Vapodest Kjeldahl distillation system (Gerhardt GmbH & Co. KG, Königswinter, Germany), where after the distilled ammonia was fixated in boric acid. Finally, a titration apparatus (718 STAT Titrino, Metrohm AG, Herisau, Switzerland) was used to titrate the distillates with 0.01 M HCl.

Chlrophyll (Chl) a, b, and c determination

After harvesting, about 0.5 g of fresh plant material was weighed into 50 mL centrifuge tubes, which were covered with aluminium foil to avoid exposure to light, and 15 mL aqueous acetone solution (*i.e.*, 90 % acetone and 10 % saturated magnesium carbonate solution (1 g $MgCO_3$ in 100 mL Milli-Q® water)) was added. The samples were then macerated with a tissue grinder and allowed to steep in the dark at 4 °C in a refrigerator for at least 2h. Afterwards, all samples were centrifuged at 3000 rpm (*i.e.*, 1660 *g*) for 15 min and 3 mL of each clarified extract was transferred into a 1 cm cuvette, where after the optical density (*i.e.*, the absorbance) of each sample extract at 750, 664, 647, and 630 nm was determined using a spectrophotometer. The optical density readings at 664, 647, and 630 nm are used to determine Chl *a*, *b*, and *c*, respectively, while the readings at 750 nm are used as a correction for sample turbidity. Equations C.1 to C.3 are applied to calculate the chlorophyll *a*, *b*, and *c* content in the extracts.

$$Chl_a = 11.85 \times (OD_{664}) - 1.54 \times (OD_{647}) - 0.08 \times (OD_{630}) \quad \textbf{(C.1)}$$

$$Chl_b = 21.03 \times (OD_{647}) - 5.43 \times (OD_{664}) - 2.66 \times (OD_{630}) \quad \textbf{(C.2)}$$

$$Chl_c = 24.52 \times (OD_{630}) - 7.60 \times (OD_{647}) - 1.67 \times (OD_{664}) \quad \textbf{(C.3)}$$

where Chl_a, Chl_b, and Chl_c [mg L^{-1}] are the concentrations of chlorophyll *a*, *b*, and *c*, respectively, and OD_{664}, OD_{647}, and OD_{630} [-], are the corrected (*i.e.*, after subtraction of the readings at 750 nm) optical density readings at 664, 674, and 630 nm, respectively.

Ag and CeO_2 ENPs dose effects on *E. canadensis*

Table C.1 – Impact of Ag ENPs or Ag^+ ions dose on *E. canadensis* biomass (ΔFW), TP, TN, and Chl *a*, *b*, and *c* content after 72 h of exposure. Data is presented as mean ± standard deviation (n = 5 for ΔFW, n = 3 for TP, and n = 2 for TN and Chl). Different letters indicate statistically significant differences ($p < 0.05$) between treatments for each parameter.

	Parameter		Ag ENPs or Ag^+ ions dose					
			0 mg L^{-1}	**0.05 mg L^{-1}**	**0.1 mg L^{-1}**	**0.25 mg L^{-1}**	**0.5 mg L^{-1}**	**1 mg L^{-1}**
Ag ENPs	**ΔFW**	**(%)**	2.1 ± 8.6 ^{a}	0.9 ± 1.6 ^{a}	-0.1 ± 2.7 ^{a}	0.7 ± 2.3 ^{a}	1.5 ± 4.1 ^{a}	0.3 ± 2.3 ^{a}
	TP	**(g kg^{-1} DW)**	7.3 ± 3.2 ^{a}	11.8 ± 0.2 ^{b}	12.2 ± 1.2 ^{b}	11.5 ± 0.2 ^{b}	11.7 ± 0.2 ^{b}	11.9 ± 1.4 ^{b}
	TN	**(g kg^{-1} DW)**	26.6 ± 3.2 ^{a}	39.5 ± 4.8 ^{a}	42.9 ± 5.6 ^{a}	37.8 ± 7.2 ^{a}	43.6 ± 6.1 ^{a}	41.1 ± 1.8 ^{a}
	Chl *a*	**(mg kg^{-1} FW)**	444 ± 20 ^{c}	337 ± 4 ^{b}	345 ± 38 ^{b}	356 ± 50 ^{b}	195 ± 32 ^{a}	206 ± 67 ^{a}
	Chl *b*	**(mg kg^{-1} FW)**	394 ± 15 ^{c}	225 ± 12 ^{b}	256 ± 13 ^{b}	231 ± 48 ^{b}	124 ± 19 ^{a}	163 ± 42 ^{ab}
	Chl *c*	**(mg kg^{-1} FW)**	52 ± 19 ^{b}	15 ± 4 ^{a}	18 ± 3 ^{a}	< 3	< 3	< 3
Ag^+ ions	**ΔFW**	**(%)**	2.1 ± 8.6 ^{a}	-1.5 ± 1.3 ^{a}	2.1 ± 2.7 ^{a}	-2.4 ± 3.1 ^{a}	0.7 ± 2.9 ^{a}	-1.6 ± 2.6 ^{a}
	TP	**(g kg^{-1} DW)**	7.3 ± 3.2 ^{a}	9.2 ± 0.8 ^{ab}	11.9 ± 1.7 ^{ab}	9.8 ± 0.6 ^{ab}	12.1 ± 0.8 ^{ab}	13.9 ± 3.3 ^{b}
	TN	**(g kg^{-1} DW)**	26.6 ± 3.2 ^{a}	30.8 ± 8.5 ^{a}	38.0 ± 3.9 ^{a}	22.3 ± 0.3 ^{a}	34.0 ± 6.1 ^{a}	37.1 ± 4.6 ^{a}
	Chl *a*	**(mg kg^{-1} FW)**	444 ± 20 ^{c}	435 ± 40 ^{c}	204 ± 27 ^{ab}	300 ± 48 ^{b}	220 ± 40 ^{ab}	136 ± 6 ^{a}
	Chl *b*	**(mg kg^{-1} FW)**	394 ± 15 ^{c}	317 ± 63 ^{bc}	127 ± 20 ^{a}	209 ± 54 ^{ab}	132 ± 41 ^{a}	82 ± 11 ^{a}
	Chl *c*	**(mg kg^{-1} FW)**	52 ± 19 ^{b}	31 ± 16 ^{a}	< 3	< 3	< 3	< 3

Data presented as "<" indicate values below the detection limit (DL).

Table C.2 – Impact of CeO_2 ENPs or Ce^{3+} ions dose on *E. canadensis* biomass (ΔFW), TP, TN, and Chl *a*, *b*, and *c* content after 72 h of exposure. Data is presented as mean ± standard deviation (n = 5 for ΔFW, n = 3 for TP, and n = 2 for TN and Chl). Different letters indicate statistically significant differences ($p < 0.05$) between treatments for each parameter.

	Parameter		CeO_2 ENPs or Ce^{3+} ions dose					
			0 mg L^{-1}	**0.5 mg L^{-1}**	**1 mg L^{-1}**	**5 mg L^{-1}**	**10 mg L^{-1}**	**50 mg L^{-1}**
CeO_2 ENPs	**ΔFW**	**(%)**	2.1 ± 8.6 [a]	1.9 ± 3.5 [a]	2.4 ± 1.8 [a]	1.6 ± 3.3 [a]	1.6 ± 4.4 [a]	3.6 ± 5.7 [a]
	TP	**(g kg^{-1} DW)**	7.3 ± 3.2 [a]	8.3 ± 0.8 [a]	7.9 ± 0.9 [a]	8.0 ± 1.0 [a]	8.9 ± 1.0 [a]	8.3 ± 0.6 [a]
	TN	**(g kg^{-1} DW)**	26.6 ± 3.2 [a]	29.1 ± 4.2 [a]	34.3 ± 0.3 [a]	25.5 ± 1.8 [a]	26.8 ± 2.4 [a]	26.5 ± 0.3 [a]
	Chl *a*	**(mg kg^{-1} FW)**	444 ± 20 [a]	393 ± 40 [a]	348 ± 7 [a]	465 ± 34 [a]	458 ± 89 [a]	372 ± 45 [a]
	Chl *b*	**(mg kg^{-1} FW)**	394 ± 15 [a]	289 ± 22 [a]	262 ± 43 [a]	401 ± 33 [a]	402 ± 38 [a]	328 ± 146 [a]
	Chl *c*	**(mg kg^{-1} FW)**	52 ± 19 [a]	29 ± 8 [a]	31 ± 21 [a]	48 ± 28 [a]	67 ± 49 [a]	57 ± 32 [a]
Ce^{3+} ions	**ΔFW**	**(%)**	2.1 ± 8.6 [a]	1.5 ± 4.3 [a]	-1.1 ± 3.8 [a]	0.4 ± 4.1 [a]	2.8 ± 1.3 [a]	-0.5 ± 6.8 [a]
	TP	**(g kg^{-1} DW)**	7.3 ± 3.2 [a]	8.6 ± 1.4 [a]	8.2 ± 1.9 [a]	7.9 ± 0.9 [a]	8.2 ± 0.5 [a]	6.5 ± 1.1 [a]
	TN	**(g kg^{-1} DW)**	26.6 ± 3.2 [a]	30.7 ± 7.6 [a]	29.5 ± 6.6 [a]	26.4 ± 4.5 [a]	20.9 ± 5.8 [a]	35.0 ± 4.2 [a]
	Chl *a*	**(mg kg^{-1} FW)**	444 ± 20 [a]	385 ± 21 [a]	403 ± 24 [a]	377 ± 38 [a]	466 ± 88 [a]	455 ± 46 [a]
	Chl *b*	**(mg kg^{-1} FW)**	394 ± 15 [b]	265 ± 41 [ab]	273 ± 12 [ab]	222 ± 12 [a]	346 ± 74 [ab]	304 ± 60 [ab]
	Chl *c*	**(mg kg^{-1} FW)**	52 ± 19 [a]	19 ± 15 [a]	20 ± 7 [a]	33 ± 9 [a]	37 ± 3 [a]	9 ± 6 [a]

Ag and CeO_2 ENPs depletion in complex aqueous media in the presence of *E. canadensis*

Table C.3 – Change in plant biomass (ΔFW) of *E. canadensis* incubated in different aquatic media during 72 h, with and without (Control) exposure to 0.1 mg L^{-1} Ag ENPs and Ag^{+} ions, or 1 mg L^{-1} CeO_2 ENPs and Ce^{3+} ions (mean ± standard deviation, n = 5). Different letters indicate statistically significant differences ($p < 0.05$) between samples for each treatment, while significant deviations ($p < 0.05$) from the Control for each water sample are also denoted with an asterisk.

	Parameter	Tap water	10 % Hoagland's	MB	GG	CC
Control	**ΔFW (%)**	-1.7 ± 1.8 ^{a}	-0.1 ± 3.7 ^{a}	3.4 ± 5.1 ^{a}	3.9 ± 6.1 ^{a}	5.2 ± 1.7 ^{a}
Ag ENPs	**ΔFW (%)**	3.8 ± 1.6 ^{ab,*}	0.5 ± 3.8 ^{ab}	-0.7 ± 2.6 ^{a}	7.9 ± 4.6 ^{b,*}	5.2 ± 5.9 ^{ab}
Ag^{+} ions	**ΔFW (%)**	0.1 ± 2.6 ^{a}	-2.0 ± 4.1 ^{a}	1.0 ± 3.1 ^{a}	-0.5 ± 2.9 ^{a}	1.0 ± 5.3 ^{a}
CeO_2 ENPs	**ΔFW (%)**	1.3 ± 2.6 ^{a}	3.5 ± 3.4 ^{ab}	2.7 ± 2.1 ^{ab}	5.3 ± 3.6 ^{ab}	7.9 ± 3.3 ^{b}
Ce^{3+} ions	**ΔFW (%)**	0.7 ± 1.5 ^{a}	-2.3 ± 3.4 ^{a}	-0.5 ± 1.2 ^{a}	2.9 ± 2.1 ^{ab}	6.9 ± 5.7 ^{b}

Appendix D

Supplementary information to Chapter 6

"Factors affecting interactions of Ag and CeO_2 nanoparticles with (re)suspended sediments"

Blank sediments

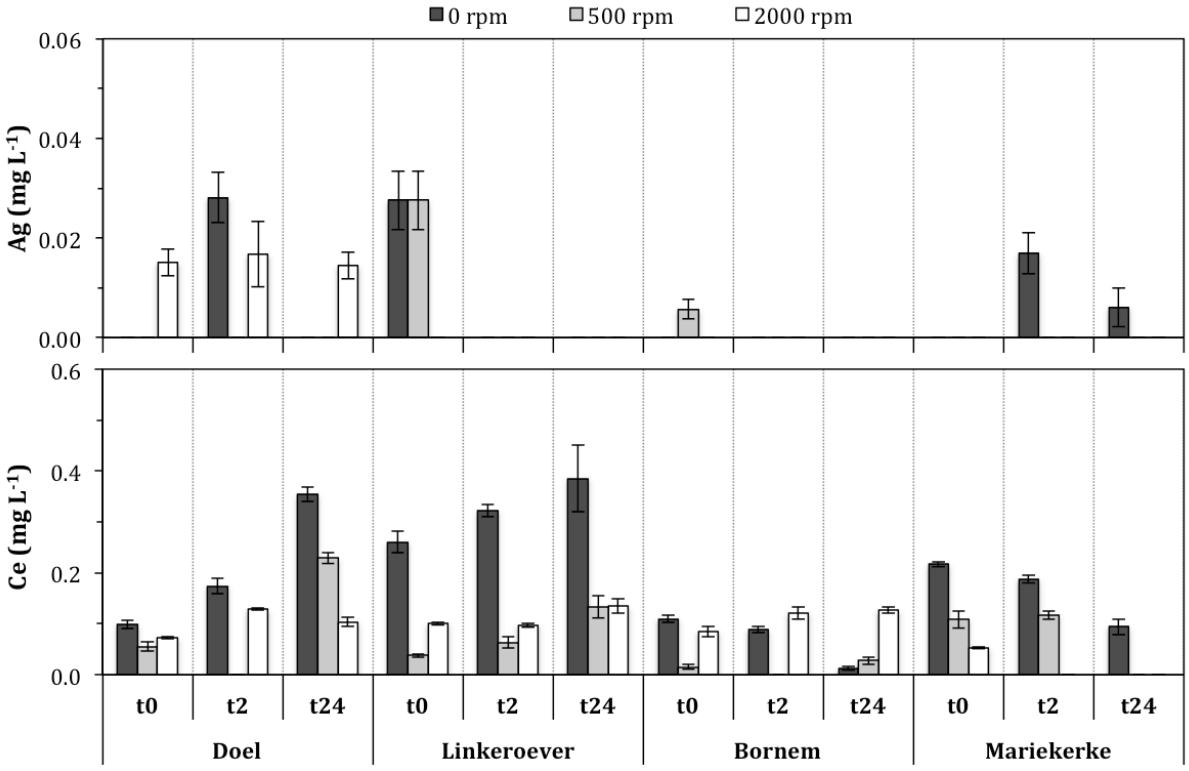

Figure D.1 – Silver (top graph) and cerium (bottom graph) concentrations determined in the liquid phase of blank sediment suspensions, as affected by centrifugation speed, after centrifugation for 10 min. The speed of 0 rpm represents 10 min of gravitational settling. (Data shown are mean values, missing bars denote values below the detection limit (DL_{Ag} = 12 μg L^{-1}; DL_{Ce} = 25 μg L^{-1}), error bars indicate standard deviations, n = 3)

Pearson correlation analysis data

Table D.1 – Pearson correlation analysis results for the relationship between TOC content (*Y*) and amount of suspended matter (*X*), remaining in the liquid phase of blank sediment suspensions.

Sediment	Regression equation	Correlation coefficient (*r*)	Statistical significance (*p*)
Doel	$Y = 101.85\,X - 48.85$	0.999 **	< 0.0005
Linkeroever	$Y = 34.12\,X + 57.26$	0.996 **	< 0.0005
Bornem	$Y = 77.82\,X - 14.13$	0.998 **	< 0.0005
Mariekerke	$Y = 101.85\,X - 48.85$	0.981 **	< 0.0005
OVERALL	$Y = 63.51\,X + 15.00$	0.919 **	< 0.0005

** Correlation is significant at the 0.01 level (2-tailed).

Table D.2 – Pearson correlation analysis results for the relationship between the relative amount of silver (*Y*) and the suspended matter content (*X*), remaining in the liquid phase of sediment suspensions spiked with Ag^+ ions.

Sediment	Regression equation	Correlation coefficient (*r*)	Statistical significance (*p*)
Doel	$Y = 0.039\,X - 0.036$	0.735 *	0.024
Linkeroever	$Y = 0.092\,X + 0.016$	0.970 **	< 0.0005
Bornem	$Y = 0.172\,X - 0.084$	0.979 **	< 0.0005
Mariekerke	$Y = 0.032\,X - 0.017$	0.980 **	< 0.0005
OVERALL	$Y = 0.044\,X + 0.018$	0.612 **	< 0.0005

** Correlation is significant at the 0.01 level (2-tailed).

* Correlation is significant at the 0.05 level (2-tailed).

Table D.3 – Pearson correlation analysis results for the relationship between the relative amount of silver (*Y*) and the suspended matter content (*X*), remaining in the liquid phase of sediment suspensions spiked with Ag ENPs.

Sediment	Regression equation	Correlation coefficient (*r*)	Statistical significance (*p*)
Doel	$Y = 0.105\,X - 0.048$	0.900 **	0.001
Linkeroever	$Y = 0.090\,X + 0.227$	0.895 **	0.001
Bornem	$Y = 0.305\,X - 0.118$	0.992 **	< 0.0005
Mariekerke	$Y = 0.048\,X - 0.003$	0.946 **	< 0.0005
OVERALL	$Y = 0.065\,X + 0.115$	0.434 **	0.008

** Correlation is significant at the 0.01 level (2-tailed).

Table D.4 – Pearson correlation analysis results for the relationship between the relative amount of cerium (*Y*) and the suspended matter content (*X*), remaining in the liquid phase of sediment suspensions spiked with Ce^{3+} ions.

Sediment	Regression equation	Correlation coefficient (*r*)	Statistical significance (*p*)
Doel	$Y = 0.161\,X - 0.118$	0.995 **	< 0.0005
Linkeroever	$Y = 0.160\,X + 0.087$	0.973 **	< 0.0005
Bornem	$Y = 0.111\,X - 0.054$	0.974 **	< 0.0005
Mariekerke	$Y = 0.023\,X - 0.019$	0.989 **	< 0.0005
OVERALL	$Y = 0.083\,X - 0.030$	0.644 **	< 0.0005

** Correlation is significant at the 0.01 level (2-tailed).

Table D.5 – Pearson correlation analysis results for the relationship between the relative amount of cerium (*Y*) and the suspended matter content (*X*), remaining in the liquid phase of sediment suspensions spiked with CeO_2 ENPs.

Sediment	Regression equation	Correlation coefficient (*r*)	Statistical significance (*p*)
Doel	$Y = 0.267\,X - 0.050$	0.994 **	< 0.0005
Linkeroever	$Y = 0.233\,X + 0.207$	0.956 **	< 0.0005
Bornem	$Y = 0.182\,X - 0.049$	0.958 **	< 0.0005
Mariekerke	$Y = 0.108\,X - 0.010$	0.950 **	< 0.0005
OVERALL	$Y = 0.186\,X + 0.070$	0.651 **	< 0.0005

** Correlation is significant at the 0.01 level (2-tailed).

Table D.6 – Pearson correlation analysis results for the relationship between the relative amount of silver (*Y*) and the TOC content (*X*), remaining in the liquid phase of sediment suspensions spiked with Ag^{+} ions.

Sediment	Regression equation	Correlation coefficient (*r*)	Statistical significance (*p*)
Doel	$Y = 0.0004\,X - 0.054$	0.745 *	0.021
Linkeroever	$Y = 0.003\,X + 0.167$	0.961 **	< 0.0005
Bornem	$Y = 0.002\,X - 0.054$	0.993 **	< 0.0005
Mariekerke	$Y = 0.0007\,X - 0.057$	0.985 **	< 0.0005
OVERALL	$Y = 0.0005\,X + 0.033$	0.467 **	0.004

** Correlation is significant at the 0.01 level (2-tailed).

* Correlation is significant at the 0.05 level (2-tailed).

Table D.7 – Pearson correlation analysis results for the relationship between the relative amount of silver (*Y*) and the TOC content (*X*), remaining in the liquid phase of sediment suspensions spiked with Ag ENPs.

Sediment	Regression equation	Correlation coefficient (*r*)	Statistical significance (*p*)
Doel	$Y = 0.001\,X - 0.099$	0.901 **	0.001
Linkeroever	$Y = 0.003\,X + 0.075$	0.900 **	0.001
Bornem	$Y = 0.004\,X - 0.060$	0.982 **	< 0.0005
Mariekerke	$Y = 0.001\,X - 0.069$	0.981 **	< 0.0005
OVERALL	$Y = 0.0008\,X + 0.124$	0.382 *	0.021

** Correlation is significant at the 0.01 level (2-tailed).

* Correlation is significant at the 0.05 level (2-tailed).

Table D.8 – Pearson correlation analysis results for the relationship between the relative amount of cerium (*Y*) and the TOC content (*X*), remaining in the liquid phase of sediment suspensions spiked with Ce^{3+} ions.

Sediment	Regression equation	Correlation coefficient (*r*)	Statistical significance (*p*)
Doel	$Y = 0.002\,X - 0.041$	0.994 **	< 0.0005
Linkeroever	$Y = 0.005\,X + 0.349$	0.966 **	< 0.0005
Bornem	$Y = 0.001\,X - 0.035$	0.988 **	< 0.0005
Mariekerke	$Y = 0.005\,X - 0.045$	0.962 **	< 0.0005
OVERALL	$Y = 0.001\,X + 0.025$	0.595 **	< 0.0005

** Correlation is significant at the 0.01 level (2-tailed).

Table D.9 – Pearson correlation analysis results for the relationship between the relative amount of cerium (*Y*) and the TOC content (*X*), remaining in the liquid phase of sediment suspensions spiked with CeO_2 ENPs.

Sediment	Regression equation	Correlation coefficient (*r*)	Statistical significance (*p*)
Doel	$Y = 0.003\,X - 0.179$	0.996 **	< 0.0005
Linkeroever	$Y = 0.007\,X + 0.190$	0.967 **	< 0.0005
Bornem	$Y = 0.002\,X - 0.013$	0.937 **	< 0.0005
Mariekerke	$Y = 0.002\,X - 0.142$	0.944 **	< 0.0005
OVERALL	$Y = 0.003\,X + 0.071$	0.629 **	< 0.0005

** Correlation is significant at the 0.01 level (2-tailed).

Table D.10 – Pearson correlation matrix presenting the correlation coefficients (*r*) and statistical significances (*p*) between the relative amounts of Ag^+ ions, Ag ENPs, Ce^{3+} ions, and CeO_2 ENPs remaining in the supernatant of the sediment suspensions, and sediment physicochemical properties.

		pH	EC	OM	$CaCO_3$	TN	CEC	DOC	TP	Sand	Silt	Clay	Cl^-
Ag^+ ions	***r***	0.481	-0.285	-0.617 *	0.550	-0.642 *	-0.607 *	-0.695 *	-0.691 *	0.470	-0.369	-0.490	-0.045
	p	0.114	0.370	0.033	0.064	0.024	0.036	0.012	0.013	0.201	0.328	0.150	0.897
Ag ENPs	***r***	0.712 **	0.040	-0.702 *	0.741 **	-0.775 **	-0.732 **	-0.781 **	-0.860 **	0.521	-0.307	-0.680 *	0.303
	p	0.009	0.902	0.011	0.006	0.003	0.007	0.003	< 0.0005	0.151	0.421	0.030	0.366
Ce^{3+} ions	***r***	0.969 **	0.511	-0.439	0.912 **	-0.615 *	-0.533	-0.546	-0.799 **	0.134	0.194	-0.555	0.757 **
	p	< 0.0005	0.090	0.154	< 0.0005	0.033	0.074	0.066	0.002	0.732	0.617	0.096	0.007
CeO_2 ENPs	***r***	0.962 **	0.525	-0.134	0.917 **	-0.339	-0.245	-0.258	-0.578 *	-0.153	0.444	-0.302	0.748 **
	p	< 0.0005	0.080	0.678	< 0.0005	0.280	0.442	0.418	0.049	0.695	0.232	0.396	0.008

** Correlation is significant at the 0.01 level (2-tailed).

* Correlation is significant at the 0.05 level (2-tailed).

Table D.11 – Pearson correlation matrix presenting the correlation coefficients (*r*) and statistical significances (*p*) between the relative amounts of Ag^+ ions, Ag ENPs, Ce^{3+} ions, and CeO_2 ENPs remaining in the supernatant of the sediment suspensions, and sediment main and trace elements content.

		Ca	K	Na	Mg	Cd	Cr	Ni	Fe	Mn	Pb	Cu	Zn	Al	As
Ag^+ ions	***r***	0.437	-0.461	0.027	-0.425	-0.603 *	-0.600 *	-0.635 *	-0.561	-0.584 *	-0.680 *	-0.654 *	-0.647 *	-0.602 *	-0.249
	p	0.155	0.131	0.933	0.169	0.038	0.039	0.027	0.058	0.046	0.015	0.021	0.023	0.038	0.435
Ag ENPs	***r***	0.617 *	-0.523	0.352	-0.345	-0.786 **	-0.722 **	-0.773 **	-0.643 *	-0.728 **	-0.809 **	-0.796 **	-0.802 **	-0.698 *	-0.243
	p	0.033	0.081	0.262	0.273	0.002	0.008	0.003	0.024	0.007	0.001	0.002	0.002	0.012	0.447
Ce^{3+} ions	***r***	0.934 **	-0.398	0.787 **	0.178	-0.772 **	-0.528	-0.620 *	-0.378	-0.581 *	-0.663 *	-0.648 *	-0.701 *	-0.457	0.149
	p	< 0.0005	0.200	0.002	0.580	0.003	0.077	0.032	0.225	0.048	0.019	0.023	0.011	0.135	0.645
CeO_2 ENPs	***r***	0.964 **	-0.127	0.786 **	0.468	-0.581 *	-0.245	-0.344	-0.071	-0.304	-0.403	-0.380	-0.453	-0.167	0.379
	p	< 0.0005	0.694	0.002	0.125	0.048	0.444	0.273	0.827	0.336	0.194	0.223	0.140	0.605	0.224

** Correlation is significant at the 0.01 level (2-tailed).

* Correlation is significant at the 0.05 level (2-tailed).

Appendix E

Supplementary information to Chapter 7

"Fate of Ag and CeO_2 nanoparticles in soil suspensions and effect of natural organic matter on CeO_2 nanoparticles stability"

Blank soils

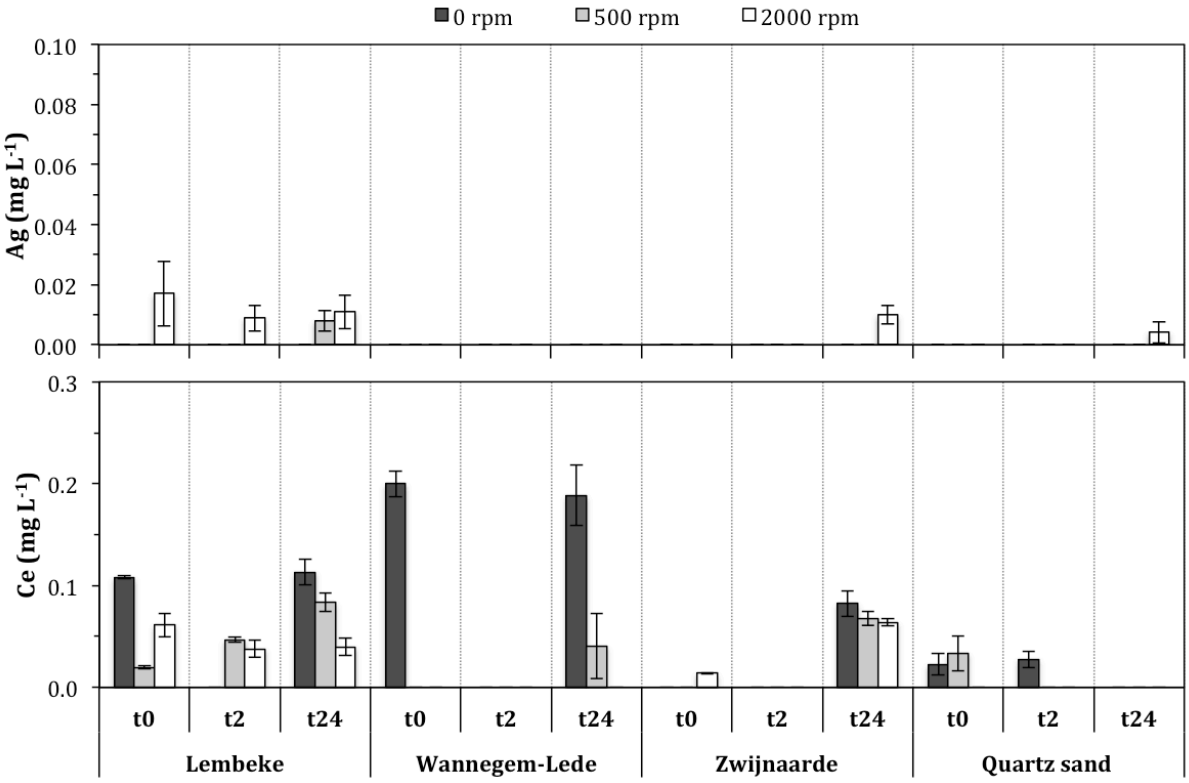

Figure E.1 – Silver (top graph) and cerium (bottom graph) concentrations determined in the liquid phase of blank soil suspensions, as affected by centrifugation speed, after centrifugation for 10 min. The speed of 0 rpm represents 10 min of gravitational settling. (Data shown are mean values, missing bars denote values below the detection limit (DL_{Ag} = 12 μg L^{-1}; DL_{Ce} = 25 μg L^{-1}), error bars indicate standard deviations, n = 3)

Pearson correlation analysis results

Table E.1 – Pearson correlation analysis results for the relationship between TOC content (*Y*) and amount of suspended matter (*X*), remaining in the liquid phase of blank soil suspensions.

Soil	Regression equation	Correlation coefficient (*r*)	Statistical significance (*p*)
Lembeke	$Y = 544.90\ X - 94.80$	0.986 **	< 0.0005
Wannegem-Lede	$Y = 55.82\ X + 22.64$	0.992 **	< 0.0005
Zwijnaarde	$Y = 235.45\ X + 22.83$	0.996 **	< 0.0005
OVERALL	$Y = 44.41\ X + 101.45$	0.460 *	0.016

** Correlation is significant at the 0.01 level (2-tailed).

* Correlation is significant at the 0.05 level (2-tailed).

Table E.2 – Pearson correlation analysis results for the relationship between the relative amount of silver (*Y*) and the suspended matter content (*X*), remaining in the liquid phase of soil suspensions spiked with Ag^+ ions.

Soil	Regression equation	Correlation coefficient (*r*)	Statistical significance (*p*)
Lembeke	$Y = 0.223\ X - 0.027$	0.955 **	< 0.0005
Wannegem-Lede	$Y = 0.087\ X + 0.028$	0.987 **	< 0.0005
Zwijnaarde	$Y = 0.098\ X + 0.022$	0.961 **	< 0.0005
OVERALL	$Y = 0.088\ X + 0.029$	0.971 **	< 0.0005

** Correlation is significant at the 0.01 level (2-tailed).

Table E.3 – Pearson correlation analysis results for the relationship between the relative amount of silver (*Y*) and the suspended matter content (*X*), remaining in the liquid phase of soil suspensions spiked with Ag ENPs.

Soil	Regression equation	Correlation coefficient (*r*)	Statistical significance (*p*)
Lembeke	$Y = 0.239\ X + 0.469$	0.894 **	0.001
Wannegem-Lede	$Y = 0.035\ X + 0.699$	0.891 **	0.001
Zwijnaarde	$Y = 0.055\ X + 0.834$	0.559	0.118
OVERALL	$Y = 0.041\ X + 0.697$	0.332	0.091

** Correlation is significant at the 0.01 level (2-tailed).

Table E.4 – Pearson correlation analysis results for the relationship between the relative amount of cerium (*Y*) and the suspended matter content (*X*), remaining in the liquid phase of soil suspensions spiked with Ce^{3+} ions.

Soil	Regression equation	Correlation coefficient (*r*)	Statistical significance (*p*)
Lembeke	$Y = 0.228\ X + 0.034$	0.979 **	< 0.0005
Wannegem-Lede	$Y = 0.023\ X - 0.015$	0.979 **	< 0.0005
Zwijnaarde	$Y = 0.082\ X + 0.006$	0.899 **	0.001
OVERALL	$Y = 0.003\ X + 0.069$	0.048	0.812

** Correlation is significant at the 0.01 level (2-tailed).

Table E.5 – Pearson correlation analysis results for the relationship between the relative amount of cerium (*Y*) and the suspended matter content (*X*), remaining in the liquid phase of soil suspensions spiked with CeO_2 ENPs.

Soil	Regression equation	Correlation coefficient (*r*)	Statistical significance (*p*)
Lembeke	$Y = 0.439\ X + 0.535$	0.951 **	< 0.0005
Wannegem-Lede	$Y = 0.067\ X + 0.254$	0.917 **	< 0.0005
Zwijnaarde	$Y = -0.046\ X + 0.919$	-0.495	0.175
OVERALL	$Y = -0.059\ X + 0.721$	-0.277	0.162

** Correlation is significant at the 0.01 level (2-tailed).

Table E.6 – Pearson correlation analysis results for the relationship between the relative amount of silver (*Y*) and the TOC content (*X*), remaining in the liquid phase of soil suspensions spiked with Ag^{+} ions.

Soil	Regression equation	Correlation coefficient (*r*)	Statistical significance (*p*)
Lembeke	$Y = 0.0004\ X + 0.015$	0.991 **	< 0.0005
Wannegem-Lede	$Y = 0.0015\ X + 0.007$	0.992 **	< 0.0005
Zwijnaarde	$Y = 0.0004\ X + 0.0143$	0.997 **	< 0.0005
OVERALL	$Y = 0.0006\ X + 0.030$	0.593 **	0.001

** Correlation is significant at the 0.01 level (2-tailed).

Table E.7 – Pearson correlation analysis results for the relationship between the relative amount of silver (*Y*) and the TOC content (*X*), remaining in the liquid phase of soil suspensions spiked with Ag ENPs.

Soil	Regression equation	Correlation coefficient (*r*)	Statistical significance (*p*)
Lembeke	$Y = 0.0004\,X + 0.513$	0.931 **	< 0.0005
Wannegem-Lede	$Y = 0.0006\,X + 0.685$	0.894 **	0.001
Zwijnaarde	$Y = 0.0002\,X + 0.830$	0.584	0.098
OVERALL	$Y = 0.0004\,X + 0.684$	0.271	0.172

** Correlation is significant at the 0.01 level (2-tailed).

Table E.8 – Pearson correlation analysis results for the relationship between the relative amount of cerium (*Y*) and the TOC content (*X*), remaining in the liquid phase of soil suspensions spiked with Ce^{3+} ions.

Soil	Regression equation	Correlation coefficient (*r*)	Statistical significance (*p*)
Lembeke	$Y = 0.0004\,X + 0.077$	0.979 **	< 0.0005
Wannegem-Lede	$Y = 0.0004\,X - 0.023$	0.956 **	< 0.0005
Zwijnaarde	$Y = 0.0003\,X - 0.001$	0.901 **	0.001
OVERALL	$Y = 0.0004\,X + 0.010$	0.695 **	< 0.0005

** Correlation is significant at the 0.01 level (2-tailed).

Table E.9 – Pearson correlation analysis results for the relationship between the relative amount of cerium (*Y*) and the TOC content (*X*), remaining in the liquid phase of soil suspensions spiked with CeO_2 ENPs.

Soil	Regression equation	Correlation coefficient (*r*)	Statistical significance (*p*)
Lembeke	$Y = 0.0007\,X + 0.619$	0.971 **	< 0.0005
Wannegem-Lede	$Y = 0.0012\,X + 0.230$	0.892 **	0.001
Zwijnaarde	$Y = -0.0002\,X + 0.920$	-0.470	0.202
OVERALL	$Y = 0.001\,X + 0.532$	0.381 *	0.050

** Correlation is significant at the 0.01 level (2-tailed).

* Correlation is significant at the 0.05 level (2-tailed).

Table E.10 – Pearson correlation matrix presenting the correlation coefficients (*r*) and statistical significances (*p*) between the relative amounts of Ag^{+} ions, Ag ENPs, Ce^{3+} ions, and CeO_2 ENPs remaining in the supernatant of the soil suspensions, and soil properties.

		pH	EC	OM	TN	CEC	DOC	TP	Sand	Silt	Clay
Ag^{+} ions	***r***	0.216	-0.700 *	-0.985**	-0.974**	-0.928**	-0.707*	-0.919**	0.359	0.979**	0.920**
	p	0.499	0.011	< 0.0005	< 0.0005	< 0.0005	0.033	< 0.0005	0.342	0.001	0.003
Ag ENPs	***r***	0.787 **	-0.135	-0.401	-0.347	-0.514	0.369	-0.340	0.041	0.388	0.532
	p	0.002	0.676	0.197	0.269	0.088	0.329	0.279	0.916	0.448	0.219
Ce^{3+} ions	***r***	-0.119	-0.922**	-0.937**	-0.931**	-0.981**	-0.152	-0.997**	0.649	-0.595	-0.759*
	p	0.712	< 0.0005	< 0.0005	< 0.0005	< 0.0005	0.696	< 0.0005	0.059	0.213	0.048
CeO_2 ENPs	***r***	-0.352	0.555	0.947**	0.938**	0.846**	0.681*	0.831**	-0.211	-0.965**	-0.960**
	p	0.262	0.061	< 0.0005	< 0.0005	0.001	0.044	0.001	0.586	0.002	0.001

** Correlation is significant at the 0.01 level (2-tailed).

* Correlation is significant at the 0.05 level (2-tailed).

Table E.11 – Pearson correlation matrix presenting the correlation coefficients (*r*) and statistical significances (*p*) between the relative amounts of Ag^{+} ions, Ag ENPs, Ce^{3+} ions, and CeO_2 ENPs remaining in the supernatant of the soil suspensions, and soil's main and trace elements content.

		Ca	K	Na	Mg	Cr	Ni	Fe	Mn	Pb	Cu	Zn	Al
Ag^{+} ions	***r***	0.843**	-0.322	-0.340	-0.268	0.967**	0.949**	-0.279	0.953**	-0.212	0.660	0.580	-0.464
	p	0.004	0.308	0.280	0.399	< 0.0005	< 0.0005	0.379	< 0.0005	0.584	0.053	0.101	0.128
Ag ENPs	***r***	0.664	0.025	-0.467	0.090	0.392	0.468	0.101	0.453	0.899**	0.839**	0.889**	0.011
	p	0.051	0.939	0.126	0.781	0.297	0.204	0.755	0.221	0.001	0.005	0.001	0.973
Ce^{3+} ions	***r***	-0.845**	-0.661*	-0.562	-0.620*	-0.618	-0.690*	-0.629*	-0.682*	-0.768*	-0.955**	-0.980**	-0.772**
	p	0.004	0.019	0.057	0.032	0.076	0.040	0.028	0.043	0.016	< 0.0005	< 0.0005	0.003
CeO_2 ENPs	***r***	-0.885**	0.142	0.205	0.086	-0.965**	-0.956**	0.099	-0.960**	0.094	-0.726*	-0.666*	0.294
	p	0.001	0.661	0.523	0.790	< 0.0005	< 0.0005	0.759	< 0.0005	0.811	0.027	0.050	0.353

** Correlation is significant at the 0.01 level (2-tailed).

* Correlation is significant at the 0.05 level (2-tailed).

Appendix F

Supplementary information to Chapter 8

"Impact of carboxymethyl cellulose coating on FeS nanoparticles stability, transport, and mobilization potential of trace metals present in soils and sediment"

Synthesis and characterization of FeS ENPs

Table F.1 – Impact of CMC and FeS concentration on the *Z*-average size of the synthesized nanoparticles. (mean value ± standard deviation, *n* = 3)

No.	Synthesis condition	Hydrodynamic diameter (nm)
1	500 mg L^{-1} FeS, 0.05 % CMC	154.5 ± 5.8
2	50 mg L^{-1} FeS, 0.05 % CMC	757.6 ± 19.0
3	50 mg L^{-1} FeS, 0.005 % CMC	519.9 ± 13.2
4	500 mg L^{-1} FeS, 0 % CMC	NM

NM: not measureable via PCS analysis due to the large size and rapid settling of the particulates from solution.

Soil and sediment characterization

Table F.2 – Physicochemical properties of the different soil/sediment samples. (mean ± standard deviation, *n* = 3)

Parameter		S1	S2	S3
pH-H_2O	**(-)**	7.68 ± 0.09	6.83 ± 0.01	7.55 ± 0.03
EC	**(μS cm^{-1})**	221.7 ± 2.1	86.4 ± 26.7	930 ± 11
CEC	**($cmol_c$ kg^{-1})**	4.03 ± 0.03	7.20 ± 0.29	24.3 ± 0.2
OM	**(%)**	2.20 ± 0.10	4.84 ± 0.17	9.35 ± 0.13
$CaCO_3$	**(%)**	4.00 ± 0.80	NM	10.2 ± 0.5
TN	**(g kg^{-1})**	0.29 ± 0.01	0.22 ± 0.04	3.41 ± 0.02
TP	**(mg kg^{-1})**	601 ± 16	0.08 ± 0.01	2.89 ± 0.03
Sand	**(%)**	76.5	88	26.0 ± 0.1
Silt	**(%)**	17.4	8	47.3 ± 0.5
Clay	**(%)**	6.1	4	26.7 ± 0.7

NM: not measured.

Table F.3 – Major and trace elements content of the different soil/sediment samples. (mean value ± standard deviation, *n* = 3)

Element		S1	S2	S3
Ca	**(g kg^{-1})**	68.2 ± 4.9	1.45 ± 0.04	47.1 ± 0.2
Mg	**(g kg^{-1})**	4.82 ± 0.41	0.30 ± 0.01	5.87 ± 0.09
K	**(g kg^{-1})**	0.62 ± 0.02	0.47 ± 0.01	5.78 ± 0.19
Na	**(mg kg^{-1})**	155 ± 9	31.1 ± 3.0	497 ± 9
Al	**(g kg^{-1})**	6.47 ± 0.17	2.90 ± 0.06	21.1 ± 0.84
Fe	**(g kg^{-1})**	8.58 ± 0.11	1.75 ± 0.04	40.1 ± 0.4
As	**(mg kg^{-1})**	10.4 ± 3.3	< 10	28.5 ± 1.5
Cd	**(mg kg^{-1})**	< 0.4	11.3 ± 0.5	3.84 ± 0.11
Co	**(mg kg^{-1})**	< 4.0	< 4.0	5.33 ± 0.73
Cr	**(mg kg^{-1})**	11.8 ± 0.4	8.33 ± 0.41	41.7 ± 1.1
Cu	**(mg kg^{-1})**	38.7 ± 1.5	31.6 ± 1.1	61.0 ± 0.8
Hg	**(mg kg^{-1})**	20.8 ± 0.7	0.44 ± 0.01	0.61 ± 0.01
Mn	**(mg kg^{-1})**	341 ± 30	47.1 ± 0.8	1068 ± 8
Ni	**(mg kg^{-1})**	22.1 ± 0.3	2.8 ± 0.3	33.3 ± 1.6
Pb	**(mg kg^{-1})**	38.2 ± 2.9	273 ± 17	87.7 ± 1.5
Zn	**(mg kg^{-1})**	61.8 ± 2.1	651 ± 17	455 ± 2

Data presented as "<" indicate values below the detection limit (DL).

Leaching of trace metals: batch experiments

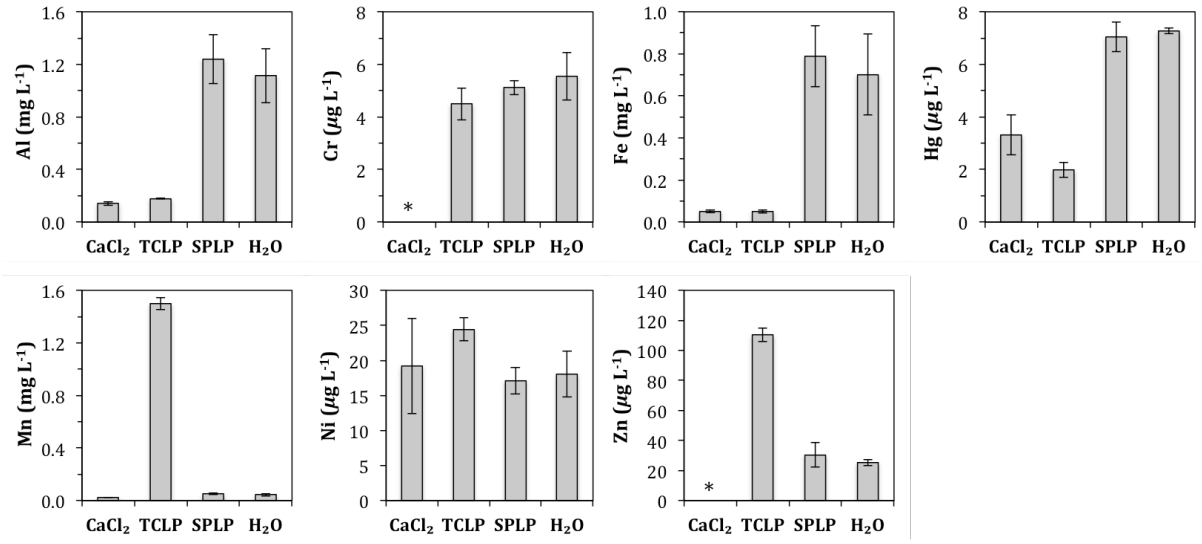

Figure F.1 – Leaching of trace metals from S1 upon extraction with $CaCl_2$, TCLP, or SPLP solution, or with Milli-Q® water. (Bars represent mean values, values below the detection limit are either indicated with an asterisk or were omitted from the figure (DL_{As} = 100 μg L^{-1}; DL_{Cd} = 4.0 μg L^{-1}; DL_{Co} = 40 μg L^{-1}; DL_{Cr} = 4.0 μg L^{-1}; DL_{Cu} = 10 μg L^{-1}; DL_{Pb} = 40 μg L^{-1}; DL_{Zn} = 20 μg L^{-1}), error bars denote standard deviations, *n* = 3)

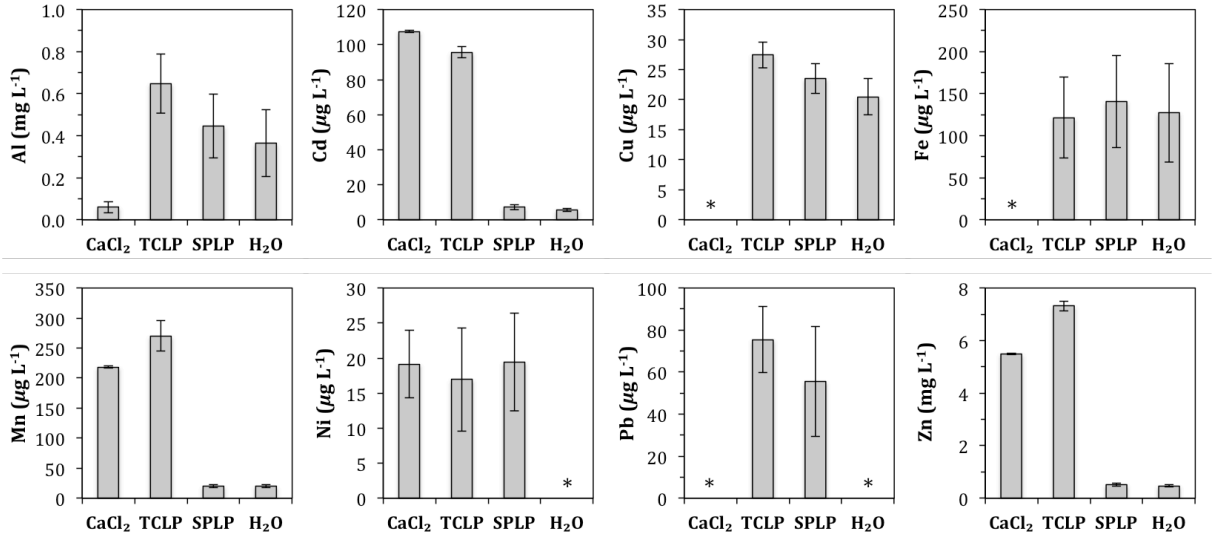

Figure F.2 – Leaching of trace metals from S2 upon extraction with $CaCl_2$, TCLP, or SPLP solution, or with Milli-Q® water. (Bars represent mean values, values below the detection limit are either indicated with an asterisk or were omitted from the figure (DL_{As} = 100 μg L^{-1}; DL_{Co} = 40 μg L^{-1}; DL_{Cr} = 4.0 μg L^{-1}; DL_{Fe} = 40 μg L^{-1}; DL_{Ni} = 12 μg L^{-1}; DL_{Pb} = 40 μg L^{-1}), error bars denote standard deviations, n = 3)

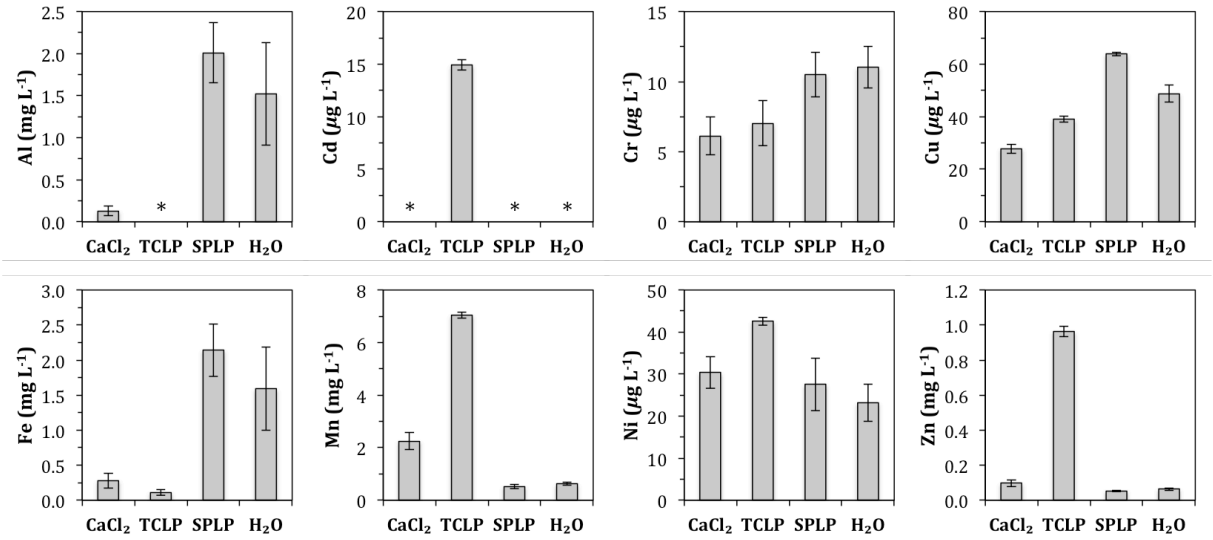

Figure F.3 – Leaching of trace metals from S3 upon extraction with $CaCl_2$, TCLP, or SPLP solution, or with Milli-Q® water. (Bars represent mean values, values below the detection limit are either indicated with an asterisk or were omitted from the figure (DL_{Al} = 50 μg L^{-1}; DL_{As} = 100 μg L^{-1}; DL_{Cd} = 4.0 μg L^{-1}; DL_{Co} = 40 μg L^{-1}; DL_{Pb} = 40 μg L^{-1}), error bars denote standard deviations, n = 3)

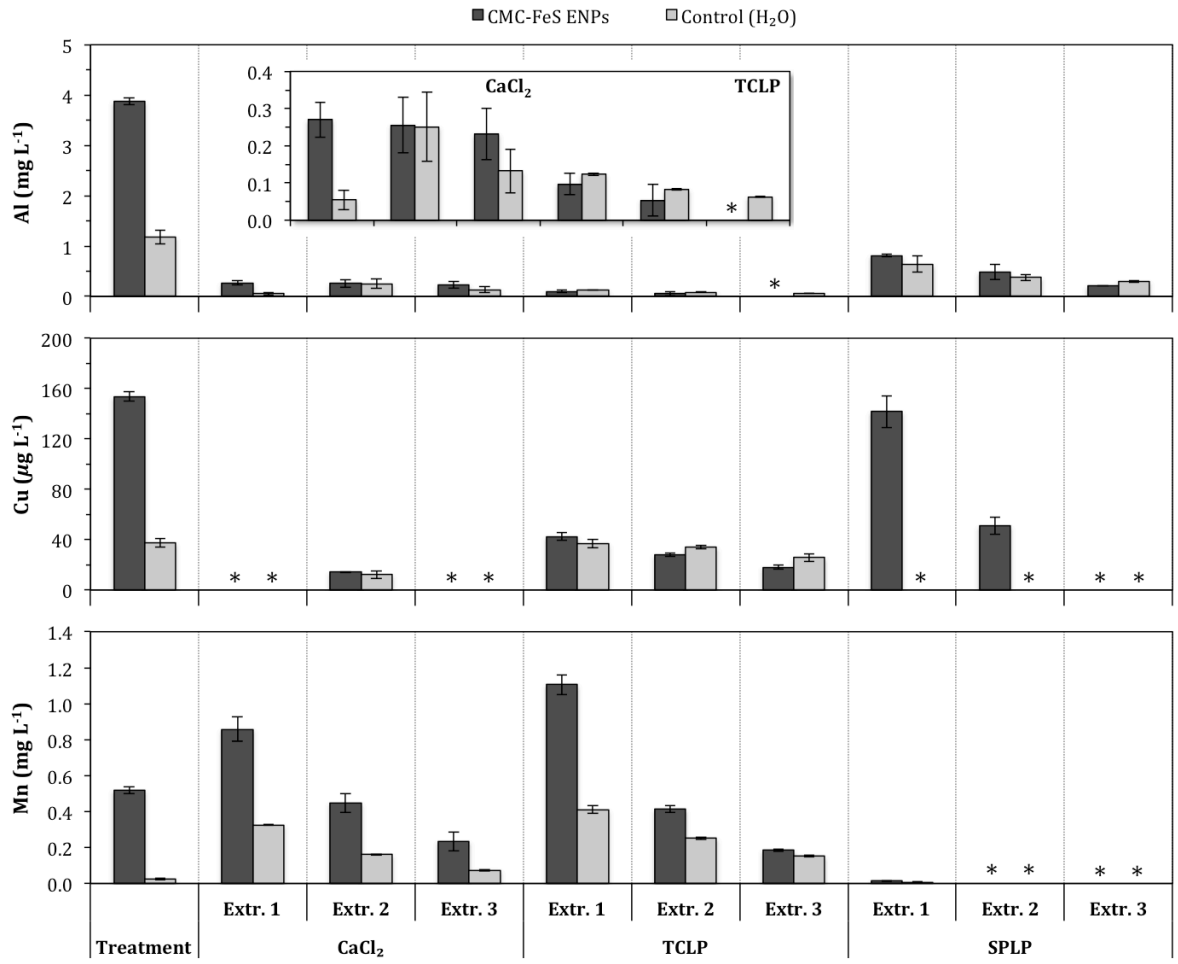

Figure F.4 – Leaching of Al, Cu, and Mn upon treatment of S2 with 500 mg L^{-1} CMC-FeS ENPs, and following a threefold sequential extraction of the treated soil residue with $CaCl_2$, TCLP, or SPLP solution. Milli-Q® water was used for the control treatment. The inset in the top graph shows a close-up of the sequential extraction of Al using $CaCl_2$ or TCLP solution. (Bars represent mean values, values below the detection limit are indicated with an asterisk (DL_{Al} = 50 μg L^{-1}; DL_{Cu} = 10 μg L^{-1}; DL_{Mn} = 5.0 μg L^{-1}), error bars denote standard deviations, n = 3)

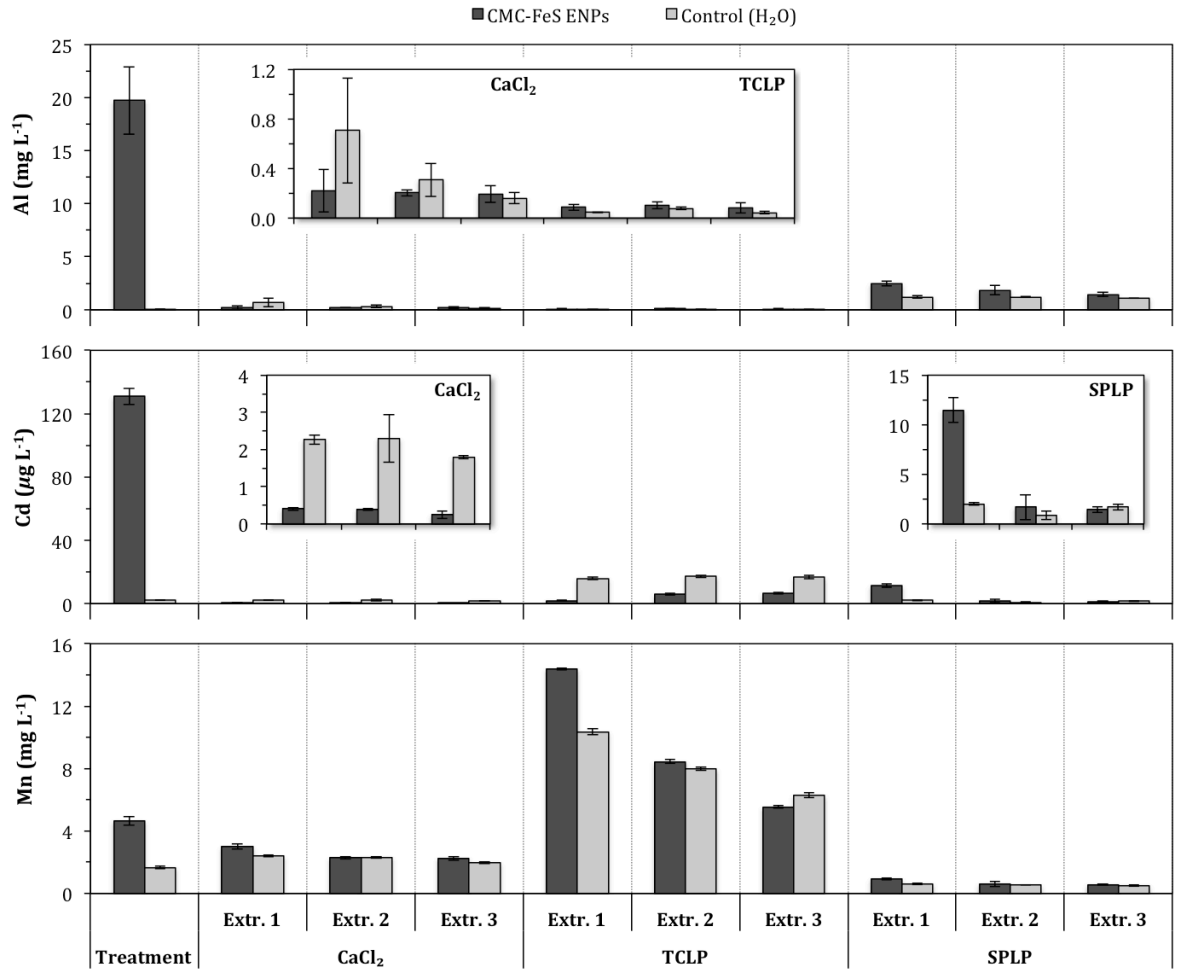

Figure F.5 – Leaching of Al, Cd, and Mn upon treatment of S3 with 500 mg L^{-1} CMC-FeS ENPs, and following a threefold sequential extraction of the treated sediment residue with $CaCl_2$, TCLP, or SPLP solution. Milli-Q® water was used for the control treatment. The insets show close-ups of the sequential extraction of Al using $CaCl_2$ or TCLP solution (top graph), and of Cd using $CaCl_2$ or SPLP solution (middle graph). (Bars represent mean values, error bars denote standard deviations, n = 3)

Appendix G

Supplementary information to Chapter 9

"Partitioning behaviour of Ag nanoparticles in suspensions of field-incubated sediment under controlled redox conditions"

Ag ENPs characterization data

Table G.1 – Characterization information of the 40 nm NanoXact™ citrate- and polyvinylpyrrolidone-coated silver nanoparticles (Cit-Ag and PVP-Ag ENPs).

Parameter	Unit	Cit-Ag ENPs	PVP-Ag ENPs
Particle diameter	**(nm)**	40.6 ± 4.1	39.0 ± 5.2
Hydrodynamic diameter	**(nm)**	42.5	54.2
Surface area	**(m^2 g^{-1})**	13.8	14.2
Zeta (ζ) potential	**(mV)**	-39.4	-44.3
Particle concentration	**(particles mL^{-1})**	5.9 x10^{10}	6.8 x 10^{10}
Mass concentration	**(mg Ag mL^{-1})**	0.022	0.023
Solution pH	**(-)**	7.7	5.7
Particle surface	**N/A**	Sodium citrate	PVP
Solvent	**N/A**	Aqueous 2 mM Citrate	Milli-Q® water

Characterization data kindly provided by nanoComposix Europe.

N/A: not applicable

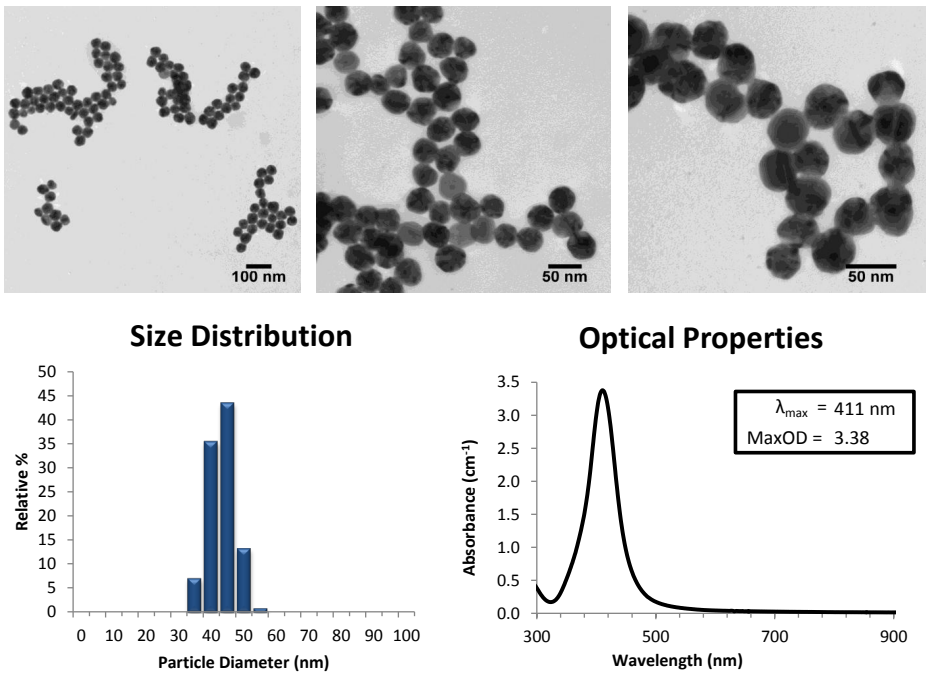

Figure G.1 – TEM images (top), particle size distribution (bottom left), and UV-Vis absorption spectrum (bottom right) of the 40 nm NanoXact™ citrate-coated silver nanoparticles (Cit-Ag ENPs) dispersed in aqueous 2 mM citrate solution, kindly provided by nanoComposix Europe.

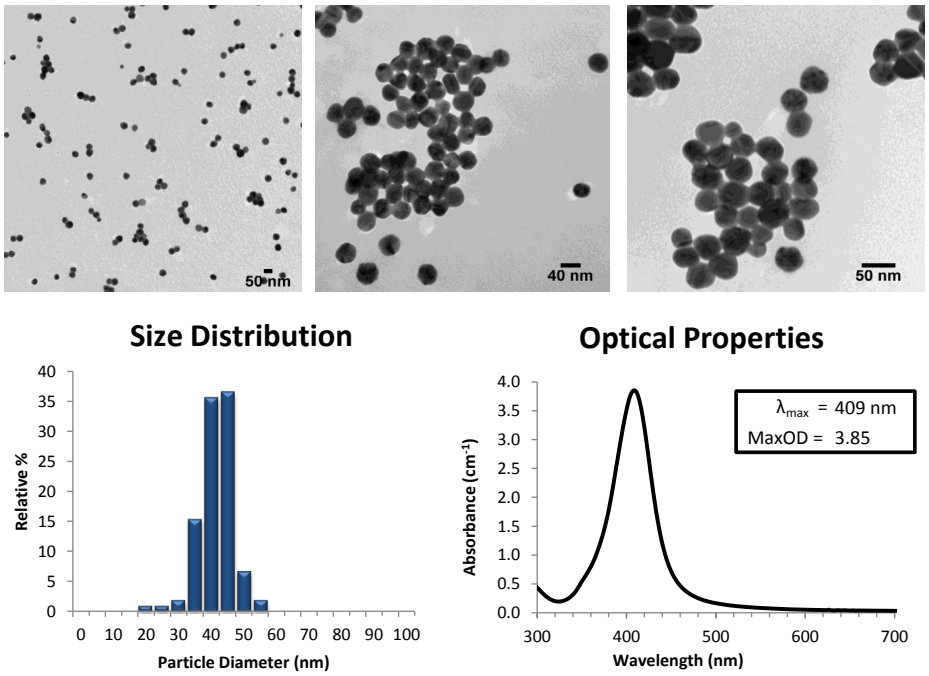

Figure G.2 – TEM images (top), particle size distribution (bottom left), and UV-Vis absorption spectrum (bottom right) of the 40 nm NanoXact™ polyvinylpyrrolidone-coated silver nanoparticles (PVP-Ag ENPs) dispersed in Milli-Q® water, kindly provided by nanoComposix Europe.

Partitioning behaviour and fate of Ag ENPs in (re)suspended sediment under controlled redox conditions

Table G.2 – Silver content remaining in the supernatant of untreated sediment suspensions (*i.e.*, controls), after 24, 72, 144, 168, and 192 h of MC incubation under O_2 or N_2/O_2 redox conditions. The supernatants were obtained from centrifuging 50 mL slurry samples at 1000 rpm for 10 min. Data is presented as mean ± standard deviation (n = 1).

Sediment type	Redox condition	Ag (μg L^{-1})				
		24 h	72 h	144 h	168 h	192 h
Dry	O_2	2.1	1.5	2.1	-	2.4
Oxic fresh	O_2	3.9	3.5	3.6	-	2.3
Dry	N_2/O_2	2.6	3.2	2.3	3.1	2.9
Anoxic fresh	N_2/O_2	2.8	3.6	3.2	3.1	3.5

Table G.3 – Total organic carbon (TOC), inorganic carbon (IC), chloride (Cl^-), and sulphate (SO_4^{2-}) content in 0.45 μm filtrates of the supernatant of untreated sediment suspensions (*i.e.*, controls), after 24, 72, 144, 168, and 192 h of MC incubation under O_2 or N_2/O_2 redox conditions. The supernatants were obtained from centrifuging 50 mL slurry samples at 1000 rpm for 10 min. (n = 1)

Sediment type	Redox condition	Parameter		24 h	72 h	144 h	168 h	192 h
Dry	O_2	TOC	(mg L^{-1})	-	167	162	-	130
		IC	(mg L^{-1})	-	17	18	-	22
		Cl^-	(mg L^{-1})	50	58	67	-	72
		SO_4^{2-}	(mg L^{-1})	182	447	643	-	692
Oxic fresh	O_2	TOC	(mg L^{-1})	64	66	66	-	58
		IC	(mg L^{-1})	26	33	23	-	30
		Cl^-	(mg L^{-1})	10	14	21	-	25
		SO_4^{2-}	(mg L^{-1})	84	113	154	-	183
Dry	N_2/O_2	TOC	(mg L^{-1})	230	233	234	186	174
		IC	(mg L^{-1})	14.8	22	20	31	19
		Cl^-	(mg L^{-1})	45	58	61	69	67
		SO_4^{2-}	(mg L^{-1})	162	195	190	251	394
Anoxic fresh	N_2/O_2	TOC	(mg L^{-1})	123	135	132	135	121
		IC	(mg L^{-1})	60	43	17	12	11
		Cl^-	(mg L^{-1})	36	40	50	54	63
		SO_4^{2-}	(mg L^{-1})	65	62	48	65	96

NO_3^- and PO_4^{3-} concentrations were generally below 1.4 and 1.5 mg L^{-1}, respectively.

Table G.4 – Total organic carbon (TOC), inorganic carbon (IC), chloride (Cl^-), and sulphate (SO_4^{2-}) content in 0.45 μm filtrates of the supernatant of sediment suspensions treated with 200 μg L^{-1} Ag^+ ions, after 24, 72, 144, 168, and 192 h of MC incubation under O_2 or N_2/O_2 redox conditions. The supernatants were obtained from centrifuging 50 mL slurry samples at 1000 rpm for 10 min. (mean ± standard deviation, n = 3)

Sediment type	Redox condition	Parameter		24 h	72 h	144 h	168 h	192 h
Dry	**O_2**	**TOC**	**(mg L^{-1})**	242 ± 3.8	186 ± 7.8	157 ± 7.6	-	94.9 ± 39.2
		IC	**(mg L^{-1})**	11.6 ± 0.5	22.6 ± 1.9	36.4 ± 2.5	-	25.7 ± 11.7
		Cl^-	**(mg L^{-1})**	52.1 ± 3.9	59.0 ± 4.6	71.1 ± 4.6	-	78.7 ± 8.5
		SO_4^{2-}	**(mg L^{-1})**	192 ± 1.2	315 ± 21	554 ± 105	-	533 ± 124
Oxic fresh	**O_2**	**TOC**	**(mg L^{-1})**	40.9 ± 11.1	54.1 ± 6.2	50.1 ± 4.5	-	50.0 ± 5.1
		IC	**(mg L^{-1})**	12.3 ± 2.9	22.2 ± 3.8	26.6 ± 5.2	-	38.7 ± 6.1
		Cl^-	**(mg L^{-1})**	10.5 ± 0.6	16.3 ± 2.0	25.3 ± 4.3	-	31.1 ± 5.8
		SO_4^{2-}	**(mg L^{-1})**	84.3 ± 26.1	172 ± 37	225 ± 47	-	268 ± 67
Dry	**N_2/O_2**	**TOC**	**(mg L^{-1})**	220 ± 34	226 ± 20	206 ± 8	196 ± 8	187 ± 11
		IC	**(mg L^{-1})**	13.4 ± 2.3	20.1 ± 1.6	47.9 ± 1.2	22.2 ± 6.4	21.3 ± 1.4
		Cl^-	**(mg L^{-1})**	43.3 ± 4.3	56.7 ± 1.4	65.3 ± 6.4	72.7 ± 6.6	73.5 ± 8.7
		SO_4^{2-}	**(mg L^{-1})**	153 ± 35	190 ± 18	193 ± 1	235 ± 29	284 ± 115
Anoxic fresh	**N_2/O_2**	**TOC**	**(mg L^{-1})**	96.6 ± 7.9	128 ± 13	130 ± 7	124 ± 4	116 ± 6
		IC	**(mg L^{-1})**	41.1 ± 14.0	11.7 ± 7.8	9.1 ± 3.0	9.7 ± 3.0	9.3 ± 3.0
		Cl^-	**(mg L^{-1})**	37.3 ± 2.2	43.5 ± 1.4	55.0 ± 2.4	58.3 ± 3.1	63.1 ± 2.6
		SO_4^{2-}	**(mg L^{-1})**	4.5 ± 6.4	6.7 ± 7.3	7.4 ± 6.9	28.4 ± 6.8	83.1 ± 17.0

NO_3^- and PO_4^{3-} concentrations were generally below 10 and 1.4 mg L^{-1}, respectively.

Table G.5 – Total organic carbon (TOC), inorganic carbon (IC), chloride (Cl^-), and sulphate (SO_4^{2-}) content in 0.45 μm filtrates of the supernatant of sediment suspensions treated with 200 μg L^{-1} Cit-Ag ENPs, after 24, 72, 144, 168, and 192 h of MC incubation under O_2 or N_2/O_2 redox conditions. The supernatants were obtained from centrifuging 50 mL slurry samples at 1000 rpm for 10 min. (mean ± standard deviation, n = 3)

Sediment type	Redox condition	Parameter		24 h	72 h	144 h	168 h	192 h
Dry	**O_2**	**TOC**	**(mg L^{-1})**	184 ± 17	149 ± 12	136 ± 11	-	120 ± 9
		IC	**(mg L^{-1})**	14.8 ± 4.4	24.4 ± 11.3	24.8 ± 12.2	-	20.2 ± 5.7
		Cl^-	**(mg L^{-1})**	47.6 ± 2.7	56.8 ± 1.4	63.3 ± 2.8	-	68.6 ± 3.6
		SO_4^{2-}	**(mg L^{-1})**	186 ± 38	410 ± 139	588 ± 133	-	632 ± 77
Oxic fresh	**O_2**	**TOC**	**(mg L^{-1})**	57.8 ± 7.4	54.3 ±3.6	44.3 ± 0.4	-	48.4 ± 4.5
		IC	**(mg L^{-1})**	14.9 ± 5.8	22.5 ± 6.0	28.0 ± 1.2	-	34.8 ± 1.8
		Cl^-	**(mg L^{-1})**	11.6 ± 0.1	18.5 ± 0.2	28.3 ± 2.9	-	36.7 ± 0.9
		SO_4^{2-}	**(mg L^{-1})**	75.1 ± 16.2	201 ± 31	258 ± 41	-	300 ± 41
Dry	**N_2/O_2**	**TOC**	**(mg L^{-1})**	211 ± 44	230 ± 16	188 ± 46	186 ± 11	187 ± 17
		IC	**(mg L^{-1})**	13.0 ± 1.3	20.2 ± 1.6	40.9 ± 2.2	21.7 ± 2.3	16.8 ± 2.1
		Cl^-	**(mg L^{-1})**	37.8 ± 12.5	57.6 ± 1.4	59.2 ± 0.5	72.7 ± 6.6	65.9 ± 3.3
		SO_4^{2-}	**(mg L^{-1})**	147 ± 49	181 ± 21	182 ± 1	235 ± 29	283 ± 85
Anoxic fresh	**N_2/O_2**	**TOC**	**(mg L^{-1})**	110 ± 9	136 ± 11	125 ± 32	129 ± 20	122 ± 16
		IC	**(mg L^{-1})**	52.6 ± 3.8	18.9 ± 11.1	14.6 ± 13.8	14.3 ± 7.6	10.6 ± 1.5
		Cl^-	**(mg L^{-1})**	35.6 ± 0.7	42.8 ± 2.0	48.4 ± 2.9	51.9 ± 3.8	54.7 ± 3.6
		SO_4^{2-}	**(mg L^{-1})**	35.9 ± 21.9	35.2 ± 24.9	32.7 ± 23.2	107 ± 123	179 ± 158

NO_3^- and PO_4^{3-} concentrations were generally below 1.8 and 1.6 mg L^{-1}, respectively.

Table G.6 – Total organic carbon (TOC), inorganic carbon (IC), chloride (Cl^-), and sulphate (SO_4^{2-}) content in 0.45 μm filtrates of the supernatant of sediment suspensions treated with 200 μg L^{-1} PVP-Ag ENPs, after 24, 72, 144, 168, and 192 h of MC incubation under O_2 or N_2/O_2 redox conditions. The supernatants were obtained from centrifuging 50 mL slurry samples at 1000 rpm for 10 min. (mean ± standard deviation, n = 3)

Sediment type	Redox condition	Parameter		24 h	72 h	144 h	168 h	192 h
Dry	**O_2**	**TOC**	**(mg L^{-1})**	198 ± 15	181 ± 19	144 ± 3	-	115 ± 5
		IC	**(mg L^{-1})**	14.1 ± 4.2	25.7 ± 9.5	21.1 ± 7.9	-	20.4 ± 4.1
		Cl^-	**(mg L^{-1})**	49.6 ± 0.6	55.4 ± 1.9	61.7 ± 4.1	-	65.1 ± 4.1
		SO_4^{2-}	**(mg L^{-1})**	193 ± 25	345 ± 43	537 ± 44	-	597 ± 18
Oxic fresh	**O_2**	**TOC**	**(mg L^{-1})**	72.4 ± 7.6	66.0 ± 2.8	58.1 ± 3.3	-	55.0 ± 3.3
		IC	**(mg L^{-1})**	16.8 ± 1.7	23.3 ± 1.1	30.1 ± 5.4	-	32.9 ± 3.7
		Cl^-	**(mg L^{-1})**	11.8 ± 1.0	18.2 ± 2.7	29.1 ± 5.3	-	36.0 ± 7.3
		SO_4^{2-}	**(mg L^{-1})**	109 ± 18	259 ± 13	367 ± 14	-	401 ± 18
Dry	**N_2/O_2**	**TOC**	**(mg L^{-1})**	240 ± 3	234 ± 5	219 ± 9	187 ± 11	181 ± 14
		IC	**(mg L^{-1})**	13.1 ± 0.9	19.7 ± 4.2	49.4 ± 11.5	21.3 ± 1.4	14.8 ± 3.7
		Cl^-	**(mg L^{-1})**	46.0 ± 1.1	59.8 ± 1.6	67.2 ± 5.1	74.4 ± 4.8	76.2 ± 6.7
		SO_4^{2-}	**(mg L^{-1})**	177 ± 5	197 ± 2	251 ± 124	303 ± 113	295 ± 115
Anoxic fresh	**N_2/O_2**	**TOC**	**(mg L^{-1})**	103 ± 5	116 ± 5	130 ± 4	126 ± 4	129 ± 9
		IC	**(mg L^{-1})**	42.5 ± 21.4	17.4 ± 10.1	20.1 ± 7.3	9.3 ± 4.8	8.6 ± 6.0
		Cl^-	**(mg L^{-1})**	34.4 ± 2.1	40.0 ± 2.0	46.9 ± 7.4	52.7 ± 6.7	55.3 ± 7.5
		SO_4^{2-}	**(mg L^{-1})**	19.7 ± 20.0	18.2 ± 19.3	14.1 ± 14.7	37.3 ± 16.7	77.4 ± 13.4

NO_3^- and PO_4^{3-} concentrations were generally below 1.5 and 1.6 mg L^{-1}, respectively.

Table G.7 – Acid volatile sulphide (AVS) content of the dry and anoxic fresh sediment prior to MC incubation (t_0), and after selected times during MC incubation in the absence (Control) and presence of 200 μg L^{-1} Ag^+ ions, Cit-Ag ENPs, or PVP-Ag ENPs. (n =1)

Sediment type	**Redox condition**	**Incubation treatment**	**AVS (mg S^{2-} g^{-1} DM)**			
			t_0	**24 h**	**144 h**	**192 h**
Dry	**-**	**-**	0.02	-	-	-
	N_2/O_2	**Control**	-	-	0.13	0.05
		Ag^+ ions	-	-	0.17	-
		Cit-Ag ENPs	-	-	0.10	-
		PVP-Ag ENPs	-	-	0.15	-
Anoxic fresh	**-**	**-**	3.08	-	-	-
	N_2/O_2	**Control**	-	3.05	2.81	0.08
		Ag^+ ions	-	-	2.73	-
		Cit-Ag ENPs	-	-	2.82	-
		PVP-Ag ENPs	-	-	2.71	-

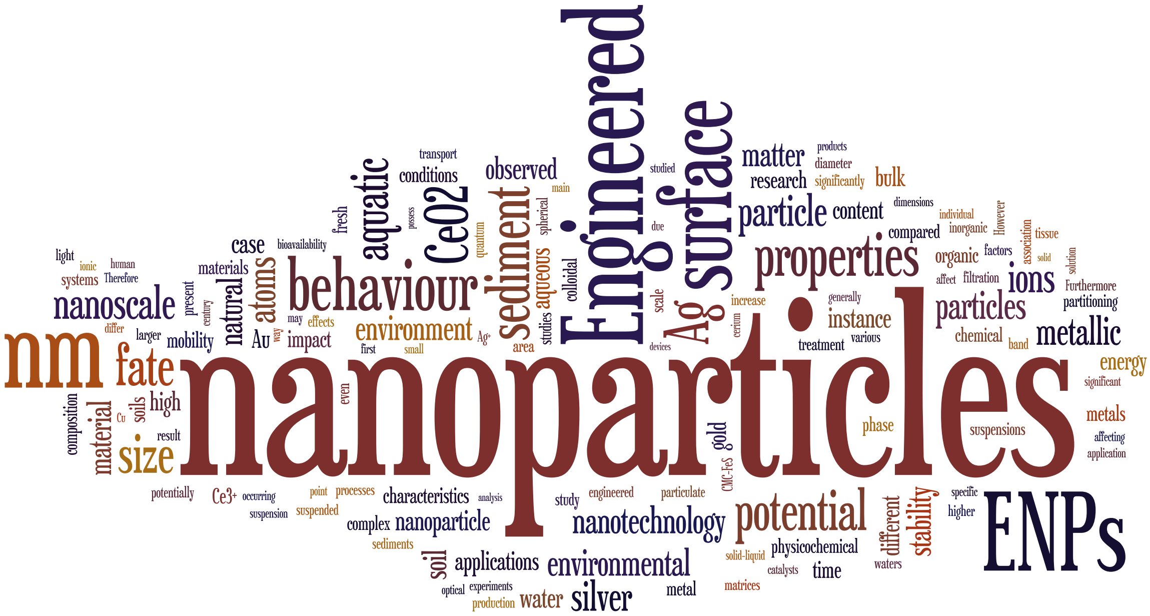

nanoparticles
Engineered
surface
behaviour
ENPs
nm
fate
properties
potential
sediment
CeO2
aquatic
nanoscale
size
particles
particle
ions
metallic
nanotechnology
environmental
silver
nanoparticle
stability
different
instance
matter
observed
atoms
natural
environment
material
high
soil
applications
water
physicochemical
characteristics
complex
bulk
energy
metals
phase
gold
Ag
Au
Ce3+